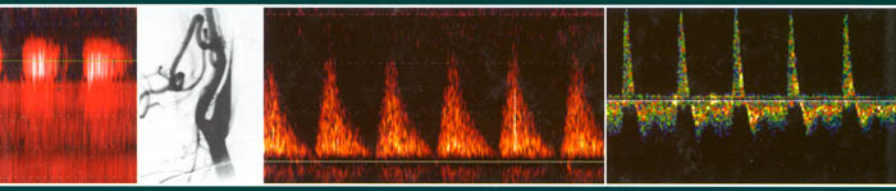

Cerebrovascular Ultrasound in Stroke Prevention and Treatment

Edited by Andrei V. Alexandrov

Foreword by James C. Grotta

FUTURA

Blackwell Publishing

Cerebrovascular Ultrasound in Stroke Prevention and Treatment

This page intentionally left blank

Cerebrovascular Ultrasound in Stroke Prevention and Treatment

EDITED BY

Andrei V. Alexandrov, MD, RVT

Assistant Professor of Neurology and Radiology
Director, STAT Neurosonology Service and
Center for Noninvasive Brain Perfusion Studies
Stroke Program, University of Texas-Houston Medical School
Houston, TX

FOREWORD BY

James C. Grotta, MD

Blackwell
Publishing

Futura, an imprint of Blackwell Publishing

© 2004 by Futura, an imprint of Blackwell Publishing

Blackwell Publishing, Inc./Futura Division, 3 West Main Street, Elmsford, New York 10523, USA
Blackwell Publishing, Inc., 350 Main Street, Malden, Massachusetts 02148-5020, USA
Blackwell Publishing Ltd, 9600 Garsington Road, Oxford OX4 2DQ
Blackwell Science Asia Pty Ltd, 550 Swanston Street, Carlton, Victoria 3053, Australia

All rights reserved. No part of this publication may be reproduced in any form or by any electronic or mechanical means, including information storage and retrieval systems, without permission in writing from the publisher, except by a reviewer who may quote brief passages in a review.

04 05 06 07 5 4 3 2 1

ISBN: 0-4051-0381-7

Library of Congress Cataloging-in-Publication Data

Cerebrovascular ultrasound in stroke prevention and treatment /
edited by Andrei V. Alexandrov; foreword by James C. Grotta.
p. ; cm.
Includes bibliographical references and index.
ISBN 1-4051-0381-7
1. Cerebrovascular disease—Ultrasonic imaging.
I. Alexandrov, Andrei V.
[DNLM: 1. Cerebrovascular Accident—ultrasonography.
2. Cerebrovascular Accident—therapy. WL 355 C4142 2003]
RC388.5.C4345 2003
616.8'107543—dc21
2003009007

A catalogue record for this title is available from the British Library

Acquisitions: Steven Korn
Production: Julie Elliott
Typesetter: Graphicraft Limited, Hong Kong
Printed and bound in Great Britain by CPI Bath, Bath

For further information on Blackwell Publishing, visit our website:
www.blackwellfutura.com
www.blackwellpublishing.com

Foreword
Ultrasound: a clinician's perspective

The greatest advances in understanding and treating stroke have occurred in the past 30 years. This progress has coincided and largely resulted from our dramatically improved ability to diagnose stroke and its subtypes, characterize its location and severity, and understand its causes rapidly, accurately and in real time. This has taken some of the charm out of clinical stroke care as the senior readers of this book will still remember even the most astute clinicians' conclusions based on a careful history and physical exam proven wrong at the postmortem table. But the positive benefits of technology and improved diagnostic capability far exceed our nostalgia for the 'good old days' when we relied mainly on our clinical acumen. What constitutes our improved ability to diagnose stroke? Unlike many other diseases, precise diagnosis of stroke depends almost entirely on imaging.

Our diagnostic capability took its greatest leap forward with the development of brain imaging, first with X-ray computed tomography, and more recently with magnetic resonance imaging. Brain imaging has enabled us to quickly and accurately differentiate between infarct and hemorrhage, determine the location and surmise the probable cause, and establish the age and severity of most strokes rapidly and painlessly. Brain imaging is now the first step in stroke diagnosis and treatment, and has been called the 'EKG of stroke'. This technology is now available in the vast majority of hospitals in the developed world and, more than any other component of our clinical management, distinguishes 21st century stroke care.

Physiologic imaging developed almost concomitantly with structural brain imaging. Our ability to investigate cerebral blood flow and metabolism using radio-labeled tracers enabled us to see that acute and chronic stroke is a dynamic and potentially reversible process that would eventually yield to timely and precise therapeutic intervention. Pioneering studies using xenon and positron emitting isotopes demonstrated reduced cerebral blood flow distal to chronic extracranial and intracranial occlusion or vasospasm, and, most importantly, revealed the 'ischemic penumbra' of reversibly damaged brain tissue in acute stroke patients that has yielded so far to timely reperfusion and, at least experimentally, to so called 'neuroprotective' therapies targeting downstream consequences of interrupted blood flow. Furthermore, the linkage of cerebral blood flow and metabolism discovered with physiologic imaging has generated our ability to carry out 'functional imaging'. This technology is not only helping us understand the functional anatomy of simple and complex behaviors, but has also given visible proof of the plasticity of brain function. This has given a huge boost to research into treatment aimed at amplifying stroke recovery.

Imaging the vascular bed is the third critical aspect of stroke diagnosis. The seductive complexity of the brain draws our attention, but the stroke clinician must never lose sight of the fact that stroke is first and foremost a disease of the blood vessels nourishing that organ. Vascular imaging has been available to clinicians longer than our ability to image the brain parenchyma. Catheter arteriography can reveal the anatomy of extracranial and intracranial occlusive disease, aneurysms and arterio-venous malformations, and for decades has been a standard part of the preoperative evaluation of patients with severe forms of these conditions. However, it was not until the advent of 'non-invasive' techniques, using ultrasound and more recently magnetic resonance and CT-angiography, that vascular imaging has become part of the routine evaluation of all stroke patients. Such testing has become critical to answer essential clinical questions that impact management of every stroke patient such as the cause of bleeding in patients with intracranial hemorrhage, and the precise location, nature and severity of arterial occlusion or narrowing in patients with transient ischemic attack or ischemic stroke.

Contents

Contributors

Robert J. Adams, MD
Reagents Professor of Neurology
Department of Neurology
Medical College of Georgia
Augusta, GA

Andrei V. Alexandrov, MD, RVT
Assistant Professor of Neurology and Radiology.
Director, STAT Neurosonology Service and
Center for Noninvasive Brain Perfusion Studies
Stroke Program, University of Texas-Houston
Medical School
Houston, TX

Fahmi M. Al-Senani, MD
Associate Consultant
King Faisal Specialist Hospital and Research Center
Riyadh, Saudi Arabia

Eva Bartels, MD
Professor of Neurology
Director, Cerebrovascular Ultrasound
Georg-August University
Gottingen, Germany

W. Scott Burgin, MD
Assistant Professor of Neurology and Radiology
University of Rochester
Rochester, NY

Sergio Calleja, MD
Attending Physician, Department of Neurology
Hospital Central Universitario de Asturias
Oviedo, Spain

Ioannis Christou, MD
Internist and Director
Stroke Prevention Outpatient Clinic and
3rd Internal Medicine Department
Hellenic Air Forces VA General Hospital
Athens, Greece

Andrew M. Demchuk, MD, FRCPC
Assistant Professor of Neurology
Department of Clinical Neurosciences
University of Calgary
Calgary, Alberta, Canada

Ashraf El-Mitwalli, MD, PhD
Assistant Lecturer
Neurology Department
Mansoura Faculty of Medicine
Mansoura, Egypt

Anthony Estrera, MD
Assistant Professor
Department of Cardio-thoracic and Vascular Surgery
The University of Texas—Houston Medical School
Houston, TX

Robert A. Felberg, MD
Director, Stroke Program
Department of Neurology
Ochsner Clinic
New Orleans, LA

Zsolt Garami, MD
Fellow in Neurosonology and Senior Sonographer
Stroke Treatment Team
The University of Texas—Houston Medical School
Houston, TX

Anne M. Jones, RN, BSN, RVT, RDMS
Lecturer, Department of Neurology
Wake Forrest University Medical Center
Winston-Salem, NC

Marc Malkoff, MD
Associate Professor and Director
Neurocritical Care
Stroke Treatment Team,
The University of Texas—Houston Medical School

Joseph Nates, MD, FCCM
Associate Professor of Anesthesiology and Critical Care Medicine
Department of Critical Care Medicine
Division of Anesthesiology Critical Care Medicine
University of Texas MD Anderson Cancer Center
Houston, TX

Marsha M. Neumyer, BS, RVT
Assistant Professor of Surgery
The Pennsylvania State University College f Medicine
Director, Vascular Diagnostic Laboratory Section
The Penn State Vascular Institute
Milton S. Hershey Medical Center
Hershey, PA

David W. Newell, MD
Professor of Neurosurgery,
Department of Neurological Surgery
Director, Seattle Stroke Center
University of Washington
Seattle, WA

Fenwick T. Nichols III, MD
Professor, Department of Neurology
Medical College of Georgia
Augusta, GA

Joseph F. Polak, MD, MPH
Associate Professor of Radiology
Brigham and Women's Hospital
Harvard Medical School
Boston, MA

Disya Ratanakorn, MD
Associate Professor of Neurology
Division of Neurology, Department of Medicine
Faculty of Medicine Ramathibodi Hospital
Mahidol University
Bangkok, Thailand

Hazim Safi, MD
Professor and Chairman
Department of Cardio-thoracic and Vascular Surgery
The University of Texas—Houston Medical School
Houston, TX

Joon Song, MD
Associate Professor of Neuroradiology
Department of Radiology
The University of Texas—Houston Medical School
Houston,TX

Charles H. Tegeler, MD
Professor of Neurology
Head, Section on Stroke and Cerebrovascular Disease
Director, Neurosonology Laboratory
Department of Neurology
Wake Forest University School of Medicine
Winston-Salem, NC

Ken Uchino, MD
Assistant Professor
Stroke Institute
University of Pittsburgh
Pittsburgh, PA

Anne W. Wojner, PhD, CCRN
Assistant Professor
Department of Neurology
Director, Neuroscience Critical Care Training
Stroke Treatment Team
The University of Texas-Houston Medical School
Houston, TX

The advantages of ultrasound for vascular diagnosis are well known. It is a fast, portable, non-invasive, repeatable and inexpensive technique. The application of ultrasound to clinical stroke care over the past decades has revealed a number of clinical determinations that are best made by this technique and that directly impact on clinical decision-making. Among various clinical situations, the most established ones include:

- the early detection and characterization of extracranial atherosclerosis and occlusive disease especially at the carotid bifurcation,
- the consequences of proximal arterial occlusive disease on the distal cerebral vasculature,
- the natural history and response to treatment of acute arterial occlusion that causes hyperacute stroke,
- the detection of microemboli associated with cardiac and aortic pathology and carotid artery surgical manipulation (and perhaps gauging response to anti-platelet therapy),
- selection of children with sickle cell disease for blood transfusion as an effective tool in primary stroke prevention, and
- the time course and reversibility of cerebral vasospasm after subarachnoid hemorrhage.

Portable ultrasound machines and handy monitoring sets made it possible to bring this technology to the bedside and observe remarkable flow changes in stroke patients in real time. However, the field of ultrasonic diagnosis also has it detractors and limitations. For many applications, ultrasound has not been thoroughly tested for its utility, accuracy and validity in multicenter studies. While the benefits of using this methodology for the above indications, as well as for others that undoubtedly will emerge as our exploration of stroke disease continues, may seem self-evident to those of us who live with ultrasound technology and use it every day, this is not so evident to others. Careful outcomes research investigating the accuracy and cost benefit of ultrasound is needed to establish the utility of this technique for any clinical situation where we surmise that it should be routine. Many such studies have been carried out and have established the value of ultrasound, particularly for the clinical issues listed above. This book should help identify where such data exist, and more importantly, where more data is still needed.

Finally, early ultrasound technology was indirect, had poor resolution and had high rates of false-positive and false-negative results. Even now, the technique is 'operator dependent' in terms of the accuracy and validity of its results. While, in fact, to some extent these concerns are true of all diagnostic imaging, these limitations have been particularly true of ultrasound. Newer technology has provided significant advances in this regard, but it is necessary for each and every laboratory to maintain strict quality control in order to maximize the information that this powerful technology can provide. This textbook provides a major advance in that regard. Written by experts in the field, it will provide sonographers with the tools needed to enhance the confidence of clinicians in utilizing ultrasound technology and the clinicians with additional information how to implement this technology in their everyday decision-making.

James C. Grotta, MD
Houston, TX

Preface

This book is about vascular examination of patients suffering from stroke and the relevance of this information to management decisions. This book is for clinicians who are eager to learn, prepared to observe and would not stop explorations.

Ultrasound sharpens the clinician's ear and provides a stethoscope, an observation tool. And, like a microscope, an ultrasound probe needs a scientist to point it in the right direction. However, to paint a global picture, a complex ultrasound system also needs an artist to bring the art and science of medicine together. Ultrasound enables us to monitor the cardiovascular system and brain responses to treatment in real time, a blessing on the way to develop stroke therapies, and a handy tool to tailor treatment when the current evidence is meager.

I am indebted to my friends and colleagues who spent immeasurable time sharing their expertise in this book. Working with the Stroke Treatment Team is a thrill, and this book is the result of many observations, often at obscene hours, that made us believe that stroke is treatable.

Andrei V. Alexandrov, MD
Houston, TX

Acknowledgements

I joined the University of Texas Stroke Treatment Team in 1996, and never regret the loss of lifestyle or many sleepless nights. I'm fortunate to work with Team members who would race day or night to see and treat acute stroke patients, breaking all speed limits and meeting any strict time windows. With countless hours spent together in the emergency department, angio rooms, specialized care units and late night diners, we shared thoughts and debated various ways to treat acute cerebral ischemia.

These observations would never have happened without Jim Grotta, a visionary for stroke treatment, who started this Team and lead us to the highest percentage of consecutive stroke patients being treated with thrombolytics to date, and without those who made this happening in Houston, current and former Team members who are now heading their own Stroke Teams in the United States, Canada, and other countries (I apologize for not listing the many more Stroke Team members who worked hard in Houston prior to 1996): Fahmi Al-Senani, Alex Brunser, Scott Burgin, Sergio Calleja, Morgan Campbell, Chin-I Chen, Oleg Chernyshev, David Chiu, Ioannis Christou, Andrew Demchuk, Ashraf El-Mitwalli, Robert Felberg, Zsolt Garami, Christiana Hall, Susan Hickenbottom, Yasuki Iguchi, Jennifer Ireland, Scott Kasner, Derk Krieger, Lise Labiche, Marc Malkoff, Robert Mikulik, Lewis Morgenstern, Elizabeth Noser, Nicholas Okon, Paisith Piriyawat, Marc Ribo, Hashem Shaltoni, Ken Uchino, Carlos Villar-Cordova, Teddy Wein, Frank Yatsu.

The words Stroke Treatment Team will remain just words without nurses, who are responsible for daily care for patients and who carry out our clinical trials. Our Team is blessed with outstanding nurses who keep physicians on their toes: Patti Bratina, Sheila Ford, Dawn Matherne, Robin Saiki, Sandi Shaw, Dora Vital, Anne Wojner.

The Team will never be complete without our interventionalists, cardiovascular surgeons, neurosurgeons, critical care and emergency physicians and research faculty: Jaroslaw Aronowski, Eddy Cacayourin, Linda Chi, Guy Clifton, Tony Estrera, Brent King, Dong Kim, Steve Koch, Bill Maggio, Joseph Nates, David Robinson, Hazim Safi, Richard Smalling, Joon Song, Roger Strong, Dennis Vollmer.

This work would also have been impossible without the Houston Fire Department, City Paramedics and the many Emergency Room nurses and physicians, and neurology residents.

PART I

How to perform ultrasound tests

This page intentionally left blank

CHAPTER 1

Cerebrovascular anatomy and principles of extracranial ultrasound examination

Marsha M. Neumyer, BS, RVT *& Andrei V. Alexandrov,* MD, RVT

Introduction

Over the past four decades, a variety of non-invasive tests and clinical applications have been developed for detection and monitoring of cerebrovascular disease [1–10]. The goals of non-invasive cerebrovascular testing are to differentiate normal from diseased arteries, identify all categories of stenosis, localize the disease process including occlusions, detect progression of disease, detect and quantify cerebral embolism, demonstrate the morphologic characteristics of an atherosclerotic plaque, and assess the potential of the collateral circulation to maintain cerebral blood flow. Although not all of these goals are currently met by a single test procedure, a combination of extracranial and intracranial tests can meet the demand.

Mastering cerebrovascular ultrasound requires knowledge of anatomy, physiology of cardiovascular and nervous systems, fluid dynamics and pathologic changes in a variety of cerebrovascular disorders [11–21], as well as basic ultrasound physics and instrumentation [22–24]. These textbooks cover several, sometimes overlapping areas that are important in both performing the ultrasound examination and interpreting the results.

The aim of this book is to describe the methods of cerebrovascular ultrasound testing, practical criteria for interpretation and relevance of these findings to patient management. Rapid bedside evaluation by an expert sonographer with a portable ultrasound unit is an excellent screening test that can provide an immediate impact on patient management at a lower cost and with no time delays compared to other imaging methods.

Skepticism towards ultrasonography [25] is based largely on the lack of knowledge how to perform, interpret and use the results of ultrasound tests in research and clinical practice. In addition, the accuracy of ultrasound testing is dependent on the skill, knowledge and experience of sonographers. The practice of ultrasound (both performance and interpretation) should be a mandatory part of the residency training for physicians of different specialties. Sonographers have to meet the requirements set by the board examinations of the American Registry of Diagnostic Medical Sonographers (ARDMS, www.ardms.org). Interpreting physicians have to demonstrate competence by completing the required number of hours of continuing medical education in ultrasound methods and supervised interpretation of a set number of cases for each imaging modality. These requirements are outlined in the regulatory documents of the Intersocietal Commission of Accreditation of Vascular Laboratories (ICAVL, www.icavl.org). The American Society of Neuroimaging (www.asnweb.org) also offers a peer-reviewed multiple-choice proficiency examination in neurosonology that covers physics, clinical application and interpretation of the carotid/vertebral and transcranial ultrasound methods. Finally, consistent application and local validation of ultrasound testing and interpretation are the keys to successful practices [26].

Unlike other current imaging tests, ultrasound offers real-time assessment of pathophysiologic changes and

monitoring of patients with cerebrovascular diseases. Often, this information finds no place in clinical decision-making because it has not been tested in randomized clinical trials. Not everything that we do as clinicians can or should be tested in these trials. Ultrasound can be very helpful in clinical decision-making if the results are provided in a timely fashion, and the practicing physicians are prepared to use this information to select the best management strategy, and often to go beyond 'proven' (often meager) standards in the best interests of the patient.

Anatomy of the cerebrovascular arterial system

When performing a vascular ultrasound examination, one must think about generated images with respect to transducer position, i.e. a sonographer should 'think in 3-D', or three-dimensions, about the vessel being investigated. A sonographer should further imagine how this arterial segment would look on an angiogram. We strongly encourage those learning and interpreting ultrasound to be familiar with cerebral angiograms [11] since invasive angiography is the gold standard for assessment of accuracy of ultrasound testing. The following section deals with normal vascular anatomy and common arterial variations.

The common carotid artery

On the right, the brachiocephalic (innominate) artery arises from the aortic arch and then bifurcates into the subclavian artery and the common carotid artery (CCA). On the left side, both the common carotid artery and the left subclavian artery originate directly from the aortic arch. The CCA is easily assessable on the neck where it runs in parallel with the jugular vein (Figure 1.1). At approximately the level of the 4th vertebrae, which is at the level of the upper border of the thyroid cartilage, the common carotid arteries bifurcate into the internal and external carotid arteries (Figure 1.2). The carotid bulb represents dilatation at the distal common carotid artery extending into the proximal internal carotid artery. The carotid bulb bears unique flow patterns yielding a boundary separation zone and its wall has numerous baro- and chemoreceptors. The size and location of the carotid bulb are variable.

Most atherosclerotic disease occurs at the level of the bifurcation due to marked changes in vessel geometry resulting in increased shear stress, fluid stagnation and increased particle residence time on the posterolateral wall of the bulb [27].

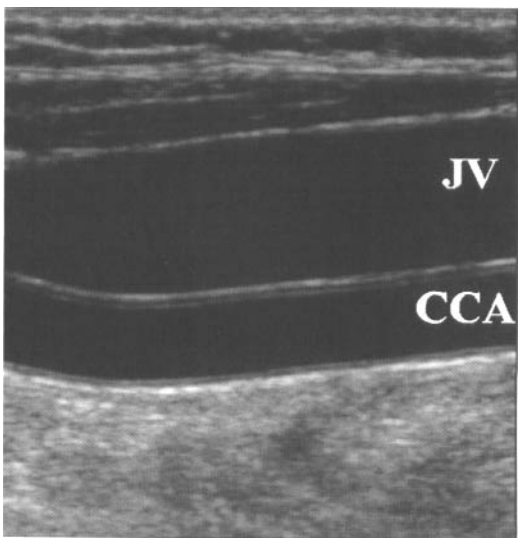

Figure 1.1 Brightness-modulated (B-mode) image of the common carotid artery (CCA) and the jugular vein (JV).

The internal carotid artery

Beyond the carotid bulb, the internal carotid artery (ICA) returns to a normal caliber (Figure 1.2) and courses in a relatively straight line up the neck into the skull to supply blood flow to the eye and brain. As a rule, the ICA has no branches within the neck. After entering the skull, the ICA makes an S-shaped curve in the region of the carotid siphon. This is an area where arterial wall dissections or atherosclerotic disease may occur. The first major branch of the ICA is the ophthalmic artery that supplies the eye. After giving off the ophthalmic artery, the ICA branches into the middle cerebral artery (MCA) and the anterior cerebral artery (ACA), a part of the circle of Willis.

The external carotid artery

The external carotid artery (ECA) supplies the muscles of the face, forehead and scalp. The ECA has eight branches on the neck, arising shortly after the bifurcation (Figure 1.2). Several of these branches, i.e. ascending pharyngeal, facial, internal maxillary and superficial temporal arteries, communicate via anastomoses with the ICA. The occipital artery is the only

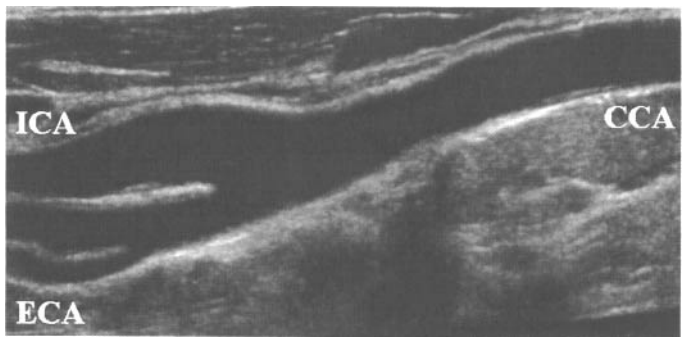

Figure 1.2 Longitudinal B-mode image of the internal carotid artery (ICA) bulb, external carotid artery (ECA) and the distal portion of the common carotid artery.

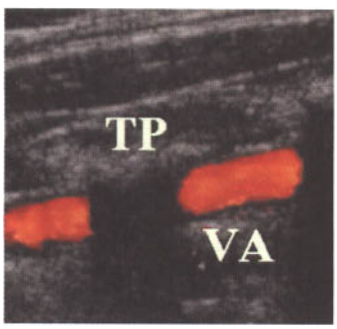

Figure 1.3 Superimposed color flow image of the vertebral artery (VA). Flow signals are present between 'shadows' on B-mode produced by vertebral transverse processes (TP).

ECA branch that communicates with the vertebral artery circulation. It is important to recognize these branches because the ECA quite often becomes a collateral source for blood flow to the brain when the ICA is critically stenosed or occluded.

The vertebral artery

The vertebral arteries arise from the subclavian arteries and pass cephalad in the neck to enter the bony canal at the C6 vertebrae. They course through the transverse processes of the vertebrae (Figure 1.3), and enter the base of the skull through the foramen magnum. At this point, the right and left vertebral arteries join together to form the basilar artery. The trunk of the basilar artery courses for 2–3 cm [11] before terminating in the posterior cerebral arteries (Figure 1.4), which make up the posterior portion of the circle of Willis.

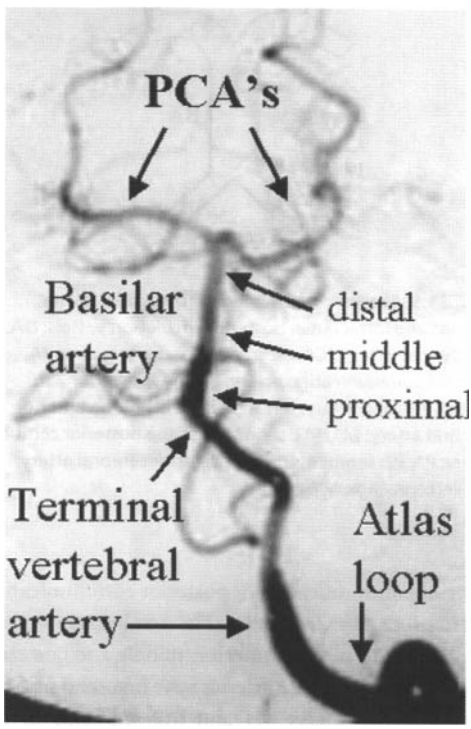

Figure 1.4 Digital subtraction angiography (DSA) demonstrates the course of the terminal vertebral, basilar and posterior cerebral (PCA) arteries on an anteroposterior projection.

The circle of Willis

The circle of Willis is a unique network of vessels located at the basis of the brain that create anastomoses between both terminal carotid arteries and posterior circulation vessels (Figure 1.5). A complete circle of Willis delivers collateral flow through the

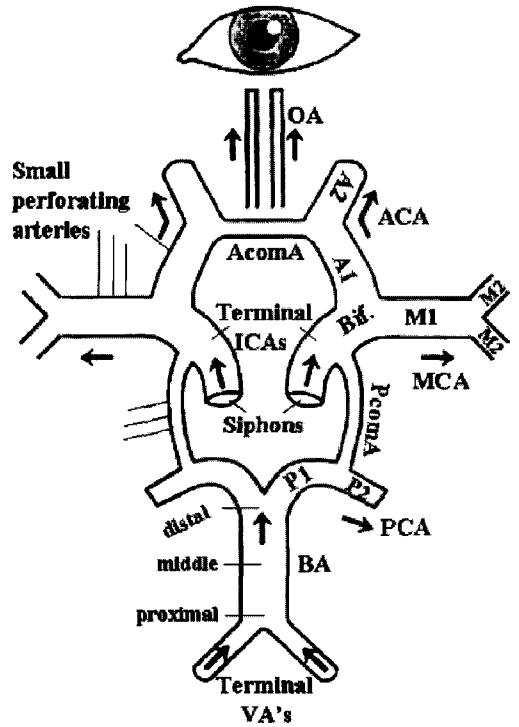

Figure 1.5 A schematic drawing of the circle of Willis, siphons and intracranial posterior circulation vessels. OA, ophthalmic artery; ICA, internal carotid artery; AcomA, anterior communicating artery; PcomA, posterior communicating artery; A1, A2, segments of the anterior cerebral artery; M1, M2, segments of the posterior cerebral artery; P1, P2, segments of the posterior cerebral artery; VA, vertebral artery.

anterior communicating or posterior communicating arteries (see also Chapter 3). The first branches of the circle of Willis include anterior, middle and posterior cerebral arteries. These arteries have first- and second-degree branches (i.e. M1 and M2 segments of the MCA [11]) that along with the intracranial vertebrobasilar system can be evaluated with cerebrovascular ultrasound through the intact skull [5].

Components of ultrasound examination

Continuous-wave (CW) Doppler

Dr Eugene Strandness first reported the use of a transcutaneous flowmeter to evaluate occlusive arterial disease in 1966 [1]. Extracranial carotid and vertebral examinations using continuous-wave (CW) Doppler were reported by Drs Merrill Spencer and Michael von Reutern and colleagues in the 1970s [2,28]. With this technology, one crystal continuously emits the signal and another crystal continuously receives returned echoes. CW Doppler displays Doppler frequency shifts and a unidirectional analog flow signal trace of maximum frequencies was originally created (Figure 1.6). Current CW systems can differentiate between positive and negative Doppler shifts and create a bidirectional spectral signal that shows flow direction as towards or away from the transducer. However, CW Doppler shows no information regarding the structure (image) or depth from which the signals originated. The advantage of this ultrasound test is its ability to display Doppler frequency shifts from moving objects without an artifact called aliasing (see 'The color flow Doppler image' below). With recent development of direct imaging and pulsed-wave Doppler methods, CW Doppler is rarely performed and is not reimbursed in the US as a *sole* test used for evaluation of the carotid vessels. Perhaps the only remaining indications for CW Doppler for carotid arteries are extensive (> 2 cm) shadowing of the bifurcation, arterial lesions extending above the level of the lower jaw, or a quick bifurcation screening before or with (not as a substitute for) direct imaging investigation. Despite recent attempts to create portable CW Doppler technology for intracranial vessels [29], this test cannot reliably differentiate flow signals from different parts of the circle of Willis. Display of flow signals from multiple vessels along the beam path is also known as range ambiguity [30].

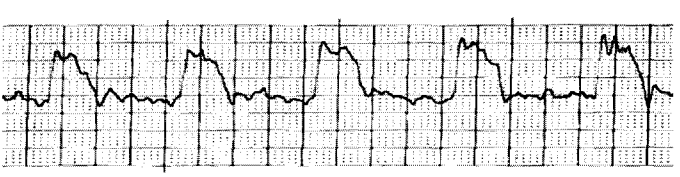

Figure 1.6 Continuous-wave (CW) Doppler was first used to produce a unidirectional analog flow signal of maximum frequencies reflected from moving blood.

The B-mode image

The B-mode (brightness) image is created from the amplitude of backscattered echo signals that are displayed in gray scale along beam propagation (depth) and the length of transducer/skin interface [22–24] (Figures 1.1 & 1.2). The gray shade of the signal on screen displays the strength of returning echo while its location relates to the depth of tissue reflector. Several crystals are sequentially activated with electronic pulses or the transducer is rotated mechanically (steering) to create multiple scan lines. The scan lines are put together to generate an image (or 'frame'). Since the average speed of sound propagation in soft tissues is 1540 m/s ('a mile per second'), multiple frames are generated in a second, creating an illusion of a real-time picture ('movie making' with ultrasound).

The maximum depth of sound penetration is determined by the emitting frequency of the ultrasound transducer, which is usually 4–12 MHz for extracranial imaging and 2–4 MHz for intracranial imaging. Higher frequencies have smaller pulse lengths and allow better spatial resolution but less penetration due to increased sound scattering. Time-gain compensation (TGC) is applied to improve visualization of structures with increasing depths of insonation. The smallest distinguishable distance between two reflectors along the ultrasound beam axis (axial resolution) is directly proportionate to the spatial length of the pulse. Lateral resolution (or resolution perpendicular to the direction of an ultrasound beam) is also dependent on transducer geometry since it is the highest in the focal zone. The focal zone is determined as the narrowest point between converging (near-field) and diverging (far-field) parts of the ultrasound beam. Note that an ultrasound scanner can create multiple focal zones to optimize different parts of the image. Therefore, linear or curved array transducers with larger surface, dynamic electronic focusing and multiple narrow-width beams have better lateral resolution.

B-mode imaging artifacts include:

1 Shadowing (no image can be generated along ultrasound beam axis behind a bright reflector). Changing transducer position and planes of insonation may minimize shadow appearance. Shadows can originate from perpendicular insonation of vessel walls, plaque calcification (Figure 1.7) and transverse vertebral processes (Figure 1.3).

2 Reverberation (multiple bright echoes that often have regular shape and layered position are displayed along the axis of ultrasound beam when echoes bounce many times between two strong reflectors).

3 Mirror image (a false image—also known as phantom image or reflection artifact—is created when obliquely scanning a strongly reflecting boundary). Vessel visualization in transverse and longitudinal planes often resolves confusion associated with this artifact.

4 Plane of section (three-dimensional structure is inadequately displayed on a two-dimensional monitor). Using imagination for three-dimensional spatial relationships, transducer position should be changed to generate adequate sectional planes.

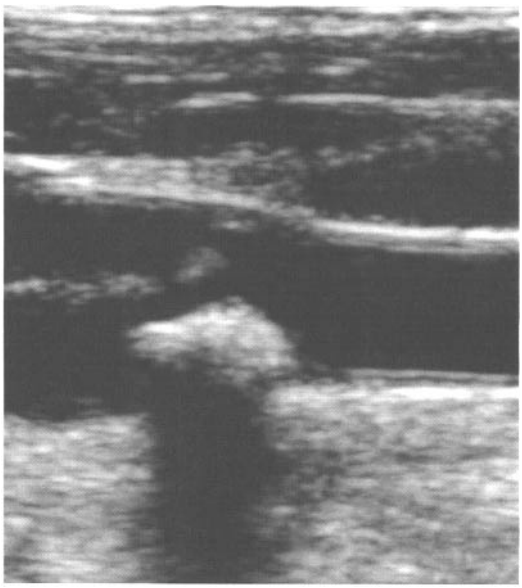

Figure 1.7 Plaque calcification produces a 'shadow' artifact on B-mode scan, or the dark area due to poor or no ultrasound penetration underneath a bright reflector.

B-mode imaging is used to identify the carotid and vertebral arteries, carotid intima–media complex, atherosclerotic plaques and anatomic anomalies. B-mode imaging can also be used to perform intracranial studies where it shows contralateral skull line, midline structures including the third ventricle, and brain parenchymal structures [31].

The color flow Doppler image

Color-coded Doppler flow imaging (CDFI) displays the average (or mean) shifts in the frequency of returned echoes backscattered from moving objects, usually red blood cells. The color scale can be manually

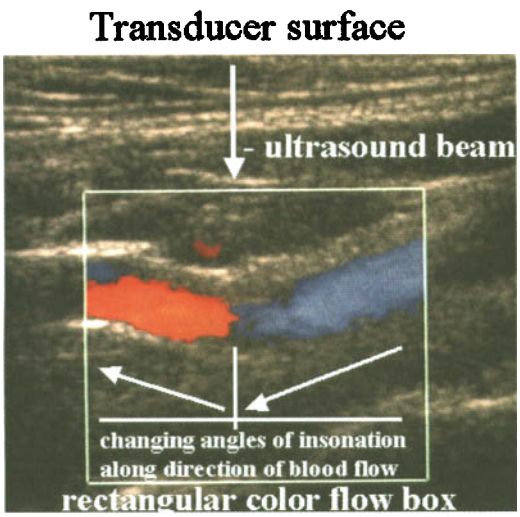

Figure 1.8 Color Doppler flow image of the common carotid artery.

selected ranging from two colors (red and blue) to a rainbow palette. At least two distinctly different colors are used to display clearly the direction of flow relative to transducer midline (Figure 1.8). According to the Doppler effect, objects moving towards the transducer will increase the frequency of backscattered echoes relative to emitted frequency and vice versa. However, color assignments are operator dependent.

Therefore, CDFI is used to identify moving blood and display the direction of flow. No Doppler frequency shift occurs at a 90° angle between the ultrasound beam and moving bloodstream (Figure 1.8). CDFI often contains artifacts:

1 Aliasing (abrupt change from the maximum velocity in one flow direction to the maximum velocity in the opposite direction without crossing zero line). It can be present in a normal vessel if the scale settings are inadequately low to display flow velocity, i.e. a sonographer uses low pulse repetition frequency (Figure 1.9). It can also be present with maximum scale settings in stenosed vessels due to elevated flow velocities. Scale setting control and comparison of vessel course and B-mode findings help to differentiate imaging artifact from pathologic finding.

2 'Bleeding' (the presence of moving blood outside the vessel). This artifact can be produced by an oblique strong reflector (mirror image) or by tissue motion

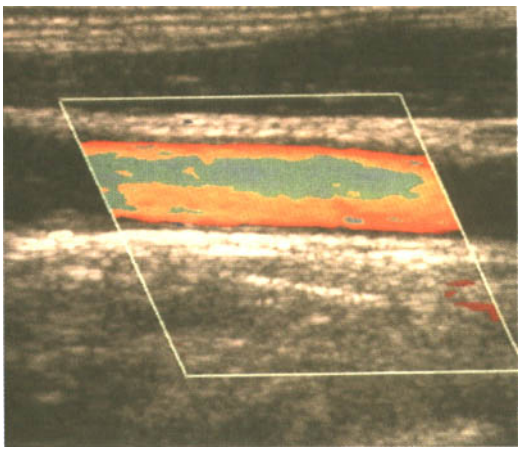

Figure 1.9 Color aliasing artifact in a normal vessel due to low pulse repetition frequency settings.

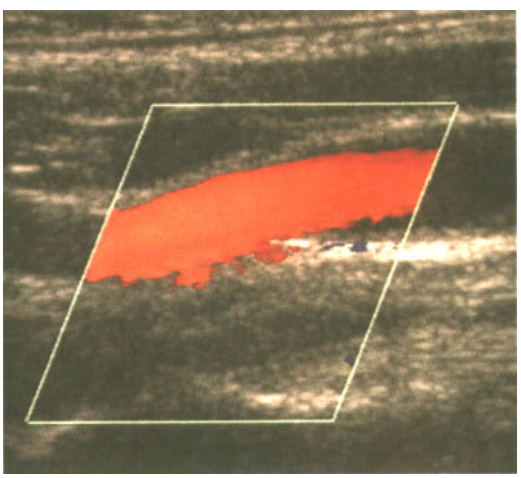

Figure 1.10 Color bleeding, or the artificial presence of blood motion outside the vessel.

adjacent to the vessel. In both circumstances, changing transducer position and color gain setting helps to optimize the image (Figure 1.10).

Occasionally, CDFI may be unable to depict blood flow since its spatial resolution is lower than B-mode image [7]. Also, there is a trade-off between B-mode and superimposed CDFI images: larger CDFI boxes require slower frame rates that decrease B-mode resolution and vice versa. CDFI may not be able to adequately display blood flow in tortuous and deep-located vessels as well as vessels affected by the low flow states, i.e. near-occlusion [20]. Other forms of flow imaging may be used in these circumstances.

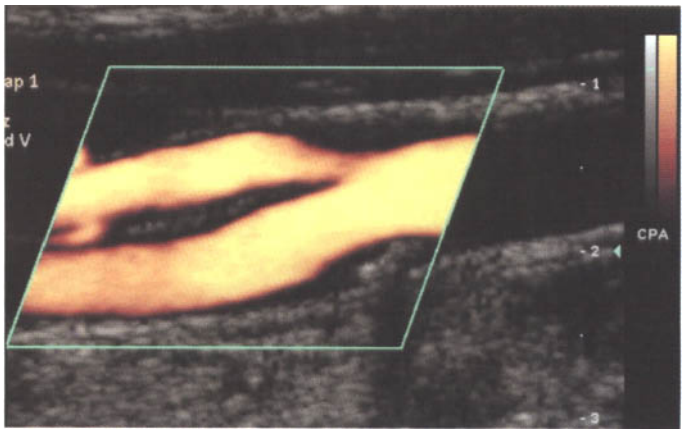

Figure 1.11 Power-mode image of the carotid bifurcation.

The power Doppler image

Power Doppler imaging displays color-coded intensities of the returned echoes that contain Doppler frequency shifts. Unlike CDFI, power mode shows direction-independent changes in the energy of signals backscattered by moving objects. Therefore, power-mode images are usually created with brightness-adjusted unicolor scales (Figure 1.11). Power-mode images show the course of the vessel without color change due to flow direction. Power mode can be used to visualize tortuous and deep-located vessels, branches and slow-moving blood [8,20]. 'Flashing' is the most common artifact that is created by tissue motion, and similarly to 'bleeding' displays artifactual flow signals outside the vessel lumen. This can be corrected by changing the gain settings and color box size.

The color velocity image

The color velocity imaging (CVI) display is similar to CDFI; however, the color-encoded velocities are derived from time-domain processing of returned echo signals [32]. For example, CVI image represents the movement of red blood cell clusters in time along the vessel course. It allows better trade-off between B-mode and color flow information in terms of image resolution due to better utilization of scan lines. CVI can also better display functional flow lumen. It is also used in some laboratories to calculate flow volume estimates in the carotid arteries.

B-flow and compound imaging

Brightness-mode display can also be used to generate flow images, since moving blood changes the strength of reflected signals relative to surrounding structures [33]. Combined with electronic focusing and multiple focal zones, such images can provide high-resolution structural scans (Figure 1.2) and superimpose flow signals in gray scale over a B-mode image (Figure 1.12). The B-flow scans avoid aliasing and offer potentially better trade-off between tissue motion and moving blood signals.

Harmonic imaging

An emitted frequency of a diagnostic ultrasound pulse wave passing through tissue can change due to reflection off a moving object (Doppler shift) or during faster sound transmission through fluid compressed at the peak intensity of the ultrasound wave (harmonics). This frequency change occurs mostly during wave propagation (less during reflection). The result is appearance of the second harmonic frequency that is twice the emitted frequency [9]. This mechanism of non-linear interaction of ultrasound with body tissues allows the use of harmonic frequencies to image tissues with and without contrast substances, and new-generation duplex scanners provide this option. Potential clinical utility of harmonic imaging in cerebrovascular ultrasound includes application of contrast agents for tissue perfusion studies including brain parenchyma, differentiation of a complete occlusion from subtotal stenosis and better delineation of plaque and vessel wall morphology [34–37].

Doppler velocity spectral display

A pulse-wave ultrasound beam can also be used to detect Doppler shift in the returned echoes since

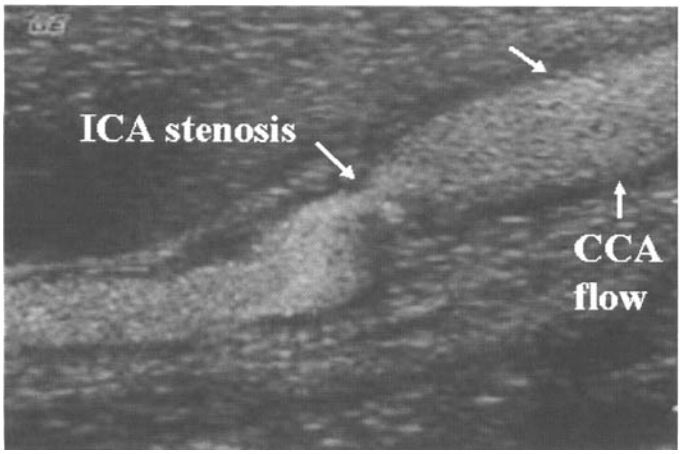

Figure 1.12 B-flow, or brightness-mode display of residual flow through the internal carotid stenosis.

moving blood or tissues will change the emitted frequency. This phenomenon is used to measure flow velocity simultaneously with structural and color flow imaging. To obtain velocity values close to the real speed of blood, angle correction is applied; this is discussed below in the 'Scanning protocol'.

Extracranial duplex ultrasound examination technique and scanning protocol

The extracranial duplex examination should include transverse and longitudinal B-mode scans of the vessels. Examination can start with transverse scanning since it allows fast identification of the CCA, jugular vein, the level of bifurcation and the presence of atherosclerotic disease [16,18,20]. The transverse examination begins with the most proximal segment of the common carotid artery following its course towards the distal portion, passing through bifurcation, and ending at the level of the mandible with visualization of the distal cervical segment of the internal carotid artery (Figure 1.13). The transverse plane permits appreciation of vessel diameter, presence of pathology and anatomic anomalies. The examination is repeated in the longitudinal plane (Figures 1.1 & 1.2), beginning again with the most proximal segment of the common carotid artery and extending the scan throughout the bifurcation, internal and external carotid arteries. The vertebral artery is examined at its origin and also in the midcervical segment of the neck (Figure 1.3).

To optimize the gray-scale image, set the dynamic range to 40–50 dB and the time-gain compensation (TGC) as appropriate to the depth of the common carotid and vertebral arteries.

Imaging in the transverse plane

1 With the patient's head turned slightly away from the side being examined, place the ultrasound probe low on the neck, anterior to the sternocleidomastoid muscle, just above the clavicle. The left side of the image should be orientated towards midline structures, i.e. trachea.

2 Locate the proximal segment of the common carotid artery (CCA) in the transverse plane. Slowly move the probe along the length of the CCA.

3 At the distal end of the CCA, locate the dilatation that identifies the carotid bulb.

4 Slowly move the probe through the region of the carotid bulb and note the bifurcation into the internal (ICA) and external (ECA) carotid arteries.

5 Follow the course of the ICA and ECA to the level of the mandible. Document any evidence of pathology, vessel tortuosity and abnormal anatomy.

Imaging in the longitudinal plane

1 Return to the proximal segment of the CCA with the ultrasound probe rotated to image in the longitudinal axis. The left side of the image should be orientated cephalad.

2 Begin with the probe placed anterior to the sternocleidomastoid muscle.

3 Image the widest longitudinal axis of the CCA by

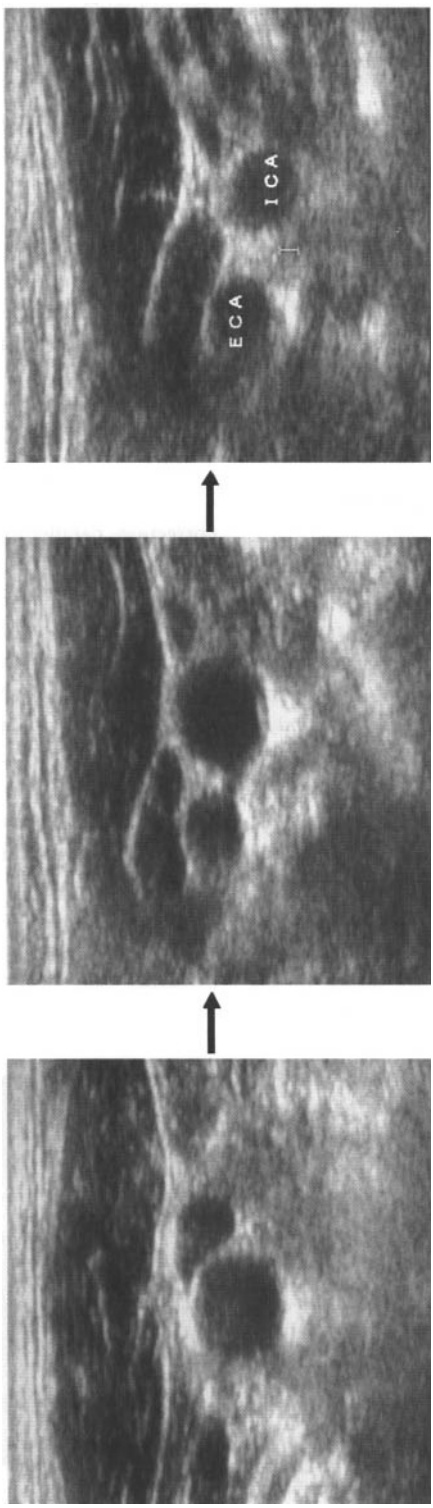

Figure 1.13 Sequential transverse views of the proximal common carotid artery (left), bifurcation (center) and distal ICA (right) with B-mode imaging.

directing the sound beam perpendicular to the anterior wall of the vessel.

4 Optimize the image so that the normal linear reflectivity of the arterial wall is apparent.

5 Slowly move the probe along the course of the vessel and into the carotid bulb.

6 With the distal CCA and bulb in view, slowly rock the transducer side to side to reveal the origins of the internal and external carotid arteries. Care must be taken to angle the probe along the origins to avoid transecting the views of each artery.

7 In turn, follow the courses of the ICA and ECA, optimizing the image for accurate evaluation of anatomy and pathology. Document any evidence of pathology, vessel tortuosity or abnormal anatomy.

Color flow ultrasound evaluation of flow dynamics

1 Return to the longitudinal image of the proximal CCA.

2 Choose the appropriate color pulse repetition frequency (PRF) by setting the color velocity scale for the expected velocities in the vessel. For normal adult arteries, the velocity range is usually around or under 100 cm/s (or 2.5 kHz Doppler frequency shift). Note that most criteria will use a 125 cm/s cut-off for velocities elevated due to carotid stenosis. Adjust the scale further to avoid systolic aliasing (low PRF) or diastolic flow gaps (high PRF or filtering) in normal vessels.

3 Optimize the color power and gain so that flow signals are recorded throughout the lumen of the vessel with no 'bleeding' of color into the surrounding tissues.

4 Avoid using large or wide color boxes since this will slow down frame rates and resolution of the imaging system. Use color boxes that cover entire vessel diameter and 1–2 cm of its length. Align the box, i.e. select appropriate color flow angle correction, according to the vessel geometry and course.

5 Slowly move the probe throughout the course of the CCA, bulb, ICA and ECA.

6 Identify and record regions of flow disturbance, inappropriately high or low velocity signals, or the absence of flow signals.

7 To find the vertebral artery, return to the CCA (longitudinal view, transducer position anterior to the sternocleidomastoid muscle). Steer the color beam towards the proximal CCA. Rock the probe slightly to the lateral aspect of the neck to image the vertebral artery as it courses through the transverse processes of the vertebrae ('shadows'). 'Heel–toe' the probe above the clavicle to image the origin of the vertebral artery as it arises from the subclavian artery. Confirm that the direction of flow in the vertebral artery is the same as in the CCA.

Doppler spectral evaluation of flow dynamics

1 Return to the longitudinal image of the CCA.

2 Use color flow image as a guide for Doppler examination (Figure 1.14).

3 Begin the examination using a Doppler sample volume size of 1.5 mm positioned in the middle of a normal vessel (Figure 1.14).

4 Consistently follow one of the choices for angle correction: parallel to the vessel walls or to the color flow jet.

5 Adjust the Doppler spectral power and gain to optimize the quality of the signal return.

6 Slowly sweep the sample volume throughout the length of the CCA, bulb, ICA and ECA.

7 Perform temporal artery tapping when insonating ECA to differentiate between the ECA and ICA flows. Also note the presence of arterial branches that may be present at the proximal ECA stem.

8 Identify regions of flow disturbance or where flow is absent.

9 Record flow patterns in the proximal and distal CCA, the proximal, mid and distal ICA and the proximal ECA at appropriate angles of insonation.

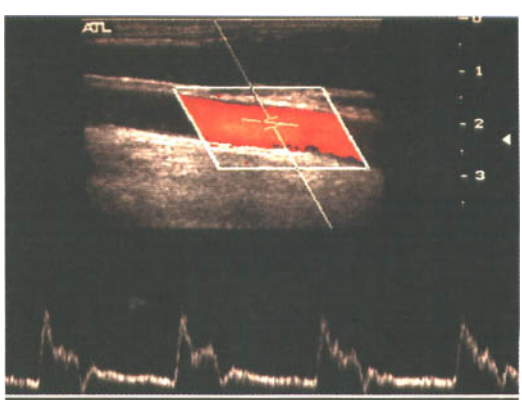

Figure 1.14 Angle-corrected velocity measurements in the common carotid artery.

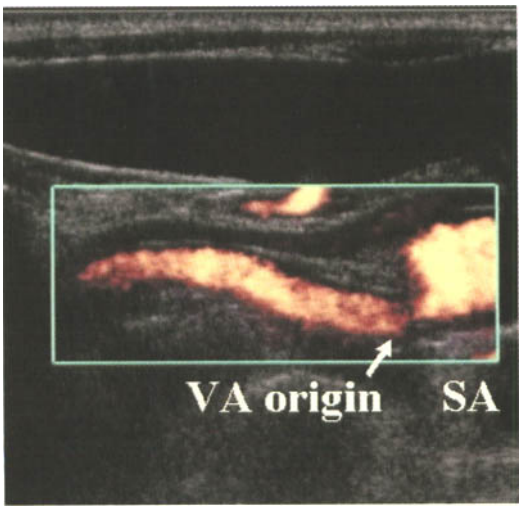

Figure 1.15 Power-mode image of the vertebral artery origin.

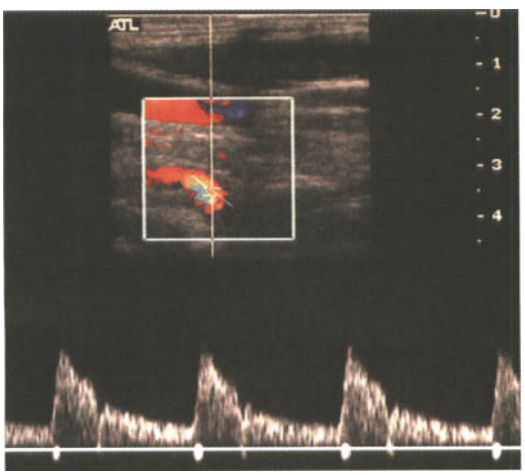

Figure 1.16 Angle-corrected velocity measurements in the vertebral artery.

Additionally, include Doppler spectral waveforms proximal, within and distal to all areas where flow abnormalities were observed.

10 Locate the origin or proximal segment of the vertebral artery (Figure 1.15). Record flow patterns, paying careful attention to flow direction. Follow accessible cervical segments of the vertebral artery (Figure 1.16). Change angulation of the color box and Doppler sample along with the course of the artery.

Extracranial duplex examination should provide the following data

1 Peak systolic velocity in all vessel segments.
2 End-diastolic velocity in all vessel segments.
3 Ratios of the ICA to CCA peak systolic velocities.
4 Documentation of the Doppler spectral waveform morphology from the CCA, ICA and ECA.
5 Flow direction and peak systolic velocity of the vertebral arteries.
6 Views demonstrating the presence and location of pathology.
7 Images of plaque morphology and surface features.

Tips to improve accuracy

1 Consistently follow a standardized scanning protocol.
2 Perform a complete examination of the carotid and vertebral arteries.
3 Sample velocity signals throughout all arterial segments accessible.
4 Use multiple scan planes.
5 Take time to optimize the B-mode, color and spectral Doppler information.
6 Videotape or create a digital file of the entire study, including sound recordings.
7 Always use the highest imaging frequencies to achieve higher resolution.
8 Account for any clinical conditions or medications that might affect velocity.
9 Integrate data from the right and left carotid and vertebral arteries.
10 Do not hesitate to admit uncertainty and list all causes for limited examinations.
11 Expand Doppler examination to intracranial vessels when indicated.

Tips for optimizing color flow set-up

1 According to standardized protocols, the carotid bifurcation should be to the left of the image. This orientation should then clearly indicate the appropriate direction of flow in the common carotid artery and jugular vein. The arterial and venous flow directions are then given color assignments with respect to flow towards or away from the transducer. Traditionally, flow towards the transducer is assigned red (common carotid) while flow away from the probe is assigned blue (jugular vein). The direction of flow relative to the probe will change if the probe is rotated 180° or if the color box is steered in the opposite direction, i.e. the vein will appear red while the artery

will appear blue. When this occurs, the color should be changed back to the original assignment to avoid confusion. It must also be noted that the color will change along the course of an artery if the flow direction varies throughout the cardiac cycle (triphasic, to–fro) or if the vessel changes direction relative to the orientation of the sound beam.

2 The zero baseline of the color bar (PRF) is set at approximately two-thirds of the range with the majority of frequencies allowed in the red direction (for flow towards the brain). This setting allows you to display higher arterial mean frequency shifts (velocities) without aliasing artifacts. You should make allowance for some flow in the reverse (blue) direction to allow for changes in flow direction (i.e. ICA bulb, poststenotic dilatation). When the transducer is rotated 180°, the color will change (note point **1** above), and the zero baseline will shift with the color changes to accommodate for flow in the forward direction. You will need to adjust both the color assignment and the zero baseline to the initial set-up for consistency.

3 The color PRF and zero baseline may need to be readjusted throughout the examination to allow for the changes in velocity that occur with tortuosity and stenosis. It is important to adjust the PRF in the following situations:

Examination of the carotid bulb. The color differentiation scale should be set to detect and clearly visualize the slower flow in the boundary separation zone. The range (PRF), however, may need to be set higher to detect increased velocities in the region adjacent to the flow divider.

In the presence of stenosis. The color PRF should be increased to display the high velocities and to avoid aliasing.

In the poststenotic zone. The color PRF should be decreased to observe the lower velocities and flow direction changes, if any, found in the region of turbulent flow just distal to the stenosis.

When bruits are encountered. The color PRF should be decreased to detect the lower frequencies associated with a bruit. Usually, the frequency of these bruits is less than 1 kHz.

When occlusion is suspected. The color PRF should be decreased to detect the preocclusive, low-velocity, high-resistance signal associated with critical stenosis or occlusion and to confirm absence of flow at the site of occlusion.

4 The color wall filter should be set as low as possible. You should note that the color wall filter may automatically increase as you increase the PRF. You may need to decrease the wall filter manually when you decrease the color PRF.

5 The ensemble length (color sensitivity) should be around 12 in systems where this is an adjustable control. You can increase the ensemble length in regions where you want more sensitive color representation. It is important to remember that the frame rate will decrease when the ensemble length is increased (see also point **8** below). There are no circumstances when the ensemble length would be decreased during an extracranial carotid duplex examination.

6 The angle of the color box should be changed to obtain the most acute Doppler angles between the scan lines and the direction of blood flow. This will result in better color display because of more suitable Doppler angles. The angle should always be equal to or less than 60°. Because linear array transducers are steered at angles of 90 and 70° from the center of the array, this may require a 'heel–toe' maneuver with the transducer on the surface of the skin to adjust the position of the vessel within the color box. An alternative would be to physically change the orientation of the transducer by 180°.

7 The desaturation of color from darker to lighter hues on the color bar indicates increasing Doppler frequency shifts, i.e. increasing velocities. Note that close to the zero baseline, the colors are the darkest. As the velocity increases, the color becomes lighter. You should select colors so that the highest frequency shifts in each direction are of high contrast to each other so that you can readily detect aliasing. For example, you could set the color selections so that low to high velocities are seen as dark blue to light green to aqua in one direction and red to orange to yellow in the opposite flow direction. Aliasing would then appear as aqua adjacent to yellow.

8 The frame rate should be kept as high as possible to capture the very rapid change in flow dynamics that occurs with stenosis, especially in the region of the carotid bulb. Remember that frame rate is affected by:

PRF—frame rate decreases with decreasing PRF;
ensemble length—increasing the color ensemble length will decrease the frame rate;
width of the color box—increased width will decrease the frame rate; and
depth—deep insonation decreases frame rate.

9 The color box should be kept to a size that is adequate for visualizing the area of interest and yet small enough to keep the frame rate at a reasonable number, approximately 15 or more to ensure adequate filling of the vessel. The frame rate is usually displayed in hertz on the monitor.

10 The color gain should be adjusted throughout the examination to detect the changing signal strength. If the color gain is not properly adjusted, some color information may be lost or too much color may be displayed. In this case, you will see color in areas where there should be no flow. The gain should initially be adjusted to an 'overgained' level, with color displayed in the tissue and then turned down until the tissue noise just disappears or is minimally present. This is the level at which all color images should be assessed. In situations where there is very low flow, or questionable occlusion, an 'overgained' level may be advantageous to show any flow that might be present, e.g. total occlusion vs. a near-occlusion or critical stenosis.

References

1 Strandness DE, McCutcheon EP, Rushmer RF. Application of a transcutaneous Doppler flowmeter in evaluation of occlusive arterial disease. *Surg Gynecol Obstet* 1966; **122** (5): 1039–45.

2 Spencer MP, Reid JM, Davis DL, Paulson PS. Cervical carotid imaging with a continuous-wave Doppler flowmeter. *Stroke* 1974; **5** (2): 145–54.

3 Barber FE, Baker DW, Nation AW, Strandness DE, Reid JM. Ultrasonic duplex echo-Doppler scanner. *IEEE Trans Biomed Eng* 1974; **21** (2): 109–13.

4 Budingen HJ, von Reutern GM, Freund HJ. Diagnosis of cerebro-vascular lesions by ultrasonic methods. *Int J Neurol* 1977; **11** (2–3): 206–18.

5 Aaslid R, Markwalder TM, Nornes H. Noninvasive transcranial Doppler ultrasound recording of flow velocity in basal cerebral arteries. *J Neurosurg* 1982; **57** (6): 769–74.

6 Spence JD, Coates RK, Pexman JA. Doppler flow maps of the carotid artery compared with the findings on angiography. *Can J Surg* 1983; **26** (6): 556–8.

7 Bogdahn U, Becker G, Schlief R, Reddig J, Hassel W. Contrast-enhanced transcranial color-coded real-time sonography. *Stroke* 1993; **24**: 676–84.

8 Rubin JM, Bude RO, Carson PL, Bree RL, Adler RS. Power Doppler US: a potentially useful alternative to mean frequency-based color Doppler US. *Radiology* 1994; **190** (3): 853–6.

9 Burns PN. Harmonic imaging with ultrasound contrast agents. *Clin Radiol* 1996; **51**: 50–5.

10 O'Leary DH, Polak JF, Kronmal RA, Manolio TA, Burke GL, Wolfson SK Jr. Carotid-artery intima and media thickness as a risk factor for myocardial infarction and stroke in older adults. Cardiovascular Health Study Collaborative Research Group. *N Engl J Med* 1999; **340** (1): 14–22.

11 Krayenbuehl H, Yasargil MG. *Cerebral Angiography*, 2nd edn. Stuttgart: Thieme, 1982.

12 Bernstein EF. *Vascular Diagnosis*, 4th edn. St. Louis: Mosby-Year Book, 1993.

13 Polak JF. *Peripheral Vascular Sonography: a Practical Guide*. Philadelphia: Williams & Wilkins, 1992.

14 Strandness DE. *Duplex Scanning in Vascular Disorders*, 2nd edn. New York: Raven Press, 1993.

15 Zweibel WJ. *Introduction to Vascular Ultrasonography*, 4th edn. St Louis: Harcourt Health Sciences, 2000.

16 von Reutern GM, Budingen HJ. *Ultrasound Diagnosis in Cerebrovascular Disease*. Stuttgart: Thieme, 1993.

17 Tegeler CH, Babikian VL, Gomez CR. *Neurosonology*. St Louis: Mosby, 1996.

18 Hennerici M, Neuerburg-Heusler D. *Vascular Diagnosis with Ultrasound. Clinical Reference with Case Studies*. Stuttgart: Thieme, 1998.

19 Hennerici M, Meairs S. *Cerebrovascular Ultrasound: Theory, Practice and Future Developments*. Cambridge: Cambridge University Press, 2001.

20 Bartels E. *Color-Coded Duplex Ultrasonography of the Cerebral Arteries: Atlas and Manual*. Stuttgart: Schattauer, 1999.

21 Babikian VL, Wechsler LR, eds. *Transcranial Doppler Ultrasonography*, 2nd edn. Woburn, MA: Butterworth Heinemann, 1999.

22 Edelman SK. *Understanding Ultrasound Physics*, 2nd edn. The Woodlands, TX: ESP, Inc, 1997.

23 Kremkau FW. *Diagnostic Ultrasound: Principles and Instruments*, 5th edn. St Louis: Harcourt Health Sciences, 1998.

24 Zagzebski JA. *Essentials of Ultrasound Physics*. St. Louis: Mosby, 1997.

25 Ringelstein EB. Skepticism toward carotid ultrasonography. A virtue, an attitude, or fanaticism? *Stroke* 1995; **26** (10): 1743–6.

26 Katanick SL. Accreditation of vascular ultrasound laboratories. In: Tegeler CH, Babikian VL, Gomez CR, eds. *Neurosonology*. St Louis: Mosby, 1996: 484–8.

27 Glagov S, Bassiouny HS, Zarnis CK, Slesers A. Morphogenesis of the atherosclerotic plaque. In: Hennerici M, Mearis S, eds. *Cerebrovascular Ultrasound: Theory, Practice and Future Developments*. Cambridge: Cambridge University Press, 2001: 117–33.

28 von Reutern GM, Pourcellot L. Cardiac cycle-dependent alternating flow in vertebral arteries with subclavian artery stenoses. *Stroke* 1978; **9** (3): 229–36.

29 Kidwell CS, Martin NA, Saver JL. A new pocket-sized transcranial ultrasound device (NeuroDop): comparison with standard TCD. *J Neuroimaging* 2000; **10** (2): 91–5.

30 Edelman SK. *Understanding Ultrasound Physics*, 2nd edn. The Woodlands, TX: ESP, Inc, 1997: 132.

31 Berg D, Siefker C, Ruprecht-Dorfler P, Becker G. Relationship of substantia nigra echogenicity and motor function in elderly subjects. *Neurology* 2001; **56** (1): 13–7.

32 Knappertz VA, Tegeler CH. Color Flow Imaging. In: Tegeler CH, Babikian VL, Gomez CR, eds. *Neurosonology*. St Louis: Mosby, 1996: 30–1.

33 Pellerito JS. Current approach to peripheral arterial sonography. *Radiol Clin North Am* 2001; **39** (3): 553–67.

34 Postert T, Federlein J, Weber S, Przuntek H, Buttner T. Second harmonic imaging in acute middle cerebral artery infarction. Preliminary results. *Stroke* 1999; **30** (8): 1702–6.

35 Eyding J, Wilkening W, Postert T. Brain perfusion and ultrasonic imaging techniques. *Eur J Ultrasound* 2002; **16** (1–2): 91–104.

36 Meyer K, Wiesmann M, Albers T, Seidel G. Harmonic imaging in acute stroke: detection of a cerebral perfusion deficit with ultrasound and perfusion MRI. *J Neuroimaging* 2003; **13** (2): 166–8.

37 Hennerici M, Meairs S. Imaging arterial wall disease. *Cerebrovasc Dis* 2000; **10** Suppl 5: 9–20.

2

CHAPTER 2

Intracranial cerebrovascular ultrasound examination techniques

Andrei V. Alexandrov, MD, RVT & *Marsha M. Neumyer*, BS, RVT

Introduction

Advances in low-frequency Doppler ultrasound as well as imaging resolution, color flow and power Doppler have led to the use of these technologies for interrogation of the intracranial circulation through intact skull. It is important for the performance of transcranial Doppler (TCD) and transcranial color duplex sonography (TCCS) to understand proper patient and transducer positioning, anatomic landmarks and appropriate scale settings, including spectral analysis, gray scale and color flow information.

TCD examination technique

A single-gate spectral transcranial Doppler (TCD) was introduced by Rune Aaslid in 1982 to non-invasively assess cerebral hemodynamics [1]. The four 'windows' for insonation (Figure 2.1) are temporal, orbital, suboccipital and submandibular [2]. The transtemporal approach allows velocity measurements in the middle (MCA), anterior (ACA), posterior (PCA) and communicating arteries [1–5]. The transorbital approach is used to insonate the ophthalmic artery (OA) and internal carotid artery (ICA) siphon. The suboccipital approach allows insonation of the terminal vertebral (VA) and basilar (BA) arteries through the foramen magnum. The submandibular approach is used to obtain ICA velocities as it enters the skull.

For a typical diagnostic TCD examination, use a fast 3–5-s sweep speed that allows details of the waveform and spectrum to be seen (Figure 2.2). To shorten the time necessary to find the window and to identify different arterial segments with a single-gate spectral TCD, the examination should begin with the maximum power and gate settings (i.e. power 100%, gate 10–15 mm) for the transtemporal and suboccipital approaches. Although this recommendation seemingly violates the rule of using ultrasound power 'as low as reasonably achievable' (ALARA), it allows the time

Image Not Available

Figure 2.1 Windows for intracranial vessel location. There are four windows of insonation: temporal, orbital, suboccipital and submandibular. (Reproduced with permission from Alexandrov AV. *Vascular Ultrasound Today* 1998; **3**: 141–60.)

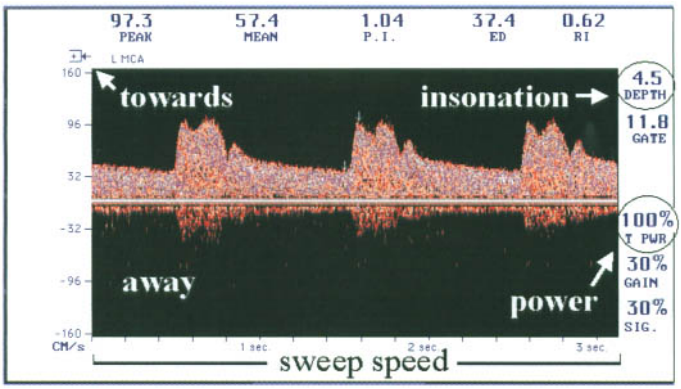

Figure 2.2 Pulsed-wave spectral waveform display. Identify flow direction, velocity scale, depth of insonation as well as sweep speed and power settings. Small arrows indicate the cardiac cycle measured to calculate the peak, mean and end-diastolic (ED) flow velocities. PI, pulsatility index (Gosling–King); RI, resistance index (Pourcellot).

necessary to find windows and to complete the examination to be shortened, thus reducing the overall patient exposure to ultrasound energy. The goals of a 'non-image-guided' single-gate spectral TCD examination are:

1 to follow the course of each major branch of the circle of Willis with spectral display;

2 to identify, optimize and store the highest velocity signals;

3 to obtain TCD spectra at at least two key points per artery (Figure 2.3); and

4 to identify, optimize and store any abnormal or unusual waveforms.

Transtemporal insonation steps (Figure 2.4)

Step 1 Set the depth at 50–56 mm (midpoint of the M1 MCA segment was established at approximately 50 mm depth [6]).

Place the probe at position 1 (Figure 2.1) above the zygomatic arch and aim it slightly upwards and anterior to the contralateral ear/window.

Find any flow signal (window), and avoid too anterior and too posterior angulation.

Find a flow signal directed towards the probe which resembles MCA flow. A normal MCA flow is a low-resistance waveform (Figure 2.2) similar to the ICA flow pattern.

By decreasing the depth, follow the signal to the distal M1 key-point of insonation without losing the signal. Often, a slight adjustment of the probe angulation is needed.

Store distal M1 MCA signal at 45 mm. If bidirectional signals are found, store the highest-velocity signal in each direction (distal M1–proximal M2 branches).

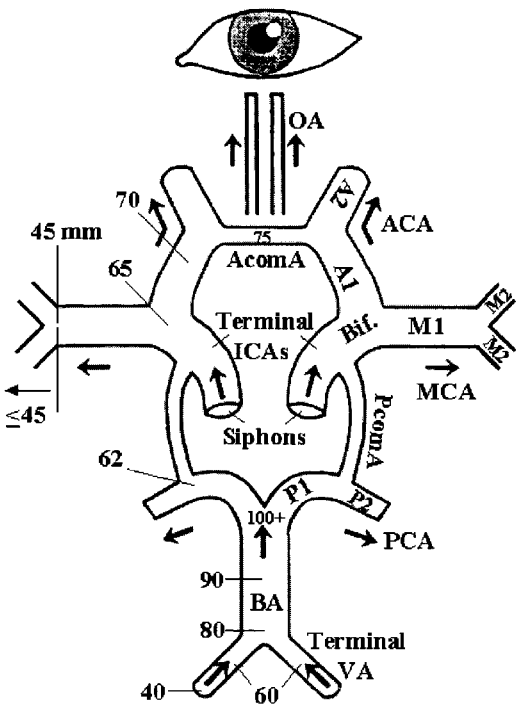

Figure 2.3 Key insonation segments and depths for transcranial Doppler examination.

Step 2 Follow the signals until they disappear at shallow 30–45-mm depths.

Store any abnormal signal.

Return to the distal M1 MCA signal.

Step 3 Follow the M1 MCA stem to its origin at 60–70-mm depths dependent on the size of adult patient skull. Pay attention to the sound and velocity changes since insonation of the terminal ICA is also possible at these depths.

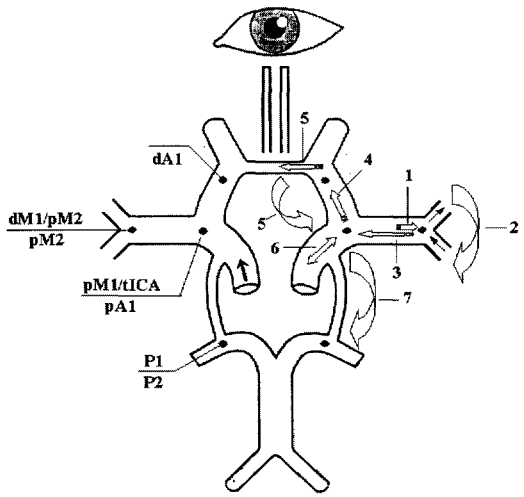

Figure 2.4 Steps for Doppler examination through the transtemporal window. Steps are represented by numbers 1 through 7. Abbreviations: dA1, distal A1 segment of the anterior cerebral artery (flow is directed away from transducer, or displayed below the baseline); dM1, distal M1 middle cerebral artery (towards transducer, above the baseline); pM2, proximal M2 (bidirectional, above and below the baseline); pM1, proximal M1 MCA; tICA, terminal internal carotid artery (both towards the transducer, above the baseline); pA1, proximal A1 anterior cerebral artery (away from transducer, below the baseline); P1, first segment of the posterior cerebral artery (towards transducer, above the baseline); P2, second segment of the posterior cerebral artery (away from transducer, below the baseline).

Find the ICA bifurcation at approximately 65 mm (range 58–70 mm in adults) and obtain both proximal M1 MCA and proximal A1 ACA signals.
Store a bidirectional signal of the bifurcation (M1/A1).

Step 4 Follow the A1 ACA signal to 70–75-mm depths.
Store the distal A1 ACA signal at 70 mm.

Step 5 Follow the distal A1 ACA signal to the midline depth range (75–80 mm). The A1 ACA signal may disappear, or a bidirectional signal may appear at the midline depth.
Store any abnormal signals.
Return to bifurcation at 65 mm.

Step 6 Find the terminal ICA signal just inferior and sometimes slightly posterior to the bifurcation at 60–65 mm. If the probe is angled inferior and anterior to the ICA bifurcation at 60–70-mm depths, the distal part of the supraclinoid siphon can be found through the temporal window.
Store any abnormal signal.
Return to the bifurcation at 65 mm.

Step 7 Set the depth at 63 mm and slowly turn the transducer posteriorly by 10–30°.
Usually there is a flow gap between the ICA bifurcation and the PCA signals.
Find PCA signals directed towards (P1) and away (P2) from the probe at a depth range of 55–75 mm.
Store the PCA signals with the highest velocity.

Transorbital insonation steps (Figure 2.5)

Step 1 Decrease power to minimum (17 mW) or 10%.
Set the depth at 50–52 mm, place the transducer over eyelid and angle it slightly medially.
Determine flow pulsatility and direction in the distal ophthalmic artery (OA).
Store the distal OA signals at 52 mm.

Step 2 Increase the depth to 60–64 mm and find the ICA siphon flow signals.
The siphon signals are usually located medially in the orbital window.
Store bidirectional signals at 62 mm (C3 or the siphon genu).
If only unidirectional signals are obtainable,

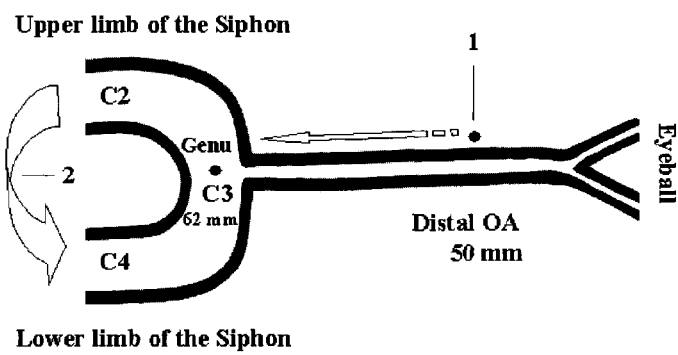

Figure 2.5 Steps 1–2 of Doppler examination through the orbital window. OA, ophthalmic artery; C2, C3, C4, sequential segments of the internal carotid artery.

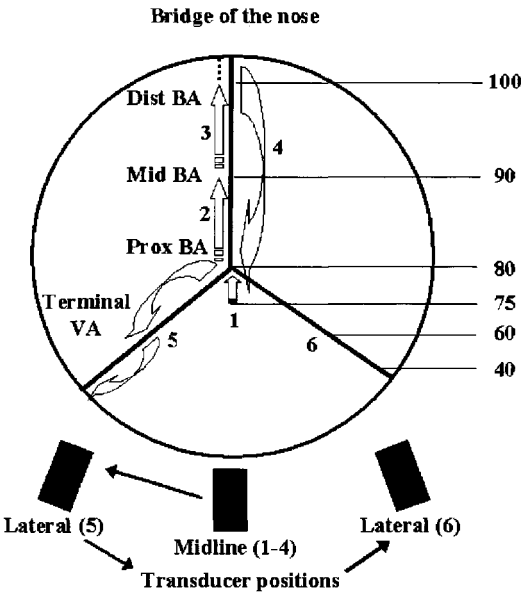

Figure 2.6 Steps 1–6 of Doppler examination through the foraminal window. BA, basilar artery; VA, vertebral artery.

store signals directed towards (C4 or the lower limb of the siphon) and away (C2 or the upper limb) from the probe.

Suboccipital insonation steps (Figure 2.6)

Step 1 Set the system back to full power.
Place the transducer at midline an inch below the edge of the skull and aim it at the bridge of the nose.
Set the depth at 75 mm (presumed location of both terminal VAs and proximal BA).
Identify a flow signal directed away from the probe, i.e. find the window.
This signal can be arbitrarily assigned to the terminal vertebral arteries (slightly lateral probe angulation) or the proximal basilar artery (medial and slightly upward angulation).
Increasing the depth, follow the flow directed away from the probe. This depth increase presumably focuses the beam on the proximal BA in most adults.
Store the proximal BA signal arbitrarily assigned to a depth of 80 mm.

Step 2 Follow the basilar artery to 90 mm (mid-BA segment).
Bidirectional signals may be found at various depths with a low-resistance flow in the cerebellar arteries directed towards the probe.
Store any abnormal signals.

Step 3 Follow the distal BA segment to a depth of 100 + mm until it disappears or is replaced by the anterior circulation signals.
Store the highest-velocity signal obtained at the most distal depth of the basilar artery insonation.

Step 4 Follow the stem of the basilar artery backwards while decreasing the depth of insonation to 80 mm and confirm previous findings.

Step 5 Place the probe about an inch laterally to the midline and aim towards the bridge of the nose or slightly towards the contralateral eye.
Find the vertebral artery (VA) flow signal directed away from the probe.
Follow the course of the terminal VA segment intracranially from 80 mm to 40 mm.
Store the VA signals at 60 mm or at the depth of the highest-velocity signal.

Step 6 Place the probe on the contralateral side an inch off the midline position.
Repeat the VA examination steps for the contralateral vessel from 80 to 40 mm.
Store the VA signals at 60 mm or at the depth of the highest-velocity signal.

Submandibular insonation steps (Figure 2.7)

Step 1 Place the probe laterally under the jaw anterior and medial to the sternocleidomastoid

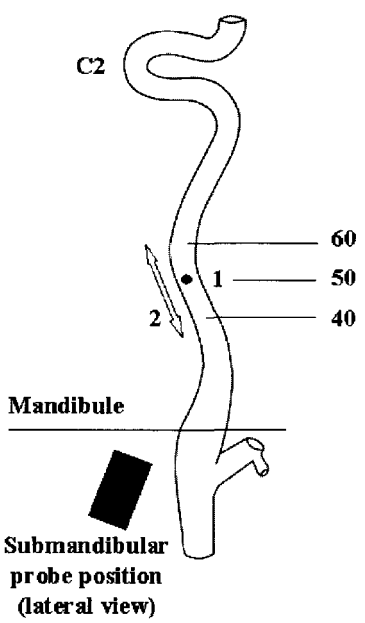

Figure 2.7 Steps 1–2 of Doppler examination through the submandibular window.

muscle. Aim the transducer upwards and slightly medially.

Set the depth at 50 mm.

Find a low-resistance flow directed away from the probe.

Step 2 Increase the depth from 50 to 60 mm and decrease to 40 mm.

Store the distal ICA signal at the depth that shows the highest-velocity signal.

At a shallow depth, perform the temporal artery tap to differentiate from the external carotid artery flow signals.

Practical advice

1 Avoid too anterior or too posterior angulation of the probe at the beginning of the transtemporal examination.

2 Do not settle on the first signal obtained. Always keep searching for higher-velocity signals.

3 Once the highest signal is found, avoid losing signals when switching the depth of insonation: follow the course of the arteries with slight angulation of the probe over the same window whenever possible. Remember the normal depth ranges (Figure 2.8) and flow direction (Figure 2.9) for the circle of Willis of an adult patient.

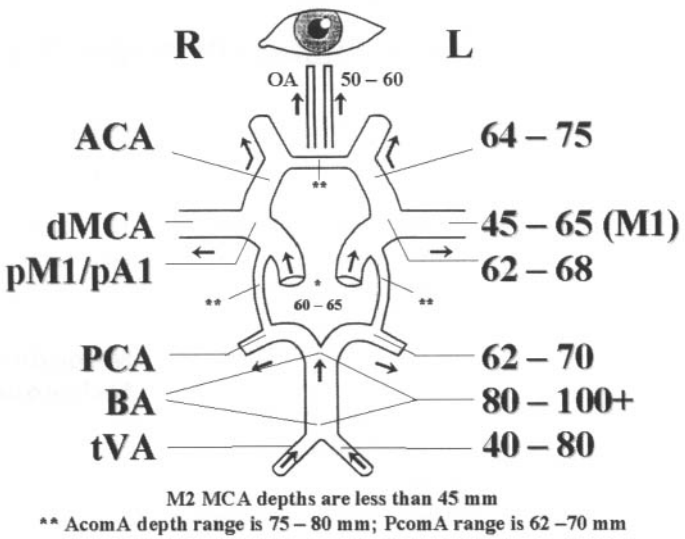

Figure 2.8 Depth ranges for insonation of the proximal intracranial arterial segments. Cerebral arteries: ACA, anterior; MCA, middle; PCA, posterior. Communicating arteries: AcomA, anterior; PcomA, posterior. OA, ophthalmic artery; BA, basilar artery; tVA, terminal vertebral artery.

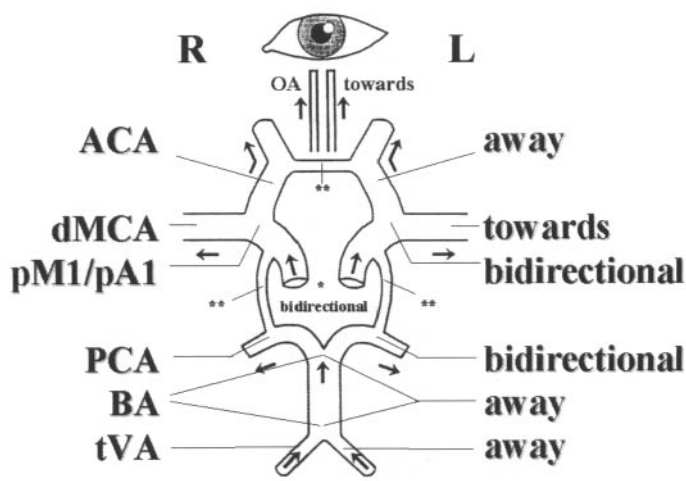

Figure 2.9 Flow direction relative to the transducer.

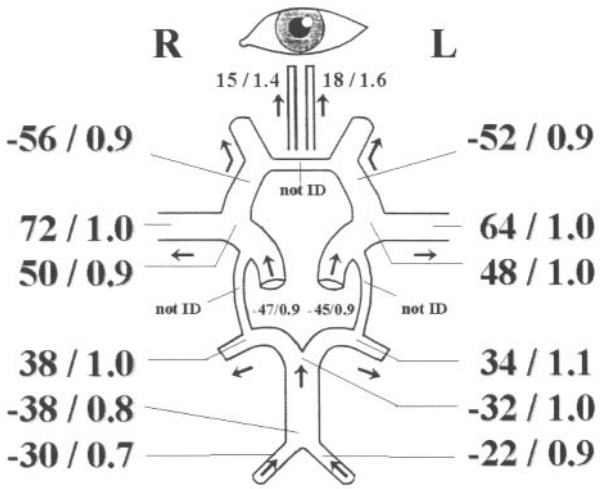

Figure 2.10 Normal transcranial Doppler examination. Values are given as mean flow velocity/pulsatility index. Minus means away from the probe. Under normal anatomic and circulatory conditions, the middle cerebral artery has the highest velocity values whereas pulsatility index differences are minimal between vessel segments.

4 Try not to take the probe off the skull until investigation of all segments through that window is completed.

5 Try not to lose arterial flow signals while switching between the segments of the same artery.

6 Memorize transducer position and angulation if patient is restless or insonation is being interrupted.

7 Use insonation across the midline to locate contralateral MCA/ACA signals if one temporal window is suboptimal, absent or not accessible.*

8 Do not overgain strong signals (background should not contain any noise signals).

9 In the case of weak signals, boost the signal and/or gain settings and apply manual measurements.

10 Perform a complete examination, document the mean flow velocities, pulsatility indices and flow direction in all major arteries (Figure 2.10), and double-check missing arterial segments.

11 Remember that vessel identification is operator dependent. Gain experience from studying normal individuals and patients with angiographically documented arterial pathology.

12 Consistently apply insonation protocol for TCD examinations. Use notes to document information pertinent to interpretation.

M-mode or PMD/TCD examination technique

Transcranial power-motion mode Doppler (PMD) was recently invented by Mark Moehring [3]. PMD, or M-mode, simultaneously displays flow intensity and direction over 6 cm or more of intracranial space (Figure 2.11). An advantage offered by this mode of insonation is display of all flow signals obtainable at a given position and direction of the transducer. The promise of PMD is to make transcranial Doppler (TCD) examination easy even for an inexperienced person since it takes a long time to acquire the skills to find windows of insonation with a single-channel spectral TCD.

PMD is combined with a single-channel spectral analysis in a new generation of transcranial Doppler systems (Figure 2.11). Using a single transducer, a clinician can search for a window of insonation without 'blindly' choosing a depth for spectral analysis and without relying on sound recognition/arm coordination. PMD shows flow signals on a color-coded, real-time display that may serve as a guide for proper spectral analysis (Figures 2.12 & 2.13). A standard PMD/TCD insonation protocol is provided below.

* Insonation across the midline can be difficult without imaging. You can measure the diameter of the patient skull to determine the midline depth. In most adults, the midline is located between 70 and 80 mm. Once you cross the midline, the vessel identification becomes reversed: contralateral A1 ACA is directed towards the probe (range 75–85 mm), while others are directed away from the probe: M1 MCA (range 85–105 + mm); terminal internal carotid artery (TICA) (80–85 mm); and P1/P2 PCA (75–83 mm). The top of the basilar segment at midline depths and the very proximal contralateral P1 PCA can be directed towards the probe from the transtemporal window.

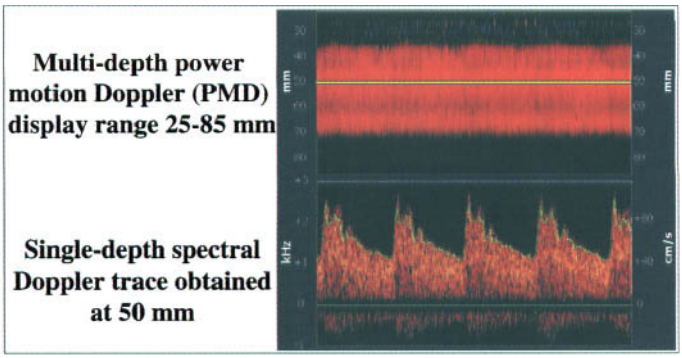

Figure 2.11 PMD/TCD display. Power-motion mode, or PMD, display combined with a single-channel transcranial Doppler (TCD) spectral analysis.

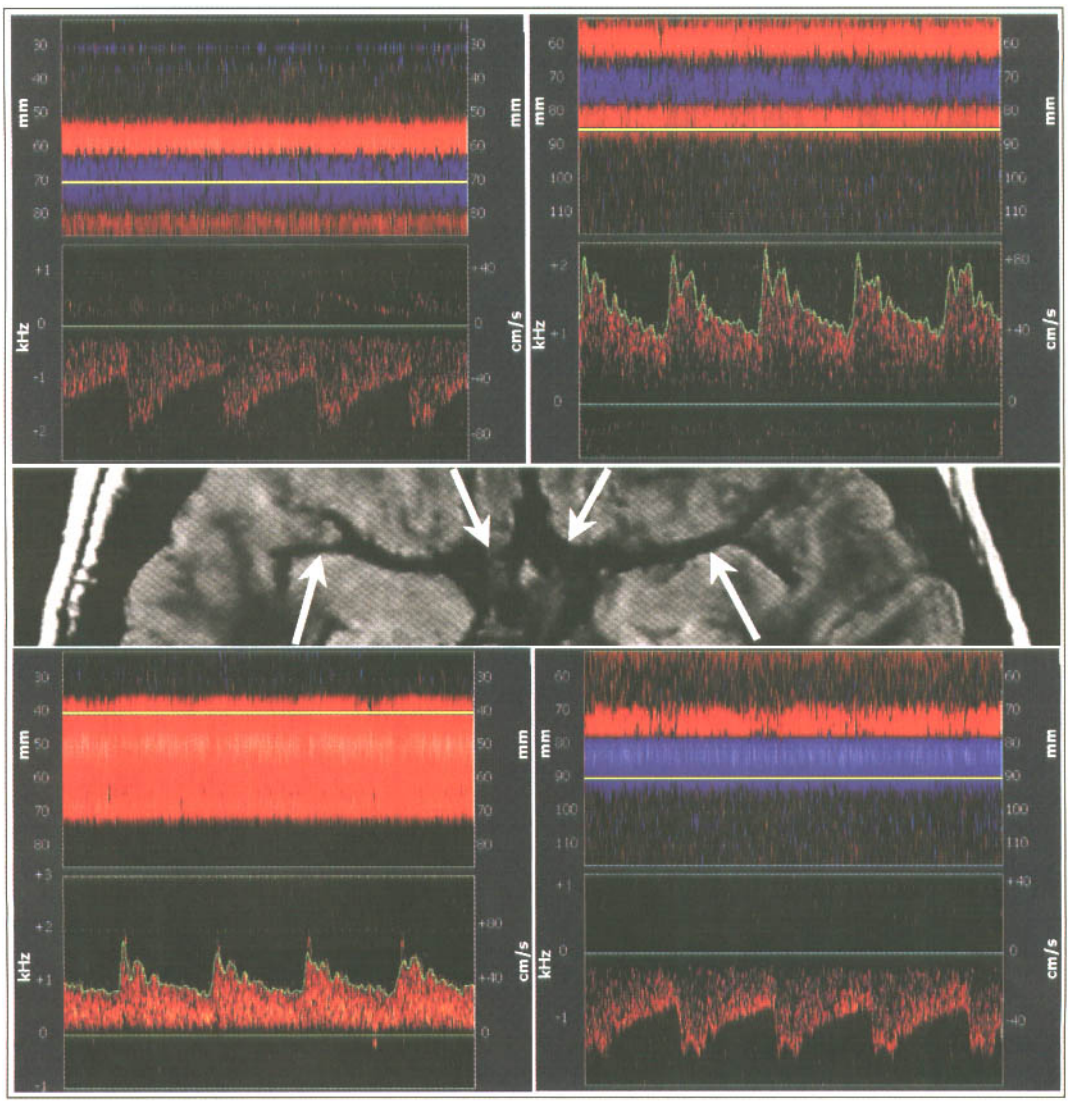

Figure 2.12 Arterial segments evaluated with PMD/TCD through the transtemporal window. PMD displays the length of arterial segment identified, i.e. proximal M2–M1, MCA and the depth of spectral analysis is displayed, i.e. 40 mm. Magnetic resonance images of the circle of Willis are provided to show location of vessel sampling (arrows).

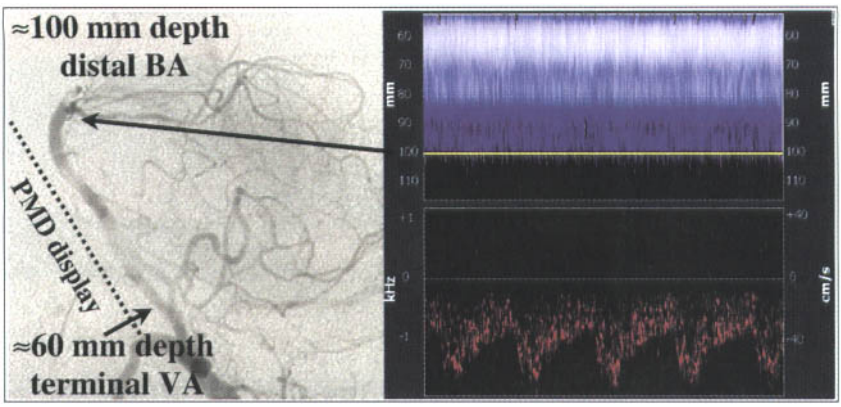

Figure 2.13 Insonation of the terminal vertebral and basilar arteries. Presumed beam path and vessel sampling depth are superimposed on a digital subtraction angiography image (left).

Useful rules to remember

1 TCD velocities do not measure cerebral blood flow volume. However, changes on TCD may correlate with changes in the cerebral blood flow.

2 Cerebral blood flow and mean flow velocities decrease with age.

3 Hypertension (including chronic) increases pulsatility of flow and may increase the mean flow velocity.

4 Hyperventilation decreases the mean flow velocity and increases pulsatility of flow.

5 Hypercapnia increases the mean flow velocity and decreases pulsatility of flow.

6 A waveform pattern is determined by various factors including cardiac output and blood pressure, as well as the brain autoregulatory or vasomotor responses and focal arterial lesions.

7 A waveform pattern can also be determined by the downstream circulatory conditions such as loss of autoregulation or elevated intracranial pressure (ICP).

8 Cerebral blood flow and mean flow velocity are inversely proportionate to vessel radius, length and blood viscosity.

9 When homologous arterial segments are compared, normal variations of up to 30% in flow velocities and pulsatility indices can be expected.

10 Variations in the angle of insonation can account for 15% and the resistance of downstream vasculature during breathing cycles for another 15% of a normal velocity/pulsatility difference.

11 Normal variations of up to 100% in flow velocities between homologous segments such as PCA or VA can be attributed to the tortuous vessel course, angle of insonation changes, anatomic variants of the circle of Willis and hypoplasia/atresia.

12 Anatomic variations of the circle of Willis are common; it is normal (symmetric, with all communicating arteries properly developed) in only about 20% of patients.

13 If an intracranial artery is not found, this finding itself does not mean that this artery is occluded.

Tips to improve accuracy

1 Perform a complete and thorough examination; store actual sound recordings when possible.

2 Try not to lose flow signals when changing the depth of insonation.

3 Target clinically involved arterial segment or suspected level of occlusion.

4 Use headphones and the maximum pulse repetition frequency possible.

5 To focus on a specific segment, decrease gate or sample volume and increase gain, if necessary.

6 Avoid mirror artifacts (do not overgain, or decrease power or sample volume) (Figure 2.14).

7 Account for medications and clinical conditions which change flow volume/velocity.

8 Do not hesitate to admit uncertainty and list all probable causes.

Previous studies have established normal values and variations for depth of insonation [1,2,4–6], and a multicenter study was performed to validate TCD findings [7]. Some variation between the depths of insonation can be expected due to the differences in patient skull diameters and sample volumes used for insonation. Regardless of which scanning protocol or

A standard PMD/spectral TCD insonation protocol for an average-size adult patient

Transtemporal insonation

1 Set PMD display at 30–80-mm depth range.
2 Apply transducer to the middle aspect of the temporal window above zygomatic arch and close to the ear lobe.
3 Maintain slightly upward and anterior angulation of the probe.
4 Set noise levels to allow minimal background signal on PMD display.
5 If no flow signals appear, advance transducer in slow circular movements towards the anterior temporal window.
6 While advancing transducer, keep changing probe angulation from the anterior to perpendicular direction relative to the temporal bone.
7 Find a window with maximum spatial presence of the middle cerebral artery (MCA) flow signature between 30 and 70 mm depths. In other words, attempt to fill the PMD screen with color flow signals over the MCA depth range.
8 Readjust the probe angulation to detect flow signals in the M2 MCA segments (depths 30–45 mm), terminal ICA (depths 60–70 mm) and anterior cerebral artery (ACA, depths 60–75 mm).
9 Return to the view of the MCA origin and slightly rotate transducer 10–30° posteriorly and downwards to detect flow in the posterior cerebral artery (PCA depth range is 60–70 mm).
10 At all transducer positions, note whether the contralateral flow signals can be displayed (depth ≥ 75 mm in most adults).
11 Sequentially advance TCD sample volume with 1-mm steps over all arterial segments detected by PMD to display spectral information.

Transorbital insonation

1 Decrease the power output of the unit to 10%.
2 Set PMD depth at 30–80 mm range.
3 Place transducer over closed eyelid and angle it slightly medially.
4 Align transducer position to display flow signatures at the depth of 40–70 mm.
5 Determine pulsatility and direction of flow in the ophthalmic artery.
6 Sample spectral information from the distal ophthalmic artery (depths 40–55 mm) and ICA siphon (depths 55–70).

Transforaminal insonation

1 Set PMD depth at 60–110 mm range.
2 Place transducer suboccipitally at midline and aim towards the bridge of the nose, and detect any flow signal moving away from the probe.
3 Align transducer position to display maximum flow signatures between 75 and 100 mm.
4 Sample spectral information from the proximal (80 mm), middle (90 mm) and distal (100 + mm) portions of the basilar artery.
5 To find the terminal vertebral arteries, set PMD depth at 30–80 mm range.
5 Place transducer laterally 1–3 cm off midline and aim towards orbits. Avoid angulation to the contralateral side.
6 Sample spectral flow signals from all segments of the terminal vertebral artery and repeat examination on the other side.

Note that small sample volume for spectral TCD delivers higher intensities with a PMD/spectral TCD unit. The trade-off between sensitivity and spatial resolution may remain optimal even with a small 3-mm spectral gate.

depth ranges are adopted, a local validation of TCD findings must be performed at each laboratory.

Transcranial color duplex imaging

Transcranial color duplex sonography (TCCS) is performed with a phased array transducer. Most often the Doppler carrier frequency is in the range of 2–3 MHz with an imaging frequency of up to 4 MHz. It is important to optimize not only the B-mode image, but also the color and spectral Doppler information for accurate evaluations [8–15]. Although TCCS provides a convenient flow map, a single-channel spectral Doppler interrogation remains the mainstay of diagnosis for newer transcranial ultrasound techniques.

Image Not Available

Figure 2.14 The artifact above the baseline is produced during insonation of a normal flow in the vertebral artery (below the baseline) that acts as a bright reflector on the full-power beam path. (Reproduced with permission from Alexandrov AV. *Vascular Ultrasound Today* 1998; **3**: 141–60.)

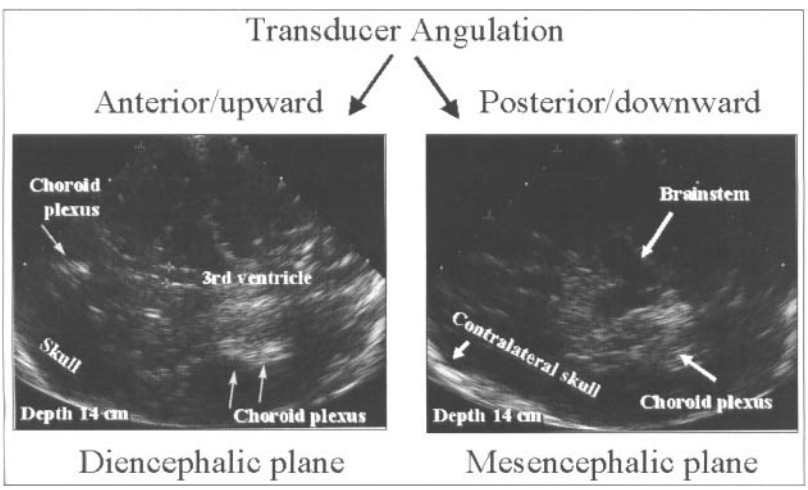

Figure 2.15 Planes of intracranial B-mode examination.

The B-mode image

The anatomic landmarks vary with the acoustic window chosen and transducer angulation (Figure 2.15). It is important to:

1 pay careful attention to the width of the sector image;

2 optimize signal return throughout the depth of the image using time-gain compensation (TGC);

3 place the focal zone at the level of the area of interest or immediately inferior to this region; and

4 achieve appropriate gray-scale contrast by adjusting the dynamic range so that echo intensity clearly defines intracranial bony and soft tissue anatomy.

The color Doppler image

The color Doppler image represents Doppler-shifted frequencies within a designated area of interest, the color box. Quite often, the entire circle of Willis can be displayed within the color box. If this is not the case, the anterior (Figure 2.16) and posterior circulation can be studied separately. It is important to:

1 optimize the color display by proper choice of colors to represent forward and reverse flow: choose contrasting colors to represent forward and reverse high-velocity signals;

2 use a high frame rate because you are expecting arterial signals with moderate antegrade velocity;

3 adjust the color gain so that the lumen of the vessels is filled without evidence of 'bleeding' of color into the surrounding tissues;

4 change the color velocity scale pulse repetition frequency (PRF) often throughout the course of the examination to detect variations in velocity that occur with vessel tortuosity, stenosis and occlusion; and

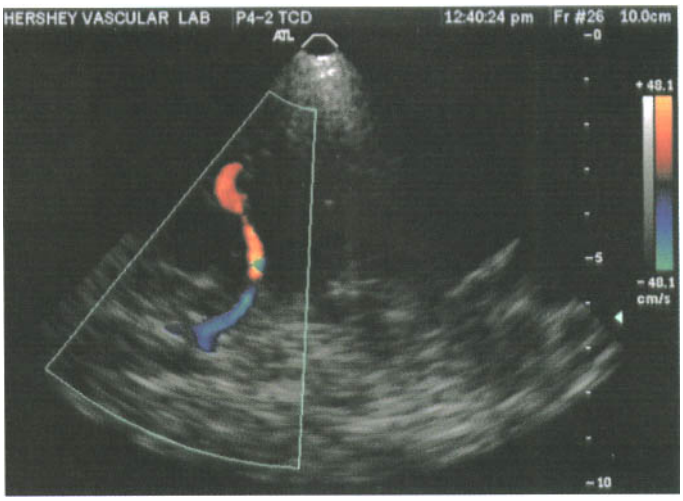

Figure 2.16 Color Doppler flow image of the anterior and middle cerebral arteries. Blue, anterior; red, middle cerebral artery.

5 keep the wall filter as low as possible so that detection of low-velocity, low-amplitude signals will not be overlooked.

Doppler spectral analysis

The Doppler spectral display contains the diagnostic information similar to 'non-image-guided' TCD. However, TCCS allows angle correction and the velocity values will be different from a non-image-guided TCD that assumes a zero angle of insonation [16,17]. The TCCS display should document the peak systolic velocity, the maximum mean flow velocity, end-diastolic velocity, the resistance index (RI) and the pulsatility index (PI). It is important to:

1 use adequate Doppler power to allow penetration but to limit the duration of high power use;
2 employ a low wall filter so that low-velocity, low-amplitude signals can be detected;
3 vary the sample volume size, velocity scale and Doppler gain to obtain characteristic and accurate spectral information from the intracranial arteries;
4 align the angle of insonation with a longer (0.5–1-cm) display of color jet [17];
5 correlate audible Doppler signal with the spectral display for *all* accessible arterial segments; and
6 if you use *TCD* criteria, change the angle of insonation to *0° for all vessels.*

TCCS examination technique

Unlike transcranial Doppler, the TCCS examination allows visualization of anatomic landmarks and spatial course of the arteries that is helpful for vessel identification. By complementing the duplex examination with color flow or power Doppler and, when available, three-dimensional imaging (Figure 2.17), the course of the arteries can be traced and angle-corrected velocities determined.

Figure 2.17 Three-dimensional power Doppler image of the circle of Willis.

The acoustic windows that are employed for TCD are also useful for TCCS, i.e. transtemporal, orbital and foraminal. An additional frontal window has recently been described to insonate the origins of A2 ACA segments [18].

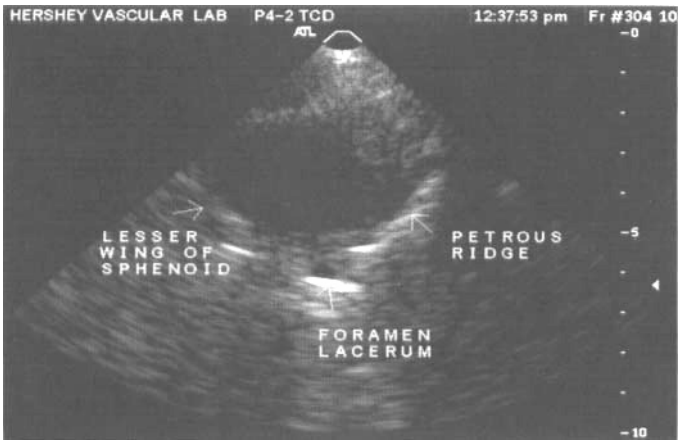

Figure 2.18 Landmarks for transtemporal B-mode examination.

Using the transtemporal approach, the examiner should look for the petrous ridge of the temporal bone, the cerebral falx, the supracellar cistern, the 3rd ventricle and the cerebral peduncles as anatomic landmarks [19]. From the suboccipital window, the examiner should find the foramen magnum and the occipital bone. Imaging through the orbit should reveal the globe and optic nerve. These are useful anatomic landmarks that allow you to select transducer position over the best achievable window, optimize image quality and direct interrogation toward structures that surround arteries intracranially.

Using the transtemporal window

1 The study is initiated with the patient lying in the supine position with the head straight.

2 It is best for the examiner to sit or stand behind the patient, with their arm or elbow resting on the pillow beside the patient's ear.

3 Place the ultrasound transducer on the temporal bone in the preauricular area anterior to the ear and cephalad to the zygomatic arch. The left side of the image should display the frontal portion of the intracranial structures.

4 Angle the transducer slightly superiorly to visualize the anterior cerebral circulation. You should note that the ipsilateral anterior circulation is at the top of the image and that you can quite often see through the midline of the brain to visualize the contralateral anterior circulation. Although infrequent in the majority of patients, you may occasionally visualize the posterior circulation as well. When this is possible, the posterior circulation will appear to the right of the monitor while the anterior circulation lies to the left.

5 Begin the examination at an image depth of 12–16 cm. This will allow visualization of the contralateral skull and interrogation of the entire intracranial field in most adults.

6 Using B-mode imaging, you should be able to identify the lesser wing of the sphenoid bone extending anteriorly and the petrous ridge of the temporal bone extending posteriorly (Figure 2.18).

7 From this point, angle the transducer slightly superiorly to image falx and peduncles. This will establish the midline structures.

8 Reduce the imaging depth to 8–10 cm to study the ipsilateral anterior circulation. Set the color controls to allow for equal forward and reverse flow velocities and steer the color box straight down from center.

9 Use as narrow a width of the color box as possible to interrogate the middle cerebral artery to the level of the bifurcation. This will increase the frame rate and prevent aliasing of signals in normal arteries. Although angle correction may be possible over short segments of arteries, it is best to maintain a 0° angle of insonation to prevent overestimation of peak and/or mean velocities.

10 Using color flow imaging, follow the course of the middle cerebral artery to its bifurcation. You may need to angle the probe slightly anteriorly and superiorly to image the anterior cerebral artery (ACA). The normal ACA will be displayed in blue as it courses away from the transducer toward the midline of the brain (Figure 2.16). The A2 segment can occasionally be visualized extending anteriorly.

11 When sampling in the region of the bifurcation, the terminal segment of the internal carotid artery (ICA) can be visualized by tilting the transducer

slightly inferiorly. Although blood flow is most commonly toward the transducer, the flow direction relative to the ultrasound beam can vary in this often-tortuous segment.

12 Angle the ultrasound beam slightly posteriorly and inferiorly to image the posterior cerebral artery (PCA) and posterior communicating artery (PComA), if present. This can be achieved by steering the box so that it is positioned over the peduncles. You should note that the PCA wraps around the peduncle. Flow towards the transducer is commonly assigned to the P1 PCA segment and flow away from the transducer is considered to represent P2 PCA segment distal to the origin of the PComA. Given the depth of the PCA and the relatively low velocity, the color scale (PRF) may need to be reduced in order to optimize the return signal. If you are able to visualize the termination of the basilar artery, you may be able to image both the ipsilateral (red) and contralateral (blue) P1 segments.

13 The anterior communicating artery (AComA) cannot usually be differentiated from the neighboring ACAs because of its small size. Keeping in mind the anatomy and the appropriate angulation of the sound beam relevant to the axis of the vessels, you should be able to image the functioning PComA, which is of longer length, as it connects the anterior and posterior segment of the circle.

Using the suboccipital window

1 Have the patient sit up on a chair or lie on their side with the head tilted forward ('bring your chin to your chest') to image the vertebral and basilar arteries. This creates an easily accessible acoustic window between the cranium and the atlas of the vertebral column. The transducer should be placed slightly to the right or left of midline with the beam angled toward the bridge of the nose. The first structure that you will encounter is the large anechoic foramen magnum. Surrounding this you will see the brightly echogenic rim of the occipital bone. Blood flow will normally be away from the transducer in the vertebral arteries and a Y-shaped color flow image of the vertebrobasilar junction can be visualized at 6–8 cm depth (Figure 2.19).

2 Examine Doppler spectra of the vertebral arteries along their course to the confluence forming the basilar artery. You may see the posterior inferior cerebellar arteries (PICAs) branching from the vertebral arteries. Because these small branches course toward the transducer, they should appear in red. It is important to standardize your imaging protocol so that, if you cannot image both vertebral arteries together, the right and left vertebral arteries always appear in the same location on the color flow image. It is our custom to orientate the transducer so that the right vertebral artery appears to the right of the image and the left vertebral to the left of the image.

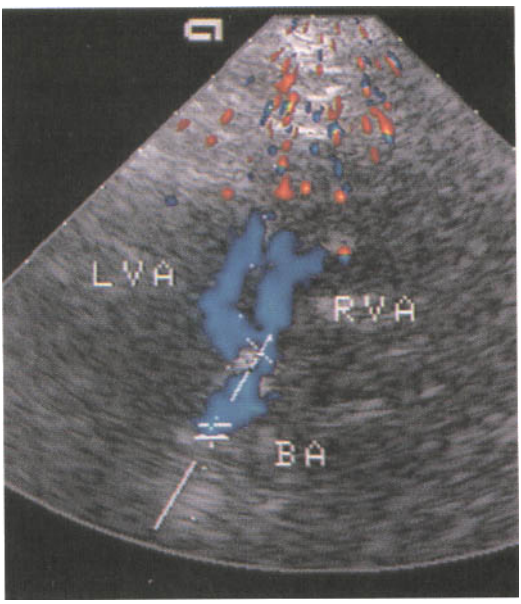

Figure 2.19 'Y'-sign. Color Doppler flow image of the vertebral confluence and the proximal basilar artery. (Image courtesy of Dr Eva Bartels.)

3 From the level of the vertebral arteries, angle the transducer slightly inferiorly and superiorly to visualize the basilar artery (BA). The BA is most commonly imaged at a depth of 7–11 cm [19]. You may have to point the transducer upwards to image the distal portion of the BA up to its bifurcation using the foraminal approach. Since color flow depth range may be less than B-mode, a single-gate spectral Doppler interrogation of the distal BA depth may be performed without a color box. Note that this portion of the BA can be visualized using the transtemporal approach or with the help of ultrasound contrast substances.

Using the orbital window

To access the ophthalmic artery (OA) and the carotid siphon, the transorbital window should be chosen. Because the sound beam is passing through a fluid-filled chamber at relatively high acoustic output levels, there is legitimate concern for ocular damage due to heat absorption and cavitation. It is very important to know the Food and Drug Administration

(FDA)-approved guidelines for choice of transducer and power settings for the ultrasound systems that you are using for transorbital studies and to adhere to these guidelines. The current FDA derated maximum acoustic output levels for ophthalmic imaging are a spatial peak temporal average (SPTA) intensity of 17 mW/cm^2 and a mechanical index (MI) of 0.28. Transorbital insonation steps are as follows.

1 The ultrasound probe is placed over the closed eyelid, which is covered with acoustic gel. The patient is asked to look inferiorly and toward the contralateral side. It is important to standardize your scanning protocol so that the nasal aspect of the eye corresponds to the orientation marker on the probe. This is kept constant for both the right and left eyes.

2 The globe appears as a dark anechoic structure in the center of the image. The optic nerve appears as an anechoic tube extending from the globe into the far field of the image (Figure 2.20). The distal portion of the ophthalmic artery will appear slightly medially at a depth of 3–5 cm. Blood flow is normally directed toward the transducer with relatively high resistance compared to intracranial vessels. You will note sharpened peak systolic and slightly lower diastolic flow components (Figure 2.20).

3 The carotid siphon can be imaged at a depth of 6–7 cm. The direction of blood flow will vary with the segments interrogated (parasellar, genu, supraclinoid). Flow signals are bidirectional at the genu, toward the sound beam in the parasellar segment and away from the sound beam in the supraclinoid segment.

Using the submandibular window

During a routine extracranial cerebrovascular examination, the cervical portion of the internal carotid artery (ICA) can be imaged to the level of the ramus of the mandible. To access the segment of the ICA distal to this level, place the transducer at the angle of the mandible and angle it toward the head and slightly medially. The distal ICA can be imaged at a depth of 3–6 cm with flow away from the transducer. To apply the Lindegaard ratio [20], a measurement of the ICA flow should be taken at 0° angle of insonation.

Advantages of TCCS over non-imaging techniques

With transcranial imaging, the examiner is able to visualize anatomic landmarks and spatial relationship of the vessels that can be used for identification of the arteries in the circle of Willis (see Chapter 3). This leads to increased confidence in the accuracy of the examination. The course of tortuous arteries can be followed, arterial branching can be identified, and the terminal vertebral arteries can be differentiated (left and right) leading to positive evaluation of the basilar artery. Using color flow imaging, the examiner is able to detect regions of disturbed flow, and immediately suspect focal stenosis or occlusion, arteriovenous malformations or large aneurysms. The study can be complemented with power Doppler and three-dimensional reconstruction to assure complete evaluation of all segments of the circle of Willis. Additionally, when performed in combination with extracranial duplex evaluation, this technology has enhanced our clinical approach to patients presenting with acute stroke and has a potential to increase our ability to differentiate between ischemic and hemorrhagic stroke [21].

Limitations of TCCS

To ensure a complete and accurate examination, the sonographer must use his or her knowledge of intracranial anatomy and complete a single-gate spectral analysis even without complete color visualization of the circle of Willis. In other words, *spectral analysis must be performed at depths that may contain arterial flow signals even if these segments are not or only poorly visualized with color flow imaging.* It is particularly applicable to vessel tortuosity when an out-of-plane position may result in no color flow signal, yet an attempt must be made to detect flow in this area. It must be kept in mind that several ultrasound techniques are being used to create the gray-scale image of the intracranial anatomy, the color flow image of the cerebral vasculature and the spectral display of flow patterns in the intracranial arteries and veins. It places high demand on frame rate and processing capacity of the duplex scanner. Because the bone in the region of the transtemporal window will attenuate the ultrasound beam, TCCS offers fewer successful non-contrast-enhanced studies compared to the non-imaging TCD techniques. TCCS should not be used as a screening test for cerebral aneurysms [22,23]. Furthermore, fewer diagnostic criteria are available for detection and grading of intracranial disease with TCCS [24,25]. Although TCCS allows assessment of intracranial veins, thrombosis and arteriovenous malformations [26–28], the reliability and clinical utility of TCCS in this setting is still unknown.

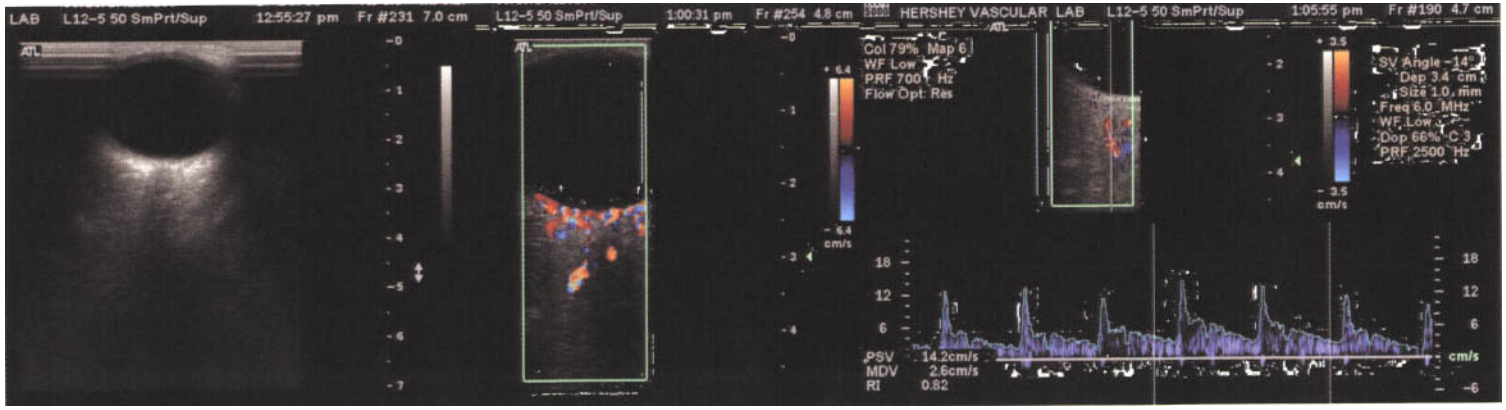

Figure 2.20 Steps of transorbital examination. B-mode of the eye and optic nerve (left), B-mode plus color Doppler flow (center), angle-corrected velocimetry of the ophthalmic artery (right).

Although the advantages of transcranial color flow imaging compared to the non-imaging studies are recognized, current high-resolution duplex ultrasound systems do not facilitate portable bedside evaluations as yet. Recognition of imaging artifacts and complete Doppler spectral interrogation are the keys to reducing operator-dependent failures of TCCS.

References

1 Aaslid R, Markwalder TM, Nornes H. Noninvasive transcranial Doppler ultrasound recording of flow velocity in basal cerebral arteries. *J Neurosurg* 1982; **57**: 769–74.

2 Otis SM, Ringelstein EB. The transcranial Doppler examination: principles and applications of transcranial Doppler sonography. In: Tegeler CH, Babikian VL, Gomez CR, eds. *Neurosonology*. St Louis: Mosby, 1996: 140–55.

3 Moehring MA, Spencer MP. Power M-mode transcranial Doppler ultrasound and simultaneous single gate spectrogram. *Ultrasound Med Biol* 2002; **28**: 49–57.

4 Aaslid R. *Transcranial Doppler Sonography*. Wien: Springer Verlag, 1986: 39–59.

5 Hennerici M, Rautenberg W, Sitzer G, Schwartz A. Transcranial Doppler ultrasound for the assessment of intracranial arterial flow velocity—Part 1. Examination technique and normal values. *Surg Neurol* 1987; **27** (5): 439–48.

6 Monsein LH, Razumovsky AY, Ackerman SJ, Nauta HJ, Hanley DF. Validation of transcranial Doppler ultrasound with a stereotactic neurosurgical technique. *J Neurosurg* 1995; **82** (6): 972–5.

7 Babikian V, Sloan MA, Tegeler CH, DeWitt LD, Fayad PB, Feldmann E, Gomez CR. Transcranial Doppler validation pilot study. *J Neuroimaging* 1993; **3**: 242–9.

8 Bogdahn U, Becker G, Schlief R, Reddig J, Hassel W. Contrast-enhanced transcranial color-coded real-time sonography. *Stroke* 1993; **24**: 676–84.

9 Schoning M, Buchholz R, Walter J. Comparative study of transcranial color duplex sonography and transcranial Doppler sonography in adults. *J Neurosurg* 1993; **78**: 776–84.

10 Schoning M, Walter J. Evaluation of the vertebrobasilar-posterior system by transcranial color duplex sonography in adults. *Stroke* 1992; **23**: 1577–82.

11 Giovagnorio F, Quaranta L, Bucci MG. Color Doppler assessment of normal ocular blood flow. *J Ultrasound Med* 1993; **12**: 473–7.

12 Fujioka KA, Gates DT, Spencer MP. A comparison of transcranial Doppler imaging and standard static pulse wave Doppler in the assessment of intracranial hemodynamics. *J Vasc Technol* 1994; **18**: 29–35.

13 Bartels E, Fuchs HH, Flugel KA. Color Doppler imaging of basal cerebral arteries: normal reference values and clinical applications. *Angiology* 1995; **46** (10): 877–84.

14 Baumgartner RW, Schmid C. Comparative study of power-based versus mean frequency-based transcranial color-coded duplex sonography in normal adults. *Stroke* 1996; **27**: 101–4.

15 Kenton AR, Martin PJ, Evans DH. Power Doppler: an advance over color Doppler for transcranial imaging? *Ultrasound Med Biol* 1996; **22**: 313–7.

16 Bartels E, Flugel KA. Quantitative measurements of blood flow velocity in basal cerebral arteries with transcranial duplex color-flow imaging. A comparative study with conventional transcranial Doppler sonography. *J Neuroimaging* 1994; **4** (2): 77–81.

17 Giller GA. Is angle correction correct? *J Neuroimaging* 1994; **4**: 51–2.

18 Stolz E, Kaps M, Kern A, Dorndorf W. Frontal bone windows for transcranial color-coded duplex sonography. *Stroke* 1999; **30** (4): 814–20.

19 Bartels E. *Color-Coded Duplex Ultrasonography of the Cerebral Arteries: Atlas and Manual*. Stuttgart: Schattauer, 1999.

20 Lindegaard KF, Nornes H, Bakke SJ, Sorteberg W, Nakstad P. Cerebral vasospasm diagnosis by means of angiography and blood velocity measurements. *Acta Neurochir (Wien)* 1989; **100** (1–2): 12–24.

21 Becker GM, Winkler J. Differentiation between ischemic and hemorrhagic stroke by transcranial color-coded real-time sonography. *J Neuroimaging* 1993; **3**: 41–7.

22 Baumgartner RW, Mattle HP. Transcranial color-coded duplex sonography in cerebral aneurysms. *Stroke* 1994; **25**: 2429–34.

23 White PM, Wardlaw JM, Teasdale E, Sloss S, Cannon J, Easton V. Power transcranial Doppler ultrasound in the detection of intracranial aneurysms. *Stroke* 2001; **32** (6): 1291–7.

24 Baumgartner RW, Mattle HP, Schroth G. Assessment of > 50% and < 50% intracranial stenosis by transcranial color-coded duplex sonography. *Stroke* 1999; **30**: 87–92.

25 Lien LM, Chen WH, Chen JR, Chiu HC, Tsai YF, Choi WM, Reynolds PS, Tegeler CH. Comparison of transcranial color-coded sonography and magnetic resonance angiography in acute ischemic stroke. *J Neuroimaging* 2001; **11** (4): 363–8.

26 Stolz E, Kaps M, Domdorf W. Assessment of intracranial venous hemodynamics in normal individuals and patients with cerebral venous thrombosis. *Stroke* 1999; **30**: 70–5.

27 Becker G, Bogdahn U. Transcranial color-coded real-time sonography in intracranial veins. Normal values of blood flow velocities and findings in superior sagittal sinus thrombosis. *J Neuroimaging* 1995; **2**: 1196–9.

28 Becker GM, Winkler J. Imaging of cerebral arteriovenous malformations by transcranial colour-coded real-time sonography. *Neuroradiology* 1990; **32**: 280–8.

3

CHAPTER 3

Color flow anatomy of the circle of Willis

Eva Bartels, MD & *Andrei V. Alexandrov*, MD, RVT

Introduction

Sir Thomas Willis, in his landmark book published in 1664, described the anatomy of basal intracranial vessels (Figure 3.1). In the first half of the 20th century, Egar Monis introduced invasive cerebral angiography that enables the visualization of these arteries in humans and still remains the gold standard for other imaging modalities. Recent technology advances in computed tomography (CT) and magnetic resonance (MR) imaging allow non-invasive and three-dimensional reconstruction of these vessels.

Transcranial color flow imaging with ultrasound provides a fast way to visualize the spatial course and flow direction in the arteries of the circle of Willis in a two-dimensional plane image in real time. A three-dimensional reconstruction of ultrasound data is also possible with newer generations of duplex scanners

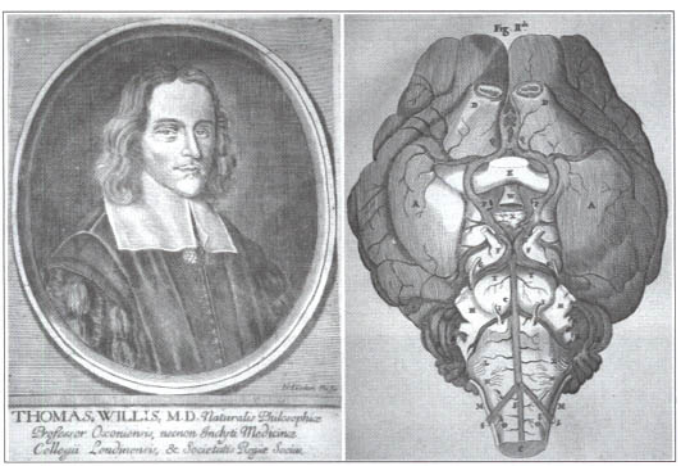

Figure 3.1 Sir Thomas Willis (1621–75), an English physician, anatomist and physiologist. He was Professor of Natural Philosophy at Oxford, England, 1660–75. Willis studied the anatomy of the central nervous system and the circulation of the blood. His landmark text, *Cerebri Anatome*, 1664, was reproduced many times and developed into a pocket-size standard textbook for medical students. Photos of the portrait and drawing of the brain were made by Dr Alexandrov at the Tirgu Mures Library in Romania. The textbook contains remarkable drawings by Sir Christopher Wren, a famous architect of the 17th century. Sir Thomas Willis described the arterial circle at the base of the brain and its function. He was the first to use the term 'reflex action'. Willis attempted to correlate the knowledge of anatomy, physiology and biochemistry with clinical findings in neuropathology. Willis proposed that the choroid plexus was responsible for the absorption of cerebrospinal fluid. Later, in *De Anima Brutorum*, 1672, he proposed that the corpus striatum received all sensory information, while the corpus callosum was associated with imagination and the cerebral cortex with memory.

that allow such data acquisition. Although transcranial color duplex sonography (TCCS) is not yet readily available at the bedside in most institutions, rapid development of digital and computer-based ultrasound technologies will soon make a fast three-dimensional assessment of the circle of Willis a reality.

This chapter offers self-assessment material to determine recognition of basic color flow transcranial findings. These patterns are helpful in recognizing normal anatomy and typical artifacts. Correct answers and discussion points are provided at the end of the chapter.

Questions

Question 1. Identify the arteries and brain structures shown in Figure 3.2.

Question 2. The change in color assignment of the distal middle cerebral artery (MCA) flow (location 1, Figure 3.2) represents:

A Aliasing
B Range ambiguity
C Stenosis
D Tortuousity
E Reversal

Question 3. Figure 3.3 provides keys to vessel identification using transcranial color flow imaging. The appearance of the distal right MCA in a color flow image in Figure 3.3 is likely due to:

A Range ambiguity
B Branching
C Vasodilatation
D Arteriovenous malformation
E Aneurysm

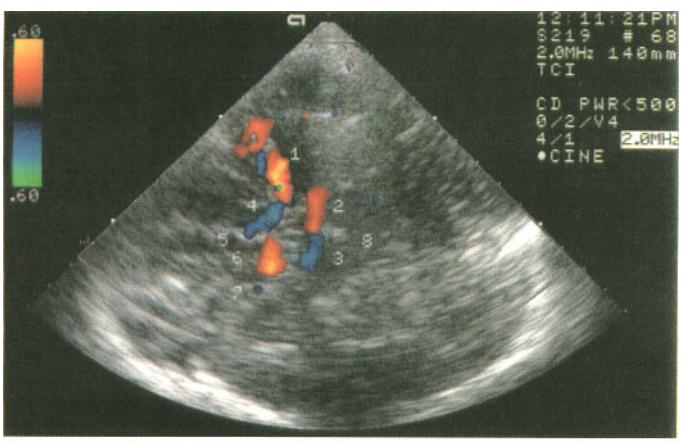

Figure 3.2 Color flow image of the circle of Willis. See Question 1 and answer for explanation.

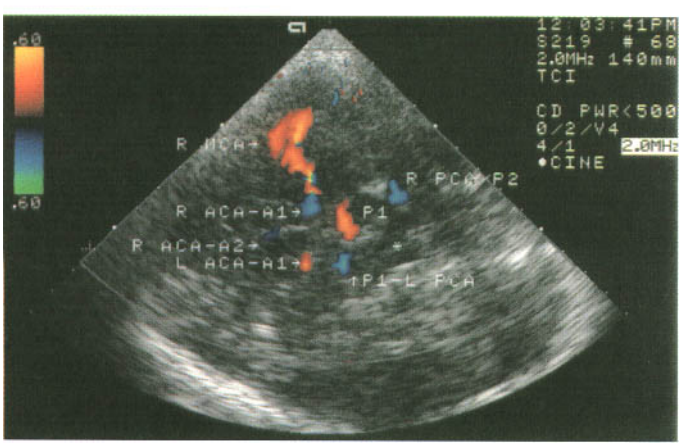

Figure 3.3 Color flow appearance of the proximal arterial segments with temporal insonation. See Question 3 and answer for explanation.

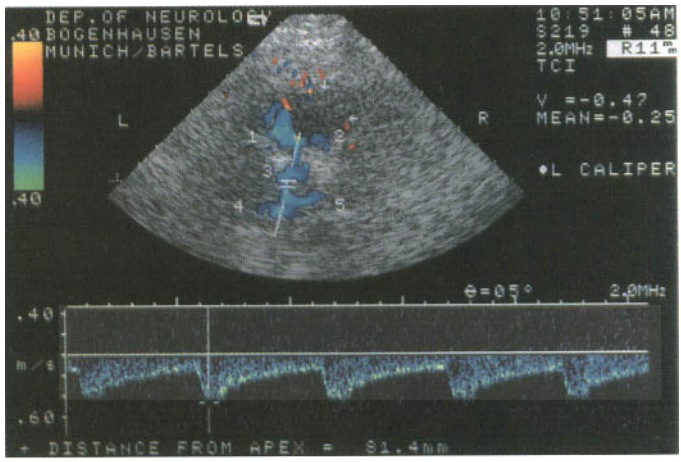

Figure 3.4 Color flow examination through the suboccipital window. See Question 4 and answer for explanation.

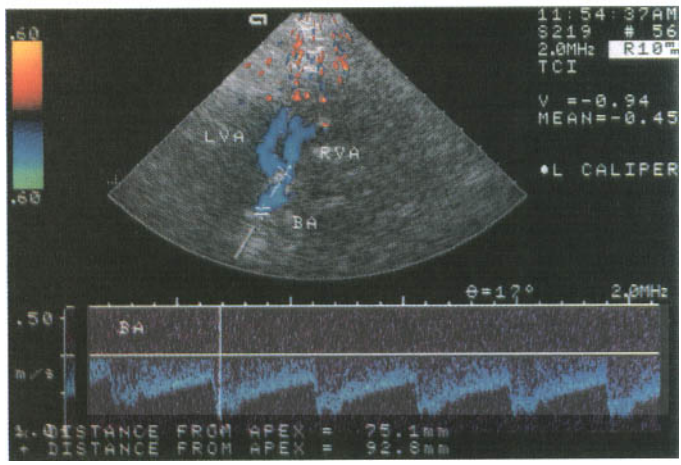

Figure 3.5 Color flow imaging of the basilar artery. See Question 6 and answer for explanation.

Question 4. Figure 3.4 shows suboccipital TCCS examination through the foramen magnum. Identify the arteries numbered on Figure 3.4.

Question 5. As shown in Figure 3.4, changes in the basilar artery diameter are due to:

A Stenosis
B Compression
C Tortuosity
D Low flow
E Atresia

Question 6. Figure 3.5 shows a color flow-guided Doppler interrogation of the mid-to-distal basilar artery segment. The depths of visualization of the basilar artery are 75–92 mm. The Doppler gate is placed at 92.8 mm. The color flow image of the vertebrobasilar system shown in Figure 3.5 is called:

A Mosaic pattern
B To-and-fro flow
C Slosh phenomenon
D Double lumen sign
E Y-sign

Question 7. As shown in Figure 3.6, the proximal basilar artery is found at the depth of 67 mm. The Doppler spectrum shows arterial flow pattern. In Figure 3.6, identify the artery interrogated with Doppler gate.

A Posterior inferior cerebellar artery
B Anterior inferior cerebellar artery
C Superior inferior cerebellar artery
D Terminal right vertebral artery
E Right posterior cerebral artery

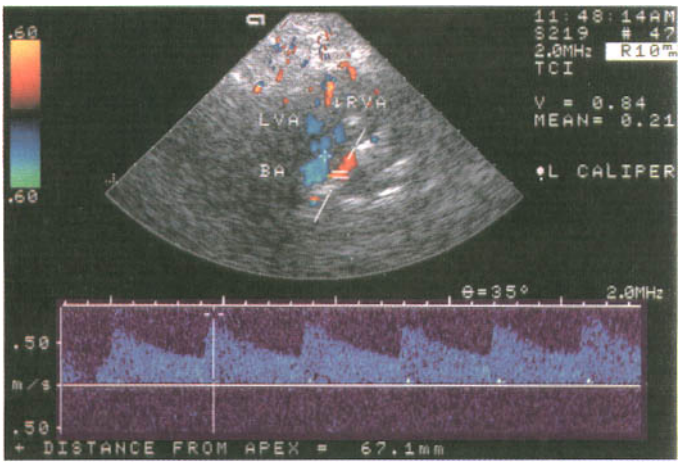

Figure 3.6 Angle-corrected velocity measurement through the foraminal window. See Question 7 and answer for explanation.

Correct answers

Question 1. Matching correct answers are:
1 Distal M1 MCA
2 P1 posterior cerebral artery (PCA)
3 Contralateral PCA
4 A1 anterior cerebral artery (ACA)
5 A2 ACA
6 Contralateral A1 ACA
7 Contralateral MCA
8 Brainstem
The key to vessel identification in this image is to orientate yourself in the image. First, recognize that the top of the image sector represents the area where transducer is applied to the temporal bone window. White dots on the sector margins represent depth of insonation scale with 1-cm units. Color flow assignment is provided in the color bar scale in the left portion of the screen. Therefore, each color flow signal can be interpreted as to its depth location and flow direction towards or away from the transducer. Finally, visual recognition of a typical distribution of the branches of the circle of Willis represents the major advantage of TCCS.

Question 2. Correct answer is **D**.
There are two areas of color flow changes in the MCA. The first area is located at its proximal portion and represents aliasing likely due to relatively low color flow velocity scale. Note that in this area the color changes abruptly from light red to green and this is consistent with the wraparound phenomenon in maximum Doppler frequencies, i.e. aliasing. The second area is in the distal MCA portion (location 1) and the color changes from dark red to dark blue. In other words, the color flow assignment changed by crossing the baseline. This happens with the tortuous course of the vessel or bidirectional flow at arterial bifurcations where one vessel is continuing its spatial course towards the transducer and another one is directed away from it.

Question 3. Correct answer is **B**.
The distal MCA appears to increase its diameter and the origin of two vessels can be visualized. This is a normal appearance of the M2 MCA subdivision where both M2 branches are still directed towards the transducer. The second best answer is range ambiguity since the wavelength of a 2-MHz Doppler carrying frequency is 0.77 mm, that is, comparable to the MCA dimensions. Some scatter of ultrasound can be expected, leading to artifactual appearance of color flow vessel edges. Therefore, current TCCS technology may not be used to measure MCA diameter with the precision necessary to calculate percentage stenosis or flow volume. Finally, an arteriovenous malformation (AVM) should be considered as a part of the differential diagnosis since it may result in the appearance of relatively large vessels at the level of the proximal MCA. Spectral Doppler interrogation (either at 60° or, preferably, at 0° angle of insonation) of suspicious areas may provide further information.

Question 4. Matching correct answers are:
1 Left vertebral artery (VA)
2 Right VA

3 Basilar artery
4 Cerebellar branch
5 Cerebellar branch

This image represents a normal appearance of the terminal VA junction and basilar artery stem. These vessels are very tortuous and sometimes only segmental assessment is possible. The main advantage of TCCS is direct visualization of the terminal VAs, side-to-side differentiation and differentiation of the terminal VA and proximal BA segments as well as terminal VA portion that is not possible with TCD.

Question 5. Correct answer is **C.**

The basilar artery can be found with a suboccipital transducer position and ultrasound beam direction towards the bridge of the nose. The distal basilar artery climbs along the brainstem and pons to branch off at the level of the cerebral peduncles. This spatial course produces a substantial change in the angle of insonation and out-of-the-plane vessel position that lead to changes in the velocity and vessel diameter measurements. Finally, the basilar artery seems to increase its diameter on color flow image at the points where cerebellar arteries branch off its stem.

Question 6. Correct answer is **E.**

This image represents a classical flow pattern called the 'Y'-sign that describes a normal junction of the terminal vertebral arteries. This is not an image of a double lumen flow since both proximal flow signals are of equal velocity and continuation that implies equal resistance to flow in both vessels. The term 'double lumen' usually refers to a pathologic condition, for example, with arterial dissection where one color jet represents a true lumen and another one indicates the false lumen, usually with a decreased and/or high-resistance flow pattern.

Question 7. Correct answer is **B.**

This image shows a branch of the basilar artery that has flow direction towards the transducer. This color flow pattern indicates a cerebellar branch. The posterior inferior cerebellar artery (PICA) usually arises from the terminal VA segment as it is clearly visualized on the image proximal to the vertebral junction. The anterior inferior cerebellar artery (AICA) arises from the proximal basilar artery stem. In order to decide which part of the basilar artery was imaged, the depth indicating the proximal basilar artery is given. Since the basilar artery is at least 2 cm long in most adults, the color flow image represents a branch that originates within 1 cm of the basilar artery origin, thus representing the AICA. Ideally, to clearly differentiate between the AICA and the superior cerebellar artery (SCA), an image of the distal basilar artery should be obtained, showing either the presence of another more distal branch or at least the extent of the basilar artery stem. The SCA usually branches off the distal basilar artery before the P1 posterior cerebral artery origin. However, SCA detection requires high resolution TCCS equipment and is operator dependent.

This page intentionally left blank

PART II

Hemodynamic principles

This page intentionally left blank

4 CHAPTER 4

Integrated assessment of systemic and intracranial hemodynamics

Anne W. Wojner, PhD, CCRN

Introduction

Hemodynamics is a term used to describe the flow of blood through the vascular system. The measurement and augmentation of hemodynamics requires an understanding of complex physiologic mechanisms that foster systemic autoregulation, the body's ability to adjust blood flow despite marked changes in arterial blood pressure. Autoregulation is dependent upon complex mechanisms that enable rapid detection of flow alterations coupled with multisystem responses that aim to maintain optimal perfusion, especially to critical organ systems. Chief among these mechanisms is augmentation of myocardial performance through intrinsic and extrinsic means.

Today, an understanding of systemic hemodynamic principles coupled with a sound understanding of safe augmentation measures is essential to the neuroscience clinician. Management of many neurovascular conditions often hinges on augmentation of systemic hemodynamic parameters to enhance intracranial blood flow, perfusion and brain tissue oxygenation. The coexistence of cardiac conditions such as acute myocardial ischemia or infarction, coronary artery disease, cardiac valvular anomalies and dysrhythmias frequently challenges safe augmentation of systemic flow parameters in neuroscience patients; yet, the heart and systemic vasculature may be enslaved to drive intracranial perfusion when the clinician safely and accurately uses technology and clinical skills to continuously monitor the effects of his or her care.

This chapter will examine principles associated with systemic and intracranial hemodynamics and the methods commonly used in a critical care setting to assess hemodynamic function. Correlated continuous monitoring of systemic and intracranial hemodynamics provides a means for ongoing assessment of circulatory adequacy, perfusion and overall tissue oxygenation, promoting sound clinical management of complex flow-related issues. The chapter will conclude with case studies in correlated assessment and management of neuroscience patients.

Principles of blood flow

The circulatory system is a closed circuit made up of two major components, the systemic and pulmonary circulation. An understanding of blood flow through these circuits must be supported by discussion of the physical characteristics of blood, and the interrelationship of *pressure*, *resistance* and *flow*. Manipulation of pressure and resistance variables within the cardiovascular system directly affects blood flow parameters, and serves as the basis for clinical hemodynamic augmentation.

Blood *viscosity* is primarily determined by hematocrit, the percentage of blood that is made up of cells. An increase in hematocrit results in an increase in friction between successive layers of blood, slowing down its propagation velocities and amplifying the pressure necessary to drive blood through the systemic circulation. When combined with reduced internal vessel diameter, an increase in blood viscosity may significantly impair blood flow.

Flow of blood through vessels is primarily determined by two factors:

1 differences in pressure ($P_1 - P_2$) between the two ends of a vessel; and

2 vascular resistance to flow.

Ohm's law is often used to describe flow through the vascular system. Simply put, it states that blood flow is directly proportional to the pressure difference, but inversely proportional to the resistance:

$$\text{blood flow} = \Delta \text{ pressure} \div \text{resistance}.$$

The amount of muscle tension within the vascular bed necessary to maintain specific flow pressures varies significantly. The *law of Laplace* describes this, stating that the muscle tension (T) needed to maintain a specific pressure (P) is reduced as the radius (R) is decreased:

$$P = T/R.$$

The smaller the blood vessel diameter, the less tension is required to maintain a given pressure within the vessel [1]. Applied to human anatomy, the degree of wall tension necessary to maintain perfusion pressure in the aorta would be approximately 10 000 times that necessary to maintain pressure within a capillary bed.

Resistance, or impediment to flow, cannot be measured directly, and is derived by measurements of blood flow and pressure difference within a vessel. Varying degrees of resistance occur in vessels throughout the body. Resistance is a product of changing vessel diameters coupled with proportional increases in blood viscosity, as well as the cross-sectional area of vascular beds. The resistance associated with changes in vessel diameter affects the movement of blood flow through a phenomenon known as streamlining or laminar flow [1]. *Laminar flow* describes the parabolic movement of blood in layers within a blood vessel; the layer closest to the vessel wall moves at the slowest velocity, while larger vessels with multiple layers exhibit increased rates of flow at the core of the vessel. *Turbulent flow* occurs when blood moves at the same time in a cross-wise and streamlined fashion. Turbulence is typically the product of obstructions to flow, passage of blood over a rough surface, or a sharp change in the direction of flow; it results in an eddy current, with an increase in friction and resistance.

Poiseuille's law is often used to describe the impact of resistance on blood flow; it states that the flow (Q) of a fluid through a tube is directly proportional to the pressure difference that exists between two ends of a tube ($P_1 - P_2$) to the fourth power of the radius of the tube (r^4), and is inversely proportional to length of the tube (L) and the viscosity of the fluid (n):

$$Q = \pi(P_1 - P_2)r^4/8Ln$$

where $\pi/8$ serves as a proportional geometric value [1].

Poiseuille's law illustrates how resistance increases in direct proportion to viscosity and vessel length, but decreases in direct proportion to vessel diameter and pressure gradient; in other words, the diameter of a blood vessel is the most significant contributor of all to the rate of blood flow through a vessel.

The interrelatedness of these concepts in the production of varying rates of blood flow can be illustrated by changes in arterial pressure. An increase in arterial pressure increases the force propelling blood and also distends vessel walls, thereby reducing vascular resistance; the result is an increase in blood flow. Similarly, a drop in arterial pressure results in reduced forward flow secondary to a decrease in vessel diameter from reduced arterial stretch, accompanied by an increase in resistance to flow; blood viscosity further contributes to a decline in flow during low pressure states as sluggish movement fosters clumping of cells and additional flow resistance.

The cardiac cycle

The cardiac cycle represents the sequential electrical and mechanical events that occur within a single heart beat, namely systole and diastole. At normal heart rates approximately two-thirds of the cardiac cycle consist of diastolic events, allowing for muscle relaxation and filling of the ventricles. Figure 4.1 illustrates the events of the cardiac cycle and corresponding pressure changes associated with blood flow through the heart.

Ventricular systole consists of three phases.

In phase 1, also known as *isovolumetric contraction*, the ventricles begin the process of contraction, building wall tension against closed semilunar (aortic and pulmonic) valves. The increase in pressure inside the ventricles causes the atrioventricular (mitral and tricuspid) valves to snap closed.

In phase 2, also known as *rapid ventricular ejection*, ventricular pressures exceed those within the aorta and pulmonary arteries, causing the semilunar valves to open as well as ejection of blood under intense pressure.

During phase 3, the *reduced ejection phase*, blood ejection slows considerably and intraventricular pressures drop sharply as contraction ends, causing

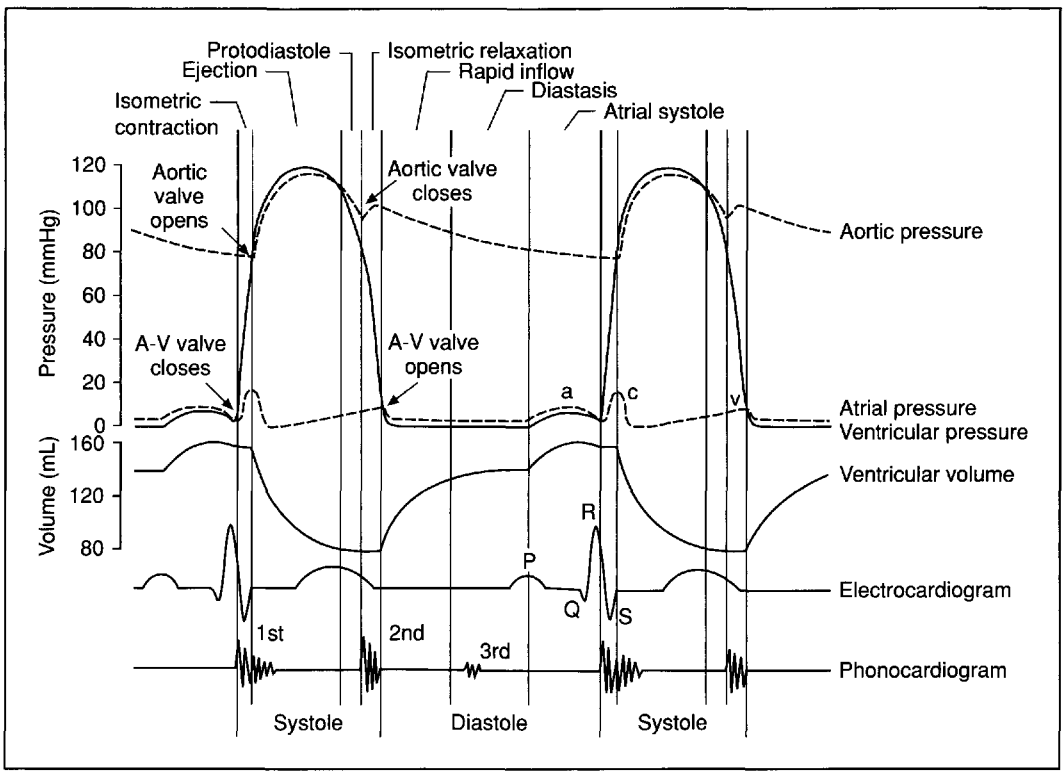

Figure 4.1 Electrical and mechanical events of the cardiac cycle. Note the interrelationship of the electrical and mechanical events in the cardiac cycle including heart sounds recorded by phonocardiogram and intraventricular volumes. From [1].

the semilunar valves to close when aortic and pulmonary artery pressures again exceed those within the ventricle.

Under normal resting conditions ventricular systole results in a stroke volume of approximately 70–80 mL, constituting about 60% of left ventricular end-diastolic volume [2].

Right ventricular (RV) and left ventricular (LV) performance differs significantly during systole due to the physical structure of these very different pumps. The RV exhibits a large surface area capable of moving like a bellows to promote swift ejection of blood to the low-resistance pulmonary system. Because muscle lengthening and shortening are less important contributors to RV contraction, changes within the pulmonary bed that increase resistance are likely to stifle ventricular performance, producing reduced RV output and a back-up in intracardiac right heart preload to the systemic venous circulation. The LV has a relatively small surface area and is capable of reducing and increasing its internal chamber circumference through muscle shortening and lengthening [2].

Application of the law of Laplace to LV performance demonstrates that wall tension is minimized as chamber size (radius) decreases; in patients exhibiting LV dilatation and hypertrophy, significant wall tension is required, amounting to intense myocardial oxygen consumption. A similar clinical picture is illustrated through examination of the process of volume loading; when intraventricular preload exceeds an optimal level, the resulting ventricular dilatation requires significant wall tension to maintain optimal chamber pressures and forward flow into the high-resistance aorta. The result of significant ventricular dilatation, whether due to excessive fluid hydration, pathologic dilatation or hypertrophy, is often the same: congestive failure with backflow to the pulmonary bed and pulmonary edema.

Ventricular diastole consists of four phases.

In phase 1, also called *isovolumetric relaxation*, ventricular pressure drops dramatically without a change in volume. When ventricular pressure decreases below that within the atria, the atrioventricular valves open, initiating the next phase.

In phase 2, also called the *rapid filling stage* or the early diastolic filling phase of the ventricles, the low intraventricular pressures present in phase 2 produce a phenomenon known as diastolic suction or recoil, which contributes to rapid blood flow and ventricular filling. When tachycardia is present, diastolic suction/recoil plays a significant role in maintaining ventricular filling despite a shortened filling time.

In phase 3, the *period of diastasis* is initiated when blood flow ceases and is marked by an equalization of ventricular and atrial pressures. When the diastolic phase is shortened due to an increase in heart rate, phase 3 may not be present as the process continues on to phase 4.

In phase 4, also called the *period of atrial contraction* or late ventricular diastole, heart rate, PR interval length and atrial preload determine the amount of blood that fills the ventricles during atrial kick. Under normal resting circumstances, preload contributed through atrial kick will not greatly affect overall ventricular volumes; but, in periods of stress, loss of atrial kick through processes such as atrial fibrillation may result in a decrease in ventricular preload by as much as 18% or more [2].

The arterial system should be viewed as a pressure reservoir that is capable of converting intermittent systolic and diastolic pressures into relatively constant flow through the *Windkessel effect* [1,3]. This effect describes the arterial system's ability to receive pulsatile energy transmission from the heart during systolic ejection and convert this to continuous pulsating waves that foster movement of blood through the systemic circulation. *Distensibility* is the primary factor responsible for maintaining the Windkessel effect's pulsatile transmission; the greater the distensibility or elasticity of the arterial system, the better the blood flow throughout the circuit. Distensibility and the subsequent elastic recoil of arterial vessels provides for constant forward flow during the diastolic phase of the cardiac cycle, thereby reducing *systemic vascular resistance* (SVR) and the workload of the heart during systole. As elasticity is reduced through processes such as atherosclerosis or chronic hypertension, resistance to flow from the left heart during systole increases, prompting the need for greater wall tension and an increase in LV workload.

Figure 4.2 represents an arterial waveform with the phases of the cardiac cycle identified. As noted previously, the arterial system is capable of maintaining a constant pressure within the vascular system, despite the dynamic events of the cardiac cycle. Because this constant pressure is a more accurate portrayal of physiologic systemic arterial pressure, calculation and assessment of mean arterial pressure (MAP) serves as a more reliable marker of systemic arterial pressure [1,2]. MAP was first calculated by recording the area

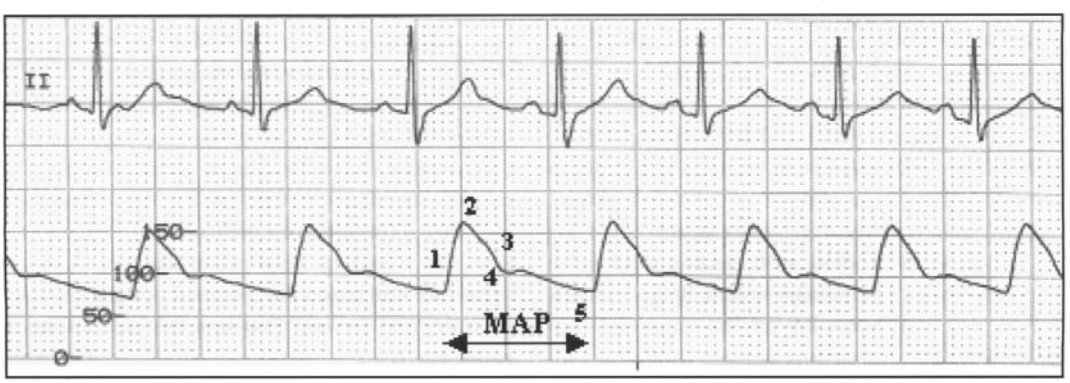

Figure 4.2 Phases of the cardiac cycle arterial waveform. Key to arterial waveform: 1, isovolumetric contraction; 2, peak systolic pressure (PSP); 3, reduced systolic ejection; 4, dicrotic notch; 5, end-diastolic pressure (EDP). Note: measurement of arterial pressure is performed by taking PSP over EDP; arterial pressure = 160/80 mmHg; mean arterial pressure (MAP) measured by area under the waveform (107 mmHg).

under the arterial pressure curve and dividing the area by the concurrent time period. A more simplistic calculation of MAP is:

$$\text{MAP} = (\text{systolic pressure} - \text{diastolic pressure}) \div 3 + \text{diastolic pressure}.$$

It is important to note that, as the pulsatile wave is transmitted across the arterial bed, systolic peak pressures may rise by as much as 20–40 mmHg from baseline aortic root pressure, due to an increase in resistance and arterial pulse pressure.

Pulse pressure, or the difference between systolic and diastolic pressures, may be used to assess arterial capacitance [2]. Normal pulse pressure is approximately 50 mmHg. In the absence of sepsis accompanied by low diastolic pressures, significant elevations of pulse pressure above this point signify reduction in arterial compliance due to processes such as atherosclerosis and/or chronic hypertension, and are associated with increased LV workload due to high resistance to flow. Because arterial compliance directly affects LV workload and the amount of resistance to blood flow during LV systole, pulse pressure may also be used to reflect stroke volume, the amount of blood ejected with each ventricular contraction. When it is used in this manner, the clinician must critically examine not only systolic and diastolic arterial pressures but also changes in other accompanying parameters to determine the underlying cause.

For example, a narrowed/decreased pulse pressure occurs in both hypovolemic and cardiogenic shock signifying decreased cardiac output in the face of elevated SVR; this finding is typically accompanied by low systolic pressures, a normal or often elevated diastolic pressure, an increase in heart rate and delayed capillary refill. Distinct changes in pulse pressure may also be detected in septic shock; pulse pressure may widen or elevate signifying high cardiac output and low SVR, and is accompanied by low diastolic pressures reflective of vasodilatation.

Arterial perfusion and venous return

Within the microcirculation, much of the arterial pressure head dissipates allowing for sufficient pressure gradients to promote forward flow. Dilatation and constriction of precapillary sphincters, thoroughfare channels and arterioles promote precise control of blood flowing through capillary networks to match cellular metabolic needs. Diffusion is primarily promoted by solute concentration and pressure gradients. According to the *Starling equilibrium*, filtration and reabsorption across capillary walls depend on the interrelation of four forces:

1 capillary pressure of approximately 30 mmHg which exerts a force to promote filtration through capillary walls;

2 interstitial fluid pressure of approximately 3 mmHg which through maintenance of a slightly negative pressure pulls fluid into the interstitial space;

3 interstitial fluid colloid osmotic pressure of approximately 8 mmHg which promotes osmotic fluid shifts into the interstitium; and

4 plasma colloid pressure (oncotic pressure) of approximately 28 mmHg which promotes capillary reabsorption [1].

Other factors affecting the exchange of substances across the capillary wall include viscosity of the filtrate and the integrity of the capillary wall.

The venous system serves as a volume reservoir of variable capacity as well as a conduit system for blood flow. Right atrial pressure or *central venous pressure* (CVP) is regulated by the following three contributing factors:

1 total blood volume;

2 the heart's ability to optimally pump blood; and

3 the capacitance of the venous system.

Under normal circumstances atmospheric pressure approximates CVP (CVP = 0). An increase in total blood volume, reduced left and/or right ventricular pump performance or maximized venous capacitance will result in an elevated CVP.

Intrinsic cardiac determinants of blood flow

Cardiac output (CO) is defined as the amount of blood that is pumped by the left ventricle into the aorta each minute. Normally in adults, the volume of blood pumped by the left ventricle each minute is 4–8 L, with an average cardiac output of approximately 5 L/min. Cardiac output varies according to body size; because of this, *cardiac index* (CI) is a measure that is used to estimate the proportion of blood flow to body surface area (BSA):

$$\text{CI} = \text{CO}/\text{BSA}.$$

Normal values for CI are 2.8–4.2 L/min/m^2; an average CI for a healthy 70-kg male is approximately 3 L/min/m^2.

Cardiac output is calculated as:

$$CO = \text{heart rate} \times \text{stroke volume}.$$

Stroke volume (SV) is the amount of blood ejected from the left ventricle with each contraction. Stroke volume is calculated as:

$$SV = \text{left ventricular end-diastolic volume} - \text{residual left ventricular blood volume}.$$

The residual left ventricular blood volume is determined immediately following systole. The average adult exhibits a stroke volume of 60–100 mL/ventricular contraction [3,4].

The CO equation (heart rate × SV) highlights the dependency of CO on heart rate and factors that influence stroke volume, namely preload, contractility and afterload. To maintain CO within an adequate range, heart rate and/or stroke volume must respond through adjustment of contractile rate or the amount of blood filling the left ventricle for ejection. Spontaneous electrical pacemaker activity, termed automaticity, normally controls adult heart rate in the sinoatrial (SA) node at a rate between 60 and 100 beats per minute. A decrease in CO produces a rapid, dynamic response in heart rate in an attempt to maintain adequate systemic blood flow.

Heart rate augmentation produces distinct processes that may enhance or exacerbate a decline in myocardial performance. Increased heart rates produce an increased cellular influx of calcium into the sarcoplasmic reticulum resulting in an improved myocardial contractile function. This process is called the *Treppe phenomenon*, and is capable of offsetting the reduction of left ventricular diastolic filling time occurring in tachycardia [2,3]. As heart rates increase beyond those typical of SA node-mediated responses, diastolic filling time declines sharply; combined with a rise in metabolic substrate production, contractile function is sharply diminished, producing a decrease in CO.

Preload. The term preload is defined as the volume of blood distending the left ventricle at the end of diastole (end-diastolic volume—EDVol). Since EDVol exerts a pressure within the ventricular system, the term end-diastolic pressure (EDP) is also used to reflect preload [1–4]. Preload is determined by the following three factors:

1 total blood volume/venous return;
2 vascular resistance/capacitance; and
3 myocardial contractility.

Heart rate influences left ventricular preload as EDVol is dependent on the time devoted to diastolic filling which shortens in proportion to increases in heart rate. For example, at a heart rate of 70 beats/min, diastole represents about 60% of the cardiac cycle, resulting in optimal end-diastolic filling, but at a heart rate of 200 beats/min, diastole comprises only 35% of the cardiac cycle [3].

Contractility. Left ventricular contractility or pump strength is the terminology used to reflect myocardial muscle shortening and the development of muscle tension. A number of extrinsic factors contribute to myocardial contractility, termed *positive inotropic agents.* These substances include:

1 intrinsic circulating sympathetic amines and other synthetic inotropes;
2 thyroid hormone; and
3 minerals such as calcium and magnesium.

The *Frank–Starling law* [5,6] (also called the length–tension relationship) describes the relationship between preload and resulting contractile force, relating muscle fiber lengthening to the development of tension. Simply stated, optimal myocardial tension is the product of optimal muscle fiber lengthening; lengthening of left ventricular muscle fibers by EDV is directly proportionate to the amount of tension and subsequent contractile force that is produced during systole. Figure 4.3 illustrates the relationship

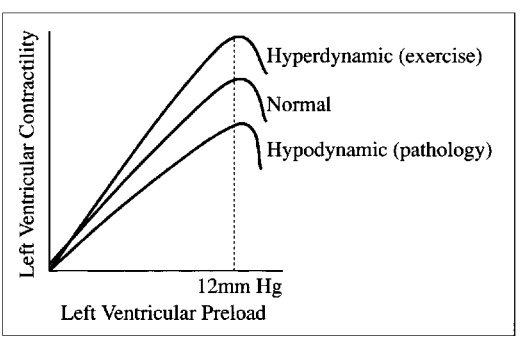

Figure 4.3 Relationship between preload and contractility. Note myocardial stretch and resulting contractile force in response to preload pressure.

between preload (muscle lengthening) and myocardial contractility. The normal adult left ventricle responds optimally to EDV between 10 and 12 mmHg, producing a corresponding myocardial fiber length of 2.2 μm [3]; pressures exceeding this are associated with a decrease in the interdigitation of actin and myosin filaments, with a reduction in contractile site activation (descending limb of the Frank–Starling curve).

Afterload. Left ventricular afterload refers to wall tension, and reflects the SVR in the aorta that the ventricle must overcome to eject its volume [3,4]. An important distinction must be made between left ventricular afterload and SVR. Afterload itself cannot be measured directly in clinical practice, but what is known is that ventricular wall tension must rise to a level that will allow forward flow through the resistance of the systemic arterial bed beyond the aortic valve. During early systole, this is accomplished by building wall tension with the aortic valve in a closed position in phase 1 of ventricular systole (isovolumetric contraction); this phase represents the point of the cardiac cycle responsible for more than 50% of myocardial oxygen consumption [1,3]. Once wall tension has been optimized and intraventricular pressure significantly rises, the aortic valve opens, enabling forward thrust of blood into the arterial system. Because SVR represents the amount of resistance that the ventricle must build tension against to enable forward flow, SVR serves as a calculated clinical measure that may be used to reflect left ventricular afterload.

Similar to left ventricular afterload, right ventricular afterload is reflected in the calculated measurement of pulmonary vascular resistance (PVR) [3]. Because the pulmonary vasculature is normally a low-resistance system, right ventricular afterload is usually an insignificant contributor to overall myocardial oxygen consumption.

Factors capable of influencing left ventricular afterload include a variety of systemic conditions including body temperature, hypertension, altered aortic distensibility due to atherosclerotic changes, blood viscosity and alterations in vascular resistance due to bacterial endotoxins and severe immune system responses with significant histamine release. Intrinsic cardiac contributors to afterload include structural alterations such as aortic valve stenosis.

Contributors to right ventricular afterload include entities that produce pulmonary hypertension such as chronic obstructive pulmonary disease, pulmonary embolism and use of positive end-expiratory pressure mechanical ventilation settings. Similar to the left heart, an intrinsic cardiac contributor would be pulmonic valve stenosis.

Arterial blood pressure (ABP) is derived from CO and SVR, and intrinsic mechanisms exist to maintain ABP when CO or SVR become altered. Under most circumstances CO and SVR have an inverse relationship. When cardiac output falls due to reduced contractility or preload values, SVR will increase in an attempt to maintain ABP within normal parameters. Because of this, use of ABP for rapid detection of clinical changes often provides poor clinical information, as blood pressure may appear normal in the face of early clinical deterioration. When SVR increases due to a primary reduction of contractility, compromised left ventricular function precludes an ability to overcome the increased resistance, stifling forward flow even further. In this scenario, use of medications or devices that reduce SVR may be beneficial, such as sodium nitroprusside in combination with a positive inotropic agent and/or intra-aortic balloon counterpulsation [7]. Similarly, when CO falls due to significant blood loss (alterations in preload), SVR will again increase to maintain ABP; once circulating blood volume is replaced, SVR returns to normal. In sepsis or meningitis, SVR is often significantly reduced, resulting in low vascular resistance to left ventricular outflow. The ventricle compensates with increases in CO often above normal values, and transcranial Doppler often shows a general velocity increase above normal values with low-resistance waveforms. When preload is adequately maintained in this scenario, use of pressors to maintain ABP can often be entirely avoided.

Calculation of SVR requires measurement of the following variables: mean arterial pressure (MAP), right atrial pressure (RAP or CVP) and CO. The formula for SVR is:

$$SVR = (MAP - RAP) \times 80 \div CO.$$

Calculation of PVR requires measurement of pulmonary artery mean pressure (PAM), pulmonary artery wedge pressure (PAWP) and CO. The formula for PVR is:

$$PVR = (PAM - PAWP) \times 80 \div CO.$$

Table 4.1 Reflexes influencing vasomotor response.

Reflex	*Anatomic location*	*Cardiac/vasomotor response*
Bainbridge reflex	Right atrium of the heart; accelerator receptors	Tachycardia initiated by increased right atrial pressure with receptor distension
Baroreceptor reflex (Marey's law of the heart)	Aortic arch and carotid sinus	Increased arterial pressure stimulates vagal fibers which produces bradycardia and reduced ventricular contractility
Chemoreceptors	Aortic arch and carotid bodies	Hypoxia, hypercapnia and/or acidosis stimulate receptors to produce tachycardia

Neuroendocrine mediation of cardiac output

The autonomic nervous system plays an important role in augmenting heart contractility, preload and afterload. Vagus nerve fibers innervate the SA node and atrioventricular (AV) conduction tissue. When stimulated, parasympathetic fibers result in reduced SA node automaticity, prolongation of impulse conduction time through the AV node and decreased ventricular contractile force [1,2].

Sympathetic nerve fibers are prevalent throughout the myocardium and the arterial vascular system. Sympathetic *β_1-receptors* within the myocardium increase the rate of firing of the SA node, conduction velocity and myocardial contractility when stimulated by intrinsic sympathetic amines such as norepinephrine, epinephrine and dopamine [1,2]. Stimulation of β_1-receptors may produce an increase in CO up to 20–30% from baseline, primarily as a result of inotropic augmentation [2]. Sympathetic *β_2-receptors* within vascular smooth muscle produce vasodilatation when stimulated by selective adrenergic agents, reducing LV afterload to enhance forward flow. Stimulation of *α_1-receptors*, also located in vascular smooth muscle, results in vasoconstriction [1,2].

Within the central nervous system, the pons and the ventrolateral medulla both play a role in cardiac and vasomotor function. Stimulation of pressor regions within the brainstem produces an increase in heart rate, contractility and blood pressure. When the depressor regions are stimulated, profound bradycardia associated with a reduction in myocardial contractility and blood pressure may result. Cortical, limbic and hypothalamic-mediated responses to environmental stimuli may also have a profound influence on myocardial performance [1,2]. Table 4.1 identifies a number of *reflexes that influence vasomotor response.* Cardiac and respiratory reflexes are very closely related; a decrease in pH associated with an increase in P_aCO_2 results in vasodilatation, while an increase in pH with a decrease in P_aCO_2 typically produces some degree of vasoconstriction.

Vasodilatation leads to:

1 decrease in peripheral resistance;
2 decrease in flow pulsatility; and
3 increase in blood flow velocity.

Vasoconstriction leads to:

1 increase in peripheral resistance;
2 increase in flow pulsatility; and
3 decrease in blood flow velocity.

Hormones may also contribute to alterations in myocardial performance and circulatory mechanisms. Antidiuretic hormone (ADH or vasopressin) may be released from the posterior pituitary in response to decreases in CO associated with a presumed need for volume. In addition to promoting water reabsorption, ADH also possesses potent vasoconstrictive properties. Atrial natriuretic factor (ANF), which possesses both salt- and water-excreting properties, may also be released in response to significant atrial muscle fiber stretch associated with hypervolemia [1,2]. Despite its salt- and water-wasting properties, clinical studies have demonstrated the main benefit of ANF release to be associated with arterial and venous vasodilatation, which foster reduction of preload and afterload [8,9]. Aldosterone release is also stimulated by a decrease in CO promoting increased renal tubule reabsorption of sodium and water [1,2].

Microcirculatory flow mechanisms are also mediated by neural control systems. Local blood flow is regulated through arteriole resistance vessels and

mechanisms that augment changes in venous capacitance and return. Vasodilating and vasoconstricting prostaglandins also play a role in the augmentation of peripheral circulation, as do endothelial factors such as nitric oxide (NO) which may enhance vasodilatation in response to a number of triggers [10].

Bedside assessment of systemic hemodynamics

Assessment of systemic hemodynamic parameters necessitates measurement and interpretation of both non-invasive data from the clinical examination and, when possible, invasive data collected from monitoring technology. For the purposes of this chapter, data specific to those affecting stroke volume and systemic tissue oxygenation will be reviewed; combining these data with those obtained from ECG monitoring and the general physical examination provides an overall picture of systemic hemodynamic status which may be used to direct hemodynamic augmentation.

A common but inappropriate practice of accepting values from the numeric display of a bedside monitor, instead of those determined by reading a static graph paper tracing, often places the clinician at risk of misinterpretation of hemodynamic data [3,4,11,12]. All bedside monitor values must be verified against those produced on a graphic strip, as bedside monitors do not always provide accurate waveform values, despite their use of respiratory algorithms. This is especially true when respiratory artifacts and/or abnormal waveform morphology related to intrinsic pathology are present. If the clinician is able to simultaneously freeze the ECG and hemodynamic waveform on the bedside monitor, use of a cursor to accurately determine waveform values may be substituted for a paper strip [11,12].

As mentioned earlier, stroke volume is derived from three primary contributors, preload, contractility and afterload. Measures of preload consist of both non-invasive data as well as those obtained through central monitoring systems. Perhaps one of the most undervalued measures of preload and one that is generally simplistic, is determination of *jugular venous pressure* (JVP). Because of the proximal location of the right internal jugular vein, measurement of pressures there directly reflect right atrial pressure [3]. To measure JVP, follow these steps:

- Position the patient at a 45° angle with the head and neck in a neutral aligned position.
- Compress the jugular vein at the point just above the clavicle; release pressure and observe filling of the venous column—if it fills from the top, measurement of JVP will not reliably estimate cardiac preload.
- Identify the following reference points: the top of the fluid column (the meniscus)—reference point; and the angle of Louis (sternal angle)—zero point.
- Measure the vertical distance between the angle of Louis and the meniscus; because the sternal angle lies 5 cm above the right atrium, add the number of cm of JVP elevation above the angle of Louis to 5 to calculate an estimation of CVP.

Additional assessments related to JVP inspection include noting the presence of *Kussmaul's sign* and assessment of hepatojugular reflex. To assess presence of Kussmaul's sign add the following steps to the procedure listed above:

- Have the patient take a deep breath.
- Observe movement of the meniscus (or the top filling point of the jugular vein) on inspiration.
- Determine a decrease or increase in the filling level.

Normally on inspiration, intrathoracic pressure decreases, resulting in a decrease in the meniscus level. Kussmaul's sign reflects a pathologic increase in meniscus level on inspiration related to decreased cardiac compliance from processes such as congestive failure or cardiac tamponade [3]. Assessment of *hepatojugular reflex* involves the addition of the following steps to the procedure:

- Ask the patient to breathe normally.
- Apply pressure to the right upper quadrant of the abdomen for 10 s; note a rise in JVP filling level and assess whether the rise is sustained throughout the application of pressure, or is transient despite pressure application with a return to prepressure levels.

Normal findings should include a transient rise of JVP with a return to normal level while pressure continues to be applied. A sustained elevation of JVP throughout the pressure application process signifies a significant increase in LV preload, except in the presence of RV infarction [3]. Lastly, while JVP reflects preload, the clinician assessing JVP data must consider the dynamic interplay between preload, contractility and afterload to correctly determine the meaning of preload elevations.

Invasive hemodynamic monitoring modalities are often useful in the assessment of preload and other variables associated with stroke volume. Normal values and formulas for *invasive cardiac indices* are listed

Table 4.2 Invasive cardiac parameters: formulas and normal values.

Adapted from Whalen DA, Kelleher RM. Cardiovascular patient assessment. In: Kinney MR, Dunbar SB, Brooks-Brunn JA, Molter N, Vitello-Cicciu JM, eds. *AACN Clinical Reference for Critical Care Nursing*, St. Louis: Mosby, 277–318.

in Table 4.2. Insertion of a CVP line or pulmonary artery (PA) catheter provides the clinician with an improved ability to directly measure preload parameters in an accurate manner. Because invasive catheters require use of transducers to convert mechanical pressures to numeric data, it is important to make note of *principles associated with transducer maintenance and monitoring.*

1 A fluid interface between catheter and transducer coupled with non-distensible, stiff tubing must be maintained to promote accurate transmission of pressure waves; clinicians must ensure systems are bubble free and supported by pressure that prevents a back-up of blood into the line. Secondly, the phlebostatic axis, measured at the level of the tricuspid valve, provides the only known place in the body where central pressures are not influenced by hydrostatic pressure. Because of this, transducer systems used to measure pressures within the heart and arterial system must be leveled and zeroed to atmospheric pressure at the phlebostatic axis to ensure accuracy in measurement. The phlebostatic axis is located at the 4th intercostal space or at the point of half the anterior/posterior diameter of the chest, when the patient is placed in a supine position between 0 and 60° head of bed elevation [3].

2 An important point must be emphasized here due to a practice often observed in neuroscience units of moving the arterial pressure transducer to the level of the foramen of Monro. This practice originated as a method that aimed to approximate MAP within the brain for use in the calculation of cerebral perfusion pressure (CPP); it is not based on physiologically sound principles of hemodynamic monitoring given the actual location of the catheter in the peripheral arterial bed, coupled with the complex hemodynamics of the intracranial arterial system which can in no way be measured by a simple adjustment of transducer height. Placement of the transducer zero point at any level other than the phlebostatic axis will result in only one finding: distorted pressure values that are not accurate and meaningful in the course of clinical management.

3 To ensure accuracy in invasive hemodynamic measurements, the transducer/monitoring system's dynamic response should be tested. Dynamic response

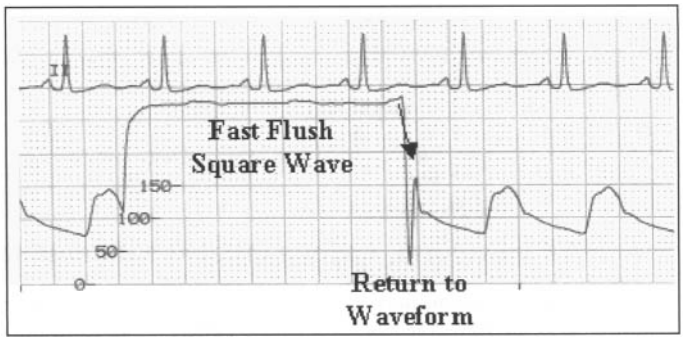

Figure 4.4 Square wave test with optimal response. Steps to assess square wave: 1, fast-flush system and release; 2, count number of small boxes occurring before return of waveform; 3, divide number of small boxes into paper speed (25 mm/s). Note: One small box before return of waveform; 25/1 = 25 Hz. Ideal frequency response = ≥ 25 Hz.

is the ability of the system to reproduce accurately variations in pressure occurring within the vasculature. It is tested through performance of a fast flush and assessed by the square wave produced. Figure 4.4 provides an example of the correct response to fast flushing of the catheter. Testing of dynamic response prevents misinterpretation of data obtained from invasive catheters in that overdampened waveforms will underestimate systolic pressures and overestimate diastolic pressures, while spiked, underdampened waveforms typically overestimate systolic pressures [11,12].

4 Interpretation of invasive hemodynamic data should be performed with caution. Measurements of pressures within the thoracic cavity are subject to the influence of respiration and pressure changes occurring with the respiratory cycle. The point of end-expiration provides the only time during the respiratory cycle that is minimally influenced by changes in intrathoracic pressure [3,4,11,12], making measurement at this point critical to the determination of accurate data. In patients breathing without mechanical ventilation, end-expiration is generally the high point on a waveform just before the inspiratory dip as illustrated in Figure 4.5. But, in patients receiving positive pressure mechanical ventilation, end-expiration may be measured at different points on a waveform depending on the ventilator settings and the presence or absence of spontaneous respiratory effort (Figure 4.6). Use of simultaneous end-tidal CO_2 monitoring (capnography or partial end tidal CO_2, $PETCO_2$) assists with rapid and accurate detection of end-expiration in patients receiving mechanical ventilation [12].

Direct measurement of CVP can be performed through placement of a catheter into the right atrium,

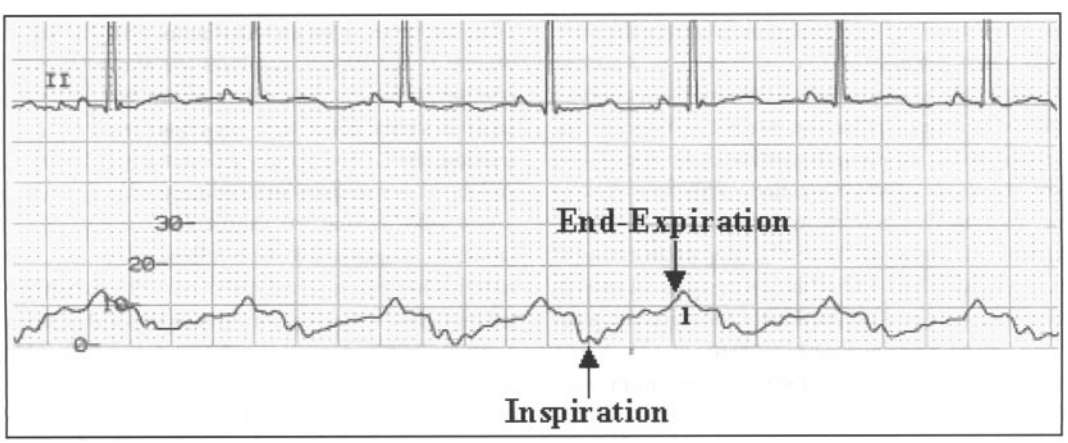

Figure 4.5 End-expiratory measurement in a patient spontaneously breathing without mechanical ventilation (central venous pressure (CVP) waveform). Key for CVP waveform: 1, A-wave at end-expiration. Note: Measurement of CVP is performed by taking the mean of the A-wave; CVP = 10 mmHg; measurement taken at incorrect point on waveform would have underestimated CVP at 5–7 mmHg.

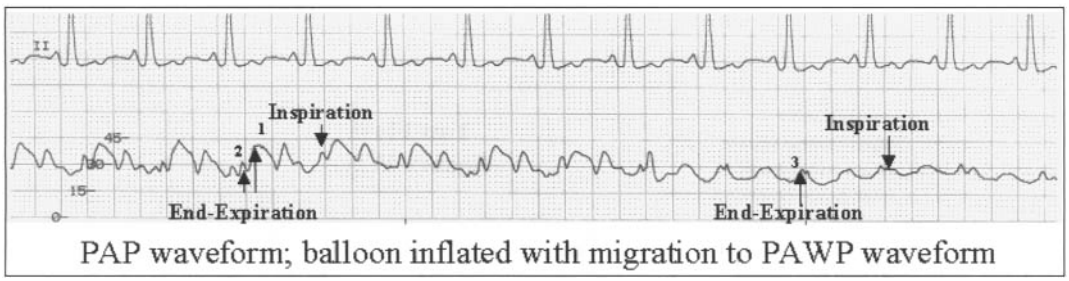

Figure 4.6 End-expiratory measurement in a patient on positive pressure mechanical ventilation (pulmonary artery pressure (PAP) and pulmonary artery wedge pressure (PAWP) waveforms). Key for PAP waveform (left): 1, peak systolic pressure (PSP); 2, end-diastolic pressure (EDP). Note: Measurement of PAP is performed by taking PSP over EDP at end-expiration; PAP = 42/28 mmHg; measurement during inspiration would have overestimated pressures at 45/32 mmHg. Key for PAWP waveform (right): 3, A-wave. Note: Measurement of PAWP is performed by taking the mean of the A-wave; PAWP = 22 mmHg; measurement during inspiration would have overestimated pressure at 28 mmHg.

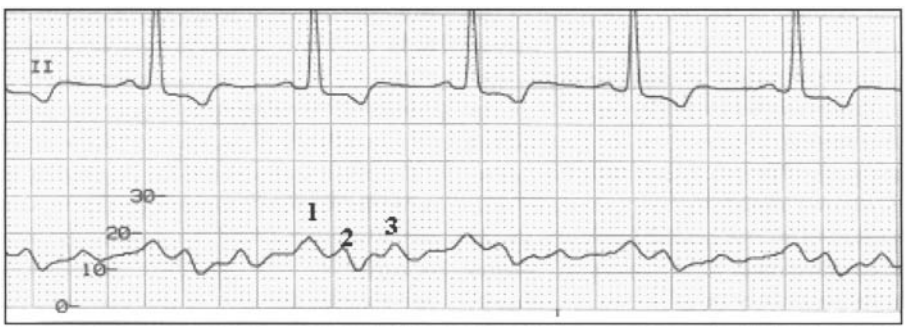

Figure 4.7 Central venous pressure (CVP) waveform. Key for CVP waveform: 1, A-wave; 2, C-wave; 3, V-wave. Note: Measurement of CVP is performed by taking the mean of the A-wave; CVP = 16 mmHg.

or by insertion of a pulmonary artery (PA) catheter with measurement of central pressures from the proximal port. Normal CVP varies from 2 to 6 mmHg; Figure 4.7 illustrates a right atrial waveform obtained by CVP catheter. Note the distinct waveforms that reflect specific events in the cardiac cycle. The A-wave reflects right atrial contraction, while the C-wave occurs with closure of the tricuspid valve, and the V-wave reflects atrial filling and bulging of the tricuspid valve during right ventricular contraction. Normally, the A-wave is the most prominent wave present, while the C-wave may be absent entirely [11,12]. A very large V-wave is often suggestive of tricuspid valve regurgitation and can be further assessed by auscultation of a systolic ejection murmur at the 4th intercostal space left sternal border.

Pulmonary artery wedge pressure (PAWP) is another measurement of preload, and provides a more accurate picture of LV end-diastolic volume than measures taken within the right atrium (Figure 4.8). The waves present in the PAWP waveform are of similar morphology to those in the CVP waveform, but reflect left heart processes; the A-wave represents left atrial contraction, the C-wave occurs with mitral valve closure, and the V-wave reflects atrial filling and bulging of the mitral valve during left ventricular systole [11,12]. Similarly, a giant V-wave is often associated with mitral valve regurgitation and is typically accompanied by a systolic ejection murmur at the cardiac apex. Normal PAWP pressure is between 4 and 12 mmHg [3]. The presence of giant V-waves often causes clinicians to misinterpret left atrial waveforms as pulmonary artery waveforms, but can be easily identified with ECG correlates as a pathologic waveform.

Figure 4.7 identifies the correct technique for *measurement of right atrial pressures*, which consists of

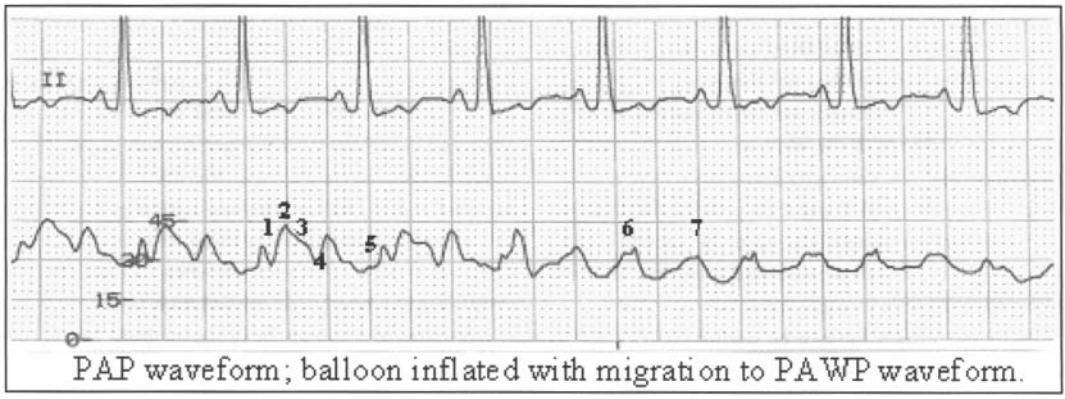

Figure 4.8 Pulmonary artery pressure waveform (PAP) and pulmonary artery wedge pressure (PAWP) waveform. Key for PAP waveform (left): 1, isovolumetric contraction; 2, peak systolic pressure (PSP); 3, reduced systolic ejection; 4, dicrotic notch; 5, end-diastolic pressure (EDP). Note: Measurement of PAP is performed by taking PSP over EDP; PAP = 42/29 mmHg. Key for PAWP waveform (right): 6, A-wave; 7, V-wave. Note: Measurement of PAWP is performed by taking the mean of the A-wave; PAWP = 27 mmHg.

averaging the peak and lower values of the A-wave. Using the ECG for correlation, the A-wave is found after the P-wave, while the V-wave occurs after the T-wave, but before the P-wave on the ECG; to easily find the V-wave on a right atrial waveform, limit assessment to the components of the waveform occurring within the TP interval on the ECG. A similar process is used to measure left atrial waveforms obtained by PA catheter in the wedge position. Because of an increase in electrical–mechanical delay, the A-wave on a PAWP waveform is usually found at or just after the QRS complex, while the V-wave occurs in close proximity to the P-wave on the ECG (Figure 4.8). When pathologic conditions are present that distort or eliminate entirely the production of an A-wave (e.g. tricuspid or mitral stenosis; dysrhythmias producing loss of atrioventricular synchrony, including pacemaker generated rhythms; atrial fibrillation), right and left atrial pressures may be read at the Z-point, which correlates with the end of the QRS complex on the ECG [11,12].

Pulmonary artery end-diastolic pressure (PAEDP) may also be used as a measure of preload (Figure 4.8). Because the volume of blood at the end of diastole in the pulmonary artery represents the volume that will ultimately fill the left heart, a relationship between PAEDP and PAWP exists. In the absence of pulmonary hypertension, there should be no more than a 6 mmHg difference between PAEDP and PAWP, with the PAEDP running only slightly higher than wedge [3,4]. Because of this constant relationship, use of the PAEDP as a substitute for PAWP is standard practice in many critical care units, lengthening the life of the catheter's balloon and preventing the need for catheter replacement due to balloon rupture. Normal PAEDP pressures run between 5 and 15 mmHg [3]; the waveform is read just before the systolic upstroke at the end of diastole when ventricular filling is complete.

As stated earlier, preload is affected by not only total blood volume, but also the pumping ability of the heart. Often with significant deterioration in myocardial contractility, preload may become elevated without the addition of fluid to circulatory volume. Hence, preload alterations may reflect indirectly poor myocardial contractility. Likewise, significant LV or RV afterload may directly alter preload values secondary to an inability of the ventricle to overcome high resistance to forward flow; preload elevates as flow is stifled.

Measurement of contractility as a contributor to stroke volume has been debated by clinicians for many years. Use of calculated variables such as ejection fraction (EF) measurements are often considered helpful by clinicians, yet others criticize these values as indirect calculated measures of contractility. Normal values for LVEF and RVEF are 60–75% and 45–50%, respectively. The bottom line is that no measure exists today to directly determine contractile force in real time. Because of this, some practitioners prefer to simply infer contractility from variables that can be measured directly such as CO or CI and preload parameters [3,4].

Measurement of afterload also relies on use of calculated variables derived from an equation which is an algebraic reformulation of Ohm's law [3]. Because ventricular afterload may not be measured directly, calculated SVR and PVR serve as a reflection of the resistance that the ventricles must overcome to eject their volume. Both SVR and PVR provide the clinician with an estimate of just how hard the ventricle must work to generate wall tension and pressures that will foster forward flow through the semilunar valves.

Increases in SVR have to be examined critically to determine their relationship with other hemodynamic parameters. Because an increase in SVR will occur in response to a decrease in CO/SV, the clinician must critically analyse the precise cause of SVR alterations to determine the necessary clinical action. Similarly, augmentation of SVR with pressor therapy to drive up perfusion pressures must be cautiously undertaken; the effect of significant LV afterload on CO and preload cannot be underestimated, especially in the face of occult or known cardiac dysfunction. Significantly low SVRs are often associated with conditions such as sepsis or systemic immune response syndrome (SIRS) that trigger events that produce widespread vasodilatory processes. Normally SVR values are 900–1600 dynes/s/cm^{-5} [3,4].

Alterations in PVR may occur in relation to therapies or pathologic conditions that produce pulmonary hypertension. The normal range for PVR is 155–255 dynes/s/cm^{-5} due to the normally low-pressure pulmonary system [3,4].

Perhaps the most useful parameter to measure in the patient requiring invasive hemodynamic monitoring is continuous mixed *venous oxygen saturation*, or S_vO_2. Data relative to body needs in oxygen supply and demand are provided by PA catheters capable of measuring S_vO_2. These data are so important that one could argue the logic behind only placing PA catheters capable of providing these data continuously. Oxygen saturation of hemoglobin in the pulmonary artery is presented by digital display; because the pulmonary artery represents the terminal point before the blood can be reoxygenated, measurement of oxygen saturation provides information on tissue uptake or the oxygen extraction demands of the body [3,4,11,12].

Four variables are essential to the assessment of S_vO_2:

1 cardiac output (CO);
2 hemoglobin;
3 arterial oxygen saturation; and
4 tissue oxygen consumption.

Delivery of oxygen, or oxygen supply, is dependent on CO, hemoglobin and arterial oxygen saturation, whereas S_vO_2 reflects tissue oxygen consumption. When tissue oxygen needs increase, the first compensatory measure exerted by the body is an attempt to increase CO. A second compensatory measure is an increase in tissue extraction, which occurs when CO changes are insufficient to meet tissue oxygenation needs [11].

Decreases in S_vO_2 may be brought about by a number of clinical phenomena that may insult oxygenation and cardiac performance in an occult manner. Chief among these are patient positioning, movement and activities of daily living which may challenge an already compromised cardiopulmonary system [3]. Real-time measurement of S_vO_2 enables assessment of the effect of these phenomena on tissue oxygenation supply and demand, promoting improved patient outcomes. Measurement of S_vO_2 along with other hemodynamic variables enables clinicians to fully gauge the need for specific therapies to augment the oxygen supply and demand equation. Normal S_vO_2 is 60–80%; significant changes in S_vO_2 of 5–10% or more for greater than 5 min warrant close clinical investigation to ensure optimal tissue oxygenation [3,11].

The use of *non-invasive CO monitoring* remains controversial. Thoracic electrical bioimpedance is one example of a measure of CO obtained by placement of external electrodes. The electrical impedance change in blood flow through the thoracic aorta is analysed producing an estimate of SV; the device multiplies the SV by heart rate to derive CO; EF can also be calculated [3]. Unfortunately, only a 'fair' to 'satisfactory' relationship has been measured between bioimpedance CO values and those obtained through PA catheter [13]; limitations include the potential for incorrect electrode placement, overestimation of CO during vasopressor therapy, aortic insufficiency and hypovolemia, and underestimation of CO during sepsis or hypertensive episodes [3]. Given these limitations, the usefulness of bioimpedance CO measures in neuroscience patient management is doubtful at best.

Relationship between systemic and intracranial hemodynamics

The brain is metabolically dependent on a continuous supply of oxygen and glucose which are delivered at a

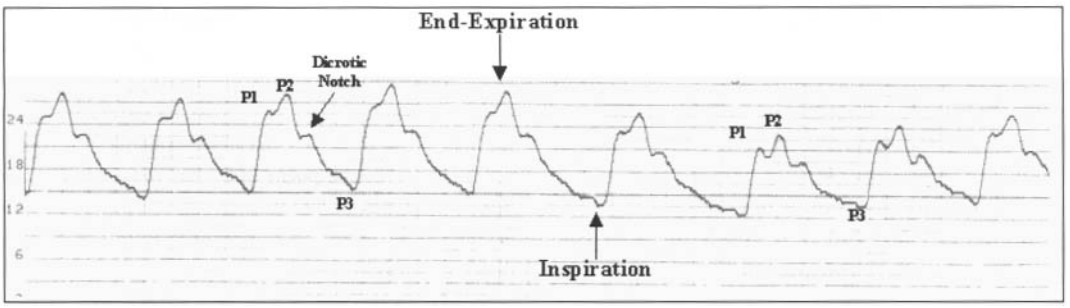

Figure 4.9 Intracranial pressure (ICP) waveform. ICP waveform with respiratory fluctuation; note drop in pressure due to decreased cardiac output during inspiratory phase. Unlike thoracic pressures which fluctuate artificially with intrathoracic respiratory pressure changes, measurement at end-expiration is not used in the calculation of ICP, as both inspiratory and expiratory pressures reflect actual pressures generated within the cranium that vary with fluctuations in cardiac output. Key to ICP waveform: P1, peak systolic pressure; P2, tidal wave; P3, end-diastolic pressure. Note: ICP is measured at the point of P2; inspiratory and expiratory P2 measurements are averaged; ICP = 26 mmHg.

rate of approximately 750 mL/min or 15% of the total CO. Resting *cerebral blood flow* (CBF) is relatively stable despite changes in CO, body position and arterial blood pressure; it amounts to approximately 50 mL per 100 g of brain tissue per minute [1]. Focal changes in CBF correlate with metabolic demands, in that activity in specific brain regions is accompanied by a focal increase in blood flow secondary to autoregulation. When autoregulatory processes are functional, the brain is capable of producing varying levels of arterial perfusion pressures across a wide range of systemic arterial pressures. When autoregulation is dysfunctional, brain perfusion pressures become dependent on systemic hemodynamic flow parameters.

The *Monro–Kellie hypothesis*, which was originally postulated in the 1800s [14], describes the relationship of the skull and its contents to pressure dynamics. Intracranial contents (brain tissue, blood and cerebrospinal fluid) interact dynamically and exert a constant pressure with the skull by their volume; the skull itself is incapable of expanding in size, so that changes in the volume of any one of the intracranial contents requires a compensatory change in the volume of another. Under normal circumstances, the dynamic compliant interaction between the intracranial contents ensures constancy of intracranial pressures (ICPs) within the normal parameters of 0–15 mmHg [15], making the brain a low-pressure, low-resistance system. When ICP is elevated, the brain's resistance to flow is increased significantly, making critically important the maintenance of optimal systemic hemodynamic performance to ensure brain tissue perfusion.

Direct measurement of *intracranial pressure* (ICP) can be performed using a variety of systems, the most reliable of which is the intraventricular catheter. Because the ventricles are fluid-filled reservoirs, transmission of intraventricular pressure waveforms to bedside monitoring systems provides an ability to view in real time the relationship of systemic hemodynamic flow parameters to intracranial pressure dynamics.

Figure 4.9 represents an intraventricular pressure waveform in a patient with normal intracranial compliance. Note the similarities in waveform morphology to an arterial waveform; this effect is produced by arterial pulsations transmitted through cerebrospinal fluid (CSF) that are subsequently superimposed on the ICP waveform. In particular, note the components reflective of the three phases of ventricular systole, namely isovolumetric contraction, rapid ventricular ejection and reduced ventricular ejection, as well as ventricular diastole. Discrete *pressure points* (P_1, P_2, P_3) define specific points on the ICP waveform that can be related to the cardiac cycle.

P_1 is referred to as the percussion wave and relates to the point of peak systolic pressure.

P_2 is called the tidal wave and relates to the reduced systolic ejection phase of the cardiac cycle on an arterial waveform, terminating in the dicrotic notch. P_2 is used to reflect intracranial arterial autoregulation of flow in that a progressive upward movement of P_2 towards P_1, or complete loss of P_2 indicates reduced arterial compliance.

P_3 is initiated immediately following the dicrotic notch on the arterial waveform, which signifies

closure of the aortic valve and the onset of ventricular diastole.

Cerebral perfusion pressure (CPP) is a measure that reflects the difference in arterial in-flow and venous outflow, typically calculated by subtracting mean venous pressure (MVP) from MAP. Calculation of CPP is performed using a modified equation that substitutes ICP for MVP as the chief resistance factor, producing the following equation:

$$CPP = MAP - ICP.$$

Optimal CPP is defined as a pressure greater than or equal to 70 mmHg [15]. Reduction in CPP causes the rate of intracranial arterial vasodilatation to increase logarithmically. Because autoregulation is an energy-dependent response, sustained periods of oxygen deprivation will devastate the response, making perfusion solely dependent on the balance between MAP and ICP.

Use of the ICP waveform to reflect arterial blood flow through the intracranial circuit requires correlation of the events of the cardiac cycle depicted on the ICP waveform with changes in the waveform morphology. The reduced ventricular ejection phase correlates with the point on the ICP waveform associated with the P_2 waveform; forward flow during this less dynamic phase of the cardiac cycle is normally augmented by changes in arterial compliance secondary to autoregulation. P_2 likely reflects an autoregulatory 'bounce' associated with varied perfusion pressures in highly elastic arterial vessels. But, in the case of atherosclerosis, chronic hypertension or increasing ICP, P_2 may be lost or approximate P_1 as the ability for elastic recoil or expansion with varying flow rates may be significantly reduced or lost entirely. As ICP continues to increase, the passive intracranial blood flow occurring during ventricular diastole meets progressively higher degrees of resistance to flow, resulting in loss of a discrete diastolic flow pattern. The overall result of significantly elevated ICP pressures is a flattening of the ICP waveform accompanied by distortion or loss of discrete pressure waves.

As mentioned previously, the hemodynamic pressure measurements originating within the thoracic cavity are subject to the influence of inspiratory and expiratory changes and must be measured at end-expiration to ensure accuracy. While inspiratory and expiratory changes often influence the pattern of ICP waveforms, these changes reflect real pressure effects and should be taken into consideration when determining pressure values. Because of its significance as a marker of intracranial arterial compliance, measurement of ICP at the point of P_2 has most commonly been advocated, although many practitioners simply calculate a mean pressure using peak systolic and end-diastolic pressure points.

Similar to the use of S_vO_2 as a marker of systemic tissue oxygenation, neuroscience practitioners use *jugular venous oxygen saturation* ($S_{jv}O_2$) to reflect global brain tissue oxygen consumption. Normal $S_{jv}O_2$ is between 55 and 70% [16]. In the absence of a sudden increase in the fraction of inspired oxygen concentration or anemia, $S_{jv}O_2$ levels greater than 75% reflect a state of hyperemia, although discrete areas of ischemia may still be present within the brain. This is a significant limitation of $S_{jv}O_2$ monitoring, in that focal ischemic findings tend to be blunted by global oxygenation measures. When $S_{jv}O_2$ levels are less than 55%, a state of oligemia is present.

An advantage to the use of $S_{jv}O_2$ is the ability to calculate additional intracranial oxygenation values, including cerebral metabolic rate ($CMRO_2$) and global cerebral oxygen extraction ratio (O_2ER). Table 4.3 provides the formulas used for oxygenation calculations that may be used to fine-tune systemic flow parameters to enhance brain tissue oxygenation. Figure 4.10 provides an example of systemic augmentation measures that may be used to enhance brain tissue oxygenation based on $S_{jv}O_2$ and ICP data.

The transcranial Doppler (TCD) waveform should be compared to the ICP values at a closed drainage position as well as to the morphology of the ICP waveform. Furthermore, TCD waveforms and velocity data should be reviewed in relation to systemic and intracranial hemodynamic parameters. TCD velocities are not the measurement of CBF, and therefore TCD can provide only indirect evidence as to whether any given therapy is successfully enhancing brain tissue perfusion. Depending on the underlying pathology (e.g. ischemic vessel thrombosis, subarachnoid hemorrhage with vasospasm, or increased ICP secondary to traumatic brain injury or intracranial hemorrhage), TCD waveform analysis in combination with assessment of intracranial and systemic hemodynamics can provide important information related to

Table 4.3 Cerebral oxygenation calculations.

Value	*Formula*
Arterial oxygen content saturation (C_aO_2)	$1.34 \times Hgb \times S_aO_2 + 0.0031 \times P_aO_2$
Jugular venous oxygen content saturation ($C_{jv}O_2$)	$1.34 \times Hgb \times S_{jv}O_2 + 0.0031 \times P_{jv}O_2$
Arteriovenous jugular oxygen content difference ($AV_{jD}O_2$) 3.5–8.1 mL/dL	$C_aO_2 - C_{jv}O_2$
Cerebral extraction of oxygen (C_EO_2) 24–42%	$S_aO_2 - S_{jv}O_2$
Cerebral metabolic rate ($CMRO_2$)	$\frac{CBF \times AV_{jD}O_2}{100}$
Global cerebral oxygen extraction ratio (O_2ER)	$S_aO_2 - S_{jv}O_2/S_aO_2$ *Alternative formula:* $\frac{C_EO_2}{S_aO_2}$

Hgb, hemoglobin; S_aO_2, arterial oxygen saturation; P_aO_2, partial pressure of arterial oxygen; $S_{jv}O_2$, jugular venous oxygen saturation; $P_{jv}O_2$, partial pressure of jugular venous oxygen; CBF, cerebral blood flow.

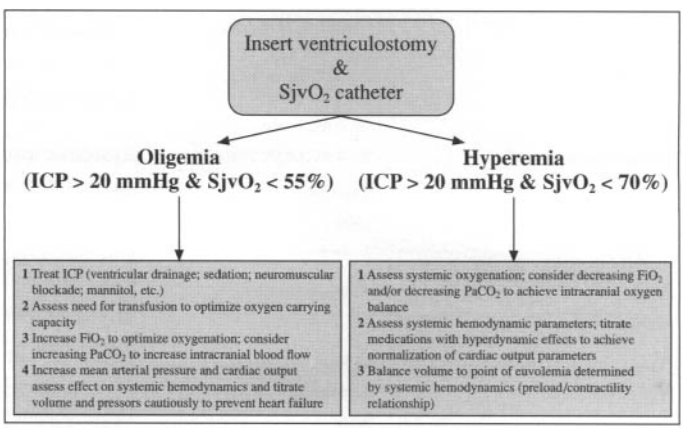

Figure 4.10 Algorithm for oxygenation and intracranial pressure (ICP) management.

safe augmentation of cardiac performance and arterial pressure.

A number of therapeutic modalities may be used to augment brain tissue perfusion, including α_1- and/or $\beta_{1,2}$-adrenergic agents such as phenylephrine, dopamine and dobutamine, as well as volume infusion, and in special circumstances intra-aortic balloon pump counterpulsation. Prescribed without complete knowledge of cardiac performance limitations and specific intracranial flow needs, these measures may produce significant harm, instead of therapeutic benefit. The case studies below provide an opportunity to utilize both systemic and intracranial hemodynamic data to direct a plan of care aimed at enhancing brain tissue perfusion.

Case studies in hemodynamic augmentation

Case 1

Diagnosis. Traumatic brain injury with diffuse axonal injury (19-year-old male, receiving neuromuscular blockade and sedation on propofol and morphine drips).

TCD waveform analysis. High-resistance waveforms in anterior and posterior circulation, pulsatility index range 1.2–1.6.

Systemic and intracranial hemodynamic parameters and oxygen calculations

Parameter	Data
Core temperature	37.8 °C
Heart rate	78 beats/min
Arterial pressure (MAP)	118/68 (67) mmHg
Cardiac output	3.8 L/min
Cardiac index	2.4 L/min/m^2
Stroke volume	48.7 mL/contraction
Stroke volume index	30.4 mL/m^2/contraction
CVP	5 mmHg
PAP	19/9
PAWP	7 mmHg
SVR	1305 dynes/s/cm^{-5}
SVRI	2067 dynes/s/cm^{-5}
S_vO_2	63%
P_aO_2	97 mmHg
S_aO_2	98%
CO_2	44 mmHg
ICP	35 mmHg
CPP	32 mmHg
$S_{jv}O_2$	45%
$A_{vjD}O_2$	10.8 mL/dL
C_EO_2	53%
O_2ER	54%

Interpretation

Elevated ICP with reduced CPP coupled with increased global brain tissue oxygen consumption due to potentially reduced intracranial blood flow. Systemic hemodynamics reflect preload pressures that are within low normal limits in the face of low CO, suggestive of suboptimal left ventricular stretch; systemic tissue oxygen consumption within low normal limits. Current fractional concentration of oxygen in inspired gas (F_iO_2) on mechanical ventilator of 40%, rate 14 breaths per minute, tidal volume 800 mL. Hemoglobin and hematocrit stable at 12.6 and 36.

Treatment

- Continue ventricular drainage; administer mannitol.
- Optimize preload : contractility relationship; administer crystalloid and consider addition of colloid (Hespan or 5% albumin) infusion to increase PAWP to 12–14 mmHg and re-evaluate hemodynamic parameters, including effect of volume on MAP.
- If MAP remains below 90 mmHg, add dopamine drip at β_1 range and titrate as needed.
- Increase ventilator rate to 18 breaths per minute; reassess CO_2.
- Administer antipyretic agent.

Systemic and intracranial hemodynamic parameters and oxygen calculations

Parameter	Data
Core temperature	36.1 °C
Heart rate	95 beats/min
Arterial pressure (MAP)	155/86 (92) mmHg
Cardiac output	5.2 L/min
Cardiac index	3.3 L/min/m^2
Stroke volume	55 mL/contraction
Stroke volume index	34 mL/m^2/contraction
CVP	11 mmHg
PAP	36/16
PAWP	14 mmHg
SVR	1246 dynes/s/cm^{-5}
SVRI	1963 dynes/s/cm^{-5}
S_vO_2	74%
P_aO_2	99 mmHg
S_aO_2	100%
CO_2	35 mmHg
ICP	24 mmHg
CPP	68 mmHg
$S_{jv}O_2$	57%
$A_{vjD}O_2$	7.9 mL/dL
C_EO_2	43%
O_2ER	43%

$A_{vjD}O_2$ arteriovenous jugular oxygen content.

Continued

Interpretation

ICP responded to mannitol and normalization of CO_2. TCD showed an improvement in flow pulsatility (pulsatility index range 0.9–1.2). Systemic hemodynamics improved with volume infusion and administration of β_1-adrenergic agent; SVR decreased in response to improved volume/contractility ratio. Improved CPP reflected in increased $S_{jv}O_2$.

Treatment

- Maintain PAWP at 14–16 mmHg; monitor urinary volume from mannitol and dopaminergic effects of dopamine infusion and replace intravascular volume as necessary.
- Maintain MAP between 90 and 100 mmHg with volume and dopamine.
- Repeat systemic hemodynamics for significant change in status.

Case 2

Diagnosis. Subarachnoid hemorrhage, postoperative Day 4 (67-year-old female, spontaneously breathing via nasal cannula at 2 L/min; vasospasm treated with hypervolemia and phenylephrine vasopressor therapy).

TCD waveform/velocity analysis. Left middle cerebral artery (MCA) vasospasm, maximum mean flow velocity 190 cm/s, Lindegaard ratio 5.2.

Systemic and intracranial hemodynamic parameters and oxygen calculations

Parameter	Data
Core temperature	36.2 °C
Heart rate	121 beats/min
Arterial pressure (MAP)	120/93 (102) mmHg
Cardiac output	3.4 L/min
Cardiac index	2.0 L/min/m^2
Stroke volume	28 mL/contraction
Stroke volume index	16.5 mL/m^2/contraction
CVP	17 mmHg
PAP	54/22
PAWP	20 mmHg
SVR	2000 dynes/s/cm^{-5}
SVRI	3400 dynes/s/cm^{-5}
S_vO_2	54%
P_aO_2	90 mmHg
S_aO_2	97%
CO_2	32 mmHg
ICP	16 mmHg
CPP	96 mmHg
$S_{jv}O_2$	58%
$A_{vjD}O_2$	7.2 mL/dL
C_EO_2	39%
O_2ER	40%

Interpretation

ICP/CPP are acceptable; $S_{jv}O_2$ reflects global brain tissue oxygen consumption, but not discrete oxygen deficits which may be occurring in the left MCA territory due to vasospasm. Myocardial performance is suboptimal due to high preload pressures with overdistention of the left ventricle and increased SVR due to both reduction of CO and direct vasoconstriction secondary to α_1-adrenergic therapy. Systemic tissue oxygenation reduced due to poor myocardial performance (increased demand with decreased supply), coupled with pulmonary infiltrates due to volume load.

Treatment

- Diuresis with furosemide to reduce PAWP to 12–14 mmHg and re-evaluate systemic hemodynamic parameters, including cardiac tolerance of MAP values between 95 and 100 mmHg.
- Consider F_iO_2 40% by simple face mask until volume overload resolved.

Systemic and intracranial hemodynamic parameters and oxygen calculations

Parameter	Data
Core temperature	36.0 °C
Heart rate	117 beats/min
Arterial pressure (MAP)	126/98 (107) mmHg
Cardiac output	3.7 L/min
Cardiac index	2.2 L/min/m^2
Stroke volume	32 mL/contraction
Stroke volume index	18.8 mL/m^2/contraction
CVP	10 mmHg
PAP	43/17
PAWP	14 mmHg
SVR	2097 dynes/s/cm^{-5}
SVRI	3527 dynes/s/cm^{-5}

Continued overleaf

S_vO_2	57%
P_aO_2	96 mmHg
S_aO_2	98%
CO_2	37 mmHg
ICP	15 mmHg
CPP	92 mmHg
$S_{jv}O_2$	58%
$A_{vjD}O_2$	6.6 mL/dL
C_EO_2	40%
O_2ER	41%

Interpretation

ICP/CPP are acceptable; $S_{jv}O_2$ reflects global brain tissue oxygen consumption, but not discrete oxygen deficits which may be occurring in the left MCA territory due to vasospasm. Repeat TCD examination shows increase in the mean flow velocity (MFV = 205 cm/s), with the Lindegaard ratio of 5.4. Myocardial performance remains suboptimal despite reduction in preload measures; contractility is unable to overcome high SVR due to a combination of low cardiac output and the vasopressor therapy necessary to optimize perfusion through stenotic arterial segments.

Treatment

- Consider intra-aortic balloon pump counterpulsation to increase cardiac output and reduce left ventricular afterload.
- Titrate vasopressor and volume according to systemic hemodynamic parameters to optimize brain tissue perfusion (target to increase CPP values, decrease the Lindegaard ratio and achieve continuous positive diastolic flow during balloon counterpulsation).

Intra-aortic balloon pump (IABP) waveform. The five points of the IABP are identified as follows (Figure 4.11, bottom waveform):

- ASP, assisted systolic pressure (balloon deflation occurs immediately before, reducing left ventricular workload);
- PAEDP, patient aortic end-diastolic pressure;
- PSP, peak systolic pressure (unassisted; no balloon deflation occurs before it);
- PDAP, peak diastolic augmented pressure (achieved through balloon inflation);
- BAEDP, balloon aortic end-diastolic pressure (reduction of afterload achieved by balloon deflation).

Note decreased diastolic perfusion pressures after

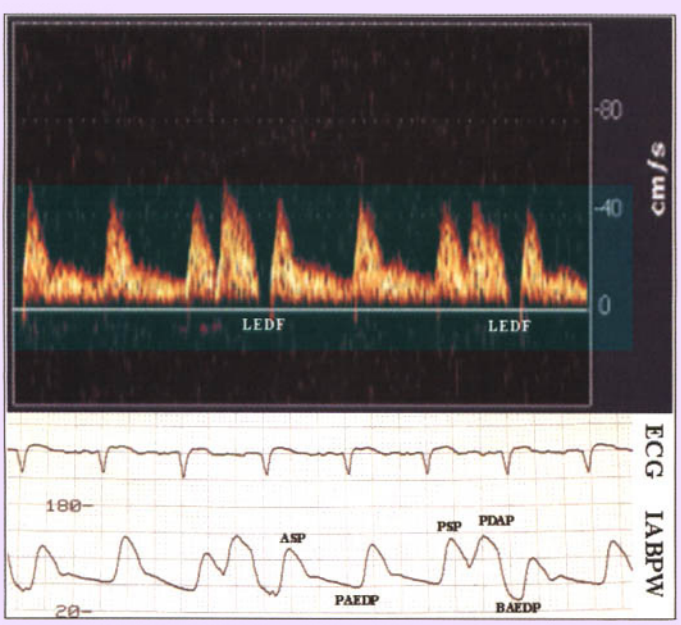

Figure 4.11 Intra-aortic balloon pump waveform (IABPW) and the middle cerebral artery velocity changes with early balloon deflation. Key to IABP waveform: ASP, assisted systolic pressure; PAEDP, patient aortic end-diastolic pressure; PSP, peak systolic pressure (unassisted); PDAP, peak diastolic augmented pressure; BAEDP, balloon aortic end-diastolic pressure; LEDF, loss of end-diastolic flow in the MCA detected by transcranial Doppler (TCD) related to early balloon deflation.

Continued

early balloon deflation resulting in relatively high resistance flow in the middle cerebral artery and likely lower CPP values (Figure 4.11).

Retimed IABP waveform for deflation immediately prior to the next systolic upstroke creates higher positive diastolic flow to the brain in all cycles and low-resistance waveforms in the middle cerebral artery (Figure 4.12).

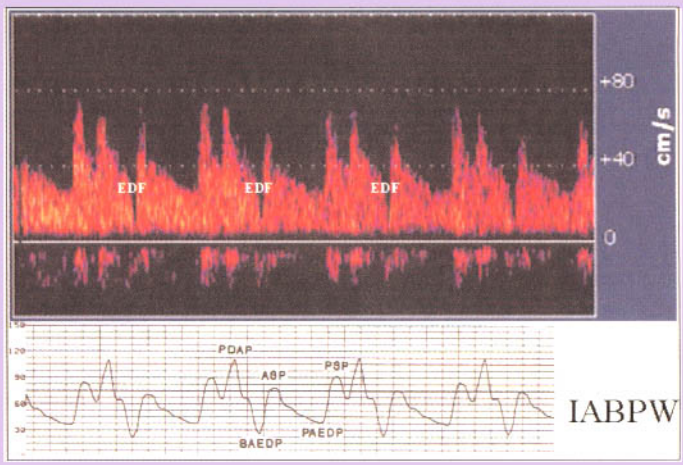

Figure 4.12 Intra-aortic balloon pump waveforms (IABPWs) with retimed balloon deflation. Key to IABP waveform: ASP, assisted systolic pressure; PAEDP, patient aortic end-diastolic pressure; PSP, peak systolic pressure (unassisted); PDAP, peak diastolic augmented pressure; BAEDP, balloon aortic end-diastolic pressure; EDF, return of end-diastolic flow and overall low-resistance flow pattern in the MCA on TCD spectral analysis following adjusted balloon deflation.

References

1 Guyton AC. *Textbook of Medical Physiology*, 9th edn. Philadelphia: W.B. Saunders, 1996.

2 Stewart SL, Vitello-Cicciu JM. Cardiovascular clinical physiology. In: Kinney MR, Dunbar SB, Brooks-Brunn JA, Molter N, Vitello-Cicccіu JM, eds. *AACN Clinical Reference for Critical Care Nursing*. St. Louis: Mosby, 2001: 249–76.

3 Whalen DA, Kelleher RM. Cardiovascular patient assessment. In: Kinney MR, Dunbar SB, Brooks-Brunn JA, Molter N, Vitello-Cicccіu JM, eds. *AACN Clinical Reference for Critical Care Nursing*. St. Louis: Mosby, 2001: 277–318.

4 Darovic GO. *Hemodynamic Monitoring: Invasive and Noninvasive Clinical Application*, 2nd edn. Philadelphia: W.B. Saunders, 1995.

5 Frank O. On the dynamics of cardiac muscle (translated by Chapman CB and Wasserman E). *Am Heart J* 1959; **58** (282): 467.

6 Starling EH. *The Linacre Lecture on the Law of the Heart*. London: Longman's Green, 1918.

7 Wojner AW. Assessing the five points of the intra-aortic balloon pump waveform. *Crit Care Nurse* 1994; **14** (3): 48–52.

8 Saito Y *et al.* Clinical application of atrial natriuretic peptide in patients with congestive heart failure: Beneficial effects on left ventricular function. *Circulation* 1987; **76**: 115–30.

9 Epsiner EA, Richards AM. Atrial natriuretic peptide, an important factor in sodium and blood pressure regulation. *Lancet* 1989; **1** (8640): 707–10.

10 Wennmalm A. Endothelial nitric oxide and cardiovascular disease. *J Intern Med* 1994; **235**: 317–27.

11 Ahrens TS, Taylor LA. *Hemodynamic Waveform Analysis*. Philadelphia: W.B. Saunders, 1992.

12 Ahrens TS. *Hemodynamic Waveform Recognition*. Philadelphia: W.B. Saunders, 1993.

13 Shoemaker WC *et al.* Multicenter trial of a new thoracic electrical bioimpedance device for cardiac output estimation. *Crit Care Med* 1994; **22** (12): 1907–11.

14 Kelli G. An account of the appearances observed in the dissection of two of the three individuals presumed to have perished in the storm of the 3rd, and whose bodies were discovered in the vicinity of Leith on the morning of the 4th November 1821 with some reflections on the pathology of the brain. *Transmissions Med Chir Sci Edinburgh* 1824; **1**: 84–169.

15 Davis AE, Briones TL. Intracranial disorders. In: Kinney MR, Dunbar SB, Brooks-Brunn JA, Molter N, Vitello-Cicccіu JM, eds. *AACN Clinical Reference for Critical Care Nursing*. St. Louis: Mosby, 2001: 685–709.

16 Sullivan J. Jugular venous oxygen saturation monitoring. Insertion, care, troubleshooting, and removal. In: Lynn-Mchale DJ, Carlson KK, eds. *AACN Procedure Manual for Critical Care*, 4th edn. St. Louis: Mosby, 2001: 570–9.

5

CHAPTER 5

Practical models of cerebral hemodynamics and waveform recognition

Andrei V. Alexandrov, MD, RVT

Introduction

Any single rule invoked to explain hemodynamics of the living brain is too simplistic or will often be proven wrong by clinical experience. To analyse the real-time flow information provided by ultrasound, a clinician often has to put together a practical model of several hemodynamic principles that will best explain the findings. When multiple explanations exist, the simplest, yet sufficient model is usually the right answer. Before making a diagnosis of pathologic changes, seek physiologic explanation in cardiovascular, respiratory and hematologic functions that always interplay and have a broad range of compensatory capacities. This chapter provides description of basic hemodynamic principles and easy-to-remember practical models that can help with interpretation and differential diagnosis.

Waveform recognition and proper description of flow findings are also essential skills for test performance and interpretation. This chapter will further guide through the basic process of identifying Doppler settings and waveform components and will provide examples of typical waveforms and flow findings. Illustrations contain typical waveforms found during transcranial Doppler (TCD) examinations. Interpretation and discussion of these findings and differential diagnoses are provided in the text.

Flow resistance

Brain function requires continuous flow through the cardiac cycle, and therefore to maintain the flow, the resistance should be low in diastole. As Billy Joel said, 'You can't go the distance with too much resistance'.

To create a positive diastolic flow, a pressure gradient should exist [1] between the arteries entering the brain and veins exiting the intracranial space. Pressure gradients determine blood flow rates. To promote antegrade flow, they exist between the common and internal carotid arteries (ICAs), between the ICA and middle cerebral artery (MCA), etc. Changes in these pressure gradients can open collaterals of the circle of Willis. The flow rate, or the flow volume per unit time, directly depends on the pressure difference described in the Hagen–Poiseuille law:

$$\text{Flow rate} = \frac{\pi(P_1 - P_2)r^4}{8\eta L}$$

where P_1 is the pressure at the beginning and P_2 the pressure at the end of the flow system, r is the radius of the lumen, π is a constant, η is the fluid viscosity and L is the length or distance that flow has to travel between the pressure points.

The Hagen–Poiseuille law does not take into account stretching of blood vessels in response to pressure or volume changes.

The flow rate is directly proportionate to the pressure difference and inversely proportionate to the resistance (or the energy loss required to propel fluid over the distance between the pressures). *Resistance*, therefore, is:

$$\text{Resistance} = K\frac{8\eta L}{\pi r^4}$$

K – is a constant ≥ 1 representing energy loss necessary

to develop an optimal flow profile in a vessel (i.e. parabolic flow). In the distributing arteries of the body, the diameter of branching vessels and the geometry of bifurcations introduce even greater energy losses.

Resistance can be changed by vasomotor activity. For example, arterioles can vasodilate to attract more collateral flow with increasing degree of a proximal occlusive disease.

Practical models

Arterial Pco_2 ↑	Arteriole diameter ↑	Resistance ↓	⇒ M1 MCA velocity ↑
Arterial Pco_2 ↓	Arteriole diameter ↓	Resistance ↑	⇒ M1 MCA velocity ↓
Degree of stenosis ↑	Blood viscosity =	Length of stenosis =	⇒ Resistance ↑
Degree of stenosis =	Blood viscosity ↑	Length of stenosis ↑	⇒ Resistance ↑

↑, Increase; =, unchanged; ↓, decrease.

Although there is a linear relationship between viscosity and resistance, blood generally behaves as a non-Newtonian fluid [2]. Blood viscosity changes with velocity gradient, heart rate, vessel geometry, hematocrit, temperature and shear stress [2].

Flow velocity

In a vessel with straight walls and no bifurcations (an oxymoron in the brain vasculature), the flow velocity and cross-sectional area are linked in a 'continuity principle' [1]:

$$A_1 \times V_1 = A_2 \times V_2$$

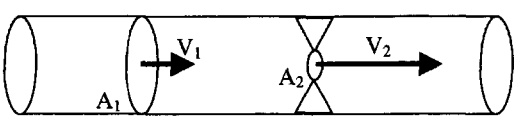

Note that the *highest* velocity exists at the *exit* from a focal stenosis. Since fluid is non-compressible, if average pressure remains the same, the V_2 velocity should increase by an amount inversely proportionate to the reduction in the vessel lumen area:

$$V_2 = \frac{A_1 V_1}{A_2} \quad \text{or} \quad V \sim \frac{1}{r^2}$$

Flow acceleration begins at the stenosis entrance where the pressure energy of flow (i.e. blood pressure) is converted into kinetic energy producing increased velocities. This conversion of energy is described by the *Bernoulli effect*:

$$P_1 - P_2 = \Delta P = {}^1/_2 \rho (V_1^2 - V_2^2),$$

where ρ is the density of blood. However, blood velocity changes with increasing degree of stenosis are more complex, i.e. the velocity is inversely proportionate also to the linear and cubic function of the residual lumen. The correlation between velocity and stenosis was described by Spencer and Reid [3] (see Chapter 6).

Practical models

Degree of stenosis ↑	Blood viscosity =	Length of stenosis =	⇒ Velocity ↑
Degree of stenosis =	Blood viscosity ↓	Length of stenosis =	⇒ Velocity ↑
Degree of stenosis =	Blood viscosity =	Length of stenosis ↑	⇒ Velocity ↓

Turbulence

The laminar structure of a normal parabolic blood flow can be disturbed by a sudden expansion of the vessel diameter, by excessive flow acceleration at the stenosis or, sometimes, by hyperemia (increased flow volume in a normal vessel or collateral channel). Turbulence refers to formation of vortices, swirling currents in various directions that disrupt the laminar boundary layers. Turbulence further contributes to energy losses along the vascular tree. The appearance of turbulence at a certain velocity threshold is determined by the *Reynolds number* (*Re*):

$$Re = \frac{2rv\rho}{\eta}$$

In other words, the higher the Reynolds number (i.e. ≥ 2000–2200 in a vessel with smooth walls) for a given velocity *v*, the higher the propensity to turbulence [1]. This propensity increases with higher density of blood and lower blood viscosity. A turbulent flow flattens the velocity profile (the higher the Reynolds number, the flatter the velocity profile).

Turbulence disrupts the relationship between pressure and flow described by the Hagen–Poiseuille law and the correlation between the degree of stenosis and velocity.

Spectral Doppler waveforms provide general evidence for the disturbance of flow; however, the waveforms do not provide quantitative measurements of turbulence. Several flow changes can be found simultaneously in a vessel that contains turbulent flow: low-frequency systolic bruits and bidirectional noise, flattening of the waveform and appearance of a 'plug-like' flow [1].

Practical models

Velocity ↑	Blood viscosity =	Degree of stenosis ↑	⇒ Turbulence ↑
Velocity =	Blood viscosity ↑	Degree of stenosis =	⇒ Turbulence ↓

Vasomotor reactivity (VMR)

Cerebral blood flow (CBF) rates change with vasodilatory or constricting stimuli that affect the diameter of brain resistance vessels. As a rule, the smaller the diameter of the arterial branches, the greater the capacity of these vessels to constrict or dilate. These changes also directly affect the velocity and waveforms in the proximal branches of the circle of Willis. The middle cerebral artery (MCA) velocity changes by 3–4% per mmHg change in end-tidal CO_2 [4]. However, it is important to remember that:

$$\text{flow velocity} \neq \text{CBF}.$$

Although the velocity is *not* flow volume [5], Newell and Aaslid state that the flow velocity can reflect CBF and the velocity *change* can be proportionate to the changes in CBF if:

1 the angle of insonation remains constant;
2 the perfused territory remains the same; and
3 the effect of only one stimulus is observed [6].

Moreover, according to Kontos [5], to calculate flow volume through an intracranial vessel, its diameter should be precisely measured at the time of velocity assessment, and this cannot be accomplished with current ultrasound methods.

However, TCD can easily quantify the response of cerebral vessels to carbon dioxide. Markus described a simple measurement of the MCA velocity response to 30 s of breath-holding [7] termed the *breath-holding index* (BHI)

$$\text{BHI} = \frac{\text{MFV}_{\text{baseline}} - \text{MFV}_{\text{end}}}{\text{MFV}_{\text{baseline}}} \times \frac{100}{\text{seconds of breath-holding}}$$

where *MFV* is mean flow velocity. Silvestrini *et al.* prospectively evaluated BHI in case-controlled studies and showed that impaired VMR can help to identify patients at higher risk of stroke who have asymptomatic carotid stenosis or previously symptomatic carotid occlusion [8,9].

Practical model

Blood viscosity =	Blood pressure =	Degree of stenosis ↑	⇒ Vasomotor reactivity ↓

Decreased VMR suggests failure of collateral flow to adapt to the stenosis progression.

Cerebral autoregulation

A change in perfusion pressure leads to a proportionate change in flow volume. The brain, however, developed an intrinsic mechanism that adjusts the vascular resistance to maintain CBF constant in the physiologic range of blood pressure (BP) (50–150 mmHg for normotensive individuals) [10]. Giller *et al.* showed that a BP decrease of 30 mmHg caused compensatory dilatation of the M1 MCA segment by 4% and M2 MCA segment by 20% [4]. Autoregulation guards the brain with the continuous supply of water, glucose and oxygen necessary for its function. Both VMR and autoregulation coexist and override each other when invoked by various stimuli. As a result, complex dynamic changes in the waveform shape and velocity values can be observed in a short time with breathing cycles, changes of cardiac output, coughing, sneezing, etc.

Autoregulation also decreases distal resistance to flow in the long term when a proximal arterial

obstruction develops. When autoregulation has already set the cerebral vessels to maximal dilatation, no vasomotor response is induced by breath-holding, and any significant drop in BP, blood oxygenation or dehydration can cause hypoperfusion or ischemia [11].

Cerebral autoregulation can be accomplished through a fast-acting myogenic mechanism to immediately compensate for changing perfusion status [10]. The *Bayliss effect (myogenic mechanisms)* postulates that smooth muscles of the resistance vessels respond to changes in the transmural pressure to increase or restrict the incoming flow. A long-term regulation of CBF is likely corrected by various *metabolic mechanisms* and vasoactive substances providing feedback and regulatory action. Regardless of the priority of each mechanism or the existence of other mechanisms (i.e. neurogenic, etc.), cerebral autoregulation can be disturbed by head trauma or cerebral ischemia, and its non-invasive measurement with ultrasound is still being developed.

Arterial bifurcation and flow distribution

Arterial stenosis or occlusion display flow features predicted by the principles governing resistance and velocity only when the lesion is single, short in length and located at segments with no bifurcations. The brain attempts to compensate for arterial lesions by utilizing multiple bifurcations and regulatory mechanisms that redistribute flow around the obstruction. To bring the flow around the lesion, the brain vessels neighboring the obstruction dilate to create a pressure gradient between the proximal open vessel and the vessels distal to the obstruction. This pressure gradient is responsible for the collateral flow through a competent circle of Willis that can maintain an ICA occlusion symptom free in some patients.

As a general rule, a collateral channel opens when a lesion is located proximal to its origin, and a pressure gradient develops between the donor arteries and the recipient vessels.

Several factors can disturb the regulatory mechanisms and the ability of brain vasculature to maintain adequate perfusion. Systemic blood pressure and cardiac output may decrease, the patient may become dehydrated, platelet function may be activated, an embolus can lodge in the distal vasculature and spreading tissue edema can change overall resistance to flow. The key to interpreting a variety of cerebrovascular ultrasound findings is to put together the previous hemodynamic models with flow changes observed at bifurcations and check for flow diversion pathways to compensate for obstructive lesions.

Practical model of an acute distal M1MCA occlusion

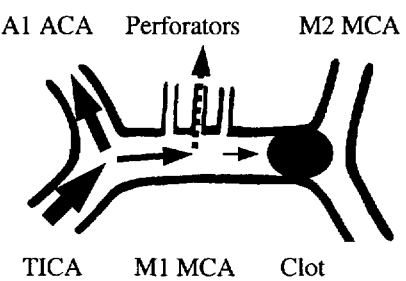

Velocity (branching vessel) ↑	Velocity (stem with bifurcations) =	Velocity (at the clot) ↓
Reasons		
Collateral channels	Low-resistance bifurcations	Increased resistance

In the case of a distal M1 MCA occlusion, the anterior cerebral artery (ACA) can serve as a flow redistribution channel to deliver blood to the MCA territory via transcortical collaterals. The lenticulostriatal arteries, or perforators may also serve as a low-resistance channel that can deliver blood to the internal capsule and more distally via the ascending branches. These flow phenomena may account for variable stroke severity with the distal M1 MCA occlusion and relatively normal or slightly decreased proximal M1 MCA velocity (see also 'Select clinical applications and clinical vignettes').

These simple models can help in memorizing the effects of the most important factors that determine velocity and pulsatility of flow. Flow models that are invoked to explain actual flow findings should be corrected with respect to patient condition, vital signs, medications and waveform morphology.

Practical models			TCD	Condition
Blood viscosity ↑	BP =	Stenosis (none or =)	⇒ Velocity ↓, PI ↑	Dehydration, pulmonary shunt
Blood viscosity ↓	BP =	Stenosis (none or =)	⇒ Velocity ↑, PI ↓	Hydration, anemia
Acute BP ↑	Blood viscosity =	Stenosis (none)	⇒ Velocity ↑, PI ↑	Hypertension (effect of dopamine)
Acute BP ↓	Blood viscosity =	Stenosis (none)	⇒ Velocity ↓, PI ↓	Hypotension, collapse
Chronic BP ↑	Proximal stenosis (none)		⇒ Velocity ↑, PI ↑	Effect of chronic hypertension
Chronic BP ↓	Proximal stenosis (none)		⇒ Velocity ↓, PI = or ↓	Congestive heart failure
Cardiac output ↑	Blood viscosity =	Spasm (no)	⇒ Velocity ↑, PI ↑	Normal autoregulation (liver failure)
Cardiac output ↑	Blood viscosity =	Spasm (no)	⇒ Velocity ↑, PI↓	Altered autoregulation (head trauma)
Cardiac output ↑	Blood viscosity =	Spasm (yes)	⇒ Velocity ↑, PI ↑	HHH therapy (success)
Cardiac output ↑	Blood viscosity =	Spasm (yes)	⇒ Velocity ↑, PI ↓↓	HHH therapy (failure)
Degree of stenosis ↑	Length of stenosis =	BP =	⇒ Velocity ↑	Focal stenosis progression
Degree of stenosis ↓	Length of stenosis =	BP =	⇒ Velocity ↓	Focal stenosis regression
Length of spasm ↑	Degree of spasm =	BP =	⇒ Velocity = or ↓	Diffuse vasospasm
Length of spasm ↓	Degree of spasm =	BP =	⇒ Velocity = or ↑	Focal vasospasm

↑, Increase; =, unchanged; ↓, decrease; PI, the pulsatility index (Gosling); HHH, hypertension–hemodilution–hypervolemia.

How to read waveforms

The flow waveform represents time dependence of blood flow velocity on cardiac activity [12]. Waveform recognition during Doppler examination starts with hearing the flow signal followed by visual analysis of the signal appearance on screen. Steps to optimize flow signals depend largely on this immediate recognition of the waveform and sonographer skills. Reading any ultrasound findings starts with orientation on screen and identification of machine settings. For Doppler examination, these simple and essential components include:

1 transducer and sample volume (gate) positioning;
2 flow direction;
3 angle of insonation;
4 scale settings; and
5 sweep speed.

For the purposes of this chapter, all Doppler recordings were obtained with a large (13-mm) sample volume at assumed zero angle of insonation. Flow signals towards the probe are displayed above baseline with a constant sweep speed. Scale settings, gain and baseline position were adjusted when necessary.

First, using the following five steps, identify the components of a cardiac cycle (Figure 5.1):

1 beginning of systole;
2 peak velocities during systole (peak systole);
3 diacrotic notch (closure of the aortic valve signalling the beginning of diastole);
4 end-diastolic velocities (end-diastole); and
5 the shape and magnitude of flow deceleration during the cardiac cycle.

Second, determine whether the measurements provided by automated software or manual placement are representative of the waveforms found. Doppler flow signal optimization is checked by the following:

1 signal-to-noise ratio (i.e. background should contain no or minimal noise);
2 envelope (or waveform follower) does not over- or underestimate velocities;
3 scale settings are adequate to display maximum velocities;
4 baseline (zero line) is positioned to avoid aliasing or sufficiently separate signals;
5 signal intensity is equal during recording sweep.

Third, the waveform recognition will depend on

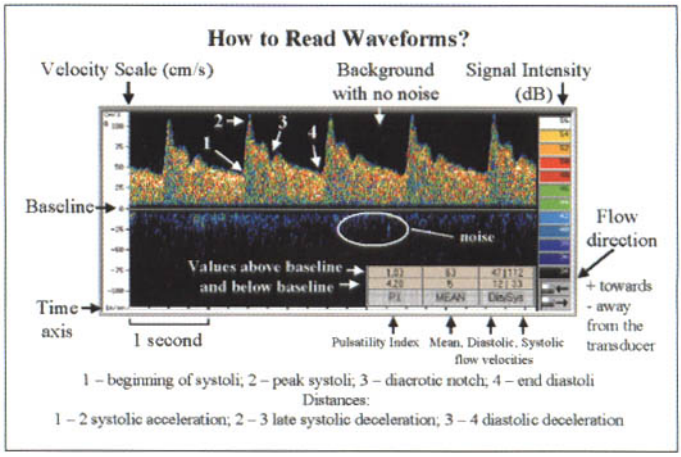

Figure 5.1 Keys to waveform presentation.

identification of the following components of an optimized Doppler signal:

1 early systolic upstroke (sharp or slow, delayed);

2 late systolic and diastolic deceleration (continuous, stepwise or flattened);

3 shape of the waveform (smooth, sharpened or flattened);

4 systolic/diastolic velocity difference (flow pulsatility); and

5 other components of the Doppler spectrum (bruit, spectral narrowing, embolic signals, etc.).

Specific waveforms

Normal findings

Case history. An asymptomatic 32-year-old man with arterial blood pressure 130/80 (Figure 5.2).

Interpretation. This waveform shows a sharp systolic flow acceleration and stepwise deceleration with positive end-diastolic flow. The end-diastolic velocity falls between 20 and 50% of the peak systolic velocity values, and this finding indicates low resistance to arterial flow.

Case history. An asymptomatic 32-year-old man with arterial blood pressure 130/80 (Figure 5.3).

Interpretation. This recording shows a bidirectional signal with simultaneous sharp systolic upstrokes and similar stepwise deceleration in both flow directions. Both waveforms show low-resistance flow patterns obtained at the ICA bifurcation.

Increased pulsatility of flow

Case history. A 65-year-old man with a new onset aphasia and chronic hypertension (Figure 5.4).

Interpretation. The waveform above baseline has a rapid systolic upstroke and a rounded peak systolic complex followed by a stepwise flow deceleration. The end-diastolic velocities below 30% of peak systolic values indicate relative increase in flow resistance. If flow

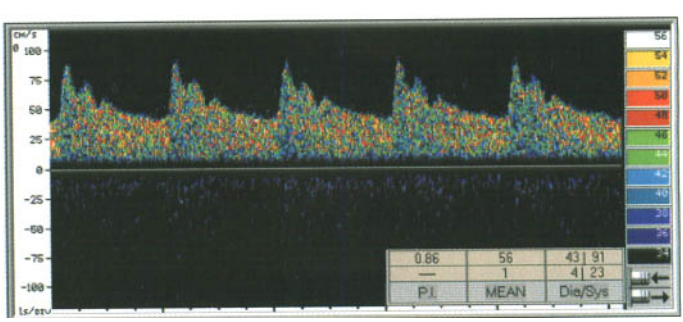

Figure 5.2 A low-resistance unidirectional flow signal.

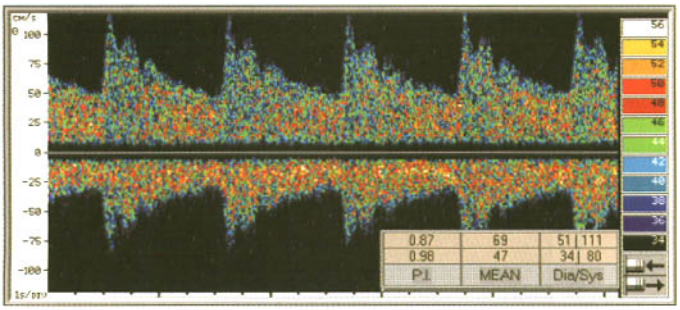

Figure 5.3 A low-resistance bidirectional flow signal.

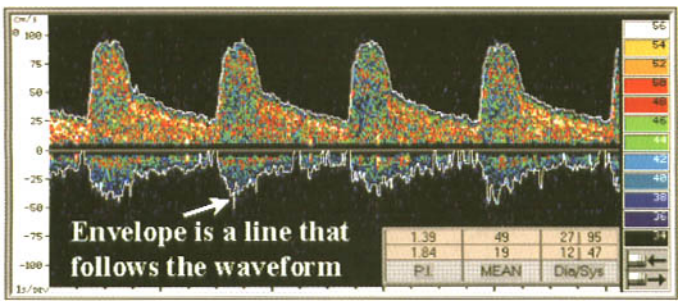

Figure 5.4 Increased resistance to flow with chronic hypertension.

pulsatility is relatively similar in branching and contralateral vessels, a pulsatile waveform with normal or elevated mean flow velocity indicates normal vessel patency at the site of insonation and is not suggestive of a distal arterial occlusion. A weak flow signal below baseline in Figure 5.4 is not optimized and measurements are erroneous.

The effects of chronic hypertension on intracranial Doppler recordings may include:

1 increase in flow pulsatility [13] (pulsatility index values of ≥ 1.2 at the University of Texas STAT Neurosonology Laboratory); and

2 relative mean flow velocity increase above age-expected values.

Kidwell *et al.* showed that a relative increase in the Gosling pulsatility index above 1.17 correlates with the presence of silent brain damage on MRI in patients with chronic hypertension [14].

Case history. A 37-year-old man with closed traumatic brain injury (TBI) and intracranial pressure 52 mmHg (Figure 5.5).

Interpretation. The flow signal above baseline shows sharp systolic upstrokes followed by sharp deceleration indicating an overall increased resistance to flow.

Despite elevated pulsatility index (PI) in a young individual free of chronic hypertension (PI = 1.2), this high resistance waveform in the middle cerebral artery indicates normal patency of its proximal segment. This patient with traumatic brain injury (TBI) had

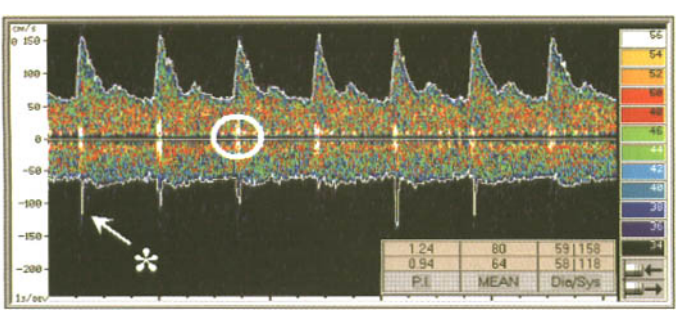

Figure 5.5 A complex waveform indicating flow to both high- and low-resistance vascular beds.

intracranial pressure of 52 mmHg that produced increased resistance in the distal vascular bed. Elevated pulsatility index values were observed in patients with increased intracranial pressure [15]. The Doppler spectrum shows sharpening of the waveform due to faster flow deceleration. At the same time, the waveform above baseline also has a substantial diastolic flow indicating that some of this flow may be directed to a low-resistance vascular bed. This can happen in patients with TBI because both edematous (bruised) and normally perfused tissues may be present within the MCA territory. Furthermore, brain areas may be present with disturbed autoregulation or unequal distribution of ICP and mass effect. The waveform above baseline resembles a common carotid waveform because the CCA supplies both low- and high-resistance vascular beds.

The flow signal below baseline has a low-resistance flow pattern flow seen in a vein. A loud thump-like early systolic sound (circled) is present due to vessel wall motion. This bright reflector disturbs spectral analysis and causes the envelope to spike (marked with *) leading to errors in automated velocity and pulsatility measurements below baseline.

Case history. A 35-year-old man with subarachnoid hemorrhage (Grade II, Day 2) and liver failure (Figure 5.6).

Interpretation. Both waveforms above and below the baseline have sharp systolic upstrokes and an abrupt flow deceleration. These pulsatile waveforms with the end-diastolic velocities within 20–25% of peak systolic values indicate high resistance to arterial flow. The difference in automated calculations of PI (PI below baseline is higher than above baseline) is attributable to the weakness of the signal directed away from the probe and the underestimation of the diastolic velocity by the envelope (last full cycle on the right).

This patient with subarachnoid hemorrhage has an even more pulsatile waveform (PI = 1.7). The differential diagnosis includes increased intracranial pressure, vasospasm and systemic conditions. Although hydrocephalus can be expected to develop by 48 h after the bleeding, this patient has normal ICP values (continuous ventricular drainage and invasive ICP monitor) at the time of TCD examination. A vasospasm that may produce these waveforms at M1 and A1 segment origins should affect both MCA and ACA territories and this will be an unlikely event on Day 2. Finally, the patient does not hyperventilate since he is alert and breathing room air at a normal pace. In this case, increased PI values and a sharp pulsatile waveform are seen due to autoregulatory vasoconstriction of the distal arterial bed in response to spontaneously increased cardiac output (cardiac index = 7) in a young patient with liver failure.

Case history. A 42-year-old woman with closed traumatic brain injury (Figure 5.7).

Interpretation. The waveforms above baseline show a regular heart rate with variable velocities (sharp systolic upstrokes, stepwise deceleration, low resistance). Marked velocity fluctuations can spontaneously occur every four cardiac cycles due to breathing. A cycle with the highest velocities (*) can be used for manual calculations.

Flow velocity and pulsatility fluctuations can also be caused by altered autoregulation (the patient has traumatic brain injury) and changes in the intracranial pressure. Blood flow velocity measurements can also be partially affected by changes in the angle of insonation (transducer positioning and, to a lesser degree, vessel pulsation and motion). Changes in flow pulsatility and waveform shape, as seen in this patient, are unlikely to be affected by the angle of insonation.

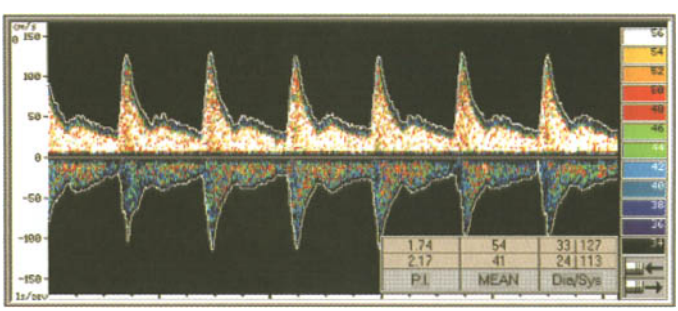

Figure 5.6 Increased pulsatility of flow at a bifurcation.

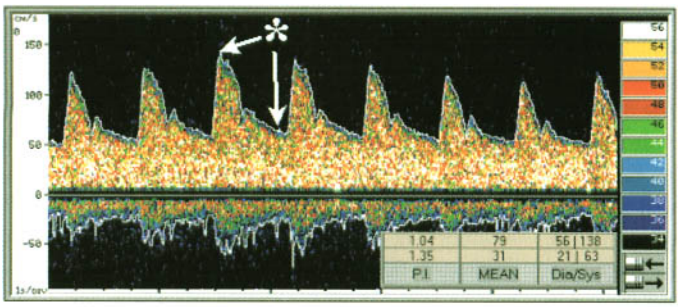

Figure 5.7 Variable velocity and pulsatility.

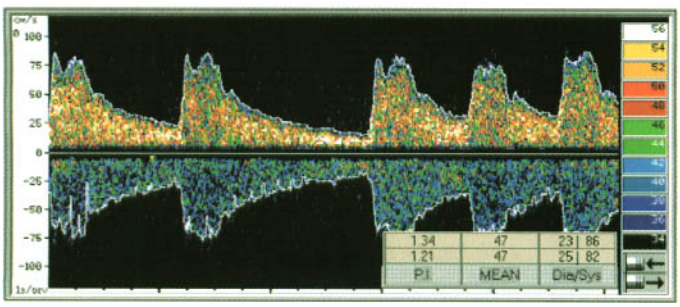

Figure 5.8 Extrasystole.

Irregular heart rhythm

Case history. A 54-year-old man with an acute small cortical stroke and left ventricular hypertrophy (LVH) (Figure 5.8).

Interpretation. Waveforms above and below the baseline have sharp upstrokes, arrival of maximum systolic velocities towards the end of systole and stepwise flow deceleration. The end-diastolic velocities fall below 30% of peak systole due to irregular heart rate: this also affects estimation of flow resistance (increased values of PI calculated with envelope tracings) from only 2–5 cycles' averaged values. A single cycle may be selected for manual measurements.

Measurements that are affected by irregular heart rate include:

1 velocity (underestimation); and
2 pulsatility (overestimation).

A prolonged pause between cardiac contractions (seen in the second cycle, Figure 5.8) leads to lower than usual end-diastolic velocities that artificially decrease the velocity and increase pulsatility index values. Avoid including in measurements the compensatory pauses after extrasystole; or, if extrasystoles are too frequent, a higher number of cardiac cycles should be averaged using slower sweep speeds or manual measurements of the highest velocity cycle should be used.

Case history. A 60-year-old woman with recent transient ischemic altack (TIA) and atrial fibrillation (Figure 5.9).

Interpretation. Waveforms towards the probe have irregular arrival of cardiac cycles with sharp upstrokes

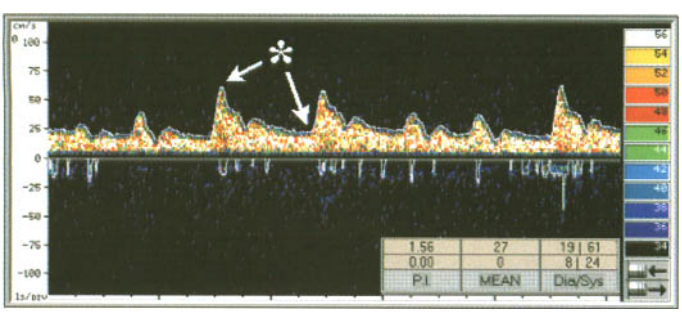

Figure 5.9 Atrial fibrillation.

and variable velocities. As a practical rule, a cycle with the highest velocities (marked as *) can be used for manual calculations. However, estimation of flow resistance and representative mean velocity is difficult since the pulse rate and cardiac output are affected.

This a typical waveform obtained from a patent middle cerebral artery in a patient with atrial fibrillation. This waveform can be easily recognized if there is no cardiac cycle similar to the other. Yet, overall it is a low-resistance flow recording since end-diastolic velocity exceeds 30% of peak systole during every cycle taken separately. PI values are overestimated since the envelope recognizes maximum peak systole and minimum end-diastole taken from separate cycles. Although averaging of 20 cardiac cycles may provide more representative velocity and pulsatility index values, it is impractical and difficult to accomplish. A less scientific but practical solution is to use manual measurements taken from a cycle with the highest peak and end-diastolic measurements that are often representative of a more synchronized cardiac contraction with better cardiac output. This approach also shortens time of examination and introduces a consistent way of recording velocities for serial studies.

Changes in the systolic flow acceleration

Case history. A 67-year-old man with resolving MCA stroke and carotid occlusion (Figure 5.10).

Interpretation. The waveform above baseline shows a delayed systolic flow acceleration, flattened systolic complex and slow diastolic deceleration. End-diastolic velocities above 50% of peak systole indicate very low flow resistance. This waveform is called a 'blunted' flow signal.

This waveform shows a delayed systolic flow acceleration that can be found in a patent vessel distal to a high-grade stenosis or occlusion [16]. The MCA usually receives either collateral flow around or residual flow through the ICA lesion and, in order to attract more flow, compensatory vasodilatation occurs to reduce overall resistance to flow (low (1.0–0.6) or very low (< 0.6) PI values). When these 'blunted' waveforms (with MFV generally above 20 cm/s) are found unilaterally, it is a sign of a proximal (ICA or terminal ICA) hemodynamically significant obstruction. If a delayed systolic flow acceleration is found in both internal carotid branches and the basilar artery, it may be a sign of reduced cardiac output (i.e. congestive heart failure).

Case history. A 73-year-old man with MCA stroke and carotid occlusion (Figure 5.11).

Interpretation. The waveform above baseline has an upward systolic upstroke. This waveform has to be compared to a non-affected vessel in order to decide if only a *slight* delay in systolic acceleration is present. In any case, this is *not* a blunted signal since a clear systolic complex is visualized.

This waveform shows only a slight delay in the systolic flow acceleration and a clear systolic complex. This type of flow acceleration can be found in patients with or without hemodynamically significant proximal arterial obstruction. When found at the MCA origin or just posteriorly to a 'blunted' MCA signal, this waveform may be attributable to the posterior communicating artery or the posterior cerebral artery with a normal systolic flow acceleration in the presence of an ICA obstruction.

Collateralization of flow

Case history. A 70-year-old woman with a recent TIA and carotid occlusion (Figure 5.12).

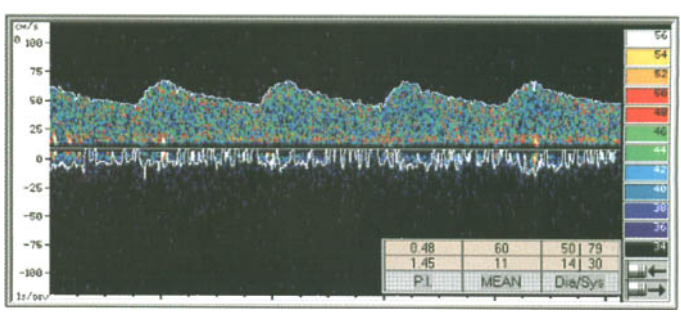

Figure 5.10 A blunted signal.

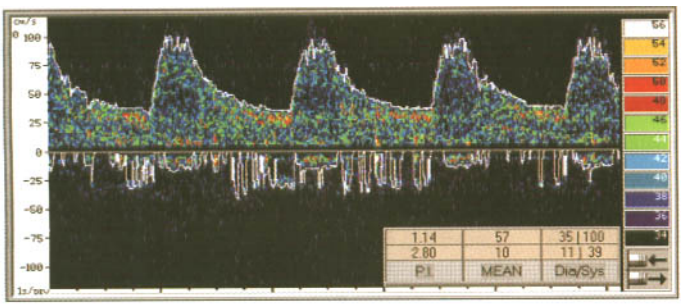

Figure 5.11 Slightly delayed systolic flow acceleration.

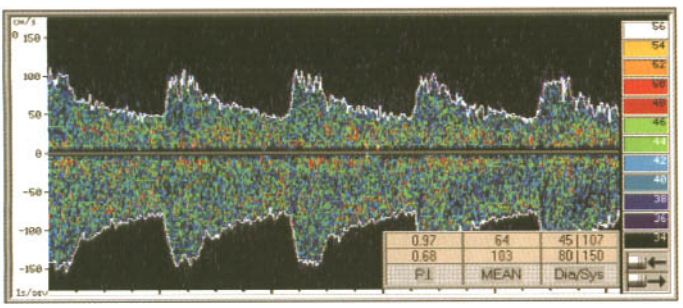

Figure 5.12 Flow diversion.

Interpretation. This tracing displays a bidirectional signal with normal systolic upstrokes. The waveform below baseline shows higher velocities and lower resistance to flow. This may represent flow diversion to a branch directed away from the probe.

This bidirectional signal represents a typical finding at the MCA/ACA bifurcation with flow diversion to the ACA being present. When the ACA becomes the donor vessel for the anterior cross-filling to compensate for a contralateral carotid obstruction, the ACA starts to supply both A2 segments and often the contralateral MCA via contralateral A1 segment reversal. This cross-filling may manifest on the donor site as the mean flow velocity difference ACA > MCA and pulsatility index ACA < MCA due to compensatory flow volume increase and vasodilatation. It is important to optimize both MCA and ACA signals to make sure that maximum Doppler shifts are compared at these vessels and not between the terminal ICA (TICA) and ACA. Simultaneous display of the terminal ICA/ACA signals may yield similar velocity differences due to a suboptimal angle of insonation with the TICA.

Aliasing and signal optimization

Case history. A 72-year-old man with a recent TIA and a moderate proximal carotid stenosis (Figure 5.13).

Interpretation. This recording shows a waveform that exceeds one half of the velocity scale (i.e. an artifact called 'aliasing'). Both envelopes show automated

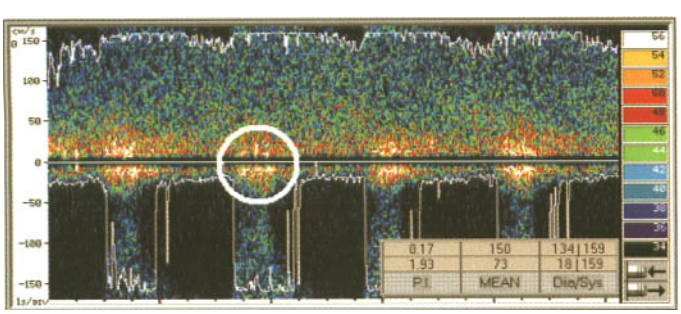

Figure 5.13 Aliasing.

recognition of the velocity values that are erroneous. This waveform also contains a low-frequency bidirectional signal heard as a bruit (circled).

This waveform is a typical pulse wave Doppler artifact [17]. This artifact inappropriately displays, or cuts off, the systolic frequencies from the top or the bottom of the spectral display. There is often an overlap in maximum velocities between the flow signals towards and away from the probe. This artifact is linked to a pulsed Doppler system handicap in velocity detection posed by the half of pulse repetition frequency (PRF) threshold (or the *Nyquist limit*) [17]. Steps to optimize this signal should include:

1 adjustment of the velocity scale to maximum possible values;

2 moving baseline ('drop the baseline', or converting the recording into a unidirectional display); and

3 reducing sample volume or gate (this may help to focus the beam at one vessel thus avoiding or reducing the impact of aliasing on the velocity measurements).

Case history. A 68-year-old man with a recent MCA stroke and MCA stenosis (Figure 5.14).

Interpretation. This waveform is an optimized signal with high velocities, bruits, normal systolic acceleration and low-resistance flow pattern. Background contains no noise and the envelope shows a good automated waveform tracing. Other data are needed to confirm whether this is a stenotic signal, i.e. focal changes in velocity along the MCA stem and comparison to the contralateral MCA velocity values.

Differential diagnosis includes a compensatory velocity increase if another large vessel lesion is present. From a single depth tracing in the intracranial vessels, it is impossible to tell whether this waveform represents a focal significant velocity increase due to stenosis, or it represents hyperemia with collateralization of flow. Shown in this figure, the MCA flow signal with a mean flow velocity of 117 cm/s was found at the site of a 50% MCA narrowing unilateral to the hemisphere affected by an ischemic stroke. If found contralateral to a proximal ICA obstruction, similar velocity findings may represent M1 MCA stenosis or flow diversion. A focal MCA stenosis is likely to be found if the distal M1 MCA velocity decelerates by more than 30%.

Case history. A 59-year-old man with an acute stroke and carotid occlusion contralateral to the side of insonation (Figure 5.15).

Interpretation. This tracing displays a bidirectional signal with minimal aliasing. Both waveforms show normal systolic upstrokes, bruits and low resistance

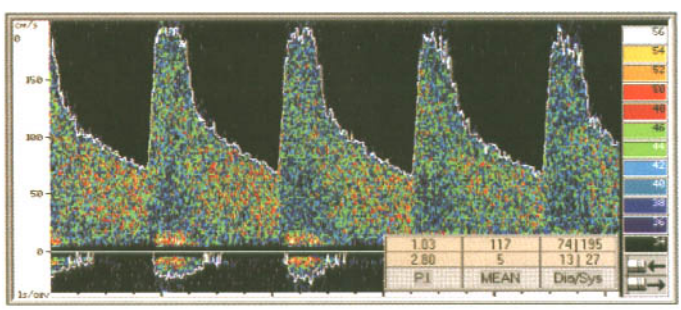

Figure 5.14 A stenotic signal.

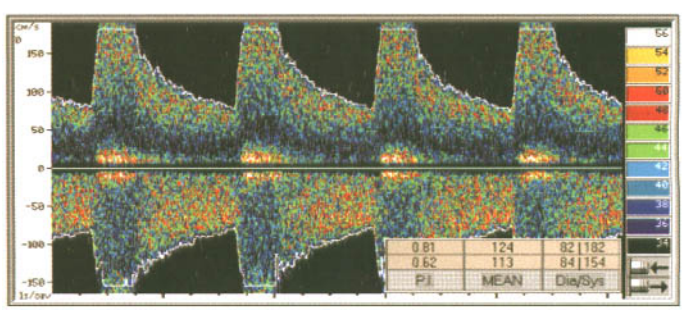

Figure 5.15 Aliasing or optimized signal?

patterns. Envelopes indicate reasonable signal optimization. Other data are needed to determine whether this is a compensatory or stenotic velocity increase.

This recording shows that bidirectional signals with elevated velocities may not be completely separated by adjustment to the maximum velocity scale values, yet both signals are reasonably optimized for measurements. These signals are both abnormal in terms of being above the age-expected velocities, and further adjustments of Doppler setting may insignificantly improve the velocity values obtained at bifurcation. The waveforms were found at the ICA bifurcation contralateral to a complete proximal ICA occlusion mostly indicating laminar flow (note changes in the intensity spectrum of the MCA waveform above baseline) and bruits at bifurcation due to compensatory flow diversion. In acute ischemic stroke, the abrupt development of carotid thrombosis may cause a significant flow diversion and opening of collateral channels. This process may result in acutely elevated velocities in the donor vessels followed by velocity decrease in the subacute and chronic phases when stroke is completed or vessel dilatation is accomplished.

Case history. A 42-year-old woman with subarachnoid hemorrhage (Day 8) (Figure 5.16).

Interpretation. This simultaneous display of four waveforms is due to a large sample volume (or gate) of insonation of 13 mm. Marked as (1), the highest velocities were likely found in a segment with maximal narrowing; (2) shows elevated velocities in another segment with less narrowing; (3) hyperemic signals likely in a proximal vessel; and (4) branch signals.

The differential diagnosis includes the presence of a mirror artifact and hyperemia.

This is a complex recording obtained in a patient with subarachnoid hemorrhage who developed a severe MCA vasospasm. The use of a large (13-mm) sample volume may produce simultaneous display of waveforms detected at different arterial segments (i.e. terminal ICA, proximal M1, mid-M1 MCA or neighboring segments with different patency). Although the highest velocities in waveform (1) are likely attributable to the site of maximum vasospasm (the mean flow velocity of 295 cm/s), the presence of mirror artifact [18] and hyperemia (as a potential cause of it being a bright reflector) should be excluded using the Lindegaard ratio [19]. The signal-to-noise ratio appears to be optimized, i.e. no noise in the background. This patient was on hypertension–hemodilution–hypervolemia (triple H) therapy and hyperemia was mostly ruled out by the Lindegaard ratio of 10 (see also Chapter 6).

Severe stenosis, acute thrombosis and occlusions

Case history. A 65-year-old man with an acute stroke and carotid thrombosis unilateral to the site of insonation (Figure 5.17).

Interpretation. This tracing displays a loud bidirectional bruit with a turbulent high-velocity signal of a stenotic origin. Minimal aliasing is present. The envelope above baseline indicates weak peak systolic tracings that lead to underestimation of the velocity increase.

Similar waveforms can be found at a severe stenosis with turbulent flow when a sample volume is positioned slightly off the vessel segment that has the highest-velocity jet. Remember that the highest-velocity jet can usually be found at the exit of a focal stenosis. By itself, this waveform is already diagnostic, showing that some flow velocities were lost to turbulence and the peak velocity values may be decreasing as disease progresses towards near-occlusion. Velocities taken from such waveforms usually underestimate the highest velocity and this may affect grading the severity of a lesion.

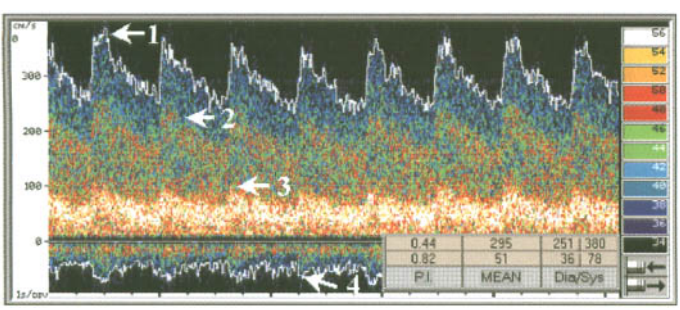

Figure 5.16 Increased velocities, multiple waveforms and severe vasospasm.

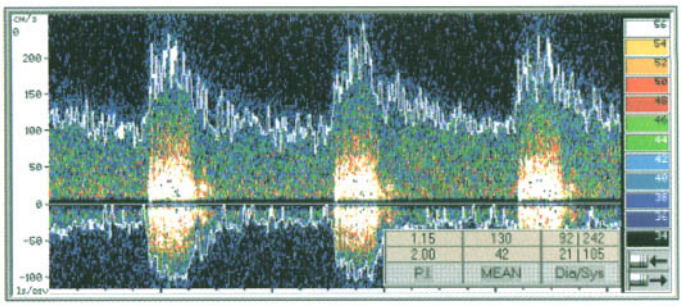

Figure 5.17 Turbulence, bruits and velocity underestimation.

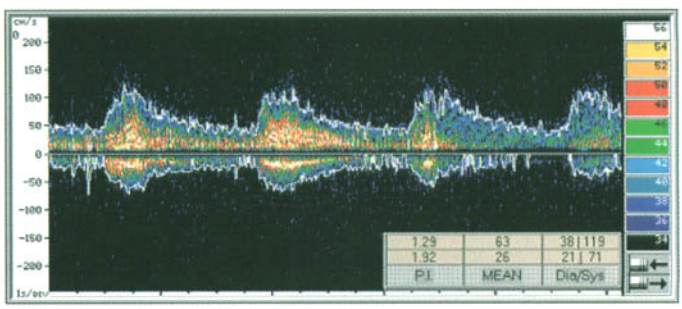

Figure 5.18 Continuous bruit and delayed systolic flow acceleration.

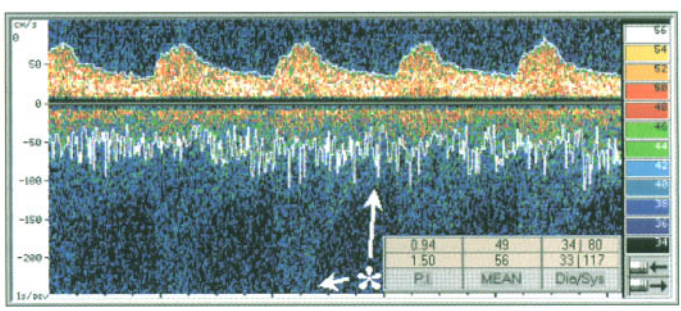

Figure 5.19 A weak signal.

Case history. A 76-year-old man with a recent TIA (Figure 5.18).

Interpretation. This tracing displays a turbulent signal of variable intensity with bidirectional bruits. This waveform can be found in a poststenotic segment. The peak systolic complex is not clearly visualized since a laminar flow profile is not re-established yet [1].

This waveform that contains bruits of variable intensity and incomplete spectral velocity tracing should alert the sonographer to expand the search for the highest-velocity jet and to suspect a subtotal stenosis with bruits of prolonged duration.

Case history. A 71-year-old woman with an ACA territory stroke and a proximal moderate carotid stenosis (Figure 5.19).

Interpretation. This tracing shows a bidirectional signal with a low-resistance waveform above baseline that is optimized and has a slightly delayed systolic upstroke. A high-velocity weak signal below baseline (marked as *) is not optimized since overgaining does not change the signal-to-noise ratio and measurements are erroneous.

This recording shows a weak signal suspicious of a focal velocity increase in a branching vessel (below baseline). If a stenosis is located deep in the intracranial vasculature (i.e. depths of insonation 65 mm or more), sound attenuation and limited pulse repetition frequency may preclude its definition and measurement. Increasing gain may help to visualize the waveform but may be insufficient (as in this case) for automated tracings since the signal-to-noise ratio in a

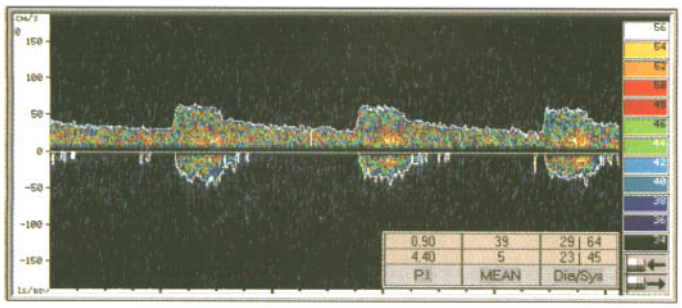

Figure 5.20 A branch occlusion.

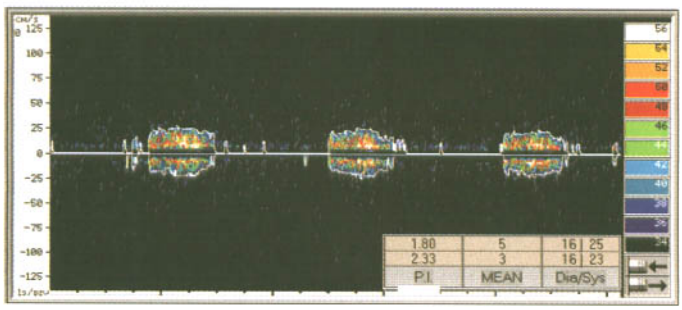

Figure 5.21 A minimal signal (systolic spike).

weak stenotic signal is low and remains unaffected. Reducing the sample volume to focus on this specific signal may also reduce sensitivity of Doppler if burst pressure is reduced. If waveforms presented in this case are detected, use manual measurements to quantify velocity increase. The use of power M-mode-guided TCD spectral assessment may lead to the sites of disturbed signals [20], and the use of contrast-enhanced ultrasound agents [21] may help to avoid this technical problem.

Case history. A 75-year-old man with an M2 MCA occlusion and ICA occlusion (Figure 5.20).

Interpretation. A low-resistance waveform above baseline has a short systolic upstroke and flattened systolic complex. Comparison with a non-affected vessel will help to determine whether this is a blunted or dampened signal (see flow grading criteria in Chapter 10). A high resistance minimal signal below the baseline has no end-diastolic flow.

This recording shows a complex signal that can be obtained in the intracranial vessels at the site of or just proximal to an arterial occlusion, affecting for example the M1–M2 MCA bifurcation. An arterial occlusion can produce a variety of residual flow signals [22] (see Chapter 10 & Part V). These waveforms can be recognized by abnormal appearances of the systolic complex and end-diastolic flow compared to the unaffected side, including absent end-diastolic flow. Nevertheless, changes in flow pulsatility and velocity are often accompanied by signs of flow diversion or compensatory velocity increase, and these findings point to hemodynamic significance of suspected arterial obstruction.

Case history. A 62-year-old woman with an M1 MCA occlusion (Figure 5.21).

Interpretation. This is a minimal bidirectional signal with no end-diastolic flow. This waveform can be representative of a residual flow signal around MCA clot if collaborated by additional findings indicating occlusion at this location. Bruits and vessel intercepting at a nearly 90° angle should be considered as a possible explanation.

This recording shows a systolic spike (or a minimal residual flow signal) obtained at the site of an acute MCA occlusion. In this case, systolic spikes with low velocities and bruit-like appearance are seen followed by periods with no diastolic flow indicating very high resistance to flow and abolishment of brain perfusion, at least during diastole. Generally, flow signals obtained at near-90° angles have some recognizable

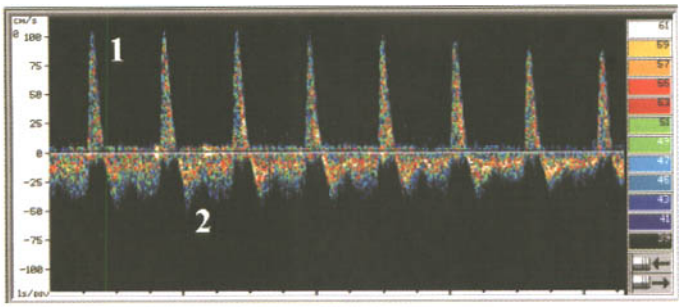

Figure 5.22 An oscillating or reverberating flow signal.

waveform components and the waveforms extending into diastole can be slightly improved by reangulation of a transducer.

Circulatory arrest

Case history. A 41-year-old woman with TBI and clinical progression to brain death (Figure 5.22).

Interpretation. Both waveforms represent an extremely high resistance to flow. Marked as (1), flow signals above baseline represent sharp spikes with abrupt flow deceleration to zero at the time of closure of the aortic valve and no positive end-diastolic flow. Marked as (2), the same blood pool reverses its direction during entire diastole producing the sign of flow reverberation or oscillation.

In this case, an extremely high resistance to flow precludes brain perfusion [15,23–25]. This waveform was observed in a patient who developed massive brain swelling with progression into cerebral circulatory arrest. If reverberating flow is found in both proximal MCAs and the basilar artery, it predicts the absence of brain perfusion that can be demonstrated by nuclear cerebral blood flow studies. Hemodynamically, this waveform indicates that all blood that passed through the sample volume towards the brain in systole was pushed out of the distal vasculature in diastole resulting in no flow passage to brain parenchyma.

References

1 von Reutern GM, Budingen HJ. *Ultrasound Diagnosis of Cerebrovascular Disease.* Stuttgart: Georg Thieme Verlag, 1993: 53–5.

2 Liepsch D. Principles and models of hemodynamics. In: Hennerici M, Meairs S, eds. *Cerebrovascular Ultrasound: Theory, Practice, and Future Developments.* Cambridge: Cambridge University Press, 2001: 27–8.

3 Spencer MP, Reid JM. Quantitation of carotid stenosis with continuous wave Doppler ultrasound. *Stroke* 1979; **10**: 326–30.

4 Giller CA, Bowman G, Dyer H, Mootz L, Krippner W. Cerebral arterial diameters during changes in blood pressure and carbon dioxide during craniotomy. *Neurosurgery* 1993; **32**: 737–42.

5 Kontos HA. Validity of cerebral arterial blood flow calculations from velocity measurements. *Stroke* 1989; **20**: 1–3.

6 Newell DW, Aaslid R, Lam A, Mayberg TS, Winn HR. Comparison of flow and velocity during dynamic autoregulation in humans. *Stroke* 1994; **25**: 793–7.

7 Markus HS, Harrison MJ. Estimation of cerebrovascular reactivity using transcranial Doppler, including the use of breath-holding as the vasodilatory stimulus. *Stroke* 1992; **23**: 668–73.

8 Sivestrini M, Vernieri F, Pasqualetti P, Matteis M, Passarelli F, Troisi E, Caltagirone C. Impaired cerebral vasoreactivity and risk of stroke in patients with asymptomatic carotid stenosis. *JAMA* 2000; **283**: 2122–7.

9 Vernieri F, Pasqualetti P, Matteis M, Passarelli F, Troisi E, Rossini PM, Caltagirone C, Silvestrini M. Effect of collateral blood flow and cerebral vasomotor reactivity on the outcome of carotid artery occlusion. *Stroke* 2001; **32**: 1552–8.

10 Guyton AC. *Textbook of Medical Physiology*, 7th edn. Philadelphia: W.B. Saunders Co, 1986: 230–43.

11 Ringelstein EB, Weiller C, Weckesser M, Weckesser S. Cerebral vasomotor reactivity is significantly reduced in low-flow as compared to thrombo-embolic infarctions: the key role of the circle of Willis. *J Neurol Sci* 1994; **121**: 103–9.

12 von Reutern GM, Budingen HJ. *Ultrasound Diagnosis of Cerebrovascular Disease.* Stuttgart: Georg Thieme Verlag, 1993: 56–62.

13 von Reutern GM, Budingen HJ. *Ultrasound Diagnosis of Cerebrovascular Disease.* Stuttgart: Georg Thieme Verlag, 1993: 52–63.

14 Kidwell CS, el-Saden S, Livshits Z, Martin NA, Glenn TC, Saver JL. Transcranial Doppler indices as a measure of diffuse small-vessel disease. *J Neuroimaging* 2001; **11**: 229–35.

15 Harders A. *Neurosurgical Applications of Transcranial Doppler Sonography*. Wien: Springer-Verlag, 1986: 117.

16 Giller CA, Mathews D, Purdy P, Kopitnik TA, Batjer HH, Samson DS. The transcranial Doppler appearance of acute carotid occlusion. *Ann Neurol* 1992; **31**: 101–3.

17 Edelman SK. *Understanding Ultrasound Physics*, 2nd edn. The Woodlands: ESP, Inc, 1997: 135.

18 Ratanakorn D, Kremkau FM, Myers LG, Meads DB, Tegeler CH. Mirror-image artifact can affect transcranial Doppler interpretation. *J Neuroimaging* 1998; **8**: 175–7.

19 Lindegaard KF, Nornes H, Bakke SJ, Sorteberg W, Nakstad P. Cerebral vasospasm diagnosis by means of angiography and blood velocity measurements. *Acta Neurochir (Wien)* 1989; **100** (1–2): 12–24.

20 Moehring MA, Spencer MP. Power M-mode transcranial Doppler ultrasound and simultaneous single gate spectrogram. *Ultrasound Med Biol* 2002; **28**: 49–57.

21 Ries F, Honisch C, Lambertz M, Schief R. A transpulmonary contrast medium enhances the transcranial Doppler signal in humans. *Stroke* 1993; **24**: 1903–9.

22 Demchuk AM, Burgin WS, Christou I, Felberg RA, Barber PA, Hill MD, Alexandrov AV. Thrombolysis in brain ischemia (TIBI) transcranial Doppler flow grades predict clinical severity, early recovery, and mortality in patients treated with tissue plasminogen activator. *Stroke* 2001; **32**: 89–93.

23 Ropper AH, Kehne SM, Wechsler L. Transcranial Doppler in brain death. *Neurology* 1987; **37**: 1733–5.

24 Petty GW, Mohr JP, Pedley TA, Tatemichi TK, Lennihan L, Duterte DI, Sacco RL. The role of transcranial Doppler in confirming brain death: sensitivity, specificity, and suggestions for performance and interpretation. *Neurology* 1990; **40**: 300–3.

25 Ducrorq X, Hassler W, Moritake K, Newell DW, von Reutern GM, Shiogai T, Smith RR. Consensus opinion on diagnosis of cerebral circulatory arrest using Doppler-sonography. Task Force Group on cerebral death of the Neurosonology Research Group of the World Federation of Neurology. *J Neurol Sci* 1998; **159**: 145–50.

PART III

Criteria for interpretation

This page intentionally left blank

6

CHAPTER 6

Diagnostic criteria for cerebrovascular ultrasound

Andrei V. Alexandrov, MD, RVT & *Marsha M. Neumyer,* BS, RVT

Introduction

Laboratory accreditation, such as that offered by the Intersocietal Commission for the Accreditation of Vascular Laboratories (ICAVL, www.icavl.org), requires documentation and consistent application of the diagnostic criteria for interpretation of cerebrovascular studies [1]. The diagnostic criteria in this chapter represent a summary of previously published criteria for extra- and intracranial ultrasound and those internally generated by the STAT Neurosonology Service, UT-Stroke Treatment Team and the Vascular Laboratory, PennState University College of Medicine, Milton S. Hershey Medical Center. These criteria can be used as a template to establish and accredit a vascular laboratory; however, any ultrasound laboratory should perform local validation of the accepted criteria [1]. We also review pertinent correlative imaging tests and their clinical applicability.

The required *diagnostic criteria for cerebrovascular ultrasound* include [1,2]:

1. normal extracranial and intracranial findings;
2. carotid stenosis and plaque formation;
3. carotid occlusion and dissection;
4. vertebral artery stenosis or occlusion;
5. intracranial arterial stenosis;
6. arterial spasm;
7. hyperemia;
8. collateral flow patterns and flow directions;
9. cerebral embolization;
10. increased intracranial pressure;
11. cerebral circulatory arrest;
12. intracranial arterial occlusion; and
13. subclavian steal syndrome.

Normal extracranial and intracranial findings

Laminar flow

Under normal conditions, when blood flows at a steady rate through a long, smooth vessel, it flows in streamlines, i.e. laminae, or layers, with the fastest-moving cells flowing in the center of the bloodstream [3] (Figure 6.1). Cells adjacent to the arterial wall experience inertial pull and shear stresses [4] as they rub against the wall and cells moving in neighboring layers. Blood flow velocities will be quite slow adjacent to the wall, and both forward and reverse flow can be seen. This velocity gradient and low frequency spectrum is detected when the Doppler sample volume is placed near the vessel wall. Therefore, a sample volume comparable to or larger than vessel diameter can display *spectral broadening* in a normal vessel with laminar and undisturbed flow because the velocity gradient through the entire vessel lumen is sampled (Figure 6.1). For example, all normal transcranial Doppler recordings have spectral broadening since sample volume of ≥ 3 mm covers the entire middle cerebral artery stem. Therefore, we no longer use the term 'spectral broadening' as an independent diagnostic criterion for disease without other direct imaging findings.

Arterial wall pulsation

Systolic ejection of blood occurs at the highest blood pressure, and the arterial wall moves outward during this phase of the cardiac cycle. This expansion of the vessel lumen occurs due to compliance of the vessel wall, and the energy stored in the vessel wall

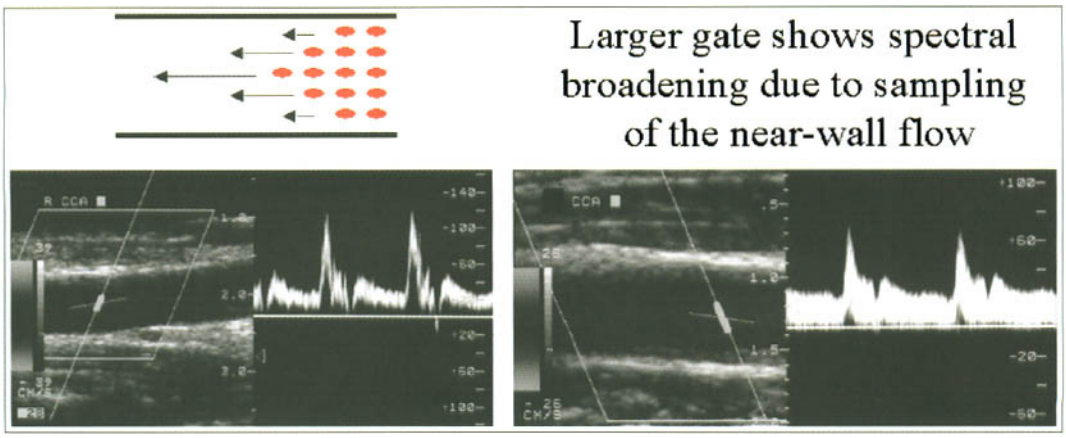

Figure 6.1 Laminar flow. Arrows represent velocity vectors. Faster moving blood is present in the midstream of parabolic flow.

determines the so-called compliance flow [5]. During the deceleration phase of systole, the arterial wall moves inward, forcing the layers closer together. This inward movement and crowding of the cell layers causes the cells to move at a narrow range of velocities in the center stream. During diastole, the resting phase of the cardiac cycle with the lowest blood pressure values, the cells are spinning around, with their movement between layers expressed as a spectrum of low flow velocities. Pressure gradient along the vessel length determines the so-called resistance flow. Therefore, during outward vessel wall pulsation, the laminae move apart, allowing forward flow to occur with little or no disruption. Thus, arterial flow waveforms represent the sum of resistance and compliance flow [5]. Accurate depiction of a disturbance of the arterial wall pulsation on a B-mode image may be the first indirect sign of arterial obstruction.

Normal flow in the common carotid artery

Approximately 80% of the blood flow from the common carotid artery (CCA) will enter the low-resistance vascular circulation of the brain and eye, resulting in 300–400 mL being delivered to the brain via each internal carotid every minute [6]. For this reason, the CCA waveform will largely mimic the flow patterns in the internal carotid artery (ICA). This is evidenced by positive diastolic flow (above the zero baseline) associated with flow to the low-resistance circulation of the ICA. Like the external carotid artery (ECA), the common carotid artery will demonstrate the sharp systolic peak, rapid systolic deceleration and relatively low diastolic flow typical of the high-resistance external carotid artery flow pattern (Figure 6.2).

Normal flow in the internal carotid artery

Due to cerebral autoregulation and low vascular resistance in the brain, the Doppler spectral waveforms from the ICA show a quasi-steady flow pattern with constant forward diastolic flow, also described as a low-resistance flow pattern. There is rapid systolic upstroke, often with somewhat rounded peak at systole, and stepwise deceleration during diastolic runoff. This low-resistance flow pattern can be present even with a high-grade carotid stenosis (Figure 6.2).

Each ICA carries approximately 40% of the total cerebral blood flow volume [6]. The ICA flow stream adjacent to the flow divider will accelerate faster than the ECA and move cephalad throughout the cardiac cycle to meet the demands imposed by cerebral autoregulation. The geometry of the bulb results in retrograde movement of cells toward the opposite wall and oscillatory forward and reverse flow patterns, resulting in separation of the flow stream [7]. Flow is slower on the wall opposite the flow divider and therefore blood particle resident time may be increased, one of the theories supporting the pathophysiology of atherogenesis on the posterolateral wall of the bulb [8] (Figure 6.3).

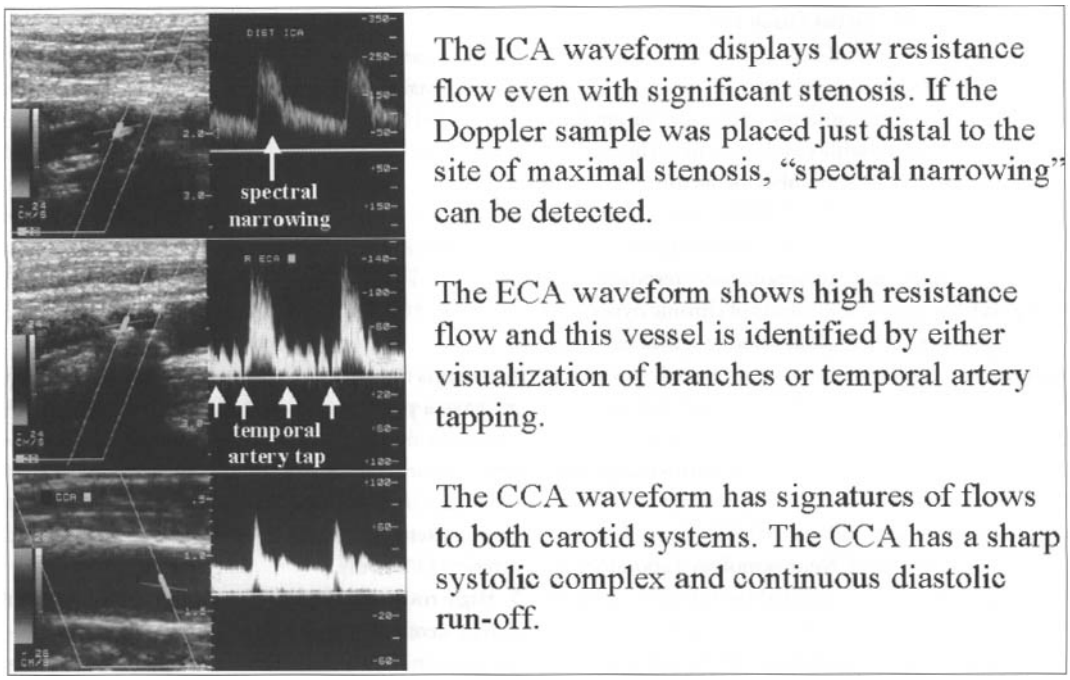

Figure 6.2 Carotid waveforms.

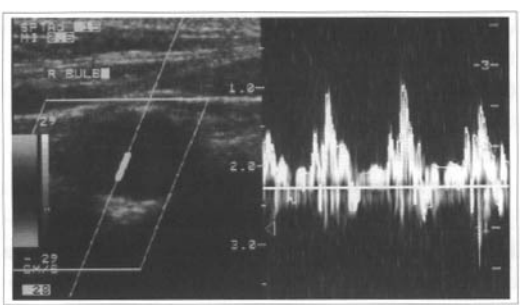

Figure 6.3 Flow separation in the internal carotid artery bulb. Doppler spectrum shows a complex low-frequency waveform with phases of reversed flow direction.

Normal flow in the external carotid artery

The ECA feeds the high-resistance vascular bed of the muscles of the face, forehead and scalp. This high resistance is expressed by the classic signature waveform demonstrating rapid systolic upstroke, rapid deceleration, sometimes with a brief flow reversal during aortic valve closure, and a low diastolic flow velocity. Note that younger individuals may have relatively low-resistance flow signatures in the ECA. The ECA flow waveform changes with rhythmic tapping on the preauricular branch of the temporal artery in most individuals [9] (Figure 6.2). However, we do *not* recommend carotid compression tests to differentiate between the ICA and ECA, nor to determine collateral channels with intracranial examination.

Normal flow in the vertebral artery

The vertebral artery (VA) supplies a low-resistance system of the brainstem and the vessels of posterior cerebral circulation. Both vertebral arteries deliver approximately 20% of total cerebral blood flow [6]. Like the ICAs, the vertebrals also have a low-resistance waveform profile; however, blood flow velocities in the VA are generally lower than in the anterior circulation vessels [6].

Often, there is a marked difference in flow velocities between the two vertebral arteries that may be attributable to dominance and/or hypoplasia of one of the vessels. An atretic vertebral artery may have a more pulsatile waveform with lower flow velocities. It is important to measure arterial blood pressure on both arms, and under normal conditions the difference between arms should not exceed 10 mmHg.

Normal intracranial flow findings

Transcranial Doppler (TCD) or duplex examination may reveal a broad range of findings including different waveforms in the anterior and posterior circulation vessels, flow pulsatility and velocities. This variety can be attributed to a number of factors including the anatomy of the circle of Willis, side differences in the angle of insonation, velocity modulation with breathing cycles and autoregulatory responses, as well as cardiac output and effects of chronic hypertension. Therefore, the absolute velocity values have less significance compared to the abnormal waveform recognition, asymmetry of intracranial findings and interrelationship of flow findings between the vessels.

Previous studies have established normal ranges for TCD measurements and analysed the value of different parameters and indices [10–15]. Based on this information, the STAT Neurosonology Laboratory at the University of Texas adopted the following criteria for *normal transcranial Doppler examination* [2].

1 Good windows of insonation, all proximal arterial segments found. 'Not found' does not mean occluded since atresia of intracranial arterial segments is common as well as suboptimal windows and angles of insonation.

2 Direction of flow and depths of insonation in adults are as shown in Table 6.1.

3 The difference between flow velocities in the homologous arteries is less than 30%: 15% is attributable to the difference in angle of insonation and another 15% to breathing cycles. However, posterior cerebral and vertebral arteries may have 50–100% difference due to dominance, hypoplasia and tortuous course. Similarly, M2 and M1 MCAs may have up to 100% variation in velocity dependent on tortuosity.

4 A normal M1 MCA mean flow velocity (MFV) does not exceed 170 cm/s in children with sickle cell disease and 80 cm/s in adults free of anemia or subarachnoid hemorrhage.

5 A normal velocity ratio: MCA ≥ ACA ≥ siphon ≥ PCA ≥ BA ≥ VA. Velocity values can be equal between these arterial segments or sometimes exceed by 5–10 cm/s, i.e. ACA > MCA, or BA > ICA, likely due to the angle of insonation or common anatomic variations.

6 Patients free of hypertension while breathing room air have a positive end-diastolic flow velocity (EDV) of approximately 25–50% of the peak systolic velocity (PSV) values and a low-resistance pulsatility index (PI) of 0.6–1.1 in all intracranial arteries. A high-resistance flow pattern (PI ≥ 1.2) is seen in the ophthalmic arteries (OAs) only.

7 High-resistance flows (PI ≥ 1.2) can be found in patent cerebral arteries with aging, chronic hypertension and increased cardiac output, and during hyperventilation.

Normal intracranial waveforms were presented in Chapter 5. Figure 6.4 illustrates the range of pulsatility index of Gosling and King [16] that can be found in the arteries supplying the brain. Note that wide variations in the velocity and pulsatility of flow can be found under normal and abnormal circulatory conditions.

Besides PI, the resistance to flow can be expressed using the resistance index (RI) described by Pourcellot [17]. This index is calculated as the ratio of (PSV – EDV)/PSV with normal values below 0.75. There is a controversy as to which index better describes the

Table 6.1 Normal depth, direction and mean flow velocities at assumed 0° angle of insonation of the arteries of the circle of Willis.

Artery	*Depth (mm)*	*Direction*	*Children**	*Adults*
M2 middle cerebral artery	30–45	Bidirectional	< 170 cm/s	< 80 cm/s
M1 middle cerebral artery	45–65	Towards	< 170 cm/s	< 80 cm/s
A1 anterior cerebral artery	62–75	Away	< 150 cm/s	< 80 cm/s
A2 anterior cerebral artery†	45–65	Towards	N/A	< 80 cm/s
Internal carotid artery siphon	60–64	Bidirectional	< 130 cm/s	< 70 cm/s
Ophthalmic artery	50–62	Towards	Variable	Variable
Posterior cerebral artery	60–68	Bidirectional	< 100 cm/s	< 60 cm/s
Basilar artery	80–100+	Away	< 100 cm/s	< 60 cm/s
Vertebral artery	45–80	Away	< 80 cm/s	< 50 cm/s

* Values are given for children with sickle cell anemia.

† A2 ACA can be found through the frontal windows with transcranial color-coded sonography (TCCS) in select patients [19].

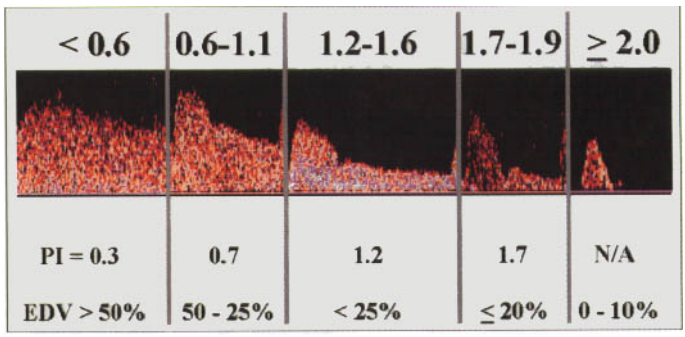

Figure 6.4 Pulsatility index (Gosling). PI = (PSV – EDV)/MFV. Normotensive individuals have PIs in the range of 0.6–1.1 while breathing room air.

Table 6.2 The risk of stroke and the severity of carotid stenosis in symptomatic patients in the NASCET trial [21].

*ICA stenosis (%)**	*Medical group (%)*	*Surgical group (%)*	*NNT*
70–99	26.1	12.9	8
50–69	22.2	15.7	15
< 50	18.7	14.9	26

* ICA stenosis is expressed as percentage diameter reduction of the residual lumen on digital subtraction angiography measured by the North American (N) method.
Medical group received antiplatelet therapy to prevent stroke; surgical group underwent carotid endarterectomy within 6 months after transient ischemic attack or minor stroke.
NNT, number of patients needed to treat to prevent one stroke.

resistance to flow since PI may be more influenced by cardiac output while RI is more reflective of the distal resistance [18]. We prefer to use mostly the pulsatility index since at our laboratory we have validated our criteria for a broad range of PI values.

Carotid stenosis and plaque formation

The risk of ischemic stroke increases proportionately to the severity of carotid stenosis (Table 6.2), and randomized carotid endarterectomy (CEA) clinical trials have shown that patients with severe carotid stenosis benefit from CEA combined with medical therapy compared to medical therapy alone [20–22].

Since less invasive interventions to prevent stroke such as angioplasty and stenting are emerging [23], it is extremely important to carefully apply the results of the clinical trials into practice to minimize risks associated with CEA. These steps include risk factor assessment and application of the specific methods of measuring carotid stenosis in patient selection for surgery. In clinical practice and laboratory accreditation, angiography is used as a gold standard for evaluation of ultrasound performance and sonographers should be familiar with its methods and pitfalls.

In reality, surgeons may select patients based on carotid duplex results alone without angiographic control [24]. These ultrasound laboratories have to rely on stenosis assessment by a surgeon who determines the residual lumen size during plaque removal and this information is often submitted for accreditation without standardized methods of measuring percentage stenosis. In fact, the true standard for measuring anatomic arterial stenosis is the planimetry of an atherosclerotic plaque removed *en bloc* at surgery [25,26] (Figure 6.5). Although impractical in the clinical setting, this standard is used as a research tool providing the measurement of carotid stenosis and plaque composition.

To perform carotid plaque planimetry [25], the specimen is placed in formalin, which decalcifies the plaque and induces uniform shrinkage by 11–13%. Then the plaque is fixed and sliced into transverse cuts to visualize the plaque internal structure and the residual lumen (Figure 6.5). The area of the tightest residual lumen (S_1) and the area of the entire lumen (S_2) are measured using software for calculation of the

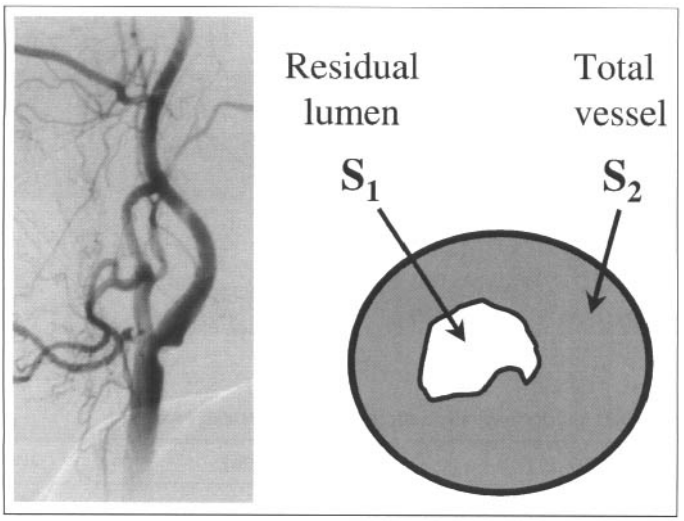

Figure 6.5 Digital subtraction angiography and plaque planimetry. S_1 is the area of the tightest residual lumen, and S_2 is the area of the entire plaque cross-section.

area of irregular-shaped objects. The anatomic stenosis is calculated using the formula:

$$\text{stenosis} = (1 - S_1/S_2) \times 100\%.$$

This method was employed in validation studies to assess the accuracy of digital subtraction angiography (DSA) and ultrasound for measuring carotid stenosis [25,26]. Overall, DSA tends to underestimate anatomic stenosis when angiographic measurements are compared to plaque planimetry [25,26].

The advantages of carotid plaque planimetry include accurate assessment of the *area,* or anatomic stenosis; and direct visualization of plaque surface configuration and its internal structure. To its disadvantage, the method is time-consuming, and it provides a post factum measurement of the stenosis.

Carotid stenosis measured by angiography

Randomized trials [20–22] used DSA as the diagnostic test to measure the degree of carotid stenosis expressed as the percentage *linear diameter* reduction of the vessel determined by strict and specific methods. To apply these methods, only one view of the tightest residual lumen (d) should be selected and the measurement sites (n) should be chosen differently for each method (Figure 6.6). The stenosis is calculated using the formula:

$$\text{ICA diameter reduction} = (1 - d/n) \times 100\%,$$

where d and n are the diameter measurements made on a hard copy in mm.

The *North American (N) method, or the 'distal' degree of stenosis,* was used in the Asymptomatic Carotid Atherosclerosis Study (ACAS) and the North American Symptomatic Carotid Endarterectomy Trial (NASCET) and refers to the distal ICA as the denominator n [27]. The measurement is made using a jeweler's eye-piece and calipers at the segment of the far-distal ICA with parallel walls beyond poststenotic dilatation (Figure 6.6).

The advantages of the N method include: its widespread use; the availability of validated diagnostic criteria for ultrasound screening; and firm prognostic data regarding the risk of stroke and benefit of CEA [28]. The disadvantages include: the underestimation of the degree of carotid stenosis by 15–25% compared to other angiographic methods and area estimates; the interobserver variability of up to 30% for the values determined for the same angiogram; and the distal ICA disease or collapse and its obscuration with ECA branches in 10–20% of consecutive angiograms [28].

The *European (E) method, or the 'local' degree of stenosis,* was employed in the European Carotid Surgery Trial (ECST) and requires drawing an imaginary outline of the ICA bulb to estimate the normal dimensions of the vessel at the site of the tightest narrowing [21]. Although there is no objective way to decide where exactly the normal vessel wall is supposed to be on the DSA image, the E method has a

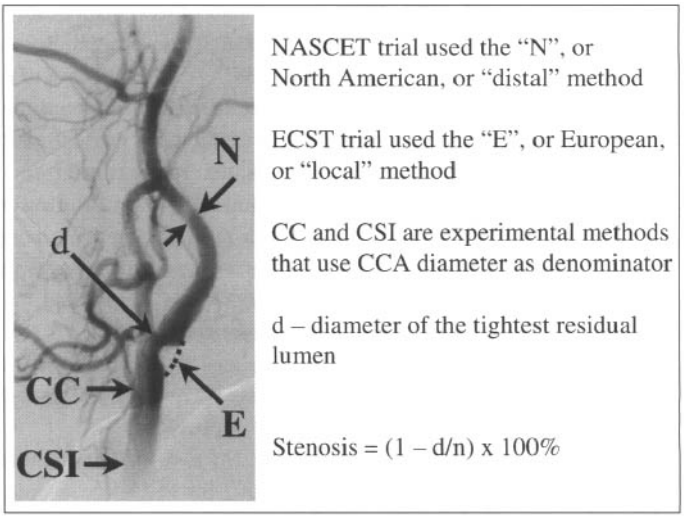

Figure 6.6 Angiographic methods of measuring carotid stenosis.

good reproducibility between experienced observers and provides stenosis values closer to anatomic stenosis than the N method. For instance, a 70% N stenosis is equal to 84% E stenosis and 90% area stenosis [25]. This is largely due to the fact that ICA bulb diameter estimate is greater than the diameter of the distal ICA in the normal vessel and its segment beyond the stenosis (Figure 6.6).

The advantages of the E method include: a good reproducibility despite its subjective nature; estimation of the stenosis closer to area values; widespread use; and firm prognostic data regarding the risk of stroke and benefit of CEA [28]. The disadvantages include: the subjective nature (guesswork) of the bulb diameter estimation; and dependency on the interpreter's experience [28].

The *common carotid (C) method* was developed to avoid the subjective nature of the E measurement [29]. The denominator *n* is derived from the disease-free distal CCA diameter which is usually well opacified and unobscured by arterial branches (Figure 6.6). In cases where the distal CCA is diseased, the CCA 3–5 cm proximal to the bifurcation may be used [30] to estimate the widest normal ICA bulb diameter (ICA bulb = 1.18 proximal CCA diameter) [31]. Both CCA sites [29,30] offer comparable diameter reduction estimates.

The advantages of the C method are: the reliability of the CCA as the measurement site since it is rarely (< 3%) affected by atherosclerosis; values close to the E method and area stenosis; the discrepancy between observers is the lowest (< 15%); and it is applicable to most consecutive angiograms [28,30]. The disadvantages include: infrequent use; fewer prognostic data available [29]; and only a few correlations with ultrasound are available [32].

These methods of measuring carotid stenosis represent indices rather than a precise measurement of disease severity since they are based on the diameter reduction estimates derived from only one angiographic projection. The residual lumen asymmetry is most common with mild to moderate carotid stenoses which, together with imaging artifacts and operator dependency, account for most of the discrepancies with other imaging modalities. Agreement between all three angiographic methods can be achieved [29], and the percentage stenosis measurements are the closest for the high-grade carotid stenoses [33]. Before magnetic resonance angiography (MRA), contrast-enhanced CT angiography (CTA) and ultrasound can supplant DSA, these imaging modalities have to be compared against DSA [34–36] to ensure that a non-invasive work-up allows prediction of the specific DSA stenosis measurements with a clinically acceptable level of accuracy relevant to the equipment and observers employed. It is necessary to perform this self-assessment validation study at each individual institution for MRA and CTA as well as for ultrasound.

Although the same methods of measuring carotid stenosis can be applied to non-invasive angiographic images, tight and tortuous residual lumen, turbulence and slow near-wall and poststenotic flows can

produce artifacts with MRA. MRA overestimates the degree of carotid stenosis compared to DSA when both are measured by the same method [34,35].

The discrepancy increases with moderate to mild carotid stenoses and arises from the differences in the residual lumen and turbulent flow visualization. The presence of a flow signal void due to turbulence or slow flow may lead to underestimation of the residual lumen with MRA, thus increasing the ratio with the local or distal denominator. However, a flow 'gap' (which appears as a segment of the vessel completely free of signal with reappearance of the signal distally) indicates greater than 60% N stenosis with sensitivity of 91% and specificity of 97% [37]. Further improvement in image resolution is necessary for MRA to achieve the precision comparable to that of DSA in measuring the residual lumen and normal vessel diameters. Despite these shortcomings, the meta-analysis of published series [38] showed that MRA has sensitivities of 0.82–0.86, specificities of 0.89–0.94, and the composite receiver–operator curve (ROC) areas of 0.91–0.92 similar to that of ultrasound when compared to DSA. MRA offers an advantage of a complete extra- and intracranial examination compared to ultrasound. A combination of carotid ultrasound and MRA is safe and it has sufficient accuracy compared to DSA in patient selection for CEA [39]. Since most outpatients with a history of transient ischemic attack undergo MRI/MRA, a combination of non-invasive screening with ultrasound and MRA appears the most common clinical pathway for patient selection. In laboratories with validated and accurate ultrasound screening, MRA offers minimal additional information for measuring the proximal ICA stenosis [40]. Some physicians reserve the use of DSA only for patients with discrepant ultrasound and MRA results.

The agreement between CTA and DSA in quantifying the degree of carotid stenosis was about 80–95% [41–43]. The limiting factors are plaque calcification, the thickness of tissue slices and imaging artifacts. Interpretation of CTA relies on good quality three-dimensional reconstruction and expertise in reading two-dimensional source images. In addition to MRA and CTA, ultrasound helps to determine extent and composition of atheromatous plaque, and offers a non-invasive real-time tool for patient follow-up. The advantages of both MRA and CTA include non-invasiveness; repeatability; and lower costs compared to DSA. The disadvantages include: imaging artifacts; inapplicability in selected patients; interinterpreter variability; overestimation of the carotid stenosis; and lack of validation in randomized trials. With these shortcomings, a local validation of the non-invasive angiographic techniques is as desirable as the quality control for ultrasound screening. The caveats in measuring carotid stenosis are known [44], and strict requirements for research study analysis [45] and everyday measurement and reporting [27] should be followed.

Carotid stenosis measured by ultrasound

B-mode imaging of carotid plaques

B-mode imaging was applied to evaluate patients with carotid disease to directly visualize plaque burden [46]. Using B-mode, a normal arterial wall can be visualized and early stages of carotid atherosclerosis can be detected, including intimal–medial thickening (IMT), fatty streak or soft plaques (Figure 6.7), and small non-stenosing plaques (Figure 6.8). As the plaque grows, it protrudes into the vessel lumen and the percentage diameter reduction of the vessel can be measured in the absence of shadowing and if the near-wall positioning of the sound beam is avoided. Percentage diameter reduction can be best measured on the longitudinal views in the presence of a plaque that causes less than 50% diameter reduction. The

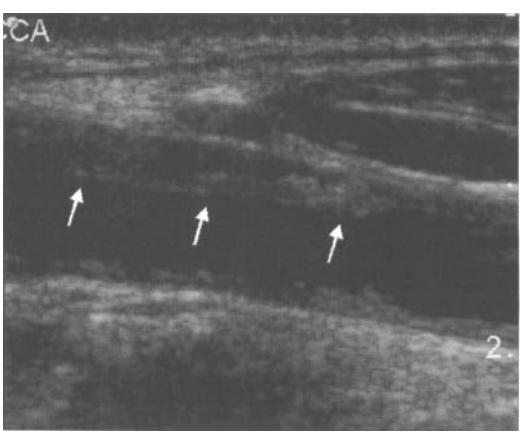

Figure 6.7 Diffiuse thickening of the intima–media complex, hypoechoic plaque or fatty streak. The B-mode image shows early signs of atheromatous disease affecting distal common carotid artery. Arrows show subintimal lipid deposits that form so-called 'fatty streak'.

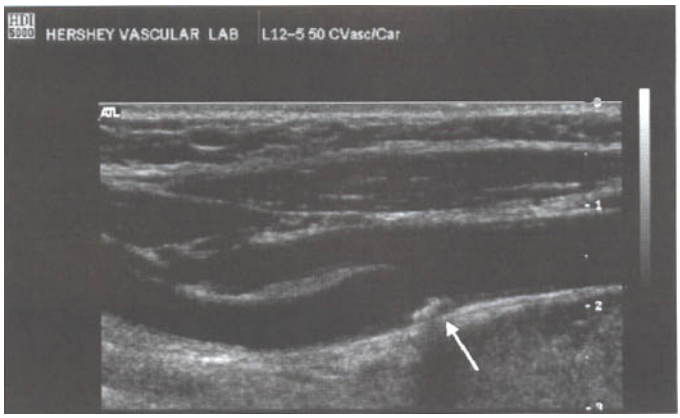

Figure 6.8 Non-stenosing plaque. A high-resolution B-mode scan of the bifurcation shows a small round plaque at the internal carotid artery origin that slightly elevates intima likely without causing any significant stenosis. This finding needs to be confirmed by color flow imaging and Doppler examination.

longitudinal views have to be compared with cross-sectional views to avoid false-positive results with near-wall beam position and overestimation of plaque protrusion. Validation studies and the impact of B-mode measurements were summarized in a consensus statement [47].

When plaque is documented, the morphology of the lesions can be characterized based on acoustic properties on a B-mode image. A *plaque description* in the report should include its:

1 location;
2 length;
3 composition; and
4 surface of the lesion.

Plaque *location* and length are given in the context of the artery or segments affected, including the length of the plaque in cm. Plaques longer than 2 cm, particularly with extensive shadowing, may lead to difficulties with grading severity of carotid stenosis since the velocity is inversely proportionate to the lesion length.

Plaque *composition* is assessed for its:

1 echogenicity (brightness);
2 texture;
3 extent; and
4 edges.

Plaque echogenicity can be described using a variety of terms and, recently, computer-assisted techniques were tested to minimize interobserver discrepancies [48–59]. To ensure consistent grading of plaque echogenicity, the B-mode image should be optimized so that the patent segment of the vessel that contains moving blood should be dark and have no reflections between the vessel walls. Color information should be discarded due to B-mode/color trade-off and particularly if a digital analysis of the image is sought. If the echoes are uniform throughout all regions of the plaque, it is considered to be acoustically homogeneous (Figure 6.9). A heterogeneous plaque has mixed areas of brightness and variations in texture (Figure 6.10). B-mode imaging is ideally suited to determine whether or not atherosclerotic plaques are acoustically homogeneous or heterogeneous.

Clearly, *homogeneous* plaques are most likely to be purely cellular in nature with little evidence of complication as determined by the presence of calcification, significant cholesterol deposition or hemorrhage. These lesions are commonly associated with intimal hyperplasia.

The presence of an acoustically *heterogeneous* plaque, however, signifies that the atherosclerotic process has become complicated. The difficulty remains in determining the correlation between heterogeneous plaques as identified by B-mode ultrasound and their ability to subsequently produce stroke symptoms. A heterogeneous plaque, without acoustic shadowing, most commonly signifies a fibrofatty lesion. The presence of calcifications usually leads to shadowing (Figure 6.10).

Fischer [59] describes *pathologic changes* that occur in carotid atherosclerotic plaques as:

1 neovascularity;
2 calcification;
3 intraplaque hemorrhage;
4 ulceration; and
5 thrombosis.

Ultrasound assessment of heterogeneous plaque provides evidence for some of these processes. As plaques age and organize, they may acquire calcium

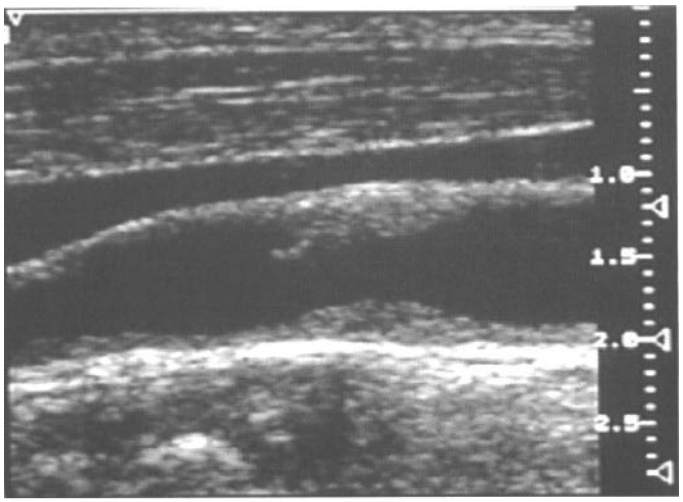

Figure 6.9 Homogeneous plaque. A concentric plaque is present on both sides of the longitudinal arterial projection. Plaque texture is uniform through its length and is moderately echogenic.

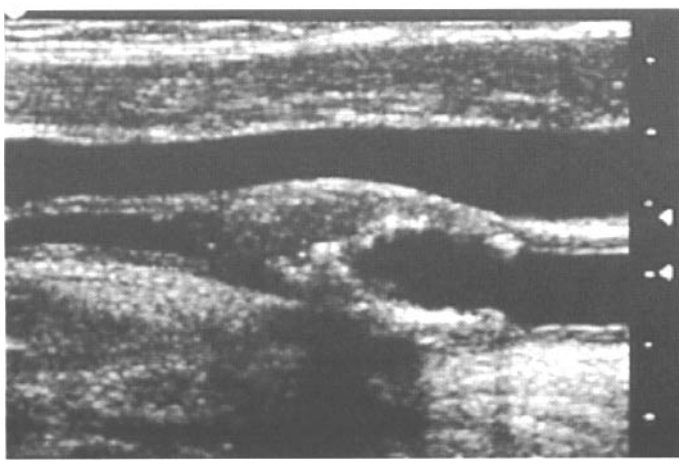

Figure 6.10 Heterogeneous plaque. The B-mode image of the internal carotid artery (ICA) bulb shows a plaque with areas of increased and decreased echogenicity as well as shadowing at the distal wall. Plaque appearance may also produce an impression of a concentric lesion or complete occlusion. This image can be caused by a plaque of only mild or low moderate stenosis since the imaging plane shows near-wall structures in the ICA bulb. Note that the distal ICA walls are not parallel (out of the image plane).

deposits that reflect ultrasound resulting in acoustic shadowing. This may prevent visualization of the arterial segment lying beneath the shadow. Anechoic or hypoechoic regions within the plaque may represent hemorrhage, lipid deposits or necrotic regions [60], and a hypoechoic plaque may predict higher risk of stroke independently of the degree of carotid stenosis [49,51,53,55]. The higher the degree of carotid stenosis, the more likely the plaque will appear heterogeneous and almost all pathologic changes can be present [59].

The *surface* of plaques can be characterized as smooth or irregular. Surface irregularity on ultrasound may suggest potential ulceration [61] and thrombogenic surface by exposing the lipid core to blood flow [59]. Characterization of the surface of lesions requires assessment at multiple image angles. It is difficult to visualize the plaque surface of a heterogeneous [62,63] and low echogenic plaque, even using the edge-enhancing techniques or gray-scale median [64]. The application of color [65,66] or B-flow or power Doppler [67] may help to delineate the residual lumen, but a trade-off between the color flow and B-mode imaging may preclude precise measurements and may fail to identify ulcerations [68]. Another uncertainty arises when slow flow or flow reversal are seen along the edges of a long and irregular plaque. This may be attributable to poststenotic dilatation or large ulceration with a crater filled with moving blood. Therefore, there is little correlation between angiographic, ultrasonographic and pathomorphologic definition of plaque ulceration [60,62,69]. Several

factors affect this agreement, including definitions and size of ulceration, superimposed thrombi and image projection. While in certain circumstances B-mode ultrasound may also be useful for identifying areas of loss of endothelial integrity, the highly subjective nature of this observation renders it unsatisfactory for routine use. Future applications include three-dimensional and four-dimensional real-time ultrasound measurements of plaque mobility and flow interfaces [70,71].

The advantages of B-mode grading of the carotid stenosis include the quantification of early atherosclerotic changes; visualization of the plaque structure and extent; and the possibility of 'on-site' diameter reduction measurements (the site similar to the E method). The disadvantages include common imaging artifacts (inappropriate gain settings, shadowing due to calcium deposition and scattering); and the inability to differentiate fresh clot from moving blood.

Color-coded flow imaging of carotid stenosis

Color Doppler flow imaging (CDFI) can help to identify vascular structures and the residual lumen [72,73]. However, CDFI alone should *not* be used for grading carotid stenosis since it displays the mean frequency shift and is therefore more prone to aliasing with inappropriate velocity scale settings (Figure 6.11) compared to angle-corrected velocimetry. On transverse images, CDFI can also demonstrate the residual lumen and area stenosis [66,74], but precise measurements are difficult due to the same trade-off between the gray-scale and color flow imaging modes as well as the sound scattering at vessel walls. The dimension of color flow residual lumen changes significantly between systole and diastole. CDFI is used to identify vessel abnormalities and the tightest residual lumen, and to adjust the Doppler angle for pulse-wave velocimetry [72,75]. Power mode can also be used for the same purposes and may offer an advantage of flow display regardless of its direction and velocity values [76] (Figure 6.12).

Angle-corrected Doppler velocimetry in carotid stenosis

The velocity is inversely proportionate to the radius of the residual lumen, stenosis length, blood viscosity and peripheral resistance [77,78]. The peak systolic velocity (PSV) is inversely proportionate to the linear, squared and cubic functions of the residual lumen radius [32], resulting in a complex polynomial curve of the third order which demonstrates this relationship (Figure 6.13). The ICA velocity starts to slowly increase when the carotid atheroma reduces the residual lumen diameter by 15–30% and the area by 30% or more [32,77,78]. However, only when atheroma results in a 50% diameter reduction of the ICA, focal flow disturbance is associated with the angle-corrected PSV of ≥ 125 cm/s (or frequency shift equal to or greater than 4 kHz) in the residual lumen [47, 77] (Table 6.3). This frequency/velocity threshold is commonly used in various criteria for grading carotid stenosis and may be modified if collateralization of flow is present [79,80].

Further velocity increase compensates for blood flow volume until it reaches approximately 60–80% diameter or 84–90% area stenosis (Figure 6.13). Typical changes in systolic and diastolic velocities as well as Doppler spectra are shown in Figure 6.14.

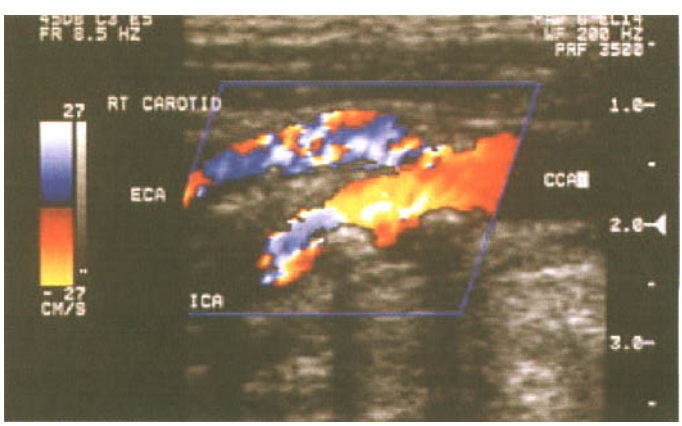

Figure 6.11 Color Doppler flow image of internal carotid artery stenosis. The velocity scale settings are low, leading to aliasing at multiple sites. However, relatively low PRF allows better delineation of plaque edges and the color flow appearance can guide the angle-corrected Doppler velocimetry.

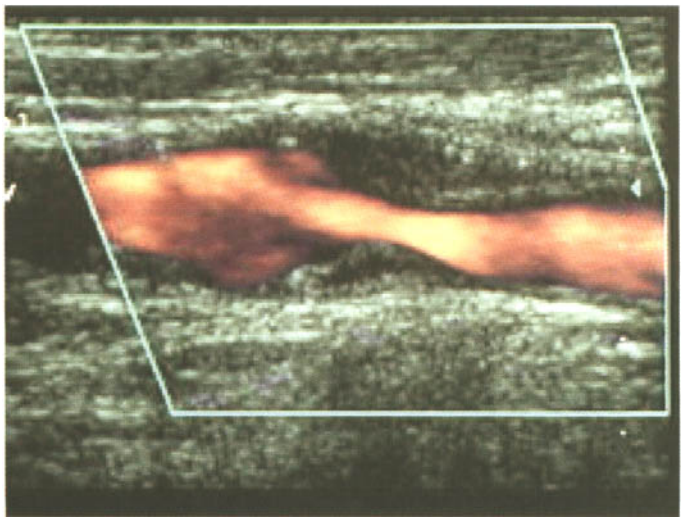

Figure 6.12 Power-mode image of carotid stenosis. This image illustrates the change in vessel diameter and flow orientation along the stenosis and in the poststenotic area. The power image identifies the exit from the stenosis where the angle-corrected Doppler velocimetry should yield the highest velocity values.

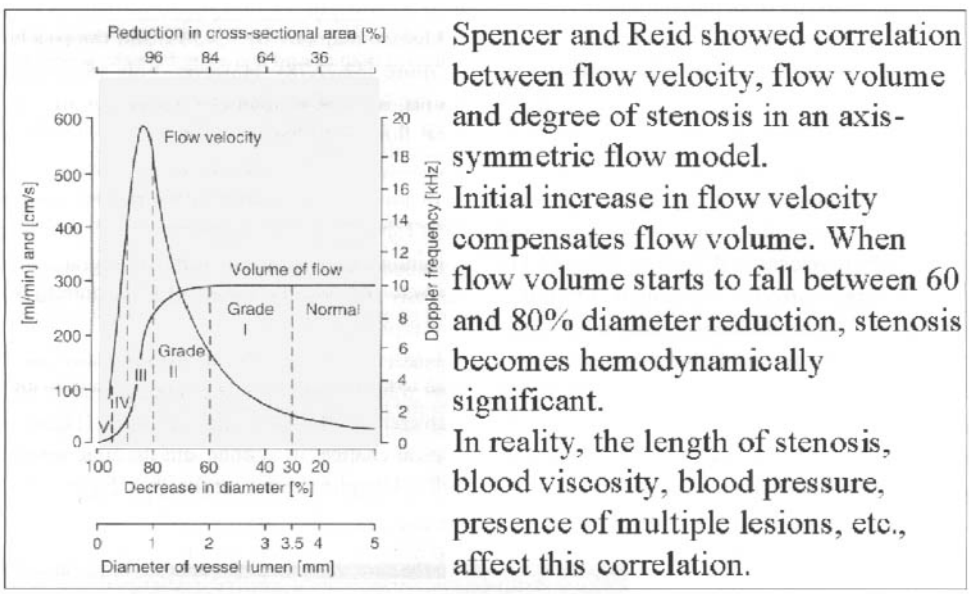

Figure 6.13 The relationship between arterial stenosis, flow and velocity.

Besides the diameter reduction, the axis asymmetry and length of the stenosis will result in flow volume reduction along the path of the lesion, and will determine the hemodynamic significance of the stenosis [77]. Therefore, although uncommon, flow volume reduction may occur with elongated stenoses of less than 70% (diameter measurements). Decreasing flow volume through a long and resistant lesion is responsible for the secondary and indirect flow changes, such as velocity deceleration, blunting of a poststenotic waveform and development of collaterals.

The advantages of Doppler velocimetry include: the direct physiologic measurement of flow acceleration at the stenosis site; its widespread use; and the availability of validated diagnostic criteria. The disadvantages include: operator dependency (angle of insonation, experience); velocity changes due to cardiac output, bilateral stenoses, flow volume reduction,

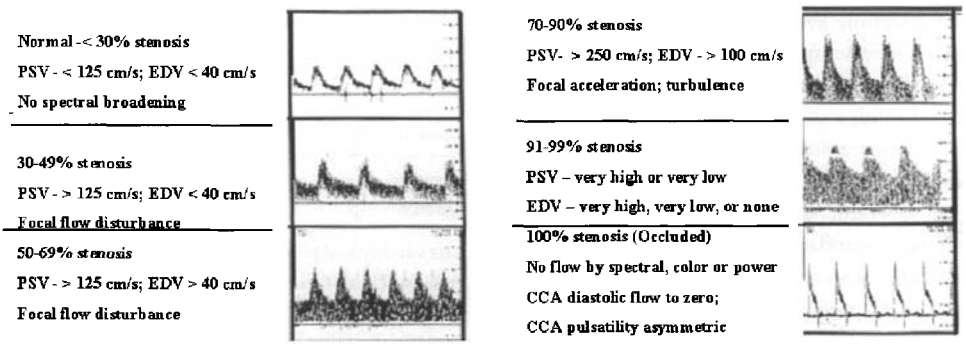

Figure 6.14 Peak systolic, diastolic and Doppler spectra with varying degrees of carotid stenosis. These criteria were developed and validated at the Vascular Laboratory, Hershey Medical Center.

Table 6.3 The Society of Radiologists in Ultrasound Consensus Criteria for Carotid Stenosis. Panelists included: Andrei Alexandrov, J. Dennis Baker, Carol Benson, Edward Bluth, Barbara Caroll, Michael Eliasziw, John Gocke, Edward Grant (Chairman), Barbara Hertzberg, Gregory Moneta, Laurence Needleman, Sandra Katanick, John Pellerito, Joseph Polak, Kenneth Roll, Douglas Wooster, Eugene Zeirler.

Stenosis range N method	*ICA PSV*	*ICA/CCA PSV ratio*	*ICA EDV*	*Plaque*
Normal	< 125 cm/s	< 2.0	< 40 cm/s	None
< 50%	< 125 cm/s	< 2.0	< 40 cm/s	< 50% diameter reduction
50–69%	125–230 cm/s	2.0–4.0	40–100 cm/s	≥ 50% diameter reduction
70–near occlusion	> 230 cm/s	> 4.0	> 100 cm/s	≥ 50% diameter reduction
Near occlusion	May be low or undetectable	Variable	Variable	Significant, detectable lumen
Occlusion	Undetectable	Not applicable	Not applicable	Significant, no detectable lumen

etc.; and equipment dependency (carrier frequency, beam geometry, etc.).

The peak systolic velocity (PSV) is mainly a function of the radius of the residual lumen as well as length of the stenosis and cardiac output. A variety of circulatory conditions influence the flow volume and velocity in CCA and ICA. In practice, individual variations of PSV and their influence on grading carotid stenosis can be reduced if the highest peak systolic velocities in the ICA and CCA are used to calculate the ICA/CCA PSV ratio [81]. The highest PSV, color flow definition of the residual lumen and ICA/CCA ratio, followed by the B-mode findings, form the basis for ultrasound grading of carotid stenosis [47,82–87].

Society of Radiologists in Ultrasound consensus criteria for carotid stenosis measurements with duplex

A multidisciplinary panel of experts was invited by the Society of Radiologists in Ultrasound to attend a 2002 consensus conference on diagnostic criteria to grade carotid stenosis with duplex ultrasound. The Consensus Panel determined a set of criteria most suitable for grading a focal stenosis in the proximal ICA (Table 6.3). It is recommended to use these criteria if a laboratory is new and seeking a set of most applicable criteria for prospective validation. If a laboratory has previously developed a set of their own criteria, validated them and continues to successfully use them in clinical practice, then there is no need to change diagnostic criteria.

Validation of ultrasound measurements of carotid stenosis

The three validated criteria for greater than 50% N carotid stenosis include [47]:

1 maximum peak systolic velocity (PSV) or Doppler frequency shift;
2 ICA/CCA ratio; and
3 B-mode measurements of diameter reduction.

These criteria were validated in several studies with good and excellent accuracy parameters [47]. This fact may partly be attributable to a publication bias

towards carefully evaluated series, and the reported accuracies may not necessarily reflect the performance of these criteria in common practice. Nevertheless, published validity of these criteria and the experience of many sonographers indicate that an accurate and consistent grading of the carotid stenosis is possible if both the operator and technical aspects of vascular imaging are standardized through a prospectively established protocol and ongoing quality control.

In order *to locally apply any published criteria*, the following information should be available from the source:

1 type of equipment;
2 carrier frequency for Doppler velocimetry, i.e. 4–7 MHz;
3 scanning parameters such as pulse repetition frequency set at the highest value; sample volume of 1.5 mm; high pass filters used to detect slow poststenotic flow and maximum frequencies in severe stenosis, i.e. 50 and 100 Hz; Doppler angle equal to or less than 60°;
4 angiographic method of imaging as gold standard, i.e. DSA, MRA or CTA;
5 measurement method employed, i.e. N, E or C methods; or residual lumen measurements during CEA.

To locally validate any diagnostic criteria, a comparison of the screening test (ultrasound) against the best available gold standard (i.e. DSA) must be made (Table 6.4), and the sensitivity, specificity and positive and negative predictive values should be calculated using the following formulae:

$$\text{sensitivity} = (A/A + C) \times 100\%;$$

$$\text{specificity} = (D/D + B) \times 100\%;$$

$$\text{positive predictive value} = (A/A + B) \times 100\%;$$

$$\text{negative predictive value} = (D/D + C) \times 100\%;$$

$$\text{accuracy} = (A + D)/(A + B + C + D) \times 100\%;$$

where A, B, C and D are given in Table 6.4. As a rule, ultrasound and angiography should be performed closely in time to avoid the influence of intraplaque hemorrhage, thrombosis or stenosis regression. The interpreters should be 'blinded' to the results of another test and ideally a prospective data collection needs to be employed.

A more precise validation may require an ROC analysis [83] which examines the trade-off between sensitivity and specificity for certain diagnostic thresholds. For example, a low PSV threshold of 4 kHz will have the best sensitivity of > 95% but a poor specificity of < 70% to predict > 50% N stenosis. A high PSV threshold of > 8 kHz for the same degree of stenosis will have moderate sensitivity of approximately 80% but the highest specificity exceeding 95%. Similar correlations are applicable to PSV thresholds expressed in cm/s [82]. Usually at least 100 observations (two measurements of the left and right carotids per patient) are required for this analysis and, to further avoid biases, measurements that represent mild, moderate and severe carotid stenoses are necessary. In the landmark studies [82,83], the PSV and ICA/CCA ratio thresholds were determined for > 70% N stenosis and, to translate the final results from the NASCET trial, additional ultrasound criteria for stenoses greater than 50% diameter reduction compared to the distal ICA should also be employed [47,86]. Note that the 50% N stenosis corresponds to 70–75% E or C stenosis.

Table 6.4 A 2 × 2 table for the calculation of accuracy parameters.

	Diagnostic test	
Screening test	*Disease +*	*Disease –*
Disease +	A	B
Disease –	C	D

The validity and predictive value of the screening test against the best available gold standard are calculated from true-postitive (A), false-positive (B), false-negative (C) and true-negative (D) values (see the text for formulas).

Validation of ultrasound criteria for different scanners

This kind of validation study is particularly difficult since different scanners used in the same laboratory have different Doppler carrying frequencies and transducer configurations [88]. The steps to validate criteria for different scanners should include:

1 identifying the reference scanner (usually the most used or previously validated machine);
2 establishing velocity difference between the scanners (use the same patient and normal controls);
3 establishing consistent scanning protocol between users and scanners;
4 prospectively comparing several studies obtained on each scanner to angiography;
5 making adjustments to local diagnostic criteria, if necessary.

These validation steps are particularly important in the laboratories with multiple sonographers and scanners. Technical supervision by a senior sonographer should provide ongoing quality control of scanning protocols and improvement of scanning techniques of new sonographers.

Since ultrasound results change with different equipment and variable circulatory conditions, diagnostic criteria should encompass prediction of the stenosis range, i.e. 50–69% as opposed to a '62.5% stenosis' measurement at ultrasound.

Additional difficulties in grading severity of carotid stenosis arise when a discrepancy is found between standard velocity criteria and B-mode and color flow findings. Note that velocities are a complex function of the entire residual lumen, whereas B-mode and color images are at best two-dimensional estimates of the same structure. New imaging techniques allow a three-dimensional reconstruction of structural and flow images and the value of this technology is being tested [70,71]. The diagnostic criteria should also include definitions for hemodynamically significant lesions as well as for grading bilateral and tandem lesions. These additional criteria are discussed below.

Hemodynamically significant ICA lesions can be present with or without significant PSV increase. They are termed 'significant' since they cause a poststenotic drop in flow volume equivalent to or greater than 80% diameter stenosis on the Spencer curve (developed for axis-symmetric and focal stenoses). The development of such a significant blood pressure gradient requires compensation via distal vasodilatation and development of collaterals. In human carotid arteries, hemodynamically significant ICA lesions are usually in the 70–99% diameter reduction range by the NASCET method or appear as elongated stenoses of variable diameter reduction, tandem lesions, near-occlusions or occlusions. Often, these lesions can only be discovered using indirect criteria for grading carotid stenosis. The *indirect criteria for hemodynamically significant carotid stenosis* include [89–97]:

1 decreased end-diastolic flow velocity in the CCA and/or ICA in the presence of a distal lesion;

2 color flow findings such as narrow and elongated residual lumen;

3 reversed flow direction in the ophthalmic artery;

4 anterior cross-filling via anterior communicating artery;

5 posterior communicating artery flow;

6 increased flow pulsatility in the unilateral CCA;

7 decreased flow pulsatility in the unilateral MCA;

8 abnormal flow acceleration and pulsatility transmission index (unilateral MCA).

Although infrequently present with less than 70% N stenosis, the indirect criteria may help to detect severe or hemodynamically significant carotid stenosis when the velocity and gray-scale findings are insufficient for diagnosis.

Postcarotid endarterectomy assessment and carotid stents

B-mode imaging of carotid arteries reconstructed after successful carotid endarterectomy [98] or stenting [99] show changes in the vessel wall consistent with suture placement or stent material. Particular attention should be paid to inspection of the wall changes at the edges of carotid reconstruction where incomplete plaque removal and residual stenosis can be found. Color flow images demonstrate flow that fills the entire lumen. Angle-corrected velocity measurement may show values above normal through the reconstructed part of the vessel likely due to flow remodeling [98,99].

Our criteria for *patent stents* include:

1 stented area shows no deformities and the vessel has parallel walls;

2 no plaque protrusion into the vessel lumen is seen at the proximal and distal ends of the stent;

3 color flow fills the entire stent lumen;

4 peak systolic velocity throughout the stent area is less than or equal to 150 cm/s.

Our criteria for *stent deformity or restenosis* include:

1 B-mode evidence for equal to or greater than 30% narrowing of the stent/vessel lumen (note that if a calcified plaque is present outside the stent with parallel walls, it may produce shadowing and false impression of vessel narrowing);

2 focal velocity increase at the point of maximal narrowing greater than 150 cm/s and prestenotic (or prestent) to stenotic segment PSV ratio of $1/\geq 2$;

3 additional evidence of plaque or thrombus formation at the site of stent deformity or at the proximal or distal ends of the stent (note that low velocities and high-resistance waveforms can be found with a subtotal obstruction of the stent).

Our criteria for *stent or postsurgical occlusion* include:

1 B-mode evidence of hypo- or hyperechoic filling of the reconstructed vessel lumen;

2 no flow signals can be obtained at the longitudinal and transverse views of the reconstructed vessel;
3 high resistance prereconstructed vessel or CCA signals.

Grading bilateral carotid stenosis

The severity of bilateral disease is difficult to grade due to compensatory flow increase in one of the carotid arteries or flow volume diversion into posterior circulation. The range of stenosis and relative contribution of compensatory flow should be mentioned for each artery. If both carotids have abnormally high peak systolic velocities, this may lead to overestimation of the stenosis if the velocity criterion is not adjusted to higher values [100] or it is used alone [87]. The following parameters may help to identify the more severely stenosed side:
1 high ICA/CCA ratio on the side of maximum stenosis;
2 low ICA/CCA ratio on the side of compensatory velocity increase;
3 collateralization of flow on TCD from the side with compensatory velocity increase toward the side with maximum narrowing;
4 reversed ophthalmic artery flow on the side of maximum stenosis;
5 abnormal poststenotic waveforms (blunted waveform, extremely turbulent flow, dampening of flow);
6 ultrasound estimates of flow volume reduction on the side of maximum stenosis.

Tandem carotid lesions

Tandem lesions in the carotid artery can lead to increased risk of perioperative stroke [101], and distal lesions may change after flow is reconstituted in the proximal ICA [102]. Recent analysis of published series suggested that tandem lesions do not affect hemodynamics as a simple summation of separate degrees of stenosis [103]. Ultrasound diagnosis of tandem lesions should therefore include careful evaluation of carotid duplex results for subtle signs of distal obstruction to flow. This may occur in the CCA if the first or second lesion, or a combination of the two, are hemodynamically significant. Often, evaluation of periorbital flows and intracranial vasculature using transcranial Doppler is required to demonstrate hemodynamic significance of lesions distal to the field of extracranial duplex [90,94,96]. These tests are of particular value when only moderate ICA stenosis is found proximally and more severe distal lesion cannot be studied directly. The report should specify all arterial segments affected, with the range of stenosis estimated for each lesion.

Our criteria for *tandem carotid lesions* in an adult patient include:
1 decreased or absent ICA end-diastolic velocity despite relatively low proximal ICA lesion severity;
2 pulsatile poststenotic ICA waveform on one side;
3 relatively low ICA PSV despite the high grade of lesion severity estimated from color and B-mode findings;
4 contralateral or posterior compensatory velocity increase discordant with the severity of a proximal ICA stenosis;
5 stenotic flow signatures and MFV > 80 cm/s, or absent ICA siphon signal through the orbit unilateral to a proximal ICA lesion;
6 anterior cross-filling or posterior communicating artery flow discordant with stenosis severity in the proximal ICA; and
7 stenotic flow signatures and MFV > 80 cm/s in the terminal ICA through the transtemporal window.
The diagnosis of a hemodynamically significant, bilateral or tandem carotid lesion becomes more certain if more than one of the above-mentioned criteria are found. Sometimes, particularly in younger patients, these flow abnormalities can be very subtle, and often the presence of just one abnormal finding raises suspicion. Since ultrasound is a screening test, different levels of certainty should be reflected in the report, i.e. possible, probable or definite presence of an ICA lesion and its severity.

The most confusing situation, i.e. a discrepancy between ultrasound and angiographic results, often occurs due to time delays between ultrasound and angiography. In our experience in stroke patients, the closer both tests are performed to the onset of symptoms the greater the agreement can be expected between them. We repeat ultrasound on admission to scheduled surgery, if more than 3 days have elapsed since angiography.

Factors that can lead to *discrepant duplex/angiography results* include:
A *Patient*
1 Arterial occlusion, clot propagation and recanalization.
2 Intraplaque hemorrhage.
3 Growth of collaterals.
B *Technique*

1 Use of different scanners.
2 Single-projection measurements.
3 Time delays between tests.

C *Operator*

1 Inconsistent scanning protocol.
2 Application of uniform criteria for different scanners without local validation.
3 Limited angiographic views and insufficient selective vessel studies.

Carotid artery occlusion and dissection

With current technologies, it is difficult to be certain of the diagnosis of a *complete* carotid artery occlusion based on ultrasound findings without invasive angiographic confirmation. In fact, when a patient appears to have complete occlusion at first-ever carotid ultrasound examination, a 'benefit of the doubt' should be given by reporting occlusion *or* 99% stenosis. If there is a minimal residual lumen and flow in the distal ICA, this can change patient management, i.e. surgery or stenting may be possible. It is preferable to obtain angiographic confirmation for complete ICA occlusion. The diagnostic accuracy of ultrasound in differentiation of complete occlusion from subtotal stenosis may be improved with contrast agents and sensitive flow imaging techniques [104–107].

The following criteria for *carotid artery occlusion* were derived from multiple studies [79,108–121] and our own observations:

1 absent flow signal in the distal ICA on flow imaging and spectral analysis;
2 high resistance 'stump' waveform with absent or reversed end-diastolic flow just proximal to the flow void area or structural lesion in the ICA (Figure 6.15);
3 drumbeat sounds of lesion motion and vessel wall covibration (usually systolic spikes of low frequency) (Figure 6.15);
4 decreased arterial wall pulsations on B-mode compared to contralateral side; and
5 delayed systolic flow acceleration, blunting of the MCA waveform, or evidence of flow diversion to a branching vessel (i.e. ECA) and/or collateralization of flow via OA, anterior communicating artery (AComA) or posterior communicating artery (PComA).

In the absence of a structural lesion in the proximal ICA and bifurcation, the absence or reversal of the diastolic flow in these segments should raise high suspicion of a distal ICA occlusion [122].

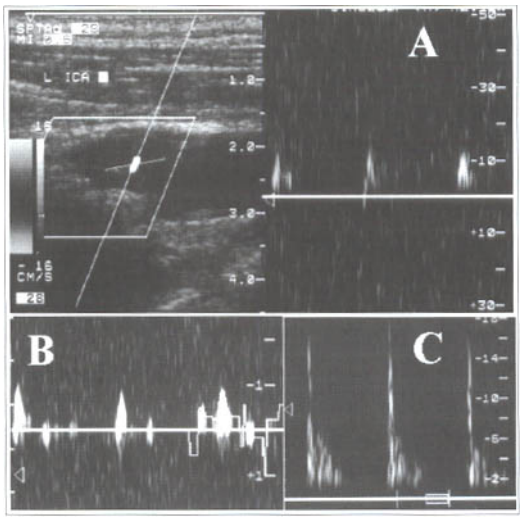

Figure 6.15 Drum-like waveforms with internal carotid artery occlusion. (a) Minimal early systolic spike; (b) systolic spike followed by vessel motion during closure of the aortic valve; (c) sharp systolic spike with no diastolic flow.

In a patient with new-onset stroke symptoms or a recent TIA, ultrasound can detect an *acute thrombosis or an embolus in the ICA* [123–126]. This can be suspected:

1 when flow signal void is found over a lesion with hypo- or anechoic intraluminal appearance (possible fresh clot on B-mode);
2 when there is high velocity in the ECA indicating flow diversion;
3 in the presence of intracranial collaterals; and
4 when microemboli are found in the MCA unilateral to ICA lesion and symptomatic brain side.

An acute thrombosis associated with carotid plaque usually shows an underlying atheroma that may be hyperechoic and have shadowing, whereas an acute embolus from the cardiac source may appear mostly hypoechoic and mobile [123,125,126].

Dissection of the ICA can be detected sonographically despite its common location at the entrance to the skull since a descending intimal flap and hemodynamic effects of an upstream lesion can be demonstrated [127–142]. ICA dissection can be suspected when:

1 an intimal flap is visualized in the ICA with abnormal flow waveforms (differentiate B-mode artifacts caused by jugular vein or other bright reflectors);

2 high resistance pulsatile flow signals are found in the ICA bulb without evidence for an atheromatous lesion;
3 two waveforms are identified in the ICA: normal (flow directed towards true lumen) and high-resistance signal with reduced velocity (false lumen);
4 reversed OA and other intracranial collaterals are found in the presence of a normal extracranial examination; and
5 microemboli are found in the MCA unilateral to a suspected carotid lesion.

Non-invasive diagnosis of ICA dissection is difficult since most of these lesions have variable locations often involving distal ICA at the entrance to the skull [143,144]. The diagnosis is often based on indirect evidence of the distal ICA lesion and may be impossible until the dissection becomes hemodynamically significant or descends to the field of insonation. Patient history often points to trauma, neck manipulation, neck pain or episodes of excessive coughing or sneezing with respiratory infection, etc. [145–147].

ICA dissections can recanalize, and this process can be documented angiographically and monitored with ultrasound [129,133,148–151]. Ultrasound criteria for *recanalization of previously dissected carotid artery* include:
1 recovery of end-diastolic flow in the distal ICA (low resistance flow);
2 return of normal systolic flow acceleration in the MCA without collateralization of flow; and
3 return of normal siphon and OA signals.

Vertebral artery stenosis or occlusion

Most vascular laboratories simply determine the presence and direction of blood flow in the midcervical vertebral artery (VA) without an extensive exploration of the VA origin and its terminal portion. Compared to carotid imaging, fewer validation studies are available for detection and quantification of the VA lesions [152–168]. However, VA stenoses, occlusions and dissections are increasingly being recognized as potential causes or risk factors for posterior circulation ischemia [152,162,169]. VA stenosis occurs more often in V3–V4 segments, followed by the origin of the vertebral artery (V0), and midcervical section (V1–V2) [170]. Direct assessment of the V3 segment with ultrasound is not possible [170]. Therefore, the diagnosis of vertebral obstruction at this level is based on finding indirect proximal signs (i.e. increased flow pulsatility and different waveforms between two sides) or distal signs (poststenotic turbulence, blunted waveform). Diagnostic criteria for direct assessment of the V4 segment will be presented below in the section on the criteria for 'Intracranial stenosis'.

During extracranial duplex examination, the assessment of the vertebral artery should include scanning the midcervical portion and attempts to visualize the proximal VA and its origin whenever possible. Diagnostic criteria for *VA stenosis* derived from previous studies [152–168] and our own experience include:
1 focal significant PSV velocity increase with a ratio between prestenotic and stenotic segments of $1/\geq 2$;
2 presence of a structural lesion, turbulence or spectral narrowing; and
3 indirect pre- or poststenotic signs (abnormal pulsatility and waveforms).

Our criteria for VA stenoses do not include a PSV cut-off since tortuosity of the proximal VA segment, compensatory velocity increase with ICA lesions [171] and VA dominance may produce relatively high velocities. The keys to diagnosis of the VA stenosis with $\geq 50\%$ diameter reduction are the terms 'focal' and 'significant'. The velocity increase should be found over a relatively short (usually 1–2 cm) segment of the VA with normal or decreased pre- and poststenotic velocities. This increased velocity should at least double the velocities found in other segments of the same VA. A hypoplastic VA is more likely to have low velocity and greater pulsatility over longer arterial segments particularly with changes in hemorheology [172].

Derived from previous studies [152–168], diagnostic criteria for *VA occlusion* include:
1 flow void area and absent pulsed Doppler signals in a segment or entire VA stem;
2 hypoechoic vessel lumen (acute and subacute occlusion); and
3 hyperechoic vessel lumen (chronic occlusion).

Occasionally, a *segmental VA occlusion* can be found [173] due to tremendous capacity of the vertebral artery to compensate via muscular collaterals. In these cases, patent distal and particularly terminal VA segments are found carrying antegrade low-resistance flow, often with delayed systolic upstroke. The latter should be differentiated from a proximal lesion of

the subclavian artery. Therefore, incomplete assessment of the VA stem can miss a short segmental occlusion.

Intracranial stenosis

Middle cerebral artery (MCA) stenosis

Primary findings include a focal significant mean flow velocity increase (MFV ≥ 80 cm/s), and/or peak systolic velocity increase (PSV ≥ 140 cm/s), and/or interhemispheric MFV difference of ≥ 30 cm/s in adults free of abnormal circulatory conditions [14,174–185]. A proximal M2–distal M1 MCA stenosis is present if the velocity increase is found at 40–50 mm [186]. A proximal M1 MCA stenosis is usually found at 55–65-mm depths in adults [187]. Chimowitz *et al.* in the prospective part of the Warfarin Aspirin Stroke and Intracranial Disease (WASID) Study [188], adopted criteria that an MCA MFV ≥ 100 cm/s indicates ≥ 50% M1 MCA diameter reduction. To improve the predictive value of 100 cm/s threshold, use the ratio with a homologous or a proximal MCA segment of ≥ 2 [183]. A ≥ 70% MCA stenosis will produce a stenotic/prestenotic ratio of 3/1 or greater (Figure 6.16).

If anemia, congestive heart failure and other circulatory conditions associated with elevated or decreased velocities are present, then a focal MFV difference of ≥ 30% between neighboring or homologous arterial segments should be applied. Adult patients with anemia or hyperthyroidism often have MCA mean flow velocities in the range of 60–110 cm/s. In children with sickle cell disease an MCA MFV of up to 170 cm/s is considered normal [12,189] (see Chapter 7).

A stenosis in the middle cerebral artery may be also suspected if indirect flow disturbances are detected by TCD. These important *additional findings* may include:

1 turbulence, or disturbed flow distal to the stenosis;
2 increased unilateral anterior cerebral artery (ACA) MFV indicating compensatory flow diversion [184, 185]. This finding may also indicate A1 ACA or an ICA bifurcation stenosis with a side-to-side ACA MFV ratio ≥ 1.2;
3 a low-frequency noise produced by non-harmonic covibrations of the vessel wall and musical murmurs due to harmonic covibrations producing pure tones; and
4 microembolic signals found in the distal MCA.

If FVs are increased throughout the M1 MCA stem, the differential diagnosis includes MCA stenosis, terminal ICA or siphon stenosis, hyperemia or compensatory flow increase in the presence of contralateral ICA stenosis, ACA occlusion or incorrect vessel identification.

MCA subtotal stenosis or near-occlusion

A critical stenosis produces a focal FV decrease or a 'blunted' MCA waveform with slow or delayed systolic acceleration, slow systolic flow deceleration, low velocities and MFV MCA < ACA or any other intracranial artery [190,191].

Decreased or minimal flow velocities with slow systolic acceleration can be found due to a tight elongated MCA stenosis or thrombus causing near-occlusion, or

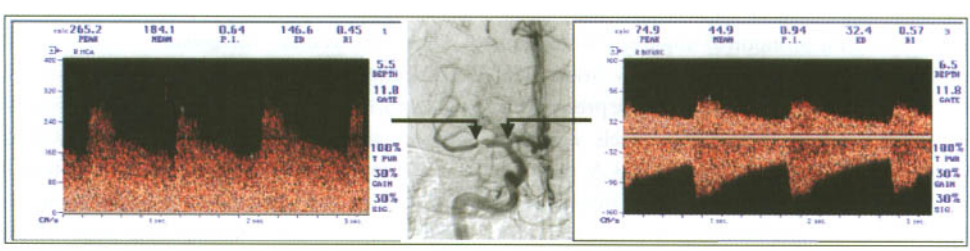

Figure 6.16 A severe M1 middle cerebral artery stenosis. Although validated velocity criteria indicate > 50% MCA stenosis, other signs suggest in fact ≥ 80% lesion: increased end diastolic velocity and flow diversion to ACA.

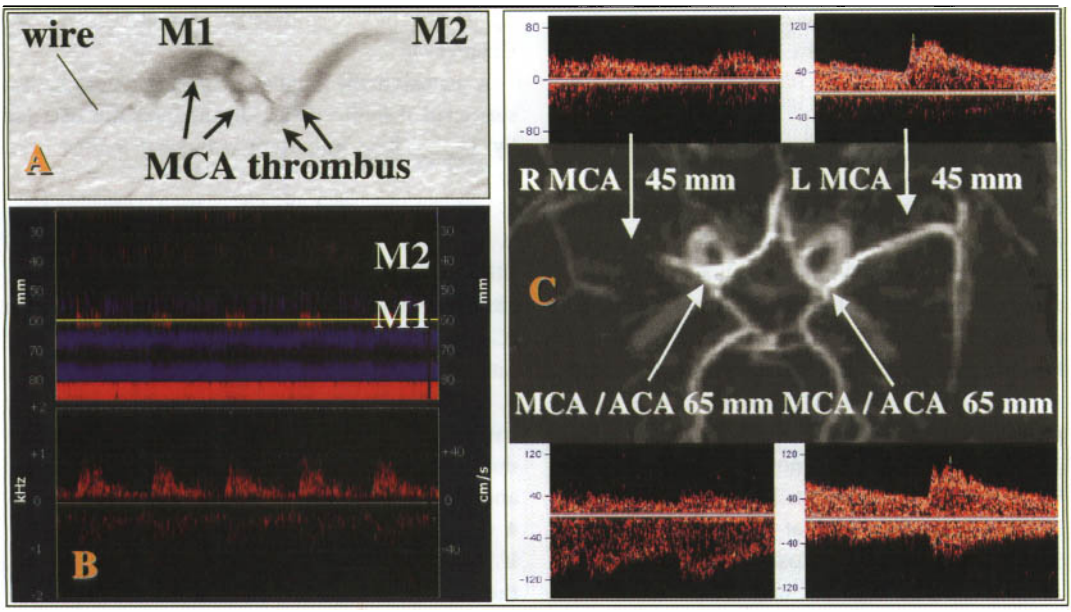

Figure 6.17 Acute M1 MCA near-occlusion. (a) digital subtraction image of residual flow around 'sausage'-like thrombus in the MCA. (b) Spectral analysis shows a dampened residual flow signal in the proximal M1 MCA at the depth of 60 mm. M-mode displays this signal as a high resistance antegrade flow signature at 60 mm. M-mode displays other vessels including low resistance flows in both ACAs at the depths of 62–85 mm, low resistance flow to a branch of the M1 segment at the depths of 50–60 mm (either early anterior temporal branch or perforators), and antegrade residual flow signal in one of the M2 branches at the depths of 30–40 mm. (c) Spectral TCD findings include a blunted right M1 MCA signal, a 2:1 left to right MCA MFV ratio, compensatory velocity increase in the right ACA (R ACA MFV > L MCA MFV), and a normal left MCA systolic flow acceleration. MRA shows a flow signal void due to slow and diminished flow in the mid-M1 segment with some flow reconstitution in the distal branches.

a proximal ICA obstruction [90,91,93]. The 'blunted' waveform is common in patients with acute ischemic stroke, particularly in those presenting with a hyperdense MCA sign on non-contrast CT scan or a flow gap on MRA (Figure 6.17; also see the criteria for 'Arterial occlusion').

A false-positive diagnosis of MCA subtotal stenosis can occur because of problems with vessel identification and a suboptimal angle of insonation. Incorrect probe angulation and shallow insonation usually lead to these errors. To confirm the presence of a flow-limiting lesion, branching vessels need to be evaluated. Note that an M1–M2 MCA subtotal stenosis is usually accompanied by flow diversion to the ACA and/or compensatory flow increase in the PCA indicating transcortical collateralization of flow [190,191].

Anterior cerebral artery (ACA)

Primary findings in an ACA stenosis include a focal significant ACA FV increase (ACA > MCA) and/or ACA MFV ≥ 80 cm/s, and/or a ≥ 30% difference between the proximal and distal ACA segments, and/or a ≥ 30% difference compared to the contralateral ACA [14,190]. Collateralization via the AComA can be excluded by a normal contralateral ACA flow direction and the absence of stenotic signals at 75 mm. Usually, an A1 ACA stenosis can be detected at 62–75 mm.

The differential diagnosis includes anterior cross-filling due to proximal carotid artery disease [114,116,120]. Additional findings may include turbulence and a flow diversion into the MCA and/or compensatory flow increase in the contralateral ACA.

Decreased or minimal flow velocities at the A1 ACA origin may indicate a suboptimal angle of insonation from the unilateral temporal window, an atretic or tortuous A1 ACA segment and A1 ACA near-occlusion. Since the A2 ACA segment cannot be assessed directly by TCD, its obstruction can be suspected only if a high-resistance flow is found in the distal dominant A1 ACA segment (70–75 mm).

Common errors include incorrect vessel identification (terminal ICA vs. ACA) and velocity underestimation (suboptimal angle of insonation, poor window, weak signals).

Terminal ICA and ICA siphon

The paracellar and supraclinoid ICA segments are difficult to examine in their entirety. An orbital examination may reveal stenotic flow directed towards or away from the probe at 58–64 mm in adults. The terminal ICA bifurcation is located at 60–75 mm from the transtemporal window. A terminal ICA/siphon stenosis produces a focal significant MFV increase ICA MFV ≥ 70 cm/s, and/or an ICA > MCA, and/or a ≥ 30% difference between arterial segments [14,192].

The differential diagnosis includes moderate proximal ICA stenosis and/or compensatory flow increase with contralateral ICA stenosis. Additional findings in the presence of an ICA stenosis may include turbulence, blunted unilateral MCA, OA MFV increase and/or flow reversal with low pulsatility. The ICA siphon MFVs may decrease due to siphon near-occlusion (a blunted siphon signal), or distal obstruction (i.e. MCA occlusion or increased ICP).

Common errors include vessel identification (MCA vs. ICA), deep (> 65 mm) transorbital insonation and collateralization of flow misinterpreted as an arterial stenosis.

Posterior cerebral artery (PCA)

A PCA stenosis produces a focal significant FV increase resulting in a PCA MFV > ACA or ICA; and/or a PCA MFV ≥ 50 cm/s in adults [14,193]. The PCA is located at 58–65 mm; the P1 segment is directed towards the probe, the P2 segment is directed away from the probe. The differential diagnosis includes collateral flow via the PComA and siphon stenosis. Using transcranial duplex imaging, it may be possible to differentiate PCA stenosis from collateralization of flow using the peak systolic velocity [194]. Additional findings may include turbulence and a compensatory flow increase in the MCA.

Common sources of error include unreliable vessel identification, the presence of an arterial occlusion and a top-of-the-basilar stenosis.

Basilar artery (BA)

Primary findings in the presence of a BA stenosis include a focal significant velocity increase where a MFV BA > MCA or ACA or ICA, and/or MFV BA ≥ 60 cm/s in adults, and/or there is ≥ 30% difference between arterial segments [14,165,195–197]. Although the depth range for basilar segments varied between previous studies [195,196], it is also dependent on the size of the neck and skull, and the technician's ability to insonate the distal basilar artery with failure rates far less than 30% [196]. Our depth criteria are the following: the proximal basilar artery is located at ≥ 75 mm, the mid-BA segment is located at 90 mm, and the distal BA is found at 100 mm in most adults [187,198]. The differential diagnosis includes terminal VA stenosis if elevated velocities are found proximally. If elevated velocities are found throughout the BA stem, the differential diagnosis includes compensatory flow increase. With the latter, VA FVs are also elevated.

Basilar artery subtotal stenosis or near-occlusion produces a focal FV decrease (≤ 30% difference between arterial segments and/or BA < VA) resulting in a blunted waveform [190,193,199]. The differential diagnosis includes fusiform basilar artery with or without thrombus since enlarged vessel diameter may reduce flow velocities. If end-diastolic flow is absent, the differential diagnosis includes BA occlusion.

Additional findings may include:

1 turbulence and disturbed signals distal to the stenosis;

2 compensatory flow increase in VAs and posterior inferior cerebellar arteries (PICAs) indicating cerebellar collateralization; and

3 collateral supply via PComA(s) to PCA(s) and reversed distal basilar artery.

Common sources of error include tortuous basilar ('not found' does not always mean obstructed), elongated BA obstruction and distal BA lesions that were not reached by TCD insonation. Application of power Doppler, ultrasound contrast and duplex imaging may help detection of the distal basilar segment, tortuosity and distal branches [200,201]. Also, a collateral flow from the posterior to anterior circulation in the presence of carotid lesions may increase flow velocity changes associated with mild stenosis and/or tortuosity. In the case of flow collateralization, the dominant vertebral artery velocities are also increased [171].

Terminal vertebral artery (VA)

Primary findings with intracranial VA stenosis include

a focal significant velocity increase [165] where MFV VA > BA, and/or MFV VA ≥ 50 cm/s (adults), and/or there is ≥ 30% difference between VAs or its segments [2,14]. A terminal VA stenosis may also present as a high-resistance (PI ≥ 1.2) flow in one of the vertebral arteries, and/or a blunted or minimal flow signal [199]. The terminal VA is found at 40–75 mm, dependent on the size of the neck and skull. To detect > 50% intracranial stenoses, the peak systolic velocity criteria were also developed for angle-corrected duplex ultrasound of the vertebral and other intracranial arteries [202].

The differential diagnosis includes proximal BA or contralateral terminal VA stenoses and a compensatory flow increase in the presence of a contralateral VA occlusion or carotid stenosis [171].

Additional findings may include:

1 turbulence or disturbed flow signal distal to the stenosis;

2 a compensatory flow increase in the contralateral vertebral artery or its branches (cerebellar collaterals); and

3 low BA flow velocities (hemodynamically significant lesion, hypoplastic contralateral VA) and low-resistance flow distal to stenoses (compensatory vasodilatation).

Common sources of error include a compensatory flow increase due to hypoplastic contralateral VA, low velocities in both VAs due to suboptimal angle of insonation, extracranial VA stenosis or occlusion with well-developed muscular collaterals, elongated VA stenosis/hypoplasia and incorrect vessel identification, e.g. posterior inferior cerebellar artery.

Arterial stenosis: summary

An intracranial stenosis should be suspected when the normal hierarchy of flow velocities is disrupted, i.e. MCA ≥ ACA ≥ ICA ≥ PCA ≥ BA ≥ VA by the mean flow velocity difference greater than 20% between these arteries, i.e. BA > MCA and focal velocity elevation (Table 6.5). TCD can reliably detect stenoses located in the M1 MCA, ICA siphon, terminal vertebral arteries, proximal basilar arteries and P1 PCA. The reported sensitivity ranges are 85–90%, specificity 90–95%, positive predictive values (PPV) 85%, negative predictive values (NPV) 98%, with lower accuracy parameters for the posterior circulation. TCD sensitivity for measuring velocity without aliasing is limited in patients with deep (> 65 mm) stenoses due to low pulse repetition frequency of TCD instruments [13,14,203]. Stenoses of M2, A2 and P2 segments are difficult to find due to suboptimal angle of insonation or unknown location. Intracranial collaterals and hyperemia may mimic stenotic flow.

Arterial vasospasm and hyperemia

Arterial vasospasm is a complication of subarachnoid hemorrhage (SAH), which becomes symptomatic in more than 25% of patients leading to a delayed ischemic deficit (DID) [204]. DID usually occurs when vasospasm results in a severe (≤ 1 mm) intracranial arterial narrowing, producing flow depletion with extremely high velocities [205]. Vasospasm may affect proximal stems and distal branches of intracranial arteries, with the most common locations being the MCA/terminal ICA, bilateral ACA and basilar artery [206]. Vasospasm may coexist with hydrocephalus, edema and cerebral infarction. The differential diagnosis with TCD should always consider the hyperdynamic state that we will refer to as *hyperemia*. Hyperemia may be induced by spontaneous cardiovascular responses to SAH or induced by hypertension–hemodilution–hypervolemia (HHH) therapy [207]. Although inadequate, the term 'hyperemia' is used to describe velocity changes on TCD. The flow velocity

Table 6.5 Maximum mean flow velocity thresholds (assumed zero angle of insonation) for a focal intracranial arterial stenosis on transcranial Doppler.

Artery	*Depth (mm)*	*Velocity (cm/s)*	*Velocities for WASID ≥ 50% stenosis*
M1–M2 middle cerebral artery	30–65	≥ 80	≥ 100 cm/s (in addition, use 1/2 ratio)
A1 anterior cerebral artery	60–75	≥ 80	N/A
Internal carotid artery siphon	60–65	≥ 70	≥ 90 cm/s (in addition, use 1/2 ratio)
Posterior cerebral artery	60–72	≥ 50	N/A
Basilar artery	80–100+	≥ 60	≥ 70 cm/s (in addition, use 1/2 ratio)
Vertebral artery	40–80	≥ 50	≥ 70 cm/s (in addition, use 1/2 ratio)

Table 6.6 Transcranial Doppler criteria for grading proximal middle cerebral artery (MCA) vasospasm.

Mean flow velocity (MFV) (cm/s)	*MCA/ICA MFV ratio*	*Interpretation*
< 120	≤ 3	Hyperemia
> 80	3–4	Hyperemia + possible mild spasm
≥ 120	3–4	Mild spasm + hyperemia
≥ 120	4–5	Moderate spasm + hyperemia
≥ 120	5–6	Moderate spasm
≥ 180	6	Moderate-to-severe spasm
≥ 200	≥ 6	Severe spasm
> 200	4–6	Moderate spasm + hyperemia
> 200	3–4	Hyperemia + mild (often residual) spasm
> 200	< 3	Hyperemia

measured by TCD is not a direct measurement of cerebral blood flow volume [208]. However, focal or global velocity changes can help differentiate between spasm and hyperemia. Both conditions may coexist, since most SAH patients with spasm routinely receive HHH therapy.

Although quantitative criteria have been studied extensively, grading vasospasm severity is difficult, and the interpretation of TCD findings should be individualized. Daily TCDs may detect considerable flow velocity and pulsatility changes that should be related to the patient's clinical condition, medications, blood pressure, time after Day 0 and intracranial pressure (ICP) findings.

Proximal vasospasm in any intracranial artery results in a focal (or diffuse along one or two branching segments) elevation of MFVs without parallel FV increase in the feeding extracranial arteries (intracranial/extracranial vessel ratio ≥ 3). *Distal vasospasm* in any intracranial artery may produce a focal pulsatile flow (PI ≥ 1.2) indicating increased resistance distal to the site of insonation. No MFV increase may be found since vasospasm is located distal to the site of insonation [209]. *Additional findings* may include daily changes in velocities, ratios and PIs during the first 2 weeks but particularly pronounced during the critical Days 3–7 after the onset of SAH.

MCA-specific criteria (see Table 6.6)

The MCA findings on TCD have been most rigorously validated and correlated with the diameter of the residual lumen on DSA [205,210–213]. According to Lindegaard, MCA MFV ≥ 200 cm/s predicts a residual lumen of 1 mm or less [205]. The differential diagnosis includes hyperemia, combination of vasospasm and hyperemia in the same vessel, residual vasospasm and hyperemia. Unlike focal atherosclerotic lesions, vasospasm may affect longer segments of the terminal ICA and MCA. Vasospasm may be unequally distributed along the MCA stem and branches. However, the presence of hyperdynamic cardiovascular state and HHH therapy may promote high velocities even in the presence of severe spasm affecting multiple segments.

Table 6.7 Predictors of adverse outcomes in patients with subarachnoid hemorrhage: transcranial Doppler findings indicating vasospasm progression and intracranial pressure (ICP) changes.

Parameter	*Values*
Velocity	Early appearance of MCA MFV ≥ 180 cm/s
	Rapid (> 20% or + > 65 cm/s) daily MFV rise during critical Days 3–7
Ratio	MCA/ICA ratio ≥ 6
Pulsatility	Abrupt appearance of high-resistance
	PI ≥ 1.2 due to increased ICP (hydrocephalus)
	Appearance of PI ≥ 1.2 due to distal spasm

MCA, middle cerebral artery; MFV, mean flow velocity; ICA, internal carotid artery; PI, pulsatility index.

Prognostically unfavourable findings on TCD are summarized in Table 6.7. These criteria were modified from a review by Sloan [204].

Criteria for vasospasm in other intracranial arteries

Grading vasospasm severity in arteries other than the MCA is difficult [204,214]. Sloan suggested reporting vasospasm in these arteries as possible, probable and definite [204] (Table 6.8). The key indicator of

Table 6.8 Sloan's optimized criteria for grading vasospasm (VSP) in intracranial arteries.

Artery/mean flow velocity	*Possible VSP**	*Probable VSP**	*Definite VSP**
Internal carotid artery	> 80	> 110	> 130
Anterior cerebral artery	> 90	> 110	> 120
Posterior cerebral artery	> 60	> 80	> 90
Basilar artery	> 70	> 90	> 100
Vertebral artery	> 60	> 80	> 90

* After hyperemia has been mostly ruled out by the focal velocity increase and by the intracranial artery/extracranial ICA ratio ≥ 3 except for posterior circulation vessels.
Optimized criteria were modified from the review by Sloan [204].

a significant vasospasm is a focal, asymmetric and disproportionate velocity increase that may occur in an artery distant from the aneurysm site or blood clot collection on CT. The differential diagnosis includes hyperemia and its combination with vasospasm in these arteries.

An ongoing individual correlation of DSA with same-day TCD findings may improve the accuracy of TCD in detecting vasospasm onset. A focal and disproportionate to therapy increase in flow velocities indicates the development of vasospasm. For example, an MCA MFV increase by +50 cm/s may indicate 20% diameter reduction of the vessel, and since FV is inversely proportionate to the vessel radius, a 30% diameter reduction usually doubles the velocity on TCD [215]. Therefore, TCD may be more sensitive to intracranial artery diameter changes than angiography, particularly in the early phases of spasm development. Since TCD is a screening tool, the criteria should be adjusted to a higher sensitivity to detect any degree of vasospasm in order to institute HHH therapy. At the same time, higher specificity threshold should be used for severe vasospasm to minimize the number of false-negative angiograms, particularly if TCD is used to select patients for angioplasty.

In our experience, vasospasm that affects the basilar artery stem, PCAs or ACAs may cause compensatory velocity increase in the MCAs with low Lindegaard ratios. Therefore, a complete daily TCD examination may reveal more significant hemodynamic changes that can be used to identify patients with spasm in arteries other than the MCA.

Hyperemia

Hyperemia is suspected with elevated velocities in the intracranial and feeding extracranial vessels (Table 6.6). Hyperemic changes on TCD are common in patients with SAH receiving HHH therapy. The use of the Lindegaard ratio [212] and new flow and area indices [216] may help to minimize false-positive TCD results and better predict the diameter of the residual lumen on angiography.

Otherwise, hyperperfusion syndrome may develop after carotid endarterectomy or angioplasty due to limited or impaired capacity of the brain to regulate restored blood flow volume [217–220]. Patients frequently experience headache and seizures. TCD often shows ≥ 30% increase in MCA MFV unilateral to the reconstructed carotid artery and low-pulsatility waveforms compared to the contralateral side, indicating decreased capacity of distal vasculature to regulate the re-established flow volume. Pulsatility index may decrease > 20% compared to the contralateral side. These changes can often be found during surgery immediately after cross-clamp release. Spencer diagnosed hyperperfusion when the MCA MFV is 1.5 times the precross-clamp values and persists at that level without corrective measures [221].

Collateral patterns and flow direction

TCD can directly detect the following collateral channels [222–226]:

1 anterior cross-filling via the anterior communicating artery;
2 posterior communicating artery; and
3 reversed ophthalmic artery.

The intracranial collateral channels are dormant under normal circulatory conditions. A collateral channel opens when a pressure gradient develops between the two anastomosing arterial systems. TCD can detect some of these collateral pathways: reversed OA, anterior cross-filling via AComA, and PComA flow either

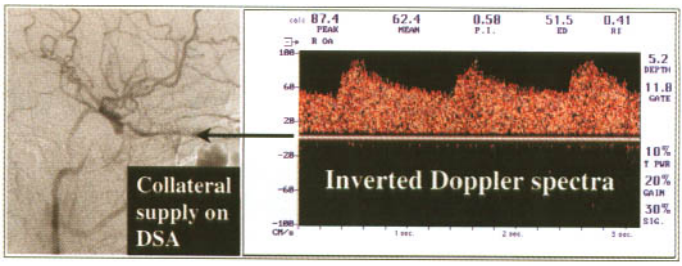

Figure 6.18 A reversed ophthalmic artery (OA). Collateral flow via reversed OA (arrow) has a low-resistance pulsatility index (0.58) and flow direction away from the probe (inverted image).

to or from the anterior circulation [222–226]. Flow direction will depend on the direction of collateralization. When present, collateral flow patterns rarely imply anatomic variants but, most often, the presence of a flow-limiting lesion proximal to the recipient arterial system and the origin of the collateral channel.

The direction of flow indicates which arterial system is the *donor* (the source of flow) and which is the *recipient* (the collateral flow destination) [14]. TCD provides information on functioning collateral channels and direction of collateral flow. An expanded battery of TCD parameters may be used to refine the evaluation of the severity of ICA lesions, particularly when multiple lesions are found or the applicability of other tests is limited due to the presence of the distal ICA lesions [94,96].

Reversed ophthalmic artery

Primary findings. An abnormal OA signal includes low-pulsatility flow directed primarily away from the probe via a transorbital window at 50–62-mm depth (Figure 6.18). Check vessel identification since an ICA siphon flow signal can mimic reversed OA in the presence of low-velocity OA signals.

Additional findings may include no substantial difference in MFVs detected in the OA and siphon; high velocities in the ICA siphon suggesting either a high-grade proximal ICA and/or siphon stenosis; and no flow signals at depths ≥ 60 mm suggesting an ICA occlusion.

Interpretation. If the reversed OA is the only abnormal finding, this indicates possible proximal ICA occlusion or severe stenosis. Occasionally, this may be the only sign of an ICA dissection or occlusion. If a reversed OA is found with a delayed systolic flow acceleration in the unilateral MCA, there is a probable proximal ICA occlusion or severe stenosis. If a reversed OA is found with at least one other collateral channel (anterior cross-filling, or PComA) there is a definite proximal ICA occlusion or high-grade stenosis.

Common sources of error include shallow or deep OA insonation, ICA dissection with considerable residual flow, terminal ICA occlusion distal to the OA origin and retrograde filling of the ICA siphon with normal OA direction. Furthermore, a normal OA direction does not rule out proximal ICA obstruction.

Anterior communicating artery

Collateral flow through the AComA cannot be reliably distinguished from the neighboring ACAs due to the smaller AComA length and diameter compared to a large sample volume. Therefore, we report the anterior cross-filling via AComA as opposed to the velocity and direction of flow in the AComA itself.

Anterior cross-filling:

1 elevated A1 ACA MFVs on the donor side presenting as ACA > MCA and/or donor ACA MFVs > 1.2 times greater than contralateral ACA;

2 possible stenotic-like flow at 70–80 mm directed away from the donor side; and

3 a normal or low MFV in A1 ACA of the recipient side with or without A1 flow reversal (Figure 6.19).

The *differential diagnosis* includes distal A1 ACA stenosis, and compensatory flow increase if one A1 segment is atretic. Identification of the reversed A1 segment depends on the skill of the operator.

Interpretation:

1 If only elevated donor ACA velocities are found, the differential diagnosis includes A1 ACA stenosis and atresia of the contralateral A1 segment. With the latter, the donor A1 segment supplies both A2 segments (may be present in normal individuals due to anatomic variations of the circle of Willis as well as in patients with ICA or MCA obstructive lesions).

2 If an elevated donor ACA velocity is found with

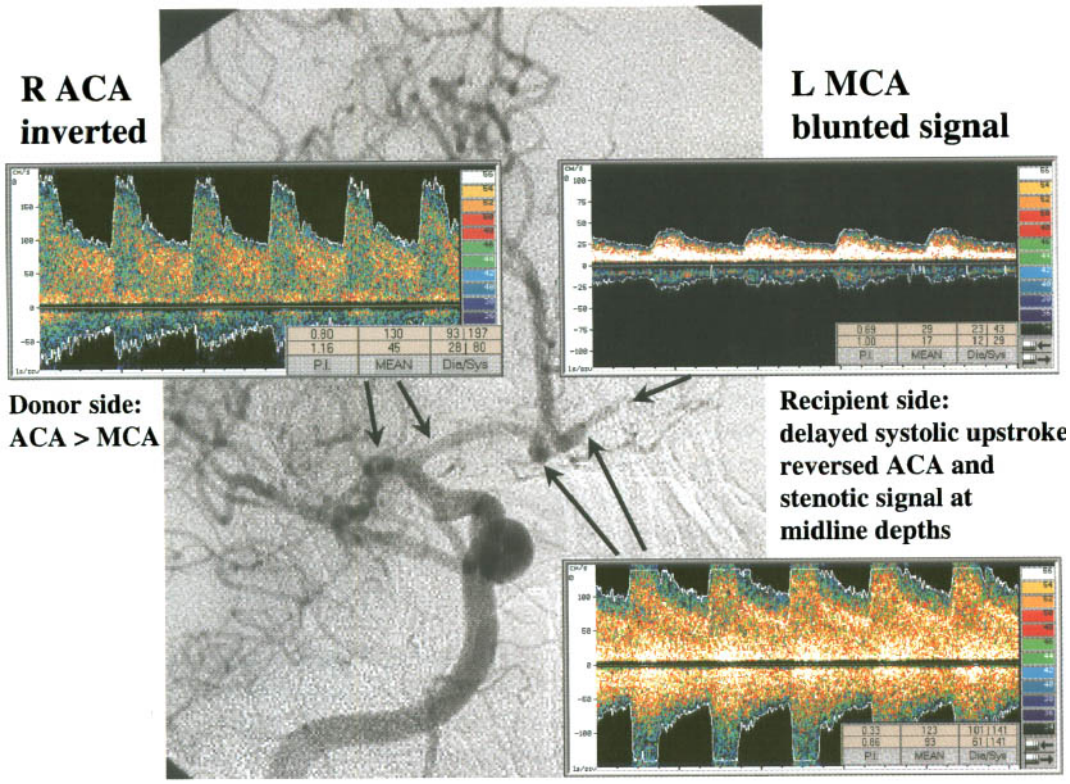

Figure 6.19 *Anterior cross-filling via anterior communicating artery (AComA).* Transcranial Doppler shows elevated velocities in the contralateral ACA > MCA (upper left Doppler spectra) of the donor site and elevated velocities at midline depths with reversed unilateral A1 ACA flow direction (lower right spectra). Bidirectional stenotic flow signals at midline depth likely include AComA and proximal A2 ACA flows (arrows). Recipient MCA has delayed systolic flow acceleration and a blunted flow signal (upper right image).

stenotic flow at midline depths, the differential diagnosis includes distal A1 stenosis, ICA siphon stenosis and cross-filling via the AComA.

3 If an elevated donor ACA MFV is found with a reversed contralateral A1, this indicates probable proximal ICA stenosis.

4 If an elevated donor ACA MFV is found with stenotic-like flow at midline depths and a reversed contralateral A1 ACA, there is a definite proximal ICA stenosis or occlusion.

Posterior communicating artery

The PComA connects the posterior and anterior cerebral arterial systems and can be detected by TCD since it usually has a considerable length > 5 mm and a favorable angle of insonation. When functioning, it may be detected as a flow signal consistently present at varying depths from 60 to 75 mm via the transtemporal approach. Under normal conditions, this area has no detectable flow when the sonographer switches from the ICA bifurcation posteriorly to locate the PCA. The direction of flow in PComA corresponds to collateralization: anterior to posterior collateral flow is directed away from the probe, whereas the posterior to anterior collateral flow is directed towards the probe. Vessel identification is difficult since the PComA and PCA are prone to anatomic variations.

Collateralization via PComA. Flow signals directed either away from or towards the probe with posterior angulation of the transducer over the temporal window are consistently found at 60–75 mm (Figure 6.20). The velocity range is similar to or higher than those detected in the M1 MCA and ICA bifurcation (anterior to posterior collateral flow), or basilar artery (posterior to anterior collateral flow). A possible stenotic-like flow signal may be found at 60–75 mm with similar probe angulation. The differential diagnosis includes the terminal ICA or PCA stenoses.

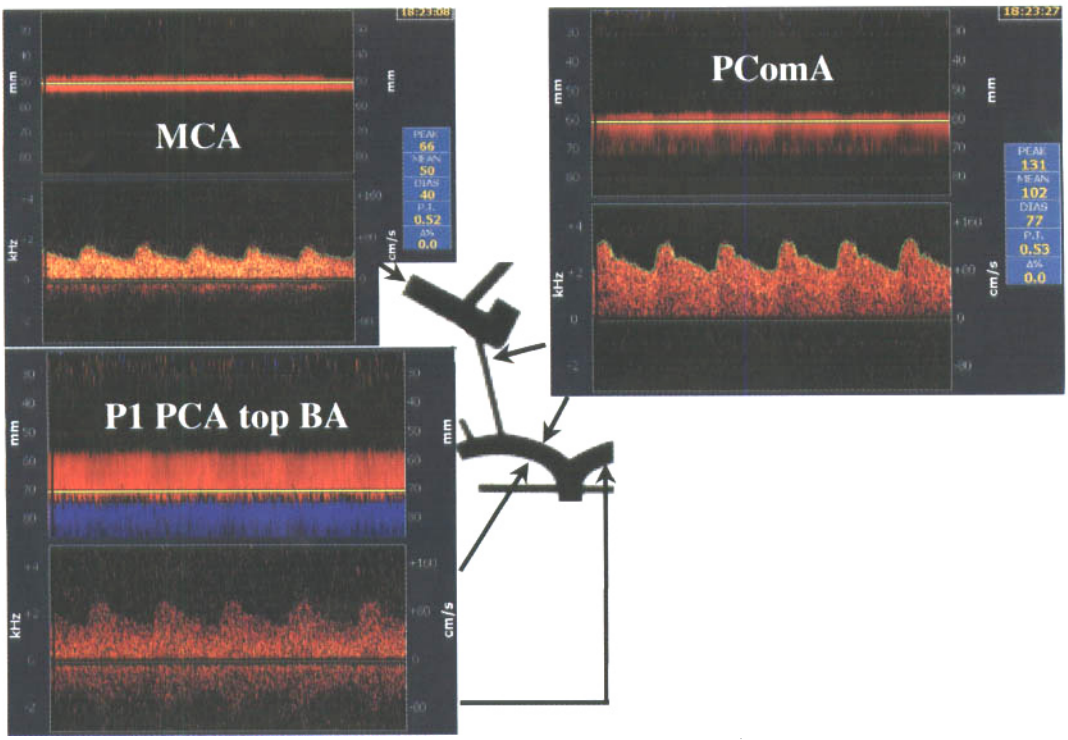

Figure 6.20 Collateralization of flow via posterior communicating artery (PComA). PComA has an MFV that is usually greater than the velocity in the recipient artery where the delayed systolic flow acceleration can also be found. Lower left PMD-TCD image shows top of the basilar bifurcation into P1 PCA segments at midline depths.

Cerebral embolization

Ultrasound can detect embolism in real time [227], and TCD can detect this process in the cerebral vessels [221,228,229]. TCD is used to monitor carotid and cardiac surgery, angioplasty/stenting and stroke patients with presumed cardiac or arterial sources for brain embolization. Some institutions use TCD as an established monitoring tool, and some still regard this application as investigational.

The microembolic signals (MES) detected by TCD are asymptomatic since the size of the particles producing them is usually comparable to or even smaller than the diameter of brain capillaries [230]. However, the MES cumulative count is related to the incidence of neurophycologic deficits after cardiopulmonary bypass [228,231,232] and stroke after carotid endarterectomy [221,229,233–235], and the significance of MES as a risk factor for ischemic stroke is emerging.

It is important to know how to detect and identify MES. Occasionally, a sonographer may be the only witness to cerebral microembolization during a routine examination and this finding may suggest a vascular origin of the neurologic event and point to the potential sources of embolism (heart chambers and septum, aortic arch, arterial stenosis or dissection) [236–243].

Strict standards should be followed when an interpreter documents and reports microemboli on TCD [244]. The gold standard for MES identification still remains the on-line interpretation of real-time, video- or digitally taped flow signals [244–246]. The spectral recording should be obtained with minimal gain at a fixed angle of insonation with a small (< 10 mm) sample volume. The probe should be maintained with a fixation device during at least 0.5–1 h monitoring. The use of a two-channel simultaneous registration and a prolonged monitoring period may improve the yield of the procedure. Multigated or multiranged registration at different insonation depths may improve differentiation of embolic signals from artifacts. Like in fishing, using multiple lines may yield a better catch during the same period of time.

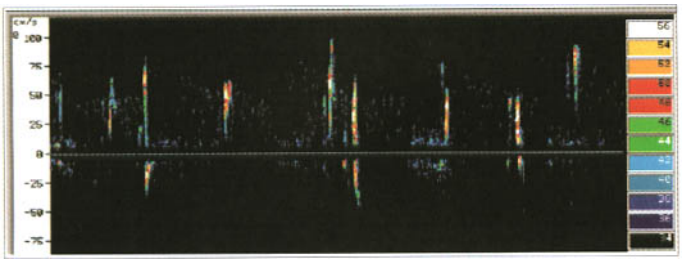

Figure 6.21 Microembolic signals. The consensus definition is provided in the text. A single-gate spectral transcranial Doppler recording of the middle cerebral artery flow shows multiple high-intensity transient and primarily unidirectional signals after intravenous injection of agitated saline in a patient with right-to-left cardiac shunt.

According to the International Cerebral Hemodynamics Society definition [247], *microembolic signals (MES)* have the following characteristics (Figure 6.21):

1 random occurrence during the cardiac cycle;
2 brief duration (usually < 0.1 s);
3 high intensity (> 3 dB over background);
4 primarily unidirectional signals (if fast Fourier transformation is used); and
5 audible component (chirp, pop).

According to Ringelstein and the international panel of experts [244], quality control of studies that report microemboli should include documentation of the following 14 parameters: ultrasound device; transducer frequency, type and size; insonated artery; insonation depth; algorithms for signal intensity measurement; scale settings; detection threshold; axial length of sample volume; fast Fourier transform (FFT) size (number of points used); FFT length (time); FFT overlap; transmitted ultrasound frequency; high-pass filter settings; and the recording time. There is an agreement that no current system of automated embolus detection has the required sensitivity and specificity for clinical use. Therefore, the interpreting physician has to review every stored signal, listen to the sound characteristics, determine the difference between the signal and background (dB), and attempt to determine the source of microemboli.

Increased intracranial pressure (ICP)

A normal low-resistance intracranial waveform is detected by TCD since the brain is a low-resistance vascular system with normal or low ICP values. When ICP increases up to the diastolic pressure of the resistance vessels, EDV decreases and flow deceleration occurs more rapidly, and the changes on TCD are noted with ICP values of 20 mmHg or higher [248–258]. The following changes can be observed on *TCD with increasing ICP*:

1 end-diastolic velocity decrease;
2 pulsatility index increase (PI ≥ 1.2 for previously normotensive young individuals);
3 resistance index increase;
4 shortening of the trans-systolic time; and
5 decrease in peak and mean flow velocities.

When ICP becomes greater than diastolic blood pressure but less than systolic pressure, the result is either a triphasic waveform as seen in the peripheral arteries, or a sharply peaked systolic signal and an absent end-diastolic component. Further increase in ICP may lead to cerebral circulatory arrest (Figure 6.22).

Increased ICP may result in high-resistance waveforms: PI ≥ 1.2, decreased or absent EDV, and triphasic or reverberating flow. We use the following algorithm that may help to differentiate among the mechanisms of increased resistance to flow.

If PI is ≥ 1.2 and positive end-diastolic flow is present:
A in all arteries: hyperventilation; increased cardiac output, hypertension; increased ICP;
B unilaterally: compartmental ICP increase; stenoses distal to the site of insonation;
C in one artery: distal obstruction (hypoplasia, spasm, stenosis, edema).

If PI is ≥ 2.0 and end-diastolic flow is absent:
A in all arteries: arterial occlusion; extremely high ICP; possible arrest of cerebral circulation;
B unilaterally: compartmental ICP increase, occlusion distal to insonation site;
C in one artery: distal obstruction (occlusion, severe spasm, edema).

Cerebral circulatory arrest

Progressive elevation of ICP due to brain edema or mass effect produces stepwise compression of small and large intracranial arteries eventually leading to cerebral circulatory arrest (Figure 6.22). A prolonged absence of brain perfusion can be detected using

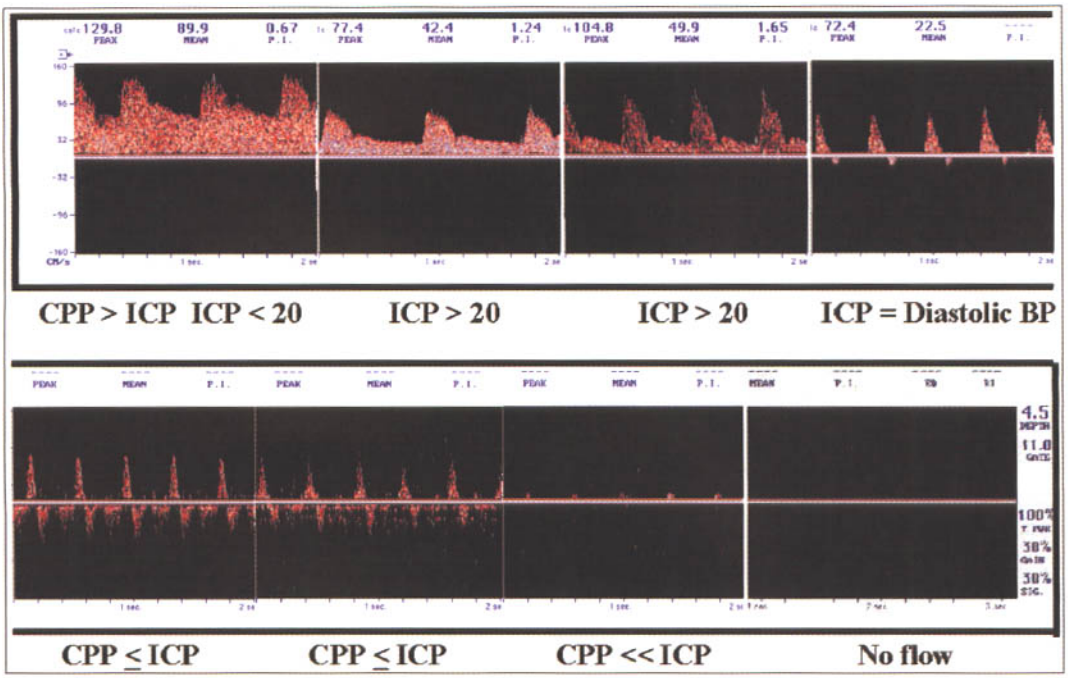

Figure 6.22 Increased ICP and cerebral circulatory arrest. ICP, intracranial pressure; CPP, cerebral perfusion pressure.

oscillating (reverberating) flow pattern, systolic spike or absent flow signals [259–271], and this process will lead to brain death [272]. TCD is a reliable tool to confirm cerebral circulatory arrest with accuracy parameters close to 100% at experienced centers [259–271].

Based on previous published studies, reviews and criteria [259–272], and our own clinical experience, we developed the following algorithm if *cerebral circulatory arrest is suspected*:

1 Document arterial blood pressure at the time of TCD examination.

2 Positive MCA or BA end-diastolic flow = no cerebral circulatory arrest.

3 Absent end-diastolic flow = uncertain cerebral circulatory arrest (too early or too late).

4 Reversed minimal end-diastolic flow = possible cerebral circulatory arrest (continue monitoring).

5 Reverberating flow = probable cerebral circulatory arrest (confirm in both MCAs at 50–60 mm and BA at 80–90 mm, then monitor arrest for 30 min).

TCD *cannot* be used to diagnose brain death since this is a clinical diagnosis [272]. TCD can be used to confirm cerebral circulatory arrest in adults and children *except* in infants less than 6 months [259–271]. TCD can be used to monitor progressive flow changes towards cerebral circulatory arrest. Once a reverberating signal is found it should be monitored for at least 30 min in both MCAs and BA to avoid false-positive findings. Also, avoid insonation of bifurcations, i.e. MCA/ACA, since bidirectional reverberating signals may overlap creating an illusion of positive EDV.

A transient cerebral circulatory arrest can occur in patients with SAH and head trauma due to A-waves of ICP. TCD can also be used to determine the appropriate time for other confirmatory tests (i.e. to minimize studies with residual cerebral blood flow), and to discuss the consequent issues with the patient's family.

Arterial occlusion

The diagnosis of acute intracranial arterial occlusion with TCD is more complex and yields more information about intracranial thrombus than described in previously published criteria [176,273–279]. Unlike chronic complete occlusion, acute arterial occlusion is a dynamic process associated with residual flow and, at times, only partial flow obstruction. It is probably best to call acute occlusion as "lesion amenable for intervention" in acute stroke patients.

The operator must be experienced, and the best results are usually obtained for the M1 MCA, terminal ICA/siphon and basilar artery. The main requirement is a good window of insonation and to prove this, other patent arteries should be identified through the same approach, or a contrast agent should be used. Besides no detectable signals at the site of complete occlusion or velocity asymmetry between the homologous segments on TCD in acute ischemic stroke [176,273–279], a variety of flow signals around the thrombus (Figure 6.23) can be detected [280]. To determine the presence of an acute arterial occlusion, it is extremely important to depart from a simplistic concept of asymmetry in flow velocities between affected and non-affected sides. An acute lesion may represent a complete occlusion, subtotal stenosis or partial yet hemodynamically significant flow obstruction. Instead of relying on velocity measurements, the TCD examiner should pay attention to flow waveforms, and signs of flow diversion or collateralization. This approach leads to a greater yield of abnormal TCD findings that are highly predictive of the presence of a thrombus at urgent angiography [190,281].

To achieve better sensitivity to slow and weak flow, a single-gate spectral TCD system should be set at maximum allowed power and a large (12–15 mm) sample volume. A power motion Doppler/TCD system should be set at the depth range of presumed arterial occlusion and a small (3 mm) spectral TCD sample volume. In approximately 75% of cases with acute intracranial occlusion, some residual flow signals can be detected from presumed clot location [280,281]. Waveform morphology discloses more information about clot location, hemodynamic significance of obstruction and resistance in the distal vasculature than velocity difference by itself. Moreover, if the MCA on the affected side has a MFV of 30% or less than the non-affected side and it also has delayed systolic flow acceleration, these findings point to a proximal ICA obstruction and not necessarily the MCA lesion [199]. Further waveform analysis of the distal MCA and PCA is required to establish the presence of an additional lesion in the MCA. Waveform analysis also allows determination of possible patency of small perforating arteries in the proximal MCA stem [282]. This finding is often helpful in explaining distribution of the neurologic deficits in the acute stroke patient. Demchuk *et al.* developed the thrombolysis in brain ischemia (TIBI) flow grading system (Figure 6.23) to predict the success of intracranial clot lysis and short-term improvement after ischemic stroke [280]. The definitions are provided below. For more information see Chapter 10.

An acute occlusion is more likely to be found with recent stroke symptoms or fluctuating neurologic deficits and signs of flow diversion and elevated velocities in the branching vessels. A chronic occlusion is often associated with well-developed major collateral channels and lower velocities.

Based on the previous studies [176,273–279] and our own correlations with invasive angiography, Demchuk *et al.* described detailed criteria for intracranial occlusions on TCD [280,283]. For the diagnosis of *MCA occlusion,* the abnormal waveforms have to be found between 40 and 65 mm via the transtemporal approach (Figures 6.24–6.26).

Secondary findings are:

1 flow diversion/compensatory velocity increase in the unilateral ACA and/or PCA;

2 no flow signals from the ACA and ICA with PCA flow identified (possible 'T'-type terminal ICA occlusion (Figure 6.26));

3 diastolic flow and overall velocity decrease from the TICA to the distal MCA.

These findings help to localize MCA occlusion, i.e. M2 MCA, distal M1 MCA, proximal M1 MCA with or without residual flow to perforators, or extending from the TICA (Figures 6.24–6.26). If findings are uncertain or multiple lesions are suspected, these findings need to be confirmed by insonation across the midline from the contralateral temporal window when time permits (see also fast track insonation protocol).

With *intracranial or terminal ICA occlusion (C1–C2 segments),* the abnormal waveforms are found at 62–70 mm via the transorbital approach. For example, with ICA occlusion above the origin of the ophthalmic artery, a high-resistance or dampened ICA siphon signal can be found transorbitally (Figure 6.27). The hallmark of an isolated distal ICA occlusion is the presence of patent MCA signals (normal or blunted) throughout M1–proximal M2 stems and the presence of collateralization of flow indicating a hemodynamically significant lesion in the ICA.

With a *proximal ICA occlusion,* the most common findings include a blunted MCA signal and reversed OA (Figure 6.28), or absent orbital signals from the OA and ICA siphon. TCD by itself cannot differentiate

Image Not Available

Figure 6.23 Thrombolysis in brain ischemia (TIBI) residual flow grades. (Reprinted with permission from the Health Outcomes Institute, the Woodlands, TX.)

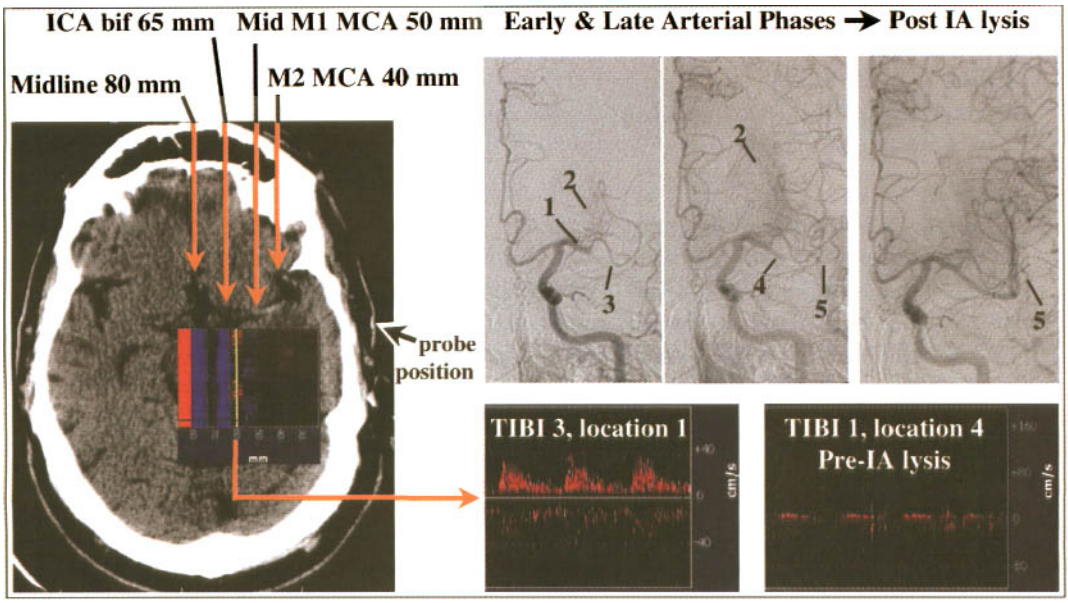

(a)

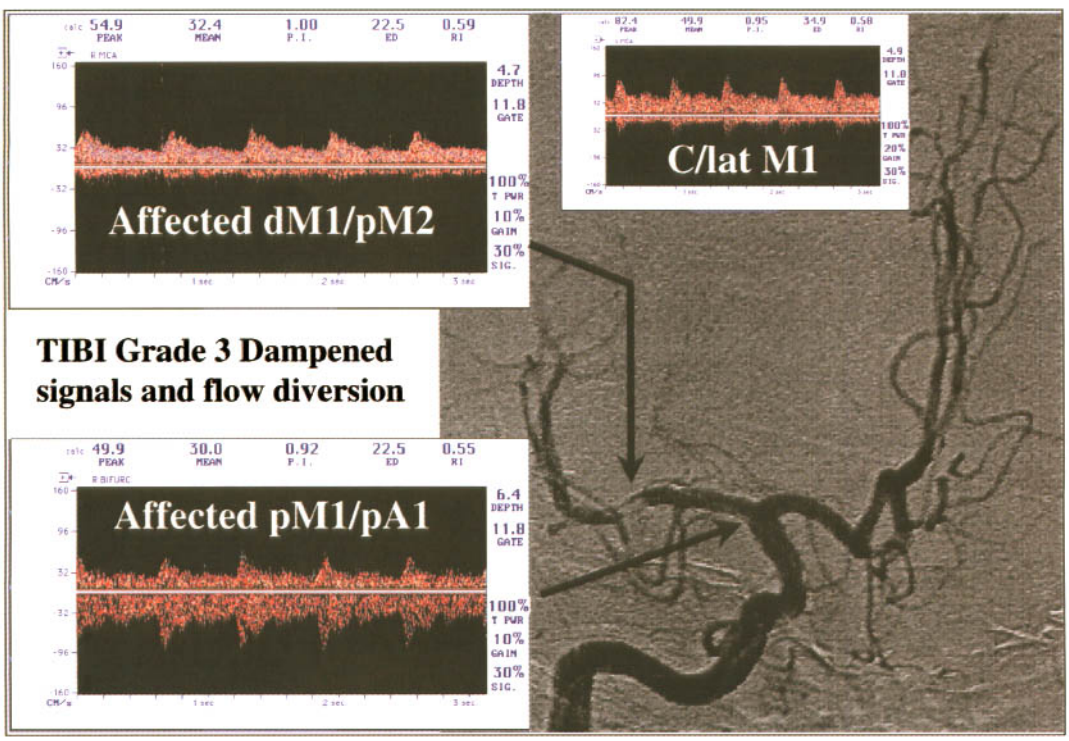

(b)

Figure 6.24 Different levels and residual signals with MCA occlusion. (a) TIBI blunted and minimal signals correlation with early and late angiographic phases showing acute mid-M1 MCA occlusion. (b) TIBI dampened flow signal in a patient with acute thrombus in M2 MCA subdivision.

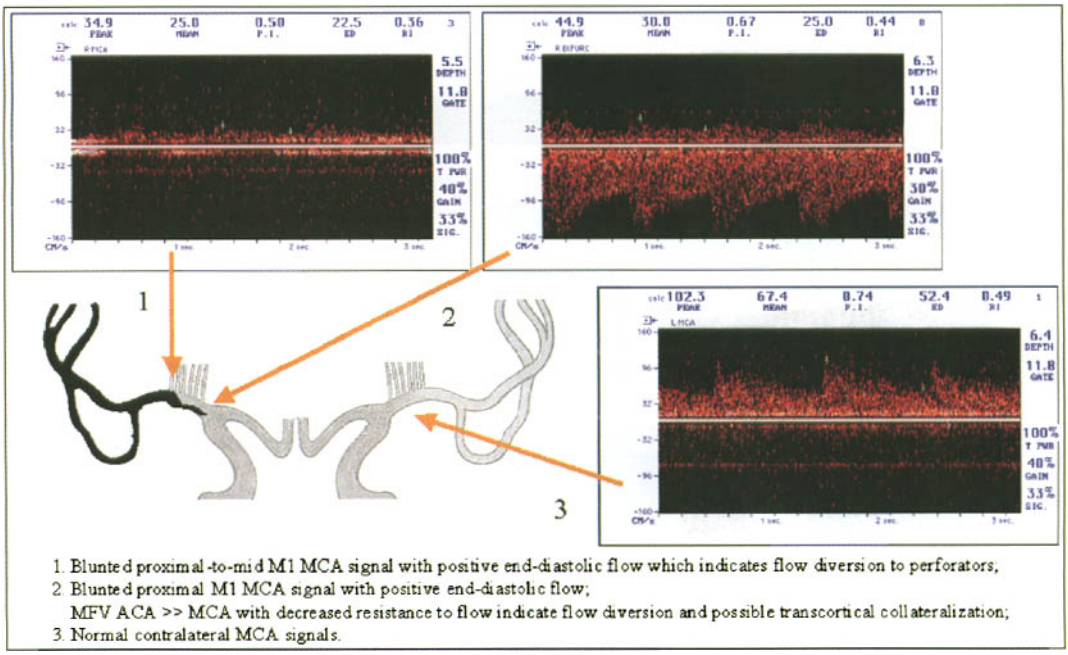

Figure 6.25 A common appearance of an acute proximal M1 middle cerebral artery (MCA) occlusion. Since the residual flow appears to be present up to the mid M1 MCA depths, differential diagnosis includes a subtotal stenosis. In the case of an acute obstruction with fresh clot, the residual flow signals may change rapidly and will depend on recanalization or reocclusion processes. (Reprinted with permission from Demchuk *et al.* [283].)

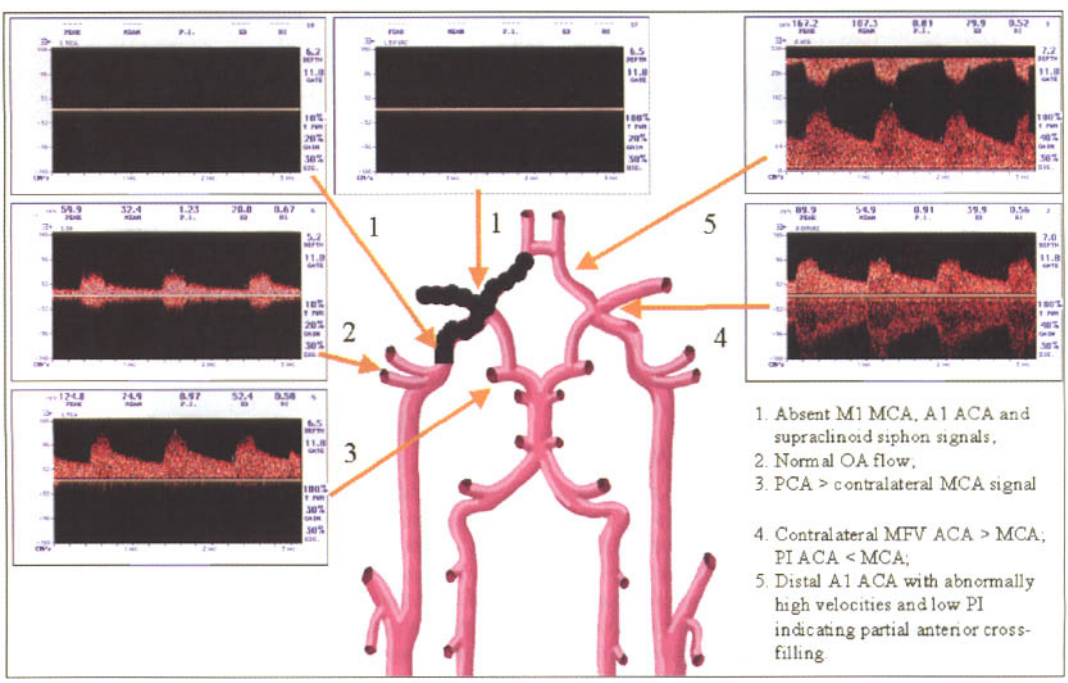

Figure 6.26 Carotid 'T'-type occlusion on transcranial Doppler. (Reprinted with permission from Demchuk *et al.* [283].)

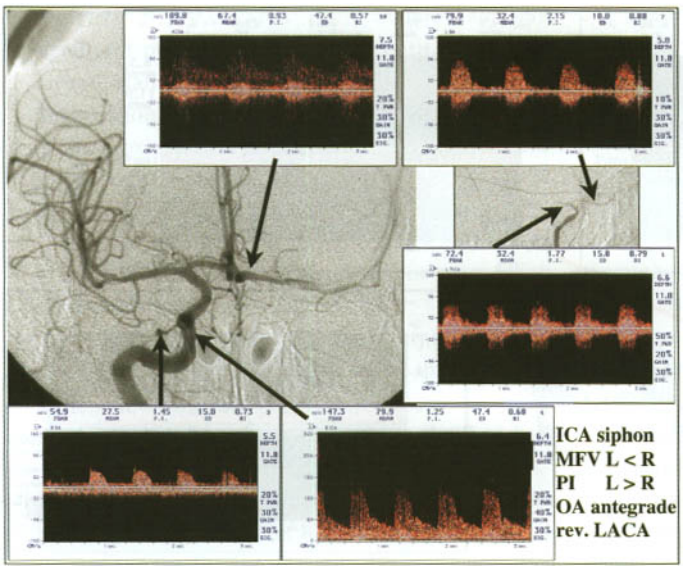

Figure 6.27 Intracranial internal carotid artery occlusion (C1–C2 segments). TCD shows antegrade flow in the left OA and dampened TIBI grade 3 signals in the left TICA through the orbital window compared to contralateral side. DSA shows anterior cross-filling with early mass-effect (left image), and diminution of flow in C2 segment distal to the OA origin (right image).

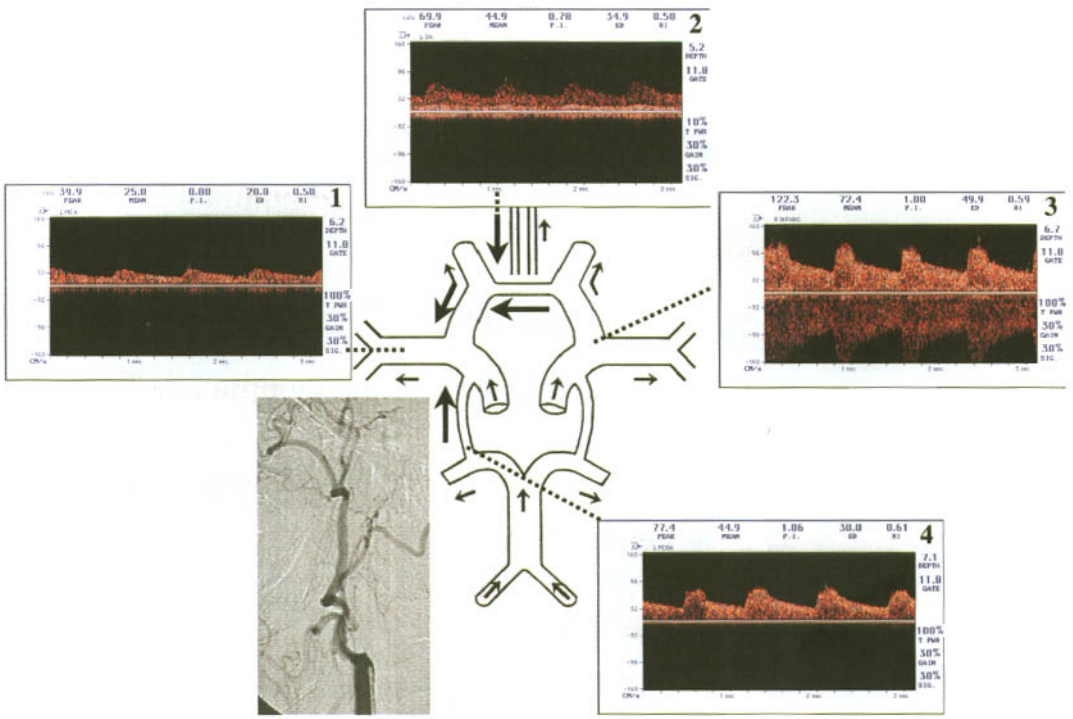

Figure 6.28 Proximal internal carotid artery (ICA) occlusion. The most common site of a proximal ICA occlusion is its extracranial portion particularly at the level of the bulb (bottom left DSA image). If only transcranial Doppler is performed without angiographic correlation, the location of a hemodynamically significant ICA obstruction can only be reported as proximal to the ophthalmic artery origin. Correlation with direct extracranial ultrasound imaging studies is necessary to determine the presence of an occlusion or a hemodynamically significant stenosis in the proximal ICA. **1** blunted signal in the MCA unilateral to ICA occlusion; **2** reversed ophthalmic artery (inverted image); **3** contralateral ACA > MCA indicating collateralization of flow via anterior cross-filling; **4** unilateral P1 PCA or PComA flow (normal systolic flow acceleration, MFV PCA > MCA suggesting functional PComA or transcortical collateralization of flow).

complete ICA occlusion from hemodynamically significant proximal high-grade stenosis, and direct carotid examination should be employed to answer this question. TCD can help to determine an extension of the proximal ICA occlusion into the supraclinoid siphon or terminal ICA, tandem MCA/ICA lesions and the presence of collateral channels.

Secondary findings for any ICA occlusion site include:
1 collateral flow in the PComA and/or cross-filling via the AComA;
2 contralateral ICA compensatory velocity increase; and
3 possible frequent microemboli in the unilateral TICA or MCA.

With an *occlusion in the basilar artery*, the abnormal waveforms are found at 80–100+ mm via the transforaminal approach (Figure 6.29). Arbitrarily, the proximal BA is located at 80 mm, the midbasilar at 90 mm and the distal at 100+ mm depth.

Secondary findings may include;
1 a flow velocity increase in one or both VAs or PICAs indicating cerebellar collateral flow;
2 a high-resistance flow signal in one or both VAs indicating proximal BA occlusion;
3 a high-resistance flow signal at the origin of the BA indicating distal BA occlusion;
4 retrograde (low-resistance, stenotic) flow towards the probe at the top of the BA (proximal BA occlusion collateralized via PComAs);
5 functional PComAs with flow directed away from the probe via the temporal window; and
6 low distal BA velocities with top-of-the basilar occlusion.

TCD diagnosis of distal basilar occlusion or subtotal stenosis without obvious PComA or cross-cerebellar flows is particularly challenging [284,285]. CT angiography or three-dimensional contrast-enhanced transcranial Doppler or duplex imaging with color and power modes may be techniques of choice if distal basilar occlusion is suspected [284–286]. Special caution must be paid to the situation when only relatively low distal BA velocities are found without any other abnormal findings.

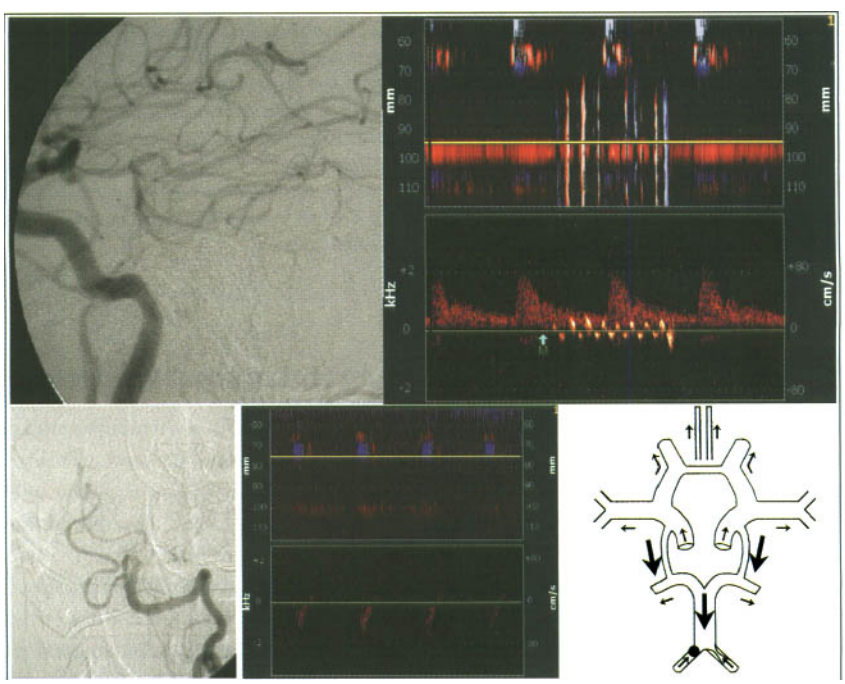

Figure 6.29 Basilar artery occlusion. Top left DSA image shows reversed filling of the distal basilar from carotid injection in a patient with right-sided hemiparesis and total NIHSS score of 11 points. Top right image shows reversed flow in the top of the basilar with response to carotid artery vibration. Bottom right DSA image shows occlusion of the proximal basilar and the left terminal vertebral artery in the presence of an artetic right VA (image not shown). Bottom middle image shows reverberating flow pattern in the left terminal VA. Bottom right graph of the circle of Willis summarizes flow findings.

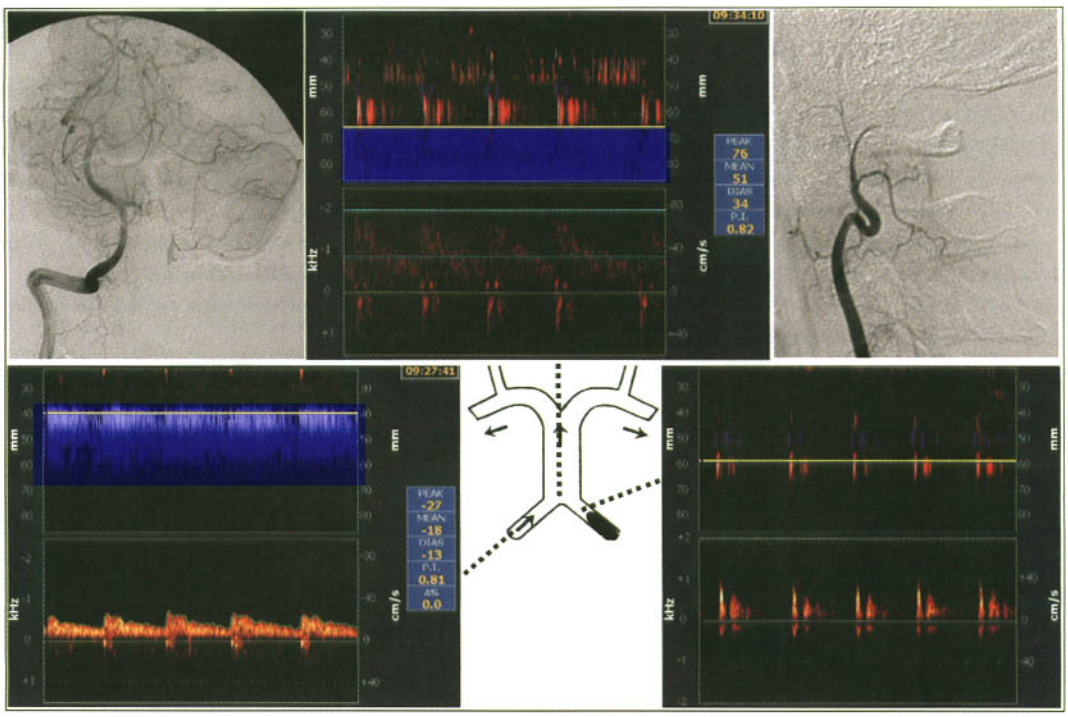

Figure 6.30 Terminal vertebral artery occlusion due to dissection at the skull entrance in a 22-year-old man complaining of dizziness and headache after lifting a heavy object. Top left DSA image shows retrograde filling of the left terminal vertebral artery and posterior inferior cerebellar arteries from the right VA injection. Upper middle image shows low-resistance flow at the junction of the vertebral arteries and the proximal basilar (PMD depth range 65–85 mm), low resistance inverted spectral waveform and high resistance systolic spikes directed towards the probe in reversed left terminal VA. Top right DSA image shows tapering of the left VA flow with dissection at the skull entrance. Bottom left image shows low resistance flow in the right VA upon entering intracranial space. Bottom right image provides a close-up of a high resistance minimal flow signal in the reversed part of the left terminal VA just distal to its occluded segment at the atlas loop.

The diagnosis of *vertebral artery (VA) occlusion* is difficult to establish using TCD alone since an extracranial segmental occlusion may be present [287]. The most accurate diagnosis with TCD can be made for a terminal VA occlusion [156]; however, the sensitivity of abnormal flow findings is only about 60% [283,287,288]. Normal intracranial TCD examination cannot completely rule out VA occlusion, particularly with a proximal location of a segmental and collateralized VA occlusion, or hypoplasia [288]. Figure 6.30 shows terminal VA occlusion. Secondary findings may include normal flow signals directed towards the probe on the side of occlusion indicating collateralization of flow from the other side and filling of PICAs.

Subclavian steal syndrome

Subclavian steal is a hemodynamic condition of reversed flow in one vertebral artery to compensate for a proximal hemodynamic lesion in the unilateral subclavian artery [289]. Thus, blood flow is diverted or 'stolen' from the brain to feed the arm. Subclavian steal is usually an accidental finding since it rarely produces neurologic symptoms. If the patient is asymptomatic, it is called 'subclavian steal phenomenon' and it usually indicates a widespread atherosclerosis in aortic branches. If symptoms of vertebrobasilar ischemia are present, it is called 'subclavian steal syndrome' [289].

Subclavian steal is well studied with ultrasound [290–311]. When steal is present at rest, the main

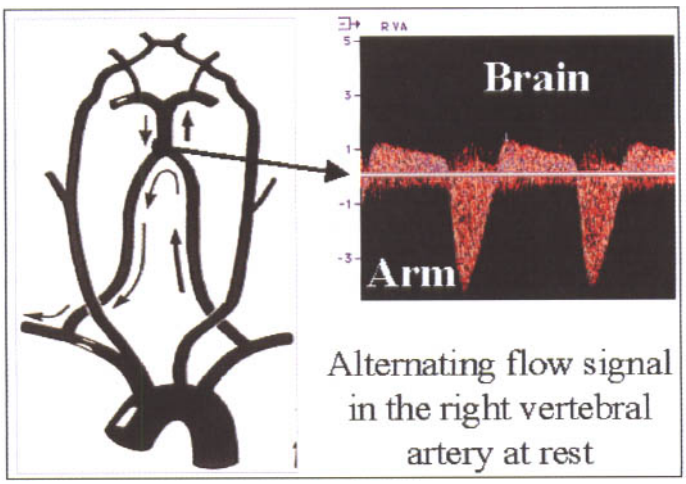

Figure 6.31 Subclavian steal: hemodynamic pathway and waveform.

findings include a difference in blood pressure between arms of ≥ 20 mmHg and, usually, systolic flow reversal (alternating flow signal or absent diastolic flow) in the 'stealing' vertebral artery as well as a low-resistance flow in the donor artery (Figure 6.31). Right-to-left subclavian steal is found in 85% of cases due to the anatomic differences in the origin of these arteries.

If the BP difference between the arms is 10–20 mmHg and the steal waveforms are not present at rest, or flow reversal is incomplete, the hyperemia test should be performed to provoke the steal and to augment flow reversal. The cuff should be inflated to over systolic BP values and flow reduction to the arm should be maintained for about 1–1.5 min (maximum 3 min, if tolerated by the patient). This duration of arterial compression produces ischemia in the arm. The cuff should be quickly released and any augmentation of flow should be monitored by TCD. Once the cuff is released, the blood flow enters tissues with increased metabolic demand produced by a short period of ischemia. Greater demand for blood flow augments the steal and alternating flow can be visualized for a short period of time in the recipient vertebral artery.

The final interpretation

The final interpretation of a non-invasive ultrasound examination should contain, at a minimum:

1 date of the examination;
2 clinical indications;
3 a description of the test that was performed;
4 a statement of the data obtained;
5 reasons for limited evaluation (if not complete);
6 interpretation of the ultrasound examination data;
7 a comparison with results from previous examinations; and
8 clinical implications of this study.

References

1 ICAVL. *Accreditation Material.* Columbia, MD, 1997.
2 Alexandrov AV, Tegeler CH. Diagnostic criteria for transcranial Doppler sonography: a model for quality assurance and laboratory accreditation. *Vasc Ultrasound Today* 1999; **4**: 1–24.
3 Guyton AC. *Textbook of Medical Physiology*, 7th edn. Philadelphia: W.B. Saunders Co., 1986: 209–10.
4 Liepsch D. Principles and models of hemodynamics. In: Hennerici M, Meairs S, eds. *Cerebrovascular Ultrasound: Theory, Practice, and Future Developments.* Cambridge: Cambridge University Press, 2001: 27–8.
5 von Reutern GM, Budingen HJ. *Ultrasound Diagnosis of Cerebrovascular Disease.* Stuttgart: Georg Thieme Verlag, 1993: 56–62.
6 Toole JF. *Cerebrovascular Disorders*, 4th edn. New York: Raven Press, 1990: 28–49.
7 Perktold K, Karner G. Computational principles and models of hemodynamics. In: Hennerici M, Meairs S, eds. *Cerebrovascular Ultrasound: Theory, Practice, and Future Developments.* Cambridge: Cambridge University Press, 2001: 63–76.
8 Glagov S, Bassiouny HS, Zarins CK, Slesers A. Morphogenesis of the atherosclerotic plaque. In: Hennerici M, Meairs S, eds. *Cerebrovascular Ultrasound: Theory, Practice, and Future Developments.* Cambridge: Cambridge University Press, 2001: 117–33.

9 von Reutern GM, Budingen HJ. *Ultrasound Diagnosis of Cerebrovascular Disease*. Stuttgart: Georg Thieme Verlag, 1993: 76–80.

10 Lindegaard KF, Bakke SJ, Grolimund P, Aaslid R, Huber P, Nornes H. Assessment of intracranial hemodynamics in carotid artery disease by transcranial Doppler ultrasound. *J Neurosurg* 1985; **63**: 89–8.

11 Hennerici M, Rautenberg W, Schwartz A. Transcranial Doppler ultrasound for the assessment of intracranial arterial flow velocity—Part I. Examination technique and normal values. *Surg Neurol* 1987; **27**: 439–48.

12 Adams RJ, Nichols FT, Figueroa R, McKie V, Lott T. Transcranial Doppler correlation with cerebral angiography in sickle cell disease. *Stroke* 1992; **23**: 1073–7.

13 Otis SM, Ringelstein EB. The transcranial Doppler examination: principles and applications of transcranial Doppler sonography. In: Tegeler CH, Babikian VL, Gomez CR, eds. *Neurosonology*. St Louis: Mosby, 1996: 140–55.

14 Babikian V, Sloan MA, Tegeler CH, DeWitt LD, Fayad PB, Feldmann E, Gomez CR. Transcranial Doppler validation pilot study. *J Neuroimaging* 1993; **3**: 242–9.

15 Bragoni M, Feldmann E. Transcranial Doppler indices of intracranial hemodynamics. In: Tegeler CH, Babikian VL, Gomez CR, eds. *Neurosonology*. St Louis: Mosby, 1996: 129–39.

16 Gosling RG, King DH. Arterial assessment by Doppler-shift ultrasound. *Proc R Soc Med* 1974; **67**: 447–9.

17 Pourcellot L. Applications cliniques de l'examen Doppler transcutane. Les colloques de l'institute national de la santé et de la recherche medicale. *INSERM* 1974: 213–40.

18 Michel E, Zernikow B. Gosling's pulsatility index revisited. *Ultrasound Med Biol* 1998; **24**: 597–9.

19 Stolz E, Kaps M, Kern A, Dorndorf W. Frontal bone windows for transcranial color-coded duplex sonography. *Stroke* 1999; **30** (4): 814–20.

20 North American Symptomatic Carotid Endarterectomy Trial Collaborators. Beneficial effect of carotid endarterectomy in symptomatic patients with high-grade carotid stenosis. *N Engl J Med* 1991; **325**: 445–53.

21 European Carotid Surgery Trialists' Collaborative Group. Randomised trial of endarterectomy for recently symptomatic carotid stenosis: final results of the MRC European Carotid Surgery Trial (ECST). *Lancet* 1998; **351**: 1379–87.

22 Executive Committee of the Asymptomatic Carotid Atherosclerosis Study. Endarterectomy for asymptomatic carotid artery stenosis. *JAMA* 1995; **273**: 1421–8.

23 Gomez CR. Carotid angioplasty and stenting: new horizons. *Curr Atheroscler Rep* 2000; **2**: 151–9.

24 Gertler JP, Cambria RP, Kistler JP, Geller SC, MacDonald NR, Brewster DC, Abbott WM. Carotid surgery without arteriography: noninvasive selection of patients. *Ann Vasc Surg* 1991; **5**: 253–6.

25 Alexandrov AV, Bladin CF, Maggisano R, Norris JW. Measuring carotid stenosis: time for a re-appraisal. *Stroke* 1993; **24**: 1292–6.

26 Pan XM, Saloner D, Reilly LM, Bowersox JC, Murray SP, Anderson CM, Gooding GA, Rapp JH. Assessment of carotid artery stenosis by ultrasonography, conventional angiography, and magnetic resonance angiography: correlation with ex vivo measurement of plaque stenosis. *J Vasc Surg* 1995; **21**: 82–8.

27 Fox AJ. How to measure carotid stenosis? *Radiology* 1993; **186**: 316–8.

28 Alexandrov AV, Bladin CF, Murphy J, Hamilton P, Maggisano R. Clinical applicability of methods to measure carotid stenosis. *J Stroke Cerebrovasc Dis* 1994; **4**: 258–61.

29 Rothwell PM, Gibson RJ, Slattery J, Sellar RJ, Warlow CP. Equivalence of measurements of carotid stenosis. A comparison of three methods on 1001 angiograms. European Carotid Surgery Trialists' Collaborative Group. *Stroke* 1994; **25**: 2435–9.

30 Bladin CF, Alexandrov AV, Murphy J, Maggisano R, Norris JW. Carotid Stenosis Index: a new method of measuring carotid stenosis. *Stroke* 1995; **26**: 230–4.

31 Williams MA, Nicolaides AN. Predicting the normal dimensions of the internal and external carotid arteries from the diameter of the common carotid artery. *Eur J Vasc Surg* 1986; **1**: 91–6.

32 Alexandrov AV, Brodie DS, McLean A, Murphy J, Hamilton P, Burns PN. Correlation of peak systolic velocity and angiographic measurement of carotid stenosis revisited. *Stroke* 1997; **28**: 339–42.

33 Bladin CF, Alexandrova NA, Murphy J, Alexandrov AV, Maggisano R, Norris JW. The clinical value of methods to measure carotid stenosis. *Int Angiol* 1996; **16**: 252–9.

34 Vanninen RL, Manninen HI, Partanen PK, Tulla H, Vainio PA. How should we estimate carotid stenosis using magnetic resonance angiography? *Neuroradiology* 1996; **38**: 299–305.

35 Fox AJ. How should we estimate carotid stenosis using magnetic resonance angiography? *Neuroradiology* 1997; **39**: 532–3.

36 Cumming MJ, Morrow IM. Carotid artery stenosis: a prospective comparison of CT angiography and conventional angiography. *AJR* 1994; **163**: 517–23.

37 Heiserman JE, Zabramnski JM, Drayer BP, Keller PJ. Clinical significance of the flow gap in carotid magnetic resonance angiography. *J Neurosurg* 1996; **85**: 384–7.

38 Blakely DD, Oddone EZ, Hasselbad V, Simel DL, Matchar DB. Noninvasive carotid artery testing. A

meta-analytic review. *Ann Intern Med* 1995; **122**: 360–7.

39 Kent KC, Kuntz KM, Patel MR, Kim D, Klufas RA, Whittemore AD, Polak JF, Skillman JJ, Edelman RR. Perioperative imaging strategies for carotid endarterectomy. An analysis of morbidity and cost-effectiveness in symptomatic patients. *JAMA* 1995; **274**: 888–93.

40 Erdoes LS, Marek JM, Mills JL, Berman SS, Whitehill T, Hunter GC, Feinberg W, Krupski W. The relative contributions of carotid duplex scanning, magnetic resonance angiography, and cerebral arteriography to clinical decision making: a prospective study in patients with carotid occlusive disease. *J Vasc Surg* 1996; **23**: 950–6.

41 Leclerc X, Godefroy O, Pruvo JP, Leys D. Computed tomographic angiography for the evaluation of carotid artery disease. *Stroke* 1995; **26**: 1577–81.

42 Post K, Eckstein HH, Hoffmann E, Volke A, Post S, Allenberg JR, Kauffmann GW. The accuracy of angiography and CT angiography of the carotid bifurcation compared to macro-morphological correlation. *Rofo Fortschr Geb Roentgenstr Neuen Bildgeb Verfahr* 1996; **164**: 196–200 [in German].

43 Link J, Brossman J, Panselin V, Gluer CC, Heller M. Common carotid bifurcation: preliminary results of CT angiography and color-coded duplex sonography compared with digital subtraction angiography. *AJR* 1997; **168**: 361–5.

44 Bousser MG. Benefits from carotid surgery? Yes, but . . . *Cerebrovasc Dis* 1992; **2**: 122–6.

45 Rothwell PM, Pendlebury ST, Wardlaw J, Warlow CP. Critical appraisal of the design and reporting of studies of imaging and measurement of carotid stenosis. *Stroke* 2000; **31**: 1444–50.

46 Comerota AJ, Cranley JJ, Cook SE. Real-time B-mode carotid imaging in diagnosis of cerebrovascular disease. *Surgery* 1981; **89**: 718–29.

47 deBray JM, Glatt B. Quantitation of atheromatous stenosis in the extracranial internal carotid artery. *Cerebrovasc Dis* 1995; **5**: 414–26.

48 Paivansalo M. Ultrasound terminology. *Europ Med Ultrason* 1984; **6**: 3–4.

49 Johnson JM, Kennely M, Decesare D, Morgan S, Sparrow A. Natural history of asymptomatic carotid plaque. *Arch Surg* 1985; **120**: 1010–2.

50 Ruthlein VM, Spengel FA. Diagnosis of symptomatic plaque in the carotid arteries of patients with neurologic ischemia symptoms. *Bildebung* 1987–89; **56**: 19–22 [in German].

51 Sterpetti AV, Schultz RD, Feldhaus RJ, Davenport KL, Richardson M, Farina C, Hunter WJ. Ultrasonic features of carotid plaque and the risk of subsequent neurologic deficits. *Surgery* 1988; **104**: 652–60.

52 Gray-Weale AC, Graham JC, Burnett JR, Byrne K, Lusby RJ. Carotid artery atheroma: comparison of preoperative B-mode ultrasound appearance with carotid endarterectomy specimen pathology. *J Cardiovasc Surg (Torino)* 1988; **29**: 676–81.

53 Widder B, Paulat K, Hackspacher J, Hamann H, Hutschenreiter S, Kreutzer C, Ott F, Vollmar J. Morphological characterization of carotid artery stenoses by duplex scanning. *Ultrasound Med Biol* 1990; **16**: 349–54.

54 Geroulakos G, Ramaswami G, Nicolaides A, James K, Labropoulos N, Belcaro G, Holloway M. Characterization of symptomatic and asymptomatic carotid plaques using high-resolution real-time ultrasonography. *Br J Surg* 1993; **80**: 1274–7.

55 Polak JF, Shemanski L, O'Leary DH *et al.* Hypoechoic plaque at US of the carotid artery: an independent risk factor for incident stroke in adults aged 65 years or older. Cardiovascular Health Study. *Radiology* 1998; **208**: 649–54.

56 Sabetai MM, Tegos TJ, Nicolaides AN, El-Atrozy TS, Dhanjil S, Griffin M, Belcaro G, Geroulakos G. Hemispheric symptoms and carotid plaque echomorphology. *J Vasc Surg* 2000; **31**: 39–49.

57 el-Barghouty N, Geroulakos G, Nicolaides A, Androulakis A, Bahal V. Computer-assisted carotid plaque characterization. *Eur J Vasc Endovasc Surg* 1995; **9**: 389–93.

58 Pedro LM, Pedro MM, Goncalves I, Carneiro TF, Balsinha C, Fernandez E, Fernadez R, Fernandez E, Fernandez J. Computer-assisted carotid plaque analysis: characteristics of plaques associated with cerebrovascular symptoms and cerebral infarction. *Eur J Vasc Endovasc Surg* 2000; **19**: 118–23.

59 Fisher M. Carotid plaque morphology in symptomatic and asymptomatic patients. In: Caplan LR, Shifrin EG, Nicolaides AN, Moore WS, eds. *Cerebrovascular Ischemia: Investigation and Management.* London: Med-Orion, 1996: 19–24.

60 Schulte-Altendorneburg G, Droste DW, Haas N, Kemeny V, Nabavi DG, Furezi L, Ringelstein EB. Preoperative B-mode ultrasound plaque appearance compared with carotid endarterectomy specimen histology. *Acta Neurol Scand* 2000; **101**: 188–94.

61 Wolverson MK, Bashiti HM, Peterson GJ. Ultrasonic tissue characterization of atheromatous plaques using a high resolution real time scanner. *Ultrasound Med Biol* 1983; **9**: 599–609.

62 O'Leary DH, Holen J, Ricotta JJ, Roe S, Schenk EA. Carotid bifurcation disease: prediction of ulceration with B-mode US. *Radiology* 1987; **162**: 523–5.

63 Bluth EI, McVay LV, Merritt CR, Sullivan MA. The identification of ulcerative plaque with high resolution

duplex carotid scanning. *J Ultrasound Med* 1988; **7**: 73–6.

64 Tegos TJ, Kalomiris KJ, Sabetai MM, Kalodiki E, Nicolaides AN. Significance of sonographic tissue and surface characteristics of carotid plaques. *AJNR Am J Neuroradiol* 2001; **22**: 1605–12.

65 Steinke W, Els T, Hennerici M. Comparison of flow disturbances in small carotid atheroma using a multigate pulsed Doppler and Doppler color flow imaging. *Ultrasound Med Biol* 1992; **18**: 11–8.

66 Steinke W, Hennerici M, Rautenberg W, Mohr JP. Symptomatic and asymptomatic high-grade carotid stenoses in Doppler color-flow imaging. *Neurology* 1992; **42**: 131–8.

67 Steinke W, Meairs S, Reis S, Hennerici M. Sonographic assessment of carotid artery stenosis. Comparison of power Doppler imaging and color Doppler flow imaging. *Stroke* 1996; **27**: 91–4.

68 Sitzer M, Muller W, Rademacher J, Seibler M, Hort W, Kniemeyer HW, Steinmetz H. Color-flow Doppler-assisted duplex imaging fails to detect ulceration in high grade internal carotid artery stenosis. *J Vasc Surg* 1996; **23**: 461–5.

69 Droste DW, Karl M, Bohle RM, Kaps M. Comparison of ultrasonic and histopathological features of carotid artery stenosis. *Neurol Res* 1997; **19**: 380–4.

70 Schminke U, Motsch L, Hilker L, Kessler C. Three-dimensional ultrasound observation of carotid artery plaque ulceration. *Stroke* 2000; **31**: 1651–15.

71 Meairs S, Hennerici M. Four-dimensional ultrasonographic characterization of plaque surface motion in patients with symptomatic and asymptomatic carotid artery stenosis. *Stroke* 1999; **30**: 1807–13.

72 Sliwka U, Rother J, Steinke W, Hennerici M. The value of duplex sonography in cerebral ischemia. *Bildebung* 1991; **58**: 182–91 [in German].

73 Tschammler A, Landwehr P, Hohmann M, Moll R, Wittenberg G, Lackner K. Color-coded duplex sonography of the extracranial arteries supplying the brain: diagnostic significance and sources of error compared in comparison with i.a. DSA. *Rofo Fortschr Geb Roentgenstr Neuen Bildgeb Verfahr* 1991; **155**: 452–9.

74 Bray JM, Galland F, Lhoste P, Nicolau S, Dubas F, Emile J, Pillet J. Color Doppler and duplex sonography and angiography of the carotid bifurcations. Prospective, double-blind study. *Neuroradiology* 1995; **37**: 219–24.

75 Hetzel A, Eckenweber B, Trummer B, Wernz M, von Reutern GM. Color-coded duplex ultrasound in pre-occlusive stenoses of the internal carotid artery. *Ultraschall Med* 1993; **14**: 240–6 [in German].

76 Steinke W, Reis S, Artemius N, Schwartz A, Hennerici M. Power Doppler imaging of carotid stenosis. Comparison with color Doppler flow imaging and angiography. *Stroke* 1997; **28**: 1981–7.

77 Spencer MP, Reid JM. Quantitation of carotid stenosis with continuous wave (C-W) Doppler ultrasound. *Stroke* 1979; **10**: 793–8.

78 Bendick PJ. Hemodynamics of arterial narrowing and occlusion. *J Vasc Technol* 1994; **18**: 235–40.

79 Widder B, von Reutern GM, Neuerburg-Heusler D. Morphologic and Doppler sonographic criteria for determining the degree of stenosis of the internal carotid artery. *Ultraschall Med* 1986; **7**: 70–5 [in German].

80 AbuRhama AF, Richmond BK, Robinson PA, Khan S, Pollack JA, Alberts S. Effect of contra-lateral severe stenosis or carotid occlusion on duplex criteria of ipsilateral stenoses: comparative study of various duplex parameters. *J Vasc Surg* 1995; **22**: 751–61.

81 Blackshear WM, Phillips DJ, Chikos PM, Harley JD, Thiele BL, Strandness DE. Carotid artery velocity patterns in normal and stenotic vessels. *Stroke* 1980; **11**: 67–71.

82 Moneta GL, Edwards JM, Chitwood RW, Taylor LM, Lee RW, Cummings CA, Porter JM. Correlation of North American Symptomatic Carotid Endarterectomy Trial (NASCET) angiographic definition of 70–99% internal carotid stenosis with duplex scanning. *J Vasc Surg* 1993; **17**: 152–7.

83 Hunink MG, Polak JF, Barlan MM, O'Leary DH. Detection and quantification of carotid artery stenosis: efficacy of various Doppler velocity parameters. *Am J Roentgenol* 1993; **160**: 619–25.

84 Soulez G, Therasse E, Robillard P, Fontaine A, Denbow N, Bourgouin P, Oliva VL. The value of internal carotid systolic velocity ratio for assessing carotid artery stenosis with Doppler sonography. *Am J Roentgenol* 1999; **172**: 207–12.

85 Paivansalo M, Leinonen S, Turunen J, Tikkakoski T, Suramo I. Quantification of carotid artery stenosis with various Doppler velocity parameters. *Rofo Fortschr Geb Rontgenstr Neuen Bildgeb Verfahr* 1996; **164**: 108–13.

86 Neschis DG, Lexa FJ, Davis JT, Carpenter JP. Duplex criteria for determination of 50% or greater carotid stenosis. *J Ultrasound Med* 2001; **20** (3): 207–15.

87 Ray SA, Lockhart SJ, Dourado R, Irvine AT, Burnand KG. Effect of contralateral disease on duplex measurements of internal carotid artery stenosis. *Br J Surg* 2000; **87**: 1057–62.

88 Daigle RJ, Stavros AT, Lee RM. Overestimation of velocity and frequency values by multielement linear array Dopplers. *J Vasc Technol* 1990; **14**: 206–13.

89 Blackshear WM, Lamb SL, Kollipara VS, Anderson JD, Murtagh FR, Shah CP, Farber MS. Correlation of hemodynamically significant internal carotid stenosis with pulsed Doppler frequency analysis. *Ann Surg* 1984; **199**: 475–81.

90 Lindegaard K, Bakke S, Grolimund P, Aaslid R, Huber P, Nornes H. Assessment of intracranial hemodynamics

in carotid artery disease by transcranial Doppler ultrasound. *J Neurosurg* 1985; **63**: 890–8.

91 Schneider P, Rossman M, Bernstein E, Torem S, Ringelstein E, Otis S. Effect of internal carotid artery occlusion on intracranial hemodynamics: transcranial Doppler evaluation and clinical correlation. *Stroke* 1988; **19**: 589–93.

92 Cantelmo N, Babikian V, Johnson W, Samaraweera R, Hyde C, Pochay V. Correlation of transcranial Doppler and noninvasive tests with angiography in the evaluation of extracranial carotid disease. *J Vasc Surg* 1990; **11**: 786–92.

93 Giller CA, Mathews D, Purdy P, Kopitnik TA, Batjer HH, Samson DS. The transcranial Doppler appearance of acute carotid artery occlusion. *Ann Neurol* 1992; **31**: 101–3.

94 Wilterdink JL, Feldmann E, Furie KL, Bragoni M, Benavides JG. Transcranial Doppler ultrasound battery reliably identifies severe internal carotid artery stenosis. *Stroke* 1997; **28**: 133–6.

95 Can U, Furie KL, Suwanwela N, Southern JF, Macdonald NR, Ogilvy CS, Buonanno FS, Koroshetz WJ, Kistler JP. Transcranial Doppler ultrasound criteria for hemodynamically significant internal carotid artery stenosis based on residual lumen diameter calculated from en bloc endarterectomy specimens. *Stroke* 1997; **28**: 1966–71.

96 Christou I, Felberg RA, Demchuk AM, Grotta JC, Burgin WS, Malkoff M, Alexandrov AV. Accuracy parameters of a broad diagnostic battery for bedside transcranial Doppler to detect flow changes with internal carotid artery stenosis or occlusion. *J Neuroimaging* 2001; **11**: 236–42.

97 Reynolds PS, Greenberg JP, Lien LM, Meads DC, Myers LG, Tegeler CH. Ophthalmic artery flow direction on color flow duplex imaging is highly specific for severe carotid stenosis. *J Neuroimaging* 2002; **12**: 5–8.

98 Roederer GO, Langlois Y, Chan AT, Breslau P, Phillips DJ, Beach KW, Chikos PM, Strandness DE. Post-endarterectomy carotid ultrasonic duplex scanning concordance with contrast angiography. *Ultrasound Med Biol* 1983; **9**: 73–8.

99 Robbin ML, Lockhart ME, Weber TM, Vitek JJ, Smith JK, Yadav J, Mathur A, Iyer SS, Roubin GS. Carotid artery stents: early and intermediate follow-up with Doppler US. *Radiology* 1997; **205**: 749–56.

100 AbuRahma AF, Richmond BK, Robinson PA, Khan S, Pollack JA, Alberts S. Effect of contralateral severe stenosis or carotid occlusion on duplex criteria of ipsilateral stenoses: comparative study of various duplex parameters. *J Vasc Surg* 1995; **22**: 751–61.

101 Rouleau PA, Huston J III, Gilbertson J, Brown RD Jr, Meyer FB, Bower TC. Carotid artery tandem lesions: frequency of angiographic detection and consequences for endarterectomy. *AJNR Am J Neuroradiol* 1999; **20**: 621–5.

102 Day AL, Rhoton AL, Quisling RG. Resolving siphon stenosis following endarterectomy. *Stroke* 1980; **11**: 278–81.

103 Guppy KH, Charbel FT, Loth F, Ausman JI. Hemodynamics of in-tandem stenosis of the internal carotid artery: when is carotid endarterectomy indicated? *Surg Neurol* 2000; **54**: 145–52.

104 Sitzer M, Furst G, Siebler M, Steinmetz H. Usefulness of an intravenous contrast medium in the characterization of high-grade internal carotid stenosis with color Doppler-assisted duplex imaging. *Stroke* 1994; **25** (2): 385–9.

105 Furst G, Saleh A, Wenserski F, Malms J, Cohnen M, Aulich A, Neumann-Haefelin T, Schroeter M, Steinmetz H, Sitzer M. Reliability and validity of noninvasive imaging of internal carotid artery pseudoocclusion. *Stroke* 1999; **30** (7): 1444–9.

106 Ferrer JM, Samso JJ, Serrando JR, Valenzuela VF, Montoya SB, Docampo MM. Use of ultrasound contrast in the diagnosis of carotid artery occlusion. *J Vasc Surg* 2000; **31**: 736–41.

107 Jung EM, Kubale R, Clevert DA, Lutz R, Rupp N. B-flow and contrast medium-enhanced power Doppler (Optison (R))—preoperative diagnosis of high-grade stenosis of the internal carotid artery. *Rofo Fortschr Geb Rontgenstr Neuen Bildgeb Verfahr* 2002; **174**: 62–9 [in German].

108 Maroon JC, Campbell RL, Dyken ML. Internal carotid artery occlusion diagnosed by Doppler ultrasound. *Stroke* 1970; **1**: 122–7.

109 Muller HR. The diagnosis of internal carotid artery occlusion by directional Doppler sonography of the ophthalmic artery. *Neurology* 1972; **22**: 816–23.

110 Hill SL, Christie A, McDannald ER, Donato AT, Martin D. Noninvasive differentiation of carotid artery occlusion from high-grade stenosis. *Am Surg* 1987; **53**: 84–93.

111 Bodily KC, Phillips DJ, Thiele BL, Strandness DE. Noninvasive detection of internal carotid artery occlusion. *Angiology* 1981; **32**: 517–21.

112 Ringelstein EB, Zeumer H, Angelou D. The pathogenesis of strokes from internal carotid artery occlusion. Diagnostic and therapeutical implications. *Stroke* 1983; **14**: 867–75.

113 Bishop CC, Powell S, Insall M, Rutt D, Browse NL. Effect of internal carotid artery occlusion on middle cerebral artery blood flow at rest and in response to hypercapnia. *Lancet* 1986; **1**: 710–2.

114 Schneider PA, Rossman ME, Bernstein EF, Torem S, Ringelstein EB, Otis SM. Effect of internal carotid artery occlusion on intracranial hemodynamics. Transcranial Doppler evaluation and clinical correlation. *Stroke* 1988; **19**: 589–93.

115 Giller CA, Steig P, Batjer HH, Samson D, Purdy P. Transcranial Doppler ultrasound as a guide to graded therapeutic occlusion of the carotid artery. *Neurosurgery* 1990; **26**: 307–11.

116 Kuwert T, Hennerici M, Langen KJ, Herzog H, Kops ER, Aulich A, Rautenberg W, Feinendegen LE. Compensatory mechanisms in patients with asymptomatic carotid artery occlusion. *Neurol Res* 1990; **12**: 89–93.

117 Yasaka M, Omae T, Tsuchiya T, Yamaguchi T. Ultrasonic evaluation of the site of carotid axis occlusion in patients with acute cardioembolic stroke. *Stroke* 1992; **23**: 420–2.

118 Lee TH, Ryu SJ, Chen ST, Tseng KJ. Comparison between carotid duplex sonography and angiography in the diagnosis of extracranial internal carotid artery occlusion. *J Formos Med Assoc* 1992; **91**: 575–9.

119 Hetzel A, Eckenweber B, Trummer B, Wernz M, von Reutern GM. Color-coded duplex ultrasound in pre-occlusive stenoses of the internal carotid artery. *Ultraschall Med* 1993; **14** (5): 240–6 [in German].

120 Muller M, Hermes M, Bruckmann H, Schimrigk K. Transcranial Doppler ultrasound in the evaluation of collateral blood flow in patients with internal carotid artery occlusion: correlation with cerebral angiography. *AJNR Am J Neuroradiol* 1995; **16**: 195–202.

121 AbuRahma AF, Pollack JA, Robinson PA, Mullins D. The reliability of color duplex ultrasound in diagnosing total carotid artery occlusion. *Am J Surg* 1997; **174**: 185–7.

122 Lee TH, Ryu SJ, Chen ST, Chan JL. Carotid ultrasonographic findings in intracranial internal carotid artery occlusion. *Angiology* 1993; **44**: 607–13.

123 Kimura K, Yonemura K, Terasaki T, Hashimoto Y, Uchino M. Duplex carotid sonography in distinguishing acute unilateral atherothrombotic from cardioembolic carotid artery occlusion. *AJNR Am J Neuroradiol* 1997; **18** (8): 1447–52.

124 Delcker A, Diener HC, Wilhelm H. Source of cerebral microembolic signals in occlusion of the internal carotid artery. *J Neurol* 1997; **244** (5): 312–7.

125 Kimura K, Yasaka M, Minematsu K, Wada K, Uchino M, Yonemura K, Ogata J, Yamaguchi T. Oscillating thromboemboli within the extracranial internal carotid artery demonstrated by ultrasonography in patients with acute cardioembolic stroke. *Ultrasound Med Biol* 1998; **24** (8): 1121–4.

126 Eudo M, de Bray JM. Floating thrombus in the carotid. *J Radiol* 2000; **81**: 1713–4 [in French].

127 de Bray JM, Dubas F, Joseph PA, Causeret H, Pasquier JP, Emile J. Ultrasonic study of 22 cases of carotid artery dissection. *Rev Neurol (Paris)* 1989; **145** (10): 702–9 [in French].

128 Hennerici M, Steinke W, Rautenberg W. High-resistance Doppler flow pattern in extracranial carotid dissection. *Arch Neurol* 1989; **46** (6): 670–2.

129 Kaps M, Dorndorf W, Damian MS, Agnoli L. Intracranial haemodynamics in patients with spontaneous carotid dissection. Transcranial Doppler ultrasound follow-up studies. *Eur Arch Psychiatry Neurol Sci* 1990; **239** (4): 246–56.

130 Steinke W, Schwartz A, Hennerici M. Doppler color flow imaging of common carotid artery dissection. *Neuroradiology* 1990; **32** (6): 502–5.

131 Sturzenegger M. Ultrasound findings in spontaneous carotid artery dissection. The value of duplex sonography. *Arch Neurol* 1991; **48** (10): 1057–63.

132 de Bray JM, Lhoste P, Dubas F, Emile J, Saumet JL. Ultrasonic features of extracranial carotid dissections: 47 cases studied by angiography. *J Ultrasound Med* 1994; **13** (9): 659–64.

133 Steinke W, Rautenberg W, Schwartz A, Hennerici M. Noninvasive monitoring of internal carotid artery dissection. *Stroke* 1994; **25** (5): 998–1005.

134 Desfontaines P, Despland PA. Dissection of the internal carotid artery: aetiology, symptomatology, clinical and neurosonological follow-up, and treatment in 60 consecutive cases. *Acta Neurol Belg* 1995; **95** (4): 226–34.

135 Sturzenegger M, Mattle HP, Rivoir A, Baumgartner RW. Ultrasound findings in carotid artery dissection: analysis of 43 patients. *Neurology* 1995; **45** (4): 691–8.

136 Babikian VL, Forteza AM, Gavrilescu T, Samaraweera R. Cerebral microembolism and extracranial internal carotid artery dissection. *J Ultrasound Med* 1996; **15** (12): 863–6.

137 Srinivasan J, Newell DW, Sturzenegger M, Mayberg MR, Winn HR. Transcranial Doppler in the evaluation of internal carotid artery dissection. *Stroke* 1996; **27** (7): 1226–30.

138 Bassetti C, Carruzzo A, Sturzenegger M, Tuncdogan E. Recurrence of cervical artery dissection. A prospective study of 81 patients. *Stroke* 1996; **27** (10): 1804–7.

139 Koennecke HC, Trocio SH Jr, Mast H, Mohr JP. Microemboli on transcranial Doppler in patients with spontaneous carotid artery dissection. *J Neuroimaging* 1997; 7 (4): 217–20.

140 Giroud M, Lemesle M, Madinier G, Manceau E, Osseby GV, Dumas R. Stroke in children under 16 years of age. Clinical and etiological difference with adults. *Acta Neurol Scand* 1997; **96** (6): 401–6.

141 Rommel O, Niedeggen A, Tegenthoff M, Kiwitt P, Botel U, Malin J. Carotid and vertebral artery injury following severe head or cervical spine trauma. *Cerebrovasc Dis* 1999; **9** (4): 202–9.

142 Sidhu PS, Chauduri KR, Khaw KT. Moyamoya disease mimicking a spontaneous internal carotid artery dissection on Doppler ultrasound. *Eur Radiol* 2000; **10** (1): 149–53.

143 O'Dwyer JA, Moscow N, Trevor R, Ehrenfeld WK, Newton TH. Spontaneous dissection of the carotid artery. *Radiology* 1980; **137** (2): 379–85.

144 Houser OW, Mokri B, Sundt TM Jr, Baker HL Jr, Reese DF. Spontaneous cervical cephalic arterial dissection and its residuum: angiographic spectrum. *AJNR Am J Neuroradiol* 1984; **5** (1): 27–34.

145 Mokri B, Sundt TM Jr, Houser OW, Piepgras DG. Spontaneous dissection of the cervical internal carotid artery. *Ann Neurol* 1986; **19** (2): 126–38.

146 Baumgartner RW, Arnold M, Baumgartner I, Mosso M, Gonner F, Studer A, Schroth G, Schuknecht B, Sturzenegger M. Carotid dissection with and without ischemic events: local symptoms and cerebral artery findings. *Neurology* 2001; **57** (5): 827–32.

147 Beletsky V, Norris JW. Spontaneous dissection of the carotid and vertebral arteries. *N Engl J Med* 2001; **345** (6): 467.

148 Markwalder TM, Starrett RW, Mumenthaler M. Spontaneous bilateral recanalization in bilateral internal carotid artery occlusion. *Stroke* 1980; **11** (1): 95–8.

149 Bogousslavsky J, Regli F, Despland PA. Spontaneous dissecting aneurysms of the internal carotid artery. Prospective evaluation of the prognosis and arterial repermeation in 14 cases. *Rev Neurol (Paris)* 1984; **140** (11): 625–36 [in French].

150 Kasner SE, Hankins LL, Bratina P, Morgenstern LB. Magnetic resonance angiography demonstrates vascular healing of carotid and vertebral artery dissections. *Stroke* 1997; **28** (10): 1993–7.

151 Engelter ST, Lyrer PA, Kirsch EC, Steck AJ. Long-term follow-up after extracranial internal carotid artery dissection. *Eur Neurol* 2000; **44** (4): 199–204.

152 Ringelstein EB, Zeumer H, Hundgen R, Meya U. Angiologic and prognostic evaluation of brain stem injuries. Clinical, Doppler-sonographic and neuroradiological findings. *Dtsch Med Wochenschr* 1983; **108** (43): 1625–31 [in German].

153 Davis PC, Nilsen B, Braun IF, Hoffman JC Jr. A prospective comparison of duplex sonography vs angiography of the vertebral arteries. *AJNR Am J Neuroradiol* 1986; 7 (6): 1059–64.

154 Winter R, Biedert S, Staudacher T, Betz H, Reuther R. Vertebral artery Doppler sonography. *Eur Arch Psychiatry Neurol Sci* 1987; **237** (1): 21–8.

155 Touboul PJ, Mas JL, Bousser MG, Laplane D. Duplex scanning in extracranial vertebral artery dissection. *Stroke* 1988; **19** (1): 116–21.

156 De Bray JM, Blard JM, Tachot C, Ledemeney M, Davinroy M. Transcranial Doppler ultrasonic examination in vertebro-basilar circulatory pathology. *Mal Vasc* 1989; **14** (3): 202–5 [in French].

157 Delcker A, Diener HC. The value of color duplex for sonography of the vertebral artery. *Vasa Suppl* 1991; **33**: 204–5 [in German].

158 Bartels E. Duplex sonography of the vertebral arteries. 2. Clinical application. *Ultraschall Med* 1991; **12** (2): 63–9 [in German].

159 Trattnig S, Schwaighofer B, Hubsch P, Schwarz M, Kainberger F. Color-coded Doppler sonography of vertebral arteries. *J Ultrasound Med* 1991; **10** (4): 221–6.

160 Schneider PA, Rossman ME, Bernstein EF, Ringelstein EB, Torem S, Otis SM. Noninvasive evaluation of vertebrobasilar insufficiency. *J Ultrasound Med* 1991; **10** (7): 373–9.

161 Bartels E, Fuchs HH, Flugel KA. Duplex ultrasonography of vertebral arteries: examination, technique, normal values, and clinical applications. *Angiology* 1992; **43** (3 Part 1): 169–80.

162 Delcker A, Diener HC, Timmann D, Faustmann P. The role of vertebral and internal carotid artery disease in the pathogenesis of vertebrobasilar transient ischemic attacks. *Eur Arch Psychiatry Clin Neurosci* 1993; **242** (4): 179–83.

163 Sturzenegger M, Mattle HP, Rivoir A, Rihs F, Schmid C. Ultrasound findings in spontaneous extracranial vertebral artery dissection. *Stroke* 1993; **24** (12): 1910–21.

164 Bartels E, Flugel KA. Evaluation of extracranial vertebral artery dissection with duplex color-flow imaging. *Stroke* 1996; **27** (2): 290–5.

165 de Bray JM, Missoum A, Dubas F, Emile J, Lhoste P. Detection of vertebrobasilar intracranial stenoses: transcranial Doppler sonography versus angiography. *J Ultrasound Med* 1997; **16** (3): 213–8.

166 de Bray JM, Penisson-Besnier I, Dubas F, Emile J. Extracranial and intracranial vertebrobasilar dissections: diagnosis and prognosis. *J Neurol Neurosurg Psychiatry* 1997; **63** (1): 46–51.

167 de Bray JM, Pasco A, Tranquart F, Papon X, Alecu C, Giraudeau B, Dubas F, Emile J. Accuracy of color-Doppler in the quantification of proximal vertebral artery stenoses. *Cerebrovasc Dis* 2001; **11** (4): 335–40.

168 Droste DW, Junker K, Stogbauer F, Lowens S, Besselmann M, Braun B, Ringelstein EB. Clinically silent circulating microemboli in 20 patients with carotid or vertebral artery dissection. *Cerebrovasc Dis* 2001; **12** (3): 181–5.

169 Caplan LR, Amarenco P, Rosengart A, Lafranchise EF, Teal PA, Belkin M, DeWitt LD, Pessin MS. Embolism from vertebral artery origin occlusive disease. *Neurology* 1992; **42** (8): 1505–12.

170 Bartels E. *Color-Coded Duplex Ultrasonography of the Cerebral Vessels*. Stuttgart: Schattauer, 1999: 118.

171 Nicolau C, Gilabert R, Garcia A, Blasco J, Chamorro A, Bru C. Effect of internal carotid artery occlusion on vertebral artery blood flow: a duplex ultrasonographic evaluation. *Ultrasound Med* 2001; **20** (2): 105–11.

172 Oder B, Oder W, Lang W, Marschnigg E, Deecke L. Hypoplasia, stenosis and other alterations of the

vertebral artery: does impaired blood rheology manifest a hidden disease? *Acta Neurol Scand* 1998; **97** (6): 398–403.

173 Besson G, Vallee B, Mimassi N, Person H, Garre H. Disabling segmental occlusion of the vertebral artery. Surgical treatment using a venous bypass from the external carotid to the C1–C2 portion of the vertebral artery (2 cases). *Neurochirurgie* 1981; **27** (1): 59–64 [in French].

174 Lindegaard KF, Bakke SJ, Aaslid R, Nornes H. Doppler diagnosis of intracranial artery occlusive disorders. *J Neurol Neurosurg Psychiatry* 1986; **49**: 510–8.

175 de Bray JM, Joseph PA, Jeanvoine H, Maugin D, Dauzat M, Plassard F. Transcranial Doppler evaluation of middle cerebral artery stenosis. *J Ultrasound Med* 1988; 7 (11): 611–6.

176 Ley-Pozo J, Ringelstein EB. Noninvasive detection of occlusive disease of the carotid siphon and middle cerebral artery. *Ann Neurol* 1990; **28**: 640–7.

177 Schwarze JJ, Babikian V, DeWitt LD, Sloan MA, Wechsler LR, Gomez CR, Pochay V, Baker E. Longitudinal monitoring of intracranial arterial stenoses with transcranial Doppler ultrasonography. *J Neuroimaging* 1994; **4**: 182–7.

178 Rother J, Schwartz A, Rautenberg W, Hennerici M. Middle cerebral artery stenoses: assessment by magnetic resonance angiography and transcranial Doppler ultrasound. *Cerebrovasc Dis* 1994; **4**: 273–9.

179 Alexandrov AV, Bladin CF, Norris JW. Intracranial blood flow velocities in acute ischemic stroke. *Stroke* 1994; **25**: 1378–83.

180 Wong KS, Li H, Lam WW, Chan YL, Kay R. Progression of middle cerebral artery occlusive disease and its relationship with further vascular events after stroke. *Stroke* 2002; **33** (2): 532–6.

181 Segura T, Serena J, Castellanos M, Teruel J, Vilar C, Davalos A. Embolism in acute middle cerebral artery stenosis. *Neurology* 2001; **56** (4): 497–501.

182 Arenillas JF, Molina CA, Montaner J, Abilleira S, Gonzalez-Sanchez MA, Alvarez-Sabin J. Progression and clinical recurrence of symptomatic middle cerebral artery stenosis: a long-term follow-up transcranial Doppler ultrasound study. *Stroke* 2001; **32** (12): 2898–904.

183 Felberg RA, Christou I, Demchuk AM, Malkoff M, Alexandrov AV. Screening for intracranial stenosis with transcranial Doppler: the accuracy of mean flow velocity thresholds. *J Neuroimaging* 2002; **12** (1): 9–14.

184 Mattle H, Grolimund P, Huber P, Sturzenegger M, Zurbrugg HR. Transcranial Doppler sonographic findings in middle cerebral artery disease. *Arch Neurol* 1988; **45** (3): 289–95.

185 Brass LM, Duterte DL, Mohr JP. Anterior cerebral artery velocity changes in disease of the middle cerebral artery stem. *Stroke* 1989; **20** (12): 1737–40.

186 Monsein LH, Razumovsky AY, Ackerman SJ, Nauta HJ, Hanley DF. Validation of transcranial Doppler ultrasound with a stereotactic neurosurgical technique. *J Neurosurg* 1995; **82** (6): 972–5.

187 Aaslid R. *Transcranial Doppler Sonography*. Wien: Springer Verlag, 1986: 39–59.

188 Chimowitz MI, Kokkinos J, Strong J, Brown MB, Levine SR, Silliman S, Pessin MS, Weichel E, Sila CA, Furlan AJ *et al.* The Warfarin–Aspirin Symptomatic Intracranial Disease Study. *Neurology* 1995; **45** (8): 1488–93.

189 Adams RJ, McKie V, Nichols F *et al.* The use of transcranial ultrasonography to predict stroke in sickle cell disease. *N Engl J Med* 1992; **326**: 605–10.

190 Alexandrov AV, Demchuk AM, Wein TH, Grotta JC. Yield of transcranial Doppler in acute cerebral ischemia. *Stroke* 1999; **30** (8): 1604–9.

191 Alexandrov AV, Demchuk AM, Felberg RA, Grotta JC, Krieger DW. Intracranial clot dissolution is associated with embolic signals on transcranial Doppler. *J Neuroimaging* 2000; **10** (1): 27–32.

192 Hennerici M, Rautenberg W, Schwartz A. Transcranial Doppler ultrasound for the assessment of intracranial arterial flow velocity—Part 2. Evaluation of intracranial arterial disease. *Surg Neurol* 1987; **27** (6): 523–32.

193 Demchuk AM, Christou I, Wein TH, Felberg RA, Malkoff M, Grotta JC, Alexandrov AV. Specific transcranial Doppler flow findings related to the presence and site of arterial occlusion with transcranial Doppler. *Stroke* 2000; **31**: 140–6.

194 Steinke W, Mangold J, Schwartz A, Hennerici M. Mechanisms of infarction in the superficial posterior cerebral artery territory. *J Neurol* 1997; **244** (9): 571–8.

195 Kimura K, Minematsu K, Yasaka M, Wada K, Yamaguchi T. Evaluation of posterior cerebral artery flow velocity by transcranial color-coded real-time sonography. *Ultrasound Med Biol* 2000; **26** (2): 195–9.

196 Ringelstein EB. Ultrasonic diagnosis of the vertebrobasilar system. II. Transnuchal diagnosis of intracranial vertebrobasilar stenoses using a novel pulsed Doppler system. *Ultraschall Med* 1985; **6** (2): 60–7 [in German].

197 Budingen HJ, Staudacher T. Identification of the basilar artery with transcranial Doppler sonography. *Ultraschall Med* 1987; **8** (2): 95–101 [in German].

198 Volc D, Possnigg G, Grisold W, Neuhold A. Transcranial Dopplersonography of the vertebro-basilar system. *Acta Neurochir (Wien)* 1988; **90** (3–4): 136–8.

199 Alexandrov AV, Tegeler CH. Diagnostic criteria for transcranial Doppler sonography: a model for quality assurance and laboratory accreditation. *Vasc Ultrasound Today* 1999; **4**: 1–24.

200 Droste DW, Nabavi DG, Kemeny V, Schulte-Altedorneburg G, Ritter MA, Weber S, Ringelstein EB. Echocontrast enhanced transcranial colour-coded duplex

offers improved visualization of the vertebrobasilar system. *Acta Neurol Scand* 1998; **98** (3): 193–9.

201 Postert T, Federlein J, Przuntek H, Büttner T. Power-based versus conventional transcranial color-coded duplex sonography in the assessment of the vertebrobasilar-posterior system. *J Stroke Cerebrovasc Dis* 1997; **6**: 398–404.

202 Baumgartner RW, Mattle HP, Schroth G. Assessment of ≥ 50% and < 50% intracranial stenoses by transcranial color-coded duplex sonography. *Stroke* 1999; **30** (1): 87–92.

203 Hennerici M, Neuerburg-Heusler D. *Vascular Diagnosis with Ultrasound: Clinical References with Case Studies.* Stuttgart: Thieme, 1998: 96.

204 Sloan MA. Transcranial Doppler monitoring of vasospasm after subarachnoid hemorrhage. In: Tegeler CH, Babikian VL, Gomez CR. *Neurosonology.* St Louis: Mosby, 1996: 156–71.

205 Lindegaard KF, Nornes H, Bakke SJ, Sorteberg W, Nakstad P. Cerebral vasospasm after subarachnoid haemorrhage investigated by means of transcranial Doppler ultrasound. *Acta Neurochir (Wien)* 1988; **42** (Suppl.): P81–4.

206 Newell DW, Grady MS, Eskridge JM, Winn HR. Distribution of angiographic vasospasm after subarachnoid hemorrhage: implications for diagnosis by transcranial Doppler ultrasonography. *Neurosurgery* 1990; **27**: 574–7.

207 Awad IA, Carter LP, Spetzler RF, Medina M, Williams FC. Clinical vasospasm after subarachnoid hemorrhage: response to hypervolemic hemodilution and arterial hypertension. *Stroke* 1987; **18**: 365–72.

208 Kontos HA. Validity of cerebral arterial blood flow calculations from velocity measurements. *Stroke* 1989; **20**: 1–3.

209 Mizuno M, Nakajima S, Sampei T, Nishimura H, Hadeishi H, Suzuki A, Yasui N, Nathal-Vera E. Serial transcranial Doppler flow velocity and cerebral blood flow measurements for evaluation of cerebral vasospasm after subarachnoid hemorrhage. *Neurol Med Chir (Tokyo)* 1994; **34** (3): 164–71.

210 Sloan MA, Haley EC Jr, Kassell NF, Henry ML, Stewart SR, Beskin RR, Sevilla EA, Torner JC. Sensitivity and specificity of transcranial Doppler ultrasonography in the diagnosis of vasospasm following subarachnoid hemorrhage. *Neurology* 1989; **39** (11): 1514–8.

211 Newell DW, Winn HR. Transcranial Doppler in cerebral vasospasm. *Neurosurg Clin N Am* 1990; **1** (2): 319–28.

212 Lindegaard KF. The role of transcranial Doppler in the management of patients with subarachnoid haemorrhage: a review. *Acta Neurochir Suppl* 1999; **72**: 59–71.

213 Lysakowski C, Walder B, Costanza MC, Tramer MR. Transcranial Doppler versus angiography in patients with vasospasm due to a ruptured cerebral aneurysm: a systematic review. *Stroke* 2001; **32** (10): 2292–8.

214 Wozniak MA, Sloan MA, Rothman MI, Burch CM, Rigamonti D, Permutt T, Numaguchi Y. Detection of vasospasm by transcranial Doppler sonography. The challenges of the anterior and posterior cerebral arteries. *J Neuroimaging* 1996; **6** (2): 87–93.

215 Piepgras A, Hagen T, Schmiadek P. Reliable prediction of grade of angiographic vasospasm by transcranial Doppler sonography. *Stroke* 1994; **25**: 260 [abstract].

216 Giller CA, Hatab MR, Giller AM. Estimation of vessel flow and diameter during cerebral vasospasm using transcranial Doppler indices. *Neurosurgery* 1998; **42** (5): 1076–81.

217 Reigel MM, Hollier LH, Sundt TM Jr, Piepgras DG, Sharbrough FW, Cherry KJ. Cerebral hyperperfusion syndrome: a cause of neurologic dysfunction after carotid endarterectomy. *J Vasc Surg* 1987; **5** (4): 628–34.

218 Powers AD, Smith RR. Hyperperfusion syndrome after carotid endarterectomy: a transcranial Doppler evaluation. *Neurosurgery* 1990; **26** (1): 56–9.

219 Schoser BG, Heesen C, Eckert B, Thie A. Cerebral hyperperfusion injury after percutaneous transluminal angioplasty of extracranial arteries. *J Neurol* 1997; **244** (2): 101–4.

220 Dalman JE, Beenakkers IC, Moll FL, Leusink JA, Ackerstaff RG. Transcranial Doppler monitoring during carotid endarterectomy helps to identify patients at risk of postoperative hyperperfusion. *Eur J Vasc Endovasc Surg* 1999; **18** (3): 222–7.

221 Spencer MP. Transcranial Doppler monitoring and causes of stroke from carotid endarterectomy. *Stroke* 1997; **28** (4): 685–91.

222 Padayachee TS, Kirkham FJ, Lewis RR, Gillard J, Hutchinson MC, Gosling RG. Transcranial measurement of blood velocities in the basal cerebral arteries using pulsed Doppler ultrasound: a method of assessing the Circle of Willis. *Ultrasound Med Biol* 1986; **12** (1): 5–14.

223 Bass A, Krupski WC, Dilley RB, Bernstein EF, Otis SM. Comparison of transcranial and cervical continuous-wave Doppler in the evaluation of intracranial collateral circulation. *Stroke* 1990; **21** (11): 1584–8.

224 Byrd S, Wolfe J, Nicolaides A, Stansby G, Cheshire N, Thomas D, Mansfield A. Vascular Surgical Society of Great Britain and Ireland: transcranial Doppler ultrasonography as a predictor of haemodynamically significant carotid stenosis. *Br J Surg* 1999; **86** (5): 692–3.

225 Schneider PA, Rossman ME, Bernstein EF, Ringelstein EB, Otis SM. Noninvasive assessment of cerebral collateral blood supply through the ophthalmic artery. *Stroke* 1991; **22** (1): 31–6.

226 Rutgers DR, Klijn CJ, Kappelle LJ, van Huffelen AC, van der Grond J. A longitudinal study of collateral flow

patterns in the circle of Willis and the ophthalmic artery in patients with a symptomatic internal carotid artery occlusion. *Stroke* 2000; **31** (8): 1913–20.

227 Spencer MP, Campbell SD, Sealey JL, Henry FC, Lindbergh J. Experiments on decompression bubbles in the circulation using ultrasonic and electromagnetic flowmeters. *J Occup Med* 1969; **11** (5): 238–44.

228 Deverall PB, Padayachee TS, Parsons S, Theobold R, Battistessa SA. Ultrasound detection of micro-emboli in the middle cerebral artery during cardiopulmonary bypass surgery. *Eur J Cardiothorac Surg* 1988; **2** (4): 256–60.

229 Spencer MP, Thomas GI, Nicholls SC, Sauvage LR. Detection of middle cerebral artery emboli during carotid endarterectomy using transcranial Doppler ultrasonography. *Stroke* 1990; **21** (3): 415–23.

230 Brucher R, Russel D. Background and principles. In: Tegeler CH, Babikian VL, Gomez CR. *Neurosonology*. St Louis: Mosby, 1996: 231–4.

231 Clark RE, Brillman J, Davis DA, Lovell MR, Price TR, Magovern GJ. Microemboli during coronary artery bypass grafting. Genesis and effect on outcome. *J Thorac Cardiovasc Surg* 1995; **109** (2): 249–57.

232 Diegeler A, Hirsch R, Schneider F, Schilling LO, Falk V, Rauch T, Mohr FW. Neuromonitoring and neurocognitive outcome in off-pump versus conventional coronary bypass operation. *Ann Thorac Surg* 2000; **69** (4): 1162–6.

233 Jansen C, Moll FL, Vermeulen FE, van Haelst JM, Ackerstaff RG. Continuous transcranial Doppler ultrasonography and electroencephalography during carotid endarterectomy: a multimodal monitoring system to detect intraoperative ischemia. *Ann Vasc Surg* 1993; **7** (1): 95–101.

234 Ackerstaff RG, Jansen C, Moll FL, Vermeulen FE, Hamerlijnck RP, Mauser HW. The significance of microemboli detection by means of transcranial Doppler ultrasonography monitoring in carotid endarterectomy. *J Vasc Surg* 1995; **21** (6): 963–9.

235 Ackerstaff RG, Moons KG, van de Vlasakker CJ, Moll FL, Vermeulen FE, Algra A, Spencer MP. Association of intraoperative transcranial Doppler monitoring variables with stroke from carotid endarterectomy. *Stroke* 2000; **31** (8): 1817–23.

236 Georgiadis D, Grosset DG, Kelman A, Faichney A, Lees KR. Prevalence and characteristics of intracranial microemboli signals in patients with different types of prosthetic cardiac valves. *Stroke* 1994; **25** (3): 587–92.

237 Tong DC, Bolger A, Albers GW. Incidence of transcranial Doppler-detected cerebral microemboli in patients referred for echocardiography. *Stroke* 1994; **25** (11): 2138–41.

238 Tong DC, Albers GW. Transcranial Doppler-detected microemboli in patients with acute stroke. *Stroke* 1995; **26** (9): 1588–92.

239 Nabavi DG, Georgiadis D, Mumme T, Schmid C, Mackay TG, Scheld HH, Ringelstein EB. Clinical relevance of intracranial microembolic signals in patients with left ventricular assist devices. A prospective study. *Stroke* 1996; **27** (5): 891–6.

240 Sliwka U, Lingnau A, Stohlmann WD, Schmidt P, Mull M, Diehl RR, Noth J. Prevalence and time course of microembolic signals in patients with acute stroke. A prospective study. *Stroke* 1997; **28** (2): 358–63.

241 Koennecke HC, Mast H, Trocio SS Jr, Sacco RL, Thompson JL, Mohr JP. Microemboli in patients with vertebrobasilar ischemia: association with vertebrobasilar and cardiac lesions. *Stroke* 1997; **28** (3): 593–6.

242 Nadareishvili ZG, Choudary Z, Joyner C, Brodie D, Norris JW. Cerebral microembolism in acute myocardial infarction. *Stroke* 1999; **30** (12): 2679–82.

243 Rundek T, Di Tullio MR, Sciacca RR, Titova IV, Mohr JP, Homma S, Sacco RL. Association between large aortic arch atheromas and high-intensity transient signals in elderly stroke patients. *Stroke* 1999; **30** (12): 2683–6.

244 Ringelstein EB, Droste DW, Babikian VL, Evans DH, Grosset DG, Kaps M, Markus HS, Russell D, Siebler M. Consensus on microembolus detection by TCD. International Consensus Group on Microembolus Detection. *Stroke* 1998; **29**: 725–9.

245 Cullinane M, Reid G, Dittrich R, Kaposzta Z, Ackerstaff R, Babikian V, Droste DW, Grossett D, Siebler M, Valton L, Markus HS. Evaluation of new online automated embolic signal detection algorithm, including comparison with panel of international experts. *Stroke* 2000; **31** (6): 1335–41.

246 Markus HS. Transcranial Doppler ultrasound. *Br Med Bull* 2000; **56** (2): 378–88.

247 The International Cerebral Hemodynamics Society Consensus Statement. *Stroke* 1995; **26**: 1123.

248 Nornes H, Angelsen B, Lindegaard KF. Precerebral arterial blood flow pattern in intracranial hypertension with cerebral blood flow arrest. *Acta Neurochir* 1977; **38**: 187–94.

249 Harders A. *Neurosurgical Applications of Transcranial Doppler Sonography*. Wien: Springer-Verlag, 1986: 45.

250 Fischer AQ, Livingstone JN. Transcranial Doppler and real-time cranial sonography in neonatal hydrocephalus. *J Child Neurol* 1989; **4** (1): 64–9.

251 Homburg AM, Jakobsen M, Enevoldsen E. Transcranial Doppler recordings in raised intracranial pressure. *Acta Neurol Scand* 1993; **87** (6): 488–93.

252 Hanlo PW, Peters RJ, Gooskens RH, Heethaar RM, Keunen RW, van Huffelen AC, Tulleken CA, Willemse J. Monitoring intracranial dynamics by transcranial Doppler—a new Doppler index: trans systolic time. *Ultrasound Med Biol* 1995; **21** (5): 613–21.

253 Mayer SA, Thomas CE, Diamond BE. Asymmetry of intracranial hemodynamics as an indicator of mass effect in acute intracerebral hemorrhage. A transcranial Doppler study. *Stroke* 1996; **27** (10): 1788–92.

254 Lewis S, Wong M, Myburgh J, Reilly P. Determining cerebral perfusion pressure thresholds in severe head trauma. *Acta Neurochir Suppl* 1998; **71**: 174–6.

255 Richards HK, Czosnyka M, Whitehouse H, Pickard JD. Increase in transcranial Doppler pulsatility index does not indicate the lower limit of cerebral autoregulation. *Acta Neurochir Suppl* 1998; **71**: 229–32.

256 Treib J, Becker SC, Grauer M, Haass A. Transcranial doppler monitoring of intracranial pressure therapy with mannitol, sorbitol and glycerol in patients with acute stroke. *Eur Neurol* 1998; **40** (4): 212–9.

257 Czosnyka M, Smielewski P, Piechnik S, Schmidt EA, Al-Rawi PG, Kirkpatrick PJ, Pickard JD. Hemodynamic characterization of intracranial pressure plateau waves in head-injury patients. *J Neurosurg* 1999; **91** (1): 11–9.

258 Rainov NG, Weise JB, Burkert W. Transcranial Doppler sonography in adult hydrocephalic patients. *Neurosurg Rev* 2000; **23** (1): 34–8.

259 Grolimund P, Seiler RW, Mattle H. Possibilities and limits of transcranial Doppler sonography. *Ultraschall Med* 1987; **8** (2): 87–94 [in German].

260 Klingelhofer J, Conrad B, Benecke R, Sander D. Intracranial flow patterns at increasing intracranial pressure. *Klin Wochenschr* 1987; **65** (12): 542–5.

261 Kirkham FJ, Levin SD, Padayachee TS, Kyme MC, Neville BG, Gosling RG. Transcranial pulsed Doppler ultrasound findings in brain stem death. *J Neurol Neurosurg Psychiatry* 1987; **50** (11): 1504–13.

262 Ropper AH, Kehne SM, Wechsler L. Transcranial Doppler in brain death. *Neurology* 1987; **37** (11): 1733–5.

263 Hassler W, Steinmetz H, Gawlowski J. Transcranial Doppler ultrasonography in raised intracranial pressure and in intracranial circulatory arrest. *J Neurosurg* 1988; **68** (5): 745–51.

264 Bode H, Sauer M, Pringsheim W. Diagnosis of brain death by transcranial Doppler sonography. *Arch Dis Child* 1988; **63** (12): 1474–8.

265 Newell DW, Grady MS, Sirotta P, Winn HR. Evaluation of brain death using transcranial Doppler. *Neurosurgery* 1989; **24** (4): 509–13.

266 Petty GW, Mohr JP, Pedley TA, Tatemichi TK, Lennihan L, Duterte DI, Sacco RL. The role of transcranial Doppler in confirming brain death: sensitivity, specificity, and suggestions for performance and interpretation. *Neurology* 1990; **40** (2): 300–3.

267 van der Naalt J, Baker AJ. Influence of the intra-aortic balloon pump on the transcranial Doppler flow pattern in a brain-dead patient. *Stroke* 1996; **27** (1): 140–2.

268 Hennerici M, Neuerburg-Heusler D. *Vascular Diagnosis with Ultrasound: Clinical References with Case Studies.* Stuttgart: Thieme, 1998: 120.

269 Ducrocq X, Hassler W, Moritake K, Newell DW, von Reutern GM, Shiogai T, Smith RR. Consensus opinion on diagnosis of cerebral circulatory arrest using Doppler-sonography: Task Force Group on cerebral death of the Neurosonology Research Group of the World Federation of Neurology. *J Neurol Sci* 1998; **159**: 145–50.

270 Ducrocq X, Braun M, Debouverie M, Junges C, Hummer M, Vespignani H. Brain death and transcranial Doppler: experience in 130 cases of brain dead patients. *J Neurol Sci* 1998; **160** (1): 41–6.

271 Hadani M, Bruk B, Ram Z, Knoller N, Spiegelmann R, Segal E. Application of transcranial Doppler ultrasonography for the diagnosis of brain death. *Intensive Care Med* 1999; **25** (8): 822–8.

272 Wijdicks EF. The diagnosis of brain death. *N Engl J Med* 2001; **344** (16): 1215–21.

273 Lindegaard K-F, Bakke SJ, Aaslid R, Nornes H. Doppler diagnosis of intracranial occlusive disorders. *J Neurol Neurosurg Psychiatry* 1986; **49**: 510–8.

274 Grolimund P, Seiler RW, Aaslid R, Huber P, Zurbruegg H. Evaluation of cerebrovascular disease by combined extracranial and transcranial Doppler sonography. Experience in 1,039 patients. *Stroke* 1987; **18**: 1018–24.

275 Halsey J. Prognosis of acute hemiplegia estimated by transcranial Doppler sonography. *Stroke* 1988; **19**: 648–9.

276 Zanette EM, Fieschi C, Bozzao L, Roberti C, Toni D, Argentino C, Lenzi GL. Comparison of cerebral angiography and transcranial Doppler sonography in acute stroke. *Stroke* 1989; **20**: 899–903.

277 Kaps M, Damian MS, Teschendorf U, Dorndorf W. Transcranial Doppler ultrasound findings in the middle cerebral artery occlusion. *Stroke* 1990; **21**: 532–7.

278 Carmelingo M, Casto L, Censori B, Ferraro B, Gazzaniga GC, Mamoli A. Transcranial Doppler in acute ischemic stroke of the middle cerebral artery territories. *Acta Neurol Scand* 1993; **88**: 108–11.

279 Razumovsky AY, Gillard JH, Bryan RN, Hanley DF, Oppenheimer SM. TCD, MRA, and MRI in acute cerebral ischemia. *Acta Neurol Scand* 1999; **99**: 65–76.

280 Demchuk AM, Burgin WS, Christou I, Felberg RA, Barber PA, Hill MD, Alexandrov AV. Thrombolysis in brain ischemia (TIBI) transcranial Doppler flow grades predict clinical severity, early recovery, and mortality in patients treated with tissue plasminogen activator. *Stroke* 2001; **32**: 89–93.

281 Burgin WS, Malkoff M, Felberg RA, Demchuk AM, Christou I, Grotta JC, Alexandrov AV. Transcranial

Doppler ultrasound criteria for recanalization after thrombolysis for middle cerebral artery stroke. *Stroke* 2000; **31**: 1128–32.

282 El-Mitwalli A, Saad M, Christou I, Malkoff M, Alexandrov AV. Clinical and sonographic patterns of tandem ICA/MCA occlusion in TPA treated patients. *Stroke* 2002; **33**: 99–102.

283 Demchuk AM, Christou I, Wein TH, Felberg RA, Malkoff M, Grotta JC, Alexandrov AV. Accuracy and criteria for localizing arterial occlusion with transcranial Doppler. *J Neuroimaging* 2000; **10**: 1–12.

284 Brandt T, Knauth M, Wildermuth S, Winter R, von Kummer R, Sartor K, Hacke W. CT angiography and Doppler sonography for emergency assessment in acute basilar artery ischemia. *Stroke* 1999; **30** (3): 606–12.

285 Klotzsch C, Bozzato A, Lammers G, Mull M, Noth J. Contrast-enhanced three-dimensional transcranial color-coded sonography of intracranial stenoses. *AJNR Am J Neuroradiol* 2002; **23** (2): 208–12.

286 Niederkorn K, Myers LG, Nunn CL, Ball MR, McKinney WM. Three-dimensional transcranial Doppler blood flow mapping in patients with cerebrovascular disorders. *Stroke* 1988; **19** (11): 1335–44.

287 Bartels E. *Color-Coded Duplex Ultrasonography of the Cerebral Vessels*. Stuttgart: Schattauer, 1999: 123–4.

288 Delcker A, Diener HC. Various ultrasound methods for studying the vertebral artery—a comparative evaluation. *Ultraschall Med* 1992; **13** (5): 213–20 [in German].

289 Toole JF. *Cerebrovascular Disorders*, 4th edn. New York: Raven Press, 1990: 199–23.

290 Voigt K, Kendel K, Sauer M. Subclavian steal syndrome. Bloodless diagnosis of the syndrome using ultrasonic pulse echo and vertebral artery compression. *Fortschr Neurol Psychiatr Grenzgeb* 1970; **38** (1): 20–33 [in German].

291 Grossman BL, Brisman R, Wood EH. Ultrasound and the subclavian steal syndrome. *Radiology* 1970; **94** (1): 1–6.

292 Reutern GM, Budingen HJ, Freund HJ. The diagnosis of obstructions of the vertebral and subclavian arteries by means of directional Doppler sonography. *Arch Psychiatr Nervenkr* 1976; **222** (2–3): 209–222 [in German].

293 von Reutern GM, Budingen HJ. Doppler sonographic study of the vertebral artery in subclavian steal syndrome. *Dtsch Med Wochenschr* 1977; **102** (4): 140–1 [in German].

294 Yoneda S, Nukada T, Tada K, Imaizumi M, Takano T. Subclavian steal in Takayasu's arteritis. A hemodynamic study by means of ultrasonic Doppler flowmetry. *Stroke* 1977; **8** (2): 264–8.

295 Pourcelot L, Ribadeau-Dumas JL, Fagret D, Planiol T. Contribution of the Doppler examination to the diagnosis of subclavian steal syndrome. *Rev Neurol (Paris)* 1977; **133** (5): 309–23 [in French].

296 Walker DW, Acker JD, Cole CA. Subclavian steal syndrome detected with duplex pulsed Doppler sonography. *AJNR Am J Neuroradiol* 1982; **3** (6): 615–8.

297 Ringelstein EB, Zeumer H. Delayed reversal of vertebral artery blood flow following percutaneous transluminal angioplasty for subclavian steal syndrome. *Neuroradiology* 1984; **26** (3): 189–98.

298 Ackerstaff RG, Hoeneveld H, Slowikowski JM, Moll FL, Eikelboom BC, Ludwig JW. Ultrasonic duplex scanning in atherosclerotic disease of the innominate, subclavian and vertebral arteries. A comparative study with angiography. *Ultrasound Med Biol Aug*, 1984; **10** (4): 409–18.

299 Pokrovskii AV, Volynskii IuD, Kuntsevich GI, Buianovskii VL, Berdikian SIA. Ultrasonic angiography in the diagnosis of lesions of the brachiocephalic branches of the aorta. *Kardiologiia* 1985; **25** (10): 82–6 [in Russian].

300 Kuperberg EB, Grozovskii IuL, Agadzhanova LP. Functional test of reactive hyperemia in the diagnosis of the vertebro–subclavian steal syndrome using ultrasonic dopplerography. *Zh Nevropatol Psikhiatr Im S S Korsakova* 1986; **86** (1): 28–34 [in Russian].

301 Bornstein NM, Norris JW. Subclavian steal: a harmless haemodynamic phenomenon? *Lancet* 1986; **2** (8502): 303–5.

302 Ackermann H, Diener HC, Dichgans J. Stenosis and occlusion of the subclavian artery: ultrasonographic and clinical findings. *J Neurol* 1987; **234** (6): 396–400.

303 Ackermann H, Diener HC, Seboldt H, Huth C. Ultrasonographic follow-up of subclavian stenosis and occlusion: natural history and surgical treatment. *Stroke* 1988; **19** (4): 431–5.

304 Klingelhofer J, Conrad B, Benecke R, Frank B. Transcranial Doppler ultrasonography of carotid-basilar collateral circulation in subclavian steal. *Stroke* 1988; **19** (8): 1036–42.

305 Bornstein NM, Krajewski A, Norris JW. Basilar artery blood flow in subclavian steal. *Can J Neurol Sci* 1988; **15** (4): 417–9.

306 Lunev DK, Pokrovskii AV, Nikitin IuM, Iunes AM. Cerebrovascular disorders in various types of the subclavian steal syndrome. *Zh Nevropatol Psikhiatr Im S S Korsakova* 1991; **91** (1): 10–4 [in Russian].

307 Nicholls SC, Koutlas TC, Strandness DE. Clinical significance of retrograde flow in the vertebral artery. *Ann Vasc Surg* 1991; **5** (4): 331–6.

308 de Bray JM, Zenglein JP, Laroche JP, Joseph PA, Lhoste P, Pillet J, Dubas F, Emile J. Effect of subclavian syndrome on the basilar artery. *Acta Neurol Scand* 1994; **90** (3): 174–8.

309 Rossum AC, Steel SR, Hartshorne MF. Evaluation of coronary subclavian steal syndrome using sestamibi imaging and duplex scanning with observed vertebral subclavian steal. *Clin Cardiol* 2000; **23** (3): 226–9.

310 Mukhtar OM, Miller AP, Nanda NC, Fuisz AR, Puri VK, Aaluri SR, Yesilbursa D, Huang WY, Ansingkar K, Ross P. Transesophageal echocardiographic identification of left subclavian artery stenosis with steal phenomenon. *Echocardiography* 2000; **17** (2): 197–200.

311 AbuRahma AF, Robinson PA, Jennings TG. Carotid-subclavian bypass grafting with polytetrafluoroethylene grafts for symptomatic subclavian artery stenosis or occlusion: a 20-year experience. *J Vasc Surg* 2000; **32** (3): 411–8.

This page intentionally left blank

PART IV

Ultrasound in stroke prevention and treatment

This page intentionally left blank

CHAPTER 7

TCD and sickle cell disease

Fenwick T. Nichols III, MD, *Robert J. Adams*, MD & *Anne M. Jones*, RN, BSN, RVT, RDMS

Introduction

Children with sickle cell disease (hemoglobin SS, or HbSS) have a significant stroke risk, with 11% of all HbSS patients developing ischemic stroke before the age of 20 [1]. These strokes primarily result from stenosis or occlusion of the distal intracranial internal carotid arteries (ICAs, Figure 7.1a) and/or proximal middle cerebral arteries (MCAs, Figure 7.1b). Many of these patients develop moya-moya phenomenon (Figure 7.1c), or a network of small collateral vessels to compensate for the ICA occlusive disease. In Japanese, 'moya-moya' means 'a puff of smoke'. This is how these small arteries appear on digital subtraction angiography in most advanced cases.

Several studies have demonstrated that transcranial Doppler (TCD) can be used to identify those children with sickle cell disease who are at increased risk of stroke [2,3]. Based upon these data, the Stroke Prevention in Sickle Cell Disease (STOP) trial was undertaken to identify children at high risk of stroke [4]. One hundred and thirty children were entered into the trial who had the time-averaged mean of the maximum (TAMM) velocities of > 200 cm/s in one or both of the MCAs or terminal ICAs at baseline TCD.

Two points must be emphasized:

1 Entry criteria for STOP required that children with HbSS had TAMM (*not* peak systolic, Figure 7.2) velocities > 200 cm/s in the MCA, and/or terminal internal carotid arteries (TICA) recorded on *two* separate

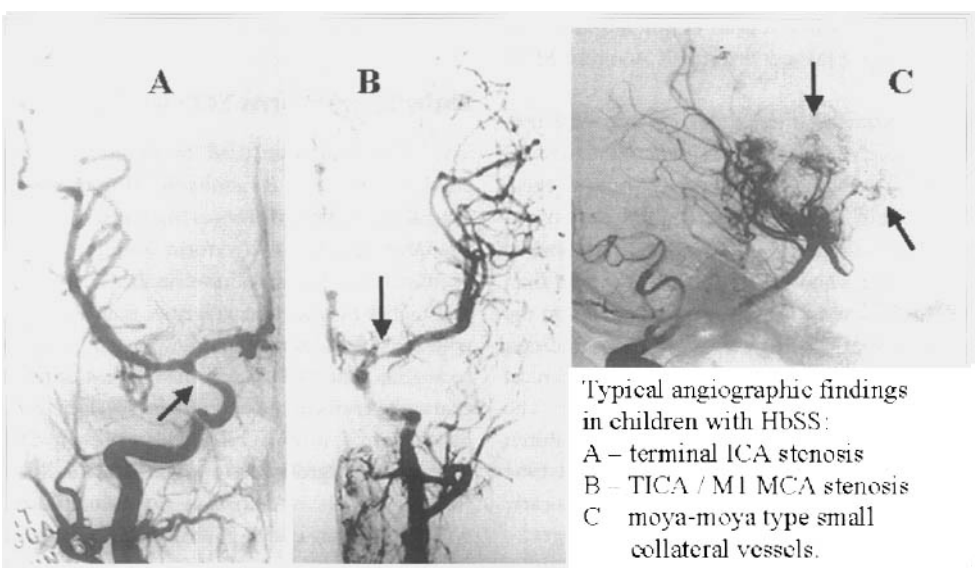

Figure 7.1 Arterial lesions and collaterals in children with sickle cell disease.

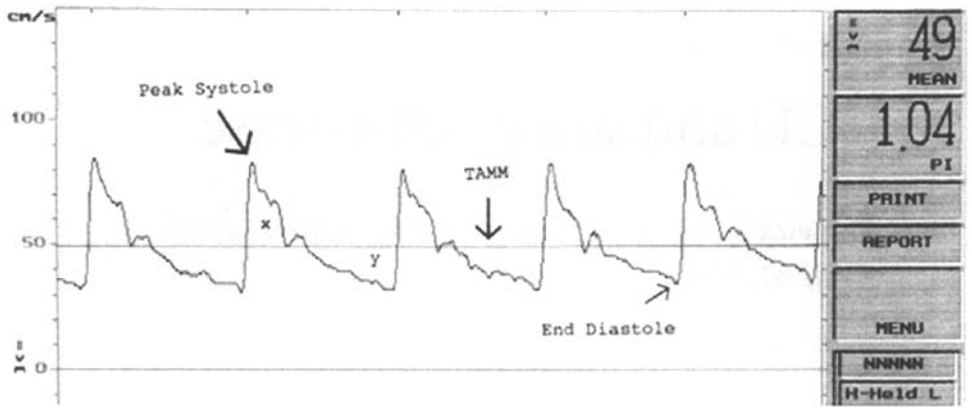

Figure 7.2 Time-averaged mean of the maximum (TAMM) line placement. This is the spectral outline as traced by the V_{max} or waveform follower. The TAMM line is placed so that the area under the V_{max} trace above the TAMM line (labelled 'x') is equal to the area below the TAMM line above the V_{max} trace (labelled 'y').

occasions separated by at least 2 weeks. A non-image-guided 2 MHz TCD was used with assumed 0° angle of insonation. The decision to require an initial examination and a subsequent confirmatory examination was made to avoid many transient physiologic variables affecting flow velocity.

2 Stroke risk was determined by velocities > 200 cm/s in the terminal ICA and/or MCA. There are no data on the stroke risk for high velocities in other vessels (anterior (ACA) or posterior (PCA) cerebral arteries); however, high velocities in these vessels are usually associated with stenosis in the terminal ICA or MCA. Therefore, discovery of high ACA or PCA velocities should prompt earlier repeat examinations in an effort to identify a missed terminal ICA and/or MCA stenosis.

Children who met these entry criteria were randomized to receive either transfusion or standard care. Over an average follow-up of about 20 months, there was one stroke in the 63 children randomized to transfusion and 11 strokes in the 67 children randomized to standard care. These results indicate a greater than 90% relative risk reduction in stroke incidence in the treated population [5]. As a result of these findings, the National Institutes of Health released a clinical alert on September 18, 1997, which stated: 'The STOP Trial confirmed that TCD can identify children with sickle cell anemia at high risk for first-time stroke. Since the greatest risk of stroke occurs in early childhood, it is recommended that children of ages 2–16 receive TCD screening. Screening should be conducted at a site where clinicians have been trained to provide TCDs of comparable quality and information content to those used in the STOP trial and to read them in a manner consistent with what was done in STOP . . . It is recommended that centers that wish to start screening children with sickle cell anemia for stroke risk do studies to compare their current equipment with STOP trial TCD equipment.' The STOP TCD scanning protocol is slightly different from that used for routine clinical TCD examinations. This chapter will describe the STOP scanning and reading technique, and discuss the rationale for its modifications. Readers interested in additional background information on TCD use in sickle cell disease are referred to the references at the end of this chapter.

How to perform TCD in children

The TCD technique used to examine children is similar to that used on adults [6]. However, there are several important differences that must be recognized in order to properly perform and interpret TCD examinations. Children have smaller head diameters and higher normal flow velocities than adults. Those with HbSS have even higher flow velocities secondary to anemia. The TCDs performed as part of the STOP trial were very focused examinations specifically adapted for children. A brief overview will be presented to provide some background as to why certain modifications were made in the examinations for these children.

TCD is a non-image-guided vascular examination in that there is no B-mode or color flow map to identify the insonated vessel and its location. Therefore it is

Table 7.1 Expected arterial depths (in mm) for different head diameters. Depths of insonation are given for ipsilateral transtemporal window of insonation.

Head diameter (cm)	MCA	MCA-1	ICA bifurcation	ACA	PCA
12	30–54	30–36	50–54	50–58	40–60
13	30–58	30–36	52–58	52–62	42–66
14	34–62	34–40	56–64	56–68	46–70
15	40–66	40–46	56–66	56–72	50–70

MCA, middle cerebral artery; MCA-1, MCA subdivision 1; ICA, internal carotid artery; ACA, anterior cerebral artery; PCA, posterior cerebral artery.

important to pay attention to the relative position and angulation of the probe, the depth of insonation and the direction of flow. Failure to do so can result in misinterpretation of the examination.

Children generally have thinner skulls than adults, so rather than the usual small and difficult-to-find ultrasonic window of the adult, the examiner may be faced with a plethora of windows. In general, the windows that lie closer to the ear, in the posterior portion of the temporal window, are preferable to those that lie more anteriorly. If the probe is placed in the more anterior portion of the transtemporal windows, it has to be angled further posteriorly to insonate any vessel. The circle of Willis is not large, and it is easy to insonate either more posteriorly or more anteriorly than intended when an unfamiliar window is used.

Since the circle of Willis is small and the windows are usually good, it is better to use a small sample volume to avoid recording flow in adjacent vessels. The signal displayed on the screen represents any flow signal within the sample volume and is not necessarily located at the exact depth displayed on the screen. The depth displayed on the screen is the depth at the midportion of the sample volume length. The sample volume width varies with the depth of insonation, being narrowest at the focal zone of the probe, and being somewhat wider at greater or lesser depths. With a 10-mm sample volume (length), the depth of insonation extends from 5 mm shallower to 5 mm deeper than the depth indicated. In a child's small circle of Willis, a 10-mm sample volume may result in unintended insonation of other arteries. This may be a particular problem when the anterior transtemporal window is used, and the probe is angled posteriorly to evaluate the PCA. A 10-mm sample volume may cross both the MCA and the PCA, making it difficult to ascertain the source of the Doppler signal. The STOP protocol specified a sample volume of 6 mm to increase confidence in the site of insonation. Decreasing sample volume length does reduce the power, but this usually is not a problem in children since less power is needed to penetrate their thinner skulls.

Children have smaller heads than adults, and consequently the depths at which vessels are identified differ (Table 7.1). If adult depth measurements are used as a basis for vessel determination serious errors may occur. Measuring the bitemporal diameter is helpful. The examiner can use either obstetric calipers or the instrument used by optometrists to determine head width when fitting eye glasses. The bitemporal skull diameter is taken by measuring the distance between the two posterior transtemporal windows. If the child's bitemporal head diameter is 13 cm, then the midline is at 65 mm, and the ICA bifurcation will be found at a depth of about 55 mm. If the probe is angled posteriorly, a bidirectional signal at 65 mm would represent the top of the basilar with flow into both PCAs; if the probe is angled anteriorly, a bidirectional signal at the midline could also represent both ACAs. For comparison, in a patient with a bitemporal diameter of 15 cm, a bidirectional signal at 65 mm would be identified as the ICA bifurcation.

In smaller head diameters, the ICA bifurcation generally lies 5–15 mm off the midline (usually about 8–10 mm). In a patient with a 13-cm bitemporal diameter, the ICA bifurcation will be found at a depth of 52–60 mm. The P1 PCA segment can be insonated from the midline depth (65 mm) to a depth of at least 50 mm, and frequently to a depth of 45 mm. This results in potential vessel identification problems, in that flow towards the probe at a depth of 55 mm could be in either the MCA or PCA. In order to verify that the flow towards the probe arises from the MCA, it is

crucial to insonate to as shallow a depth as possible. In a 13-cm diameter head, the MCA should be able to be tracked to depths of 30–35 mm, and should always be tracked to at least a depth of less than 40 mm. If flow towards the probe can be insonated from a depth of 30 mm, and tracked in 2 mm increments to a bidirectional signal at 55-mm depth, then the examiner can be confident that the vessel is the MCA. In addition, once the ICA bifurcation is identified, it is important that the examiner then angle the probe posteriorly and insonate the PCA. The PCA can then be tracked to the midline, with detection of bidirectional flow at the top of the basilar. If all of the above can be carried out, then the examiner can be confident of an accurate examination.

There is another source of bidirectional signals that is occasionally misidentified as the ICA bifurcation. These bidirectional signals can be found at MCA branch sites, either the anterior temporal artery or an early MCA bifurcation. If the head diameter nomogram is used (Table 7.1), the depth of the bidirectional signal from an MCA branch will be shallower than that expected for the ICA bifurcation.

The STOP protocol requires the MCA signal be tracked and recorded in 2-mm steps from its shallowest depth to the ICA bifurcation. The signal should be optimized at each site of insonation. The ACA signal is recorded ~ 4 mm deeper than the ICA bifurcation. The distal ICA signal is recorded ~ 4 mm deeper than the ICA bifurcation or with a slightly downward probe angulation at the depths of ICA bifurcation. Then the probe is angled posteriorly and the PCA is recorded at 2-mm increments from its shallowest depth to the top of the basilar (Table 7.1).

Due to collateral flow patterns established in response to hemodynamically significant stenoses in children with HbSS, it is particularly crucial to differentiate the MCA from the PCA. With progressive stenosis of the distal ICA, proximal ACA and/or MCA, PCA flow becomes one of the major collateral sources to leptomeningeal collaterals which then supply the distal MCA and/or ACA. In this situation, the PCA is readily insonated because of its high flow volume. The MCA may not be as easily detectable due to a high-grade stenosis or occlusion; therefore it can be easy to misidentify the PCA as the MCA unless a thorough detailed examination is performed.

Early in our use of TCD (before development of the STOP protocol), we examined a child with HbSS and moya-moya phenomenon. The PCA's strong signal was misidentified as the MCA and we assumed that the PCA could not be insonated. Angiography revealed a virtually absent MCA, with high volume flow through the PCA. With subsequent modification and close adherence to our scanning protocol, we developed very reproducible examinations, which correlate well with angiographic findings.

Factors influencing cerebral blood flow velocities

The STOP protocol is driven to determine the highest TAMM velocity (*not* peak systolic) in the MCA or terminal ICA. Because the absolute TAMM velocity is important for study classification, it is also important to recognize the physiologic, anatomic, technique and equipment variables that may affect cerebral blood flow (CBF) and flow velocities (Table 7.2).

Table 7.2 Physiologic variables affecting cerebral blood flow (CBF) and time-averaged mean of the maximum (TAMM).

Variable	Alteration	Effect on TAMM	Causes of alteration from baseline
Age	Increase	Decrease	Normal aging; decrease in CBF
Hematocrit	Decrease	Increase	Bone marrow failure; hemolysis; splenic sequestration; blood loss
	Increase	Decrease	Blood transfusion
Oxygen	Decrease	Increase	Sickle chest syndrome; pneumonia
	Increase	Minimal decrease	Oxygen administration
CO_2	Increase	Increase	Sleep; breath-holding; sedation
	Decrease	Decrease	Hyperventilation; crying
Body temperature	Increase	Increase	Fever of any cause
Glucose	Decrease	Increase	Hypoglycemia

Physiologic factors

TCD measures the velocity of blood flow, which is determined by the volume of flow over time and the luminal area of the artery. There are a number of factors influencing the volume of flow, the primary determinants being tissue requirements for oxygen and glucose delivery. Listed below is a brief overview of the various factors influencing cerebral blood flow volume.

1 *Age.* Cerebral blood flow is highest around the age of 4 years (about 85 cc/100 g tissue/min), and then declines to approximately 65 cc/100 g tissue/min at the age of 20 and to about 35 cc/100 g tissue/min at the age of 85. In addition to this gradual decline in CBF with increasing age, there is a slight increase in arterial diameter with increasing age. The net effect is that blood flow velocities are highest around the age of 4 years, and then decrease thereafter.

2 *Hematocrit.* This is a major determinant of oxygen delivery. Mild degrees of anemia do not have any significant impact on CBF, but more severe anemia causes a measurable increase in total CBF. In order to maintain adequate oxygen delivery as the hematocrit decreases, the CBF must increase. Once the hematocrit is below 30 there is a reliably detectable increase in CBF, and consequently in blood flow velocity. Sickle cell patients typically have a hematocrit of 18–25, so their CBF is higher than that of age-comparable children with normal hematocrit. The TAMM for an otherwise normal 8-year-old HbSS patient with a hemoglobin of 7 and a hematocrit of 21 is approximately 140 cm/s. In those unusual situations of elevated hematocrit there may be a decrease in CBF, sometimes due to excessive oxygen delivery or hyperviscosity.

3 *Carbon dioxide.* Arterioles on the brain surface are the resistance vessels and are important in cerebral blood flow regulation. These arterioles respond to changes in CO_2. They dilate in response to increases in carbon dioxide, allowing blood to flow more easily, thus enhancing CBF. For every 1 mm increase in CO_2, there is a 2–4% rise in CBF. Carbon dioxide plasma concentration increases in several situations, including lung disease, breath-holding or CO_2 administration. If the patient goes to sleep there may be a 2–5 mm rise in CO_2, resulting in an increase in CBF and blood flow velocity. Because of this potential sleep-induced velocity increase, children should not be allowed to sleep during the examination. The arterioles decrease in diameter with the lowering of CO_2, causing an increased resistance to flow, and decreased CBF and TAMM. As CO_2 decreases occur with hyperventilation and crying, TCD examinations should be avoided in these situations.

4 *Oxygen.* Hypoxia produces an increase in CBF in order to maintain oxygen delivery. Patients with pneumonia or other causes of lowered oxygen levels will have a compensatory increase in their CBF.

5 *Hypoglycemia.* Patients who are hypoglycemic will have a compensatory increase in CBF to increase glucose delivery to the brain. Usually, this is only a minor phenomenon and does not cause a CBF increase unless the glucose is less than 40 mg%.

6 *Fever.* Fever increases CBF by about 10% for every degree Celsius of temperature increase, so febrile patients will have elevated CBF and TCD velocities relative to their baseline.

7 *Blood pressure.* Within a broad range, the cerebral arterioles respond to changes in blood pressure to maintain a constant CBF volume. This phenomenon, referred to as autoregulation, generally prevents minor changes in blood pressure from affecting CBF. However, there are limits to autoregulation. This mechanism will fail when the blood pressure is severely elevated or depressed in acutely ill patients, significantly altering CBF.

8 *Cardiac output.* Under normal physiologic conditions, cardiac output is stable and is not a factor in CBF. However, in states of severely decreased cardiac output, such as cardiomyopathies or severe aortic stenosis, the CBF may fall. Cardiac arrhythmias may also decrease cardiac output, so third-degree heart block, or supraventricular or ventricular tachycardias may result in decreased CBF. Aortic valvular insufficiency may alter cardiac output as well, resulting in altered waveforms and possibly decreased CBF.

9 *Proximal arterial obstruction.* If there is a severe stenosis ($\geq$ 80%) affecting the source of blood to the artery being evaluated (e.g. an arterial stenosis proximal to the point of insonation), there may be a decrease in volume flow through the artery being evaluated. The severe stenosis prevents adequate flow volume delivery (resulting in lower velocity) with a low-resistance waveform. With more severe proximal stenosis, the upstroke of the waveform will become rounded.

10 *Distal arterial stenosis.* Severe arterial stenosis distal to the point of insonation causes decreased volume flow through the artery. Flow at the site of

insonation will likely have decreased velocity with a high-resistance waveform. Increased intracranial pressure will have an effect similar to distal arterial stenosis, producing increased resistance to flow at the arteriolar level.

11 *Rhythmic oscillations.* Normal individuals have periodic variations in MCA velocity occurring every 30–180 s, producing up to a 15% increase in velocity.

12 *Arteriovenous malformations (AVMs).* AVMs have no capillary bed and cause minimal resistance to flow. Insonation of a feeding artery to an AVM will demonstrate a high velocity (because of high-volume flow) with a very low resistance signal.

The STOP TCD examinations should be carried out when the child is at a 'steady state.' Although it is frequently easier to study patients when they are in hospital, many of the reasons prompting admission alter CBF. To apply STOP trial results, we do not recommend examining a child who is acutely ill, as fever, hypoxia, hypocarbia and worsened anemia may all transiently increase the TAMM, possibly resulting in a TAMM > 200 cm/s. (STOP study randomization required two TCD examinations > 200 cm/s, separated by at least 2 weeks, to avoid such problems.) Transfusion will decrease TAMM for several weeks, until the hematocrit returns towards its usual level.

Anatomic variables

1 The arteries may be very tortuous, making it difficult to obtain an optimal angle of insonation in these arteries. This may be partly addressed by probe manipulation.

2 Multiple transtemporal windows may be present and used, making examination difficult and operator dependent.

Technique and equipment variables

In general, routine clinical TCD examinations are used to detect and roughly quantify areas of stenosis. The sonographer's efforts are directed at the recognition of an abnormal area, and not necessarily the precise quantification of its severity (except in broad terms). There are several differences between routine clinical TCD examinations and the STOP protocol-based TCD examination. The STOP study used an exacting TCD scanning protocol to create a very focused reproducible examination because, based upon the Medical College of Georgia (MCG) patient cohort and STOP data, patients with TAMM velocities > 200 cm/s had a significantly increased stroke risk which could be decreased by transfusion. Therefore, the goal of the STOP TCD examination is to obtain the highest possible TAMM velocity in the MCA and/or terminal ICA and allow its reproducible measurement at follow-up. To help sonographers obtain these velocities, several modifications were made to the routine clinical TCD examination. The section below deals in detail with these variables.

Optimizing the angle of insonation

Since TCD is a non-image-guided technique, no correction to the angle of insonation can be applied to the kHz Doppler frequency shift detected during this study. As is well known, when the angle of insonation becomes larger than 15°, the kHz shift for a given velocity begins to decrease. In duplex Doppler examinations, the angle of insonation can be registered by the sonographer, so that the computer can calculate the actual velocity of flow. In TCD, the computer assumes that the angle of insonation is ideal, so that TCD cannot overestimate the velocity of flow. If the angle of insonation is 0°, the TCD-calculated velocity is accurate. If the angle of insonation is > 30°, the calculated velocity will be falsely low. In order to obtain the highest TCD velocity possible, it is necessary to attempt to optimize the angle of insonation by aiming the ultrasound beam directly down the barrel of the artery being insonated. Because the proximal MCA may have one or more curves, the examiner may have to angle (or even move) the probe as the depth of insonation is changed in order to optimally align the ultrasound beam with the vessel as the MCA stem is tracked. Children generally have generous or large acoustic windows, making it easier to make these adjustments. We have found that when the sonographer uses the STOP TCD protocol, the velocities recorded are typically higher than those recorded as part of a routine clinical examination.

Optimization of the Doppler signal (Table 7.3)

This includes recognition of the audible and visual clues indicating local high-velocity flow, as well as making appropriate scale and gain settings. As noted above, part of signal optimization is accomplished by proper transducer positioning and minor probe manipulation to achieve the best angle of insonation. STOP TCD sonographers were trained to recognize visual clues of local high-velocity flow, such as

Table 7.3 Transcranial Doppler optimization.

1 Focused examination, meticulous tracking of the middle cerebral artery course and terminal internal carotid artery.
2 Probe manipulation, angling or sliding to optimize angle of insonation.
3 Careful attention to audible cues of high velocity: 'hissing', turbulence (prompts more detailed search for high velocity).
4 Correct scale settings.
5 Sharpest waveforms.
6 Best signal-to-noise ratio.
7 Careful examination for the highest velocity.

turbulence and sudden cut-off of the waveform, plus audible clues of high velocity that may not be displayed visually on the TCD monitor. The sonographer should be able to identify characteristics of a high-velocity signal, and recognize high frequencies in the background of the audible signal that may not be displayed on screen. Turbulence (high amplitude, low-frequency/velocity, bidirectional signal that occurs at peak systole) is another audible clue to local stenosis. If the examiner hears either a high-frequency Doppler signal and/or significant turbulence, a very careful search for high velocities should be performed. It is possible to have a well-defined waveform displayed on the screen, but to hear a higher velocity in the background that is not displayed. In this situation, with probe manipulation, the higher-velocity signal can almost always be identified and displayed.

Visual display of the waveform

The examiner should also pay close attention to the visual image of the Doppler waveform. The goal is to obtain the 'cleanest', sharpest and highest-velocity signal. The examiner must locate the area of the highest velocity and then make every effort to obtain a well-defined waveform with a sharp upstroke and a sharp systolic peak. Then the examiner must focus on making the minuscule movement necessary to obtain the highest velocity at the depth being evaluated. It is a common occurrence to identify a region of high velocity, but to fail to obtain the highest velocity at the site because not enough time was spent optimizing the signal.

In clinical TCD studies, once a pathologically high velocity has been identified, most sonographers tend not to spend much time attempting to further optimize the waveform and peak velocity as it does not matter to clinical decision-making whether a child has a TAMM velocity of 150 or 190 cm/s, i.e. normal and conditional STOP values.

Waveform follower

The function of the waveform follower, or envelope, is closely tied to signal strength, optimization and gain settings. Most TCD equipment has been designed so that there is a waveform follower that will track the highest velocity displayed (V_{max}) that is above the zero line (or baseline). This waveform follower is the bright white outline that tracks the top of each of the waveforms. Some of the TCD units will also track the highest-velocity signals below the zero line. The waveform follower tracks the highest velocities, which are then used to determine the TAMM. If there is too much noise in the background, or a signal that is not strong enough for the waveform follower to recognize, the strongest signals with highest and lowest velocity amplitude will be tracked resulting in either too high or too low mean velocity measurements. As the velocities measured by the waveform follower are used to compute the peak systolic, mean and end-diastolic velocities, as well as the pulsatility and resistance indices, it is important that the displayed signal be of adequate quality for accurate tracking by the waveform follower. If the signal-to-noise ratio is poor, the computer velocity measurements may be inaccurate, and these cannot be used to apply STOP trial criteria. Thus it is important to obtain as high a signal-to-noise ratio as possible.

Instrument settings

If the gain is set too high, there will be too much background noise, and the V_{max} waveform follower will not be able to separate the actual waveform from the noise. In addition, it may sometimes result in the development of a 'mirror image' display of the waveform. Simply decreasing the gain will usually resolve these problems.

The velocity scale should be set so that the waveform fills about 0.5–0.75 of the scale to avoid aliasing. On occasion this is not possible, but every effort should be made to achieve this. In otherwise normal pediatric sickle cell patients, the TAMM velocity for the MCA is usually around 140 cm/s, so as a starting point the velocity scale should be set to display at

least 200–250 cm/s peak values in one direction. If the scale is set too low, 'wrap around' will occur, and accurate velocity measurements cannot be made. If the scale is set much too low, the velocities will completely fill the screen, and no measurable signal will be recognized.

STOP TCD scanning protocol

1 The transtemporal head diameter is measured and recorded.
2 Nomogram for expected depths for patient's head diameter is reviewed.
3 The sample volume is set to 6 mm.
4 The velocity scale is set to 200–250 cm/s.
5 The anterior TCD examination begins:
(a) The anterior temporal window is identified.
(b) The MCA signal is acquired.
(c) The MCA is tracked to as shallow a depth as possible; for most children, this should be to a depth less than 40 mm (in STOP this depth was referred to as M1 MCA, indicating the shallowest depth of the MCA that could be recorded).
(d) The TCD signal is optimized and recorded.
(e) The MCA stem is then 'tracked' by advancing the sample volume by 2-mm increments, optimizing and recording the signal.
(f) The MCA is 'tracked' (recording in 2 mm increments of depth), to the internal carotid (ICA) bifurcation, where there is a bidirectional signal (flow towards the probe is the MCA and away is the anterior cerebral artery). This signal is recorded as bifurcation (BIF).
(g) The anterior cerebral artery (ACA) is tracked to 4–6 mm deeper than the ICA bifurcation, and recorded as ACA.
(h) The sample volume depth is then returned to the ICA bifurcation, the probe is angled slightly inferiorly, the depth increased by 4–6 mm, and the Doppler flow velocity waveforms in the distal ICA are recorded, labelled as dICA.
(i) The sample depth is then returned to the ICA bifurcation, and the probe is angled slightly posteriorly until the posterior cerebral artery (PCA) is detected. The sample volume depth is then decreased to the shallowest depth at which signal can be detected.
(j) This PCA waveform is then recorded as PCA. The PCA is tracked (like the MCA in 2-mm increments, and labelled as PCA) to the midline, where bidirectional flow is identified and recorded as the top of the basilar (TOB).
(k) The opposite side is then examined (through the transtemporal window), and recorded using this same technique.
6 Posterior examination. This was performed as per standard TCD scanning protocol. As stenoses only very rarely affect the vertebrobasilar system in children with sickle cell disease, high velocities here were generally secondary to increased volume flow (collateralization of flow).
7 Ophthalmic TCD. This was not part of the STOP protocol, as small children will not generally lie quietly for a transorbital examination. However, infrequently, some abnormalities can be identified by this examination (see below).

Reading STOP TCD

The TCD unit used at participating centers in the STOP trial was a Nicolet TC 2000 model that can perform postprocessing, including adjustments of the gain settings and zero line. Reading of the STOP TCDs was standardized so that all readers set the gain and zero line to the same levels before reading the velocities. The computer-generated waveform follower (V_{max}) was used to help adjust the gain. The gain was increased or decreased until the waveform follower accurately tracked the highest identifiable velocity profile, but did not identify background noise as signal and 'spike' off the waveform. If there was signal that had aliasing, the baseline was adjusted to minimize the aliasing.

Most modern TCD equipment has software that will permit measurement of the TAMM and postprocessing of the digitally stored audio signal (i.e. soundtracks). The computer calculates TAMM from the velocities registered by the waveform follower (V_{max}) that tracks the highest velocities over time. If the waveform follower is accurately tracking the highest velocities, then the computer-calculated TAMM may be used.

Unfortunately, when there is a poor signal-to-noise ratio, the waveform follower may not accurately track the highest velocities, resulting in over- or underestimation of the TAMM. For STOP, the TAMM was measured using a visually guided technique. The gain was adjusted, usually by increasing the gain, to the

point that the waveform follower began to misidentify background noise as signal (the waveform follower would 'spike' off the waveform to noise that was misidentified as signal). The gain was then decreased to the level just below the development of 'spiking'. A cursor was then brought up onto the screen, and the TAMM measured by visual placement of the cursor.

Visual determination of the TAMM can be done reproducibly and accurately after some practice. The easiest way to explain this is to look at the waveform as if it were a mountain range with peaks (systolic) and valleys (diastolic). If you wanted to level the mountains you would draw a line across the waveforms so that if the peaks (the areas under the curve, above the line) were pushed over they would fill the valleys (the area below the line and above spectral outline, Figure 7.2). A reader can rapidly acquire the skill to accurately make this reading by doing direct comparisons between the computer-generated TAMM and the visually determined TAMM. In general, the TAMM lies at the 'shoulder' of the waveform. To minimize the effects of minor changes in velocity from irregular heart rhythm, the reader should attempt to read the TAMM across at least three waveforms. Correct and incorrect TAMM placements are given in Figures 7.3–7.6.

Using this visually guided technique, blinded repeat readings were within < 5% of the original velocities. As noted above, all STOP velocity criteria are based on TAMM. There are a number of other possible mean velocities that can be calculated. None of them are the same as TAMM. These other mean velocities include (but are not limited to) the instantaneous mean, the time average of the mean and the intensity-weighted mean. Some centers have used the following rapid calculation to arrive at the mean: add one-third of the peak systolic velocity and two-thirds of the end-diastolic velocity. We compared this calculation with the measured TAMM, and have found that this calculated mean velocity dose not match the TAMM, and is almost always lower than the TAMM.

STOP criteria and the risk of stroke in children with HbSS

The TCD examination as performed by the STOP protocol is driven to obtain the highest absolute TAMM velocity. Using the STOP TCD protocol it was found that children with HbSS with TAMM > 200 cm/s in the terminal ICA and/or MCA were at significantly increased risk of ischemic stroke and that blood transfusions decreased this risk. The TAMM velocity cut-off point of 200 cm/s was based on the Medical College of Georgia (MCG) Cohort Stroke Risk Model described by Robert Adams in 1992–96 [2,3]. This cut-off was also employed in 5000 screening TCD examinations performed on the 1934 children in the STOP screening phase [2,3].

In the MCG Cohort, children with TAMM velocities in the terminal ICA and/or proximal MCA of > 200 cm/s had a 13% per year incidence of stroke. In the STOP trial, children with velocities > 200 cm/s had a 10% per year incidence of stroke [7]. The Cooperative Study of Sickle Cell Disease collected data on 4082 sickle cell disease patients and demonstrated a risk of stroke in the pediatric sickle cell disease population of 0.5–1% per year [1]. The much higher incidence of stroke in the STOP study demonstrates that TCD can identify those at much greater risk of stroke. Stroke risk was looked at for all 1934 children screened for STOP: based on the first TCD results, with 36 months of follow-up, those with TAMM < 170 cm/s (STOP 'normal' velocities) had a 99% stroke-free survival rate; those with 170–199 cm/s (STOP 'conditional' velocities) had a 97% stroke-free survival rate; and those with > 200 cm/s (STOP 'abnormal' velocities) had an 83% stroke-free survival rate.

However, not all strokes were predicted by TCD. This may be related to other mechanisms of stroke (dissection, embolism, hypercoagulable states, small artery infarction) or to timing of TCD performance in relation to stroke development, or to failure to detect a stenosis by TCD. TCD has demonstrated itself to be a very useful tool for identifying patients with HbSS at high risk for future development of stroke, and can be used to identify those children who benefit from prophylactic transfusion.

Further guidelines on TCD performance using STOP study protocols were recently published [8], and a modest underestimation of velocities by transcranial color Doppler imaging (TCDI) compared to TCD measurements was established [9,10]. If TCDI is used, scanning protocols should be modified to obtain comparable measurements to STOP TCD instruments [9,10].

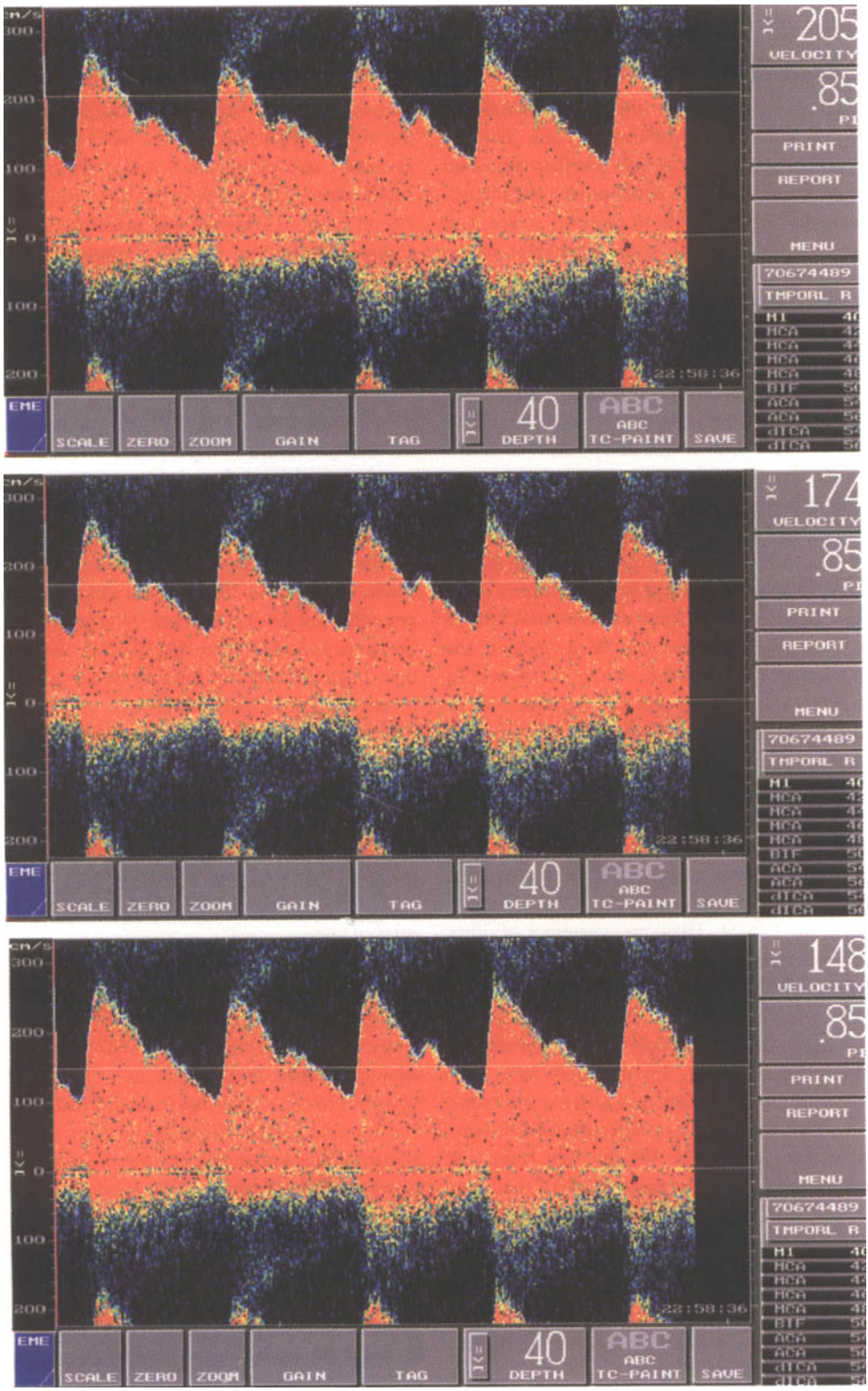

Figure 7.3 TAMM measurements. Upper spectrum: the TAMM line has been incorrectly placed resulting in too high a velocity (205 cm/s). Middle spectrum: the TAMM line has been correctly placed, with correct measurement of velocity (174 cm/s). Bottom spectrum: the TAMM line has been incorrectly placed, resulting in too low a velocity measurement (148 cm/s).

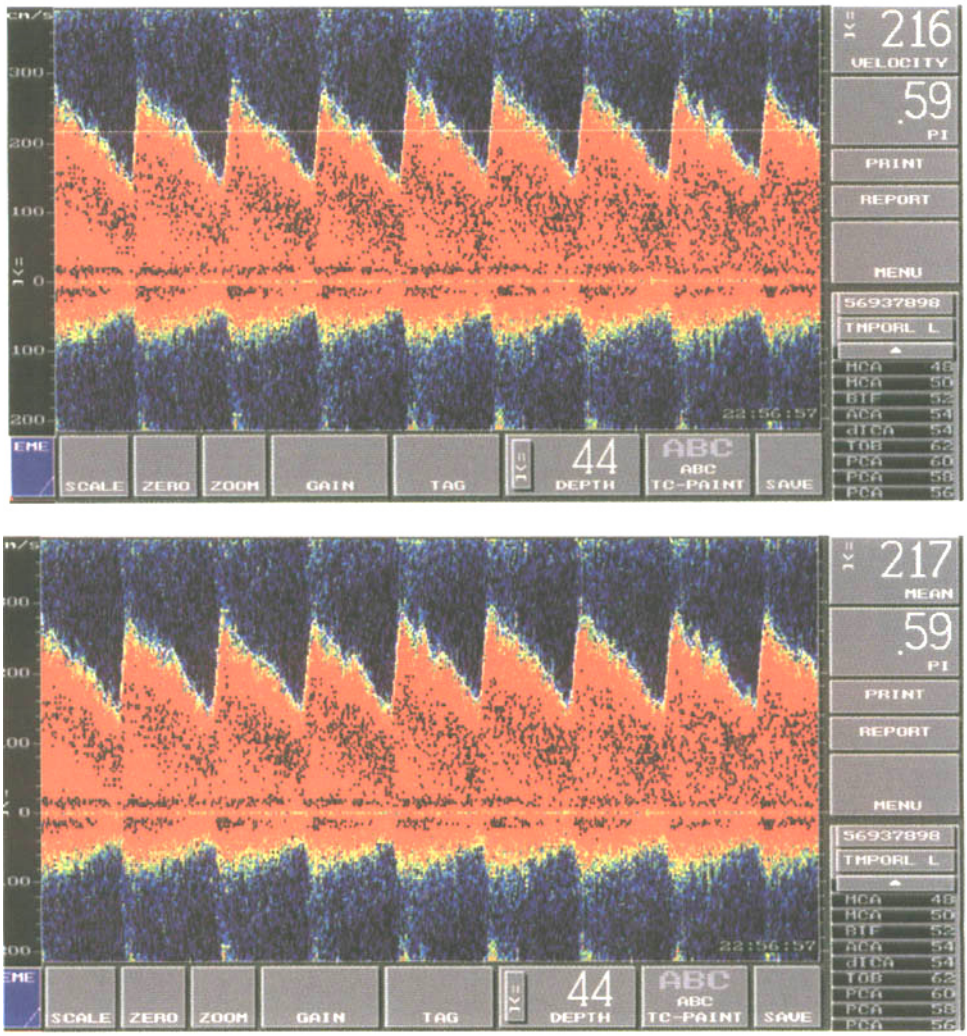

Figure 7.4 This is a well-defined waveform, with gain appropriately set. This demonstrates the correlation of computer-measured TAMM with the TAMM line. Upper spectrum: abnormal TCD study of the MCA at 44-mm depth. Lower spectrum: TAMM line has been correctly placed, measuring 216 cm/s. Same study measured by the computer using the waveform follower, with 217 cm/s.

Frequently asked questions about STOP

Question 1. What are the indications for TCD use in children with sickle cell disease?

Answer 1. TCD is used to screen children with hemoglobin SS between the ages of 2 and 16 years who have not suffered a stroke to identify those at risk for stroke.

Question 2. What are the STOP criteria for classification of TCD examinations?

Answer 2. STOP classification:

Normal: TAMM velocity < 170 cm/s

Conditional: TAMM 170–200 cm/s in the MCA and/or terminal ICA; TAMM > 170 cm/s in the PCA or ACA

Abnormal: TAMM > 200 cm/s in the MCA and/or terminal ICA

Inadequate: absent/poor acoustic window.

All studies are performed in patient's baseline 'steady state'. Do not perform studies when patient is acutely ill.

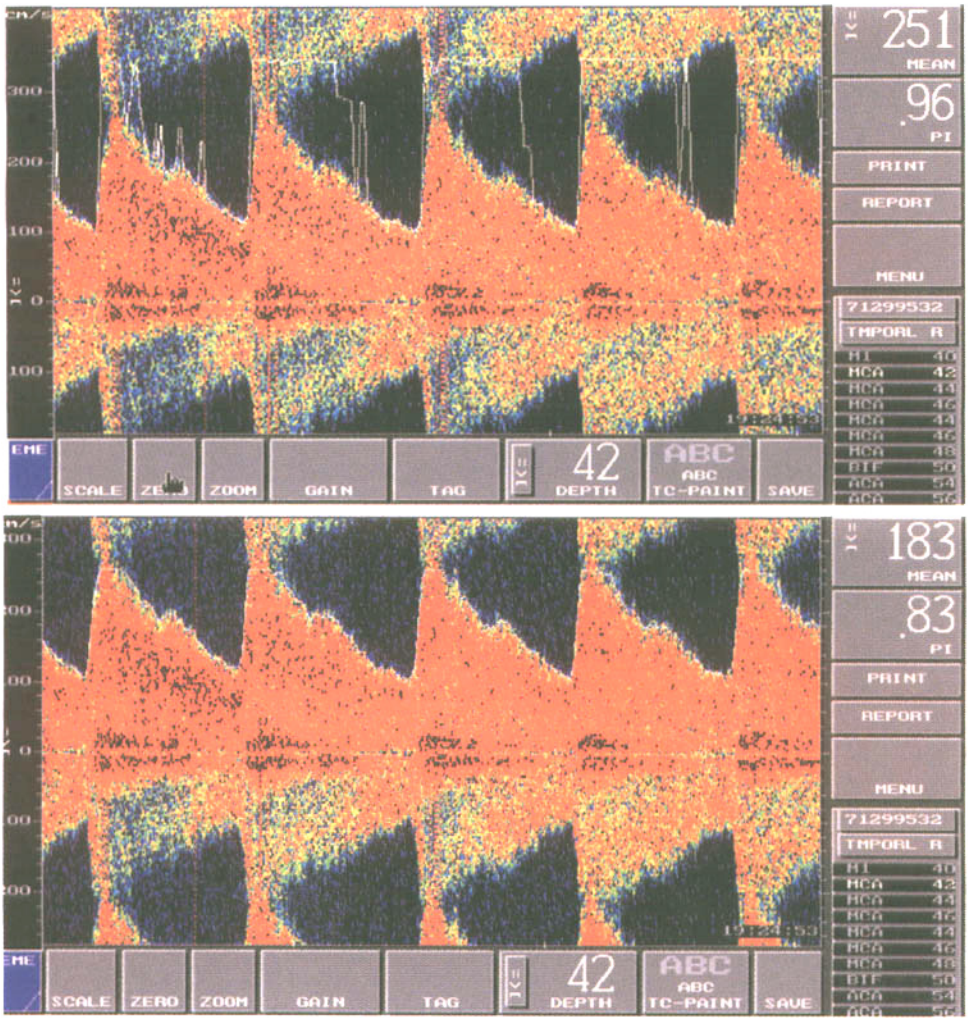

Figure 7.5 Incorrect computer-based TAMM measurement was obtained in the MCA at 42-mm depth (upper spectrum). The waveform follower (V_{max}) is not tracking the velocity profile; it is incorrectly registering the 'wrapped-around' signal as part of the waveform, resulting in a computer-measured velocity that is too high (251 cm/s), and incorrectly classifying this study as abnormal. Lower spectrum shows correct baseline adjustment for the same Doppler signal presented above. On this measurement, the baseline has been adjusted so that the aliasing no longer interferes with computer measurements. The waveform follower now accurately tracks the highest velocity of the velocity profile and correctly measures velocity at 183 cm/s.

Question 3. If a patient has one abnormal examination, when should a confirmatory (repeat) examination be performed?

Answer 3. At least 2 weeks after the initial examination. This minimizes the risk of transient elevations of TCD-measured velocities.

Question 4. If I have a child with one abnormal TCD examination, what are the chances that the child will have a second abnormal examination?

Answer 4. 85% of patients who had one abnormal TCD examination had a second examination that confirmed the abnormal velocity. Almost all of the children who had an initial examination with > 220 cm/s had a second examination that was abnormal.

Question 5. What should be done when a child has had two STOP TCD examinations with MCA or terminal ICA TAMM velocities > 200 cm/s?

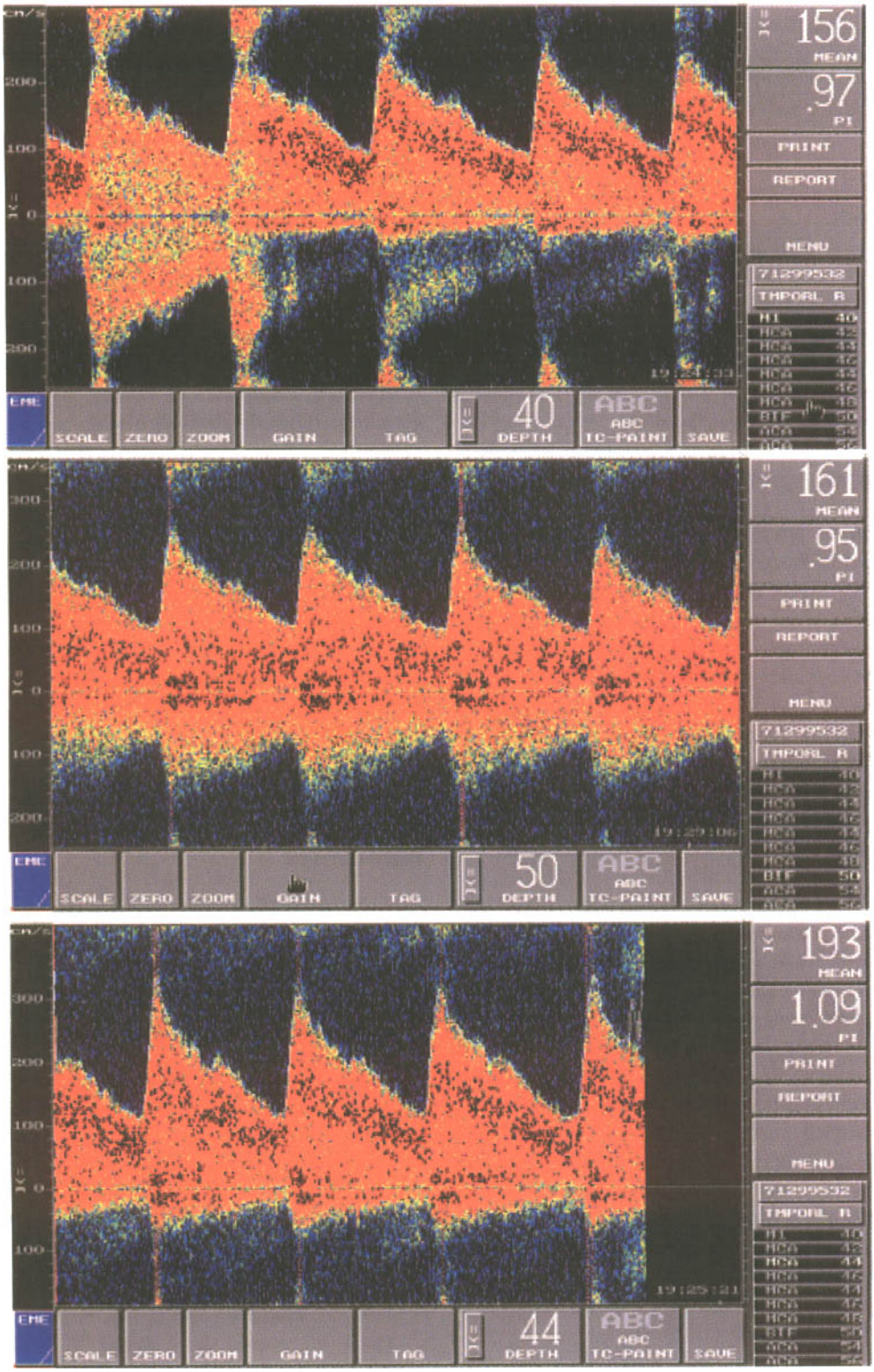

Figure 7.6 The upper spectrums show incomplete sampling. These waveforms demonstrate how a thorough examination of the MCA is necessary to identify the highest velocity. In this patient the velocities at 40 mm (upper spectrum) and 50 mm (middle spectrum) were in the normal range, i.e. 156 cm/s and 161 cm/s. A more detailed search using different aspects of the temporal window and probe manipulation demonstrated that at 44 mm there was a velocity more than 30 cm/s higher than that measured at 40 or 50 mm. This measurement led to reclassification of TAMM as high conditional, i.e. 193 cm/s.

Answer 5. Patients with two abnormal studies should be offered transfusion therapy to decrease their stroke risk.

Question 6. What is the significance of the high velocities?
Answer 6. Most of the abnormal velocities correlate with the presence of a local stenosis. Some children with abnormal velocities have normal MRAs of the intracranial circulation. These children are also at increased risk of stroke compared to the children with 'normal' velocities. It may be that the high velocity flow sets the stage for the subsequent development of stenosis, or that it is somehow associated with the process that triggers the stenosis.

Question 7. What should we expect if we screen our pediatric sickle cell population with TCD?
Answer 7. STOP TCD examinations using the protocol described in this chapter were performed on children between the ages of 2 and 16 years with sickle cell disease in 13 centers in North America. The percentages of normal, conditional, abnormal and inadequate examinations were remarkably consistent across all sites: 70% of all the TCD examinations were classified as normal; 15% of all examinations were classified as conditional; and 10% of all examinations were abnormal. Only 5% were considered inadequate.

Question 8. What about TCD in sickle cell patients who have had a stroke?
Answer 8. All of the above STOP information relates to screening children who have not had a clinically recognized stroke to identify those who are at high risk for stroke development. Once stroke develops, TCD assumes less importance. Most hematologists will begin transfusion therapy in these children once they develop stroke. Children with HbSS who have suffered a stroke may have ICA or MCA occlusions, so that the MCA on the affected side may be absent, or demonstrate very *low* velocities, rather than elevated velocities. There is not a precise cut-off, but TAMM velocities of less than 75 cm/s in non-transfused HbSS patients are very low, and raise concerns about severe proximal stenosis.

Question 9. What about TCD of the ophthalmic artery in children with sickle cell disease?
Answer 9. TCD examination of the ophthalmic arteries was not part of the STOP protocol, so there are no STOP data to directly apply to this question. However, this examination may demonstrate several abnormalities:
(a) If the patient has developed transdural collaterals from the ophthalmic to the intracranial arteries (usually ACA branch), flow in the ACA will demonstrate a low-resistance pattern rather than its usual high-resistance pattern. This is usually a late phenomenon in the development of the moya-moya pattern.
(b) If the ICA distal to the take-off of the ophthalmic is examined, abnormal high-velocity flow may be detected, as this is a frequent site of stenosis of the ICA.
(c) Reversal of flow in the ophthalmic artery is almost never seen in these patients. The stenotic lesions are almost always distal to the take-off of the ophthalmic artery, so that it cannot provide collateral flow.

Question 10. Can you provide information about the incidence of high velocities by age?
Answer 10. The highest velocities were found in younger children. Abnormal velocities by age are distributed as follows:
2–8 years 10.9%
9–12 years 9.7%
13–16 years 6.5%.

References

1 Ohene-Frempong K, Weiner SJ, Sleeper LA, Miller ST, Embury S, Moohr JW, Wethers DL, Pegelow CH, Gill FM. Cerebrovascular accidents in sickle cell disease: rates and risk factors. *Blood* 1998; **91**: 288–94.
2 Adams R, McKie V, Nichols F, Carl E, Zhang DL, McKie K, Figueroa R, Litaker M, Thompson W, Hess D. The use of transcranial ultrasonography to predict stroke in sickle cell disease. *N Engl J Med* 1992; **326**: 605–10.
3 Adams RJ, McKie VC, Carl EM, Nichols FT, Perry R, Brock K, McKie K, Figueroa R, Litaker M, Weiner S, Brambilla D. Long term risk of stroke in children with sickle cell disease screened with transcranial Doppler. *Ann Neurol* 1997; **42**: 699–704.
4 Adams RJ, McKie VC, Brambilla D *et al.* Stroke prevention trial in sickle cell anemia ('STOP'): study design. *Control Clin Trials* 1998; **9**: 110–29.
5 Adams RJ, McKie VC, Hsu L, Files B, Vichinsky E, Pegelow C, Abboud M, Gallagher D, Kutlar A, Nichols FT, Bonds DR, Brambilla D. Prevention of first stroke by transfusions in children with sickle cell anemia and abnormal results on transcranial Doppler ultrasonography. *N Engl J Med* 1998; **339**: 5–11.

6 Aaslid R, ed. *Transcranial Doppler Sonography*. Springer Verlag: New York, 1986.

7 Adams RJ, Brambilla D, Vichinsky E, Abboud M, Pegelow C, Carl E, Nichols F, Jones A, Roach S, Gallagher D, Hagner S, Granger S. Stroke prevention trial in sickle cell anemia (STOP Study). Risk of stroke in 1933 children screened with transcranial Doppler (TCD). *Stroke* 1999; **30**: 238 [abstract].

8 Nichols FT, Jones AM, Adams RJ. Stroke prevention in sickle cell disease (STOP) study guidelines for transcranial Doppler testing. *J Neuroimaging* 2001; **11**: 354–62.

9 Jones AM, Seibert JJ, Nichols FT, Kinder DL, Cox K, Luden J, Carl EM, Brambilla D, Saccente S, Adams RJ. Comparison of transcranial color Doppler imaging (TCDI) and transcranial Doppler (TCD) in children with sickle-cell anemia. *Pediatr Radiol* 2001; **31**: 461–9.

10 Bulas DJ, Jones A, Seibert JJ, Driscoll C, O'Donell R, Adams RJ. Transcranial Doppler (TCD) screening for stroke prevention in sickle cell anemia: pitfalls in technique variation. *Pediatr Radiol* 2000; **30**: 733–8.

8 CHAPTER 8

Cardiovascular risk factors and carotid ultrasound

Joseph F. Polak, MD, MPH

Introduction

Ultrasound is a technology well suited to the study of atherosclerosis. This non-invasive technology can be used to gauge the severity of carotid stenosis with the aid of Doppler waveform analysis and evaluate the extent of atherosclerotic changes on gray-scale (B-mode) ultrasound images.

Other chapters review how carotid ultrasound measurements relate to the presence of clinically overt cerebrovascular disease and how this technology can help identify candidates for carotid endarterectomy. This chapter will briefly review how Doppler velocity measurements have also been used to evaluate the presence of surgically correctable lesions in asymptomatic individuals. The value of ultrasound for evaluating atherosclerotic disease goes further. Gray-scale ultrasound images can map out moderately severe (< 50% diameter stenosis) plaque deposits or be used to measure the diffuse thickening of the carotid wall referred to as intima–media thickness (IMT). These ultrasound measures of atherosclerosis in a given individual parallel the amount and extent of exposure to cardiovascular risk factors. The extent of atherosclerotic change seen on ultrasound images is associated with the likelihood of future cardiovascular events such as stroke or myocardial infarction.

This chapter will conclude by showing how carotid ultrasound measurements of IMT can be used to quantify subclinical disease in the asymptomatic individual and to measure the response to therapeutic interventions aimed at reducing the risk of future cardiovascular events.

Doppler ultrasound and screening for significant carotid stenosis

Performance of Doppler ultrasound in multicenter clinical trials

The use of carotid ultrasound to detect the presence of 'significant' disease in asymptomatic individuals is an example of a 'screening' strategy. When used for this purpose, a Doppler velocity parameter is selected and a threshold is set in such a manner as to define a 'significant' lesion. Individuals with a significant lesion have measured Doppler velocities above the selected threshold. The accuracy of the diagnostic parameter, as an example, a peak systolic velocity above a certain value, is determined by comparison to a gold-standard measurement that quantifies disease predicted by the ultrasound test. Arteriography serves as this gold standard. As this Doppler velocity cut-off point is applied to examining a group of individuals, comparisons to a gold standard and to outcomes can then be used to determine overall efficacy. Efficacy is, however, very dependent on disease prevalence, i.e. the proportion of individuals who have a significant lesion in the group being studied.

The Asymptomatic Carotid Atherosclerosis Study (ACAS) Trial was a multicenter trial that started enrolling participants in the 1980s [1]. Carotid ultrasound played a pivotal role in ACAS since it was used to select potential candidates for enrolment in the trial. The strategy adopted by the designers of the trial was to use Doppler velocity measurements to identify individuals with a stenosis of 60% diameter or more. The investigators used carotid Doppler ultrasound as a screening test but with the intent of insuring that almost all individuals who went on to carotid

arteriography and surgery would have a lesion of at least 60% in their carotid artery. For this reason, the selected Doppler velocity threshold was set to a high enough value that 95% of selected individuals would have a lesion causing a diameter narrowing of 60% or more.

The ACAS trial showed an advantage for surgical intervention as compared to medical therapy for patients who had at least a 60% internal carotid artery stenosis [1]. In ACAS, the measured specificity of carotid ultrasound was above 97% [2]. Carotid ultrasound was, however, used according to a very strict protocol and quality control. In order to qualify, centers had to show evidence of a strong correlation between Doppler measurements and the results of carotid arteriography for 50 carotid arteries. Early results showed marked variations between centers [2], with some centers having diagnostic performance worse than what would be expected through random measurements (Figure 8.1). The diagnostic performance of carotid Doppler ultrasound improved with better instrumentation and greater care applied to the imaging protocol [3]. These results are very different from those reported for the centers participating in the NASCET study [4]. The sensitivity and specificity of carotid ultrasound in NASCET were 68% and 67% when retrospectively compared to central angiographic reading for carotid stenoses of 70% or more.

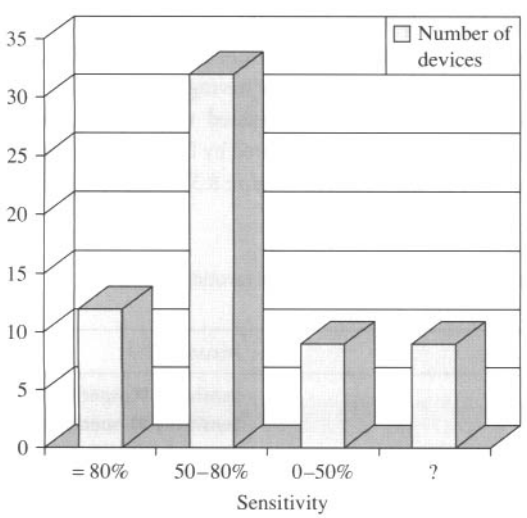

Figure 8.1 Given a specificity of 90% (chance of overcalling a stenosis less than 60% to be greater than 60%), the sensitivity of Doppler ultrasound machines evaluated in the later part of the 1980s showed inconsistent diagnostic performance.

This result, while it applies to a-one-for-all-devices peak systolic velocity (PSV) threshold for symptomatic individuals enrolled in the NASCET study, is an unacceptable performance for a screening test. The results of the carotid Doppler ultrasound studies performed without validation in the NASCET study generated some controversy. Certain methodologic issues played a role in the poor diagnostic performance of Doppler ultrasound. Because of the absence of any quality assurance program, variations in patient selection and in imaging device types and performance, and differences in the imaging protocols [4–6] likely contributed to the poor results reported for Doppler ultrasound. The obvious remedies would have included the use of a standard imaging protocol, a certification program for qualifying both sonographers and laboratories, the implementation of a quality assurance/improvement by a central coordinating/training center and adoption of locally validated screening criteria.

A central coordinating center was used by ACAS to gather the ultrasound data. In ACAS, however, carotid artery Doppler velocity measurements for grading carotid artery stenosis severity failed to show a scaling effect. The scaling effect can be looked at as means of verifying the value of a measurement method for predicting outcomes. For example, results of the NASCET study published in 1991 showed a scaling effect between the arteriographic measurement of carotid stenosis and the benefits of surgery (Figure 8.2). The greater the degree of stenosis, the greater the benefit of surgery. This can be interpreted to indicate that the risk of a future stroke increases with the degree of stenosis as measured by arteriography. In NASCET, the degree of carotid stenosis measured by Doppler velocity estimates did not relate to the benefit of surgery [4]. In ACAS, carotid ultrasound measurements did not show an association with the risk of a future stroke despite the implementation of a standard imaging protocol. However, it is possible that this may represent a selection bias in the way that these asymptomatic individuals were selected for the ACAS study since arteriographic estimates of carotid stenosis also did not show a scaling effect in this trial. The asymptomatic patients had very few events in the ACAS trial (1–2% of stroke risk per year in surgical and medical arms), and the benefits of surgery were not related to the severity of stenosis as measured on the arteriogram [1].

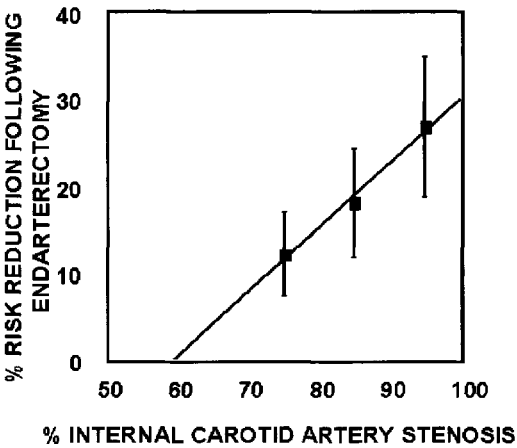

Figure 8.2 The absolute benefit (reduction in the risk of stroke) is shown for the NASCET study results published in 1991. The 'break-even' point for stenosis severity was estimated to be somewhere between 50 and 69%. This was confirmed by the results of the NASCET study published in 1998.

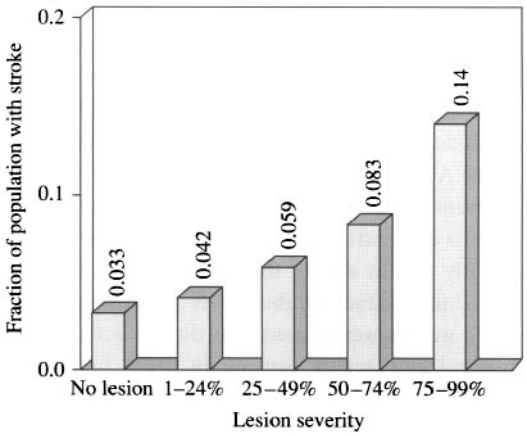

Figure 8.3 The presence of neurologic symptoms was associated with the degree of stenosis as measured with carotid ultrasound in the Cardiovascular Health Study.

It is hard to reconcile these reports from large multicenter studies with the reports coming mostly from single academic centers that show carotid Doppler velocity measurements to have high sensitivity and specificity (Table 8.1). Differences in imaging devices or imaging protocols likely had an effect on diagnostic performance of Doppler ultrasound in multicenter studies [6–8]. The paper by Kuntz *et al.* has shown that variability exists at the level of individual laboratories and for different imaging devices. The question remains whether Doppler ultrasound can be implemented at the level of more than one center and whether, with proper quality assurance protocols, Doppler ultrasound measurements relate to the risk of stroke.

Epidemiologic studies and quality assurance

The answers to some of these issues can be extracted from an epidemiologic study: the Cardiovascular Health Study (CHS) [9]. This multicenter study looked at 5888 individuals aged 65 years or more in four communities in the US. The centers participating in this study used carotid Doppler velocity measurements in an attempt to measure the severity of carotid disease. An increased risk of having stroke or transient ischemic attacks was associated with the degree of stenosis (Figure 8.3) measured by Doppler ultrasound [10]. The risk of stroke (Figure 8.3) was much greater

Table 8.1 Doppler velocity cut-off points for determining 70% or more stenosis of the internal carotid artery (ICA) consistent with NASCET [44].

Author	*Parameter(s)*	*Accuracy (%)*
Hunink *et al.* [5]	ICA PSV ≥ 230 cm/s	Sensitivity 80, specificity 90
Moneta *et al.* [45]	ICA/CCA PSV ratio ≥ 4.0	Sensitivity 91, specificity 87
Faught *et al.* [46]	ICA PSV ≥ 130 cm/s and ICA EDV ≥ 100 cm/s	Sensitivity 81, specificity 98
Neale *et al.* [47]	ICA PSV ≥ 270 cm/s and ICA EDV ≥ 110 cm/s	Sensitivity 96, specificity 91
Hood *et al.* [48]	ICA PSV ≥ 130 cm/s and ICA EDV ≥ 100 cm/s	Sensitivity 87, specificity 97
Carpenter *et al.* [49]	ICA PSV ≥ 210 cm/s or	Sensitivity 94, specificity 77
	ICA/CCA velocity ratio ≥ 3.0	Sensitivity 91, specificity 78
Chen *et al.* [50]	ICA PSV ≥ 125 cm/s and ICA EDV ≥ 135 cm/s	Sensitivity 76, specificity 93

PSV, peak systolic velocity; EDV, end-diastolic velocity; CCA, common carotid artery.

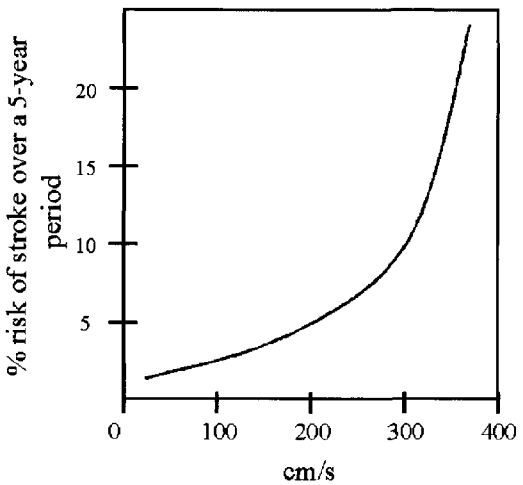

Figure 8.4 The risk of developing a stroke was shown to be directly associated to the blood flow velocity of the internal carotid artery in the Cardiovascular Health Study.

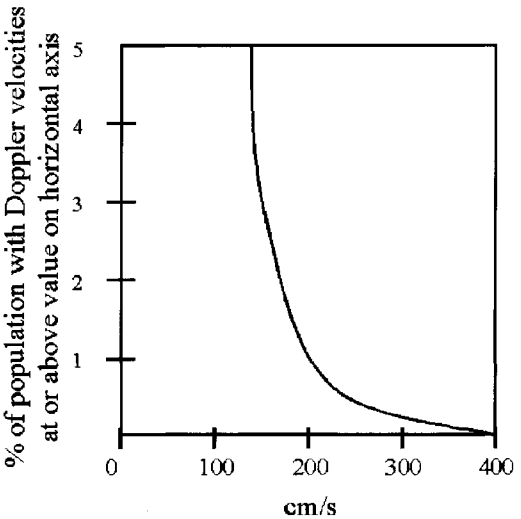

Figure 8.5 The proportion of individuals with 50% internal carotid artery stenosis was low (less than 5% in participants of the Cardiovascular Health Study). All individuals were aged 65 years or more and, for this figure, none had symptoms of cerebrovascular disease.

in subjects with velocities above 250 cm/s (75% stenosis) than for individuals with stenosis of 50–75% (Doppler velocities between 150 cm/ s and 225 cm/s) [10]. In addition, Doppler velocity measurements made in asymptomatic individuals were directly associated with the risk of a future stroke [11]. A semi-linear association was seen between Doppler velocities and incident stroke: the higher the measured Doppler velocity, the greater the chance of experiencing a subsequent stroke (Figure 8.4) during a 5-year follow-up [11]. However, the prevalence of individuals with blood flow velocities above 150 cm/s, i.e. the equivalent of a 50% diameter stenosis, was less than 5% in individuals who had no evidence of cerebrovascular symptoms (Figure 8.5) when they were evaluated with Doppler ultrasound [11].

The difference between the results of the CHS study and the results of NASCET and ACAS are, in part, explained by a very strict protocol and quality assurance program used in the CHS. The CHS study was conducted in individuals aged 65 years or more located in four very distinct geographical regions of the US. All sonographers used the same imaging device, were trained in the same imaging protocol, and were given feedback as to their technique during review of their images at a central reading center [12].

The selection of the ultrasound imaging device took place by comparing instruments from six different companies. This comparison included imaging of gray-scale phantoms, Doppler velocity phantom measurements and imaging of the same two subjects. Images obtained from all ultrasound devices were then reviewed by the six members of an Ultrasound Committee. The evaluation included image quality, focusing capability of the device, magnification factors, Doppler beam and gray-scale steering of the ultrasound image. In addition, color Doppler imaging was used as a guide for the Doppler velocity evaluations. Sonographers were trained for 2 days in a curriculum that reviewed the basics of carotid ultrasound, Doppler hemodynamics and specifics of the imaging device control panel. The trained sonographers then had to submit certification examinations that were reviewed by a co-investigator. Once certified, the sonographers were continuously informed of the quality of their examinations. Trained readers reviewed images under the supervision of the co-investigators and reported on the quality of the examinations.

Gray-scale (B-mode) imaging of the extent of atherosclerotic plaque

Much attention has been focused on the measurement of atherosclerotic plaque when determining whether a lesion is significant from the perspective of surgical interventions. However, stenotic lesions causing a 50% or more diameter stenosis have a prevalence of

less than 10% in the general population, while most lesions, if present, cause 50% or less diameter narrowing [10]. The emphasis then shifts towards a more global evaluation of the extent of carotid artery disease and possible associations with cardiovascular risk factors.

Gray-scale imaging alone, without the use of duplex or color Doppler ultrasound, has been shown to have a low sensitivity and specificity for grading the severity of carotid disease as compared to arteriography and pathology [13]. While Doppler velocity evaluations circumvent this problem in diagnostic accuracy, the gray-scale information on the carotid ultrasound imaging can still be used to evaluate the severity of carotid artery disease, especially for lesions of less than 50% diameter stenosis (where Doppler velocities are less than 150 cm/s). Plaques of low echodensity (hypoechoic or echolucent) have typically been underestimated by gray-scale imaging alone. With color Doppler imaging, the likelihood of such errors decreases [14]. The carotid ultrasound protocol of the Cardiovascular Health Study had readers blinded to the subject being studied. The degree of atherosclerotic plaque was subjectively quantified as absent (0%), 1–24% diameter narrowing, and 25–49% diameter narrowing if the Doppler velocity is less than 150 cm/s. For velocities above 150 cm/s but less than 250 cm/s, the lesion was graded as 50–74% diameter stenosis narrowing. For velocities above 250 cm/s, the stenosis was graded as 75–99% stenosis. It is understood that subtotally occluded carotid arteries can show low-amplitude blood flow signals whereas totally occluded arteries have no detectable Doppler flow signals [10]. Totally occluded carotid arteries are distinguished from subtotally occluded arteries with the aid of color Doppler imaging.

This semiquantitative scale shows an association with cardiovascular risk factors: the higher the category of plaque formation, the more an individual has cardiovascular risk factors. This observation has been made in both the Cardiovascular Health Study and the Framingham Heart Study [10,15]. Greater degrees of carotid narrowing are also associated with a higher likelihood of clinically manifest cardiovascular disease [10,16].

Cardiovascular risk factors and subclinical disease

Where did the expression 'cardiovascular risk factors' come from? After the end of World War II, public health was mostly focused on infectious diseases. In the late 1940s, a well-focused effort was directed towards understanding the factors responsible for the apparent epidemic of cardiovascular diseases in the US population. The ground-breaking Framingham Study was an example of a well-coordinated effort to measure various health parameters in a large suburban population [17]. The defined cohort, made up of volunteers, was then followed in time. With the development of cardiovascular events such as myocardial infarction and strokes, a database relating these events to certain parameters such as blood pressure and cholesterol levels was established. With time, these data generated enough events to indicate that major culprits for incident cardiovascular events included diabetes, smoking, high blood pressure and elevated cholesterol levels. These measures became recognized as risk factors for cardiovascular events and therefore risk factors for cardiovascular disease.

Cardiovascular risk factors have been identified by discovery of their association with the likelihood of developing a stroke or myocardial infarction. Plasma cholesterol levels, for example, are known to be a risk factor for myocardial infarction. The recognition that high levels of cholesterol in the blood were a risk factor came from studies that compared individuals who developed clinically overt cardiovascular events, stroke or myocardial infarction, to those who did not. In doing so, cholesterol levels were recognized as increasing the likelihood of cardiovascular events.

Cardiovascular risk factors include age, gender, diabetes, history of cigarette smoking, hypertension and plasma cholesterol levels (LDL-cholesterol in a positive fashion and HDL-cholesterol in a protective fashion). These risk factors can be further refined to include pack-years smoked, actual level of systolic blood pressure (in a positive fashion) and diastolic blood pressure and further lipoprotein subsets such as Lp(a) or apo-protein B.

The presence of carotid artery disease has served as a surrogate endpoint for the evaluation of the effects of cardiovascular risk factors. In the Framingham Study, a value of a 25% diameter stenosis in the internal carotid artery has been used as a cut-off point for identifying individuals with atherosclerotic disease [18,19]. This cut-off point has been used to study the effects of specific risk factors or risk-factor exposure over time in large populations. Data from Selhub *et al.*

[18] showed the strong association between homocysteinemia and the presence of lesions greater than 25% in the internal carotid arteries. In a publication by Wilson *et al.* [19] the presence of focal lesions in the carotids, with greater than 25% stenosis, was associated with the time course of exposure to different risk factors. The study by Wilson *et al.* clearly showed strong associations of the time exposure to different cardiovascular risk factors, mostly smoking and blood pressure, than with a single ultrasound measurement.

The presence of relatively small focal carotid lesions in the carotid system can therefore serve as a surrogate for the determination of atherosclerotic burden in individuals. These measurements are semiquantitative and subjective, yet can serve as a powerful non-invasive tool for determining the effects of risk factor exposure on the arterial system.

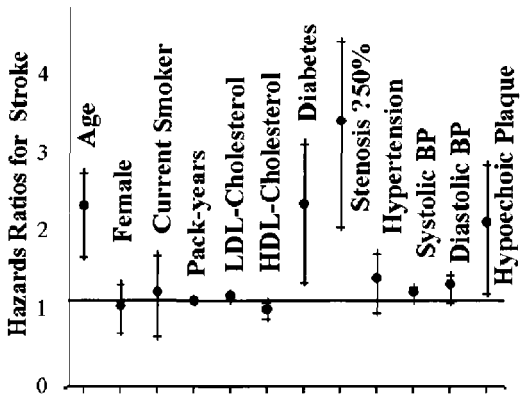

Figure 8.6 The relative risk of developing a stroke with an identified hypoechoic plaque is at least as significant as having a carotid stenosis of 50% or greater. In addition, traditional risk factors do not seem to be as important in their ability to predict incident strokes.

Plaque characterization

Early surgical series showed that the appearance of endarterectomy specimens correlated with the appearance on B-mode ultrasound, hypoechoic areas representing areas of hemorrhage [20–22]. These early studies on carotid plaque characteristics were biased to patients with high degrees of stenosis and therefore quite large plaques. The main focus of the ultrasound examination was confirming whether or not a plaque was 'dangerous' and at high risk for causing a cerebrovascular event. Studies also focused on the contour of the plaque and the capacity of ultrasound for detecting ulcerations [22,23]. The accuracy of ultrasound in such cases seems marginal, given the low accuracy for detecting ulcerations. In addition, since the patients are likely to be symptomatic, the severity of carotid stenosis is still the most important variable associated with the risk of stroke.

The concept of a vulnerable plaque in the coronary artery system has, over the years, come to be recognized as a major cause of acute myocardial infarction. According to this theory, a lipid-laden plaque will abruptly rupture into the coronary artery lumen, exposing its components to blood. Acute thrombosis would immediately take place, occluding the artery and causing a myocardial infarction. This theory is supported by observations showing that half of the plaques likely to rupture and cause thrombosis of the coronary arteries cause less than 50% diameter narrowing. Until they cause the first myocardial event, these lesions are asymptomatic and, according to recent observations with intravascular ultrasound, relatively echolucent. This process of rupture of a lipid-laden plaque (relatively hypoechoic on ultrasound imaging) is also believed to apply to the carotid system. The presence of hypoechoic carotid plaques has been related to abnormalities on computed tomograms of the brain [24]. A longitudinal prospective study has recently shown that hypoechoic lesions are also associated with the likelihood of future strokes in individuals who are asymptomatic at the time of their ultrasound examination [25]. Results of this study showed that hypoechoic plaque was a risk factor for incident stroke (Figure 8.6), a risk factor at least as important as carotid stenosis of 50% or more [25].

Although quantitative approaches for measuring plaque density are under investigation, plaque characterization has normally been done using a qualitative scoring system:

Type 1: hypoechoic, or echolucent, plaque that contains homogeneous distribution of echoes (with the exception of an echogenic rim thought to represent a fibrous cap), as shown in Figure 8.7.

Type 2: hypoechoic, or echolucent, plaque that contains a heterogeneous distribution of echoes (50% or more of the plaque has hypoechoic elements).

Type 3: hyperechoic, or echodense, plaque that contains a heterogeneous distribution of echoes (50% or more of the plaque has hyperechoic elements).

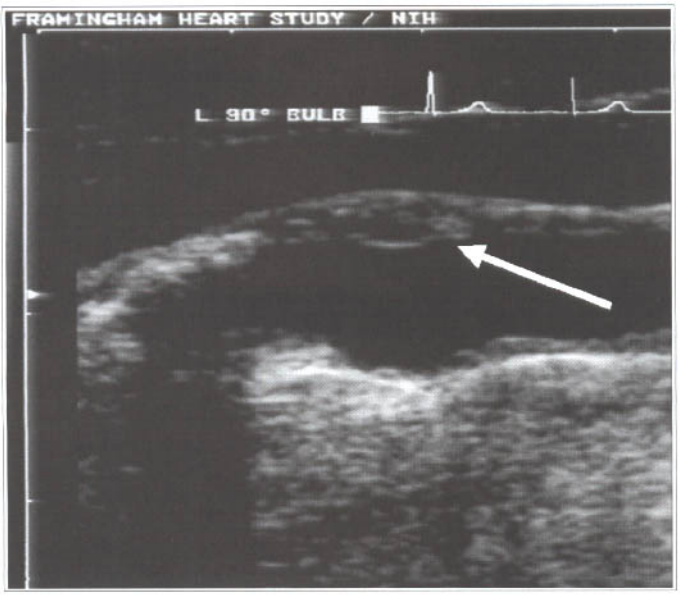

Figure 8.7 The near wall of the internal carotid artery sinus (bulb) shows a hypoechoic plaque with a rim of increased echoes. This is typical of a hypoechoic plaque.

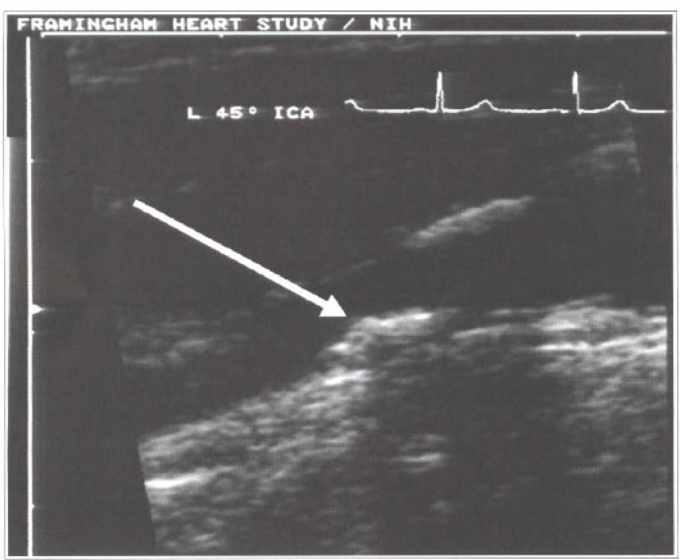

Figure 8.8 The far wall of the proximal internal carotid artery shows a dense (echogenic) plaque with strong signals. This is typical of a hyperechoic plaque.

Type 4: hyperechoic, or echodense, plaque that contains a homogeneous distribution of echoes (the plaque is made up completely of hyperechoic elements), as shown in Figure 8.8.

Type 5: calcified plaque that contains acoustic shadowing sufficiently extensive to preclude evaluation of the plaque characteristics.

The relative echogenicity of the plaques is determined by the closeness to the echoes within blood (hypoechoic) and those of the surrounding soft tissues (hyperechoic).

These metrics of carotid artery disease are currently qualitative or even semiquantitative at best. There are, however, simpler quantitative measures of the effects of atherosclerosis and risk factors that can be quantified on ultrasound images. The future of carotid ultrasound seems to be for quantitative measurements of carotid wall thickness.

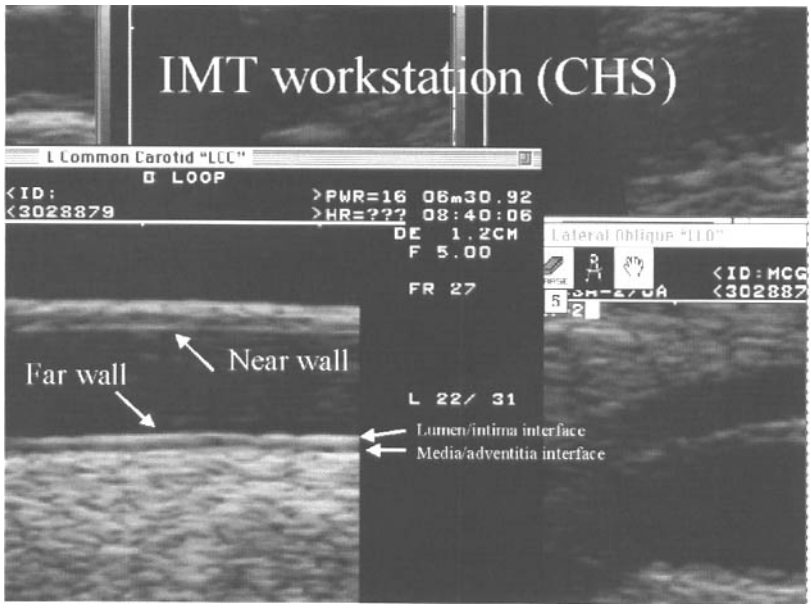

Figure 8.9 This image from a carotid ultrasound workstation shows an image with focus on the far wall of the common carotid artery. Wall thickness is measured as the distance between the leading edge of the lumen/intima interface to the media/adventitia interface.

Quantitative measures of carotid artery wall thickness

In 1986, a group of investigators pointed to a strong association between the presence of atherosclerosis and an ultrasonographic measurement of the thickness of the aortic wall. This measurement was also performed for the carotid artery wall and was shown to correlate with the presence of cardiovascular risk factors (hypercholesterolemia and smoking) [26,27]. The measurement consists of determining the distance between the leading edge of the lumen-to-wall interface of the artery and the interface between the media and adventitia on the artery wall (Figure 8.9). The combined width of this anatomic region is defined as the intima–media thickness (IMT).

Since its first evaluation *in vitro*, measurements of intima–media thickness have also been applied to large population groups. The first two studies to look at this in a systematic way were the Atherosclerosis Risk in Communities (ARIC) [28] and Kuopio heart studies [29]. Both studies showed clear associations between the presence of focal lesions in the internal carotid artery and more diffuse thickening of the arterial wall. Individuals with larger IMTs (or thicker inner layers of vessel walls) had greater numbers of cardiovascular risk factors than individuals with thinner walls.

The Cardiovascular Health Study took these measurements further and evaluated the presence of intima–media thickness within the common carotid as well as in the internal carotid arteries. These studies, with currently more than 10 years of follow-up, clearly show the very strong cross-sectional relationships between risk factors and the extent to which the wall of both the common and internal carotid arteries thickens [30]. Whereas common carotid artery wall thickening is a more diffuse process, the internal carotid artery wall thickness is a sonographic measurement of carotid plaque thickness and cholesterol deposition. As such, increased internal carotid IMT corresponds to increased degrees of carotid artery stenosis. It is therefore not surprising that measurements of internal carotid artery wall thickness correlate to the extent of subjectively graded percentage stenosis [10]. There is, however, an issue of differences in the definition of plaque and wall thickness. The size of a plaque is typically measured from the internal

elastic media to the lumen, whereas the ultrasound measurement of wall thickness is carried out from the external elastic media to the lumen.

Cross-sectional relationships between the IMT measures have further been explored and form the basis of an overall measure of subclinical cardiovascular disease [31].

IMT and prediction of incident events

IMT measurements performed in different population groups have now shown predictive power for incident events: IMT is a marker for future myocardial infarction as well as for stroke. A paper by O'Leary *et al.* in 1999 [32] showed a clear-cut scaling effect as well as excess risk with increasing thickening of the internal carotid artery and the common carotid artery as well as for a combined score adding measurements from the common and the internal carotid arteries (Figure 8.10). The predictive power of IMT measurements for stroke or myocardial infarction has also been observed by other investigators [33,34].

The technical requirements needed to perform IMT measurements are demanding.

Description of an IMT measurement protocol

IMT measurements are made at the level of the common carotid artery as well as in the proximal internal carotid artery. One protocol, used in the ARIC study, includes a sampling of the common carotid artery, and a separate sampling at the level of the common carotid bifurcation (so-called bulb) and proximal internal carotid artery. The protocol used for the Cardiovascular Health Study uses one view of the common carotid artery and three projections of the proximal internal carotid artery (to include the so-called carotid bulb). Both protocols share the fact that all imaging is done in a longitudinal plane and that the flow divider and the carotid bulb serve as anatomic markers for location of the measurements. Typically, 1-cm segments are measured in the distal common carotid artery and in the proximal internal carotid artery (bulb).

The ultrasound device and the expertise of the sonographer are important factors for obtaining precise wall thickness measurements. Comparing the results of the Cardiovascular Health Study to ARIC shows site-specific acquisition of data in greater than 97% of instances for the CHS protocol [30]. For the ARIC study, data completeness for the common carotid artery was 79%, dropping to 41% in the proximal internal carotid artery [35].

A high-resolution transducer of at least 5 MHz or higher imaging frequency is used. The ideal imaging device has not been formally identified. Different investigators have used imaging devices made by different ultrasound companies.

Image analysis and IMT as a measure of atherosclerotic burden

The simplest methodology for measuring wall thickness is the use of calipers to measure IMT directly from either a hard copy image or a digital image. Measurements made on digital images are superior to

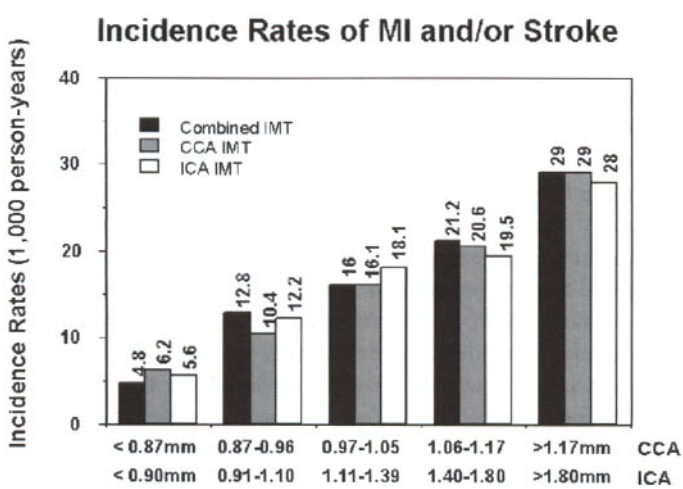

Figure 8.10 This figure shows the incident rate for stroke in individuals without evidence of cerebrovascular disease at a baseline visit. The relative risk of a stroke or myocardial infarction increases with the wall thickness of the common carotid artery (CCA) or of the internal carotid artery (ICA), or with the combined measurement of the CCA and ICA wall thickness.

measurements made on hard copy images, and more modern ultrasound devices give better measurements than the older generation of devices [36]. Although electronic calipers can be used to obtain IMT values, this approach is not as reliable as the use of a specialized workstation and sampling of a large number of points along the artery wall. Use of digital calipers on the ultrasound screen shows some relation to cardiovascular risk factors but is not as precise as measurements made using more sophisticated imaging algorithms [37].

The ARIC, CHS and Tromso investigators used specialized algorithms to measure IMT [12,38,39]. This approach decreases the variability and therefore increases the precision of IMT measurements. This translates into an increase in statistical power for detecting associations with risk factors in smaller groups of subjects. Ideally, with sufficient precision, the measurement may become precise enough to be used as a screening variable at the level of the individual patient. The traditional method of reviewing carotid images relies on human readers to review images, to identify the interfaces and to draw the contours of the wall interfaces. This approach has given support to the concept that IMT measurements are a measure of subclinical disease [40] and are predictive of future cardiovascular events [32]. Human readers also permit the inclusion of measurements of IMT in the internal carotid artery. The association between risk factors and IMT are different for measurements made in the common carotid as compared to the internal carotid artery [11,30,41]. In addition, internal carotid artery IMT measurements had predictive power for the IMT measurements made in the common carotid artery [32]. This implies that a baseline evaluation of the IMT of the common and the internal carotid arteries gives a better baseline estimate of risk for future cardiovascular events than a measurement made solely in the common carotid artery.

Image analysis and IMT as a measure of progression of atherosclerosis

Edge detection algorithms can also be applied to the processing of digitally stored carotid images. However, the performance of these edge detectors has been well evaluated for the far wall of the common carotid artery. No solid data exist for the application of this technology to either the near wall of the common carotid artery or the internal carotid artery. Phantom studies have shown some increase in the precision of IMT measurement as compared to data from human readers [42].

High-precision IMT measurements with edge detectors have found application in the serial measurement of wall thickness changes over time. Measurements using sophisticated edge detectors can track the progression or regression of atherosclerotic disease in the common carotid artery [43]. The beneficial effects of different drug therapies such as the 3-hydroxy-3-methyl-glutaryl-coenzyme A (HMG-CoA) reductase inhibitors have been clearly documented with IMT measurements. IMT increases by 0.02 mm/year in non-treated controls whereas regression of 0.01 mm/year has been shown for subjects treated with Lovastatin. While edge detector measurements work well for carotid IMT measurements, regression of wall thickness, believed to represent regression of atherosclerosis, has also been shown for IMT measurements using human reader-traced interfaces.

Carotid IMT measurements are one of the most powerful measurements of subclinical cardiovascular disease. With improvements in technology and improved edge detector software, a precise estimate of the atherosclerotic burden in individual patients seems likely in the near future.

Carotid artery protocol used at the Framingham Study

Initial scan

The purpose of the initial carotid artery scan is to orientate the sonographer to the anatomy of the carotid arteries. The transducer is held transverse and slowly swept up the neck towards and beyond the carotid bifurcation. The sonographer identifies a lateral plane where the internal jugular vein lies above the carotid artery. The sonographer should identify the distal common carotid artery, the carotid bulb, and the internal and external carotid arteries. Pulsed-wave and color Doppler are used to distinguish between the internal and external carotid arteries. The two internal anatomic landmarks, the initial dilatation that marks the origin of the carotid bulb and the most caudal end of the flow divider, should be identified. Color Doppler is used to aid in the placement of the range-gated pulse Doppler sample volume. The sonographer should identify the site of maximal wall

thickening in the near or far wall of the bulb and internal carotid artery during the initial scan. Beam steering should be used as it will help optimize interfaces by placing the echo signal at more of a right angle to the target.

Directed imaging

Obtain from the right and left sides:

1 two images: two lateral views of the distal common carotid—at peak systole and then at end-diastole;

2 two images: a lateral view of the carotid bulb and a second view at the site of maximal thickening in the carotid bulb, whether it be at any of the following imaging planes:

(a) antero-oblique
(b) lateral
(c) posterio-oblique;

3 two images: a lateral view of the internal carotid artery and a second view at the site of maximal thickening in the internal carotid artery, whether it be at any of the following imaging planes:

(a) antero-oblique
(b) lateral
(c) posterio-oblique;

4 a Doppler waveform and a peak systolic velocity in the internal carotid artery/bulb.

A lateral view is defined as a longitudinal image, 45° to the horizontal with the subject's head rotated 45° away from the side being imaged.

The three projections or scanning angles for images taken at the site of maximal thickening are the antero-oblique, lateral (45°) and posterio-oblique.

(a) Antero-oblique: the arch on the surface of the neck from the midline (trachea) to over the edge of the sternocleidomastoid muscle (from −10° to 35° to the vertical).

(b) Lateral (45°): the arch along the lateral surface of the neck, from 35° to 80° to the vertical. The sternocleidomastoid muscle can be palpated beneath this portion of the skin's surface.

(c) Posterior oblique: the arch from 80° to 135° to the vertical. The probe almost always lies just behind the posterior margin of the sternocleidomastoid muscle.

The final 45° of a complete 180° arch are not available since the patient's position and the distance to the artery from the back of the neck preclude scanning in that plane. The first 10° of the arch from the midline due to the trachea, therefore each of the three scanning arches covers a 45° segment of the neck's surface. The precise angle of the probe head should not overly concern the sonographer. Since the target is the carotid artery, once the probe is placed on the appropriate segment of the neck's surface, the scanning angle defines itself in the process of optimizing the image.

Summary

The role of carotid ultrasound is about to expand beyond that of a diagnostic test that is efficiently used in symptomatic patients, or even one where carotid Doppler ultrasound can be used to identify the asymptomatic patient with a high-grade carotid artery stenosis.

Gray-scale imaging of early plaque deposition and wall thickness is applicable to the majority of individuals with milder forms of atherosclerosis. Using IMT measurements, individuals who have suffered changes related to exposure to cardiovascular risk factors can now be identified. These individuals may profit from drug interventions and lifestyle modification at a stage early enough so that atherosclerotic changes can at least stabilize and possibly regress. The major limitations to the generalized application of this technology are the need for quality assurance protocols and measurement technologies that go beyond the scope of most diagnostic vascular laboratories. While the implementation of quality imaging for Doppler ultrasound evaluation of significant stenosis is demanding, high-resolution gray-scale imaging of the carotid wall requires even greater care.

References

1 Executive Committee for the Asymptomatic Carotid Atherosclerosis Study. Endarterectomy for asymptomatic carotid artery stenosis. *JAMA* 1995; **273**: 1421–8.

2 Howard G, Baker WH, Chambless LE, Howard VJ, Jones AM, Toole JF. An approach for the use of Doppler ultrasound as a screening tool for hemodynamically significant stenosis (despite heterogeneity of Doppler performance). A multicenter experience. Asymptomatic Carotid Atherosclerosis Study Investigators. *Stroke* 1996; **27**: 1951–7.

3 Schwartz SW, Chambless LE, Baker WH, Broderick JP, Howard G. Consistency of Doppler parameters in predicting arteriographically confirmed carotid stenosis. Asymptomatic Carotid Atherosclerosis Study Investigators. *Stroke* 1997; **28**: 343–7.

4 Eliasziw M, Rankin RN, Fox AJ, Haynes RB, Barnett HJM. Accuracy and prognostic consequences of

ultrasonography in identifying severe carotid artery stenosis. *Stroke* 1995; **26**: 1747–52.

5 Hunink MGM, Polak JF, Barlan MM, O'Leary DH. Detection and quantification of carotid artery stenosis: efficacy of various Doppler velocity parameters. *AJR* 1993; **160**: 619–25.

6 Kuntz KM, Polak JF, Whittemore AD, Skillman JJ, Kent KC. Duplex ultrasound criteria for the identification of carotid stenosis should be laboratory specific. *Stroke* 1997; **28**: 597–602.

7 Criswell BK, Langsfeld M, Tullis MJ, Marek J. Evaluating institutional variability of duplex scanning in the detection of carotid artery stenosis. *Am J Surg* 1998; **176**: 591–7.

8 Ranke C, Creutzig A, Becker H, Trappe HJ. Standardization of carotid ultrasound: a hemodynamic method to normalize for interindividual and interequipment variability. *Stroke* 1999; **30**: 402–6.

9 Fried LP, Borhani NO, Enright P *et al.* The Cardiovascular Health Study: design and rationale. *Ann Epidemiol* 1991; **1**: 263–76.

10 Polak JF, O'Leary DH, Kronmal RA *et al.* Sonographic evaluation of carotid artery atherosclerosis in the elderly: relationship of disease severity to stroke and transient ischemic attack. *Radiology* 1993; **188**: 363–70.

11 Longstreth WT Jr, Shemanski L, Lefkowitz D, O'Leary DH, Polak JF, Wolfson SK Jr. Asymptomatic internal carotid artery stenosis defined by ultrasound and the risk of subsequent stroke in the elderly. The Cardiovascular Health Study. *Stroke* 1998; **29**: 2371–6.

12 O'Leary DH, Polak JF, Wolfson SK Jr *et al.* Use of sonography to evaluate carotid atherosclerosis in the elderly. The Cardiovascular Health Study. CHS Collaborative Research Group. *Stroke* 1991; **22**: 1155–63.

13 Comerota AJ, Cranley JJ, Cook SE. Real-time B-mode carotid imaging in diagnosis of cerebrovascular disease. *Surgery* 1981; **89**: 718–29.

14 Gronholdt M-LM, Nordestgaard BG, Nielsen TG, Sillesen H. Echolucent carotid artery plaques are associated with elevated levels of fasting and postprandial triglyceride-rich lipoproteins. *Stroke* 1996; **27**: 2166–72.

15 O'Leary DH, Anderson KM, Wolf PA, Evans JC, Poehlman HW. Cholesterol and carotid atherosclerosis in older persons: the Framingham Study. *Ann Epidemiol* 1992; **2**: 147–53.

16 O'Leary DH, Polak JF, Kronmal RA *et al.* Distribution and correlates of sonographically detected carotid artery disease in the Cardiovascular Health Study. The CHS Collaborative Research Group. *Stroke* 1992; **23**: 1752–60.

17 Dawber TR. *The Framingham Study. The Epidemiology of Atherosclerotic Disease. A Commonwealth Fund Book.* Cambridge: Harvard University Press, 1980.

18 Selhub J, Jacques PF, Bostom AG *et al.* Association between plasma homocysteine concentrations and extracranial carotid-artery stenosis [see comments]. *N Engl J Med* 1995; **332**: 286–91.

19 Wilson PW, Hoeg JM, D'Agostino RB *et al.* Cumulative effects of high cholesterol levels, high blood pressure, and cigarette smoking on carotid stenosis. *N Engl J Med* 1997; **337**: 516–22.

20 Lusby RJ, Ferrell LD, Ehrenfeld WK, Stoney RJ, Wylie EJ. Carotid plaque hemorrhage. Its role in production of cerebral ischemia. *Arch Surg* 1982; **117**: 1479–88.

21 Gray-Weale AC, Graham JC, Burnett JR, Byrne K, Lusby RJ. Carotid artery atheroma: comparison of preoperative B-mode ultrasound appearance with carotid endarterectomy specimen pathology. *J Cardiovasc Surg* 1988; **29**: 676–81.

22 Bluth EI, Kay D, Merritt CR *et al.* Sonographic characterization of carotid plaque: detection of hemorrhage. *AJR Am J Roentgenol* 1986; **146**: 1061–5.

23 O'Donnell TF, Erdoes L, Mackey WC *et al.* Correlation of B-mode ultrasound imaging and arteriography with pathologic findings at carotid endarterectomy. *Arch Surg* 1985; **120**: 443–9.

24 Geroulakos G, Hobson RW, Nicolaides A. Ultrasonographic carotid plaque morphology in predicting stroke risk. *Br J Surg* 1996; **83**: 582–7 [see comments].

25 Polak JF, Shemanski L, O'Leary DH *et al.* Hypoechoic plaque at US of the carotid artery: an independent risk factor for incident stroke in adults aged 65 years or older. Cardiovascular Health Study. *Radiology* 1998; **208**: 649–54.

26 Pignoli P, Tremoli E, Poli A, Oreste P, Paoletti R. Intimal plus medial thickness of the arterial wall: a direct measurement with ultrasound imaging. *Circulation* 1986; **74**: 1399–406.

27 Poli A, Tremoli E, Colombo A, Sirtori M, Pignoli P, Paoletti R. Ultrasonographic measurement of the common carotid artery wall thickness in hypercholesterolemic patients. A new model for the quantitation and follow-up of preclinical atherosclerosis in living human subjects. *Atherosclerosis* 1988; **70**: 253–61.

28 Heiss G, Sharrett AR, Barnes R, Chambless LE, Szklo M, Alzola C. Carotid atherosclerosis measured by B-mode ultrasound in populations: associations with cardiovascular risk factors in the ARIC study. *Am J Epidemiol* 1991; **134**: 250–6.

29 Salonen R, Salonen J. Determinants of carotid intima-media thickness: a population-based ultrasonography study. *J Intern Med* 1991; **229**: 225–31.

30 O'Leary DH, Polak JF, Kronmal RA *et al.* Thickening of the carotid wall. A marker for atherosclerosis in the elderly? Cardiovascular Health Study Collaborative Research Group. *Stroke* 1996; **27**: 224–31.

31 Kuller LH, Shemanski L, Psaty BM *et al.* Subclinical disease as an independent risk factor for cardiovascular disease. *Circulation* 1995; **92**: 720–6 [see comments].

32 O'Leary DH, Polak JF, Kronmal RA, Manolio TA, Burke GL, Wolfson SK Jr. Carotid-artery intima and media thickness as a risk factor for myocardial infarction and stroke in older adults. Cardiovascular Health Study Collaborative Research Group. *N Engl J Med* 1999; **340**: 14–22.

33 Chambless LE, Heiss G, Folsom AR *et al.* Association of coronary heart disease incidence with carotid arterial wall thickness and major risk factors: the Atherosclerosis Risk in Communities (ARIC) Study, 1987–1993. *Am J Epidemiol* 1997; **146**: 483–94.

34 Hodis HN, Mack WJ, LaBree L *et al.* The role of carotid arterial intima-media thickness in predicting clinical coronary events. *Ann Intern Med* 1998; **128**: 262–9.

35 Howard G, Burke GL, Evans GW *et al.* Relations of intimal-medial thickness among sites within the carotid artery as evaluated by B-mode ultrasound. ARIC Investigators. Atherosclerosis Risk in Communities. *Stroke* 1994; **25**: 1581–7.

36 Baldassarre D, Amato M, Bondioli A, Sirtori CR, Tremoli E. Carotid artery intima-media thickness measured by ultrasonography in normal clinical practice correlates well with atherosclerotic risk factors. *Stroke* 2000; **31**: 2426–30.

37 Baldassarre D, Tremoli E, Amato M, Veglia F, Bondioli A, Sirtori CR. Reproducibility validation study comparing analog and digital imaging technologies for the measurement of intima-media thickness. *Stroke* 2000; **31**: 1104–10.

38 Bond MG, Wilmoth SK, Enevold GL, Strickland HL. Detection and monitoring of asymptomatic atherosclerosis in clinical trials. *Am J Med* 1989; **86**: 33–6.

39 Bots M, Mulder P, Hofman A, van Es G, Grobbee D. Reproducibility of carotid vessel wall thickness measurements. The Rotterdam Study. *J Clin Epidemiol* 1994; **47**: 921–30.

40 Kuller L, Borhani N, Furberg C *et al.* Prevalence of subclinical atherosclerosis and cardiovascular disease and association with risk factors in the Cardiovascular Health Study. *Am J Epidemiol* 1994; **139**: 1164–79.

41 Bots ML, Hoes AW, Koudstaal PJ, Hofman A, Grobbee DE. Common carotid intima-media thickness and risk of stroke and myocardial infarction: the Rotterdam Study. *Circulation* 1997; **96**: 1432–7.

42 Selzer RH, Hodis HN, Kwong-Fu H *et al.* Evaluation of computerized edge tracking for quantifying intima-media thickness of the common carotid artery from B-mode ultrasound images. *Atherosclerosis* 1994; **111**: 1–11.

43 Hodis HN, Mack WJ, Barth J. Carotid intima-media thickness as a surrogate end point for coronary artery disease [letter; comment]. *Circulation* 1996; **94**: 2311–2.

44 North American Symptomatic Carotid Endarterectomy Trial Collaborators. Beneficial effect of carotid endarterectomy in symptomatic patients with high-grade stenosis. *N Engl J Med* 1991; **325**: 445–53.

45 Moneta GL, Edwards JM, Chitwood RW *et al.* Correlation with North American Symptomatic Carotid Endarterectomy Trial (NASCET) angiographic definition of 70% to 99% internal carotid artery stenosis with duplex scanning. *J Vasc Surg* 1993; **17**: 152–7.

46 Faught WE, Mattos MA, van Bemmelen PS *et al.* Color-flow duplex scanning of carotid arteries: new velocity criteria based on receiver operator characteristic analysis for threshold stenoses used in the symptomatic and asymptomatic carotid trials. *J Vasc Surg* 1994; **19**: 818–28.

47 Neale ML, Chambers JL, Kelly AT *et al.* Reappraisal of duplex criteria to assess significant carotid stenosis with special reference to reports from the North American Symptomatic Carotid Endarterectomy Trial and the European Carotid Surgery Trial. *Stroke* 1994; **20**: 642–9.

48 Hood DB, Mattos MA, Mansour A *et al.* Prospective evaluation of new duplex criteria to identify 70% internal carotid artery stenosis. *J Vasc Surg* 1996; **23**: 254–61.

49 Carpenter JP, Lexa FJ, Davis JT. Determination of duplex Doppler ultrasound criteria appropriate to the North American Symptomatic Carotid Endarterectomy Trial. *Stroke* 1996; **27**: 695–9.

50 Chen JC, Salvian AJ, Taylor DC, Teal PA, Marotta TR, Hsiang YN. Predictive ability of duplex ultrasonography for internal carotid artery stenosis of 70%–99%: a comparative study. *Ann Vasc Surg* 1998; **12**: 244–7.

9 CHAPTER 9

Carotid and vertebral duplex scanning in secondary stroke prevention and stenting

Charles H. Tegeler, MD *& Disya Ratanakorn,* MD

Introduction

Stroke is the third leading cause of death in the US and is a major cause of disability in the elderly [1]. Of all strokes, about 80–85% are ischemic infarction and 15–20% are hemorrhages [2–4]. The appropriate prevention and treatment of ischemic infarction requires detection of the underlying ischemic mechanism in each patient individually. Thus, neurovascular ultrasound plays a particularly important role in patients with ischemic stroke. Carotid and vertebral duplex and transcranial Doppler ultrasonography are non-invasive methods providing a quick, safe, accurate and cost-effective way to evaluate the vascular system for potential ischemic causes. This chapter will cover clinical indications and principles of interpretation of carotid and vertebral duplex scanning, cerebrovascular stenting, integrated use, case illustrations and poststudy questions.

Carotid duplex scanning

Carotid duplex scanning is a non-invasive method used to evaluate extracranial carotid arteries, providing real-time anatomy and hemodynamic information about these vessels. The main reason to perform color-coded duplex scanning in a patient with an ischemic stroke is the detection and quantification of atherosclerotic carotid artery disease. A $\geq$ 50% carotid stenosis may be responsible for up to 25% of all ischemic strokes. Therefore, carotid duplex is considered to be the initial vascular evaluation of choice for patients who present with cerebrovascular disease. Other clinical indications include:

1 serial follow-up of known cerebrovascular disease, i.e. moderate carotid stenosis;
2 preoperative evaluation of patients with other vascular disease such as coronary artery disease and peripheral vascular diseases, and neck bruits;
3 postoperative follow-up after carotid endarterectomy and carotid stenting; and
4 assessment of pulsatile neck masses or other abnormal structures such as grafts.

Carotid duplex scanning may also be used as a screening tool for early atherosclerosis, evaluating intima–media thickness measurement in asymptomatic patients with risk factors for stroke.

Carotid duplex interpretation regarding carotid stenosis is based primarily on the hemodynamic information (blood flow velocities) provided by the duplex Doppler portion of the study. This involves image-guided placement of the Doppler sample volume, with angle correction, to obtain flow velocity information. Parameters frequently evaluated for the Doppler spectral velocities include the peak systolic and end-diastolic velocity, the ratio of velocities in the internal carotid artery (ICA) and common carotid artery (CCA), side-to-side differences, direction of flow and characteristics of the velocity waveform. These data correlate best with the percentage linear stenosis on angiography, and are key for clinical decisions regarding management with medications, surgery or intravascular intervention. The Doppler data also provide insight into the condition

of vessels both proximal and distal to the portion insonated.

The carotid duplex examination also uses information from the B-mode and color flow imaging part of the examination. This includes measurements of the intima–media thickness and plaque size; location and characteristics of plaque; anatomic variations such as tortuosity, and high and low carotid bifurcation; anatomic abnormalities such as dissection, aneurysm and intraluminal thrombus; slow flow in the vessels described as spontaneous echo contrast; and radial or longitudinal pulsation during the cardiac cycle of carotid arteries. A complete report usually also describes anatomy and hemodynamics of extracranial vertebral arteries, abnormalities in the internal jugular vein and carotid body and thyroid and other neck masses, also commenting on abnormal blood pressure or cardiac rhythm.

In the Neurosonology Laboratory at Wake Forest University School of Medicine, we report plaque sizes as minimal (> 1.0–2.0 mm), moderate (> 2.0–4.0 mm) and large (> 4.0 mm). The characteristics of plaques reported include regular, irregular or ulcerated surface; echogenicity of plaque compared to the media–adventitia signal (anechoic, hypoechoic, echogenic or hyperechoic plaques); the texture of plaque (homogenous, heterogeneous, intraplaque hemorrhage); and the presence of calcification and acoustic shadowing.

Our Neurosonology Laboratory has developed and validated the following criteria for grading carotid stenosis (Table 9.1) to predict the North American (NASCET) percentage diameter reduction measurements. When examination is performed by trained sonographers using a standard protocol, and with ongoing quality assurance, this approach can reach 90% sensitivity and specificity for identification of clinically relevant carotid stenosis. Similar results have been demonstrated by other laboratories [5–8]. The negative predictive value of the test is also high (95%). Limitations to the use of color-coded duplex ultrasound for carotid artery disease include:

1 a high carotid bifurcation;
2 very short neck;
3 extremely deeply located and/or tortuous vessels;
4 extensive (> 2 cm) acoustic shadowing; and
5 poor patient cooperation.

Vertebral duplex scanning

Vertebral duplex scanning is a non-invasive method used to evaluate extracranial vertebral arteries, providing anatomic and hemodynamic information about those vessels. Using techniques similar to those described above for the carotid arteries, the pre- and interosseous cervical segment C5–C6 part of the vertebral arteries can be insonated in 96–100% of cases, whereas the origin of the vertebral arteries can be insonated in 81–92% of cases on the right and in 65–86% of cases on the left [9,10].

Posterior circulation ischemia is quite common, particularly in the elder patient, and abnormal hemodynamics in the vertebral and basilar arteries can also affect hemodynamics observed in the carotid systems. Vertebral duplex scanning should be included as a routine part of carotid duplex ultrasonography. In addition, vertebral duplex provides not only information about the portion insonated directly, but indirect information about the proximal and distal vessel segments. Clinical indications for vertebral duplex include posterior circulation stroke or suspected transient ischemic attack, vertebral artery stenosis or occlusion, vertebral artery dissection, vertebral/subclavian steal syndrome, and unexplained anterior circulation stroke which may be caused by basilar–vertebral–subclavian steal syndrome.

Table 9.1 Flow velocity criteria used for grading carotid stenosis in the Neurosonology Laboratory at Wake Forest University School of Medicine.

Percentage diameter stenosis	PSV (cm/s)	EDV (cm/s)	ICA/CCA ratio
0–49	≤ 140	< 40	< 2
50–74	> 140	< 110	≥ 2
75–94	> 140	> 110	> 3
95–99	Variable	Variable	Variable
Occlusion	No flow	No flow	Not applicable

PSV, peak systolic velocity; EDV, end-diastolic velocity; ICA, internal carotid artery; CCA, common carotid artery.

Parameters for interpretation of vertebral duplex scanning usually include the presence and direction of flow, peak systolic and end-diastolic flow velocities, Doppler spectral waveform characteristics and the luminal diameter of the vessels. These parameters are evaluated to identify vertebral stenosis or occlusion, vertebral/subclavian steal and vertebral artery dissection, and to suspect vertebral hypoplasia. There are no established criteria for grading various degrees of extracranial vertebral artery stenosis. Nevertheless, the average normal peak systolic velocity is approximately 40–50 cm/s in the interosseous segment and approximately 64 cm/s at the vertebral artery origin [9,10].

Vertebral artery duplex scanning is very useful in the evaluation of subclavian steal syndrome which can be demonstrated by early systolic deceleration, alternating flow or total reversed flow direction of the Doppler spectral waveform at rest in the ipsilateral vertebral artery, representing different stages of subclavian steal syndrome. A latent subclavian steal phenomenon can be suspected when a potentially 'stealing' vertebral artery has an early systolic flow deceleration and a second peak velocity (Figure 9.1). A so-called 'hyperemia' test can be performed to provoke steal and induce flow reversal (Figure 9.1). Ischemia induced by inflation of the blood pressure cuff and physical exercise of the ipsilateral arm creates an increased metabolic demand and vasodilatation. Upon cuff release, vertebral duplex can uncover or confirm a steal phenomenon. Monitoring of the intracranial ipsilateral vertebral artery and basilar artery during such physiologic or evoked flow testing can help to identify patients with a true intracranial vertebral–basilar steal who may have a greater need for vascular intervention.

Carotid endarterectomy and cerebrovascular stenting

Since stroke remains the third leading cause of death in the US, prevention is of paramount importance. Many new stroke cases are due to carotid artery stenosis or obstruction [11], so carotid endarterectomy (CEA), carotid angioplasty (CA) and carotid artery stenting (CS) may play important roles in stroke prevention. Three major randomized clinical trials have established the efficacy of CEA in preventing stroke compared to antithrombotic therapy in both symptomatic patients (NASCET and ECST) with ≥ 50% stenosis and asymptomatic patients (ACAS) with > 60% carotid artery stenosis [12–14]. The greatest benefit of CEA is seen in patients with severe symptomatic carotid stenosis of ≥ 70% while the clinical relevance of CEA in an asymptomatic patient is not as widely accepted.

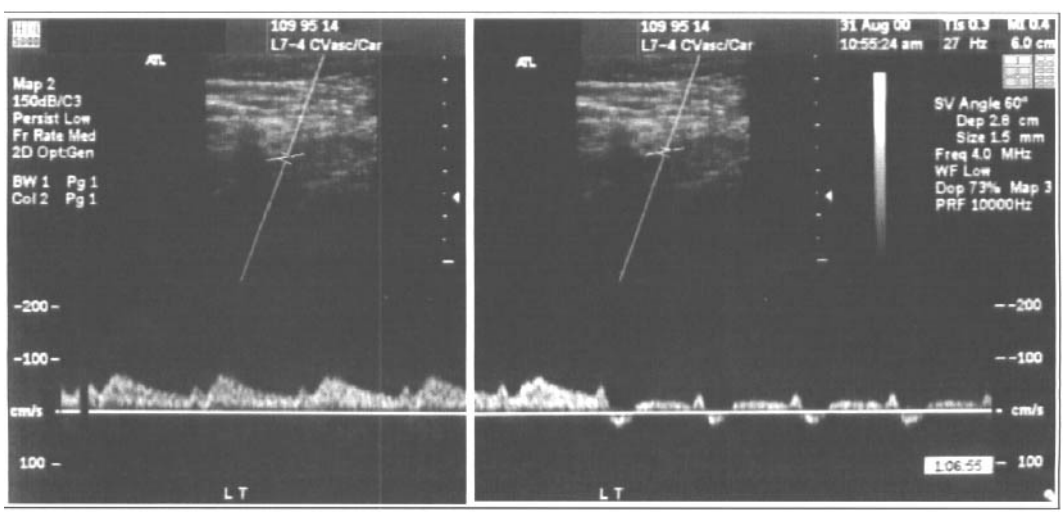

Figure 9.1 Vertebral duplex ultrasound shows systolic deceleration in the velocity spectral waveform present at rest, suggesting a latent subclavian steal (left image). A blood pressure cuff was inflated to suprasystolic values and suddenly released to perform hyperemia testing. After cuff release, a systolic flow reversal with a lower diastolic velocity was detected inducing a subclavian steal phenomenon (right image).

The NASCET trial enrolled only 0.3% of patients who underwent CEA in North America in the same time period. In the NASCET study, the incidence of major stroke, myocardial infarction or death in the surgical group was 3.1%. In ACAS, there was a 2.3% incidence of perioperative stroke or death, and a half of these complications were attributable to invasive cerebral angiography.

Due to patient selection in carotid endarterectomy trials, CEA was not performed in patients with high surgical risk for perioperative morbidity and mortality, including patients with simultaneous severe cardiac and cerebrovascular disease or other medical illness. In these patients CA and CS offer a possible alternative [11,15–17]. In patients with stenoses located in the distal ICA, restenosis after CEA, and severe carotid artery stenosis or carotid artery aneurysm caused by carotid artery dissection, CA and CS can also be used as an alternate therapy [18–20].

One study showed that elective carotid stenting in a high-risk group of patients for CEA, including 107 patients with 126 carotid arteries bearing a significant stenosis, percutaneous CA and CS was feasible. This study showed a low incidence of major stroke or death at 30 days (2.4%), low restenosis rate (4.9%) in those patients evaluated using cerebral angiography at 6-month follow-up, and low repeat intervention rates and no strokes during the follow-up period [16]. Furthermore, CA and CS can be used in the more distal part of the carotid artery, unlike CEA which can be performed only in the extracranial portion of the carotid artery. Finally, the quality of carotid stents and methods of stent deployment are constantly evolving, and these procedures become increasingly safe as clinical experience advances our understanding and techniques.

A randomized multicenter trial comparing percutaneous carotid stenting with CEA (CREST) is now underway that will compare equivalence of these procedures as well as their efficacy relative to each other. Until these results become available, CA and CS should be presented to potentially eligible patients as experimental procedures. It is paramount that a prospective institutional registry be established since there is a definite learning curve resulting in an improved safety profile over time. The use of CA or CS should be restricted to those patients who have consented to an Institutional Review Board (IRB) or ethics committee-approved protocol.

The role of cerebrovascular venous stenting has been previously described in two patients with cerebral venous occlusive disease of the major dural sinuses and high-pressure gradients across the stenoses. Cerebral venous stenting was successfully performed with substantial improvement of the venous stenosis, and substantial reversal of the pressure gradients after venous stent placement [19].

Non-invasive ultrasound testing permits visualization of vascular morphology and quantification of carotid artery stenosis, as well as characterization of hemodynamic effects. Carotid duplex scanning has been used for vascular evaluation before and serially after CA and/or CS in extracranial carotid artery stenosis, cervical carotid artery dissection and aneurysm [11,17,20,21]. Carotid duplex scanning allows visualization of the atherosclerotic lesions treated with stents and quantification of intraluminal blood flow velocity. It also allows identification of transient vasospasm, local thrombosis or dissection of the internal carotid artery at the distal end of the stent, even in the presence of normal findings on repeat cerebral angiography [17].

Integrated use of carotid and vertebral ultrasound

The decision regarding whether to investigate patients with, or at risk for, stroke or transient ischemic attack, and what tests to utilize, including neurovascular ultrasound, should be based on some key principles outlined as follows.

1 Will additional diagnostic testing, by ultrasound or any other techniques, help with the diagnosis, or affect the clinical management decisions for that specific patient? If not, then additional testing would have little clinical value, and need not be done. This is in accordance with the principle of respect for patient autonomy, e.g. a terminally ill patient with a 'do not resuscitate' (DNR) level 1 order. However, a harmless ultrasound test may be used to identify the pathogenic mechanism of stroke and thus provide information to explain to a patient's relatives why and how stroke happened. Disclosure of this information to relatives may have humanitarian value and can be obtained inexpensively and in a respectful manner with bedside ultrasound.

2 In most patients, additional testing is indicated. There are multiple techniques from which to choose,

all having roughly comparable accuracy. It is preferable to choose the safer, non-invasive, less expensive method initially, reserving the more costly, invasive or risky procedures for those that really need them. This is consistent with the principles of 'first, do no harm' and of 'adequate allocation of resources'. For example, in preparation for CEA, the choice of diagnostic testing often depends on the surgeon's preference and the accuracy of a non-invasive laboratory. Increasing numbers of surgeons are willing to operate based on the results of a non-invasive ultrasound test combined with magnetic resonance angiography, and some centers will operate based on color-coded carotid duplex alone. In such cases, carotid angiography is reserved for cases having inconclusive or conflicting results on non-invasive testing [22–24].

3 Decisions as to which test to use must be individualized for each patient, and for the local resources and expertise available. The accuracy and complication rates of the laboratories performing all diagnostic procedures should also be available if requested by the referring physician or the patient. This is in accordance with the principle of an informed consent. In addition to the routine quality assurance measures of sensitivity, specificity and accuracy, one measure of the quality of an ultrasound laboratory is whether it has been accredited by an outside organization, such as the Intersocietal Commission for the Accreditation of Vascular Laboratories (ICAVL). Another measure of quality is whether the personnel, including both the sonographers and the medical staff, are certified [25–27]. Several sonographer certification programs are available, and a physician certification in neurosonology is available through the American Society of Neuroimaging (www.asnweb.org).

We currently use ultrasound as the initial test of choice to evaluate the cerebral vessels and circulation in patients with cerebrovascular disease (Table 9.2). We often use magnetic resonance angiography or computed tomography (CT) angiography as a correlating non-invasive method, and reserve contrast angiography for those patients in whom non-invasive results are inadequate or conflicting, or where the patient is being selected for stenting [28]. We are often asked to perform serial follow-up carotid duplex scanning after CEA and stenting. The timing of carotid duplex follow-up after CEA varies between centers; however, in a patient who remains asymptomatic after surgery it can be suggested as follows:

Table 9.2 Impact of extracranial color-coded carotid duplex scannning in diagnosis and management of patients with stroke in clinical practice at Wake Forest University School of Medicine.

Extracranial color duplex scanning results
No stenosis (< 50%)
Medical treatment
Repeat study optional
50–75% stenosis
Medical treatment
Repeat 6–12 months
Study OA or ACA flow direction, and VMR
75–95% or 95–99% stenosis
Consider for CEA
Probable MRA or angiography
Study OA or ACA flow direction, and VMR
If candidate for delayed CEA treatment with AC and repeat sono prior to delayed CEA and angiography
If not CEA candidate, medical treatment
Occlusion
Medical treatment
Study OA or ACA flow direction, and VMR
If technically poor, MRA or angiography
If ongoing symptoms, repeat sono, test reserve
If ongoing symptoms for any severity of stenosis, consider embolus detection.
If > 75% stenosis, especially if ongoing symptom, consider cerebral vasoreactivity.
Consider agitated saline study for PFO in any patient with transient ischemic attack/stroke, especially those with no other identified cause.

AC, anticoagulant; ACA, anterior cerebral artery; CEA, carotid endarterectomy; MRA, magnetic resonance angiography; OA, ophthalmic artery; PFO, patent foramen ovale; VMR, vasomotor reactivity.

1 at 4 weeks;
2 at 6–12 months; and
3 every year or two thereafter.

The aims of repeated carotid testing after CEA are to:

1 look for carotid restenosis or occlusion on the side of intervention; and
2 monitor postoperative changes or disease progression on the non-operated side.

In CEA patients who have perioperative stroke or other associated complications, carotid duplex scanning is often performed immediately to look for intraluminal thrombus, intimal flap, incomplete plaque removal, carotid artery dissection and soft

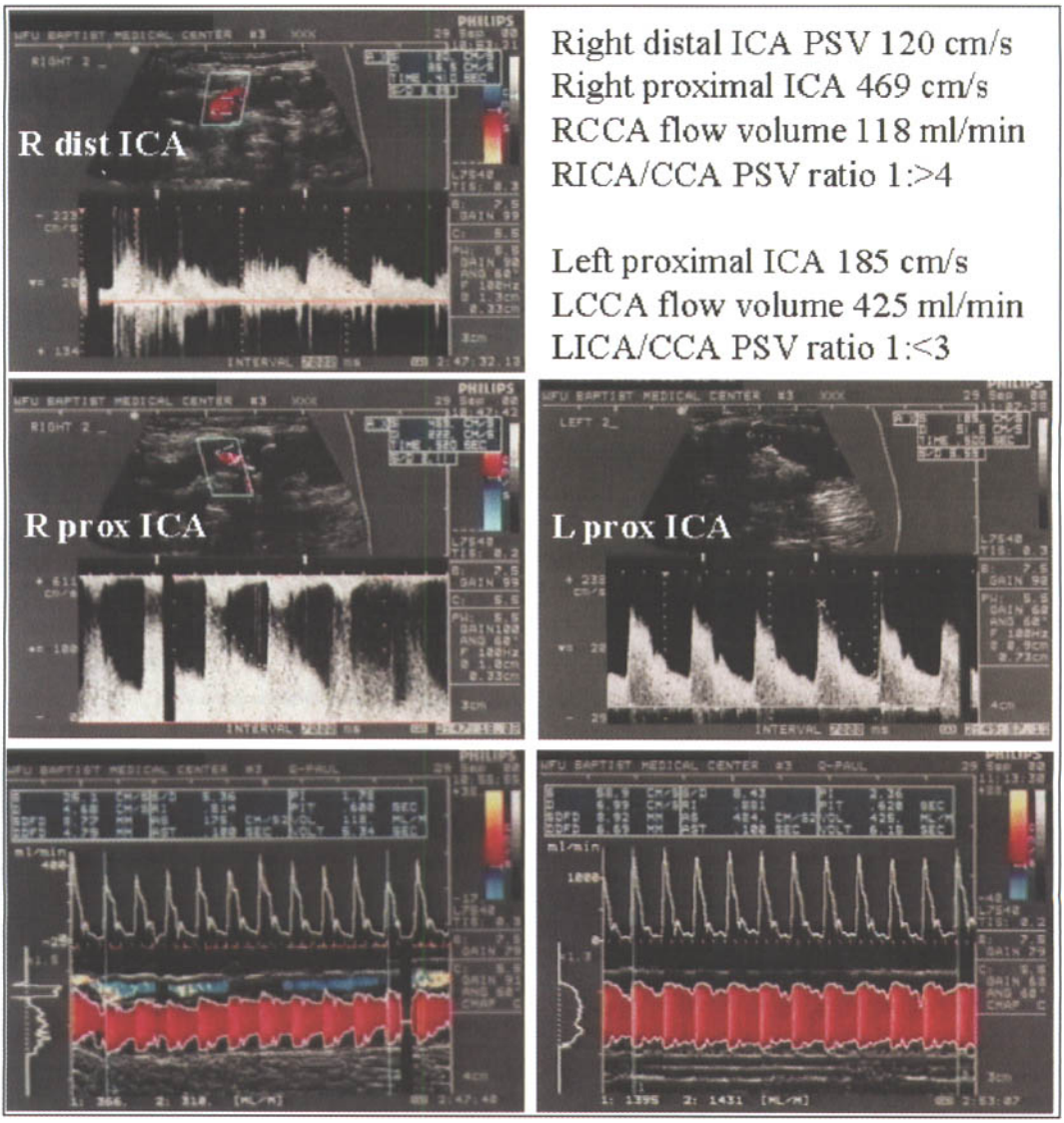

Figure 9.2 An 86-year-old white male with hypertension, coronary artery disease, carotid stenosis and hypothyroidism was evaluated for syncope following a blackout episode. Carotid duplex ultrasound showed a severe stenosis (75–95%) in the right internal carotid artery (ICA). (a) Carotid color duplex ultrasound study with very high velocities (469 cm/s systolic, 222 cm/s diastolic) at the point of aliasing at the exit of the right ICA stenosis. The following steps can be used to further optimize, or 'clean up' the recording: (i) balance transducer position with patient breathing to achieve a steady intensity of the Doppler spectrum; (ii) use a small (< 1.5 mm) gate to focus on the jet exiting the stenosis and to avoid spectral broadening; and (iii) replay the Doppler signal to select a representative sweep with the highest systolic and diastolic frequencies. (b) A color flow jet and Doppler spectrum were obtained just distal to the right ICA stenosis. This recording showed lower peak systolic velocities (120 cm/s) indicating poststenotic flow deceleration as well as turbulence and waveform dampening. Further steps to optimize this recording should be: (i) decrease Doppler gain; (ii) balance transducer to achieve stable insonation depth and to avoid tissue motion artifacts; and (iii) use a small gate to decrease the impact of tissue motion and flow reversal at the poststenotic dilatation if the signal-to-noise ratio is low. (c) Carotid duplex shows moderately increased velocities of 185 cm/s in the left ICA. If applied without correction to the ICA/CCA peak systolic velocity (PSV) ratio, these velocities alone indicate a 50–75% stenosis by the Wake Forest University criteria. However, if the right ICA has a greater than 80% stenosis, if a left-to-right anterior cross-filling via the anterior communicating artery is (*cont'd*)

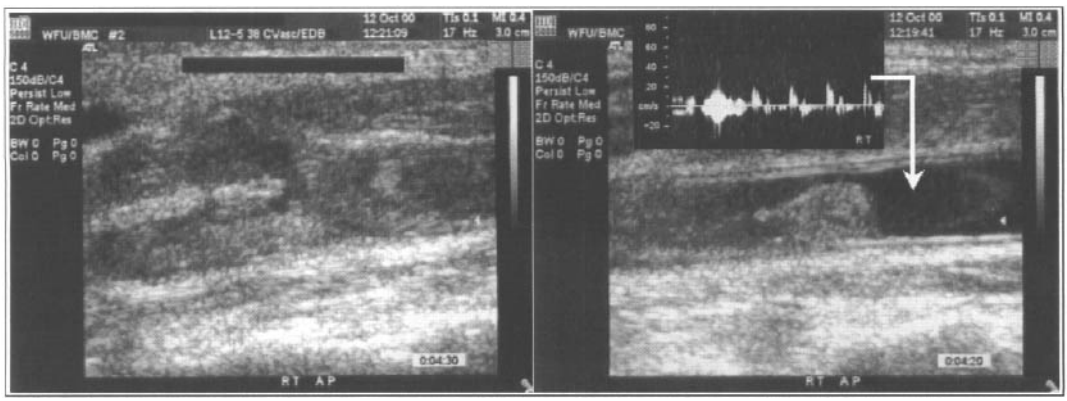

Figure 9.3 A 70-year-old woman presented with left-sided weakness and near-syncope episode following right carotid endarterectomy. Carotid duplex ultrasound shows occlusion of the right carotid system. (a) Longitudinal B-mode image of the right common carotid artery (CCA) with thrombus partially filling the lumen (right image). (b) Longitudinal B-mode image of the distal CCA, bifurcation, internal carotid artery and external carotid artery, showing lumen-filled hypoechoic echoes suggesting occlusion from thrombosis (left image). (c) Spectral Doppler of the right CCA showing low velocity and alternating flow pattern indicating more distal high-grade stenosis or occlusion (insert, right image, white arrow points to the CCA segment sampled).

tissue hematoma which may compress the vessels. These findings might prompt repeat surgery or a change in postoperative management. In CA and CS, the same protocol is usually applied.

We always attempt to perform both carotid and vertebral duplex scanning in patients sent for carotid duplex ultrasonography. We also use volume flow rate measurements in the common carotid artery, obtained with the color velocity imaging technique, to help in differentiating between collateral circulation or hyperperfusion and true stenotic flow in questionable cases. We also perform vertebral duplex studies with ischemic blood pressure cuff testing, often with additional evaluation of the intracranial vertebral and basilar artery flow velocities and directions, in all patients suspected of subclavian steal syndrome.

For the accuracy of interpretation, color-coded carotid and vertebral duplex findings are reviewed in all studies. At our laboratory, studies are videotaped for same-day review and interpretation by the medical staff. A study performed for an acute patient will be read by a staff physician shortly after completion. Finally, we advocate evaluation of the extracranial (carotid and vertebral color duplex) and intracranial (TCD or TCI) cerebral arteries as part of a complete neurovascular ultrasound examination. This provides a more complete assessment and understanding of the overall cerebral circulation, and the combination yields more clinically useful information than one or the other test performed alone.

Several typical carotid and vertebral duplex findings are provided in the case examples outlined below. Interpretation of ultrasound findings is given in figure legends.

1 Severe carotid stenosis (Figure 9.2).
2 Intraluminal thrombus on carotid duplex post CEA (Figure 9.3).
3 Subclavian steal and CCA steal with innominate artery stenosis (Figure 9.4).
4 An ulcerated plaque (Figure 9.5).

(*cont'd*) present, and the left ICA/CCA PSV ratio is less than 3, all of these findings should be interpreted as 30–59% left ICA stenosis. An additional dimension in grading the ICA stenosis can be added by utilizing the flow volume measurements. (d) The right common carotid artery (CCA) volume flow rate proximal to the severe ICA stenosis was 118 mL/min. This flow rate is significantly decreased compared to a normal range of 300–400 mL/min in an unobstructed CCA. (e) The left CCA volume flow rate was 425 mL/min. This value, in the presence of elevated peak systolic velocities, indicates compensatory velocity increase rather than bilateral severe ICA stenoses. This finding is common in the CCA or ICA contralateral to a severe ICA stenosis. If a single-vessel, single-projection carotid angiogram shows a 70% stenosis contralateral to a severe carotid lesion, the information about flow volume rates is helpful to identify which carotid is more stenosed and which one still carries some collateral flow as well as to explain the discrepancy between ultrasound and angiography in terms of estimated percentage stenosis.

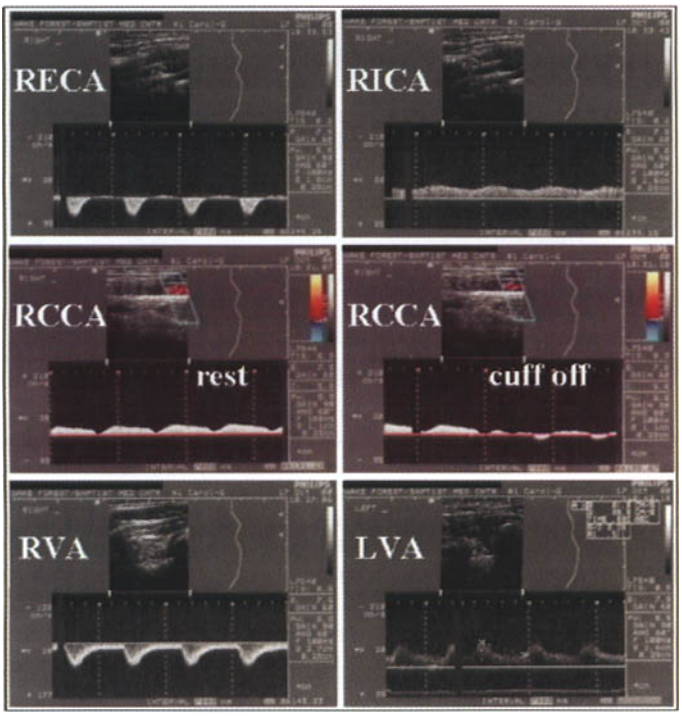

Figure 9.4 A 44-year-old male admitted for subarachnoid hemorrhage, with incidental finding on carotid duplex of innominate artery stenosis. RVA, right vertebral duplex shows manifest steal with total flow reversal; RCCA rest, right common carotid artery (CCA) color duplex shows systolic deceleration as with a latent steal; RCCA cuff off, right CCA color duplex after cuff release during ischemic cuff test shows alternating flow pattern with some actual reversal confirming latent steal; RICA, right internal carotid artery duplex shows a low-velocity signal with low pulsatility and a very low resistance appearance to the velocity waveform; RECA, right external carotid artery (ECA) duplex shows flow reversal in the ECA at rest; LVA, left vertebral duplex shows normal waveform with mildly increased velocity.

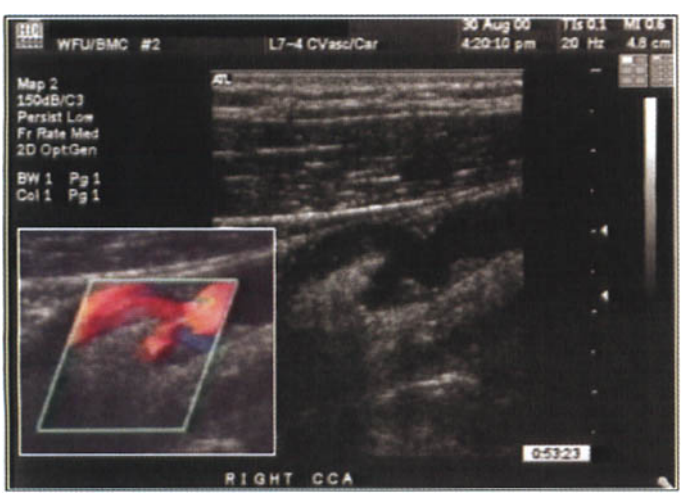

Figure 9.5 A 38-year-old woman with recurrent transient ischemic attacks (TIAs). B-mode image shows moderate and mostly hypoechoic plaque in the region of the bifurcation, with surface irregularity and possible crater in the ulcer formation. A color flow image insert shows flow reversal into the apparent crater (blue), confirming that it is indeed open to the lumen. Color flow scale setting is +28 cm/s. The finding of flow reversal within the plaque defect rules out an intraplaque hemorrhage since this is open to flow and there is no a membrane covering it. To further confirm the embolic nature of TIAs and link them to an ulcerated plaque, an embolus detection with TCD can be performed for 1 h in the right middle cerebral artery or bilaterally. If the test is positive (*i.e. unequivocally showing* several embolic signals), this patient may be a candidate for carotid endarterectomy or stenting, particularly if TIAs continue to occur despite maximum medical therapy, i.e. aspirin plus plavix or aggrenox.

References

1 American Heart Association. *1992 Heart and Stroke Facts.* Dallas, Texas.

2 Sherman DG, Dyken ML, Fisher M *et al.* Antithrombotic therapy for cerebrovascular disorders. *Chest* 1989; **95** (Suppl.): 140S–155S.

3 Cerebral Embolism Task Force. Cardiogenic brain embolism. The second part of the Cerebral Embolism Task Force. *Arch Neurol* 1989; **46**: 727–43.

4 Feldmann E. Intracerebral hemorrhage. In: Fisher M, ed. *Clinical Atlas of Cerebrovascular Disorders.* London: Mosby-Year Book Europe, 1994: 11.1–11.7.

5 Withers CE, Gosink BB, Keightley AM *et al.* Duplex carotid sonography: peak systolic velocity in quantifying internal carotid artery stenosis. *J Ultrasound Med* 1990; **9**: 345–9.

6 Beach KW, Lawrence R, Phillips DJ. The systolic velocity criterion for diagnosing significant internal carotid artery stenosis. *J Vasc Technol* 1989; **13**: 65–8.

7 Robinson ML, Sacks D, Perlmutter GS, Marinelli DL. Diagnostic criteria for carotid duplex sonography. *AJR* 1988; **151**: 1045–9.

8 Smith LL, Anderson DC, Gramith F. A step-by-step guide for validation of carotid duplex studies. *J Vasc Technol* 1993; **17**: 17–22.

9 Bartels E, Fuchs H-H, Flugel KA. Duplex ultrasonography of vertebral arteries: examination, technique, normal values, and clinical applications. *Angiology* 1992; **43**: 169–80.

10 Kuhl V, Tettenborn B, Eicke BM, Visbeck A, Meckes S. Color-coded duplex ultrasonography of the origin of the vertebral artery: Normal values of flow velocities. *J Neuroimaging* 2000; **10**: 17–21.

11 Roubin GS, Yadav S, Iyer SS, Vitek J. Carotid stent-supported angioplasty: a neurovascular intervention to prevent stroke. *Am J Cardiol* 1996; **78** (Suppl. 3A): 8–12.

12 North American Symptomatic Carotid Endarterectomy Trial Collaborators. Beneficial effect of carotid endarterectomy in symptomatic patients with high-grade carotid stenosis. *N Engl J Med* 1991; **325**: 445–53.

13 European Carotid Surgery Trialists' Collaborative Group. Randomised trial of endarterectomy for recently symptomatic carotid stenosis: final results of the MRC European Carotid Surgery Trial (ECST). *Lancet* 1998; **351**: 1379–87.

14 Executive Committee of the Asymptomatic Carotid Atherosclerosis Study. Endarterectomy for asymptomatic carotid artery stenosis. *JAMA* 1995; **273**: 1421–8.

15 Grotta J. Elective stenting of extracranial carotid arteries. *Circulation* 1997; **95**: 303–5.

16 Yadav JS, Roubin GS, Iyer S, Vitek J, King P, Jordan WD, Fisher WS. Elective stenting of the extracranial carotid arteries. *Circulation* 1997; **95**: 376–81.

17 Griewing B, Brassel F, von Smekal U, Al Ahmar MT, Kessler CH. Carotid artery stenting in patients at surgical high risk: clinical and ultrasound findings. *Cerebrovasc Dis* 2000; **10**: 44–8.

18 Yadav JS, Roubin GS, King P, Iyer S, Vitek J. Angioplasty and stenting for restenosis after carotid endarterectomy. Initial experience. *Stroke* 1996; **27**: 2075–9.

19 Marks MP, Dake MD, Steinberg GK, Norbash AM, Lane B. Stent placement for arterial and venous cerebrovascular disease: preliminary experience. *Radiology* 1994; **191**: 441–6.

20 Griewing B, Brassel F, Schminke U, Kessler CH. Angioplasty and stenting in carotid artery dissection. *Eur Neurol* 1998; **40**: 175–6.

21 Smedema JP, Saaiman A. Carotid stent-assisted angioplasty. *S Afr Med J* 1997; **87** (Suppl. 1): C9–14.

22 Shifrin EG, Bornstein NM, Kantarovsky A *et al.* Carotid endarterectomy without angiography. *Br J Surg* 1996; **83**: 1107–9.

23 Golledge J, Wright R, Pugh N, Lane IF. Colour-coded duplex assessment alone before carotid endarterectomy. *Br J Surg* 1996; **83**: 1234–7.

24 Aburahma AF, White JF III, Boland JP. Carotid endarterectomy for symptomatic carotid artery disease demonstrated by duplex ultrasonography with minimal arteriographic findings. *Ann Vasc Surg* 1996; **10**: 385–9.

25 Jones AM. Quality assurance in the vascular laboratory. In: Tegeler CH, Babikian VL, Gomez CR, eds. *Neurosonology.* St. Louis, Missouri: Mosby-Year Book, 1996: 489–93.

26 Gomez C, Kinkel P, Masdeu J *et al.* American Academy of Neurology Guidelines for Credentialing in Neuroimaging. Report from the task force on updating guidelines for credentialing in neuroimaging. *Neurology* 1997; **49**: 1734–7.

27 Masdeu JC. The American Academy of Neurology Workshop on Neuroimaging Training. American Academy of Neurology Neuroimaging Guidelines. *Neurology* 1997; **49**: 1738–40.

28 Tegeler CH, Ratanakorn D. *Neurosonology.* In: Fisher M, Bogousslavsky J, eds. *Textbook of Neurology.* Newton, MA: Butterworth-Heinemann, 1998: 101–18.

10 CHAPTER 10

Acute ischemic stroke

Andrew M. Demchuk, MD, FRCPC *& Andrei V. Alexandrov,* MD, RVT

Introduction

Intravenously administered tissue plasminogen activator (TPA) has been proven an effective therapy for ischemic stroke if initiated within 3 h from symptom onset [1]. Roughly 50% of patients treated with TPA recover in 3 months. The other 50% remain disabled or die [1]. Why 50% of the treated population does not benefit remains unclear. The likely explanation lies in the heterogeneity of ischemic stroke and the possibility of late and ineffective recanalization. Different treatment approaches may be needed depending on the location of arterial occlusion and the severity or extent of ischemic tissue damage. Ultraearly neuroimaging may provide crucial information to deal with this heterogeneity and enable therapy to be properly tailored for the individual patient. For example, recent evidence suggests early reperfusion is the key to thrombolytic benefit [2–4]. Yet only a few studies have attempted to monitor whether such a key event occurs in the early stages of acute stroke [2,4,5]. The future development of reperfusion strategies for acute stroke will require information about the status of arterial occlusion, collateral perfusion and extent and severity of ischemia in the earliest stages of treatment [3,6].

Computed tomography (CT) is the current standard imaging study in acute stroke to differentiate hemorrhagic from ischemic events. It can also provide some information regarding the extent and severity of ischemic injury by visualization of early ischemic changes that can be present at very early time points from symptom onset. The Alberta Stroke Program Early CT Score (ASPECTS) [7] helps to assess several brain regions that may be affected by ischemia (Figure 10.1). Hyperdense artery (HD) signs such as the HDMCA involving the middle cerebral artery (MCA) stem and the M2 MCA 'dot' sign [8] involving distal branches give some clues to location of occlusion and clot burden (Figure 10.2).

Early CT findings quantified using the ASPECT score can help predict complications, prognosis and likelihood of benefit with thrombolytic therapies [7]; however, CT alone does not provide definitive information regarding location of arterial occlusion as well as its persistence minutes and hours after TPA bolus. CT angiography (CTA) and magnetic resonance angiography (MRA) are modalities available to assess vessel patency in acute stroke [9,10]. However, CTA is limited by the requirement of contrast load and time delays needed for expert interpretation of source images and a three-dimensional reconstruction. MRA often demonstrates flow gaps with turbulence, high-grade stenosis, near-occlusion as well as occlusion. MRA cannot reliably identify reversed flow direction in the carotid or vertebrobasilar arteries unless special sequences are applied. Finally, neither imaging method offers the potential for continuous real-time monitoring of arterial patency. MRA is also limited by expense and the need for patient cooperation. Although critics state that magnetic resonance imaging (MRI) is the future of stroke investigation [11], the reality is that MRI is readily available to only a very small number of stroke patients and is not well tolerated in a significant number of stroke patients.

Transcranial Doppler (TCD) has the advantages of being inexpensive, portable and non-invasive and requiring minimal patient cooperation; however, TCD has not been widely accepted for use in acute stroke. The major criticism of TCD is the belief that TCD is too operator dependent to be applied to acute stroke decision-making. This chapter will outline the growing evidence that TCD is an excellent bedside tool to assess the cerebral vasculature in acute stroke.

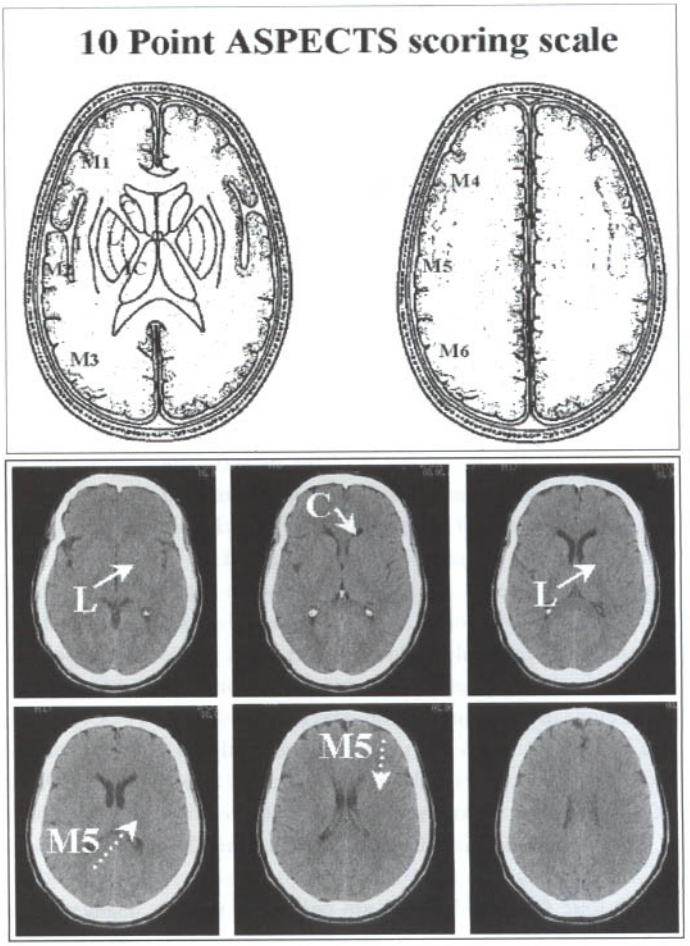

Figure 10.1 The Alberta Stroke Program Early CT Score (ASPECTS) was developed as a systematic tool to assess axial planes of ultraearly CT scans in acute middle cerebral artery (MCA) strokes. ASPECTS requires a 10-point assessment of at least four slices showing basal ganglia and four slices showing hemispheric cortex. The diagram indicates these regions as: C, caudate head; IC, internal capsule; L, lentiform nucleus; I, insular ribbon; M1, anterior MCA cortex; M2, MCA cortex lateral to the insular ribbon; M3, posterior MCA cortex; M4, M5 and M6, anterior, lateral and posterior MCA territories, respectively, approximately 2 cm superior to M1, M2 and M3 aspects and rostral to basal ganglia. Lower two rows of images demonstrate early involvement of the lentiform nucleus (L, solid arrow) and caudate head (C, solid arrow) with a total ASPECTS score of 8 points. Dotted lines indicate potential involvement of the M5 region and may be overinterpreted.

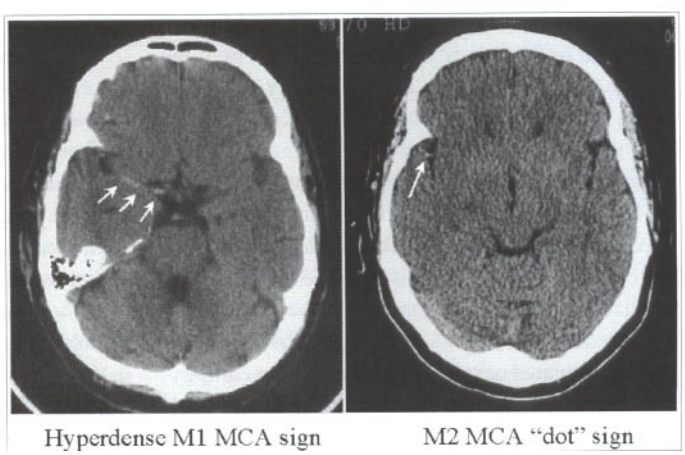

Figure 10.2 Hyperdense artery signs on a non-contrast CT scan. If present unilaterally, these signs indicate a thrombus in the M1 MCA segment (left image) or M2 subdivision (right image).

The chapter will also outline some specific situations where this modality can be helpful to the clinician now and in the future.

Fast-track insonation protocol: key to acute stroke TCD

In an effort to develop a method of rapid TCD evaluation and interpretation, a fast-track insonation protocol was developed [12]. Using such a protocol, emergency room TCD studies could be completed and interpreted within minutes at the bedside by the treating clinician, nurse or technologist. This protocol should be used only by experienced TCD users with knowledge of the clinical status of the patient. The choice of fast-track insonation steps is determined by a presumed arterial territory affected by ischemia based on clinical information. For example, if MCA symptoms are present, insonation begins with locating the MCA on the non-affected side to establish the presence of a temporal window, normal MCA waveform and velocity range. If time permits, insonation of the circle of Willis on the non-affected side should also provide the depth and velocity range for the M1 and M2 MCA segments and the internal carotid artery (ICA) bifurcation. Next, the MCA on the affected side is located with insonation starting at the mid-M1 MCA depth range, usually 56–58 mm. The waveform and systolic flow acceleration are compared to the non-affected side. If a normal MCA flow is found, the distal MCA segments are insonated (range 40–50 mm) followed by the proximal MCA and ICA bifurcation assessment (range 60–70 mm). If a 'blunted' waveform or no signals are found at 56–58 mm, the proximal MCA and ICA bifurcation are insonated before the distal segments. The absence of MCA flow signals can be confirmed by insonation across the midline from the contralateral window (depths 80–100 mm) when feasible. The ophthalmic artery (OA) flow direction and pulsatility is determined next on the affected side at depths of 52–58 mm followed by the ICA siphon assessment via the transorbital window at depths of 60–64 mm. The basilar artery (BA) is insonated next to determine whether compensatory flow velocity increase or a stenosis is present. Insonation of the vertebral arteries (VAs), OA and ICA on the non-affected side, as well as posterior cerebral arteries, is performed whenever time permits. Most studies can be accomplished within minutes and often while other patient assessment is ongoing, resulting in no time delays to treatment [12].

Yield and accuracy of TCD

Several studies have evaluated the utility of digital subtraction angiography (DSA), CTA, MRA and ultrasound in the acute stroke setting [9,10,12–16]. DSA showed complete arterial occlusion in 76% of acute stroke patients within 6 h of symptom onset [13]. Burgin *et al.* showed that a non-imaging, non-contrast-enhanced TCD had a sensitivity of 91% and a specificity of 93% compared to angiography for MCA occlusion vs. complete recanalization in patients receiving thrombolysis for ischemic stroke [17]. Based on previously published studies defining various locations of arterial occlusion, our group further developed a set of detailed diagnostic criteria and determined their accuracy parameters for the presence and location of a proximal intracranial arterial occlusion on TCD and described specific flow findings associated with intracranial occlusions [18,19].

Urgent evaluation of patients with acute ischemic stroke offers a high frequency of abnormal TCD findings such as occlusion, intracranial clot dissolution, distal embolization, reocclusion and stenosis [12,16,20]. There is no point in delaying bedside vascular assessment with TCD since this information can be especially useful at the time of initial clinical assessment of an acute stroke patient. The usefulness of this information depends on the treating physician's approach to the stroke patient and available choices between various, often experimental, treatment protocols.

We performed TCD in 130 consecutive patients in the emergency department at the time of admission neurologic examination and CT scanning [12]. Without contrast enhancement, insonation via the trans-temporal window was not possible in 15% of all patients. Despite this, overall TCD accuracy for occlusion, stenosis and normal vessel patency was 88% compared to angiography. TCD showed a proximal intra- or extracranial occlusion in 69% of thrombolysis-eligible patients within the first 6 h compared to 24% in those outside the window for thrombolysis and 0% in patients who spontaneously resolved their deficits. TCD was normal in 65% of patients with acute transient ischemic attacks (TIAs) [12].

The clinical value of this information is twofold. First, TCD evidence of occlusion helps to identify

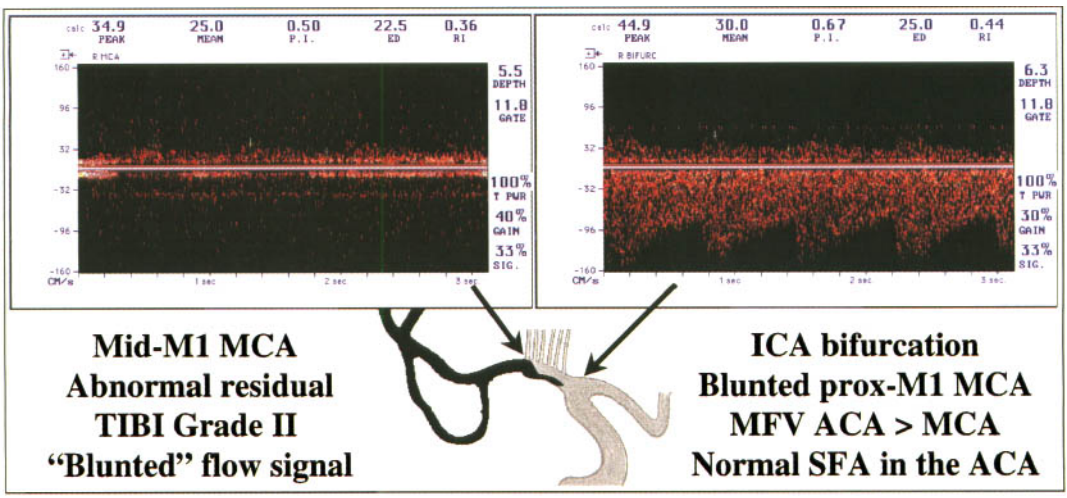

Figure 10.3 Typical spectral Doppler findings with acute M1 MCA occlusion. Transcranial Doppler shows residual flow signals at presumed thrombus location in the M1 MCA. SFA, systolic flow acceleration.

patients with acute focal neurologic deficit of an ischemic nature, and in some instances failure to identify occlusion helps to support a differential diagnosis; i.e. the presence of a pure motor syndrome and normal TCD will identify presumed lacunar syndrome, or in the presence of a headache and motor deficit, normal TCD can help suspect complicated migraine, or a functional nature of the deficit, etc. Second, the location of arterial occlusion on TCD (specific segment such as M2 or M1 MCA, terminal ICA, proximal vs. distal basilar artery) can help explain the distribution of the neurologic deficit since TCD also shows major collateral channels available to compensate for occlusion. This information helps to suspect large vessel occlusion and select the next most efficient step in ordering further diagnostic or interventional procedures despite relatively low stroke severity score and/or the clinical presence of a lacunar syndrome or relatively mild stroke severity. The presence and persistence of a large vessel occlusion or stenosis in patients with acute and spontaneously resolving deficits also point to a greater likelihood for clinical deterioration within the next 24 h [21]. These situations are described in detail in the section on specific clinical applications.

TCD occlusion criteria

The most important role of TCD in acute stroke is the determination of the presence and location of arterial occlusion [12,19] as well as of residual flow signals around the clot [22]. One of the great challenges of applying TCD to diagnose occlusion is the reliance on a complicated series of flow findings in different vessels and different depths to determine which artery is affected. To simplify this interpretation we have developed occlusion criteria based on the different flow findings of each intracranial vessel [19,22] and the extracranial internal carotid artery [23]. Figure 10.3 illustrates the criteria for a proximal MCA occlusion. The main flow finding associated with any occlusion directly assessable by TCD is an abnormal waveform at presumed clot location (see also Chapter 6 and Acute Tandem Occlusion, p. 237). Also, an acute MCA occlusion produces flow diversion to neighboring or branching vessels, and increased flow velocity can be found in the anterior cerebral artery (ACA) in approximately half of these cases [19].

These detailed diagnostic criteria were prospectively applied in 190 patients with symptoms of cerebral ischemia who also had MRA or conventional angiography at a median time of 1 h after TCD examination [18]. A total of 48 occlusions were identified by TCD, resulting in an accuracy of 92% compared to MRA or conventional angiography. Sensitivity for each individual occlusion site was above 90% with proximal ICA and MCA occlusions. Vertebral artery or basilar artery occlusion had lower sensitivity (56–60%). If TCD is normal there is at least a 94%

chance that angiographic studies will be negative [18]. This level of accuracy particularly for the anterior circulation occlusion allows the need for an immediate angiography to be ruled out in the presence of acutely normal TCD findings.

TCD grading system to measure residual flow

Coronary angiography is the mainstay vascular imaging test for acute myocardial infarction. The 'thrombolysis in myocardial infarction' (TIMI), an angiographic residual flow classification developed by cardiologists, provides significant insight into how quickly and effectively coronary thrombolysis can be accomplished [24–26]. Generally, higher amounts of residual flow around the clot predict better success of coronary thrombolysis. TIMI principles of residual flow classification were applied to cerebral angiography in the Prourokinase in Acute Stroke Trial (PROACT) [27], and this terminology is often used to describe flow findings at diagnostic cerebral angiography. Several angiographic classifications specific for brain vessels are being developed. Unlike in the coronary vessels, ultrasound assessment of brain vessels offers a unique opportunity to focus on the clot location and monitor flow signal around it due to minimal vessel motion. We therefore sought to develop a flow grading system for TCD to measure residual flow analogous to TIMI. We introduced this residual flow grading classification, called the thrombolysis in brain ischemia (TIBI) flow grades [22]. The TIBI classification grades blood flow into six groups. Grade 0 is absent, grade 1 minimal, grade 2 blunted, grade 3 dampened, grade 4 stenotic and grade 5 normal waveform (see Figure 6.23 in Chapter 6; for more information see Chapter 6 and Acute Tandem Occlusion, p. 237). The TIBI flow grade can be measured in all vessels with particular attention to the region at or just distal to the presumed site of arterial occlusion. This emergent TCD TIBI classification was evaluated in 109 patients treated with intravenous TPA [22]. Baseline TCD examination revealed a close correlation between pre-TPA National Institutes of Health Stroke Scale (NIHSS) scores and TIBI flow grades. Pre-TPA NIHSS scores were higher in TIBI grade 0 flow (median 20 points) than TIBI grade 5 flow (median 10 points). TIBI flow improvement to grade 4 or 5 occurred in 35% of initial grade 0 or 1 and 52% of initial grade 2 or 3 patients (our recent analysis of 75 patients with M1 or M2 MCA occlusions also showed that patients who had some residual flow signals were twice as likely to experience early recanalization with TPA therapy). At 24 h, the NIHSS scores were higher in follow-up TIBI grade 0 or 1 flow (median 20 points) than TIBI grade 5 flow (median 5 points). TIBI flow recovery correlated with NIHSS score improvement. NIHSS improved a median of 10 points if TIBI flow recovered from 0–1 to 4–5. Lack of flow recovery predicted worsening or no improvement. In-hospital mortality was 22% in patients with pre-TPA TIBI flow grades 0–1 and 5% in patients with pre-TPA TIBI flow grades 2–3 for anterior circulation occlusions [22].

TCD monitoring

Prolonged TCD monitoring for emboli detection and vasomotor reactivity assessment has been performed for years without any evidence of harmful effects. No adverse biologic effects have been documented for the frequencies and power ranges used in diagnostic ultrasound if applied according to safety guidelines [28]. Previous work with TCD monitoring has shown that evolution of the MCA occlusion can be followed in real time [15,29], and the recanalization process measured [30]. TCD can identify the residual flow signals to and around the clot [22], the beginning and speed of clot lysis and the timing and amount of recanalization [30]. Specific TIBI waveform changes, flow signal intensity and velocity improvement as well as embolic signals have been described during monitoring of thrombolysis or spontaneous recanalization [15,17,20,29,30]. Obtaining continuous information about the status of an arterial occlusion in acute stroke has the potential to be very helpful in further decision-making with thrombolytic therapy [31], particularly if a combined intravenous/intra-arterial drug delivery proves effective [32]. We have developed and validated detailed recanalization criteria that help determine the beginning, duration, timing and amount of recanalization in real time [30]. These examples are given in the Arterial Recanalization and Dramatic Recovery from Stroke section of the Select Clinical Applications, p. 242.

In patients with acute MCA occlusion treated with intravenous TPA, post-treatment TCD was compared with DSA or MRA [17]. Complete occlusion was

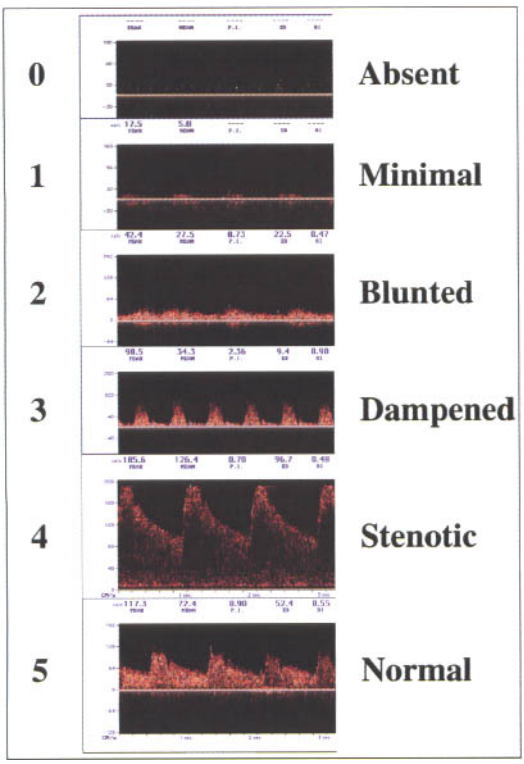

Figure 10.4 Criteria for a persisting (complete or partial) occlusion and complete recanalization after thrombolysis for ischemic stroke.

defined by absent or minimal TCD signals, partial occlusion by blunted or dampened signals, and complete recanalization by normal or low-resistance stenotic signals implying unobstructed flow distal to any residual lesion (Figure 10.4). Angiography was evaluated with the TIMI grading scale. Twenty-five patients were studied with TCD performed at 12 h and angiography at 41 h after stroke onset. Although persistent partial occlusion on TCD had high sensitivity of 100%, TIBI criteria for TIMI grade II flow had a low positive predictive value of 44%, most likely due to time delays between TCD and angiography as well as rapid evolution of partial occlusion with sluggish flow. On the other hand, TCD predicted the presence of complete occlusion on angiography (TIMI grade 0 or I) with high specificity (100%). TCD also accurately predicted angiographic findings of complete MCA recanalization with a sensitivity of 91% and specificity of 93% [17] (Figure 10.5).

Combined diagnostic TCD and CT to guide stroke therapy

Currently we combine the strengths of careful CT scan evaluation [33] with TCD information. A combination of urgent CT and bedside TCD scanning has never resulted in delays of thrombolytic therapy administration. Our pilot studies showed that these modalities can identify the target population for intra-arterial thrombolysis [17] by screening out patients with no proximal occlusion [22]. Future studies will focus on identification of candidates for mechanical clot disruptive interventions and neuroprotective therapies.

Patients with persisting occlusion are at a high risk of poor outcome and may require additional and more aggressive measures than a simple intravenous injection of TPA [31]. Also, patients may experience reocclusion [34] leading to deterioration following improvement [35], and do poorly without additional interventions (see Arterial Reocclusion and Deterioration Following Improvement in Specific Clinical Applications, p. 251).

We also hypothesize that thrombolysis is of limited value and may be dangerous if, in the presence of persisting cortical syndromes, TIBI flow is normal and no proximal occlusion is identified [22]. In our prospective observational series of 109 TPA-treated patients, 17% had no identifiable occlusion, and symptomatic hemorrhage rate in these patients was 26% [22]. These findings may indicate that recanalization has already occurred without early recovery of tissue function, and providing additional TPA to freshly infarcted tissue may be deleterious. Note that in this relatively small study group no hemorrhages occurred if patients had pure motor weakness and normal pre-TPA TCD.

Similarly, if the CT scan shows extensive early CT changes with proximal arterial occlusion on TCD that did not open rapidly, less benefit from thrombolysis can be expected, while the risk of symptomatic intracerebral hemorrhage is probably mounting with late recanalization. In addition, neuroprotective trials have been uniformly negative due to misadventures in developing effective human doses and identifying the appropriate time window and patient population for treatment. TCD therefore has given us an opportunity to start to explore the utility of real-time monitoring of arterial occlusion in acute ischemic stroke.

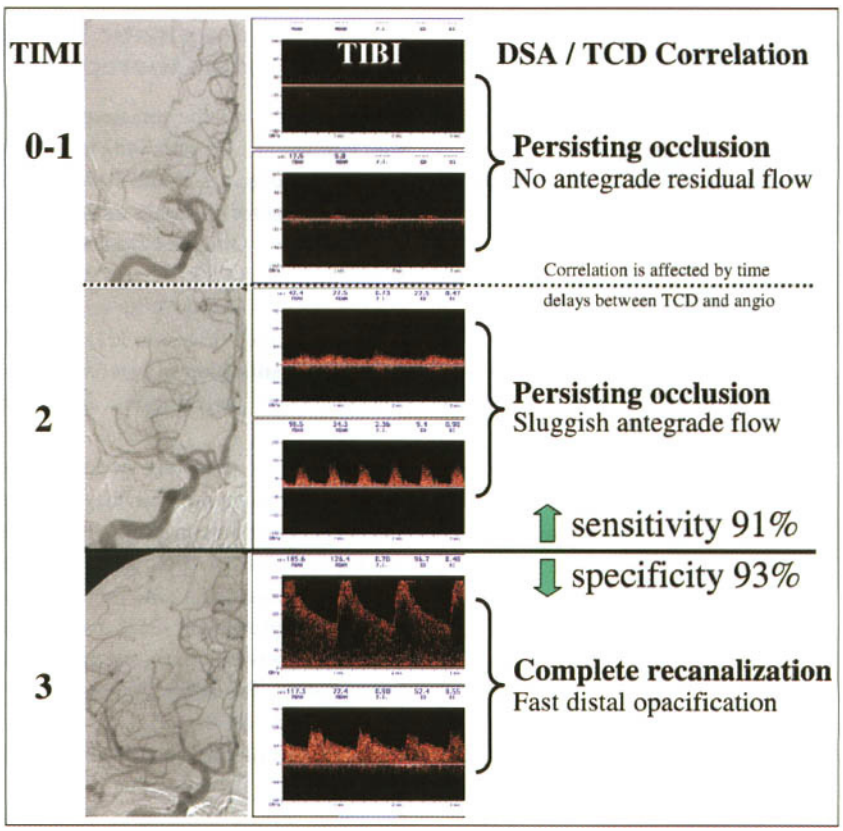

Figure 10.5 Correlation of TIMI and TIBI grading systems.

One of the most difficult patient populations to manage are those who deteriorate following improvement (DFI) during their first days of hospital admission [36]. Recent findings indicate that most DFIs occur in patients who resolved their symptoms but continue to have a proximal intra- or extracranial obstruction on TCD [21,35]. If TCD was performed within the first 6 h after symptom onset, 62% of patients with occlusion on TCD experienced DFI compared to 4% if TCD was normal [21]. With this information, one may consider close patient monitoring and aggressive management of the following parameters: blood pressure, cardiac output, head position, continuous hydration and selective use of heparin and other agents to prevent blood clotting. These examples are provided in Arterial Reocclusion and Deterioration Following Improvement in Specific Clinical Applications, p. 251. Clearly, a nihilistic approach to these patients is unsatisfactory and should be replaced by individualized assessment of vessel patency, brain perfusion status and management of the cardiovascular system.

Another exciting area of therapeutic intervention for ischemic stroke is the use of TCD for tailoring the type of thrombolytic delivery strategy. Recent evidence suggests a potential benefit from local delivery of thrombolytics via an intra-arterial approach as an alternative or addition to systemic thrombolysis in patients with MCA occlusion [27,32]. The difficulty with intra-arterial therapy is excessive use of diagnostic angiography to find patients with clot location eligible for intervention if patient selection is based only on clinical and CT findings [27]. Recent studies suggest that pretreatment NIHSS scores are sensitive to any clot presence but fail to identify specific clot location [37]. Furthermore, post-TPA-infusion NIHSS scores become less sensitive to clot presence, most likely due to recanalization that has not yet resulted in apparent clinical change [37]. Overall, an NIHSS score > 10 points readily identifies patients with

increasing thrombus burden [32], while TCD differentiates clot location, and this combined information can effectively reduce the number of negative angiograms, thereby limiting the potential for complications from this procedure in some patients and improving overall costs of intra-arterial treatment.

Another exciting potential role for TCD is patient selection for a combined approach of intravenous and intra-arterial lytic delivery that promises even higher recanalization rates and greater potential benefit for the patient [32]. This has created considerable debate as to whether one or even both therapies should be initiated in a specific situation. TCD is an ideal tool that clinicians can use themselves as a bedside aid in this decision-making. At our centers in Calgary and Houston, we initiate intravenous TPA using the National Institute of Neurological Disorders and Stroke (NINDS) rt-PA Stroke Study protocol in eligible patients irrespective of the TCD results. However, we quickly perform TCD examination before TPA bolus to identify clot presence (if any) and location. If a proximal MCA occlusion is identified, the vessel is monitored during the entire infusion and up to 2 h after bolus, when feasible. Since 75% of early recanalizations are expected to occur within the first 60 min after TPA bolus [38], an experienced sonographer can determine persisting occlusion with great certainty towards the end of a full-dose TPA infusion. If there is no substantial clinical improvement and TIBI flow grades remain unchanged towards the end of TPA infusion, the patient is taken for urgent diagnostic angiography and possible intra-arterial thrombolysis since these patients have poorer outcomes if persisting thrombus is left untreated (also see section on Arterial Reocclusion in Specific Clinical Applications, p. 251).

Therapeutic TCD

Recanalization is not achieved in a significant portion of coronary artery occlusions using systemic thrombolysis alone [31], and even lower recanalization rates have been previously demonstrated with intravenous thrombolysis in ischemic stroke. Del Zoppo *et al.* showed that only 26% of intracranial occlusions lyse partially or completely after 1 h of intravenous duteplase infusion [39]. In the PROACT II trial, only 4% of MCA clots showed complete TIMI III recanalization when urokinase was infused at the clot surface for 1 h [27].

Clinical benefit from thrombolysis is closely related to achieving early recanalization. Experimental evidence suggests that ultrasound enhances thrombolysis and increases the lytic effect of TPA, particularly if used in low MHz–kHz frequency range [40–51]. Fundamental studies by the group led by Charles Francis and by other centers showed that ultrasound exposure causes various changes such as reversible disaggregation of uncrosslinked fibrin fibers, microcavity formation in the shallow layer of thrombus, increase in the enzymatic transport of TPA improving its uptake and penetration of TPA into clots as well as residual flow enhancement with microstreaming and vessel dilatation. The effect on lysis does not appear to be mediated by thermal or cavitational effects if the mechanical index is kept below 1.

Even using 2 MHz frequency and power output under 750 mW, transcranial Doppler transmits some amount of ultrasound energy to the intracranial vessels, raising the possibility that this diagnostic modality could also enhance TPA activity [52]. Recent *in vitro* studies showed that 1 h of 1 MHz TCD helped TPA to recanalize 90% of clots compared to a 30% rate when TCD exposure was limited to 30 min [53]. Critics may point to the fact that TCD delivers insufficient energy to the clot due to tremendous attenuation of ultrasound through the skull bone and that lower frequency/low power insonation better accelerates TPA-mediated thrombolysis. Some energy is delivered through the skull to the clot/residual flow interface, since we successfully detect returned signals that display residual flow and recanalization. Grolimund studied transmission ultrasonic energy (2 MHz TCD) through the temporal bone at an average power of 135 mW [54]. He found that most skulls (with temporal window present) allowed transmission of at least 10% of beam energy. The maximum portion of energy successfully transmitted through the temporal bone was 35%. In our clinical studies, we use 2 MHz TCD beams with acoustic output powers in the 128–750 mW range. Also, the above-mentioned experiments by Francis' group suggested that the ideal frequency for ultrasound-mediated thrombolysis appears to be the 1–2.2 MHz range since kHz and MHz frequencies offer different mechanisms by which they potentiate a TPA effect.

Even if enhancement of TPA-associated clot lysis is minimal with 2 MHz standard TCD, it still deserves a randomized trial since TCD can be used for diagnostic

purposes and subsequently to monitor recanalization. If non-invasive diagnostic monitoring also has a small but independent additional effect on TPA action, TCD may help patients to achieve earlier and possibly safe recanalization. TCD may thereby prove useful to dose-control other TPA-enhancing agents and determine the time window to infuse other medications, as well as monitor the effect of other devices and frequencies.

We hypothesize that continuous 2 MHz TCD energy transmission may promote thrombolysis by simply exposing more clot surface to residual flow. When the worst residual flow signal is identified using TIBI grades, the ultrasound beam is usually focused at the intracranial clot location and its interface with surrounding, often minimal, blood flow. The ability of TCD to detect these signals indicates that ultrasonic energy was delivered to the clot, and this energy was scattered, absorbed and partially reflected at the interface since clot and moving blood have different impedances. The pressure gradient created by an ultrasound wave gives an opportunity for more TPA molecules to bind with clot fibrinogen sites, microstream along clot structures, and therefore to achieve faster recanalization without stronger mechanical vibrations, disruptions and temperature increases that may be possible with kHz frequencies or any frequency beams with a mechanical index above 1.

Our pilot clinical study assessed whether such a therapeutic effect is possible in stroke patients [4]. Stroke patients receiving intravenous TPA were monitored during infusion with portable TCD. Residual flow signals were obtained from the clot location identified by TCD. Forty patients were studied with a mean baseline NIHSS score of 19. TCD monitoring occurred for the duration of TPA infusion. Recanalization on TCD was found at 45 ± 20 min after TPA bolus. Recanalization was complete in 12 (30%) and partial in 16 (40%) patients. Dramatic recovery during TPA infusion (NIHSS score ≤ 3 points) occurred in 8 (20%) patients, all with complete recanalization. Lack of improvement or worsening was associated with no recanalization, late recanalization or reocclusion on TCD. Improvement by ≥ 10 NIHSS points or complete recovery was found in 30% of all patients at the end of TPA infusion and in 40% at 24 h. The unusually high frequency of 'on-the-table' TPA responders and a high rate of early complete recanalization raised the possibility that ultrasonic energy transmission by TCD was facilitating more rapid thrombolysis [4]. These preliminary data have provided the enthusiasm to develop a proper phase II randomized controlled trial, called CLOTBUST, to assess whether such therapeutic effect is clinically relevant. A small positive randomized trial has recently been completed with transcranial duplex technology [55].

Conclusion

TCD is an evolving acute neurovascular ultrasound technique that has both diagnostic and even therapeutic potential. Validated occlusion criteria and TIBI classification of residual flow have set the stage for the further development of this technique in acute stroke. Newer equipment using modern digital technology will simplify bone window determination, thereby easing operation for less experienced sonographers. Given the widespread availability of this equipment, increased use of this modality in acute stroke is expected.

References

1 The National Institutes of Neurological Disorders and Stroke rt-PA Stroke Study Group. Tissue plasminogen activator for acute ischemic stroke. *N Engl J Med* 1995; **333**: 1581–7.

2 Ringelstein EB, Biniek R, Weiller C, Ammeling B, Nolte PN, Thron A. Type and extent of hemispheric brain infarctions and clinical outcome in early and delayed middle cerebral artery recanalization. *Neurology* 1992; **42**: 289–98.

3 Heiss W-D, Grond M, Thiel A, von Stockhausen H-M, Rudolf J, Ghaemi M, Lottgen J, Stenzel C, Pawlik G. Tissue at risk of infarction rescued by early reperfusion: a positron emission tomography study in systemic recombinant tissue plasminogen activator thrombolysis of acute stroke. *J Cereb Blood Flow Metab* 1998; **18**: 1298–307.

4 Alexandrov AV, Demchuk AM, Felberg RA, Christou I, Barber PA, Burgin WS, Malkoff M, Wojner AW, Grotta JC. High rate of complete recanalization and dramatic clinical recovery during TPA infusion when continuously monitored by 2 MHz transcranial Doppler monitoring. *Stroke* 2000; **31**: 610–4.

5 Molina C, Montaner J, Abilleira S, Arenillas JF, Ribo M, Huertas R, Romero F, Alvarez-Sabin J. Time course of tissue plasminogen activator-induced recanalization in acute cardio-embolic stroke: a case-control study. *Stroke* 2001; **32**: 2821–7.

6 Caplan LR, Mohr JP, Kistler JP, Koroshetz W. Should thrombolytic therapy be the first-line treatment for acute ischemic stroke? Thrombolysis—not a panacea for ischemic stroke. *N Engl J Med* 1997; **337**: 1309–10.

7 Barber PA, Demchuk AM, Zhang J, Buchan AM. Validity and reliability of a quantitative computed tomography score in predicting outcome of hyperacute stroke before thrombolytic therapy. *Lancet* 2000; **355**: 1670–4.

8 Barber PA, Demchuk AM, Hudon ME, Pexman JH, Hill MD, Buchan AM. Hyperdense sylvian fissure MCA 'dot' sign: a CT marker of acute ischemia. *Stroke* 2001; **32**: 84–8.

9 Wildermuth S, Knauth M, Brandt T, Winter R, Sartor K, Hacke W. Role of CT angiography in patient selection for thrombolytic therapy in acute hemispheric stroke. *Stroke* 1998; **29**: 935–8.

10 Kenton AR, Martin PJ, Abbott RJ, Moody AR. Comparison of transcranial color-coded sonography and magnetic resonance angiography in acute stroke. *Stroke* 1997; **28**: 1601–6.

11 Warach S. Tissue viability thresholds in acute stroke: the 4-factor model. *Stroke* 2001; **32**: 2460.

12 Alexandrov AV, Demchuk AM, Wein TH, Grotta JC. The yield of transcranial Doppler in acute cerebral ischemia. *Stroke* 1999; **30**: 1605–9.

13 Fieschi C, Argentino C, Lenzi GL, Sacchetti ML, Toni D, Bozzao L. Clinical and instrumental evaluation of patients with ischemic stroke within six hours. *J Neurol Sci* 1989; **91**: 311–22.

14 Zanette EM, Fieschi C, Bozzao L, Roberti C, Toni D, Argentino C, Lenzi GL. Comparison of cerebral angiography and transcranial Doppler sonography in acute stroke. *Stroke* 1989; **20**: 899–903.

15 Kaps M, Link A. Transcranial sonographic monitoring during thrombolytic therapy. *Am J Neuroradiol* 1998; **19**: 758–60.

16 Razumovsky AY, Gillard JH, Bryan RN, Hanley DF, Oppenheimer SM. TCD, MRA, and MRI in acute cerebral ischemia. *Acta Neurol Scand* 1999; **99**: 65–76.

17 Burgin WS, Malkoff M, Felberg RA, Demchuk AM, Christou I, Grotta JC, Alexandrov AV. Transcranial Doppler ultrasound criteria for recanalization after thrombolysis for middle cerebral artery stroke. *Stroke* 2000; **31**: 1128–32.

18 Demchuk AM, Christou I, Wein TH, Felberg RA, Malkoff M, Grotta JC, Alexandrov AV. Accuracy and criteria for localizing arterial occlusion with transcranial Doppler. *J Neuroimaging* 2000; **10**: 1–12.

19 Demchuk AM, Christou I, Wein TH, Felberg RA, Malkoff M, Grotta JC, Alexandrov AV. Specific transcranial Doppler flow findings related to the presence and site of arterial occlusion with transcranial Doppler. *Stroke* 2000; **31**: 140–6.

20 Alexandrov AV, Demchuk AM, Felberg RA, Grotta JC, Krieger D. Intracranial clot dissolution is associated with embolic signals on transcranial Doppler. *J Neuroimaging* 2000; **10**: 27–32.

21 Alexandrov AV, Felberg RA, Demchuk AM, Christou I, Burgin WS, Malkoff M, Wojner AW, Grotta JC. Deterioration following spontaneous improvement: sonographic findings in patients with acutely resolving symptoms of cerebral ischemia. *Stroke* 2000; **31**: 915–9.

22 Demchuk AM, Burgin WS, Christou I, Felberg RA, Barber PA, Hill MD, Alexandrov AV. Thrombolysis in brain ischemia (TIBI) transcranial Doppler flow grades predict clinical severity, early recovery, and mortality in patients treated with tissue plasminogen activator. *Stroke* 2001; **32**: 89–93.

23 Christou I, Felberg RA, Demchuk AM, Grotta JC, Burgin WS, Malkoff M, Alexandrov AV. Accuracy parameters of a broad diagnostic battery for bedside transcranial Doppler to detect flow changes with internal carotid artery stenosis or occlusion. *J Neuroimaging* 2001; **11**: 236–42.

24 The TIMI Study Group. The thrombolysis in myocardial infarction (TIMI) trial: phase I findings. *N Engl J Med* 1985; **312**: 932–6.

25 Anderson JL. Why does thrombolysis fail? Breaking through the reperfusion ceiling. *Am J Cardiol* 1997; **80**: 1588–90.

26 Hackworthy RA, Sorensen SG, Fitzpatrick PG, Barry WH, Menlove RL, Rothbard RL, Anderson JL. Dependence of assessment of coronary artery reperfusion during acute myocardial infarction on angiographic criteria and interobserver variability. *Am J Cardiol* 1988; **62**: 538–42.

27 Furlan A, Higashida R, Wechsler L, Gent M, Rowley H, Kase C, Pessin M, Ahuja A, Callahan F, Clark WM, Silver F, Rivera F. Intra-arterial prourokinase for acute ischemic stroke. The PROACT II study: a randomized controlled trial. Prolyse in acute cerebral thromboembolism. *JAMA* 1999; **282** (21): 2003–11.

28 Barnett SB, Ter Haar GR, Ziskin MC, Rott HD, Duck FA, Maeda K. International recommendations and guidelines for the safe use of diagnostic ultrasound in medicine. *Ultrasound Med Biol* 2000; **26**: 355–66.

29 Demchuk AM, Wein TH, Felberg RA, Christou I, Alexandrov AV. Evolution of rapid middle cerebral artery recanalization during intravenous thrombolysis for acute ischemic stroke. *Circulation* 1999; **100**: 2282–3.

30 Alexandrov AV, Burgin WS, Demchuk AM, El-Mitwalli A, Grotta JC. Speed of intracranial clot lysis with intravenous TPA therapy: sonographic classification and short term improvement. *Circulation* 2001; **103**: 2897–902.

31 Christou I, Burgin WS, Alexandrov AV, Grotta JC. Arterial status after intravenous TPA therapy for

ischemic stroke: a need for further interventions. *Int Angiol* 2001; **20** (3): 208–13.

32 Lewandowski CA, Frankel M, Tomsick TA, Broderick J, Frey J, Clark W, Starkman S, Grotta J, Spilker J, Khoury J, Brott T. Combined intravenous and intra-arterial r-TPA versus intra-arterial therapy of acute ischemic stroke: Emergency Management of Stroke (EMS) Bridging Trial. *Stroke* 1999; **30**: 2598–605.

33 Pexman JH, Barber PA, Hill MD *et al.* Use of the Alberta Stroke Program Early CT Score (ASPECTS) for assessing CT scans in patients with acute stroke. *Am J Neuroradiol* 2001; **22** (8): 1534–42.

34 Alexandrov AV, Grotta JC. Arterial re-occlusion after intravenous tissue plasminogen therapy for acute ischemic stroke. *Neurology* 2002; **59**: 862–67.

35 Burgin WS, Alexandrov AV. Deterioration following improvement with TPA therapy: carotid thrombosis and re-occlusion. *Neurology* 2001; **56**: 568–70.

36 Grotta JC, Welch KM, Fagan SC, Lu M, Frankel MR, Brott T, Levine SR, Lyden PD. Clinical deterioration following improvement in the NINDS rt-PA Stroke Trial. *Stroke* 2001; **32**: 661–8.

37 Burgin WS, Wojner AW, Grotta JC, Alexandrov AV. NIH Stroke Scale as a predictor of clot presence, location, and persisting occlusion in candidates for thrombolysis. *Stroke* 2001; **32**: 324 [abstract].

38 Christou I, Alexandrov AV, Burgin WS, Wojner AW, Felberg RA, Malkoff M, Grotta JC. Timing of recanalization after TPA therapy determined by transcranial Doppler correlates with clinical recovery from ischemic stroke. *Stroke* 2000; **31**: 1812–6.

39 del Zoppo GJ, Poeck K, Pessin MS, Wolpert SM, Furlan AJ, Ferbert A, Alberts MJ, Zivin JA, Wechsler L, Busse O, Greenlee R, Brass L, Mohr JP, Feldmann E, Hacke W, Kase CS, Biller J, Gress D, Otis SM. Recombinant tissue plasminogen activator in acute thrombotic and embolic stroke. *Ann Neurol* 1992; **32**: 78–86.

40 Trubestein R, Bernard HR, Etzel F, Sobbe A, Cremer A, Stumpff U. Thrombolysis by ultrasound. *Clin Sci Mol Med* 1976; **51**: 697–8.

41 Tachibana K, Tachibana S. Ultrasonic vibration for boosting fibrinolytic effects of urokinase in vivo. *Thromb Haemost* 1981; **46**: 211 [abstract].

42 Braaten JV, Goss RA, Francis CW. Ultrasound reversibly disaggregates fibrin fibers. *Thromb Haemost* 1997; **78**: 1063–8.

43 Kondo I, Mizushige K, Ueda T, Masugata H, Ohmori K, Matsuo H. Histological observations and the process of ultrasound contrast agent enhancement of tissue plasminogen activator thrombolysis with ultrasound exposure. *Jpn Circ J* 1999; **63**: 478–84.

44 Francis CW, Onundarson PT, Carstensen EL, Blinc A, Meltzer RS, Schwarz K, Marder VJ. Enhancement of fibrinolysis in vitro by ultrasound. *J Clin Invest* 1992; **90**: 2063–8.

45 Francis CW, Blinc A, Lee S, Cox C. Ultrasound accelerates transport of recombinant tissue plasminogen activator into clots. *Ultrasound Med Biol* 1995; **21**: 419–24.

46 Suchkova V, Siddiqi FN, Carstensen EL, Dalecki D, Child S, Francis CW. Enhancement of fibrinolysis with 40-kHz ultrasound. *Circulation* 1998; **98**: 1030–5.

47 Sakharov DV, Barrertt-Bergshoeff M, Hekkenberg RT, Rijken DC. Fibrin-specificity of a plasminogen activator affects the efficiency of fibrinolysis and responsiveness to ultrasound: comparison of nine plasminogen activators in vitro. *Thromb Haemost* 1999; **81**: 605–12.

48 Rosenschein U, Gaul G, Erbel R, Amann F, Velasguez D, Stoerger H, Simon R, Gomez G, Troster J, Bartorelli A, Pieper M, Kyriakides Z, Laniado S, Miller HI, Cribier A, Fajadet J. Percutaneous transluminal therapy of occluded saphenous vein grafts: can the challenge be met with ultrasound thrombolysis? *Circulation* 1999; **99**: 26–9.

49 Akiyama M, Ishibashi T, Yamada T, Furuhata H. Low-frequency ultrasound penetrates the cranium and enhances thrombolysis in vitro. *Neurosurgery* 1998; **43**: 828–32.

50 Behrens S, Daffertshofer M, Spiegel D, Hennerici M. Low-frequency, low-intensity ultrasound accelerates thrombolysis through the skull. *Ultrasound Med Biol* 1999; **25**: 269–73.

51 Blinc A, Francis CW, Trudnowski JL, Carstensen EL. Characterization of ultrasound-potentiated fibrinolysis in vitro. *Blood* 1993; **81**: 2636–43.

52 Moehring MA, Voie AH, Spencer MP, Amory DW, Alexandrov AV. Investigation of transcranial Doppler (TCD) power output for potentiation of tissue plasminogen activator (tPA) therapy in stroke. *Cerebrovasc Dis* 2000; **10** (Suppl. 1): 9 [abstract].

53 Spengos K, Behrens S, Daffertshofer M, Dempfle CE, Hennerici M. Acceleration of thrombolysis with ultrasound through the cranium in a flow model. *Ultrasound Med Biol* 2000; **26**: 889–95.

54 Grolimund P. Transmission of ultrasound through the temporal bone. In: Aaslid R, ed. *Transcranial Doppler Sonography*. Wien: Springer Verlag, 1986: 10–21.

55 Eggers J, Koch B, Meyer K, Konig I, Seidel G. Effect of ultrasound on thrombolysis of middle cerebral artery occlusion. *Ann Neurol* 2003; **53**: 797–800.

11 CHAPTER 11

Cerebral vasospasm after subarachnoid hemorrhage

David W. Newell, MD *& Andrei V. Alexandrov,* MD, RVT

Introduction

Cerebral vasospasm is a delayed sustained contraction of the cerebral arteries, which can be induced by blood products that remain in contact with the cerebral vessel wall following subarachnoid hemorrhage (SAH) [1,2]. Vasospasm is a common complication of SAH which is often responsible for delayed ischemic neurologic deficits (DINDs) in these patients [1–4]. The most common cause of SAH is the spontaneous rupture of cerebral aneurysms [5–7]. However, SAH can also occur from other causes such as head injury and following neurosurgical operations for other lesions, and these hemorrhages can also lead to vasospasm. A more in-depth understanding of cerebral vasospasm has been possible through the development of non-invasive diagnostic techniques such as transcranial Doppler (TCD) [8,9] and techniques to measure cerebral blood flow [10–12], as well as from experimental models of vasospasm [13–15]. The pathophysiology of vasospasm and the role of TCD and blood flow studies in the diagnosis and management of patients with cerebral vasospasm will be discussed.

Biologic and physiologic aspects of vasospasm

Hemoglobin and other products from the breakdown of blood around the outside of the cerebral vessels can enter the vessel walls and induce biochemical changes leading to sustained muscular contraction, and also structural changes of the vessel characterized by collagen deposition [2]. Contractile and structural changes result in severe narrowing of the cerebral arteries that in turn can produce increased vascular resistance in the conducting vessels and secondary decreases in cerebral blood flow. Vasospasm most frequently occurs in the basal cerebral vessels as they course through the basal cisterns, which parallels the typical deposition of blood following rupture of aneurysms [4]. Occasionally, vasospasm can be found in the more distally located cerebral vessels, depending on the location of aneurysmal SAH and the location of the blood deposited around the vessels. The location and extent of the subarachnoid bleeding is determined by a non-contrast computed tomographic (CT) scan of the head (Figure 11.1). CT scans can be graded for the presence of blood using the Fischer grades [16] described in Table 11.1. The location and the thickness of the blood clots deposited in the subarachnoid space have predictive value for the risk of vasospasm and subsequent development of delayed ischemic deficits [4,16].

Vasospasm following SAH will occur and cause some degree of vessel narrowing in most patients [1,2,4,17,18]. The clinical severity of SAH measured with Hunt–Hess grades [19] (Table 11.2) or the Glasgow Coma Scale [20,21], clot burden and hydrocephalus on CT [22] and velocity changes on transcranial Doppler [23] is generally predictive of vasospasm development and progression to delayed neurologic deficits.

The majority of these patients however, do not develop vessel narrowing to the point of reducing blood flow to ischemic levels. Most patients will therefore only sustain transient mild or moderate narrowing of the cerebral vessels and undergo spontaneous resolution without development of DIND. Severe vasospasm will cause greater vessel narrowing with reduction of blood flow to ischemic thresholds and

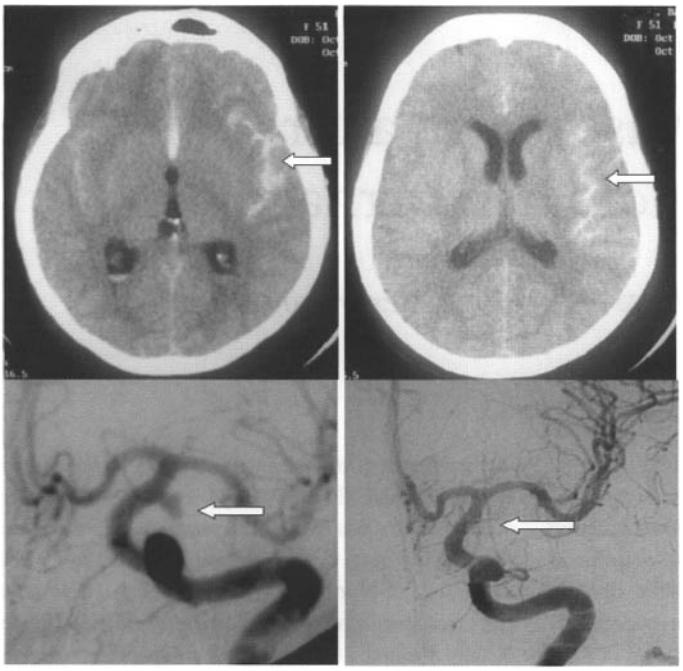

Figure 11.1 CT appearance of subarachnoid hemorrhage (SAH) and aneurysm location. (a) Illustration of a CT scan of the head (upper images) in a patient following a recent SAH illustrating thick vertical layers of blood (arrows) in the intrahemispheric and left Sylvian fissure, placing the patient at risk for vasospasm in these locations. (b) Angiogram in the same patient (lower images) showing a posterior communicating artery aneurysm before (left frame, arrow) and after clipping.

Table 11.1 Fisher grades of subarachnoid hemorrhage (SAH) on computed tomography (CT) scans.

Grade	*CT demonstration of SAH*
1	No blood detected
2	Diffuse or vertical layers < 1 mm thick
3	Localized subarachnoid clot or layers ≥ 1 mm thick
4	Intracerebral or intraventricular clot with diffuse or no SAH

Table 11.2 Hunt–Hess classification of subarachnoid hemorrhage.

Grade	*Description*
I	Asymptomatic, or mild headache with mild nuchal rigidity
II	Moderate or severe headache, nuchal rigidity, no neurologic deficit other than nerve palsy
III	Mild focal deficit, drowsiness or confusion
IV	Stupor, moderate to severe hemiparesis, possible early decerebrate rigidity and vegetative disturbances
V	Deep coma, decerebrate rigidity, moribund appearance

development of delayed ischemic neurologic deficits [24]. The onset of DIND indicates that compensatory mechanisms including recruitment of collateral circulation, autoregulation of the cerebral blood flow and increases in the oxygen extraction fraction are no longer adequate to provide sufficient blood flow.

Clinical and diagnostic features of DIND and vasospasm

The diagnosis of delayed ischemic neurologic deficit is generally made on clinical grounds, when a patient develops a new neurologic deficit, which is not explained by other causes. Delayed neurologic deterioration in patients with SAH can occur from causes other than vasospasm, including hydrocephalus, edema, hemorrhage, sepsis, electrolyte disturbance or seizures. Clinical suspicion of DINDs due to vasospasm is usually triggered by either a decreased level of consciousness or focal neurologic signs including speech deficits or weakness. Vasospasm causing frontal lobe ischemia may present as confusion, agitation, apathy or electrolyte disturbances. A so-called cerebral salt wasting syndrome, or unexplained increase in urinary output after SAH [25,26], may precede the onset of neurologic

deficits. Ischemic symptoms in the posterior circulation may be associated with a decreased level of consciousness and breathing abnormalities, or can be subtle and can include diplopia and other brainstem signs such as decreased gag reflex.

Ancillary diagnostic studies including CT scanning, TCD and blood flow measurements have a role in supporting the diagnosis of DIND since there is uncertainty in some cases whether the degree of vasospasm present in a patient is responsible for the clinical symptoms. The CT scan can rule out hydrocephalus, edema or hemorrhage as a cause for new neurologic deficits. It is also useful to ascertain whether a new infarct is present, using CT, before proceeding to endovascular therapy such as angioplasty [27] since the presence of significant infarction has been associated with increased complications following angioplasty with or without papaverine [28–31].

Post-traumatic vasospasm, or vasospasm following head injury, is now increasingly recognized as a clinical entity with potentially significant consequences [32–34]. Following trauma, bleeding in the subarachnoid space can leave blood deposited around the basal cerebral arteries, and can lead to delayed cerebral vessel narrowing and ischemia. Martin *et al.* suggested that patients with significant post-traumatic SAH be examined frequently by TCD for the presence of vasospasm as well as hypo- or hyperperfusion states after brain injury [35].

The use of transcranial Doppler and cerebral blood flow studies for vasospasm

TCD had one of its first applications in the identification of cerebral vasospasm after SAH [8,9]. TCD can be used to detect vasospasm, and the amount of blood on the CT scan correlates with the degree of subsequent velocity elevations [23]. Although TCD does not allow measurement of cerebral blood flow (CBF) [36,37], numerous studies have shown that TCD can be useful in detecting and monitoring the degree of vasospasm following SAH, in following the time course of spasm, and also for evaluating the effects of treatment for vasospasm used alone or in conjunction with CBF studies [38–42].

The degree of vasospasm in the basal vessels is inferred from the amount of acceleration of blood flow velocity through the vessels as they become narrowed [38] (Figure 11.2, Table 11.3). As a practical matter it is always important to obtain baseline TCD measurements in patients with SAH and to frequently (daily or every other day) repeat examinations throughout the hospital stay. Lindegaard *et al.* [38] showed that vasospastic middle cerebral arteries usually demonstrate velocities greater than 120 cm/s with velocity being inversely related to arterial diameter, and that velocities greater than 200 cm/s are predictive of a residual middle cerebral artery (MCA) lumen

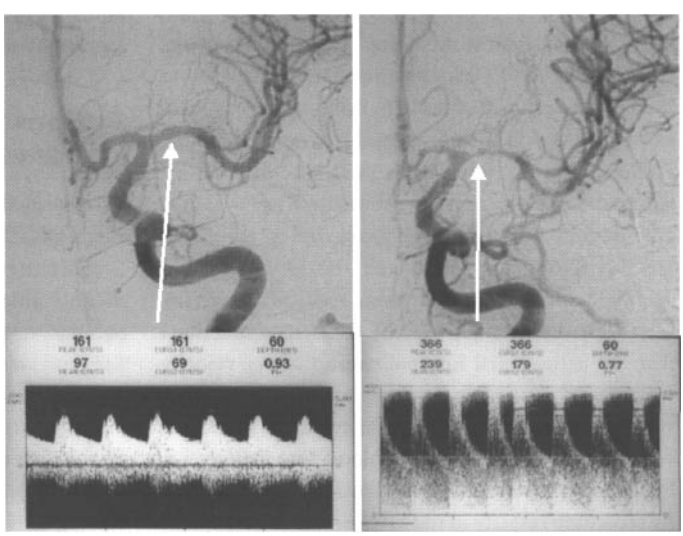

Figure 11.2 Proximal middle cerebral artery vasospasm. A left internal carotid angiogram (upper images) showed the middle cerebral arteries before (left frame) and after (right frame) the onset of vasospasm. Transcranial Doppler recordings (lower images) of the corresponding left middle cerebral blood flow velocities at baseline (left frame) before the onset of vasospasm and after development of severe spasm (right frame).

Table 11.3 Stages of vasospasm.

	Vessel narrowing	*TCD velocity*	*CBF*	*DIND*
Stage I	↑	↑	⇔	No
Stage II	↑↑	↑↑	⇔	No
Stage III	↑↑↑	↑↑↑	↓↓	No
Stage IV	↑↑↑↑	↑↑↑↑ or ↑↑↑	↓↓↓	Yes

↑, mild; ↑↑, moderate; ↑↑↑, severe; ↑↑↑↑, very severe; ⇔, no change.

TCD, transcranial Doppler; CBF, cerebral blood flow; DIND, delayed ischemic neurologic deficit.

This table shows relative changes in vessel narrowing, TCD velocities, CBF and delayed neurologic deficits according to the progressive stages of vasospasm.

diameter of 1 mm or less. Note that a normal MCA diameter is approximately 3 mm.

Single photon emission computed tomography (SPECT) is one of several methods that can be used to evaluate regional cerebral blood flow in patients with vasospasm following SAH [41]. Other methods for evaluating blood flow include xenon computed tomography (Xe-CT) [37], radioactive ^{133}Xe with external detectors, positron emission tomography (PET), and either thermodilution or laser Doppler cortical flow probes. The information gained from CBF methods can be complementary to information provided by TCD and the neurologic examination, and can be helpful in deciding on different treatment regimens in patients following SAH [42]. However, TCD mean flow velocity measurements do not allow calculation of cerebral blood flow volume and should not be substituted for CBF measurements [36,37,43,44]. TCD velocity information is helpful to predict the degree of vessel narrowing, spasm progression or regression and compensatory vasodilatation.

The changes in velocity on TCD have been correlated with vessel narrowing measured using angiography, and the best correlations are in the MCA [38,39]. Sloan *et al.* evaluated the sensitivity and specificity of TCD for vasospasm in the MCA and the vertebrobasilar system [45,46]. It is recommended that the extracranial internal carotid artery velocity be recorded also when assessing anterior circulation vasospasm due to the fact that increased or decreased velocities can also be caused by blood flow changes, i.e. hyperdynamic state with hypertension–hypervolemia. By recording velocity in the MCA and internal carotid artery (ICA), a Lindegaard ratio [47,48] between the mean flow velocities (MCA/ICA) can be calculated which may help to differentiate spasm severity and relative contribution of hyperemia (see also Chapter 6).

Vasospasm can be limited to distal vascular distributions in a relatively small percentage of cases and can be missed by TCD [49]. Although transcranial Doppler is insensitive for detecting far-distal vasospasm (i.e. M3, or distal M2 MCA), distal spasm affecting proximal M2 segments of the MCA can be detected (Figure 11.3). Far-distal spasm can often be predicted by the distribution of blood in more distal locations on the initial CT scan following SAH. Newell *et al.* reported that isolated distal vessel spasm causing significant neurologic deficit is unusual after SAH but does exist [49]. Cerebral blood flow methods such as xenon CT or SPECT are useful to confirm this diagnosis.

We employ TCD to perform daily monitoring in patients with SAH preoperatively and in the postoperative period. The routine use of blood flow studies may also be helpful in guiding therapy for vasospasm. Yonas *et al.* utilized CBF measurements with Xe-CT and have documented decreased cerebral blood flow specific to territories supplied by vasospastic vessels [43]. When combined with routine TCD detection of vasospasm, Xe-CT CBF or SPECT evaluation may prove valuable in determining which patients will ultimately benefit from angioplasty, and may also be useful to predict when earlier intervention during the asymptomatic period might be beneficial. Moreover, CBF imaging techniques such as Xe-CT and SPECT assess tissue perfusion, which complements the assessment of vessel diameter provided by TCD.

Options for treatment of vasospasm

Various medications have been evaluated in human clinical studies for their effect on reducing ischemic complications from vasospasm [3,30,31,50]. Calcium channel blockers, which are cerebral selective, have been shown to be effective in improving outcome after SAH and are now routinely used [51,52].

Another therapy which is routinely employed for the prevention and treatment of ischemic deficits following SAH is triple H therapy which denotes induced hypertension, hypervolemia and hemodilution [50]. The triple H (HHH) therapy utilizes crystalloid and colloid solutions as well as vasopressors to increase

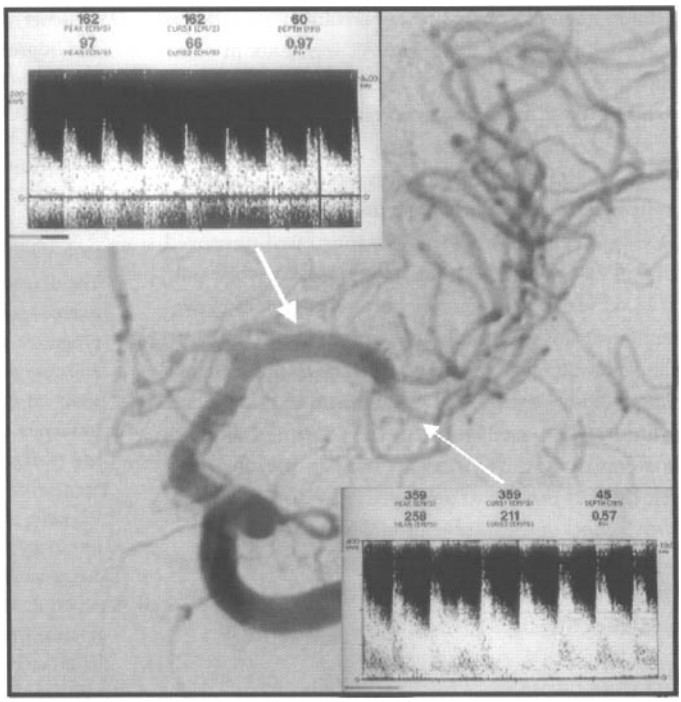

Figure 11.3 M2 middle cerebral artery (MCA) vasospasm. A left internal carotid angiogram showed improvement in vessel diameter after balloon angioplasty for a severe proximal M1 MCA vasospasm (see Figures 11.1 & 11.2). Transcranial Doppler showed mean flow velocities of 97 cm/s in the M1 MCA after angioplasty (upper waveform), and M2 MCA mean flow velocities of 258 cm/s (lower waveform), indicating development of spasm in more distal branches.

blood pressure. Therapies including HHH therapy and calcium channel blockers are often not completely effective in eliminating delayed ischemic neurologic deficits from cerebral vasospasm. Endovascular therapy using angioplasty and/or papaverine offers an additional modality for treatment in patients with vasospasm.

Zubkov first reported the use of endovascular techniques to mechanically dilate vasospastic cerebral arteries in a series of patients [27]. These encouraging results established that mechanical dilatation of cerebral arteries affected by vasospasm can result in a sustained treatment effect and thereby may benefit patients who are affected by cerebral ischemia from vasospasm. Subsequent reports from the US verified the findings of Zubkov and led to the further development of balloon angioplasty for the treatment of vasospasm [28,29].

Treatment of vasospasm with papaverine has also been recently employed with renewed interest for treatment of distal spasm that cannot be directly reached by balloon-carrying catheters. Presently, papaverine and balloon angioplasty are the most common endovascular therapies being employed in the treatment of cerebral vasospasm [30,31]. Papaverine infusion is accomplished using small repeated injections with a superselective catheter positioned just proximal to the affected area of a vessel using an infusion of 300 mg per side, or 600 mg total dose. Balloon angioplasty is performed also using transfemoral catheterization with a road mapping imaging technique available for accurate balloon placement. A soft silicone microballoon catheter is used and is introduced just proximal to the spastic segments. Papaverine can also be used as an adjunct to facilitate dilatation of vessel segments prior to the introduction of the balloon catheter. The balloon is inflated under low pressure multiple times while advancing it into the spastic segments. Careful attention is paid not to pass the catheter into a branch or a small vessel and not to overinflate the artery past the original diameter, which will minimize the risk of vessel rupture.

Angioplasty in the anterior circulation can be performed in the supraclinoid carotid arteries and proximal middle cerebral arteries including the M2 branches. Angioplasty can also be performed in both vertebral arteries, the basilar artery, proximal posterior cerebral arteries and, occasionally, the proximal superior cerebellar arteries. The anterior cerebral artery system has not previously been accessible for

balloon angioplasty, but recent advances in catheters make it possible to dilate the A1 segments in some patients.

Elliott *et al.* have observed relative improvements in CBF, using SPECT at 24 h following treatment of vasospasm, with balloon angioplasty significantly more often than with papaverine infusion [53]: 71% of vessel segment territories demonstrated improved CBF at 24 h following balloon angioplasty while only 31% of vessel segment territories showed improvement within 24 h following papaverine infusion. These results are consistent with TCD observations that balloon angioplasty is superior to papaverine infusion when used alone for the treatment of proximal vasospasm. TCD can be used to monitor flow velocities at the site of angioplasty to document sustained effect of the interventional procedure.

Recent studies also showed that TCD and other variables can monitor HHH therapy and predict outcomes after SAH [54,55].

Conclusions

The occurrence of stroke and permanent ischemic brain damage from cerebral vasospasm continues to be a clinical problem in patients following SAH and is a potentially preventable or reversible condition. Prompt recognition and treatment of this condition in part depends on accurate diagnosis that can be facilitated using TCD and cerebral blood flow studies. Although asymptomatic patient selection for early angioplasty to prevent the onset of DIND remains controversial, TCD can be used to:

1 detect asymptomatic vasospasm onset;
2 follow spasm progression and facilitate HHH therapy;
3 identify patients with severe vasospasm;
4 monitor the effect of therapies and interventions; and
5 detect spasm resolution.

References

1 Weir B, Grace M, Hansen J, Rothberg C. Time course of vasospasm in man. *J Neurosurg* 1978; **48**: 173–8.

2 Sloan MA. Cerebral vasoconstriction: physiology, pathophysiology, and occurrence in selected cerebrovascular disorders. In: Caplan LR, ed. *Brain Ischemia: Basic Concepts and Their Clinical Relevance.* London: Springer-Verlag, 1994: 151–72.

3 Fleischer AS, Raggio JF, Tindall GT. Aminophylline and isoproterenol in the treatment of cerebral vasopasm. *Surg Neurol* 1977; **8**: 117–21.

4 Kistler JP, Crowell RM, Davis KR, Heros R, Ojemann RG, Zervas T, Fisher CM. The relation of cerebral vasospasm to the extent and location of subarachnoid blood visualized by CT scan: a prospective study. *Neurology* 1983; **33**: 424–36.

5 Oldenkott P, Stolz C. Subarachnoid hemorrhage. The diagnostic guiding symptom: the blood containing liquor. Cause, clinical aspects, treatment problems and prognosis. *Med Welt* 1969; **23**: 1326–31 [in German].

6 Niizuma H, Kwak R, Otabe K, Suzuki J. Angiography study of cerebral vasospasm following the rupture of intracranial aneurysms: Part II. Relation between the site of aneurysm and the occurrence of the vasospasm. *Surg Neurol* 1979; **11**: 263–7.

7 Reynolds AF, Shaw CM. Bleeding patterns from ruptured intracranial aneurysms: an autopsy series of 205 patients. *Surg Neurol* 1981; **15**: 232–5.

8 Aaslid R, Markwalder TM, Nornes H. Noninvasive transcranial Doppler ultrasound recording of flow velocity in basal cerebral arteries. *J Neurosurg* 1982; **57**: 769–74.

9 Lindegaard KF, Nornes H, Bakke SJ, Sorteberg W, Nakstad P. Cerebral vasospasm after subarachnoid haemorrhage investigated by means of transcranial Doppler ultrasound. *Acta Neurochir (Wien)* 1988; **42** (Suppl.): P81–4.

10 Bohm E, Aronson G, Hugosson R, Grangsjo G, Ulfendahl HR, Wolgast M. Cerebral circulatory conditions in patients with ruptured aneurysms measured by an intravenous radioactive-indicator technique. *Acta Neurol Scand* 1968; **44**: 33–42.

11 Grubb RL Jr, Raichle ME, Eichling JO, Gado MH. Effects of subarachnoid hemorrhage on cerebral blood volume, blood flow, and oxygen utilization in humans. *J Neurosurg* 1977; **46**: 446–53.

12 Meyer CH, Lowe D, Meyer M, Richardson PL, Neil-Dwyer G. Progressive change in cerebral blood flow during the first three weeks after subarachnoid hemorrhage. *Neurosurgery* 1983; **12**: 58–76.

13 Barry KJ, Gogjian MA, Stein BM. Small animal model for investigation of subarachnoid hemorrhage and cerebral vasospasm. *Stroke* 1979; **10**: 538–41.

14 Rothberg CS, Weir B, Overton TR. Treatment of subarachnoid hemorrhage with sodium nitroprusside and phenylephrine: an experimental study. *Neurosurgery* 1979; **5**: 588–95.

15 Megyesi JF, Vollrath B, Cook DA, Findlay JM. In vivo animal models of cerebral vasospasm: a review. *Neurosurgery* 2000; **46**: 448–60.

16 Fischer CM, Kistler JP, Davis JM. Relation of cerebral vasospasm to subarachnoid hemorrhage visualized by

computed tomographic scanning. *Neurosurgery* 1980; **6**: 1–9.

17 Heros RC, Zervas NT, Varsos V. Cerebral vasospasm after subarachnoid hemorrhage: an update. *Ann Neurol* 1983; **14**: 599–608.

18 Mayberg MR. Cerebral vasospasm. *Neurosurg Clin N Am* 1998; **9**: 615–27.

19 Hunt WE, Hess RM. Surgical risk as related to time of intervention in the repair of intracranial aneurysms. *J Neurosurg* 1968; **28**: 14–20.

20 Teasdale G, Jennett B. Assessment of coma and impaired consciousness—a practical guide. *Lancet* 1974; **2** (7872): 81–4.

21 Teasdale GM, Murray L. Revisiting the Glasgow Coma Scale and Coma Score. *Intensive Care Med* 2000; **26**: 153–4.

22 Black PM. Hydrocephalus and vasospasm after subarachnoid hemorrhage from ruptured intracranial aneurysms. *Neurosurgery* 1986; **18**: 12–6.

23 Seiler RW, Grolimund P, Aaslid R, Huber P, Nornes H. Cerebral vasospasm evaluated by transcranial ultrasound correlated with clinical grade and CT-visualized subarachnoid hemorrhage. *J Neurosurg* 1986; **64**: 594–600.

24 Yamakami I, Isobe K, Yamaura A, Nakamura T, Makino H. Vasospasm and regional cerebral blood flow (rCBF) in patients with ruptured intracranial aneurysm: serial rCBF studies with the xenon-133 inhalation method. *Neurosurgery* 1983; **13**: 394–401.

25 Berendes E, Scherer R, Schuricht G, Rol R, Hengst K. Massive natriuresis and polyuria after triple craniocervical subarachnoid hemorrhage: cerebral salt wasting syndrome? *Anasthesiol Intensivmed Notfallmed Schmerzther* 1992; **27**: 445–8 [in German].

26 Harrigan MR. Cerebral salt wasting syndrome. *Crit Care Clin* 2001; **17**: 125–38.

27 Zubkov YN, Nikiforov BM, Shustin VA. Balloon catheter technique for dilatation of constricted cerebral arteries after aneurysmal subarachnoid hemorrhage. *Acta Neurochir (Wien)* 1984; **70**: 65–79.

28 Higashida RT, Halbach VV, Cahan LD *et al.* Transluminal angioplasty for treatment of intracranial arterial vasospasm. *J Neurosurg* 1989; **71**: 648–53.

29 LeRoux PD, Newell DW, Eskridge J, Mayberg MR, Winn HR. Severe symptomatic vasospasm: the role of immediate postoperative angioplasty. *J Neurosurg* 1994; **80**: 224–9.

30 Kaku Y, Yonekawa Y, Tsukahara T, Kazekawa K. Superselective intra-arterial infusion of papaverine for the treatment of cerebral vasospasm after subarachnoid hemorrhage. *J Neurosurg* 1992; **77**: 842–7.

31 Kassell NF, Helm G, Simmons N, Phillips CD, Cail WS. Treatment of cerebral vasospasm with intra-arterial papaverine. *J Neurosurg* 1992; **77**: 848–52.

32 Lee JH, Martin NA, Alsina G, McArthur DL, Zaucha K, Hovda DA, Becker DP. Hemodynamically significant cerebral vasospasm and outcome after head injury: a prospective study. *J Neurosurg* 1997; **87**: 221–33.

33 Zubkov AY, Pilkington AS, Bernanke DH, Parent AD, Zhang J. Posttraumatic cerebral vasospasm: clinical and morphological presentations. *J Neurotrauma* 1999; **16**: 763–70.

34 Zubkov AY, Lewis AI, Raila FA, Zhang J, Parent AD. Risk factors for the development of post-traumatic cerebral vasospasm. *Surg Neurol* 2000; **53**: 126–30.

35 Martin NA, Patwardhan RV, Alexander MJ, Africk CZ, Lee JH, Shalmon E, Hovda DA, Becker DP. Characterization of cerebral hemodynamic phases following severe head trauma: hypoperfusion, hyperemia, and vasospasm. *J Neurosurg* 1997; **87**: 9–19.

36 Romner B, Brandt L, Berntman L, Algotsson L, Ljunggren B, Messeter K. Simultaneous transcranial Doppler sonography and cerebral blood flow measurements of cerebrovascular CO_2-reactivity in patients with aneurysmal subarachnoid haemorrhage. *Br J Neurosurg* 1991; 5: 31–7.

37 Clyde BL, Resnick DK, Yonas H, Smith HA, Kaufmann AM. The relationship of blood velocity as measured by transcranial Doppler ultrasonography to cerebral blood flow as determined by stable xenon computed tomographic studies after aneurysmal subarachnoid hemorrhage. *Neurosurgery* 1996; **38**: 896–904.

38 Lindegaard KF, Nornes H, Bakke SJ, Sorteberg W, Nakstad P. Cerebral vasospasm after subarachnoid haemorrhage investigated by means of transcranial Doppler ultrasound. *Acta Neurochir (Wien) (Suppl.)* 1988; **42**: 81–4.

39 Sloan MA. *Transcranial Doppler* monitoring of vasospasm after subarachnoid hemorrhage. In: Tegeler CH, Babikian VL, Gomez CR, eds. *Neurosonology*. St Louis: Mosby, 1996: 156–71.

40 Giller CA, Purdy P, Giller A, Batjer HH, Kopitnik T. Elevated transcranial Doppler ultrasound velocities following therapeutic arterial dilation. *Stroke* 1995; **26**: 123–7.

41 Lewis DH, Eskridge JM, Newell DW, Grady MS, Cohen WA, Dalley RW, Loyd D, Grothaus King A, Young P, Winn HR. Brain SPECT and the effect of cerebral angioplasty in delayed ischemia due to vasospasm. *J Nucl Med* 1992; **33**: 1789–96.

42 Rajendran JG, Lewis DH, Newell DW, Winn HR. Brain SPECT used to evaluate vasospasm after subarachnoid hemorrhage: correlation with angiography and transcranial Doppler. *Clin Nucl Med* 2001; **26**: 125–30.

43 Yonas H, Sekhar L, Johnson SW, Gur D. Determination of irreversible ischemia by xenon-enhanced computed tomographic monitoring of cerebral blood flow in

patients with symptomatic vasospasm. *Neurosurgery* 1989; **24**: 368–72.

44 Kontos HA. Validity of cerebral arterial blood flow calculations from velocity measurements. *Stroke* 1989; **20**: 1–3.

45 Sloan MA, Haley EC, Kassell NF, Henry ML, Stewart SR, Beskin RR, Sevilla EA, Torner JC. Sensitivity and specificity of transcranial Doppler ultrasonography in the diagnosis of vasospasm following subarachnoid hemorrhage. *Neurology* 1989; **39**: 1514–8.

46 Sloan MA, Burch CM, Wozniak MA, Rothman MI, Rigamonti D, Permutt T, Numaguchi Y. Transcranial Doppler detection of vertebrobasilar vasospasm following subarachnoid hemorrhage. *Stroke* 1994; **25**: 2187–97.

47 Lindegaard KF, Nornes H, Bakke SJ, Sorteberg W, Nakstad P. Cerebral vasospasm diagnosis by means of angiography and blood velocity measurements. *Acta Neurochir (Wien)* 1989; **100**: 12–24.

48 Lindegaard KF. The role of transcranial Doppler in the management of patients with subarachnoid haemorrhage: a review. *Acta Neurochir (Suppl.)* 1999; **72**: 59–71.

49 Newell DW, Grady MS, Eskridge JM, Winn HR. Distribution of angiographic vasospasm after subarachnoid hemorrhage: implications for diagnosis by transcranial Doppler ultrasonography. *Neurosurgery* 1990; **27**: 574–7.

50 Awad IA, Carter LP, Spetzler RF, Medina M, Williams FC. Clinical vasospasm after subarachnoid hemorrhage: response to hypervolemic hemodilution and arterial hypertension. *Stroke* 1987; **18**: 365–72.

51 Barker FG, Ogilvy CS. Efficacy of prophylactic nimodipine for delayed ischemic deficit after subarachnoid hemorrhage: a metaanalysis. *J Neurosurg* 1996; **84**: 405–14.

52 Feigin VL, Rinkel GJ, Algra A, Vermeulen M, van-Gijn J. Calcium antagonists in patients with aneurysmal subarachnoid hemorrhage: a systematic review. *Neurology* 1998; **50**: 844–66.

53 Elliott JP, Newell DW, Lam DJ, Eskridge JM, Douville CM, LeRoux PD, Lewis DH, Mayberg MR, Grady MS, Winn HR. Comparison of balloon angioplasty and papaverine infusion for the treatment of vasospasm following aneurysmal subarachnoid hemorrhage. *J Neurosurg* 1998; **88**: 277–84.

54 Quereshi AI, Suarez JI, Bhardwaj A, Yahia AM, Tamargo RJ, Ulatowski JA. Early predictors of outcome in patients receiving hypervolemic and hypertensive therapy for symptomatic vasospasm after subarachnoid hemorrhage. *Crit Care Med* 2000; **28**: 824–9.

55 Quereshi AI, Sung GY, Razumovsky AY, Lane K, Straw RN, Ulatowski JA. Early identification of patients at risk for symptomatic vasospasm after aneurismal subarachnoid hemorrhage. *Crit Care Med* 2000; **28**: 984–90.

PART V

Select clinical applications and clinical vignettes

Andrei V. Alexandrov, MD, RVT

This section provides a brief overview of several clinical situations when cerebrovascular ultrasound gave important clues to pathogenesis of patient symptoms or provided valuable information that changed patient management. The doctors acknowledged in this section were my colleagues who directly participated in caring for the patients described or performed research studies focusing on these problems.

This page intentionally left blank

Typical MCA/TICA vasospasm after subarachnoid hemorrhage

With Marc Malkoff, MD

Introduction

The following case illustrates a typical course of transcranial Doppler (TCD) velocity changes in a patient who develops a unilateral (TICA/middle cerebral artery (TICA/MCA) vasospasm. Other scenarios of vasospasm development including locations in the anterior cerebral arteries (ACAs) and basilar artery are given in subsequent sections.

Besides large vessels, patients dying from acute vasospasm also had morphologic changes in small arteries, capillaries and veins at autopsy [1]. TCD offers a non-invasive tool to detect changes in large arteries before spasm becomes symptomatic [2]. TCD has the highest-accuracy parameters for vasospasm located in the MCA [2–6], and the Lindegaard ratio should be used to optimize spasm detection and its differentiation with global perfusion changes [7]. Although studies of nimodipine, a calcium channel blocker, report its effect on morbidity and mortality but not spasm incidence after subarachnoid hemorrhage (SAH) [8–10], the use of this medication may change flow parameters detected by TCD [11]. In this situation, the Lindegaard ratio should still provide supportive data for vasospasm development or progression despite relatively low velocities [7].

Case presentation

A 47-year-old white female was transferred from a community hospital to our neurointensive care unit (NICU) within 24 h after a sudden onset of the most severe headache of her life. On examination, she was alert and orientated and had no focal neurologic deficits. Computed tomography (CT) scan showed a diffuse collection of blood mostly in the supratentorial subarachnoid spaces, particularly the right Sylvian fissure (Fisher grade II SAH). She had a clinical Hunt–Hess grade II SAH, and diagnostic digital subtraction angiography (DSA) on the day of admission showed no detectable aneurysm and no early vasospasm.

Diagnostic considerations

Clinical examination and head CT are consistent with a non-traumatic SAH. Although DSA showed no intracranial aneurysm that could have been the source of bleeding, vasospasm can be expected to develop in the TICA/MCA distribution because of blood collection in the Sylvian fissure [1]. Baseline TCD was performed as soon as feasible after ventriculostomy to obtain normal velocity ranges with decompression and in close time interval with diagnostic DSA.

Ultrasound findings

Daily TCD monitoring was initiated in the NICU starting on the day of headache onset (Day 0). TCD showed a normal range of velocities in the anterior and posterior circulation vessels on Day 0, with a modest velocity increase and a slight decrease in pulsatility indices after surgical clipping of the aneurysm (Figure 1). Daily TCD follow-up showed gradual increase in the right MCA velocities from 74 cm/s postoperatively to 220 cm/s on Day 6 followed by right MCA velocity decrease after balloon angioplasty.

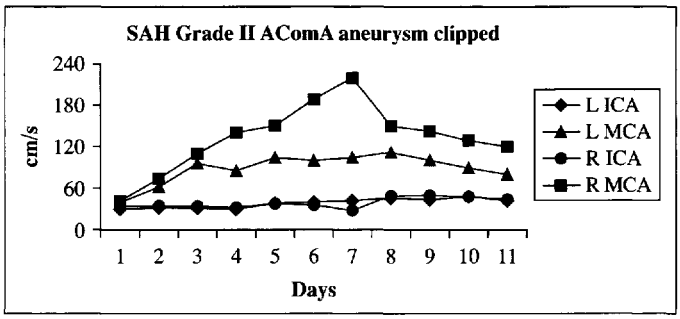

Figure 1 Mean flow velocities in internal carotid arteries and middle cerebral arteries.

Interpretation

Baseline TCD on Day 0 showed normal velocities. TCD findings on Day 1 indicate flow velocity increase and pulsatility decrease, most likely due to hydration and decompression associated with surgical clipping of the aneurysm. Day 3 was the first day of a low-moderate MCA spasm on TCD based on standard criteria for the MCA mean flow velocity and the Lindegaard ratio. Day 6 was the first day of a severe MCA spasm on TCD. Ultrasound findings on Day 7 showed velocity decrease after successful balloon angioplasty. TCD on Days 8–10 showed further velocity decrease with no significant spasm. Grading of vasospasm was performed using the mean flow velocities (MFVs) and Lindegaard (MCA/ICA MFV) ratios derived from the previous studies [2–6,11] and outlined in Chapter 6.

Correlative imaging

Repeat DSA on Day 7 showed a severe right MCA vasospasm and moderate vasospasm in the right terminal ICA and the right A1 ACA (Figure 2). Balloon angioplasty of the right terminal ICA and the M1 MCA segment was performed (Figure 2). A four-vessel diagnostic DSA was also repeated at this time and it showed no detectable aneurysm.

Differential diagnosis

This patient had no aneurysm on both baseline and repeat angiograms, yet this patient is still at risk of developing vasospasm due to blood collection in the Sylvian fissure [1]. The TICA/MCA vessels are most often affected by vasospasm after a non-traumatic SAH [1,4]. The absence of detectable aneurysm makes 'across-the-board' administration of HHH therapy problematic in such cases since with higher blood pressure there is a chance of rebleeding due to rupture of presumably existing, thrombosed and unclipped aneurysm [12,13]. TCD monitoring provides the tool to detect whether any spasm develops and to select patients for interventional procedures [14,15] and/or moderate HHH therapy in these circumstances.

The velocity difference between Day 0 and Day 1 (not shown) may also be attributable to a slow development of hydrocephalus and its alleviation by decompression after ventriculostomy. If ventriculostomy is not performed on admission or subsequent stay in the NICU, hydrocephalus may develop in some

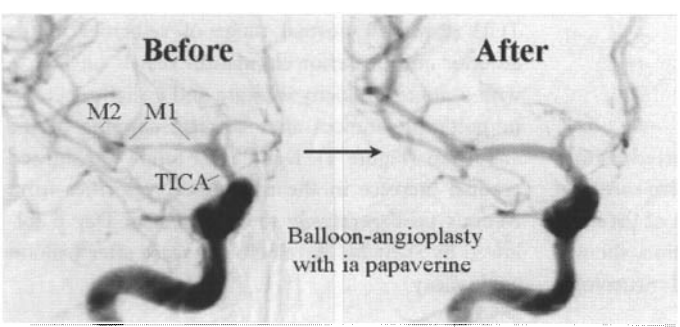

Figure 2 Balloon angioplasty with intra-arterial papaverine.

of these cases and, if ICP increases above 20 mmHg, it may produce a gradual decrease in mean flow velocities and an increase in flow pulsatility [16]. This commonly happens at Days 2–3 after headache onset.

Initial increase in velocities and elevated (> 100 cm/s) velocities bilaterally on later days may be related to 'hyperemia' with hematocrit values < 27% [17]. In this case, the Lindegaard ratio remains low, i.e. < 3. TCD findings on Day 5 indicate progression to a high-moderate MCA vasospasm (MFV 189 cm/s, Lindegaard ratio 5.3) and represent the first unfavourable prognostic sign for development of symptomatic vasospasm [18–20]. However, TCD monitoring of patients with SAH should not be limited only to MCA and ICA velocities since vasospasm may affect the TICA, ACA and other vessels. If vessels other than the MCA are affected, the MCA may have a compensatory velocity increase in the 100–180 cm/s range with relatively low ratios that may be misleading as to spasm localization and its severity (see Bilateral ACA Vasospasm and Multiple Vessel Vasospasm sections, p. 195 and p. 198).

Balloon angioplasty may restore the MCA patency but the velocity may not return to normal values [21]. This may happen due to flow reorganization through the MCA with postischemic hyperemia and dysautoregulation in the presence of hydration and hypertension therapy, if continued. Elevated ICA velocities with low Lindegaard ratios indicate persistent effect of angioplasty in terms of lumen restoration, but low pulsatility indices may indicate postischemic hyperemia and distal vasodilatation [21]. Continuing TCD monitoring after successful balloon angioplasty with papaverine may show transient velocity changes and redevelopment of spasm in some patients [22,23]. Interpretation of TCD velocity data throughout the monitoring period should be made with caution, particularly with regard to patient age [24].

Management

The patient did not undergo surgical clipping since no aneurysm was found. Oral nimodipine was administered. After TCD showed the development of low-moderate vasospasm on Day 3, a pulmonary artery (PA) catheter was placed and moderate HHH therapy (mostly fluid balance and mean arterial pressure maintenance at 100–110 mmHg) was initiated. Despite this effort, TCD showed increasing MCA velocities with increasing Lindegaard ratios through Day 6. When TCD showed severe MCA vasospasm (MFV > 200 cm/s, Lindegaard ratio > 6), a repeat angiogram was scheduled for the following day since the patient did not show any focal neurologic deficits at this point. However, the interventional radiologist was informed that, in the event of neurologic deterioration, an urgent catheter angiography and angioplasty might be required before Day 7.

DSA on Day 7 confirmed the presence of a severe MCA vasospasm, and balloon angioplasty of the right M1 MCA was performed. Intra-arterial papaverine was injected in the right M2 and A1 ACA segments but no angioplasty was performed since the degree of vasospasm in these vessels was moderate. There was a good distal contrast opacification of the A2 ACA and the contralateral ACA was largely unaffected. The four-vessel diagnostic angiography showed no detectable aneurysm on Day 7.

TCD monitoring showed a decrease in the MCA mean flow velocities and low Lindegaard ratios after angioplasty. Moderate HHH therapy was stopped and the PA catheter was removed on Day 8. TCD monitoring was discontinued on Day 11.

Follow-up

The patient was transferred from the NICU on Day 10. She returned to work 4 months after this episode.

References

1 Kassel NF, Sasaki T, Colohan ART, Nazar G. Cerebral vasospasm following aneurysmal subarachnoid hemorrhage. *Stroke* 1985; **16**: 562–8.

2 Lindegaard KF, Nornes H, Bakke SJ, Sorteberg W, Nakstad P. Cerebral vasospasm after subarachnoid haemorrhage investigated by means of transcranial Doppler ultrasound. *Acta Neurochir (Wien)* 1988; **42** (Suppl.): P81–4.

3 Sloan MA, Haley EC Jr, Kassell NF, Henry ML, Stewart SR, Beskin RR, Sevilla EA, Torner JC. Sensitivity and specificity of transcranial Doppler ultrasonography in the diagnosis of vasospasm following subarachnoid hemorrhage. *Neurology* 1989; **39** (11): 1514–8.

4 Newell DW, Grady MS, Eskridge JM, Winn HR. Distribution of angiographic vasospasm after subarachnoid hemorrhage: implications for diagnosis by transcranial Doppler ultrasonography. *Neurosurgery* 1990; **27**: 574–7.

5 Sloan MA. Transcranial Doppler monitoring of vasospasm after subarachnoid hemorrhage. In: Tegeler CH, Babikian VL, Gomez CR, eds. *Neurosonology*. St Louis: Mosby, 1996: 156–71.

6 Lysakowski C, Walder B, Costanza MC, Tramer MR. Transcranial Doppler versus angiography in patients with vasospasm due to ruptured cerebral aneurysm. A systematic review. *Stroke* 2001; **32**: 2292–8.

7 Lindegaard KF. The role of transcranial Doppler in the management of patients with subarachnoid haemorrhage: a review. *Acta Neurochir Suppl* 1999; **72**: 59–71.

8 Allen AS, Ahn HS, Preziosi TJ *et al.* Cerebral arterial spasm—a controlled trial of nimodipine in patients with subarachnoid hemorrhage. *N Engl J Med* 1983; **308**: 619–23.

9 Pickard JD, Murray GD, Illingsworth R *et al.* Effect of oral nimodipine on cerebral infarction and outcome after subarachnoid hemorrhage: British Aneurysm Nimodipine Trial. *Br Med J* 1989; **289**: 636–42.

10 Barker FG, Ogilvy CG. Efficacy of prophylactic nimodipine for delayed ischemic deficit after subarachnoid hemorrhage. A metaanalysis. *J Neurosurg* 1996; **84**: 405–8.

11 Steinmeier R, Laumer R, Bondar I, Priem R, Fahlbusch R. Cerebral hemodynamics in subarachnoid hemorrhage evaluated by transcranial Doppler sonography. Part 2. Pulsatility indices, normal reference values, and characteristics in subarachnoid hemorrhage. *Neurosurgery* 1993; **33**: 10–6.

12 Kassell NF, Peerless SJ, Durward QJ *et al.* Treatment of ischemic deficits from vasospasm with intravascular volume expansion and induced arterial hypertension. *Neurosurgery* 1982; **11**: 337–43.

13 Terada T, Komani N, Nayashi S *et al.* Hemorrhagic infarction after vasospasm due to ruptured cerebral aneurysm. *Neurosurgery* 1986; **18**: 415–9.

14 Zubkov YN, Nikiforov BM, Shustin VA. Balloon catheter technique for dilatation of constricted cerebral arteries after aneurysmal subarachnoid hemorrhage. *Acta Neurochir (Wien)* 1984; **70**: 65–79.

15 Higashida RT, Halbach VV, Cahan LD *et al.* Translumінal angioplasty for treatment of intracranial arterial vasospasm. *J Neurosurg* 1989; **71**: 648–53.

16 Klingelhofer J, Dander D, Holzgraefe M, Bischoff C, Conrad B. Cerebral vasospasm evaluated by transcranial Doppler ultrasonography at different intracranial pressures. *J Neurosurg* 1991; **75**: 752–8.

17 Sloan MA, Wozniak MA, Macko RF. Monitoring of vasospasm after subarachnoid hemorrhage. In: Babikian VL, Wechsler LR, eds. *Transcranial Doppler Ultrasonongraphy*, 2nd edn. Boston: Butterworth-Heinemann, 1999: 121.

18 Harders AG, Gilsbach JM. Time course of blood flow velocity changes related to vasospasm in the circle of Willis measured by transcranial Doppler ultrasound. *J Neurosurg* 1987; **66**: 718–28.

19 Seiler RW, Grolimund P, Aaslid R, Huber P, Nornes H. Cerebral vasospasm evaluated by transcranial ultrasound correlated with clinical grade and CT-visualized subarachnoid hemorrhage. *J Neurosurg* 1986; **64**: 594–600.

20 Grosset DG, Straiton J, McDonald I, Cockburn M, Bullock R. Use of transcranial Doppler sonography to predict development of a delayed ischemic deficit after subarachnoid hemorrhage. *J Neurosurg* 1993; **78**: 183–7.

21 Giller CA, Purdy P, Giller A, Batjer HH, Kopitnik T. Elevated transcranial Doppler ultrasound velocities following therapeutic arterial dilation. *Stroke* 1995; **26**: 123–7.

22 Livingston K, Hopkins LN. Intraarterial papaverine as an adjunct to transluminal angioplasty for vasospasm induced by subarachnoid hemorrhage. *Am J Neuroradiol* 1993; **14**: 346–7.

23 Marks MP, Steinberg GK, Lane B. Intra-arterial papaverine for the treatment of vasospasm. *Am J Neuroradiol* 1993; **14**: 822–6.

24 Torbey MT, Hauser TK, Bhardwaj A, Williams MA, Ulatowski JA, Mirski MA, Razumovsky AY. Effect of age on cerebral blood flow velocity and incidence of vasospasm after aneurismal subarachnoid hemorrhage. *Stroke* 2001; **32**: 2005–11.

Bilateral ACA vasospasm after subarachnoid hemorrhage

With Joseph Nates, MD, FCCM

Introduction

Vasospasm in the anterior cerebral arteries (ACAs) typically develops after rupture of the anterior communicating aneurysm [1–10]. It manifests as bilateral narrowing of the A1 ACA segments leading to frontal lobe ischemia. This is often difficult to recognize in drowsy patients, and may cause paraparesis in severe cases [11]. Subtle signs such as cerebral salt wasting syndrome and development of confusion can indicate the development of frontal lobe ischemia along with more obvious signs such as leg-greater-than-arm paresis, diplegia, akinesia and abulia [9,11–15]. However, akinesia and abulia may develop due to hydrocephalus and subarachnoid blood collection without ACA vasospasm.

Transcranial Doppler (TCD) has limited sensitivity for A1 ACA vasospasm and may not be able to detect any flow changes if spasm is located at A2 segments [1–10]. However, a complete insonation protocol and assessment of changes in the middle cerebral artery (MCA), Lindegaard ratio for MCA hyperemia [16] and PCA flow velocity/pulsatility may unmask distal and significant ACA vasospasm. This section illustrates a typical bilateral A1 ACA vasospasm after rupture of the anterior communicating artery aneurysm.

Case presentation

A 42-year-old white female was transferred from a community hospital to our neurointensive care unit (NICU) within 24 h after a sudden onset of the most severe headache of her life. On examination, she was alert and orientated and had no focal neurologic deficits. CT scan showed a round-shaped clot between the frontal poles as well as a diffuse collection of blood in the supratentorial subarachnoid spaces (Fisher grade III subarachnoid hemorrhage). She had a clinical Hunt–Hess grade II subarachnoid hemorrhage (SAH), and diagnostic digital subtraction angiography (DSA) on the day of admission showed a 6-mm anterior communicating artery aneurysm.

Diagnostic considerations

Clinical examination and head CT are consistent with a non-traumatic SAH. DSA showed an aneurysm at a typical location and subsequent vasospasm development can be expected in the ACA distribution. Baseline TCD was performed as soon as feasible to obtain velocity correlation with diagnostic DSA.

Ultrasound findings

Daily TCD monitoring was initiated in the NICU starting postoperatively. Mean flow velocities (MFVs) in the anterior and posterior circulation vessels on Day 1 ranged from 35 to 86 cm/s with pulsatility indices of 0.6–0.9. Daily TCD follow-up showed gradual velocity increase in both ACAs and the right MCA velocities up to 188, 204 and 164 cm/s accordingly on Day 7 (Figure 1). Right MCA/ICA MFV ratio was 2.5, and the left MCA velocity was 55 cm/s.

Interpretation

Baseline TCD on Day 1 showed detectable flows in both A1 ACAs and normal range of the mean flow velocities. Ultrasound findings on Day 7 showed abnormal velocities suggesting high-moderate or severe vasospasm in the ACA distibution. Abnormal right MCA MFV and low Lindegaard ratio suggests compensatory velocity increase in the right MCA.

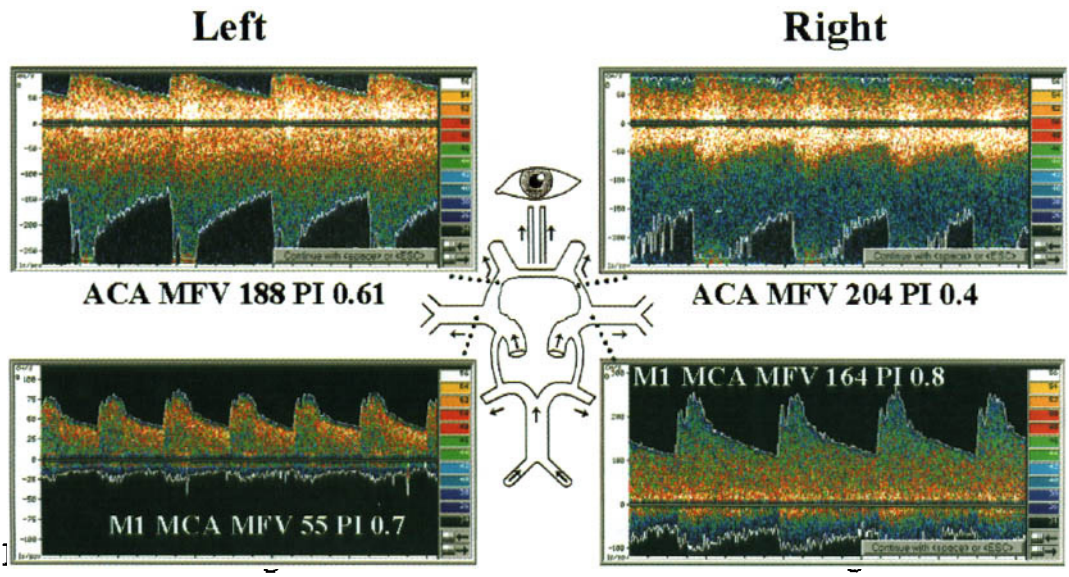

Figure 1 Transcranial Doppler findings in a patient with bilateral anterior cerebral artery vasospasm.

Correlative imaging

Repeat DSA on Day 7 showed a bilateral 'spear-headed' A1 ACA vasospasm more severe in the right ACA, and a mild narrowing in the right terminal internal carotid artery (TICA) compared to baseline DSA images. A four-vessel diagnostic DSA was also repeated at this time and it showed successful clipping of the anterior communicating artery aneurysms as well as no other detectable aneurysm.

Differential diagnosis

This patient had an aneurysm at a typical location that was the most likely source of subarachnoid hemorrhage. This patient was at risk of developing vasospasm due to medium grades of SAH severity and clot burden on CT in a typical location. On Day 4 the patient was noted to be confused, and vasospasm development was suspected.

TCD findings on Day 7 indicate progression to a high-moderate or severe ACA vasospasm or the development of a moderately severe right TICA vasospasm. The latter can produce abnormal right ACA/MCA velocities and elevated left ACA velocities if the contralateral side becomes involved in compensatory flow redistribution similar to anterior cross-filling with ICA obstructions. However, a significant right TICA spasm in this case can be ruled out by a low Lindegaard ratio of 2.5. If both ACAs become affected by significant vasospasm, the remaining pathway to compensate for these lesions is to deliver blood flow via transcortical collaterals from the MCA and PCA territories. TCD may provide indirect signs of this process by showing elevated M1–M2 MCA velocities with low Lindegaard ratio and low pulsatility indices suggesting hyperemia and distal vasodilatation. Taken together with clinical findings, these MCA/PCA velocity changes may sometimes be the only sign of significant A2 ACA vasospasm. Differential diagnosis also includes bilateral ACA vasospasm and mild MCA/TICA spasm that cannot be ruled out completely, yet it may have less clinical significance.

Management

The patient underwent craniotomy and surgical clipping of the aneurysm on Day 1 after SAH. Moderate hypertension–hemodilution–hypervolemia (HHH) therapy (mostly fluid balance and mean arterial pressure maintenance at 110 mmHg) was initiated on Day 4 after TCD detected right ACA and MCA velocity increase above 120 cm/s. TCD showed a further velocity increase that disproportionately

affected both ACAs compared to MCAs. A repeat angiogram on Day 7 confirmed the presence of a bilateral ACA, and balloon angioplasty of A1 segments was performed. Intra-arterial papaverine was injected in the A2 segments but no angioplasty was performed since the degree of vasospasm in these vessels was mild and moderate. There was a good distal contrast opacification of the A2 ACA.

Follow-up

TCD monitoring showed a decrease in the ACAs and right MCA mean flow velocities to 95–130 cm/s range after angioplasty. Moderate HHH therapy was stopped on Day 8. Her confusional state resolved by Day 9. TCD monitoring was discontinued on Day 10, and the patient was transferred from the NICU on same day. She returned to work 5 months after this episode.

References

1 Grolimund P, Seiler RW, Aaslid R, Huber P, Zurbruegg H. Evaluation of cerebrovascular disease by combined extracranial and transcranial Doppler ultrasonongraphy. Experience in 1,039 patients. *Stroke* 1987; **18**: 1018–24.

2 Newell DW, Grady MS, Eskridge JM, Winn HR. Distribution of angiographic vasospasm after subarachnoid hemorrhage: implications for diagnosis by transcranial Doppler ultrasonography. *Neurosurgery* 1990; **27**: 574–7.

3 Langlois O, Rabehenoina C, Proust F, Freger P, Tadie M, Creissard P. Diagnosis of vasospasm: comparison between arteriography and transcranial Doppler. A series of 112 comparative tests. *Neurochirurgie* 1992; **38**: 138–40 [in French].

4 Lennihan L, Petty GW, Fink ME, Solomon RA, Mohr JP. Transcranial Doppler detection of anterior cerebral artery vasospasm. *J Neurol Neurosurg Psychiatry* 1993; **56**: 906–9.

5 Wozniak MA, Rigamonti D, Sloan MA *et al.* Prevalence of anterior circulation vasospasm: a transcranial Doppler study. *Stroke* 1994; **25**: 744 [abstract].

6 Creissard P, Proust F. Vasospasm diagnosis: theoretical sensitivity of transcranial Doppler evaluated using 135 angiograms demonstrating vasospasm. Practical consequences. *Acta Neurochir (Wien)* 1994; **131**: 12–8.

7 Proust F, Hannequin D, Do Marcolino C, Auzou P, Rabehenoina C, Freger P, Creissard P. Vasospasm after rupture of aneurysms of the anterior communicating artery. Sensitivity and specificity of transcranial Doppler. *Neurochirurgie* 1995; **41**: 385–90 [in French].

8 Sloan MA. Transcranial Doppler monitoring of vasospasm after subarachnoid hemorrhage. In: Tegeler CH, Babikian VL, Gomez CR, eds. *Neurosonology*. St Louis: Mosby, 1996: 156–71.

9 Sloan MA, Wozniak MA, Macko RF. Monitoring of vasospasm after subarachnoid hemorrhage. In: Babikian VL, Wechsler LR, eds. *Transcranial Doppler Ultrasonongraphy*, 2nd edn. Boston: Butterworth-Heinemann, 1999: 109–27.

10 Jarus-Dziedzic K, Boguki J, Zub W. The influence of ruptured cerebral aneurysm localization on the blood flow velocity evaluated by transcranial Doppler ultrasonongraphy. *Neurol Res* 2001; **23**: 23–8.

11 Greene KA, Marciano FF, Dickman CA, Coons SW, Johnson PC, Mailes JE, Spetzler RF. Anterior communicating artery paraparesis syndrome: clinical manifestations and pathologic correlates. *Neurology* 1995; **45**: 45–50.

12 Berendes E, Scherer R, Schuricht G, Rol R, Hengst K. Massive natriuresis and polyuria after triple craniocervical subarachnoid hemorrhage: cerebral salt wasting syndrome? *Anasthesiol Intensivmed Notfallmed Schmerzther* 1992; **27**: 445–8 [in German].

13 Sayama T, Inamura T, Matsushima T, Inoha S, Inoue T, Fukui M. High incidence of hyponatremia in patients with ruptured anterior communicating artery aneurysms. *Neurol Res* 2000; **22**: 151–5.

14 Sviri GE, Feinsod M, Soustiel JF. Brain natriuretic peptide and cerebral vasospasm in subarachnoid hemorrhage. Clinical and TCD correlations. *Stroke* 2000; **31**: 118–22.

15 Harrigan MR. Cerebral salt wasting syndrome. *Crit Care Clin* 2001; **17**: 125–38.

16 Lindegaard KF. The role of transcranial Doppler in the management of patients with subarachnoid haemorrhage: a review. *Acta Neurochir Suppl* 1999; **72**: 59–71.

Multiple vessel vasospasm after subarachnoid hemorrhage

With Ioannis Christou, MD

Introduction

Most studies of transcranial Doppler (TCD) performance in vasospasm detection have focused on the middle cerebral artery (MCA), terminal internal carotid artery (TICA), anterior cerebral artery (ACA) and vertebrobasilar arteries [1–5]. Fewer data are available for posterior cerebral artery (PCA) vasospasm [6], and grading the severity of multiple vessel spasm remains uncertain. Further issues that may complicate vasospasm detection, follow-up and grading are:

1 involvement of distal branches not directly accessible by TCD [3];

2 late, bimodal or recurrent vasospasm development [7];

3 superimposition of flow changes due to infections that may complicate prolonged ICU stays in severe subarachnoid hemorrhage or HHH therapies [8]; and

4 development of hydrocephalus, anemia and myocardial dysfunction.

Case presentation

A 55-year-old white female was admitted to hospital 12 h after a sudden onset of the most severe headache of her life. On examination, she was alert and orientated and no focal neurologic deficits were found. A Hunt–Hess grade II subarachnoid hemorrhage (SAH) was suspected. Computed tomography (CT) scan showed diffuse collection of blood in the subarachnoid spaces and basal cisterns (Fisher grade II SAH). The patient was admitted to the neurointensive care unit (NICU), and baseline TCD was performed prior to diagnostic angiography.

Diagnostic considerations

Clinical examination and head CT are consistent with a non-traumatic SAH. Digital subtraction angiography (DSA) was performed next. Baseline TCD was performed as soon as was feasible to obtain velocity correlation with diagnostic DSA.

Ultrasound findings

A single-channel TCD was performed in the NICU. TCD showed a normal range of velocities in the anterior and posterior circulation vessels. The right vertebral artery had an alternating flow signal with a high-resistance spike directed towards the probe (Figure 1). The left vertebral artery had a low-resistance antegrade flow, while its branch (likely posterior inferior cerebellar artery, PICA) had a much higher flow resistance. The basilar artery (BA) had a normal flow direction and low-resistance flow.

Interpretation

Baseline TCD showed no evidence of vasospasm or global increase in flow pulsatility. A left-to-right steal phenomenon and high-resistance flow in a cerebellar branching artery were noted and the neuroradiology service was informed of these findings.

Correlative imaging

DSA showed a left PICA aneurysm that received flow from a reversed right terminal vertebral artery (VA) (Figure 2). This flow reversal was likely responsible for the 'steal-like' appearance of the VA flow signals. The terminal right VA and PICA appear smaller in diameter than the donor left vertebral artery. Aneurysm detection was not possible from a proximal right VA injection due to its uniformly small diameter extracranially and the first left VA injection did not clearly show the aneurysm. The

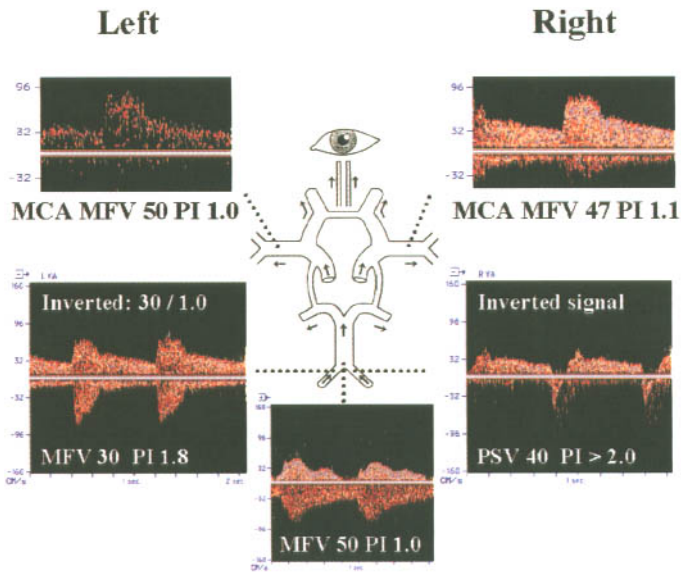

Figure 1 Baseline transcranial Doppler findings before diagnostic angiography

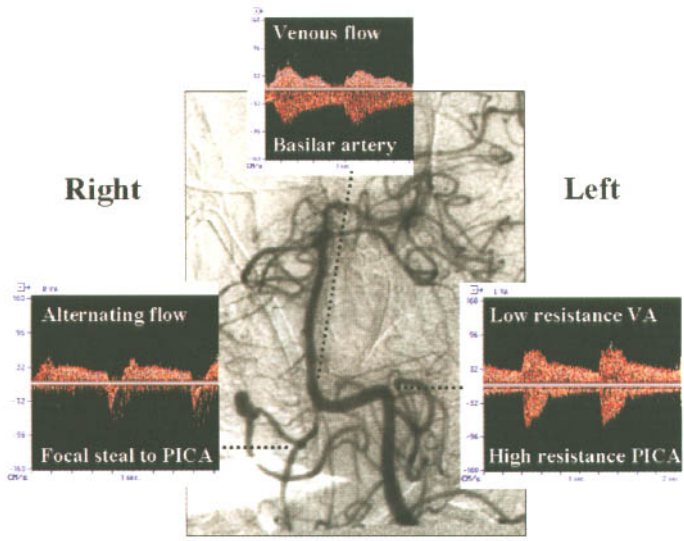

Figure 2 Transcranial Doppler waveforms, retrograde filling of the right vertebral artery and posterior inferior cerebellar artery aneurysm.

interventional neuroradiologist knew about the steal phenomenon detected by TCD and repeated selective left VA injection with more volume of contrast. The aneurysm was clearly visualized during late arterial phase in the contralateral cerebellar hemisphere.

Differential diagnosis

This is a relatively uncommon location for an intracranial aneurysm; however, no other aneurysms were found with a four-vessel DSA. The smaller diameter of the right VA and PICA may be attributed to hypoplasia since it is uncommon to see vasospasm as early as Day 1 after SAH and there were no focal velocity elevations in the terminal VAs. Also, this patient did not have a complete steal towards the subclavian artery and her right VA was barely visible at its proximal portion extracranially. This flow pattern likely existed even before the hemorrhage, since a selective left VA contrast injection opacified both cerebellar hemispheres.

Management

The patient underwent craniotomy and surgical clipping of the aneurysm on Day 2 after SAH. Repeat TCD examination showed no steal-like flow waveforms in the posterior circulation. Instead, a low-resistance flow towards the transducer was found at the depths of the terminal right VA suggesting transcerebellar collateralization of flow. Daily TCD monitoring started on Day 3, and on Day 5 it showed no evidence of proximal spasm and hyperemic flow velocities (range 77–104 cm/s) throughout the circle of Willis (Figure 3). TCD monitoring continued after the 2nd week after SAH since the patient continued to have severe headache and slowly developed even higher velocities. She received HHH therapy during the observation period. On Day 16, she became drowsy and her velocities reached maximum observed values: ACA 222 cm/s, PCA 130 cm/s, BA 109 cm/s (Figure 4). Note that the patent vertebral artery and both MCAs had elevated velocities: LVA 82 cm/s, LMCA 103 cm/s and RMCA 132 cm/s. The left VA had elevated velocities because it was the main supply of the posterior circulation flows in a patient receiving HHH therapy, and therefore its absolute velocity is high and a modified Lindegaard index for basilar vasospasm is falsely low in this situation [4,5]. The finding of bilaterally elevated MCA velocities and low Lindegaard ratios may reflect compensatory velocity increase and it may sometimes be the only indirect evidence of the vasospasm in the basilar artery. Based on clinical and TCD findings, the decision was made to repeat DSA.

DSA was performed on Day 16 after SAH. The anteroposterior projection did not show any right ACA spasm (Figure 5) due to overlapping vessels. The neuroradiologist was informed about abnormal TCD findings in the right ACA (MFV 222 cm/s), and several additional oblique shots were performed that helped to visualize a severe right A1 ACA spasm at its origin (Figure 5, arrow). However, relatively good contrast opacification of the distal ACA was seen despite this narrowing.

The basilar artery and left PCA had moderately severe vasospasm that involved the entire basilar and P1 stems (Figure 6). This length of arterial

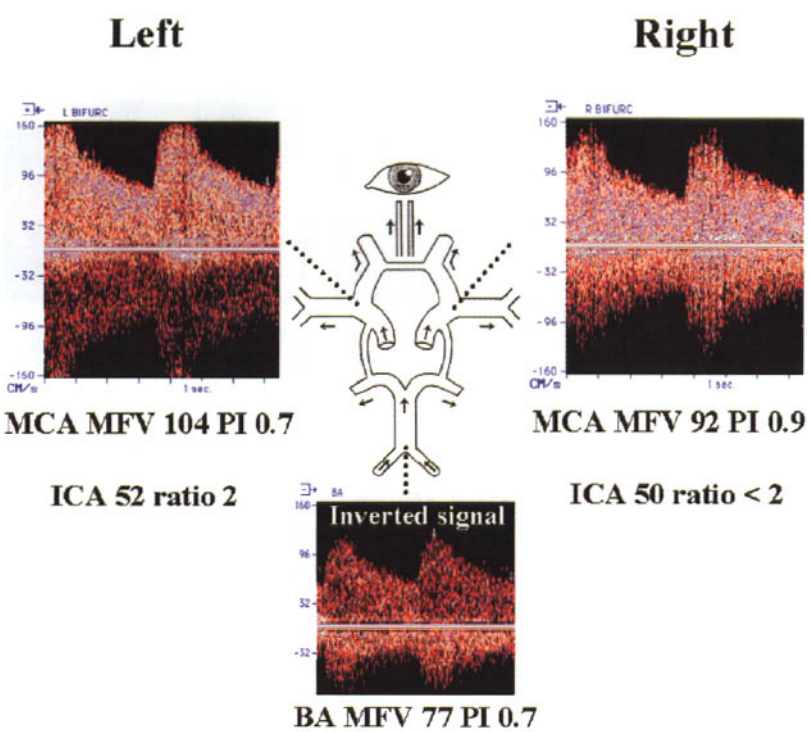

Figure 3 Hyperemic changes on transcranial Doppler.

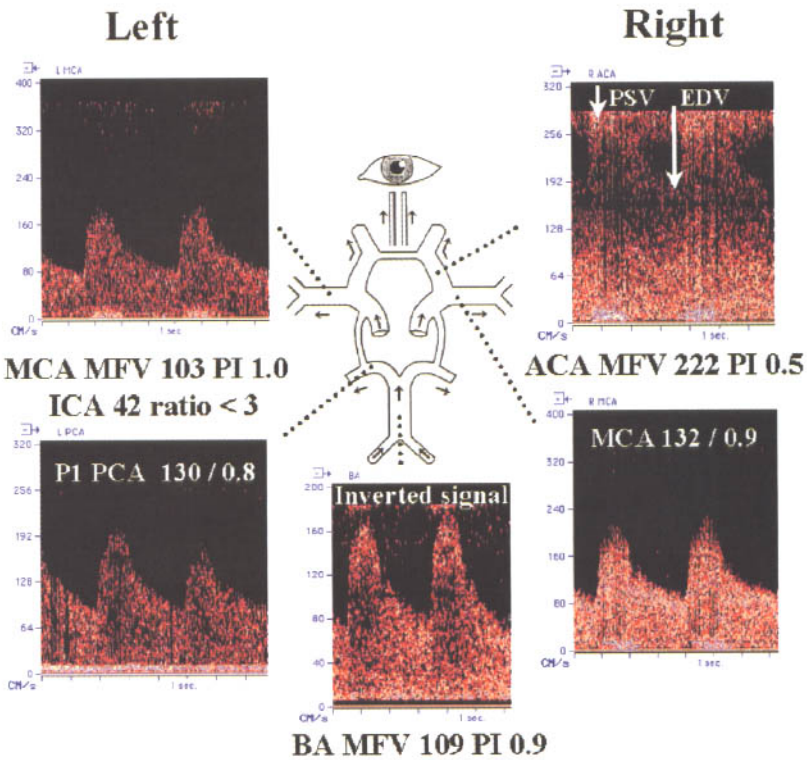

Figure 4 Abnormal transcranial Doppler velocities in multiple vessels.

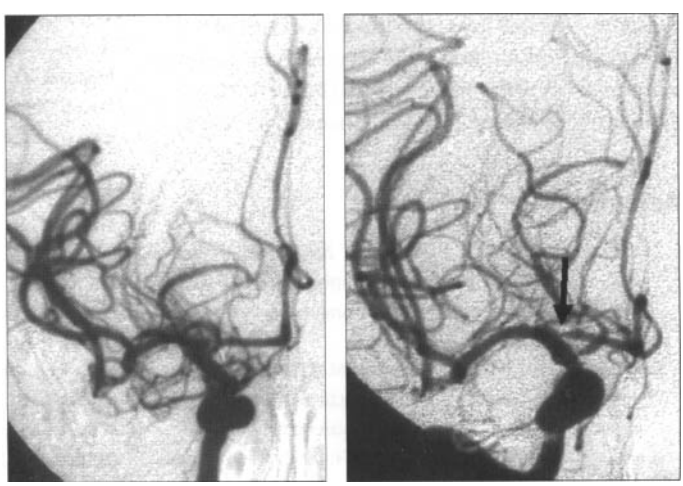

Figure 5 Projection-dependent digital subtraction angiography findings.

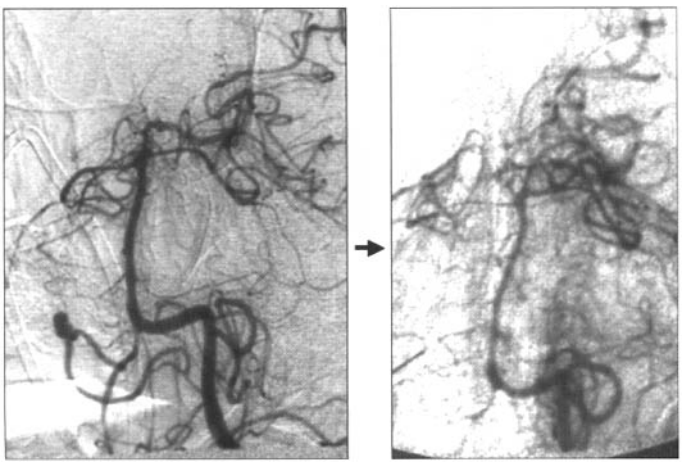

Figure 6 Basilar artery vasospasm (right) compared to baseline image (left).

narrowing resulted in relatively low TCD velocities in these vessels.

A successful balloon angioplasty was performed for the basilar artery up to the distal portion. Intra-arterial papaverine was administered for the PCA and ACA spasm locations.

Follow-up

The next day TCD showed decrease in the mean flow velocities: ACA 150 cm/s, PCA 92 cm/s, MCAs 102–107 cm/s. The basilar artery velocity decreased to 90 cm/s representing hyperemic flow with a basilar-to-vertebral velocity ratio of less than 1/1.5. The patient had no neurologic sequelae and she was transferred out of the NICU on Day 18 after SAH. At 6 months, she remained free of focal neurologic deficits.

References

1 Lysakowski C, Walder B, Costanza MC, Tramer MR. Transcranial Doppler versus angiography in patients with vasospasm due to ruptured cerebral aneurysm. A systematic review. *Stroke* 2001; **32**: 2292–8.

2 Sloan MA, Burch CM, Wozniak MA, Rothman MI, Rigamonti D, Permutt T, Numaguchi Y. Transcranial Doppler detection of vertebrobasilar vasospasm following subarachnoid hemorrhage. *Stroke* 1994; **25**: 2187–97.

3 Newell DW, Grady MS, Eskridge JM, Winn HR. Distribution of angiographic vasospasm after subarachnoid hemorrhage: implications for diagnosis by transcranial Doppler ultrasonography. *Neurosurgery* 1990; **27**: 574–7.

4 Sloan MA, Zagardo T, Wozniak MA *et al.* Sensitivity and specificity of flow velocity ratios for the diagnosis of vasospasm after subarachnoid hemorrhage: preliminary report. In: Klingelhofer J, Bartles E, Ringelstein EB, eds. *New Trends in Cerebral Hemodynamics and Neurosonology*. Amsterdam: Elsevier, 1997: 221–7.

5 Soustiel JF, Shik V, Shreiber R, Tavor Y, Goldsher D. Basilar vasospasm diagnosis: investigation of a modified 'Lindegaard Index' based on imaging studies and blood velocity measurements of the basilar artery. *Stroke* 2002; **33**: 72–7.

6 Wozniak MA, Sloan MA, Rothman MI, Burch CM, Rigatoni D, Permutt T, Numaguchi Y. Detection of vasospasm by transcranial Doppler sonography. The challenges of the anterior and posterior cerebral arteries. *J Neuroimaging* 1996; **6**: 87–93.

7 Numaguchi Y, Zoarski GH, Clouston JE, Zagardo MT, Simard JM, Aldrich EF, Cloan MA, Maurer PK, Okawara SH. Repeat intra-arterial papaverine for recurrent cerebral vasospasm after subarachnoid hemorrhage. *Neuroradiology* 1997; **39**: 751–9.

8 Sloan MA, Wozniak MA, Macko RF. Monitoring of vasospasm after subarachnoid hemorrhage. In: Babikian VL, Wechsler LR, eds. *Transcranial Doppler Ultrasonongraphy*, 2nd edn. Boston: Butterworth-Heinemann, 1999: 109–27.

Cerebral circulatory arrest

With Sergio Calleja, MD

Introduction

Brain death is a clinical diagnosis [1] and transcranial Doppler (TCD) can be used as a confirmatory tool [2,3]. Although TCD detection of oscillating flow pattern in major intracranial arteries may yield accuracy parameters close to 100% at experienced centers [3–5], false-positive TCD findings may occur and a subsequent nuclear flow scanning may reveal some residual parenchymal flow. Although this discrepancy may not affect the grave prognosis of patients with the clinical appearance of brain death, a more careful and often extended TCD examination should be performed to avoid these false-positive results.

Case presentation

A 39-year-old woman was admitted to the neurointensive care unit (NICU) with the diagnosis of Hunt–Hess grade IV subarachnoid hemorrhage (SAH). On Day 3 she was intubated and wide dilated pupils were noted on Day 4. Clinical examination on Day 5 was consistent with brain death.

Diagnostic considerations

Patients with severe grades of SAH have overall poor prognosis and increased mortality due to development of coma, vasospasm and hydrocephalus. These patients may progress to severe spasm and brain infarction before Day 7. TCD was ordered to confirm brain death after the clinical examination showed no brainstem reflexes and failed apnea test.

Ultrasound findings

As shown in Figure 1, TCD was performed according to our standard protocol for evaluation of patients with brain death. It includes assessment of the mid-M1 middle cerebral artery (MCA) flow and the proximal basilar artery flow. All three segments had reverberating (or oscillating) flow patterns.

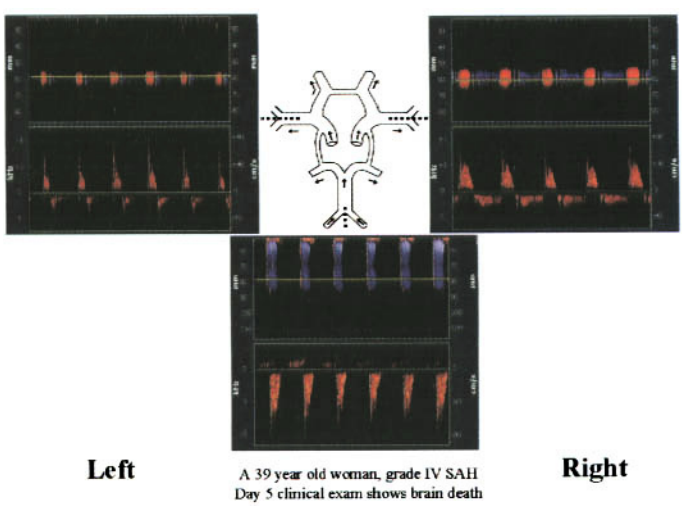

Figure 1 Spectral transcranial Doppler and M-mode findings in both M1 MCA stems and the proximal basilar artery in a patient with clinical examination consistent with brain death.

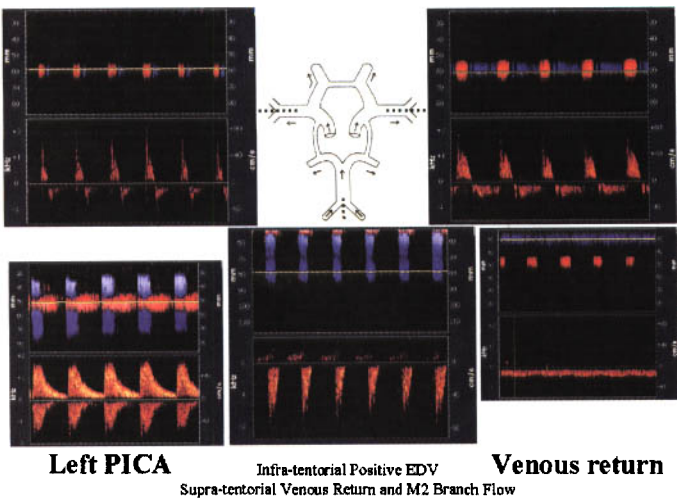

Figure 2 Spectral transcranial Doppler (TCD) and M-mode findings showing residual flow to the posterior inferior cerebellar artery (bottom left image insert), and positive venous return due to antegrade flow in an early M2 MCA branch (M-mode, bottom right image). These findings help explain a discrepancy between nuclear cerebral blood flow test and initial TCD examination.

Interpretation

TCD examination of both M1 MCAs and the proximal basilar artery was consistent with cerebral circulatory arrest at the blood pressure values of 125/60 mmHg.

Correlative imaging

Nuclear flow scan was performed at the bedside 30 min later with patient blood pressure remaining stable. It showed residual parenchymal perfusion of supratentorial structures and cerebellar hemispheres.

Differential diagnosis

At this point, incomplete arrest of cerebral circulation was diagnosed. Since the patient had non-traumatic SAH, and no surgical clipping was performed, there was no reason to suspect decompression as a possible cause of residual flow. The Camino catheter showed a minimally pulsatile waveform with intracranial pressure values of 95 mmHg in closed position. There was no cerebrospinal fluid draining in open position. All these findings suggest that residual flow seen on the nuclear flow scan occurred despite increased intracranial pressure exceeding cerebral perfusion pressure.

Management

Repeat TCD was ordered to identify the reason for false-positive findings and to detect possible sources of the residual parenchymal flow. A recommendation was made to hold the organ-harvesting protocol until confirmation of a complete cerebral circulatory arrest.

Follow-up

TCD examination was performed shortly after the nuclear flow scan and it was expanded to the MCA branches, terminal ICAs and terminal vertebral arteries. TCD showed a high-resistance waveform with positive diastolic flow in the posterior inferior cerebellar artery (PICA) and a detectable venous return in the Sylvian fissure from a transtemporal window (Figure 2). These findings indicate that the patient was evaluated early into progression of the cerebral circulatory arrest. Even though the proximal basilar artery was already affected by oscillating flow, the arrest of infratentorial circulation was still incomplete since the terminal vertebral artery branch (PICA) still had a positive diastolic flow. The arrest of supratentorial circulation was also incomplete since detectable venous return was found through the temporal window. It may occur if the MCA has early branches that are not yet affected by oscillating flow, or flow cessation is incomplete in the ACA or PCA. In this case, M-mode TCD shows a high-resistance systolic signal in the M2 MCA on the side of venous return (Figure 2, bottom right insert). Therefore, TCD examination in patients with brain death can be broadened by application of M-mode Doppler to examine branch segments in addition to major targets.

However, the presence of reverberating flow signals in the proximal MCAs and basilar artery over 30 min indicates irreversible ischemia to vital centers and grave prognosis. The impact of detection of residual parenchymal flow in this case was to delay organ harvesting by 12 h. Repeat TCD and nuclear flow scans at this time showed no positive diastolic flow or venous return and no parenchymal residual flow.

References

1 Wijdicks EF. The diagnosis of brain death. *N Engl J Med* 2001; **344** (16): 1215–21.

2 Babikian VL, Feldmann E, Wechsler LR, Newell DW, Gomez CR, Bogdahn U, Caplan LR, Spencer MP, Tegeler CH, Ringelstein EB, Alexandrov AV. Transcranial Doppler ultrasonography: year 2000 update. *J Neuroimaging* 2000; **10**: 101–15.

3 Ducrocq X, Hassler W, Moritake K, Newell DW, von Reutern GM, Shiogai T, Smith RR. Consensus opinion on diagnosis of cerebral circulatory arrest using Doppler-sonography: Task Force Group on cerebral death of the Neurosonology Research Group of the World Federation of Neurology. *J Neurol Sci* 1998; **159**: 145–50.

4 Petty GW, Mohr JP, Pedley TA, Tatemichi TK, Lennihan L, Duterte DI, Sacco RL. The role of transcranial Doppler in confirming brain death: sensitivity, specificity, and suggestions for performance and interpretation. *Neurology* 1990; **40** (2): 300–3.

5 Ducrocq X, Braun M, Debouverie M, Junges C, Hummer M, Vespignani H. Brain death and transcranial Doppler: experience in 130 cases of brain dead patients. *J Neurol Sci* 1998; **160** (1): 41–6.

Anatomic variation or a hemodynamically significant lesion?

With Eva Bartels, MD

Introduction

Sonographers and interpreting physicians usually have no problem recognizing clearly abnormal flow findings such as peak systolic velocity (PSV) of 300 cm/s in the proximal internal carotid artery (ICA) with carotid stenosis, or alternating flow signal in the vertebral artery with subclavian steal. These findings have excellent accuracy parameters in predicting pathologic findings on angiography [1–3]. However, in many patients ultrasound shows changes in flow velocity or waveforms, or on color flow images that are of marginal clinical significance, if any. This is the area where sonographers' experience and interpreters' knowledge become very important. In these cases, ultrasound interpretation will benefit from additional information that should be made available, i.e. clinical findings, magnetic resonance imaging (MRI) or computed tomography (CT) results or previous angiography, etc. This section illustrates clinical decision-making in a patient with 'soft' ultrasound findings.

Case presentation

This is a 65-year-old man who complains of newly developed several dizzy spells during the past month. He has experienced brief episodes of dizziness, lightheadedness and unsteadiness when rising quickly from a chair or when turning his head. Risk factors include chronic hypertension and smoking (he quit 3 years ago). He has not previously had a stroke or heart attack and his MRI brain scan was unremarkable.

Diagnostic considerations

Besides common causes of dizziness such as inner ear disease and syncope, the patient history points to a recent process linked to blood pressure, postural changes and neck rotation. Screening for an underlying vascular disease in the vertebrobasilar distribution seems justified.

Ultrasound findings

As shown in Figure 1, his terminal left vertebral artery has normal-flow waveforms and velocities (upper image and spectrum). Note that the velocity values were obtained using angle correction. His extracranial right vertebral artery has a high-resistance waveform (middle image and spectrum) with end diastolic flow being present but with low diastolic velocities. The transcranial color imaging (TCI) study shows flow in the right posterior communicating artery directed towards posterior circulation (bottom image). No focal extra- or intracranial stenoses were found and the rest of the ultrasound examination was unremarkable.

Interpretation

A high-resistance flow in the right vertebral artery is due to probable hypoplasia, dominant left vertebral artery, and functioning right posterior communicating artery (PComA).

Correlative imaging

MR angiography showed a small caliber of the entire

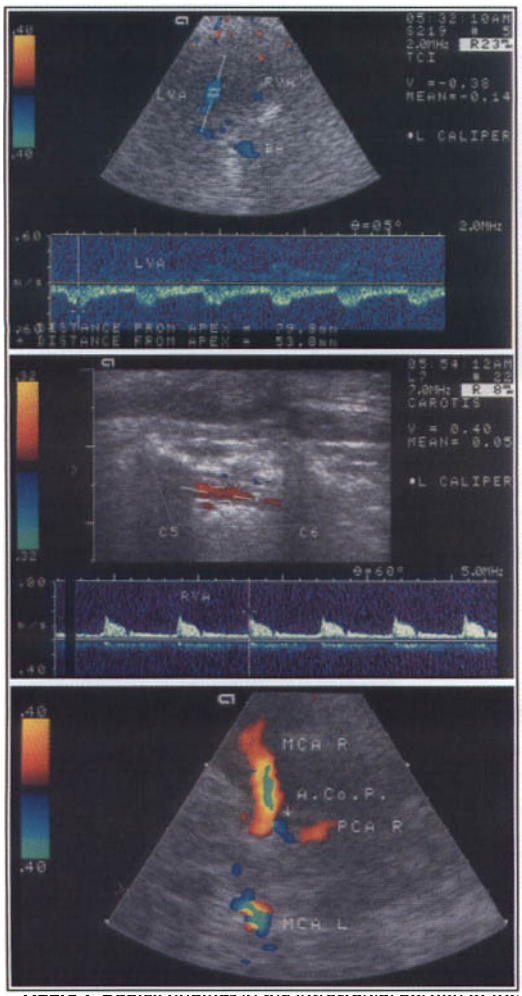

left vertebral artery (upper image); cervical portion (C5–C6 segments) of the right vertebral artery (middle image); and a functional right posterior communicating artery (A.Co.P) (bottom image).

right vertebral artery with no areas of flow void and a normal patency of the left vertebral artery. Posterior communicating arteries were present bilaterally. No previous strokes were visualized in the posterior circulation territories. Mild periventricular white matter changes were noted.

Differential diagnosis

A hemodynamically significant obstruction of the vertebral artery can produce a high-resistance waveform proximal to the lesion. Occlusions or dissections of the vertebral artery (VA) can be segmental with reconstituted flow in the terminal portion [4–10]. Note that terminal right VA flow is seen on the upper duplex image.

Hypoplasia of the vessel wall is a morphologic diagnosis, and in the clinical setting the term usually refers to a benign and uniform vessel narrowing. A small caliber of the entire vessel can produce a high-resistance waveform [4,6,9,10]. Doppler findings in this case are more consistent with hypoplasia since blood flow was found in all accessible extra- and intracranial segments of the right vertebral artery with similar waveforms as shown in the middle spectrum. Since no previous ultrasound examination is available, it is impossible to determine whether the patient had this condition before symptom onset (anatomic variation) or symptoms developed after new flow changes in the right vertebral artery.

The presence of a functional PComA may indicate hemodynamically significant obstruction in the dominant vertebral artery. However, in this case, the left vertebral artery has a low-resistance waveform and the basilar artery is filled with normal flow direction. The presence of a PComA may simply be attributable to the variable anatomy of the circle of Willis, when the posterior cerebral artery (PCA) may originate from the ICA (so called 'fetal' origin) [11]. The finding of a functioning right PComA may speculatively be attributed to:

1 transient compressions of the dominant left vertebral artery by an osteophyte with neck movement; or
2 to compensate for flow decrease in the posterior circulation with postural changes.

To confirm the first hypothesis, the PCA can be monitored using a headframe-fixed transcranial Doppler (TCD) transducer (Figure 2) [12]. The second hypothesis can be investigated using TCD monitoring with tilt table testing that may reveal a variety of responses, including mean flow velocity reduction or abnormal vasoconstriction [13–17].

However, the posterior circulation symptoms may also develop not only in patients with obstructed vertebral arteries (due to atherosclerosis or healing dissection or hypoplasia) but also in those who have recently switched their blood pressure-lowering medications and have lower than usual BP values. This patient had a BP of 165/95 prior to the time when the primary care doctor changed his medications

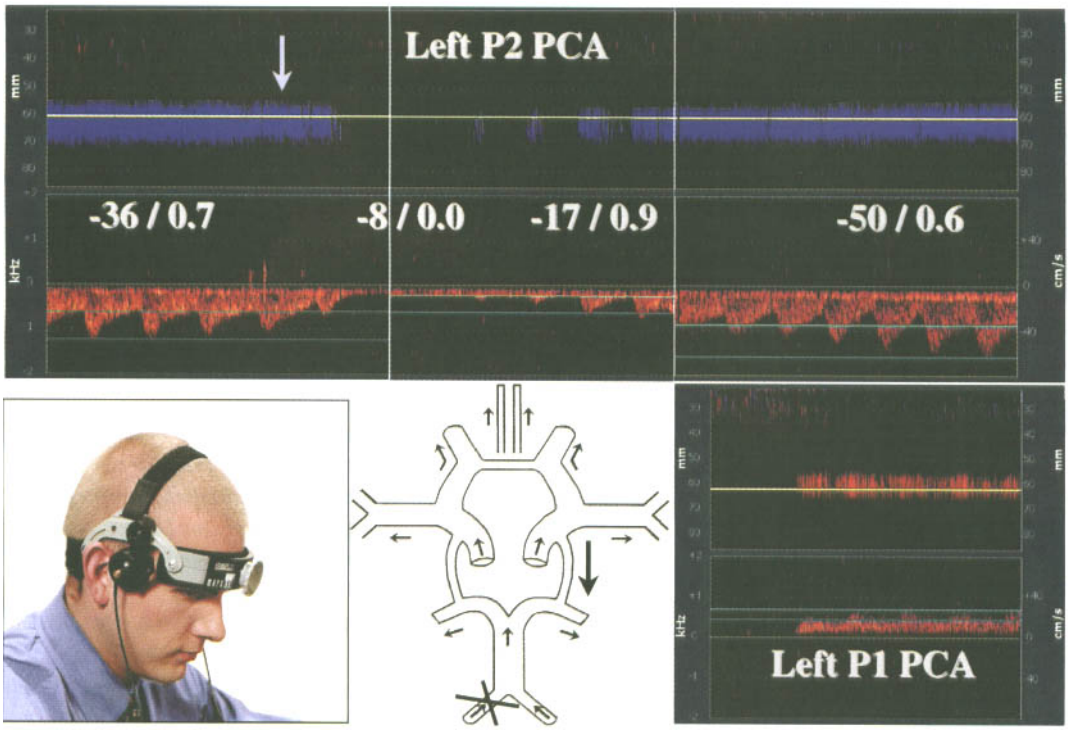

Figure 2 Sequential motion-mode and spectral transcranial Doppler recordings from P2 posterior cerebral artery during a true positive test for vertebral artery compression with head turning. Numbers indicate mean flow velocities/pulsatility (Gosling & King) indices. Arrow indicates head turn.

and achieved BP values of 150/85. The symptoms of dizziness and lightheadedness started a week later. Other factors such as reduced cardiac output, dehydration, etc. may also contribute to development of these symptoms.

Management

A recommendation was made to optimize antihypertensive medication, including potentially switching back to the ACE inhibitor and diuretic that the patient was receiving prior to symptom onset, a combination previously shown to be effective in reducing stroke risk [18]. The patient also started to take a low-dose aspirin daily.

Follow-up

Systolic and diastolic arterial BP values re-established at 160/90 mmHg, achieving approximately 10/5 mmHg BP reduction and the episodes of dizziness became less frequent. The blood pressure was cautiously lowered further over several months to achieve 140/90 mmHg values without further symptoms.

References

1 Hunink MG, Polak JF, Barlan MM, O'Leary DH. Detection and quantification of carotid artery stenosis: efficacy of various Doppler velocity parameters. *Am J Roentgenol* 1993; **160**: 619–25.

2 deBray JM, Glatt B. Quantitation of atheromatous stenosis in the extracranial internal carotid artery. *Cerebrovasc Dis* 1995; **5**: 414–26.

3 Ackerstaff RG, Hoeneveld H, Slowikowski JM, Moll FL, Eikelboom BC, Ludwig JW. Ultrasonic duplex scanning in atherosclerotic disease of the innominate, subclavian and vertebral arteries. A comparative study with angiography. *Ultrasound Med Biol* 1984; **10** (4): 409–18.

4 Reutern GM, Budingen HJ, Freund HJ. The diagnosis of obstructions of the vertebral and subclavian arteries by means of directional Doppler sonography. *Arch Psychiatr Nervenkr* 1976; **222** (2–3): 209–222 [in German].

5 Bartels E. Duplex sonography of the vertebral arteries. 2. Clinical application. *Ultraschall Med* 1991; **12** (2): 63–9 [in German].

6 Bartels E, Fuchs HH, Flugel KA. Duplex ultrasonography of vertebral arteries: examination, technique, normal values, and clinical applications. *Angiology* 1992; **43** (3 Part 1): 169–80.

7 Bartels E, Flugel KA. Evaluation of extracranial vertebral artery dissection with duplex color-flow imaging. *Stroke* 1996; **27** (2): 290–5.

8 de Bray JM, Penisson-Besnier I, Dubas F, Emile J. Extracranial and intracranial vertebrobasilar dissections: diagnosis and prognosis. *J Neurol Neurosurg Psychiatry* 1997; **63** (1): 46–51.

9 Lovrencic-Huzjan A, Demarin V, Bosnar M, Vukovic V, Podobnik-Sarkanji S. Color Doppler flow imaging (CDFI) of the vertebral arteries—the normal appearance, normal values and the proposal for the standards. *Coll Antropol* 1999; **23** (1): 175–81.

10 Oder B, Oder W, Lang W, Marschnigg E, Deecke L. Hypoplasia, stenosis and other alterations of the vertebral artery: does impaired blood rheology manifest a hidden disease? *Acta Neurol Scand* 1998; **97** (6): 398–403.

11 McCartney JP, Thomas-Lukes KM, Gomez CR. *Handbook of Transcranial Doppler*. New York: Springer, 1997: 10.

12 Sturzenegger M, Newell DW, Douville C, Byrd S, Schoonover K. Dynamic transcranial Doppler assessment of positional vertebrobasilar ischemia. *Stroke* 1994; **25** (9): 1776–83.

13 Briebach T, Fischer PA. Circulation studies and transcranial Doppler sonography in orthostatic regulation disorders. *Ultraschall Med* 1988; **9**: 223–6 [in German].

14 Hughson RL, Edwards MR, O'Leary DD, Shoemaker JK. Critical analysis of cerebrovascular autoregulation during repeated head-up tilt. *Stroke* 2001; **32** (10): 2403–8.

15 Bondar RL, Dunphy PT, Moradshahi P, Dai H, Kassam MS, Stein F, Schneider S, Rubin M. Vertical shift in cerebral autoregulation curve: a graded head-up tilt study. *Can Aeronaut Space J* 1999; **45** (1): 3–8.

16 Carey BJ, Manktelow BN, Panerai RB, Potter JF. Cerebral autoregulatory responses to head-up tilt in normal subjects and patients with recurrent vasovagal syncope. *Circulation* 2001; **104** (8): 898–902.

17 Grubb BP, Samoil D, Kosinski D, Wolfe D, Brewster P, Elliott L, Hahn H. Cerebral syncope: loss of consciousness associated with cerebral vasoconstriction in the absence of systemic hypotension. *Pacing Clin Electrophysiol* 1998; **21** (4 Part 1): 652–8.

18 PROGRESS Collaborative Group. Randomised trial of a perindorpil-based blood-pressure-lowering regimen among 6105 individuals with previous stroke or transient ischemic attack. *Lancet* 2001; **358**: 1033–41.

Subclavian steal

With Fahmi Al-Senani, MD

Introduction

Subclavian steal can be found in older patients with widespread atherosclerosis [1–3]. It manifests with an alternating flow signal in one of the vertebral arteries at rest (Figure 1) or can be augmented during hyperemia cuff test [1–5]. Since subclavian steal is rarely symptomatic, most patients have antegrade low-resistance flow in the basilar artery [5–7] despite flow reversal in one of the terminal vertebral arteries (Figure 1). The low-resistance flow in the basilar artery comes from the donor vertebral artery that feeds both the brain and contralateral arm.

Case presentation

An 86-year-old white female with past medical history of hypertension, coronary artery bypass surgery and peripheral vascular disease has been followed for several years in an outpatient clinic and vascular laboratory. She has 30–49% bilateral carotid stenoses and subclavian steal present at rest. After leaving her at home alone for a weekend, her relatives find her weak and confused and bring her to the emergency room. Upon arrival, the patient was afebrile and free of chest pain, and a 12-lead electrocardiogram (ECG) was normal. At examination, she is drowsy and has a

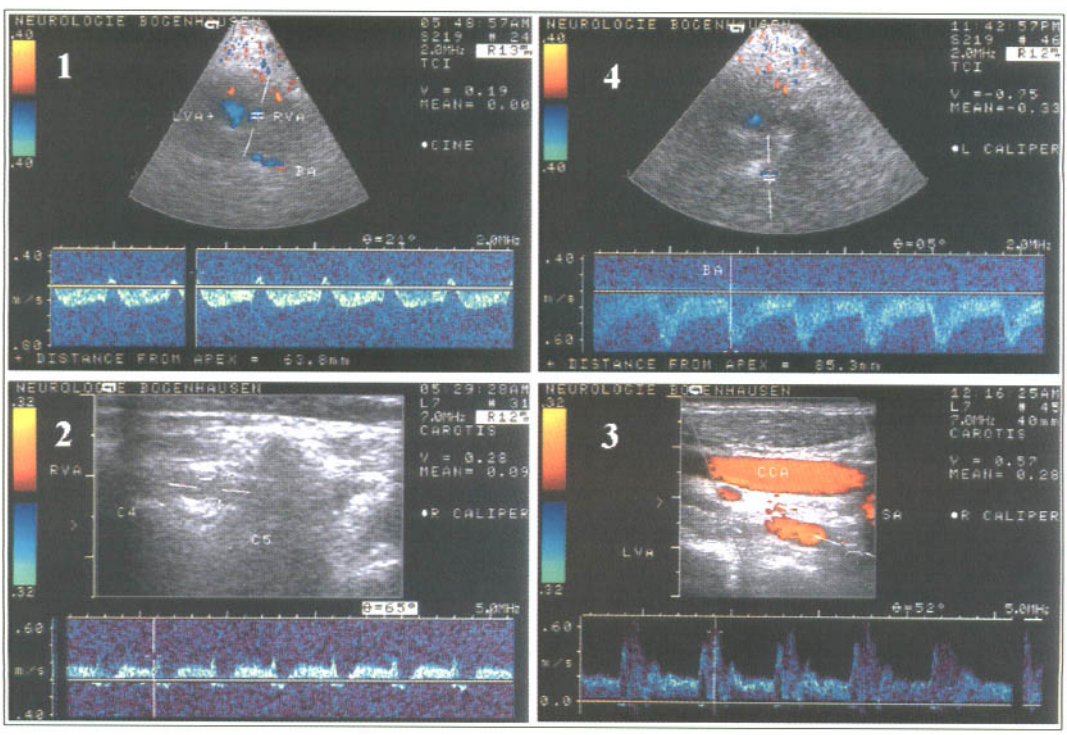

Figure 1 Color duplex findings in subclavian steal. (Upper images) Transcranial duplex findings in the left and right terminal vertebral arteries. (Lower images) Extracranial duplex findings in midcervical segments of the vertebral arteries. (Images courtesy of Dr Eva Bartels.)

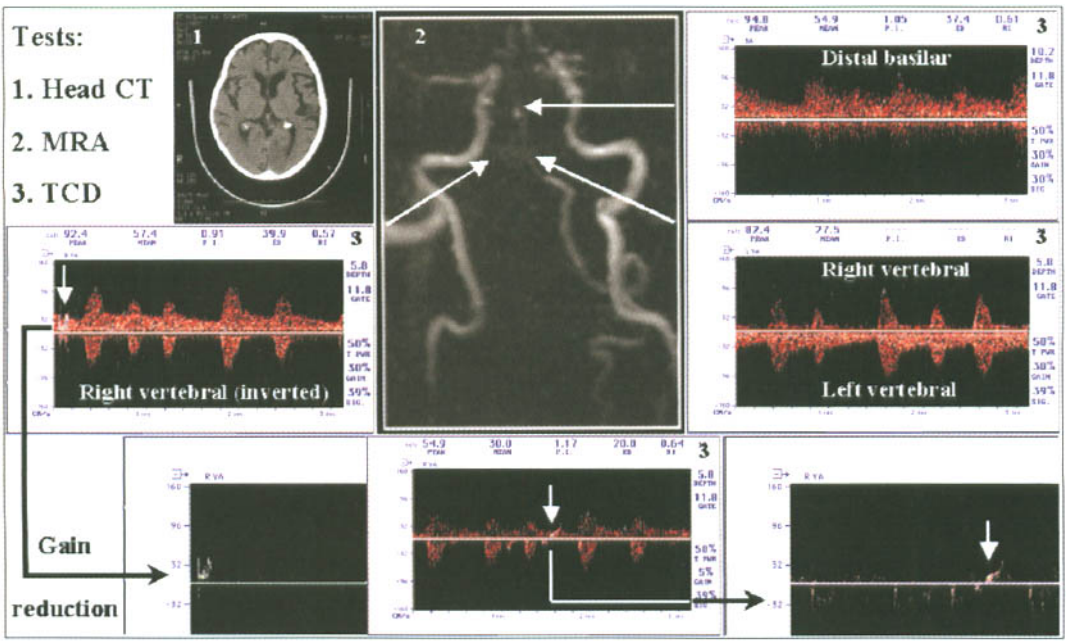

Figure 2 Computed tomography, magnetic resonance imaging and transcranial Doppler findings in an 86-year-old white woman. See text for case presentation and interpretation of findings.

new-onset hemianopsia. A non-contrast computed tomogram (CT) shows an ischemic stroke with hypoattenuation of brain tissues in the left occipital lobe (Figure 2, image 1).

Diagnostic considerations

Clinical examination and head CT are consistent with a 24–48-h-old cortical cerebral infarct in the left occipital lobe. The stroke pathogenic mechanism is probably embolic, either from an atherosclerotic lesion in the basilar or vertebral artery (artery-to-artery embolism) or from another source, i.e. heart or aortic arch. Bedside ultrasound was ordered to rapidly determine patency of the basilar artery as well as to monitor for emboli, and to confirm steal pattern.

Ultrasound findings

A single-channel non-image-guided transcranial Doppler (TCD) was performed on admission. TCD showed transient episodes of irregular heart rhythm. Multiple (up to 12/min) embolic signals (Figure 2, image 3, white arrows) were heard during routine TCD examination. The basilar artery had a low-resistance flow with unremarkable velocities. A high-resistance waveform with flow direction towards the probe was found in the right vertebral artery.

Interpretation

TCD interpretation:

1 Irregular heart rhythm (paroxysmal atrial fibrillation?).

2 Multiple brain microemboli detected in the vertebrobasilar system with frequency of up to 12/min. These emboli likely originate from a proximal source (likely heart) since emboli were heard in the left vertebral and both carotid arteries.

3 No evidence for a stenosis in the basilar artery stem.

4 A left-to-right subclavian steal phenomenon present at rest.

Correlative imaging

Magnetic resonance angiography (MRA) shows no flow in the right vertebral artery due to its reversed direction (note that venous flow is subtracted with time-of-flight MRA unless special sequencing is employed). The terminal left vertebral artery and basilar artery have areas of attenuated signal likely due to artifacts and suboptimal image reconstruction.

Differential diagnosis

Just after clinical examination and head CT scan, TCD provided real-time evidence of brain embolization, confirming that our patient had an embolic stroke. The presence of emboli in both carotid and posterior vessels points to the heart as the likely source. Transient episodes of irregular heart rhythm were not picked up on admission ECG. By chance, a sonographer witnessed paroxysms of atrial fibrillation that directed clinicians to prompt evaluation of the heart as an embolic source.

Other mechanisms such as artery-to-artery embolism were mostly ruled out by normal examination of the entire basilar artery stem. Carotid duplex helped to rule out the left vertebral stenosis at origin (data not shown). A hemodynamic stroke mechanism can also be excluded for the following reasons. In accord with previous studies [8,9], subclavian steal in our case appears to be a harmless phenomenon since it has existed for years, is present at rest and can unlikely result in a pie-shaped unilateral cortical infarction.

Management

Our patient presents outside of a conventional window for interventions for stroke and her CT scan shows hypodensity that precludes tissue rescue with thrombolysis. However, efforts should be focused on early institution of secondary stroke prevention. Although the International Stroke Trial showed a very low early recurrent stroke rate of 2% within the first 2 weeks of hospital admission [10], our patient may have endocarditis that is associated with a high recurrent stroke rate if left untreated [11,12]. An urgent echocardiogram was performed next that showed previously unrecognized endocarditis. Note that elderly patients may develop endocarditis without fever and complaints of chest pain, and stroke may herald the existence of infective endocarditis [11].

Follow-up

Anticoagulation is not indicated in patients with native valves [11–13]. After a course of antibiotic therapy to control infection and reduce the rate of recurrent stroke [11–13] was completed, Holter monitoring showed no paroxysms of atrial fibrillation and repeat TCD monitoring showed no circulating emboli. She continues to have hemianopsia; however, her daily activities have returned to prestroke level. She takes daily aspirin and is scheduled for follow-up Holter monitoring.

References

1 Toole JF. *Cerebrovascular Disorders*, 4th edn. New York: Raven Press, 1990: 199–23.

2 Reutern GM, Budingen HJ, Freund HJ. The diagnosis of obstructions of the vertebral and subclavian arteries by means of directional Doppler sonography. *Arch Psychiatr Nervenkr* 1976; **222** (2–3): 209–22 [in German].

3 Nicholls SC, Koutlas TC, Strandness DE. Clinical significance of retrograde flow in the vertebral artery. *Ann Vasc Surg* 1991; **5** (4): 331–6.

4 Ackerstaff RG, Hoeneveld H, Slowikowski JM, Moll FL, Eikelboom BC, Ludwig JW. Ultrasonic duplex scanning in atherosclerotic disease of the innominate, subclavian and vertebral arteries. A comparative study with angiography. *Ultrasound Med Biol* 1984; **10** (4): 409–18.

5 de Bray JM, Zenglein JP, Laroche JP, Joseph PA, Lhoste P, Pillet J, Dubas F, Emile J. Effect of subclavian syndrome on the basilar artery. *Acta Neurol Scand* 1994; **90** (3): 174–8.

6 Bornstein NM, Norris JW. Subclavian steal: a harmless haemodynamic phenomenon? *Lancet* 1986; **2** (8502): 303–5.

7 Bornstein NM, Krajewski A, Norris JW. Basilar artery blood flow in subclavian steal. *Can J Neurol Sci* 1988; **15** (4): 417–9.

8 Hennerici M, Klemm C, Rautenberg W. The subclavian steal phenomenon: a common vascular disorder with rare neurologic deficits. *Neurology* 1988; **38**: 669–73.

9 Ackermann H, Diener HC, Seboldt H, Huth C. Ultrasonographic follow-up of subclavian stenosis and occlusion: natural history and surgical treatment. *Stroke* 1988; **19**: 431–5.

10 International Stroke Trial Collaborative Group. The International Stroke Trial (IST): a randomised trial of aspirin, subcutaneous heparin, both, or neither among 19 435 patients with acute ischaemic stroke. *Lancet* 1997; **349**: 1569–81.

11 Hart RG, Foster JW, Luther MF, Kanter MC. Stroke in infective endocarditis. *Stroke* 1990; **21**: 695–9.

12 Paschalis C, Pugsley W, John R, Harrison MJC. Rate of cerebral embolic events in relation to antithrombotic and anticoagulant therapy in patients with bacterial endocarditis. *Eur Neurol* 1990; **30**: 87–91.

13 Levine HJ, Pauker SG, Salzman EW. Antithrombotic therapy in valvular heart disease. *Chest* 1989; **95** (Suppl.): 98S.

14 Hart RG, Kagen-Hallet K, Joerns SE. Mechanisms of intracranial hemorrhage in infective endocarditis. *Stroke* 1987; **18**: 1048–52.

Carotid dissection

With Marc Malkoff, MD

Introduction

Arterial wall dissection leads to subintimal hemorrhage, or intramural hematoma, with varying and often progressive degrees of flow obstruction due to compression of the true lumen and expansion of the false lumen [1]. Dissections of the extracranial carotid artery occurred with an annual incidence of 3.5/100 000 in a community-based population study [2]. However this number may be higher if non-disabling clinical manifestations and improvements in neuroimaging methods are taken into account. Dissections have variable clinical presentations, ranging from neck pain or headache, transient monocular blindness, partial Horner syndrome, lower cranial nerve palsies, pulsatile tinnitus or subjective bruits to acute debilitating strokes [3–9]. Dissections affecting the carotid and vertebral arteries and less frequently the aortic arch and its proximal branches are recognized as an important mechanism of ischemic strokes, particularly in the young [10]. Several etiologic theories have been proposed, including genetic predisposition for spontaneous dissections with such conditions as fibromuscular dysplasia and Marfan's syndrome; however, the trauma and mechanical stress to the arterial wall are important variables that lead to some, if not most, of detectable dissections [1,11–16]. Most arterial dissections heal spontaneously over time; however, anticoagulation is often used in these patients, and recently arterial stenting was implemented to restore patency of the true lumen early after the onset of stroke symptoms [1,17–20].

Cerebrovascular ultrasound examination in patients with suspected arterial dissection at various locations in the carotid and vertebral arteries may reveal [21–28]:

1 direct visualization of a 'double lumen' and corresponding spectral waveforms;
2 eccentric and elongated thrombus formation;
3 indirect signs of an arterial obstruction distal or proximal to the site of insonation including abnormal waveforms and oscillating patterns;
4 microembolic signals and flow diversion signs; and
5 an absence of atheromatous disease that may explain the above-mentioned findings.

Case presentation

A 42-year-old white male smoker was brought to the emergency room 24 h after onset of headache, restlessness and gradual development of left-sided weakness. On examination, he was alert and orientated and neglected his left body side. He had gaze preference and left-sided hemiparesis (arm > leg) with a National Institutes of Health Stroke Scale (NIHSS) score of 12 points. Non-contrast computed tomography (CT) showed a hyperdense right middle cerebral artery (MCA) with hypodensities in the right parietal and temporal lobes and an Alberta Stroke Program Early CT Score (ASPECTS) [29] of 4 points.

Diagnostic considerations

Clinical examination and head CT were consistent with an acute ischemic stroke. He had a hyperdense MCA sign on CT that suggested the presence of thrombus in the right M1 MCA [30]. His stroke was severe and correlated with the presumed level of intracranial arterial obstruction. No thrombolytic therapy could have been administered in this patient due to the time of onset outside any thrombolytic treatment window and the presence of hypodensity on the CT scan.

An accelerated large vessel atherosclerotic disease, carotid dissection, hypercoagulable state, paradoxical embolism and drug abuse are the usual suspected stroke mechanisms in young patients [31]. Gradual deficit onset is unlikely in an embolic stroke. Carotid

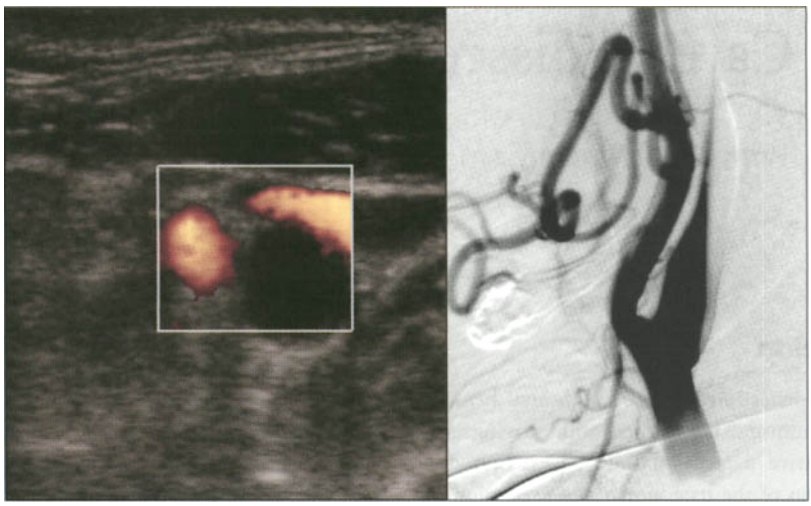

Figure 1 Carotid duplex (left image) and digital subtraction angiography (right image) in a stroke patient with an NIHSS score of 12 points.

duplex ultrasound was performed next in the emergency room.

Ultrasound findings

An extracranial examination of the right internal carotid artery (ICA) with a linear dual-frequency transducer (3–10 MHz, Sonosite, Bothell, WA) showed the following transverse image (Figure 1, left image). No flow signals were identified on power mode in a branching vessel of a larger caliber compared to two smaller vessels on the same scanning plane.

Interpretation

Although the size of the arteries may not be used as a criterion to differentiate the external from the internal carotid artery, the observed flow void was present during the entire cardiac cycle, indicating occlusion in the larger vessel. This finding corresponds to a severe stroke in the right ICA distribution with MCA occlusion. Since no atherosclerotic plaque was found at the level of bifurcation, carotid duplex is consistent with distal ICA obstruction due to dissection, intracranial ICA occlusion or embolus.

Correlative imaging

Digital subtraction angiography (DSA) was performed 1 h after carotid duplex examination and it showed tapering of the ICA lumen with a complete occlusion of the right distal ICA. A false lumen with subintimal thrombus was descending to the level of the bulb (Figure 1, right). DSA also showed a proximal right M1 MCA occlusion (not shown).

Differential diagnosis

The absence of an atheromatous plaque at the ICA bulb on ultrasound suggested either a distal ICA dissection, an intracranial ICA occlusion or an embolic occlusion. The latter is less likely to produce gradual symptom onset. A distal ICA atheromatous occlusion or carotid dissection at the entrance to the skull was therefore suspected. Additional ultrasound examination revealed flow reversal in the ophthalmic artery, pointing to occlusion location between the ICA bulb and the knee of the ICA siphon. A careful history was obtained from relatives regarding any trauma or mechanical stress to the head and neck. It turned out that the patient had undergone a lengthy dental surgical procedure 2 days prior to symptom onset. His neck was hyperextended for about 2 h during dental surgery.

Based on carotid duplex screening and clinical information, DSA was performed next to confirm the presence and extent of carotid dissection as well as the degree of arterial obstruction.

Management

This patient presents outside a conventional window for intravenous thrombolysis for stroke. A large hypodensity on CT scan makes spontaneous hemorrhagic transformation very likely [32]. If heparin is administered, and bleeding occurs, heparinization can be blamed by the principle 'guilt by association'. Urgent stenting of the true lumen is an experimental revascularization procedure [19] that may be very risky in the setting of completed acute infarction. Hypothermia and decompression [33,34] are two potential experimental options that may be considered in this situation.

After discussion with the family about the potential risks and benefits of these procedures, it was elected not to perform any of these interventions, and the patient was admitted for observation to the Stroke Unit. He did not receive heparin acutely, and he did not develop brain herniation. He was discharged home with an NIHSS score of 10 points on warfarin (target international normalized ratio (INR) 2–2.5). He is being cared for by his family, and remained disabled with a Rankin score of 3 at 3 months' follow-up.

References

1 Saver JL, Easton JD. Dissections and trauma of cervicocerebral arteries. In: Barnett HJM, Mohr JP, Stein BM, Yatsu FM, eds. *Stroke: Pathophysiology, Diagnosis, and Management*, 2nd edn. New York: Churchill Livingstone, 1998: 769–86.

2 Schievnik WI, Mokri B, Whisnant JP. Internal carotid dissection in a community in Rochester, Minnesota 1987–1992. *Stroke* 1993; **24**: 1678–80.

3 Bladin PF. A clinical and angiographic study of early diagnosis, natural history, and pathophysiology of cerebral lesions. *Vasc Surg* 1974; **8**: 203–23.

4 Fischer CM. The headache and pain of spontaneous carotid dissection. *Headache* 1982; **22**: 60.

5 Francis KR, Williams DP, Troost BT. Facial numbness and dysesthesia: new features of carotid artery dissection. *Arch Neurol* 1987; **44**: 345–246.

6 Sturzennegger M, Huber P. Cranial nerve palsies in spontaneous carotid artery dissection. *J Neurol Neurosurg Psychiatry* 1993; **56**: 1191–9.

7 Biousse V, D'Anglejan-Chatillon J, Massiou H, Bousser MG. Head pain in non-traumatic carotid artery dissection; a series of 65 patients. *Cephalgia* 1994; **14**: 33–6.

8 Biousse V, D'Anglejan-Chatillon J, Touboul PJ, Amarenco P, Bousser MG. Time course of symptoms in extracranial carotid artery dissections. A series of 80 patients. *Stroke* 1995; **26**: 235–9.

9 Bogousslavsky J, Despland PA, Regli F. Spontaneous carotid dissection with acute stroke. *Arch Neurol* 1987; **44**: 137–40.

10 Bogousslavsky J, Pierre P. Ischemic stroke in patients under age 45. *Neurol Clin* 1992; **10**: 113–24.

11 Anderson CA, Collins CJ, Rich NM, McDonald PT. Spontaneous dissection of the internal carotid artery associated with fibromuscular dysplasia. *Am Surg* 1980; **46**: 263–6.

12 Desfontaines P, Despland PA. Dissection of the internal carotid artery: aetiology, symptomatology, clinical and neurosonological follow-up, and treatment in 60 consecutive cases. *Acta Neurol Belg* 1995; **95**: 226–34.

13 Austin MG, Schaefer RF. Marfan's syndrome, with unusual blood vessel manifestations. *Arch Pathol Lab Med* 1957; **64**: 205.

14 Mayer SA, Rubin BS, Starman BJ, Byers PH. Spontaneous multivessel cervical artery dissection in a patient with a substitution of alanine for glycine (G13A) in the α1(I) chain of type I collagen. *Neurology* 1996; **47**: 552–6.

15 Grau AJ, Buggle F, Steichen-Weihn C, Heindl S, Banerjee T, Seitz R, Winter R, Forsting M, Werle E, Bode C, Nawroth PP, Becher H, Hacke W. Clinical and biochemical analysis in infection-associated stroke. *Stroke* 1995; **26**: 1520–6.

16 Beletsky V, Norris JW. Spontaneous dissection of the carotid and vertebral arteries. *N Engl J Med* 2001; **345**: 467.

17 McNeil DH, Dreisback J, Marsden RJ. Spontaneous dissection of the internal carotid artery: its conservation management with heparin sodium. *Arch Neurol* 1980; **37**: 54–5.

18 Kasner SE, Hankins LL, Bratina P, Morgenstern LB. Magnetic resonance angiography demonstrates vascular healing of carotid and vertebral artery dissections. *Stroke* 1997; **28**: 1993–7.

19 Butterworth RJ, Thomas DJ, Wolfe JH, Mansfield AO, Al-Kutoubi A. Endovascular treatment of carotid dissecting aneurysms. *Cerebrovasc Dis* 1999; **9**: 242–7.

20 Zetterling M, Carlstrom C, Konrad P. Internal carotid artery dissection. *Acta Neurol Scand* 2000; **101**: 1–7.

21 de Bray JM, Dubas F, Joseph PA, Causeret H, Pasquier JP, Emile J. Ultrasonic study of 22 cases of carotid artery dissection. *Rev Neurol (Paris)* 1989; **145**: 702–9 [in French].

22 Hennerici M, Steinke W, Rautenberg W. High-resistance Doppler flow pattern in extracranial carotid dissection. *Arch Neurol* 1989; **46** (6): 670–2.

23 Kaps M, Dorndorf W, Damian MS, Agnoli L. Intracranial haemodynamics in patients with spontaneous carotid dissection. Transcranial Doppler ultrasound follow-up studies. *Eur Arch Psychiatr Neurol Sci* 1990; **239** (4): 246–56.

24 Steinke W, Schwartz A, Hennerici M. Doppler color flow imaging of common carotid artery dissection. *Neuroradiology* 1990; **32** (6): 502–5.

25 Sturzenegger M. Ultrasound findings in spontaneous carotid artery dissection. The value of duplex sonography. *Arch Neurol* 1991; **48** (**10**): 1057–63.

26 de Bray JM, Lhoste P, Dubas F, Emile J, Saumet JL. Ultrasonic features of extracranial carotid dissections: 47 cases studied by angiography. *J Ultrasound Med* 1994; **13** (9): 659–64.

27 Hoffman M, Sacco RL, Chan S, Mohr JP. Noninvasive detection of vertebral artery dissection. *Stroke* 1993; **24**: 815–9.

28 Cals N, Devuyst G, Jung DK, Afsar N, de Freitas G, Despland PA, Bogousslavsky J. Uncommon ultrasound findings in traumatic extracranial dissection. *Eur J Ultrasound* 2001; **12**: 227–31.

29 Barber PA, Demchuk AM, Zhang J, Buchan AM. Validity and reliability of a quantitative computed tomography score in predicting outcome of hyperacute stroke before thrombolytic therapy. *Lancet* 2000; **355**: 1670–**4**.

30 Bastianello S, Pierallini A, Colonnese C, Brughitta G, Angeloni U, Antonelli M, Fantozzi LM, Fieschi C, Bozzao L. Hyperdense middle cerebral artery CT sign. Comparison with angiography in the acute phase of ischemic supratentorial infarction. *Neuroradiology* 1991; **33**: 207–11.

31 Blecic S, Bogousslavsky J. Stroke in young adults. In: Barnett HJM, Mohr JP, Stein BM, Yatsu FM, eds. *Stroke. Pathophysiology, Diagnosis, and Management*, 2nd edn. New York: Churchill Livingstone, 1998: 1001–12.

32 Toni D, Fiorelli M, Bastianello S, Saccjetti ML, Sette G, Argentino C, Montinaro E, Bozzao L. Hemorrhagic transformation of brain infarct: predictability in the first 5 hours from stroke onset and influence on clinical outcome. *Neurology* 1996; **46**: 341–5.

33 Schwab S, Georgiadis D, Berruschot J, Schellinger PD, Graffanino C, Mayer SA. Feasibility and safety of moderate hypothermia after massive hemispheric infarction. *Stroke* 2001; **32**: 2033–5.

34 Demchuk AM. Hemicraniectomy is a promising treatment in ischemic stroke. *Can J Neurol Sci* 2000; **27**: 274–7.

Carotid thromboembolism

With Ken Uchino, MD

Introduction

Embolism from a proximal source can occur in the setting of atrial fibrillation, myocardial infarction, aortic arch atheroma, right-to-left shunting and other probable sources [1]. Most emboli pass through precerebral vessels to lodge in the intracranial vasculature causing perfusion failure. Occasionally, however, a large thrombus may obstruct the proximal internal carotid artery (ICA) and its more distal fragment may propagate to the middle cerebral artery (MCA), causing neurologic deficits of variable degrees [2].

Urgent carotid revascularization was proposed as a potential intervention for crescendo transient ischemic attack (TIA) or stroke in evolution, but it appears risky in patients with acute cerebral ischemia [3,4]. Intravenous anticoagulation may be initiated early in stroke patients with atrial fibrillation without large evolving infarctions [5–8].

Case presentation

A 42-year-old black woman was brought to the emergency room 16 h after onset of headache and left-sided weakness. On examination, she was alert and orientated and neglected her left body side. She had gaze preference and left-sided hemiparesis (arm > leg) with a National Institutes of Health Stroke Scale (NIHSS) score of 12 points. Non-contrast computed tomography (CT) shows hypoattenuation in the right MCA territory and an Alberta Stroke Program Early CT Score (ASPECTS) [9] of 5 points.

Diagnostic considerations

Clinical examination and head CT are consistent with an acute ischemic stroke. No thrombolitic therapy could have been administered in this patient due to time of onset and the presence of hypodensity on the CT scan.

She developed her deficit abruptly and an embolic stroke mechanism was suspected. Transcranial Doppler (TCD) and carotid duplex ultrasound were performed next in the emergency room.

Ultrasound findings

TCD showed a blunted TIBI flow grade II signal in the right MCA and left-to-right anterior cross-filling via the anterior communicating artery. An extracranial examination of the right ICA with a linear dual-frequency transducer (3–10 MHz, Sonosite, Bothell, WA) showed the following images (Figure 1). The right ICA bulb was filled with an axis-asymmetric intraluminal mass with homogenous and slightly hypoechoic structure. Locations 1, 2, 3 and 4 indicate velocity sampling along the right ICA and common carotid artery (CCA). Doppler examination showed normal velocity range with slight delay in systolic flow acceleration in the right ICA just distal to the lesion. Right external carotid artery (ECA) and contralateral carotid examinations (Figure 1) were unremarkable.

Interpretation

Carotid ultrasound showed a thrombus in the right ICA bulb causing a hemodynamically significant obstruction to flow. Collateral supply was present through the anterior communicating artery, and no proximal MCA occlusion was found at 16 h after stroke onset.

Correlative imaging

Magnetic resonance angiography (MRA) was performed 1.5 h after carotid duplex examination and

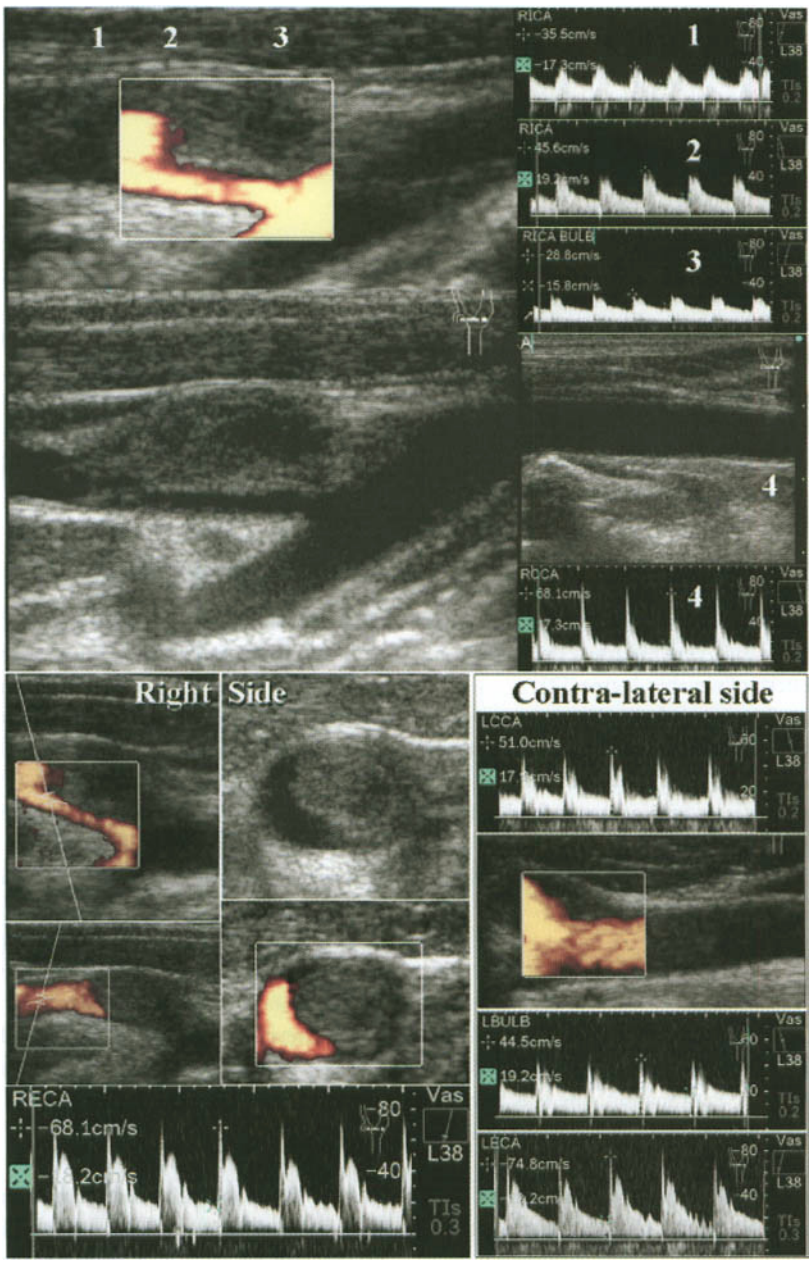

Figure 1 Duplex ultrasound findings in a stroke patient with an NIHSS score of 12 points. The upper images illustrate findings in the right bifurcation and the common carotid artery. The numbers 1, 2, 3 and 4 indicate locations where spectral Doppler waveforms were obtained: 1, proximal internal carotid artery (ICA); 2, distal bulb; 3, proximal bulb; and 4, midportion of the right common carotid artery (CCA). The angle correction in the ICA, transverse projection of the right ICA and the right external carotid artery (ECA) waveforms are shown in the bottom left set of images. The left CCA, left ICA bulb and left ECA waveforms as well as longitudinal B-mode and power-mode image of the left bifurcation are shown in the bottom right set of images.

it showed a small ICA lumen at the level of the bulb and reconstituted distal ICA and MCA flows. Transesophageal echocardiography and other tests did not reveal possible sources of embolism. Coagulation work-up was unremarkable.

Differential diagnosis

The lesion appearance on B-mode scan is typical of an intraluminal thrombus. The crescent-moon-like appearance of the residual lumen and the asymmetric non-circumferential lesion make atheroma an unlikely diagnosis. Furthermore, the intraluminal lesion was moving with arterial wall pulsations, and this real-time observation makes the diagnosis of a fresh thrombus more likely. Atheromatous lesions of this size should decrease vessel wall pulsations and be present on near and far vessel walls.

Management

This patient presents outside a conventional window for intravenous thrombolysis for stroke. Despite the evidence of a thrombus in the ICA bulb, anticoagulation with heparin was not initiated due to a large hypodensity on CT scan. Urgent carotid embolectomy or stenting, hypothermia and decompression were potential experimental options that were discussed with the patient and family who elected not to have any of these interventions performed. The patient was admitted for observation to the Stroke Unit. She did not develop brain herniation. Repeat carotid duplex examination before discharge showed normal vessel patency.

Follow-up

Her NIHSS score was 9 points at 1 week after stroke. She takes aspirin and slow-release dipyridamole [10]. She remains disabled with a Rankin score of 3 at 1.5 months' follow-up, and is being cared for by her family.

References

1 Sacco RL, Toni D, Mohr JP. Classification of ischemic stroke. In: Barnett HJM, Mohr JP, Stein BM, Yatsu FM, eds. *Stroke: Pathophysiology, Diagnosis, and Management*, 2nd edn. New York: Churchill Livingstone, 1998: 341–54.

2 El-Mitwalli A, Saad M, Christou I, Malkoff M, Alexandrov AV. Clinical and sonographic patterns of tandem ICA/MCA occlusion in TPA treated patients. *Stroke* 2002; **33**: 99–102.

3 Mead GE, Murray H, Farrell A, O'Neill PA, McCollum CN. Pilot study of carotid surgery for acute stroke. *Br J Surg* 1997; **84**: 990–2.

4 Brandl R, Brauer RB, Maurer PC. Urgent carotid endarterectomy for stroke in evolution. *Vasa* 2001; **30**: 115–21.

5 Hart RG, Coull BM, Hart D. Early recurrent embolism associated with nonvalvular atrial fibrillation: a retrospective study. *Stroke* 1983; **14**: 688–93.

6 Kelley RE, Berger JR, Alter M, Kovacs AG. Cerebral ischemia and atrial fibrillation: prospective study. *Neurology* 1984; **34**: 1285–91.

7 Albers GW, Bittar N, Young L, Hattemer CR, Gandhi AJ, Kemp SM, Hall EA, Morton DJ, Yim J, Vlasses PH. Clinical characteristics and management of acute stroke patients with atrial fibrillation admitted to US University hospitals. *Neurology* 1997; **48**: 1598–604.

8 Chamorro A, Vila N, Ascaso C, Blanc R. Heparin in acute stroke with atrial fibrillation: clinical relevance of very early treatment. *Arch Neurol* 1999; **56**: 1104–8.

9 Barber PA, Demchuk AM, Zhang J, Buchan AM. Validity and reliability of a quantitative computed tomography score in predicting outcome of hyperacute stroke before thrombolytic therapy. *Lancet* 2000; **355**: 1670–4.

10 Diener HC, Cunha L, Forbes S, Silvenius J, Smets P, Lowenthal A. European Stroke Prevention Study 2. Dipyridamole and acetylsalicylic acid in secondary prevention of stroke. *J Neurol Sci* 1996; **143**: 1–10.

Monitoring carotid endarterectomy

With Anthony Estrera, MD

Introduction

Carotid endarterectomy (CEA) was introduced by Eastcott [1], and its efficacy and durability were established in two large randomized trials for symptomatic patients with carotid stenosis [2,3]. The number needed to treat to prevent one stroke is 8/1 for symptomatic patients with ≥ 70 carotid stenosis, and 15/1 for those with 50–69% stenosis [4]. In asymptomatic patients, the overall risk of stroke is low, i.e. 2% per year, and CEA offers a small protection by reducing it to 1% per year if complication rate from angiography and surgery is ≤ 2% [5]. Perioperative complications from CEA in symptomatic patients amounted to 6.5% in the NASCET trial [6] and are even higher in general practice [7].

Non-invasive monitoring of CEA can identify patients developing ischemia during surgery. Cerebral blood flow measurements [8,9], electroencephalography (EEG) [9–14], evoked potentials [15,16], cerebral oximetry [17,18], direct stump pressure measurements [19,20] and ultrasound [21–25] can be used for this purpose. If CEA is performed under local anaesthesia, patient status can also be checked with repeat clinical examinations [26]. EEG and cerebral oximetry are very sensitive to the development of cerebral ischemia even before clinical changes become apparent [9–18]; however, these methods can miss ischemia, particularly with general anesthesia [27,28], and are limited in their ability to determine the mechanism by which ischemia develops. Ultrasound can provide sensitivity equal to EEG to detect cerebral ischemia [28], and demonstrates in real time the mechanism by which ischemia has developed, i.e. embolism, hypoperfusion, thrombosis or hyperperfusion [29]. Although multicenter randomized trials of monitoring techniques targeted to reduce perioperative stroke or transient ischemic attack (TIA) are lacking, several prospective studies showed very low complication rates with monitoring compared to historic controls [29–32], and a single-center randomized trial investigated reduction of microemboli after CEA as a surrogate marker for the risk of perioperative stroke [33,34]. A theoretical case presented below demonstrates a variety of previously reported typical transcranial Doppler (TCD) findings during CEA [21–25,28–32], their online interpretation, and responses to prevent possible complications.

Case presentation

A 68-year-old man with a past history of hypertension, smoking and leg claudication had a sudden onset of slurred speech and right arm weakness lasting for 10 min with complete resolution. On examination, he has no neurologic symptoms. Carotid ultrasound showed an 80% left internal carotid artery (ICA) stenosis and a 30% right ICA stenosis. Magnetic resonance imaging (MRI) showed no diffusion abnormalities, and MR angiography showed a flow gap in the left ICA bulb.

Diagnostic considerations

Clinical examination and vascular imaging studies are consistent with a severe carotid stenosis in a patient with recent TIA. The motor symptoms and possible speech impairment point to left hemispheric TIA. This patient appears to be an appropriate candidate for left carotid endarterectomy, and CEA under general anesthesia is scheduled.

Ultrasound findings preclamp

The left middle cerebral artery (MCA) flow signals were identified with TCD at a depth of 55 mm and a

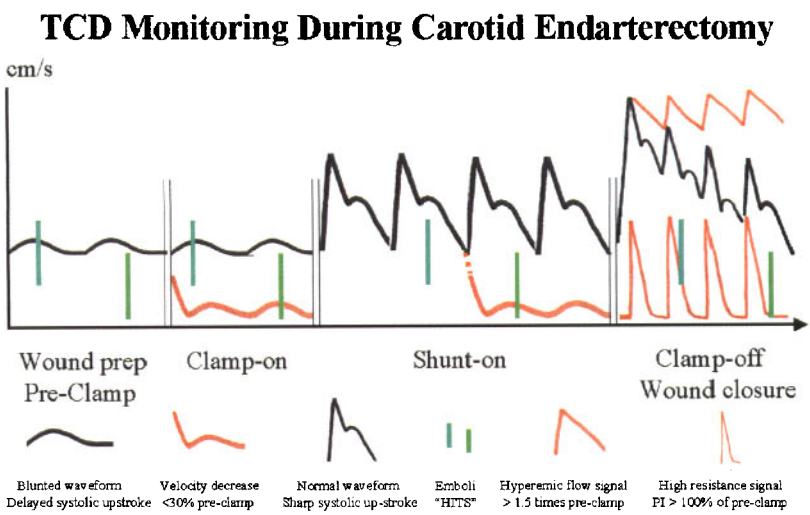

Figure 1 Composite sketch of MCA velocity and signal intensity changes during CEA.

2-MHz transducer was fixed for continuous monitoring using a Marc series headframe (Spencer Technologies, Seattle, WA). Ultrasound findings are summarized in a graph (Figure 1) where solid black lines identify waveforms detected during uncomplicated course of the CEA and grey lines indicate flow changes that necessitate correction. The interpretation of TCD findings provided below, differential diagnosis and possible corrective measures were derived from previous publications [21–25,28–33].

During wound preparation and left carotid exposure, TCD monitoring showed a blunted left MCA flow signal and numerous embolic signals of short duration and variable velocities.

Interpretation, differential diagnosis and management

TCD showed a delayed systolic flow acceleration in the MCA ipsilateral to a severe carotid stenosis since this is a flow-limiting lesion and the MCA is dilated in an attempt to attract collateral flow.

The differential diagnosis includes:

1 Vessel misidentification, i.e. terminal ICA or posterior cerebral artery (PCA) vs. MCA flow detection if sample volume is 10 mm or greater and transducer angulation is not slightly upwards and anterior.

2 ICA stenosis progression if a presurgical TCD showed normal systolic flow acceleration in the MCA. If a blunted flow signal was present on baseline TCD and a reduction of the MCA flow velocities was noted, this finding could be attributable to the changes in the angle of insonation and cerebral blood flow reduction due to general anesthesia.

3 Waveform/velocity changes due to lowering of blood pressure and decrease in cardiac output/brain metabolic demand with general anesthesia.

TCD also showed numerous embolic signals before surgical dissection of the carotids. The differential diagnosis includes:

1 Spontaneous embolization from the active carotid plaque since in patients with symptomatic carotid stenosis TCD can detect on average four embolic signals per hour in the MCA unilateral to a severe symptomatic ICA stenosis [35].

2 Spontaneous embolization from a proximal source, i.e. artificial heart valves, heart chambers or aortic arch atheroma. In this situation, an assessment of the contralateral MCA flow signals may reveal similar or higher rates of embolic signals [36,37] unrelated to the carotid stenosis or surgical maneuvers.

3 Embolic signals that appear in relation to surgical maneuvers. For example, skin preparation, surgical skin dissection and carotid exposure may cause mechanical compression of very soft plaques and dislodge microparticles from the plaque surface or pre-exposed core [29]. In this case, nurses and surgeons may consider more gentle skin and wound preparation and modification of carotid exposure techniques. This observation may be particularly useful for surgical residents in training.

Ultrasound findings with carotid clamping

The left MCA flow waveform and velocity did not change after carotid cross-clamping, and several embolic signals were detected at and in a few seconds after cross-clamping.

Interpretation, differential diagnosis and management

No change in the flow velocities after cross-clamping can be expected if the MCA unilateral to the severe carotid stenosis is not dependent on the residual flow through the lesion and collateralization of flow occurs through the communicating arteries. However, the differential diagnosis should include erroneous vessel identification, e.g. PCA, that will not show significant changes with carotid clamping.

The appearance of several embolic signals can also be expected since clamping may dislodge microparticles due to mechanical stress to the vessel wall. The worrisome explanation may be that the clamp was not advanced distally enough to compress the vessel beyond the edge of carotid plaque. Nevertheless, these embolic signals represent microscopic particles that probably do not cause any detectable damage unless they are too numerous and are associated with a significant velocity decrease.

TCD can also detect a significant drop in the unilateral MCA velocity (red line). This flow phenomenon can be expected in patients whose MCA flow is still dependent on the residual flow through the proximal carotid stenosis, particularly if an 'isolated MCA' is present. These flow findings can be expected if presurgical angiography showed the absence of intracranial collaterals with an incomplete circle of Willis ('trapped' MCA). The differential diagnosis includes:

1 Blood pressure (BP) drop. Arterial BP reading or assessment of the contralateral MCA waveform can help to identify this reason.

2 Transducer displacement. Therefore the use of a firm and reliable fixation device is of paramount importance.

A flow velocity decrease on TCD can be transient, therefore requiring no immediate corrective action. Although it usually takes just a few seconds, it may take up to 2 min for the MCA flow velocity to recover after cross-clamping due to recruitment of additional collaterals [38].

A TCD velocity decrease is considered significant if it falls below 30% of the preclamp values [29]. To trust the numeric output of a TCD unit, the flow signal should be optimized, and the online readings should be taken at the end of the sweep. If flow signals are weak, the sonographer should know how to measure the velocity manually, calculate the mean flow velocity values, and quickly estimate the velocity change. Experienced observers can estimate the velocity change by visual inspection of the real-time display, and some surgeons would prefer to see the display or to have this information available for them as soon as possible.

A TCD velocity decrease below 30% of the preclamp value may be dangerous for the patient if it persists over 2 min. This velocity drop indicates:

1 lack of collateral recruitment [29,38]; or

2 a significant decrease in cerebral blood flow since the angle of insonation has remained constant [29,39,40].

This information can be helpful to identify potential candidates for selective shunting.

Although studies have shown that placement of shunts during every surgery may result in lower complication rates, data are yet insufficient to determine whether selective or routine shunting result in improved outcomes [41]. In this case, the information presented below can help to identify problems with shunt function during CEA.

Ultrasound findings after shunt placement

Shunt insertion resulted in left MCA flow velocity increase and improved systolic flow acceleration. A few embolic signals were also detected.

Interpretation, differential diagnosis and management

TCD showed improvement in the early systolic flow acceleration since the shunt delivers blood flow using a unilateral carotid artery and the hemisphere becomes less dependent on the collateral flow. TCD findings of increased flow velocities are likely associated with higher flow rate through the MCA since the angle of insonation remained unchanged.

TCD also showed several embolic signals during and after shunt placement. The differential diagnosis includes:

1 Harmless air microbubbles since shunt placement introduces minuscule amounts of air into the arterial tree and these bubbles are so small in size that they can pass through the brain circulation into the venous collectors without causing detectable brain damage.
2 Particulate embolization with plaque fragments or microthrombi that may originate from or form at the shunt edges during its preparation and insertion. Shunt placement may also cause a small mechanical stress to the vessel wall or to the plaque edges if present at the site of insertion.
3 Spontaneous embolization from a proximal source that could have been present before surgery.
Since embolic signals were not associated with a significant velocity decrease, their size was likely too small to cause any significant obstruction to flow and no immediate action is required. However, persistence of multiple emboli without any proximal source includes the following differential algorithm:
1 Shunt placement still allows air entrance into the circulation. Tightening of vessel wall incision around shunt insertion sites may be considered.
2 The distal shunt edge may be dislodging plaque components if a distal plaque formation is present. Distal ICA inspection may be performed.
3 The distal shunt position may cause turbulence with formation of microcavitation bubbles. Shunt alignment with the vessel and its position may be revised.
4 Shunt placement reintroduces a greater flow volume into the distal ICA and this flow may be dislodging microparticles, particularly if distal or intracranial ICA disease is present.

During shunting, TCD can show a sudden velocity drop below preclamp values (red line). The differential diagnosis for this finding includes:
1 Transducer displacement. The sonographer should pay attention to changes in patient head position and surgical manipulations to make sure that these flow findings are not due to an artifact.
2 Blood pressure drop. Use arterial blood pressure reading to identify this mechanism.
3 Kink of the shunt. A surgeon may have repositioned the shunt and this may cause the shunt lumen to embed into the vessel wall. A simple shunt reorientation over the surgical field may restore the flow.
4 Shunt thrombosis. Despite its rare occurrence, this possibility should be considered since the motionless blood in the shunt cannot be distinguished from the moving blood with a simple visual inspection. If shunt thrombosis is present, its patency should be quickly restored to avoid distal hypoperfusion and/or embolization.

Ultrasound findings after shunt and cross-clamp removal

The left MCA flow velocity immediately increased to above preclamp and on-shunt values. Over the next minute, the flow velocities gradually decreased by approximately 50%, and stabilized at values within a 30% difference from the contralateral side (data not shown).

The waveform showed vertical systolic upstroke, i.e. normal flow acceleration. Several embolic signals were detected within the first 2 min of cross-clamp release.

Interpretation, differential diagnosis and management

TCD showed a transient hyperemic response after normal flow was re-established in the carotid artery. Usually there is a short phase of decreased flow velocities associated with shunt removal, and a transient velocity increase can be expected after clamp removal.

If the velocity increase is ≥ 1.5 times the preclamp values, it may indicate hyperperfusion [29]. If this velocity increase persists over 2 min without a trend towards velocity decrease, the differential diagnosis includes:
1 a benign finding, if overall mean flow velocity does not exceed 80 cm/s or 130% of the contralateral side;
2 velocity increase with blood pressure increase due to passive autoregulation; or
3 potential development of the hyperperfusion syndrome, if the velocity increase persists for over 2 min.
Potential measures that can be used to prevent hyperperfusion early after cross-clamp release include:
1 hyperventilation or increased oxygenation;
2 pharmacologic blood pressure decrease; and
3 partial ICA cross-clamp and slow release.
The latter measure can be used to temporarily limit the incoming flow and slowly increase its amount over time, and thus to 'remind' the brain to autoregulate the incoming flow.

TCD often detects emboli early after cross-clamp release. The presence of embolic signals may be attributable to the following sources:
1 air microbubbles, trapped or introduced by manipulations with shunt and cross-clamp removal;

2 spontaneous emboli from a proximal source; or
3 particulate emboli, originating at the incompletely removed plaque edges or thrombus in the ICA.

It can be expected that several emboli (usually microbubbles) will be detected upon cross-clamp release. After spontaneous embolization from a cardiac or aortic source has been excluded, the persistence of frequent emboli is worrisome. If the continuing presence of emboli is associated with re-establishment of a blunted MCA waveform or a significant velocity decrease, surgical revision is warranted. If these TCD findings were obtained after wound closure, i.e. in the recovery room, a duplex ultrasound examination of the extracranial carotids can be performed to detect the presence of a fresh thrombus in the ICA.

Shortly after cross-clamp release, TCD can show a spiky high-resistance signal in the MCA (red line) [31]. This is an abnormal waveform that indicates high resistance to flow at the site or just distal to insonation depth. The abrupt appearance of this flow signal is rare and indicates thromboembolism in the MCA. In this situation, an urgent angiography may be performed to visualize the site and extent of occlusion and this patient may be a candidate for an experimental intra-arterial intervention, i.e. thrombolysis, mechanical clot disruption or removal.

Follow-up

This patient underwent successful and uneventful left carotid endarterectomy. Repeat carotid duplex 2 weeks after surgery showed no residual stenosis in the left ICA, and a mild (approximately 30%) right ICA stenosis. Repeat duplex examinations were scheduled at 1 month and 6 months after surgery. The patient receives aspirin 350 mg [42] and clopidogrel 75 mg daily [43], and remains asymptomatic during follow-up. However, the safety of combining aspirin and clopidogrel has come into question with the results of the CURE trial [44,45].

References

1 Eastcott HHG, Pickering GW, Rob CG. Reconstruction of internal carotid artery in a patient with intermittent attacks of hemiplegia. *Lancet* 1954; ii: 954.

2 North American Symptomatic Carotid Endarterectomy Trial Collaborators. Beneficial effect of carotid endarterectomy in symptomatic patients with high-grade carotid stenosis. *N Engl J Med* 1991; 325: 445–53.

3 European Carotid Surgery Trialists' Collaborative Group. Randomised trial of endarterectomy for recently symptomatic carotid stenosis: final results of the MRC European Carotid Surgery Trial (ECST). *Lancet* 1998; 351: 1379–87.

4 Barnett HJ, Taylor DW, Eliasziw M, Fox AJ, Ferguson GG, Haynes RB, Rankin RN, Clagett GP, Hachinski VC, Sackett DL, Thorpe KE, Meldrum HE. Benefit of carotid endarterectomy in patients with symptomatic moderate or severe stenosis. North American Symptomatic Carotid Endarterectomy Trial Collaborators. *N Engl J Med* 1998; 339: 1415–25.

5 Executive Committee of the Asymptomatic Carotid Atherosclerosis Study. Endarterctomy for asymptomatic carotid artery stenosis. *JAMA* 1995; 273: 1421–8.

6 Ferguson GG, Eliasziw M, Barr HW, Clagett GP, Barnes RW, Wallace MC, Taylor DW, Haynes RB, Finan JW, Hachinski VC, Barnett HJ. The North American Symptomatic Carotid Endarterectomy Trial: surgical results in 1415 patients. *Stroke* 1999; 30: 1751–8.

7 Chaturvedi S, Aggarwal R, Murugappan A. Results of carotid endarterectomy with prospective neurologist follow-up. *Neurology* 2000; 26 (55): 769–72.

8 Sundt TM. The ischemic tolerance of neural tissue and the need for monitoring and selective shunting during carotid endarterectomy. *Stroke* 1983; 14: 93–8.

9 Sharbrough FM, Messik JM, Sundt TM. Correlation of continuous electroencephalograms with cerebral blood flow measurements during carotid endarterectomy. *Stroke* 1973; 4: 674–83.

10 Blackshear WM, Di Carlo V, Seifert KB, Connar RG. Advantages of continuous electroencephalographic monitoring during carotid surgery. *J Cardiovasc Surg* 1986; 27: 146–53.

11 Cho I, Smullens SN, Streletz LJ, Fariello RG. The value of intraoperative EEG monitoring during carotid endarterectomy. *Ann Neurol* 1986; 20: 508–12.

12 Blume WT, Ferguson GG, McNeil DK. Significance of EEG changes at carotid endarterectomy. *Stroke* 1986; 17: 891–7.

13 McCarthy WJ, Park AE, Koushanpour E, Pearce WH, Yao JS. Carotid endarterectomy. Lessons from intraoperative monitoring—a decade of experience. *Ann Surg* 1996; 224: 291–307.

14 Balotta E, Daigau G, Saladini M *et al.* Results of electroencephalographic monitoring during 369 consecutive carotid artery revascularizations. *Eur Neurol* 1997; 37: 43–7.

15 Kearse LA, Brown EN, McPeck K. Somatosensory evoked potential sensitivity relative to electroencephalography for cerebral ischemia during carotid endarterectomy. *Stroke* 1992; 23: 498–505.

16 Haupt WF, Horsch S. Evoked potential monitoring in carotid surgery: a review of 994 cases. *Neurology* 1992; **42**: 835–8.

17 Duncan LA, Ruckley CV, Wildsmith JAW. Cerebral oximetry: a useful monitor during carotid artery surgery. *Anesthesiology* 1995; **50**: 1041–5.

18 Samra SK, Dorje P, Zelenock GB, Stanley JC. Cerebral oximetry in patients undergoing carotid endarterectomy under regional anesthesia. *Stroke* 1996; **27**: 49–55.

19 Cherry KJ Jr, Roland CF, Hallett JW Jr *et al.* Stump pressure, the contralateral carotid artery, and electroencephalographic changes. *Am J Surg* 1991; **162**: 185–9.

20 Harada RN, Comerota AJ, Good GM, Hashemi HA, Hulihan JF. Stump pressure, electroencephalographic changes, and the contralateral carotid artery: another look at selective shunting. *Am J Surg* 1995; **170**: 148–53.

21 Padayachee TS, Gosling RG, Bishop CC, Burnand K, Browse NL. Monitoring middle cerebral artery blood flow velocity during carotid endarterectomy. *Br J Surg* 1986; **73**: 98–100.

22 Steiger HJ, Schaffler L, Boll J, Liechti S. Results of microsurgical carotid endarterectomy: a prospective study with transcranial Doppler and EEG monitoring, and selective shunting. *Acta Neurochir [Wien]* 1989; **100**: 31–8.

23 Spencer MP, Thomas GI, Nicholls SC, Sauvage LR. Detection of middle cerebral artery emboli during carotid endarterectomy using transcranial Doppler ultrasonography. *Stroke* 1990; **21**: 415–23.

24 Ackerstaff RGA, Jansen C, Moll FL *et al.* The significance of emboli detection by means of transcranial Doppler ultrasonography monitoring in carotid endarterectomy. *J Vasc Surg* 1995; **21**: 415–23.

25 Cantelmo NL, Babikian VL, Samaraweera RN *et al.* Cerebral microembolism and ischemic changes associated with carotid endarterectomy. *J Vasc Surg* 1998; **27**: 1024–31.

26 Benjamin ME, Silva MB Jr, Watt C *et al.* Awake patient monitoring to determine the need for shunting during carotid endarterectomy. *Surgery* 1993; **114**: 673–81.

27 Haupt WF, Erasmi-Korber H, Lanfermann H. Intraoperative recording of parietal SEP can miss hemodynamic infarction during carotid endarterectomy: a case study. *Electroencephalogr Clin Neurophysiol* 1994; **92**: 86–8.

28 Arnold M, Sturzenegger M, Schaffler L, Seiler R. Continuous intraoperative monitoring of middle cerebral artery flow velocities and electroencephalography during carotid endarterectomy. *Stroke* 1997; **28**: 1345–50.

29 Spencer MP. Transcranial Doppler monitoring and causes of stroke from carotid endarterectomy. *Stroke* 1997; **28**: 685–91.

30 Jansen C, Ramos LM, van Heesewijk JP, Moll FL, van Guijn J, Ackerstaff RG. Impact of microembolism and hemodynamic changes in the brain during carotid endarterectomy. *Stroke* 1994; **25**: 992–7.

31 Ackerstaff RG, Moons KG, van de Vlasakker CJ, Moll FL, Vermeulen FE, Algra A, Spencer MP. Association of intraoperative transcranial Doppler monitoring variables with stroke from carotid endarterectomy. *Stroke* 2000; **31**: 1817–23.

32 Babikian VL, Canthelmo NL. Cerebrovascular monitoring during carotid endarterectomy. *Stroke* 2000; **31**: 1799–801.

33 Levy CR, O'Malley HM, Fell G *et al.* Transcranial Doppler detected cerebral microembolism following carotid endarterectomy. High intensity signal loads predict postoperative cerebral ischemia. *Brain* 1997; **120**: 621–9.

34 Kaposzta Z, Baskerville PA, Madge D, Fraser S, Martin JF, Markus HS. L-arginine and S-nitrosoglutathione reduce embolization in humans. *Circulation* 2001; **103**: 2371–5.

35 Siebler M, Kleinschmidt A, Sitzer M, Steinmetz H, Freund HJ. Cerebral microembolism in symptomatic and asymptomatic high-grade internal carotid artery stenosis. *Neurology* 1994; **44**: 615–8.

36 Georgiadis D, Grosset DG, Kelman A, Faichney A, Lees KR. Prevalence and characteristics of intracranial microembolic signals in patients with different types of prosthetic cardiac valves. *Stroke* 1994; **25**: 587–92.

37 Sliwka U, Job FP, Wissuwa D. *et al.* Occurrence of transcranial Doppler high-intensity transient signals in patients with potential cardiac sources of embolism: a prospective study. *Stroke* 1995; **26**: 2067–70.

38 Babikian VL, Canthelmo NL, Wijman CAC. Neurovascular monitoring during carotid endarterectomy. In: Babikian VL, Wechsler LR, eds. *Transcranial Doppler Ultrasonography*, 2nd edn. Boston: Butterworth-Heinemann, 1999: 233.

39 Kontos HA. Validity of cerebral arterial blood flow calculations from velocity measurements. *Stroke* 1989; **20**: 1–3.

40 Aaslid R, Lindegaard KF, Sorteberg W, Nornes H. Cerebral autoregulation dynamics in humans. *Stroke* 1989; **20**: 45.

41 Counsell C, Salinas R, Naylor R, Warlow C. Routine or selective carotid artery shunting for carotid endarterectomy (and different methods of monitoring in selective shunting). *Cochrane Database Syst Rev* 2000; **2**: CD000190.

42 Taylor DW, Barnett HJ, Haynes RB, Ferguson GG, Sackett DL, Thorpe KE, Simard D, Silver FL, Hachinski V, Clagett GP, Barnes R, Spence JD. Low-dose and high dose acetylsalicylic acid for patients undergoing carotid endarterectomy: a randomized controlled trial. ASA Carotid Endarterectomy (ACE) Trial Collaborators. *Lancet* 1999; **353**: 2179–84.

43 CAPRIE Steering Committee. A randomized, blinded trial of clopidogrel versus aspirin in patients at risk of ischaemic events. *Lancet* 1996; **348**: 1329–32.

44 Yusuf S, Zhao F, Mehta SR, Chralavicius S, Tongoni G, Fox KK and the Clopidogrel in Unstable Angina to Prevent Recurrent Events Trial Investigators. Effects of clopidogrel in addition to aspirin in patients with acute coronary syndromes without ST-segment elevation. *N Engl J Med* 2001; **345**: 494–502.

45 Albers GW, Amarenco P. Combination therapy with clopidogrel and aspirin: can the CURE results be extrapolated to cerebrovascular patients? *Stroke* 2001; **32**: 2948.

Brain retroperfusion

With Zsolt Garami, MD *& Hazim Safi,* MD

Introduction

Three primary mechanisms cause injury to brain tissues after cardiac and aortic operations:

1 'mechanical' injury from cerebral embolism;

2 blood flow alterations leading to reperfusion injury; and

3 environmental, pharmacologic and patient-related factors influencing postoperative state [1].

Besides other methods that extend safe circulatory arrest, i.e. cerebroplegia, antegrade perfusion via the innominate artery and hypothermia, retrograde cerebral perfusion (RCP) was initially suggested to reverse massive air embolism [2] and later developed to maintain cerebral blood flow during surgical repairs involving the aortic arch [3]. Recently, a transvenous brain retroperfusion procedure was also applied in acute ischemic stroke in an attempt to reverse ischemic damage [4].

At surgery, RCP is performed during profound hypothermic circulatory arrest that by itself offers neuroprotection [5]. When added to profound hypothermic circulatory arrest, RCP significantly reduced neurologic dysfunction providing superior brain protection [6–8]. The mechanisms by which RCP may offer additional neuroprotection include:

1 brain oxygenation;

2 removal of toxic metabolites;

3 a more even and extensive cooling of brain tissues;

4 protection against reperfusion injury; and

5 time extension of safe circulatory arrest [4,6,7].

To deliver blood to the brain in a retrograde fashion, the superior vena cava is cannulated and connected to a bypass machine. In a few seconds on bypass, a trickle blood flow appears from the brachiocephalic arteries descending to the aorta. It has been a matter of controversy as to whether this blood reaches the brain tissue or is being shunted from venous collectors to large intracranial arteries. Without ultrasound monitoring, it is not clear how the bypass pressure and flow volume settings should be adjusted to achieve blood flow delivery to the brain since electroencephalography (EEG) shows no cerebral electrical activity due to hypothermia. It has also been a matter of controversy as to whether capillary bed is perfused during RCP [9,10].

Although transcranial Doppler (TCD) cannot directly access parenchymal perfusion of the brain, it can detect typical flow reversal in the proximal middle cerebral artery (MCA) in animal models of RCP [11]. In humans, the TCD beam can be steadily focused on the M2 or M1 MCA and the direction of flow in these segments can change with effective retroperfusion [12–15]. However, failure to reverse flow on TCD occurred in up to 40% of patients undergoing RCP in previous studies [12–15]. Perhaps this lack of flow reversal on TCD should be used to change or optimize perfusion settings to achieve flow reversal in basal cerebral arteries.

We routinely monitor aortic surgeries with TCD and detect flow reversal in the M2–M1 MCA segments during RCP. We were able to achieve a 100% detection of flow reversal in MCAs in the presence of temporal windows, and in other arteries if these windows were absent [16]. If no reversal was achieved with initial low-volume RCP, the volume was raised up to 600 cc until flow reversal was detected by TCD. The following case illustrates intraoperative flow findings.

Case presentation

A 70-year-old man with a past history of hypertension, atrial fibrillation and leg claudication had continuing episodes of chest pain. The aortocoronary angiography showed a large ascending aorta aneurysm.

Diagnostic considerations

Clinical examination and angiography are consistent with an ascending aortic aneurysm that necessitates surgical repair. In order to protect the brain and maintain the bypass of blood, brain retroperfusion and hypothermia to 15 °C was administered. EEG showed progression to electric silence with decreasing temperature. After isolectric EEG was obtained, RCP was initiated for the duration of surgical repair of the ascending aorta.

Ultrasound findings

TCD showed a low-resistance flow towards the transducer in the MCA before bypass initiation (Figure 1, upper left image). The first aortic cross-clamp produced a cluster of embolic signals (Figure 1). Note that more signals are seen on M-mode display than on a single-channel TCD since M-mode simultaneously displays several vessels and shows emboli course in both time and space. The MCA flow signal intensity increases during bypass initiation (Figure 1) since a

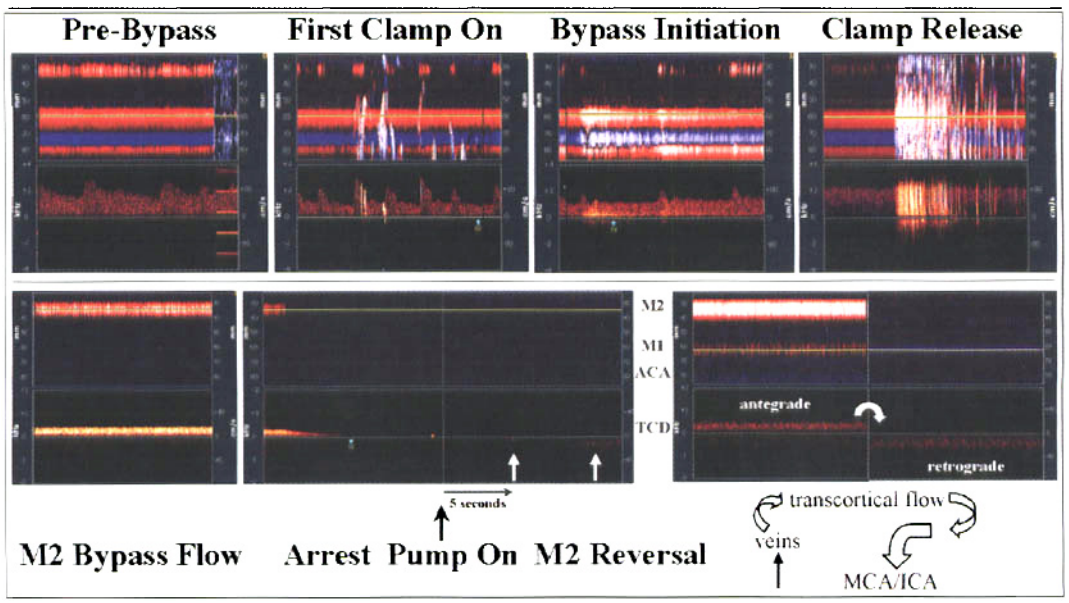

Figure 1 Prebypass (upper left image) flow has a low-resistance signature on the M-mode transcranial Doppler (TCD) that also shows antegrade M2, M1 MCA flows as well as the A1 ACAs' flow. The artifact at the end of the sweep is caused by electrical cautery.

'First clamp-on' image displays multiple embolic signals in both MCA and ACAs. Note that M-mode provides tracks of emboli in time and space. Emboli can be mapped to the arterial branches they pass by depth and direction as well as time delays along the horizontal axis. M-mode display yields more emboli than a single-gate spectral TCD.

'Bypass initiation' image shows changes in systolic acceleration towards non-pulsatile perfusion as well as changes in flow signal intensity due to introduction of a new pool of blood with different impedance.

'Clamp release' image shows a shower of emboli (mostly air microbubbles) passing towards the brain.

'M2 bypass flow' (lower left image) is a non-pulsatile antegrade flow at the 30–40 mm depths with transtemporal insonation. During induction of a complete arrest of cerebral circulation, M2 flow signals disappear on M-mode display first since at any given depth M-mode is less sensitive than a single-gate spectral TCD display. The flow signals on spectral TCD disappear last, indicating a complete arrest of cerebral circulation with bypass pump being turned off.

After the pump has been turned on (arrow), flow signals appear in the M2 MCA approximately 5 s later. The flow direction is reversed, implying that this flow has reached the MCA by retrograde filling of its branches from the venous circulation. The 5-s delay may be caused by the time necessary to fill up the veins since these vessels have the greatest intracranial compartmental capacity to accommodate for flow volume. The reversed flow signals are much weaker in intensity and have slower velocities since these parameters are indirectly proportionate to the flow volume which is reduced during retroperfusion.

Finally, a low-intensity retrograde flow establishes through the M1 MCA (bottom right image), and a diagram illustrates the passage of blood from venous collectors to the proximal intracranial arteries of the circle of Willis.

new pool of blood with different impedance is being introduced into the circulation. The aortic clamp release produced a shower of embolic signals that likely represent air microbubbles (Figure 1, upper right image).

The bottom row of images (Figure 1) shows M2 MCA flow on normal bypass, during hypothermia and cessation of antegrade perfusion (Arrest) followed by initiation of brain retroperfusion and subsequent reversal in flow direction. Note that reversed flow appears 5–10 s after the retroperfusion pump has been turned on and this flow has decreased signal intensity compared to antegrade prearrest flow.

Interpretation

TCD showed flow reversal in the M2 MCA upon initiation of RCP. This flow appeared within a few seconds' delay after the retroperfusion pump was turned on. This is likely due to the time necessary to fill intracranial veins that normally hold 70% of the total cerebral blood flow volume. After the veins are filled, a trickling flow establishes towards the arteries and it becomes detectable as a reversed M2–M1 flow signal with slower velocities and less intensity due to the low volume of retrograde moving blood.

Correlative studies

EEG showed no neuronal activities when brain temperature reached its hypothermic target and no activity was also detected during retroperfusion, even in the presence of detectable and reversed MCA flow.

Differential diagnosis

Detection of reversed MCA signals is not attributable to artifact or venous flow since the interface and angle of insonation did not change during the observation period. The reversed MCA signals have appeared between 10 and 20 s after RCP initiation, which is earlier than previously reported [15]. The MCA velocity and strength of reversed MCA signals changed in response to pump volume settings and head positioning (data not shown). TCD signals tended to disappear when volume (not pressure) of retrograde-infused blood decreased and when the patient's head was placed below 0°. These findings point to the significance of filling the intracranial veins to the maximum compartmental capacity in order to establish retrograde flow. Once established, this flow becomes sensitive to head positioning since gravitational force may be working against brain retroperfusion.

TCD detection of multiple embolic signals during bypass surgery has been studied extensively [17–20]. The cannula and bypass blood may contain numerous air microbubbles detectable by TCD. Their appearance correlates with surgical manipulations and quality of filtering systems. The size of these bubbles has been shown to be small enough to pass through brain vasculature without causing harm. However, a cumulative number of these embolic signatures may be related to neuropsychologic deficits after bypass surgery. Also, brain embolization with lipid aggregates may be responsible for small capillary–arteriolar dilatations (SCADs), and these microcirculatory lesions may be the pathomorphologic substrate of neurologic dysfunction after bypass surgery [18,19]. Since TCD cannot yet differentiate gaseous from solid, particularly lipid, emboli, the value of merely emboli counting remains uncertain.

Management

During surgery and brain retroperfusion the pump volume settings were increased to 600 cc when reversed TCD flow signals appeared and remained stable through the procedure. Head positioning below 0° was performed for a brief period of time and the MCA flow recovered upon return to the supine position.

Follow-up

This patient underwent successful surgical repair of ascending aortic aneurysm and recovered without signs of stroke. He remained symptom free at a follow-up visit 1 month after surgery.

References

1 Swain, JA. Cardiac surgery and the brain. *N Engl J Med* 1993; **329**: 1119–20.

2 Mills NL, Ochsner JL. Massive air embolism during cardiopulmonary bypass. Causes, prevention, and management. *J Thorac Cardiovasc Surg* 1980; **80**: 708–17.

3 Ueda Y, Miki S, Kusuhara K, Okita Y, Tahata T, Yamanaha K. Deep hypothermic systemic circulatory

arrest and continuous retrograde cerebral perfusion for surgery of aortic arch aneurysm. *Eur J Cardiothorac Surg* 1992; **6**: 36–41.

4 Frazee JG, Luo X, Luan G, Hinton DS, Hovda DA, Shiroishi MS, Barcliff LT. Retrograde transvenous neuroperfusion: a back door treatment for stroke. *Stroke* 1998; **29**: 1912–6.

5 Gillinov AM, Redmond JM, Zehr KJ *et al.* Superior cerebral protection with profound hypothermia during circulatory arrest. *Ann Thorac Surg* 1993; **55**: 1432–9.

6 Safi HJ, Iliopoulos DC, Gopinath SP, Hess KR, Asimacopoulos PJ, Bartoli S, Raskin RA, Shaibani AT, Laveque CM, Yawn DH. Retrograde cerebral perfusion during profound hypothermia and circulatory arrest in pigs. *Ann Thorac Surg* 1995; **59**: 1107–12.

7 Safi HJ, Brien HW, Winter JN *et al.* Brain protection via cerebral retrograde perfusion during aortic arch aneurysm repair. *Ann Thorac Surg* 1993; **56**: 270–6.

8 Safi HJ, Letsou GV, Iliopoulos DC, Subramaniam MH, Miller CH, Hassoun H, Asimacopoulos PJ, Baldwin JC. Impact of retrograde cerebral perfusion on ascending aortic and arch aneurysm repair. *Ann Thorac Surg* 1997; **63**: 1601–7.

9 Ehrlich MP, Hagl C, McCullough JN, Zhang N, Shiang H, Bodian C, Griepp RB. Retrograde cerebral perfusion provides negligible flow through brain capillaries in the pig. *J Thorac Cardiovasc Surg* 2001; **122**: 331–8.

10 Pagano D, Boivin CM, Faroqui MH, Bonser RS. Surgery of thoracic aorta with hypothermic circulatory arrest: experience with retrograde perfusion via superior vena cava and demonstration of perfusion. *Eur J Cardiothorac Surg* 1996; **10**: 833–8.

11 Razumovsky AY, Tseng EE, Hanley DF, Baumgartmer WA. Cerebral hemodynamic changes during retrograde brain perfusion in dogs. *J Neuroimaging* 2001; **11**: 171–8.

12 Sakahashi H, Hashimoto A, Aomi S, Tokunaga H, Koyanagi T, Imamaki M, Tagusari O, Hirai M, Satoh M, Koyanagi H. Transcranial Doppler measurement of middle cerebral artery blood flow during continuous retrograde cerebral perfusion. *Nippon Kyobu Geka Gakkai Zasshi* 1994; **42**: 1851–7 [in Japanese].

13 Quigley RL, Fuller BC, Sampson LN, Reitknecht FL. Passive retrograde cerebral perfusion during routine cardiac valve surgery reverses middle cerebral artery blood flow and reduces risk of stroke. *J Heart Valve Dis* 1997; **6**: 288–91.

14 Tanoue Y, Tominaga R, Ochiai Y *et al.* Comparative study of retrograde and selective cerebral perfusion with transcranial Doppler. *Ann Thorac Surg* 1999; **67**: 672–5.

15 Wong C, Bonser RS. Retrograde perfusion and true reverse brain blood flow in humans. *Eur J Cardiothorac Surg* 2000; **17**: 597–601.

16 Garami Z, Estrera A, Scheinbaum R, Calleja S, Chernyshev O, Uchino K, Malkoff M, Alexandrov AV, Safi H. Monitoring of cerebral blood flow with power mode Doppler TCD during retrograde cerebral perfusion. *Cerebrovasc Dis* 2002; **13** (Suppl. 4): 38.

17 Clark RE, Brillman J, Davis DA, Lovell MR, Price TR, Magovern GJ. Microemboli during coronary artery bypass grafting. Genesis and effect on outcome. *J Thorac Cardiovasc Surg* 1995; **109** (2): 249–57.

18 Stump DA, Kon NA, Rogers AT, Hammon JW. Emboli and neuropsychological outcome following cardiopulmonary bypass. *Echocardiography* 1996; **13**: 555–8.

19 Brown WR, Moody DM, Challa VR, Stump DA. Histologic studies of brain microemboli in humans and dogs after cardiopulmonary bypass. *Echocardiography* 1996; **13**: 559–66.

20 Brown WR, Moody DM, Challa VR, Stump DA, Hammon JW. Longer duration of cardiopulmonary bypass is associated with greater numbers of cerebral microemboli. *Stroke* 2000; **31**: 707–13.

MCA stenosis

With Robert A. Felberg, MD

Introduction

Intracranial stenotic lesions are increasingly recognized as a significant risk factor for ischemic stroke, and genetic predisposition of certain ethnic groups has been described [1–3]. Several velocity thresholds were previously proposed to identify a significant middle cerebral artery (MCA) stenosis [4–7]. These criteria include, but are not restricted to, mean flow velocity (MFV) of 100 cm/s, MFV of 120 cm/s and peak systolic velocity (PSV) of 140 cm/s. A single velocity threshold does not account for obvious effects of age and hematocrit on velocity. Therefore, in addition to the highest velocity value, we suggest using a ratio between this velocity and the velocity in a homologous vessel or a non-affected segment of the same vessel [8].

As a rule for a vessel with straight walls, a 50% diameter reduction doubles the velocity and a 70% stenosis triples the velocity at the exit of stenosis compared to a prestenotic segment (Figure 1) or to the contralateral side.

Chimowitz *et al.* in the Warfarin Aspirin Stroke in Intracranial Disease (WASID) trial identified a significant MCA stenosis at 50% diameter reduction or greater [9,10]. The Stroke Outcomes and Neuroimaging (SONIA) project prospectively validates MFV thresholds for transcranial Doppler (TCD) to achieve a greater than 80% positive predictive value of ultrasound screening (E. Feldmann 2001, personal communication). Wong and colleagues are using PSV cut-offs in their prospective studies [3]. The following examples illustrate false-positive and true-positive results of ultrasound screening for ≥ 50% MCA stenosis.

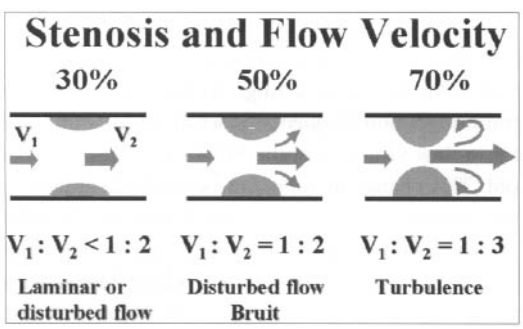

Figure 1 The relationship between pre- and poststenotic velocities in a vessel with straight walls and no bifurcations.

Figure 2 shows TCD findings in a 71-year-old hypertensive female 2 days after ischemic stroke in the right MCA that resulted in hemiparesis. If a 100-cm/s MFV threshold is applied alone, TCD indicates a 50% right MCA stenosis. An angiogram shows some degree of a proximal M1 stenosis but not sufficient to measure a 50% diameter reduction using the WASID method. According to the WASID method [9,10], the diameter of the residual lumen should be measured using high-precision calipers on a hard copy angiographic film. Then, a normal or reference diameter has to be measured in one of the three following locations (Figure 3). This location has to have a normal vessel segment with parallel walls and free of atheroma. If location 1 is affected, then the observer selects location 2. If location 2 is also affected, only then is location 3 used:

1 same artery proximal to the stenosis;
2 same artery distal to the stenosis;
3 feeding artery.

As presented in this case (Figures 2 & 3), TCD showed an abnormal result for a 71-year-old patient with a stroke. The source of false-positive TCD findings is transient velocity increase due to recanalization and/or hemodilution and anticoagulation that this patient received in hospital. Often, velocities decrease after the 1st week of stroke and a follow-up TCD may show different results. Also, digital subtraction angiography may underestimate stenosis severity since only one projection was used and a normal M1 segment proximal to the lesion was not available for calculations. A comparison of the residual lumen to the second-choice

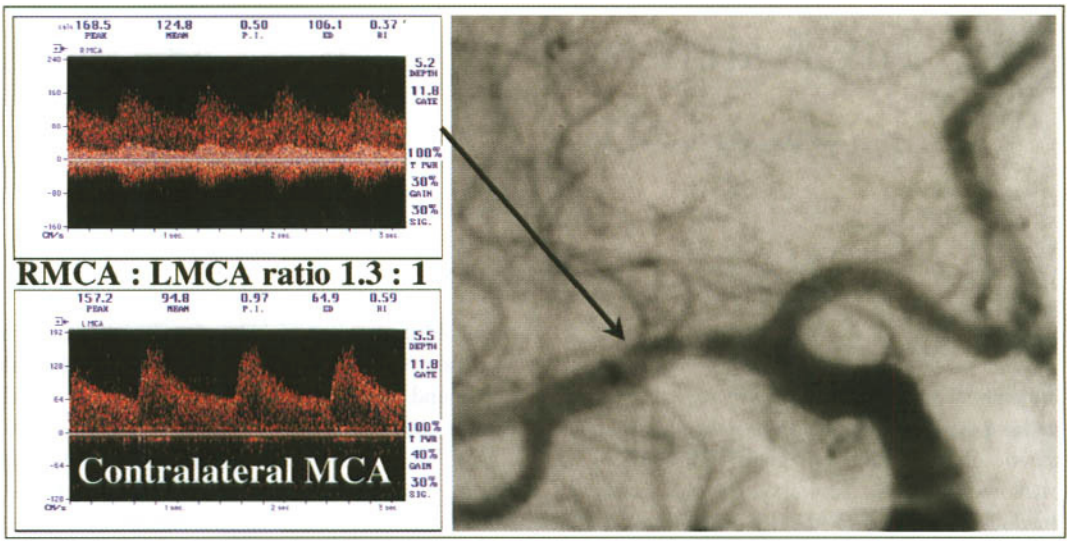

Figure 2 A false-positive transcranial Doppler diagnosis of middle cerebral artery stenosis of > 50% by the WASID criteria.

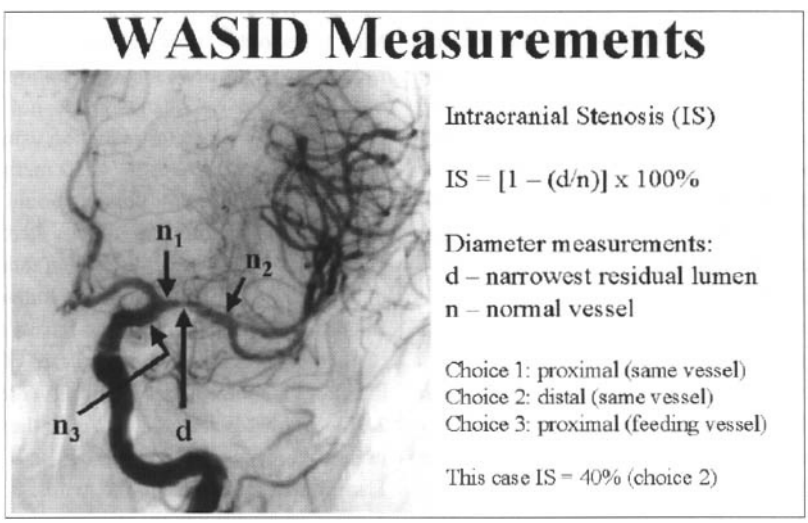

Figure 3 WASID measurements of intracranial stenosis.

measurement (M1 distal to the lesion) yields only a 40% diameter reduction. Nevertheless, the M1 lesion appears not to be hemodynamically significant since there is a good and rapid contrast opacification of the distal MCA branches and there is no blunting of the distal MCA waveform and no signs of flow diversion to the anterior or posterior cerebral artery (ACA or PCA) on TCD.

Transcranial color sonography (TCCS) can also be used to detect MCA stenosis [11]. As shown in Figure 4, courtesy of Dr Eva Bartels, a focal velocity elevation may present with color aliasing even with high color flow scale settings. In this case, color flow pulse repetition frequency is set at 80 cm/s and the mean flow velocities in the MCA exceed this threshold. This change in color can be easily identified by the examiner and will help guide spectral Doppler interrogation. If angle correction is applied, then the velocity value detected by TCCS will be higher than those measured by TCD. Very few angle-corrected diagnostic criteria are available for TCCS studies of intracranial disease [11]. To apply TCD criteria to

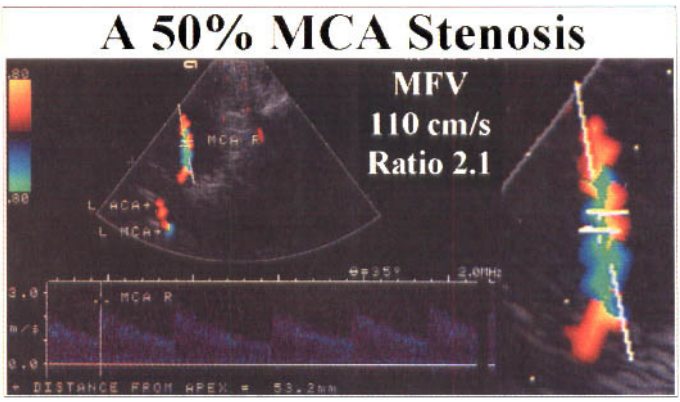

Figure 4 Transcranial color-coded duplex findings indicating approximately 50% M1 middle cerebral artery stenosis. A zoomed image (right) illustrates color aliasing and angle correction. (Image courtesy of Dr Eva Bartels.)

TCCS, a 0° angle should be used. In this case (Figure 4), MFV was measured at 100 cm/s when a 0° angle was applied. Regardless of angle correction, the velocity ratio of 2.1 in this case points to approximately 50% MCA diameter reduction (comparison to a proximal right M1 MCA segment and contralateral side).

Color appearance of the MCA flow cannot be used to measure percentage stenosis since the reduction in vessel size can be produced not only by the lesion itself but also by out-of-scanning-plane vessel position due to a tortuous course of the MCA. Also, color flow image may leave an impression of no diameter reduction due to overgaining and bleeding artifact as well as relatively comparable size of the wavelength and vessel dimensions and sound scattering at the vessel walls.

TCCS can identify which MCA segment (distal M1 or M2) is affected. Color flow imaging clearly shows the proximal, middle and distal portions of the M1 MCA segment and the origins of the M2 branches. Without imaging, uncertainty arises due to variability of head sizes and vessel location. Using TCD for an average-size adult patient, we arbitrarily assign the proximal M1 MCA lesions to depths of 65–55 mm, mid-to-distal M1 at 55–45 mm [12] and M2 subdivision branches at depths less than 45 mm. If a stenotic signal is found at 65–60-mm depth, the differential diagnosis includes the terminal ICA stenosis and collateralization of flow through the posterior communicating artery or ACA flow reversal.

A single-gate TCD can miss MCA stenoses located in the M2 segments, particularly if insonation depths were limited to 65–45 mm. An example of a stenosis located at shallow depths and visualization of associated turbulence with M-mode TCD are shown in Figure 5.

Case presentation

A 47-year-old white male with past medical history of hypertension, smoking and diabetes presented to the emergency room at 45 min after sudden onset of left-sided weakness. On examination, he is alert and shows no signs of neglect. He is plegic on his left side and the NIHSS score is 8. A non-contrast computed tomography (CT) scan is normal, and the ASPECTS score is 10. The risks and benefits of intravenous tissue plasminogen activator (TPA) therapy are being explained to the patient. During this, the patient spontaneously starts to move his left extremities, regaining full strength at 1 h after the onset of symptoms. In 2 min, he starts to complain of inability to move his left arm and leg again. After a short period of weakness, he regains full strength again, and this fluctuation of his deficit occurs several times over a span of 10 min.

Diagnostic considerations

Clinical examination and head CT are consistent with an acute and potentially reversible ischemic event. The patient was a candidate for intravenous TPA therapy before spontaneous improvement. Subsequent deterioration makes him eligible for thrombolysis again; however, the risk-to-benefit ratio of thrombolysis in patients with crescendo transient ischemic attacks (TIAs) is unclear. Furthermore, the symptoms of pure motor weakness may be psychogenic or, in the case of cerebral ischemia, the stroke pathogenic mechanism may be lacunar or due to a thrombus in a large vessel. Lesion localization is also uncertain, i.e. anterior vs. posterior circulation vessels. Bedside ultrasound was

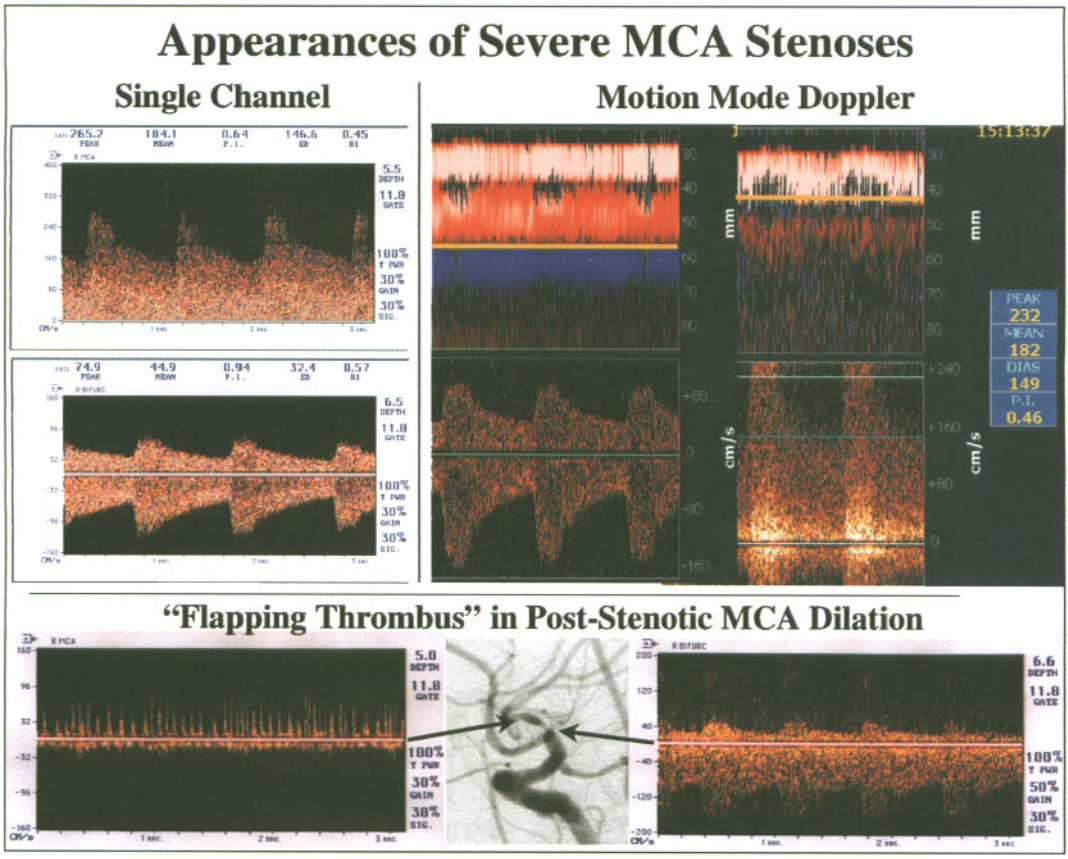

Figure 5 Severe MCA stenoses may have focal significant elevation of velocities as shown in top left case using single-channel TCD instrument. M1 MCA MFV is 184 cm/s vs. 45 cm/s at M1 origin (ratio 4.1). Top right case illustrates severe M2 MCA subdivision stenosis with bruit and focal velocity elevation at 42 mm. Both single-channel and M-mode studies demonstrate significant elevation of MCA end-diastolic velocities indicating the severity of arterial narrowing above 80% diameter reduction. Bottom series of images illustrate TCD findings in a patient presenting with acutely resolving left-sided weakness and reverberating flow signal in the M1 MCA (bottom left image). During each cardiac cycle, 7–9 flow reverberations are present indicating that a mobile lesion in the M1 MCA is acting like a valve. This flow signature was likely produced by a 'flapping' thrombus trapped in a post-stenotic dilatation demonstrated by DSA (bottom middle image) shortly after recanalization was completed and a residual severe proximal MCA stenosis has been identified as the likely source of thrombosis. All cases have evidence of flow diversion to ACA indicating hemodynamic significance of MCA stenoses.

ordered to rapidly determine patency of the right middle artery as the most likely vessel to be affected. The aim was to perform TCD during redevelopment of symptoms since at this time TCD may yield different results.

Ultrasound findings

A single-channel non-image-guided TCD was performed when the patient redeveloped left-sided weakness. TCD showed a focal velocity increase in the proximal-to-middle portion of the right M1 MCA with MFV of 215 cm/s at the depth of 55 mm (Figure 6, upper images). Clusters of multiple embolic signals (Figure 6, upper Doppler spectrum) were heard during routine TCD examination. These signals were too numerous to count and they caused marked interference with the spectral velocity analysis. However, each embolic signature had a short duration and high intensity and was uniformly slow moving (note clusters in the low-frequency range). This type of embolism appearance in real time has been described

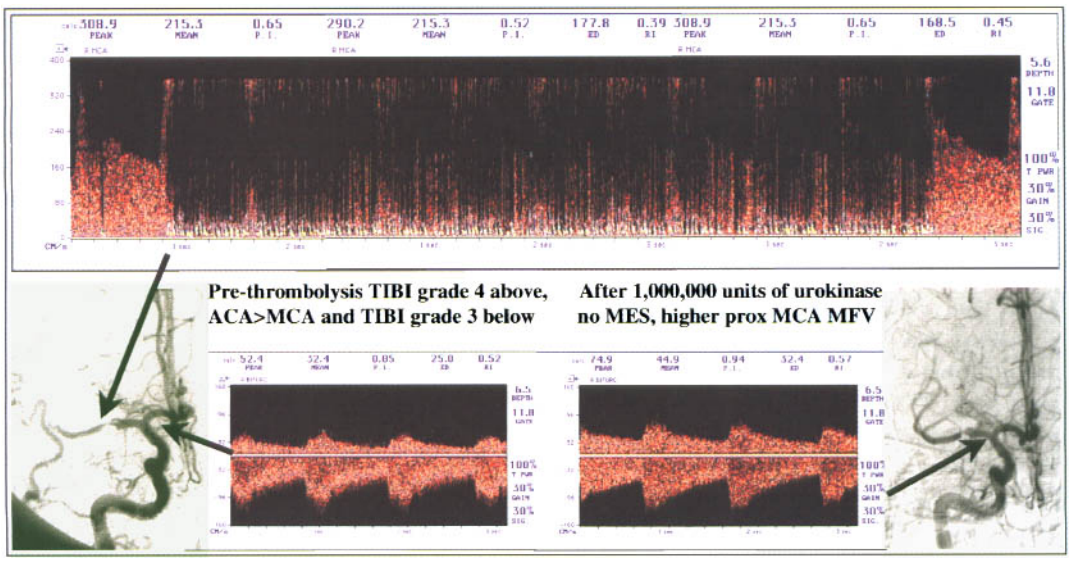

Figure 6 Severe M1 MCA stenosis and clusters of microembolic signals (MES) in a patient with crescendo TIAs. Upper image show single-channel recording of focal significant elevation of M1 MCA velocities and clusters of MES moving slowly through the sample volume (high intensity, short duration, unidirectional signals near baseline). Bottom left DSA image shows severe M1 MCA stenosis and obstruction of the M2 subdivision flow due to artery-to-artery embolism. Bottom left TCD spectra shows dampened proximal M1 MCA signal and flow diversion to ACA prior to intra-arterial procedure. Bottom right TCD spectra shows increase in the proximal M1 MCA MFV and persistence of flow diversion to the ACA after successful intra-arterial thrombolysis of distal occlusion with urokinase. Bottom left DSA image shows residual severe M1 MCA stenosis after distal thrombolysis.

by Siebler *et al.* and Segura *et al.* in the setting of MCA stenosis and focal MCA symptoms [13,14]. Wong and his group also reported embolic signals at the site just distal to the MCA stenosis and observed velocity changes as the embolus was dislodged from the lesion surface [15]. The low spectral frequency and curtain-like appearance of embolic signals in our case indicate active emboligenic surface associated with a significant MCA narrowing.

Interpretation

A severe (≥ 80% diameter reduction) mid-M1 right MCA stenosis with continuing unstable clot dissolution presenting with clusters of high-intensity embolic signals and flow diversion to the right ACA.

Correlative imaging

Digital subtraction angiography (DSA) was performed 50 min later and it showed a severe mid-M1 MCA stenosis and TIMI grade I occlusion of the M2 branches (Figure 6).

Differential diagnosis

TCD provides evidence for an ischemic nature of the recurrent neurologic deficit and points to a high-grade stenotic lesion in the MCA as the source of artery-to-artery embolization. This lesion may be atherosclerotic or embolic in origin. The absence of embolic signals in the contralateral MCA makes a proximal source of embolization (i.e. heart) unlikely. The absence of emboli in the right TICA and the proximal M1 MCA indicates a focal mid-M1 MCA lesion as a source of embolization.

Management

Although our patient presents within a conventional window for intravenous thrombolysis with TPA and each new episode of focal weakness makes him eligible for this therapy, insight into the underlying pathogenesis made us consider urgent diagnostic angiography as the next most appropriate step. DSA will help to select patient treatment dependent on the nature of the lesion, i.e. a thrombus, atheroma or dissection. DSA showed a high-grade M1 MCA stenosis likely of

atherosclerotic origin and thrombi in the M2 MCA branches. Intra-arterial urokinase was administered and TIMI grade III recanalization was achieved (Figure 6). The patient was offered an experimental angioplasty for the residual mid-M1 MCA stenosis which he declined.

Follow-up

At the time of diagnostic DSA the patient again had hemiplegia. After thrombolysis he regained strength and no symptom recurrence was noted in the next 48 h. Repeat TCD showed an MFV of 184 cm/s with ratio > 4 consistent with a ≥ 80% residual MCA stenosis. No embolic signals were detected distal to the stenosis at 24 h, 48 h and discharge. After 4 days on heparin, the patient was offered to start taking coumadin which he declined. He left hospital without neurologic deficit and started to take 350 mg of aspirin daily.

The decision to offer heparin and coumadin was made since a greater than 50% MCA stenosis bears at least a 7% per year risk of stroke in a retrospective WASID study [9]. More recent prospective studies support these findings and put a significant intracranial stenosis along the line of other major risk factors for stroke [16,17]. The question whether anticoagulation or antiplatelet therapy is efficacious in secondary stroke prevention will be answered in a randomized phase of the WASID study. The use of low-molecular-weight heparinoids is promising for early treatment and secondary stroke prevention in the patient population with high prevalence of intracranial disease [18], and this approach is being tested in an ongoing FISS-TRIS randomized trial (R. Kay, personal communication). There are also preliminary data that statins help reduce severity of the MCA lesions on MRA and possibly the number of recurrent strokes attributable to the artery-to-artery embolism (K. S. Wong *et al.* 2002, unpublished data).

References

1 Sacco RL, Kargman DE, Gu Q, Zamanillo MC. Race-ethnicity and determinants of intracranial atherosclerotic cerebral infarction. The Northern Manhattan Stroke Study. *Stroke* 1995; **26**: 14–20.

2 Wityk RJ, Lehman D, Klag M, Coresh J, Ahn H, Litt B. Race and sex differences in the distribution of cerebral atherosclerosis. *Stroke* 1996; **27**: 1974–80.

3 Wong KS, Huang YN, Gao S, Lam WW, Chan YL, Kay R. Intracranial stenosis in Chinese patients with acute stroke. *Neurology* 1998; **50**: 812–3.

4 de Bray JM, Joseph PA, Jeanvoine H, Maugin D, Dauzat M, Plassard F. Transcranial Doppler evaluation of middle cerebral artery stenosis. *J Ultrasound Med* 1988; **7**: 611–6.

5 Babikian V, Sloan MA, Tegeler CH, DeWitt LD, Fayad PB, Feldmann E, Gomez CR. Transcranial Doppler validation pilot study. *J Neuroimaging* 1993; **3**: 242–9.

6 Rorick MB, Nichols FT, Adams RJ. Transcranial Doppler correlation with angiography in detection of intracranial stenosis. *Stroke* 1994; **25**: 1931–4.

7 Alexandrov AV, Bladin CF, Norris JW. Intracranial blood flow velocities in acute cerebral ischemia. *Stroke* 1994; **25**: 1378–83.

8 Felberg RA, Christou I, Demchuk AM, Malkoff M, Alexandrov AV. Screening for intracranial stenosis with transcranial Doppler: the accuracy of mean flow velocity thresholds. *J Neuroimaging* 2002; **12**: 9–14.

9 Chimowitz MI, Kokkinos J, Strong J, Brown MB, Levine SR, Silliman S, Pessin MS, Weichel E, Sila CA, Furlan AJ. The Warfarin-Aspirin Symptomatic Intracranial Disease Study. *Neurology* 1995; **45**: 1488–93.

10 Samuels OB, Joseph GJ, Lynn MJ, Smith HA, Chimowitz MI. A standardized method for measuring intracranial arterial stenosis. *AJNR Am J Neuroradiol* 2000; **21**: 643–6.

11 Baumgartner RW, Mattle HP, Schroth G. Assessment of ≥ 50% and < 50% intracranial stenoses by transcranial color-coded duplex sonography. *Stroke* 1999; **30**: 87–92.

12 Monsein LH, Razumovsky AY, Ackerman SJ, Nauta HJ, Hanley DF. Validation of transcranial Doppler ultrasound with a stereotactic neurosurgical technique. *J Neurosurg* 1995; **82** (6): 972–5.

13 Siebler M, Steinmetz H. Microemboli detection in patients with intracranial artery disease. In: Klingelhofer J, Bartels E, eds. *New Trends in Cerebral Hemodynamics and Neurosonology*. Amsterdam: Elsevier Science, 1997: 412–5.

14 Segura T, Serena J, Molíns A, Dávalos A. Clusters of microembolic signals: a new form of cerebral microembolism presentation in a patient with middle cerebral artery stenosis. *Stroke* 1998; **29**: 722–4.

15 Gao S. Novel observations of the characteristics of real-time genesis of thromboembolism in middle cerebral artery stenosis detected by transcranial Doppler. *J Neuroimaging* 2002; **12**: 196 [abstract].

16 Segura T, Serena J, Castellanos M, Teruel J, Villar C, Davalos A. Embolism in acute middle cerebral artery stenosis. *Neurology* 2001; **56**: 497–501.

17 Wong KS, Li H, Lam WWM, Chan YL, Kay R. Progression of middle cerebral artery occlusive disease and its relationship with further vascular events after stroke. *Stroke* 2002; **33**: 532–6.

18 Kay R, Wong KS, Yu YL *et al.* Low-molecular-weight heparin for the treatment of acute ischemic stroke. *N Engl J Med* 1995; **333**: 1588–90.

Acute tandem occlusion

With Ashraf El-Mitwalli, MD, PhD *& Joon Song*, MD

Introduction

Previously proposed criteria for intracranial occlusions mostly focused on the absence of flow signals at presumed thrombus location and/or velocity asymmetry between homologous segments, i.e. middle cerebral arteries (MCAs) [1–8]. A complete arterial occlusion should produce no detectable flow signals, and this is particularly true when a chronic proximal internal carotid artery (ICA) occlusion is evaluated with Doppler ultrasound. However, with acute occlusion by an embolus or *in situ* thrombosis, some residual flow to or around the thrombus may exist due its irregular shape, relatively soft composition and systolic pressures that cause additional distension of arterial walls. An acute occlusion may therefore present with a variety of waveforms on transcranial Doppler (TCD) representing this residual flow [9].

In cardiology, the thrombolysis in myocardial infarction (TIMI) flow grading system was developed to assess the residual flow with invasive angiography [10]. The amount of residual flow predicts success of coronary thrombolysis [11] since tissue plasminogen activator (TPA) binds to fibrin sites at the clot surface and increasing amounts of residual flow bring more TPA to the clot. Unlike coronary arteries that are small and move considerably with heart contractions, the proximal branches of the circle of Willis are more steadily positioned and can be easily targeted with ultrasound [12]. We have developed the thrombolysis in brain ischemia (TIBI) flow grading system to evaluate residual flow non-invasively [9] and monitor thrombus dissolution in real time [13,14]. The TIBI system expands previous definitions of an acute arterial occlusion by focusing the examiner's attention on relatively weak signals with abnormal-flow waveforms that can be found along arterial stems filled with thrombi [9,13]. TIBI flow grades correlate with stroke severity and mortality as well as the likelihood of recanalization and clinical improvement [9].

Acute arterial occlusion is a dynamic process since thrombus can propagate, break up or rebuild within seconds or minutes, thereby changing the degree of arterial obstruction [15–17]. When we use the term acute occlusion, we mean that there is a hemodynamically significant obstruction to flow and these ultrasound findings suggest that if an urgent angiography is performed, it will likely show an arterial lesion that may be amenable to intervention. Furthermore, ultrasound may suggest that more than one occlusion is present in the same patient, e.g. tandem lesions in the ICA and MCA [18], or vertebral and basilar artery.

Bedside ultrasound examination in acute cerebral ischemia can help to:

1 identify flow obstruction or thrombus presence;
2 determine thrombus location(s);
3 assess collateral supply;
4 find the worst residual flow signal; and
5 monitor recanalization and reocclusion.

Case presentation

A 65-year-old white male with past medical history of previous myocardial infarction, hypertension and smoking presented to the emergency room at 90 min after sudden onset of left-sided weakness. On examination, he is alert, orientated and follows commands. He has a partial gaze preference and left-sided hemiparesis (arm > leg) with a National Institutes of Health Stroke Scale (NIHSS) score of 5 points. Non-contrast computed tomography (CT) shows a slightly hyperdense distal right MCA with no early ischemic changes in brain tissue with an Alberta Stroke Program Early CT Score (ASPECTS) of 10 points [19]. A decision to initiate standard intravenous TPA therapy was made according to the NINDS rt-PA Stroke Study criteria [20], and irrespective of the pre-TPA TCD results presented below. A TPA bolus is given at 122 min after stroke onset. At the end of TPA infusion, his NIHSS score is 2 points.

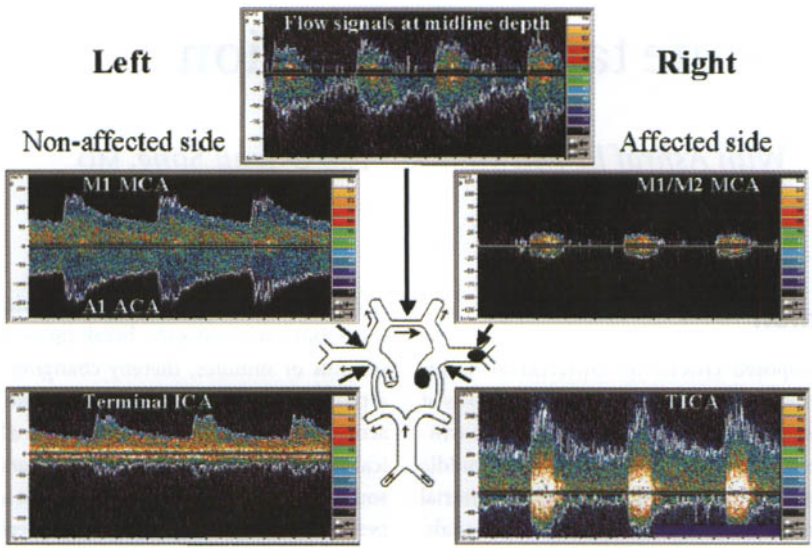

Figure 1 Transcranial Doppler waveforms in a patient with acute tandem ICA/MCA occlusion.

Diagnostic considerations

Clinical examination and head CT are consistent with an acute and potentially reversible ischemic event [19,20]. The patient is a candidate for a standard intravenous TPA therapy within the first 3 h after stroke onset since he has an NIHSS score of 5 points without signs of symptom resolution [20]. He has a hyperdense MCA sign on CT that suggests the presence of thrombus in the distal M1 MCA or M2 subdivision [21]; however, the severity of stroke is relatively mild for this level of obstruction. Gaze preference and weakness distribution indicate cortical location of ischemia while involvement of the right MCA usually produces lower NIHSS scores compared to the same lesions in the left MCA. In other words, there is no clinical indication that his clot burden may be far greater than just an MCA branch. Bedside ultrasound was ordered to rapidly determine whether any proximal occlusion was present, and whether other flow findings such as an early and partial recanalization, the distal MCA clot location, higher TIBI grades of residual flow, and flow diversion may explain his relatively low NIHSS score [18].

Ultrasound findings

A single-channel TCD showed a minimal mid-M1 flow signal at the depth of 50 mm (TIBI grade 1, Figure 1), positive diastolic flow in the proximal MCA, and a stenotic flow signal with harsh systolic bruits at the depths of the terminal ICA, posterior communicating and posterior cerebral arteries. No flow signals were obtained from the right siphon and ophthalmic artery through the transorbital window. On the contralateral side, TCD showed flow diversion to the anterior cerebral artery (ACA) (mean flow velocity (MFV) MCA < ACA; pulsatility MCA > ACA).

Interpretation

TCD showed:

1 an acute right M1–M2 subdivision occlusion with patent proximal right M1 MCA segment at perforators;

2 a hemodynamically significant, possibly acute right ICA obstruction likely extending from the neck; and

3 functioning collateral channels including left-to-right anterior cross-filling via the anterior communicating (AComA) and the right posterior communicating arteries.

Correlative imaging

Digital subtraction angiography (DSA) was performed 2 h after TPA bolus and it showed an occlusion of the right ICA at the bulb and patent proximal right M1 MCA filled through intracranial collaterals.

There was a blush of contrast to the perforating arteries. A partial distal M1 MCA occlusion was seen with TIMI grade II flow. Despite tandem occlusions, there was a good accumulation of contrast in the right MCA territory during the capillary phase.

Differential diagnosis

TCD findings may also be produced by an MCA or terminal ICA occlusion with pre-existing atretic unilateral A1 ACA. In the latter case, one might expect to find a partial anterior cross-filling via AComA to supply both A2 ACA segments that existed before acute occlusion. The incomplete circle of Willis does not usually lead to the MFV increase to stenotic values, and the contralateral ACA > MCA MFV findings suggest either a suboptimal angle of insonation, i.e. comparison of TICA and ACA velocities, or at least partial anterior cross-filling. If no isolated MCA or ACA stenosis is present, it is possible to rule out the potential technical error of sampling TICA instead of MCA by comparison of the highest ACA and the highest MCA velocities at depths other than ICA bifurcation. The ACA velocity usually exceeds MCA velocities by 10–20% or more when it supplies more than just A2 ACA territories [1,2,6].

The presence of a stenotic signal in the terminal ICA may indicate the development of a new collateral channel as well as some residual stenotic flow around thrombus in the terminal ICA. A positive diastolic flow at the M1 MCA origin suggests flow to the nearest bifurcation, and perforating arteries originating from the M1 stem before M2 branches. This finding of positive diastolic flow at M1 origin often helps to explain paresis (as opposed to plegia) in the arm and leg in the presence of tandem ICA/MCA occlusion. TCD and DSA findings correlate well and explain relatively low NIHSS scores in patients with tandem ICA/MCA occlusions [18].

The proximal right ICA occlusion may be acute or chronic. The presence of the M1 subdivision occlusion and stenotic terminal ICA signals suggest acute carotid thrombosis with M1 MCA embolization from a more proximal lesion. Other findings that can strengthen this hypothesis include TCD detection of emboli in the carotid branches and fluctuating patency of the MCA. Carotid duplex may show a hypoechoic intraluminal zone on B-mode with no color or Doppler flow signals, and tenuous residual flow in the proximal ICA. These findings would favor an acute proximal ICA occlusion with pre-existing atheromatous disease.

Management

This patient presents in a conventional window for intravenous thrombolysis for stroke. Intravenous TPA may lyse distal M1/M2 MCA occlusions but is far less successful in dissolving thrombus in the proximal ICA [22,23]. Lower NIHSS scores and early recovery are related to collateralization of flow and resumption of the MCA flow in patients with tandem occlusions [18,23]. Our data also indicate that TCD shows flow signal improvement in only 10% of ICA occlusions treated with intravenous TPA, and that complete ICA recanalization is rare without intra-arterial intervention [23]. Therefore, TCD screening of patients with tandem occlusion may help to find patients suitable for combined intravenous/intra-arterial thrombolysis if this strategy proves successful in clinical trials [24].

Besides thrombolysis, this patient needs careful monitoring of blood pressure, fluid regimen and patency of the proximal MCA since the presence of a proximal ICA obstruction may lead to reocclusion and deterioration following initial improvement [16,17,25].

TCD cannot differentiate a complete ICA occlusion from a high-grade stenosis [26]. After receiving systemic thrombolytic therapy, this patient is a candidate for early diagnostic angiography to determine the degree and nature of the proximal ICA obstruction. A complete occlusion can be differentiated from near-occlusion if a catheter is placed at the bulb and contrast is injected directly at the obstruction site. If some residual flow is present in the ICA, this patient may be a candidate for intra-arterial thrombolysis, new experimental clot-disrupting devices and angioplasty of residual stenosis [27]. If a severe residual ICA stenosis is found after thrombolysis, this information is helpful to tailor secondary stroke prevention strategies, e.g. carotid endarterectomy. This patient may also be a candidate for early anticoagulation and/or stenting if these modalities prove effective in future clinical trials.

Follow-up

This patient improved by the end of TPA infusion (no gaze preference, full leg strength and a total NIHSS

score of 2 points). Partial MCA recanalization with TIMI grade II flow was seen at 2.5 h after TPA bolus. Invasive angiography also showed a complete proximal ICA occlusion at the bulb. Repeat CT at 20 h after stroke onset showed no hemorrhagic transformation or hypoattenuation in the right MCA territory. Intravenous heparin was started 24 h after TPA bolus, even though this indication has not been confirmed or disproved in randomized clinical trials [28]. A weight-based nomogram can be used for this purpose that allows fewer mistakes in dose adjustments [29]. Repeat TCD at 48 h showed complete distal MCA recanalization and intracranial collateral flow compensating for ICA occlusion. Heparin was discontinued on Day 4 after symptom onset. He was discharged home on aspirin combined with slow-release dipyridamole and pravastatin. His modified Rankin score at 3 months was 0.

References

1 Lindegaard K-F, Bakke SJ, Aaslid R, Nornes H. Doppler diagnosis of intracranial occlusive disorders. *J Neurol Neurosurg Psychiatry* 1986; **49**: 510–8.

2 Grolimund P, Seiler RW, Aaslid R, Huber P, Zurbruegg H. Evaluation of cerebrovascular disease by combined extracranial and transcranial Doppler sonography. Experience in 1,039 patients. *Stroke* 1987; **18**: 1018–24.

3 Halsey J. Prognosis of acute hemiplegia estimated by transcranial Doppler sonography. *Stroke* 1988; **19**: 648–9.

4 Zanette EM, Fieschi C, Bozzao L, Roberti C, Toni D, Argentino C, Lenzi GL. Comparison of cerebral angiography and transcranial Doppler sonography in acute stroke. *Stroke* 1989; **20**: 899–903.

5 Kaps M, Damian MS, Teschendorf U, Dorndorf W. Transcranial Doppler ultrasound findings in the middle cerebral artery occlusion. *Stroke* 1990; **21**: 532–7.

6 Ley-Pozo J, Ringelstein EB. Noninvasive detection of occlusive disease of the carotid siphon and middle cerebral artery. *Ann Neurol* 1990; **28**: 640–7.

7 Carmelingo M, Casto L, Censori B, Ferraro B, Gazzaniga GC, Mamoli A. Transcranial Doppler in acute ischemic stroke of the middle cerebral artery territories. *Acta Neurol Scand* 1993; **88**: 108–11.

8 Razumovsky AY, Gillard JH, Bryan RN, Hanley DF, Oppenheimer SM. TCD, MRA, and MRI in acute cerebral ischemia. *Acta Neurol Scand* 1999; **99**: 65–76.

9 Demchuk AM, Burgin WS, Christou I, Felberg RA, Barber PA, Hill MD, Alexandrov AV. Thrombolysis in Brain Ischemia (TIBI) transcranial Doppler flow grades predict clinical severity, early recovery, and mortality in patients treated with tissue plasminogen activator. *Stroke* 2001; **32**: 89–93.

10 The TIMI Study Group. The Thrombolysis in Myocardial Infarction (TIMI) trial: phase I findings. *N Engl J Med* 1985; **312**: 932–6.

11 Anderson JL. Why does thrombolysis fail? Breaking through reperfusion ceiling. *Am J Cardiol* 1997; **80**: 1588–90.

12 Alexandrov AV, Demchuk AM, Felberg RA, Christou I, Barber PA, Burgin WS, Malkoff M, Wojner AW, Grotta JC. High rate of complete recanalization and dramatic clinical recovery during TPA infusion when continuously monitored by 2 MHz transcranial Doppler monitoring. *Stroke* 2000; **31**: 610–4.

13 Burgin WS, Malkoff M, Felberg RA, Demchuk AM, Christou I, Grotta JC, Alexandrov AV. Transcranial Doppler ultrasound criteria for recanalization after thrombolysis for middle cerebral artery stroke. *Stroke* 2000; **31**: 1128–32.

14 Alexandrov AV, Burgin WS, Demchuk AM, El-Mitwalli A, Grotta JC. Speed of intracranial clot lysis with intravenous TPA therapy: sonographic classification and short term improvement. *Circulation* 2001; **103**: 2897–902.

15 Demchuk AM, Wein TH, Felberg RA, Christou I, Alexandrov AV. Evolution of rapid middle cerebral artery recanalization during intravenous thrombolysis for acute ischemic stroke. *Circulation* 2000; **100**: 2282–3.

16 Burgin WS, Alexandrov AV. Deterioration following improvement with TPA therapy: carotid thrombosis and re-occlusion. *Neurology* 2001; **56**: 568–70.

17 Alexandrov AV, Grotta JC. Arterial re-occlusion in stroke patients treated with intravenous tissue plasminogen activator. *Neurology* 2002; **59**: 862–67.

18 El-Mitwalli A, Saad M, Christou I, Malkoff M, Alexandrov AV. Clinical and sonographic patterns of tandem ICA/MCA occlusion in TPA treated patients. *Stroke* 2002; **33**: 99–102.

19 Barber PA, Demchuk AM, Zhang J, Buchan AM. Validity and reliability of a quantitative computed tomography score in predicting outcome of hyperacute stroke before thrombolytic therapy. *Lancet* 2000; **355**: 1670–4.

20 The National Institutes of Neurological Disorders and Stroke rt-PA Stroke Study Group. Tissue plasminogen activator for acute ischemic stroke. *N Engl J Med* 1995; **333**: 1581–7.

21 Barber PA, Demchuk AM, Hudon ME, Pexman JH, Hill MD, Buchan AM. Hyperdense sylvian fissure MCA 'dot' sign: a CT marker of acute ischemia. *Stroke* 2001; **32**: 84–8.

22 Rudolf J, Neveling M, Grond M, Schmulling S, Stenzel C, Heiss WD. Stroke following internal carotid artery occlusion—a contra-indication for intravenous thrombolysis? *Eur J Neurol* 1999; **6**: 51–5.

23 Christou I, Felberg RA, Demchuk AM, Burgin WS, Grotta JC, Malkoff M, Alexandrov AV. Intravenous tissue plasminogen activator and flow improvement in acute ischemic stroke patients with internal carotid artery occlusion. *J Neuroimaging* 2002; **12**: 119–23.

24 Lewandowski CA, Frankel M, Tomsick TA, Broderick J, Frey J, Clark W, Starkman S, Grotta J, Spilker J, Khoury J, Brott T. Combined intravenous and intra-arterial r-TPA versus intra-arterial therapy of acute ischemic stroke: *Emergency Management* of *Stroke (EMS) Bridging Trial. Stroke* 1999; **30**: 2598–605.

25 Alexandrov AV, Felberg RA, Demchuk AM, Christou I, Burgin WS, Malkoff M, Wojner AW, Grotta JC. Deterioration following spontaneous improvement: sonographic findings in patients with acutely resolving symptoms of cerebral ischemia. *Stroke* 2000; **31**: 915–9.

26 Wilterdink JL, Feldmann E, Furie KL, Bragoni M, Benavides JG. Transcranial Doppler ultrasound battery reliably identifies severe internal carotid artery stenosis. *Stroke* 1997; **28**: 133–6.

27 Song JK, Cacayorin ED, Campbell MS, Fisher S, Malkoff MD, Alexandrov AV, Grotta JC. Intracranial balloon angioplasty of acute terminal internal carotid artery occlusion. *AJNR* 2002; **23**: 1308–12.

28 Hart RG, Easton JD. Do we really need a better way to give heparin in acute cerebral ischemia? *Stroke* 2002; **33**: 659–60.

29 Toth C, Voll C. Validation of a weight-based nomogram for the use of intravenous heparin in transient ischemic attack or stroke. *Stroke* 2002; **33**: 670–4.

Arterial recanalization and dramatic recovery from stroke

With Robert A. Felberg

Introduction

Arterial recanalization indicates successful thrombolysis and often precedes early clinical improvement in ischemic stroke [1–6]. Together with clot dissolution, the timing of recanalization determined *in vitro* represents an outcome measure of thrombolysis when clot is exposed to tissue plasminogen activator (TPA) with or without externally applied ultrasound [7–10]. This is often determined as the time of complete clot dissolution with washout to distal vasculature and veins. In human stroke, the timing of maximum completeness of recanalization on transcranial Doppler (TCD) correlates with clinical recovery as predicted from animal models [11]. However, recanalization is a process that often begins many minutes before restoration of cerebral blood flow [12] since TPA binding and activity on the clot surface are proportionate to the area exposed to blood flow. Once recanalization starts, clot softens and partially dissolves, allowing some (often minimal) residual flow improvement. This flow brings more TPA to bind with fibrinogen sites. This continuous process facilitates clot lysis and improves residual flow until the clot breaks up under the pressure of arterial blood pulsations [12]. Therefore, the speed of clot lysis can be measured through the duration of flow improvement assessed by the thrombolysis in brain ischemia (TIBI) residual flow signals [13] and other parameters such as intensity of flow signals, appearance of microembolic signals, velocity and pulsatility changes, etc. [12]. The speed of recanalization in human stroke is associated with early improvement and long-term outcome [12,14]. The speed, timing and amount of recanalization are several parameters of thrombolysis that can be determined with online ultrasound monitoring.

To measure the speed and completeness of intracranial clot lysis, it is important to determine the beginning of arterial recanalization using the five parameters (Figure 1):

1 waveform change by ≥ 1 TIBI residual flow grade (e.g. absent to minimal, minimal to blunted, etc. signal improvement);
2 appearance of embolic signals (transient high-intensity signals of variable duration);
3 flow velocity improvement by ≥ 30% at a constant angle of insonation;
4 signal intensity and velocity improvement of variable duration at constant skull/probe interface and gain/sample volume/scale settings; and
5 appearance of flow signals with variable (≥ 30%) pulsatility indices and amplitude of systolic peaks.

Once the recanalization process has started, TCD can detect the arrival of the highest TIBI flow grade that will indicate completion of recanalization (Figure 2).

Using these sonographic parameters, TCD can measure the:

1 beginning;
2 duration (or speed);
3 timing to maximum completeness; and
4 amount of arterial recanalization (complete, partial, none).

In patients who experience partial or complete thrombus dissolution, arterial recanalization can be classified as [12] (Figure 3):

1 sudden (abrupt appearance of a normal or stenotic low-resistance signal);
2 stepwise (flow improvement over 1–29 min); and
3 slow (≥ 30 min).

In patients receiving intravenous thrombolysis, recanalization began at a median time of 17 min and reached maximum TIBI flow grades at 35 min after TPA bolus, with mean duration of recanalization of 23 ± 16 min. In this study [12], recanalization was sudden in 12%, stepwise in 53% and slow in 35% patients. At 24 h, 80%, 30% and 13% of patients in these respective

Figure 1 Signs of the beginning and continuation of arterial recanalization:
1 waveform improvement by 1 or more TIBI residual flow grade: the first set illustrates flow changes from a minimal to blunted waveform (appearance of positive end-diastolic flow and rounded systolic complex);
2 appearance of embolic signals: the second set of waveforms illustrate dampened and normal flow signals with multiple transient high-intensity signals of variable duration with characteristic chirp or pop-like sounds (arrows);
3–4 flow velocity improvement by 30% or more or the signal intensity improvement: this set shows flow tracing obtained at a constant angle of insonation with mean flow velocity improvement from 15 cm/s to 30 cm/s preceded by the improvement in the strength (brightness) of the residual flow signal (middle set);
5 appearance of flow signals with variable (> 30%) amplitude of systolic peaks and pulsatility: a turbulent high-frequency, high-resistance stenotic flow signal (bottom left); variable velocities with transient appearance of flow in a branching vessel below the baseline (arrow) (bottom right).
(From Alexandrov AV *et al.* [12], with permission.)

Image Not Available

Image Not Available

Figure 2 Sequential flow changes with complete MCA recanalization during systemic thrombolysis. (Reproduced with permission from Demchuk AM *et al. Circulation* 2000; **100**: 2282–2283.)

Frame 1 A minimal flow signal in the proximal MCA at the time of intravenous rt-PA bolus (13 : 02).

Frames 2–3 Early restoration of flow signals with increasing frequencies and microembolic signals after 30 min of continuous intravenous rt-PA infusion (arrow).

Frame 4 A turbulent stenotic signal with audible chirping components suggesting continuing clot dissolution.

Frame 5 Hyperemic flow with velocities elevated above age-expected values and relatively low pulsatility (Gosling–King pulsatility index 0.73) indicating distal vasodilatation.

Frame 6 Hyperemic flow with velocities elevated above age-expected values and normal pulsatility (Gosling–King pulsatility index 0.93) showing a proximal MCA reperfusion with distal vasomotor response.

Figure 3 Speed of arterial recanalization.
I Sudden recanalization (abrupt appearance of normal or stenotic low-resistance signal). (a) Transcranial Doppler (TCD) shows minimal signal in middle cerebral artery (MCA) at time of tissue plasminogen activator (TPA) bolus. (b) At 31 min after bolus, first improvement in signal intensity was noticed and marked as 'beginning' of recanalization. (c) In less than 5 s, first low-resistance signal was detected with normal waveform and 30 s later (d), strong normal flow velocity signal was detected. Recanalization started at 31 min after TPA bolus, its duration was 35 s and timing of complete recanalization of distal M1 MCA segment (TIMI grade III equivalent) was 32 min after TPA bolus.
II Stepwise recanalization (flow improvement over 1–29 min). (a) TCD shows minimal signal in mid- to distal M1 MCA at time of TPA bolus. (b) Nine minutes later, TCD shows first improvement in amplitude of systolic velocities (beginning of recanalization); however, absence of end-diastolic velocities still indicates minimal TIBI flow signal and persisting occlusion. (c) At 14 min, positive end-diastolic flow is detected with rounded systolic shape of waveform (TIBI blunted signal) with flow improvement by 1 TIBI grade. Note high-intensity bruits during each cardiac cycle with possible embolic signals. (d) At 16 min, TCD shows high-resistance turbulent stenotic signals with elevated and variable systolic velocities that are replaced by normal waveforms at 18 min. (e) At this point, TCD findings indicate that M1 MCA patency at site of insonation is restored. Further improvement in flow velocity, pulsatility and strength of signal was detected between 18th and 20th minutes after bolus (f), indicating continuous flow recovery, presumably due to distal clot migration beyond M2 MCA bifurcation. TCD shows beginning of recanalization at 9 min, duration of 11 min, and timing of complete (TIMI grade III equivalent) recanalization at 20 min after TPA bolus.
III Slow recanalization (30–60 min). (a) At time of TPA bolus, TCD shows minimal flow signal at M1 MCA origin (above baseline) and flow signal below baseline from proximal A1 anterior cerebral artery (ACA) with mean flow velocity of 24 cm/s. (b) At 12 min after bolus, slow positive end-diastolic flow appears in proximal M1 MCA, indicating beginning of recanalization. Decrease in ACA flow signal may indicate clot movement or break-up at its proximal part. Variable M1 MCA and A1 ACA flow velocities with dampened TIBI flow grade are seen during next 40 min (c) with arrival of dampened flow signal with highest mean flow velocity of 28 cm/s and improved A1 ACA velocities of 54 cm/s at 54 min after TPA bolus (d). TCD findings indicate beginning of recanalization at 12 min, duration of 42 min, and timing of partial (TIMI grade II equivalent) recanalization with continuing flow diversion to ACA at 54 min after TPA bolus. (From Alexandrov AV *et al.* [12], with permission.)

recanalization groups had NIHSS scores of 0–3 points. Slow or partial recanalization with dampened TIBI flow signals was found in 53% of patients with total NIHSS scores ≥ 10 points at 24 h. Complete recanalization occurred faster (median 10 min) than partial recanalization (median 30 min), most likely due to changing velocities and intensity of flow signals in the latter group.

Therefore, rapid arterial recanalization is associated with better short-term improvement, mostly likely because of faster and more complete clot break-up with low resistance of the distal circulatory bed. Slow (≥ 30 min) flow improvement and dampened TIBI flow signals are less favorable prognostic signs. This information on TCD may help with selection of patients for additional pharmacologic or interventional treatment [12].

Recanalizations that occur between 5 and 7 h after cardioembolic stroke may lead to symptomatic

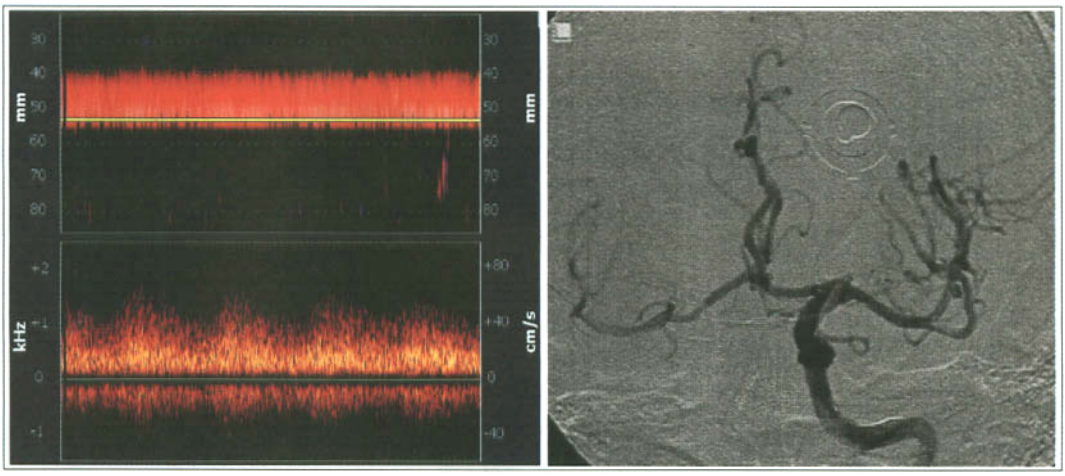

Figure 4 Blunted signal with mean flow velocity of 50 cm/s indicating complete M1 MCA recanalization with persisting proximal ICA occlusion. DSA image shows a TIMI grade III flow in the M1 MCA through the anterior cross-filling.

hemorrhage [15]. Figure 2 shows a complete stepwise M1 middle cerebral artery (MCA) recanalization at 5.5 h after stroke onset that preceded rapid clinical deterioration due to massive intracerebral hemorrhage leading to death within 24 h after stroke onset.

It is important to remember that TIBI grades 2–3 indicate partial and TIBI grades 4–5 indicate complete recanalization compared to angiography [16]. Note that normal or increased diastolic flow velocities in patients with stenotic signals indicate low resistance in the distal circulatory bed and unobstructed distal contrast opacification (TIMI grade III flow equivalent [17]). A blunted signal with mean velocities usually exceeding 20 cm/s can be seen in patients with complete MCA recanalization but persisting proximal ICA occlusion (TIMI grade III flow equivalent) (Figure 4).

Acute stroke patients receiving standard intravenous TPA therapy have been noted to occasionally experience early dramatic recovery (DR) that shortly follows early recanalization [18]. We define DR as an improvement by ≥ 10 NIHSS points or an improvement to ≤ 3 NIHSS points at the end of the hour-long infusion [19]. We also extended clinical and sonographic monitoring time up to 2 h after TPA bolus since the neurologic deficit often continues to evolve during the 2nd hour after bolus with reocclusion [20].

In our study [21], DR was observed in 12/53 (22%) TPA-treated and TCD-monitored patients. The DR group and non-DR group had equivalent age (68–70 years) and baseline NIHSS score (median score of 18 points). The time to bolus showed a non-significant trend towards earlier treatment in the DR group (DR 114 ± 44 min vs. non-DR 127 ± 30 min, NS).

The residual flow impairment due to MCA occlusion by TCD TIBI criteria was equivalent at baseline. At the end of infusion, TCD flow grades were significantly improved in the DR group (DR 3.9 ± 1.4 vs. non-DR 2.5 ± 1.7, $P = 0.01$). Approximately 70% of patients with early complete recanalization experience DR and this benefit is sustained at 3 months in two-thirds of patients.

At the end of infusion, the DR group showed a significant improvement in NIHSS scores (DR 4 ± 5 vs. non-DR 16 ± 7, $P < 0.001$). This difference was still seen at 24 h (DR 4 ± 6 vs. non-DR 15 ± 9, $P < 0.001$). Patients who experienced a DR during TPA infusion sustained this benefit at long-term follow-up of ≥ 3 months (modified Rankin scores DR 2 ± 2.5 vs. non-DR 4.2 ± 4.5, $P = 0.03$).

There was a consistent pattern and time course of recovery observed during the infusion. Certain deficits recovered early during infusion and had a complete recovery in ≥ 50% of patients. Gaze deviation recovered first, followed by sensory recovery and motor leg strength recovery. Arm motor strength recovery occurred next, but was often incomplete at the end of infusion.

Certain deficits showed a tendency to improve late in the infusion and often had only a partial improvement. These included facial motor strength and

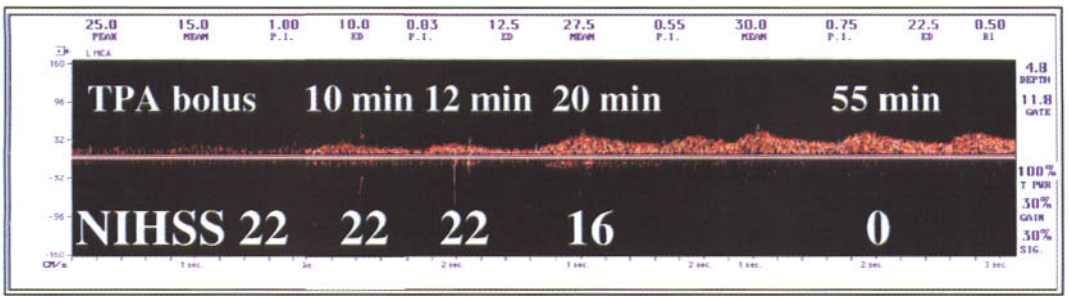

Figure 5 Stepwise recanalization of the M1 MCA segment with dramatic recovery during TPA infusion.

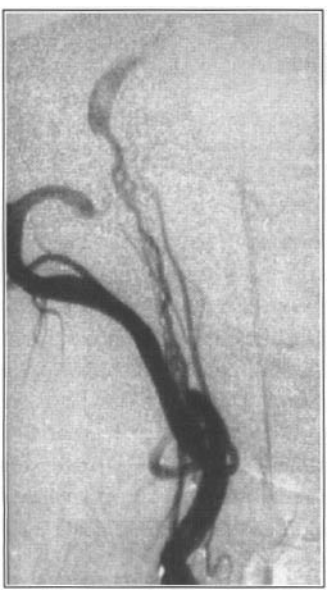

Figure 6 Delayed recanalization of ICA occlusion after successful treatment with intravenous TPA. DSA image shows formation of multiple small channels that carry antegrade flow to the siphon.

aphasia. Dysarthria tended not to improve by the end of infusion [21].

The consistent time course and pattern of DR is intriguing. These patients all had MCA syndromes with TCD-confirmed occlusions pretreatment. Topographically, only 2/12 DR patients had occlusion of the terminal ICA (TICA). All others had patent anterior cerebral arteries (ACAs) with occlusion located in the proximal M1/M2 MCA segments by our TCD criteria. As the clot lyses, a stepwise return of flow from the proximal to distal MCA is observed, leading to TIBI flow grade improvement. This predictable and measurable event suggests two alternative theories as to the mechanism of early DR [21].

The first of these models involves restoration of collateral flow during clot dissolution or clot migration to distal branches similar to the phenomenon previously observed at angiography by Minematsu *et al.* [3]. They observed migration of an MCA embolus followed by clinical improvement similar to DR and termed it a 'spectacular shrinking deficit'. The deficits that recover early (gaze deviation, leg strength and sensory loss) are cortically represented in regions abutting border zone perfusion with the ACA and posterior cerebral artery (PCA). Although there was no evidence of ACA involvement by TCD criteria in 10/12 patients, it is possible that the most proximal aspect of the thrombus was partially obstructing the proximal ACA, thus preventing flow diversion to the ACA and the development of a sufficient pressure gradient between the ACA and MCA territories. As the most proximal portion of the thrombus lysed or clot propagated distally, some transcortical collateral flow was restored. The regions in the border zone are reperfused first, followed by cortical regions located more centrally in the ischemic penumbra. In a typical M1 MCA occlusion, facial motor strength and language might be located deep in this region, explaining the lack of early recovery of these functions.

The second model of DR involves reperfusion of the small perforators originating from the M1 MCA and TICA and supplying the internal capsule and thalamus. As the proximal region of the thrombus lysed, flow was restored directly to the perforators that, in turn, restored function to the supplied regions of the thalamus and internal capsule. The functional anatomy of the internal capsule is controversial and may be variable. Anatomy of the circle of Willis is variable as well. Descending fibers from the frontal eye field are represented in the anterior limb, with motor fibers represented in the posterior limb of the internal capsule.

As the flow to small perforators is restored (positive diastolic flow at the depths corresponding to the M1 MCA origin, TIBI grades 2–3), a stepwise return in function of anterior and posterior limbs of the internal capsule as well as the thalamus may occur. This could explain the clinical pattern of recovery and why functions represented at different locations within the internal capsule and some cortical functions, such as language, recovered later during the infusion. Some long perforating arteries may reach the cortex and provide some flow to penumbral areas. Based on clinical and neuroanatomic correlation, the internal capsule would seem to recover function from a lateral to medial pattern. Although this is counterintuitive, the variable anatomy of the arterial supply to these regions and the significance of supply from TICA and ACA perforators may further contribute to different patterns and time course of DR [21].

Case presentation

A 69-year-old man with past history of hypertension and unstable angina had a sudden onset of right-sided weakness and inability to speak at lunch with his family. Upon arrival, he had forced gaze deviation, global aphasia, hemianopsia and right-sided hemiplegia. His pretreatment NIHSS score was 22. A non-contrast computed tomography (CT) scan showed no hemorrhage, and ASPECTS score was 8 with early ischemic changes in gray–white matter differentiation and sulcal effacement. The decision to give standard TPA therapy was made according to the NINDS rt-PA Stroke Study criteria. TPA bolus was given at 2 h after stroke onset (Figure 5). Diagnostic TCD was completed before bolus, the worst residual flow signal was identified in the distal M1 MCA, and continuous monitoring was performed for the duration of TPA infusion.

Diagnostic considerations

Clinical examination and head CT are consistent with an acute ischemic event. Despite his stroke severity (NIHSS > 20 points), this patient is a candidate for a standard intravenous TPA therapy within the first 3 h after stroke according to the NINDS rt-PA Stroke Study [22]. Early ischemic changes were found on pretreatment CT. However, these changes (loss of gray–white matter differentiation and sulcal effacement) are potentially reversible with successful thrombolysis and were not predictive of stroke outcome in the NINDS rt-PA Stroke Study [23]. Extensive changes such as hypodensity, involvement of more than one-third of the MCA territory and a low (< 7 points) ASPECTS score change the risk/benefit ratio for thrombolysis [24–26]. Gaze preference, global aphasia, hemianopsia and right-sided hemiplegia indicate involvement of the entire left MCA and raise clinical suspicion of a proximal MCA occlusion since a total NIHSS score of ≥ 10 points is predictive of a proximal thrombus presence at angiography [27]. Bedside ultrasound was ordered to rapidly document proximal MCA occlusion, to determine whether an ICA occlusion was also present, and to start monitoring TPA infusion.

Ultrasound findings

At the time of bolus, TCD showed a low-intensity blunted left M1 MCA flow signal (Figure 5, left frame). Ten minutes later, microembolic signals were detected. The left MCA mean flow velocity (MFV) increased from 15 cm/s to 28 cm/s at 20 min. At 55 min after bolus, the left MCA MFV was 30 cm/s; however, the systolic flow acceleration was still delayed. TCD also showed a reversed ophthalmic artery and the anterior and posterior communicating artery flows.

Interpretation

TCD showed:

1 a tenuous residual flow in the left MCA indicating its occlusion;

2 stepwise and complete MCA recanalization during TPA infusion; with

3 persisting hemodynamically significant left ICA obstruction proximal to the ophthalmic artery origin; and

4 functional collateral channels including left posterior communicating artery and a reversed left ophthalmic artery.

Correlative imaging

Digital subtraction angiography (DSA) was performed 24 h after stroke onset. DSA showed complete occlusion of the left ICA at the bulb, and a patent left MCA filled through intracranial collaterals.

Differential diagnosis

TCD findings may also be produced by a low flow state in maximally dilated MCA due to a thrombus in the proximal left ICA. TPA therapy may have helped to lyse the distal part of this thrombus and improve collateral flow via anterior and posterior communicating arteries. Nevertheless, this patient experienced a complete MCA recanalization that manifested with microembolic signals and signal intensity and velocity improvement, particularly between 10 and 20 min after TPA bolus.

Management

This patient was treated with standard TPA therapy within the first 3 h after stroke onset. Despite persistence of the left ICA occlusion, flow resumption in the MCA resulted in dramatic and complete recovery of brain functions by the end of TPA infusion. If symptom resolution is stable, the risk of immediate intra-arterial intervention may outweigh possible benefits. Therefore, a non-invasive confirmation of a complete ICA occlusion may help to rule out the need for urgent invasive angiography. This can be accomplished with contrast-enhanced CT angiography and/or carotid duplex scanning.

If this patient redevelops stroke symptoms and his repeat CT scan shows no hemorrhage or hypoattenuation, he again becomes eligible for thrombolytic therapy.

Nevertheless, careful monitoring of blood pressure and MCA patency is necessary during the next 24 h since MCA flow may be dependent of cerebral perfusion pressure distal to ICA occlusion, and blunting of the MCA waveform indicates delayed arrival of collateral flow with maximal MCA dilatation to attract this flow. Retrospectively, this waveform pattern was associated with higher risk of stroke in patients with carotid artery disease [28,29].

This patient may also be a candidate for anticoagulation at 24 h if he experiences fluctuating neurologic deficit in the presence of stable arterial blood pressure and persisting carotid occlusion. In the Trial of Org 10172 in Acute Stroke Treatment (TOAST), a subgroup with large vessel atherosclerotic lesions showed better outcomes after early anticoagulation with low-molecular-weight heparin [30].

Follow-up

Repeat neurologic examination during TPA infusion showed that gaze deviation disappeared first, followed by speech and motor function improvement. This patient recovered completely by the end of TPA infusion. DSA showed a complete left ICA occlusion. He received heparin during his hospital stay, and completed a 3-month course of coumadin. He receives aspirin 350 mg and clopidogrel 75 mg [31] and pravastatin [32]. His modified Rankin score at 3 months and 1 year was 0. He remains asymptomatic and no further intervention was considered at this time (extra–intracranial anastomoses failed to prevent stroke in one trial [33]). However, if his ICA remains permanently occluded, and a hemodynamic compromise may subsequently develop, there may be a potential role for bypass surgery in the future [34,35].

Although oxygen extraction fraction on positron emission tomography best represents the status of cerebral hemodynamics [34,35], this test is expensive and is not widely available. A variety of other tests were introduced to evaluate intracranial hemodynamics using the phenomenon of vasomotor reactivity (VMR) [36–41] including CO_2 reactivity with TCD, acetazolamide testing with TCD and cerebral blood flow scanning techniques, and the breath-holding index (BHI). The latter is the simplest way of challenging VMR if the patient is compliant and capable of holding breath for 30 s. This index is calculated using the mean flow velocities obtained by TCD before breath-holding (baseline) and at the end of 4 s of breathing after 30 s of breath-holding:

$$\text{BHI} = \frac{\text{MFV}_{\text{baseline}} - \text{MFV}_{\text{end}}}{\text{MFV}_{\text{baseline}}} \times \frac{100}{\text{seconds of breath-holding}}$$

The patient should be able to hold his or her breath voluntarily for at least 24 s, and preferably 30 s. The following steps can help the patient complete this task. First, explain in detail what needs to be accomplished, and demonstrate yourself that no major chest excursions should be made at the beginning and end of breath-holding. Major chest volume changes with forced breathing change intrathoracic pressure and may affect velocity and flow pulsatility. Second, announce to the patient 10-s intervals after breath-holding has started. This helps the patient to be more confident that he or she can complete the task. Use envelope or average mean velocities from 4 s after the

patient started to breathe (i.e. optimized signals from entire display if the sweep speed was set at 4–5 s).

BHI values of less than 0.69 are predictive of risk of stroke in patients with asymptomatic severe ICA stenoses and symptomatic occlusions [42,43]. This TCD test does not require any gas monitoring equipment or intravenous injections. Although subjectivity of patient effort and the unknowns of blood gas concentration make this test probably least reliable, it has been prospectively validated to predict clinical outcomes in steno-occlusive ICA disease, and BHI may represent a screening test in the outpatient clinic to identify patients with impaired vasomotor reactivity. Further imaging investigations and clinical trials will determine the need for surgery in this setting [44,45].

Two years later the patient remains symptom free and repeat duplex ultrasound showed reappearance of flow in the proximal ICA. Digital subtraction angiogram was performed (Figure 6). At present it is uncertain if this delayed recanalization warrants further intervention.

References

1 Jones TH, Morawetz RB, Crowell RM, Marcoux FW, FitzGibbon SJ, DeGirolami U, Ojemann RG. Thresholds of focal cerebral ischemia in awake monkeys. *J Neurosurg* 1981; **54**: 773–82.

2 Memezawa H, Smith ML, Siesjo BK. Penumbral tissues salvaged by reperfusion following middle cerebral artery occlusion in rats. *Stroke* 1992; **23**: 552–9.

3 Minematsu K, Yamaguchi T, Omae T. 'Spectacular shrinking deficit': rapid recovery from a major hemispheric syndrome by migration of an embolus. *Neurology* 1992; **42**: 157–62.

4 Baird AE, Donnan GA, Austin MC, McKay WJ. Early reperfusion in the 'spectacular shrinking deficit' demonstrated by single-photon emission computed tomography. *Neurology* 1995; **45**: 1335–9.

5 Ringelstein EB, Biniek R, Weiller C, Ammeling B, Nolte PN, Thron A. Type and extent of hemispheric brain infarctions and clinical outcome in early and delayed middle cerebral artery recanalization. *Neurology* 1992; **42**: 289–98.

6 Heiss W-D, Grond M, Thiel A, von Stockhausen H-M, Rudolf J, Ghaemi M, Lottgen J, Stenzel C, Pawlik G. Tissue at risk of infarction rescued by early reperfusion: a positron emission tomography study in systemic recombinant tissue plasminogen activator thrombolysis of acute stroke. *J Cereb Blood Flow Metab* 1998; **18**: 1298–307.

7 Lauer CG, Burge R, Tang DB, Bass BG, Gomez ER, Alving BM. Effect of ultrasound on tissue-type plasminogen activator-induced thrombolysis. *Circulation* 1992; **86**: 1257–64.

8 Akiyama M, Ishibashi T, Yamada T, Furuhata H. Low-frequency ultrasound penetrates the cranium and enhances thrombolysis in vitro. *Neurosurgery* 1998; **43**: 828–32.

9 Suchkova V, Siddiqi FN, Carstensen EL, Dalecki D, Child S, Francis CW. Enhancement of fibrinolysis with 40-kHz ultrasound. *Circulation* 1998; **98**: 1030–5.

10 Behrens S, Daffertshoffer M, Spiegel D, Hennerici M. Low-frequency, low-intensity ultrasound accelerates thrombolysis through the skull. *Ultrasound Med Biol* 1999; **25**: 269–73.

11 Christou I, Alexandrov AV, Burgin WS, Wojner AW, Felberg RA, Malkoff M, Grotta JC. Timing of recanalization after TPA therapy determined by transcranial Doppler correlates with clinical recovery from ischemic stroke. *Stroke* 2000; **31**: 1812–6.

12 Alexandrov AV, Burgin WS, Demchuk AM, El-Mitwalli A, Grotta JC. Speed of intracranial clot lysis with intravenous TPA therapy: sonographic classification and short term improvement. *Circulation* 2001; **103**: 2897–902.

13 Demchuk AM, Burgin WS, Christou I, Felberg RA, Barber PA, Hill MD, Alexandrov AV. Thrombolysis in Brain Ischemia (TIBI) transcranial Doppler flow grades predict clinical severity, early recovery, and mortality in patients treated with tissue plasminogen activator. *Stroke* 2001; **32**: 89–93.

14 Labiche LA, Al-Senani F, Grotta JC, Wojner AW, Malkoff M, Alexandrov AV. Is the benefit of early recanalization sustained at 3 months? A prospective cohort study. *Stroke* 2002.

15 Molina C, Montaner J, Abilleira S, Arenillas JF, Ribo M, Huertas R, Romero F, Alvarez-Sabin J. Time course of tissue plasminogen activator-induced recanalization in acute cardio-embolic stroke: a case-control study. *Stroke* 2001; **32**: 2821–7.

16 Burgin WS, Malkoff M, Felberg RA, Demchuk AM, Christou I, Grotta JC, Alexandrov AV. Transcranial Doppler ultrasound criteria for recanalization after thrombolysis for middle cerebral artery stroke. *Stroke* 2000; **31**: 1128–32.

17 The TIMI Study Group. The Thrombolysis in Myocardial Infarction (TIMI) trial: phase I findings. *N Engl J Med* 1985; **312**: 932–6.

18 Demchuk AM, Felberg RA, Alexandrov AV. Clinical recovery from acute ischemic stroke after early reperfusion of the brain with intravenous thrombolysis. *N Engl J Med* 1999; **340**: 894–5.

19 Alexandrov AV, Demchuk AM, Felberg RA, Christou I, Barber PA, Burgin WS, Malkoff M, Wojner AW, Grotta JC. High rate of complete recanalization and dramatic clinical recovery during TPA infusion when continuously monitored by 2 MHz transcranial Doppler monitoring. *Stroke* 2000; **31**: 610–4.

20 Alexandrov AV, Grotta JC. Arterial re-occlusion in stroke patients treated with intravenous tissue plasminogen activator. *Neurology* 2002; **59**: 862–67.

21 Felberg RA, Okon NJ, El-Mitwalli A, Burgin WS, Grotta JC, Alexandrov AV. Early dramatic recovery during IV-TPA infusion: clinical pattern and outcome in acute MCA stroke. *Stroke* 2002; **33**: 1301–7.

22 The National Institutes of Neurological Disorders and Stroke rt-PA Stroke Study Group. Tissue plasminogen activator for acute ischemic stroke. *N Engl J Med* 1995; **333**: 1581–7.

23 Patel SC, Levine SR, Tilley BC, Grotta JC, Lu M, Frankel M, Haley EC, Brott TG, Broderick JP, Horowitz S, Lyden PD, Lewandowski CA, Marler JR, Welch KM. Lack of clinical significance of early ischemic changes on computed tomography in acute stroke. *JAMA* 2001; **286**: 2830–8.

24 Davalos A, Toni D, Iweins F, Lesaffre E, Bastianello S, Castillo J. Neurological deterioration in acute ischemic stroke: potential predictors and associated factors in the European Cooperative Acute Stroke Study (ECASS) I. *Stroke* 1999; **30**: 2631–6.

25 Larrue V, von Kummer RR, Muller A, Bluhmki E. Risk factors for severe hemorrhagic transformation in ischemic stroke patients treated with recombinant tissue plasminogen activator: a secondary analysis of the European–Australasian Acute Stroke Study (ECASS II). *Stroke* 2001; **32**: 438–41.

26 Barber PA, Demchuk AM, Zhang J, Buchan AM. Validity and reliability of a quantitative computed tomography score in predicting outcome of hyperacute stroke before thrombolytic therapy. *Lancet* 2000; **355**: 1670–4.

27 Lewandowski CA, Frankel M, Tomsick TA, Broderick J, Frey J, Clark W, Starkman S, Grotta J, Spilker J, Khoury J, Brott T. Combined intravenous and intra-arterial r-TPA versus intra-arterial therapy of acute ischemic stroke. Emergency Management of Stroke (EMS) Bridging Trial. *Stroke* 1999; **30**: 2598–605.

28 Giller CA, Mathews D, Purdy P, Kopitnik TA, Batjer HH, Samson DS. The transcranial Doppler appearance of acute carotid artery occlusion. *Ann Neurol* 1992; **31**: 101–3.

29 Hartmann A, Mast H, Thompson JL, Sia RM, Mohr JP. Transcranial Doppler waveform blunting in severe extracranial carotid artery stenosis. *Cerebrovasc Dis* 2000; **10**: 33–8.

30 Adams HP, Bendixen BH, Leira E, Chang KC, Davis PH, Woolson RF, Clarke WR, Hansen MD. Antithrombotic treatment of ischemic stroke among patients with occlusion or severe stenosis of the internal carotid artery: a report of the Trial of Org 10172 in Acute Stroke Treatment (TOAST). *Neurology* 1999; **53**: 122–5.

31 CAPRIE Steering Committee. A randomized, blinded trial of clopidogrel versus aspirin in patients at risk of ischaemic events. *Lancet* 1996; **348**: 1329–32.

32 LIPID Study Group. Prevention of cardiovascular events and death with pravastatin in patients with coronary heart disease and a broad range of initial cholesterol levels. The Long-Term Intervention with Pravastatin in Ischaemic Disease (LIPID) Study Group. *N Engl J Med* 1998; **339**: 1349–57.

33 The EC/IC Bypass Study Group. Failure of extracranial–intracranial arterial bypass to reduce the risk of ischemic stroke: results of an international randomized trial. *N Engl J Med* 1985; **313**: 1191–200.

34 Powers WJ, Grubb RL, Raichle M. Clinical results of extracranial–intracranial bypass surgery in patients with hemodynamic cerebrovascular disease. *J Neurosurg* 1989; **70**: 61–7.

35 Powers WJ. Cerebral hemodynamics in ischemic cerebrovascular disease. *Ann Neurol* 1991; **29**: 231–40.

36 Bishop CCR, Powell S, Insall M *et al.* Effect of internal carotid artery occlusion on middle cerebral artery blood flow at rest and in response to hypercapnia. *Lancet* 1986; **29**: 710–2.

37 Ringelstein EB, Sievers C, Ecker S *et al.* Noninvasive assessment of CO_2-induced cerebral vasomotor response in normal individuals and patients with internal carotid artery occlusions. *Stroke* 1988; **19**: 962–9.

38 Sorteberg W, Lindegaard KF, Rootwelt K, Dahl A, Nyberg-Hansen R, Nornes H. Effect of acetazolamide on cerebral blood flow velocity and regional cerebral blood flow in normal subjects. *Acta Neurochir* 1989; **97**: 139–45.

39 Kleiser B, Widder B. Course of carotid artery occlusions with impaired cerebrovascular reactivity. *Stroke* 1992; **23**: 171–4.

40 Webster MW, Makaroun MS, Steed DL *et al.* Compromised cerebral blood flow reactivity is a predictor of stroke in patients with symptomatic carotid artery occlusive disease. *J Vasc Surg* 1995; **21**: 338–44.

41 Markus HS, Harrison MJ. Estimation of cerebrovascular reactivity using transcranial Doppler, including the use of breath-holding as the vasodilatory stimulus. *Stroke* 1992; **23**: 668–73.

42 Silverstrini M, Vernieri F, Pasqualetti P, Matheis M, Passarelli F, Triosi E, Caltagirone C. Impaired vasosmotor reactivity and risk of stroke in patients with asymptomatic carotid artery stenosis. *JAMA* 2000; **283**: 2122–7.

43 Vernieri F, Pasqualetti P, Matheis M, Passarelli F, Triosi E, Rossini PM, Caltagirone C, Silvestrini M. Effect of collateral flow and cerebral vasomotor reactivity on the outcome of carotid artery occlusion. *Stroke* 2001; **32**: 1552–8.

44 Adams HP, Powers WJ, Grubb RL, Clarke WR, Woolfson RF. Preview of a new trial of extracranial-to-intracranial arterial anastomosis: the carotid occlusion surgery group. *Neurosurg Clin N Am* 2001; **12**: 613–24.

45 Derdeyn CP, Videen TO, Yundt KD, Fritsch SM, Carpenter DA, Grubb RR, Powers WJ. Variability of cerebral blood flow volume and oxygen extraction: stages of cerebral hemodynamic impairment revisited. *Brain* 2002; **125**: 595–607.

Arterial reocclusion and deterioration following improvement

With W. Scott Burgin, MD

Introduction

The NINDS rt-PA Stroke Study defined deterioration following improvement (DFI) as a decline in the National Institutes of Health Stroke Scale (NIHSS) score by > 2 points after an initial improvement by > 2 points. This was observed in 13% of enrolled patients [1]. DFI just recently became a subject of research while previous studies focused on predictors of overall deterioration in acute stroke. Early progression of stroke symptoms was linked to cerebral edema and hypoattenuation on pretreatment computed tomography (CT) scan [2] as well as the asymmetry of blood flow velocities and no-flow signs on transcranial Doppler (TCD) [3]. As many as 91% of patients evaluated within the first 5 h after stroke onset had subsequent worsening of the neurologic deficit if angiography showed persisting extracranial and/or intracranial occlusion [4]. Early reocclusion (RO) as a mechanism of stroke progression and DFI was observed in real time when thrombolysis was monitored by TCD and serial neurologic examinations [5].

To diagnose arterial reocclusion with ultrasound, it is important to rule out other potential causes of early clinical deterioration in acute stroke patients. Clinical worsening may also occur due to cardiopulmonary decompensation that decreases cerebral perfusion pressure, and intracerebral hemorrhage that complicates tissue plasminogen activator (TPA) treatment in 6.4% of patients [6]. However, neither hemorrhagic transformation of cerebral infarct nor decrease in systolic blood pressure within the first 24 h were independent predictors of early stroke progression in the European Cooperative Stroke Study (ECASS) I [2].

Sonographically RO was described as a decrease in flow signals by ≥ 1 TIBI grade on TCD display and stable vital signs (Figure 1). Repeat CT should be considered (even in a case of sonographic deterioration without clinical changes) to rule out hemorrhagic transformation (Figure 1). Indications for repeat CT scanning in acute stroke patients usually include stroke symptom progression or deterioration following improvement by more than 4 NIHSS points, and evidence of flow worsening on TCD with or without clinical changes.

In one series [7], early reocclusion occurred in 27% of patients treated with a standard 0.9 mg/kg dose of TPA. RO is a process that can start spontaneously before TPA bolus or any time thereafter. If TCD monitoring is initiated 5–25 min before TPA bolus, TCD can show development of RO in 25% of these patients even before TPA is given. After TPA infusion begins, TCD monitoring can show reocclusion in 19% of these patients in the next 30 min, and in another 19% by the end of TPA infusion. Finally, another 37% of patients reocclude within 60–120 min after TPA bolus.

Complete or partial recanalization on TCD usually precedes reocclusion since some residual flow worsening is necessary for TCD diagnosis of RO. Thus, RO occurs in 22% of patients with complete (TIBI grade 4–5) recanalization and 41% of patients with partial (TIBI 2–3) recanalization [7]. Prior to RO, those patients have earlier median timing of recanalization compared to those who recanalized without RO: 130 min vs. 180 min after stroke onset. RO carries a relatively poor prognosis. Within 2h of TPA bolus only 25% of patients with RO have subsequent complete recanalization, 19% have partial recanalization and 56% have no early recanalization.

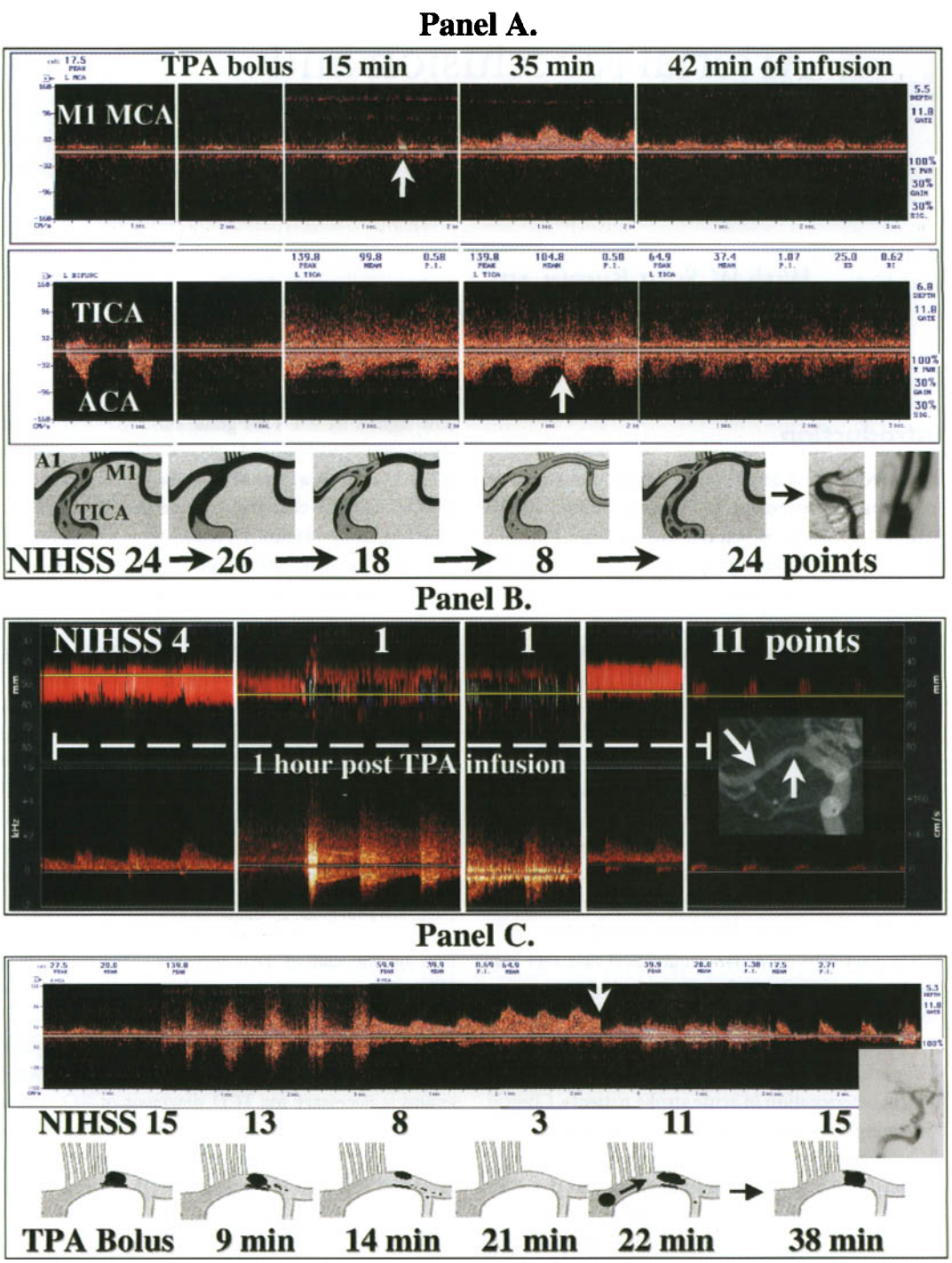

Figure 1 Panel A. A 42-year-old right-handed woman was seen 80 min, after the acute onset of right hemiplegia, global aphasia, eye deviation to the left, and a right homonymous hemianopsia (NIHSS score 24). TCD showed a proximal M1 MCA and A1 anterior cerebral artery (ACA) occlusion (panel A, top left Doppler spectra labeled M1 MCA, TICA and ACA). Second set of Doppler spectra (left to right) shows rapid progression to the terminal internal carotid artery (TICA) occlusion at the time of TPA bolus. At this time, the patient became drowsy

Patients with RO tend to have lower median prebolus NIHSS scores of 13.5 points compared to 17 points in the rest of TPA-treated patients. However at 2 and 24 h, the NIHSS scores are higher than in patients with RO compared to stable recanalization: 14 vs. 9 points and 16 vs. 6 points, respectively.

Clinical deterioration by NIHSS ≥ 4 points within the first 24 h is observed in approximately 15–20% of our TPA-treated patients. Reocclusion was seen in two-thirds of these patients: 50% in the RO group vs. 10% in those with either no or stable recanalization. There is also a trend to higher rates of symptomatic intracerebral hemorrhage (SICH) with RO: 12.5% of patients with RO had SICH compared to 2% in the rest of the TPA-treated patients. In-hospital mortality was 25% in the RO group and 3% in the non-RO group, respectively.

At 3 months, a good outcome (modified Rankin scores 0–1) was achieved by 8% of patients with no early recanalization, by 33% of patients with RO and by 50% of patients with stable recanalization. Mortality at follow-up was 42% in patients with no recanalization, 33% in patients with RO and 8% in patients with stable recanalization.

These results suggest that at least one-quarter of TPA-treated patients may experience early RO despite systemic thrombolytic therapy. Compared to stable recanalization, RO leads to higher mortality and a less favorable outcome. Reocclusion occurs more often in patients with early and partial recanalization leading to deterioration of the neurologic deficit and higher mortality. However, patients with RO may have better long-term outcomes than patients without any early recanalization [7]. Perhaps some degree of residual flow to the brain tissue that is detectable prior to RO provides additional time to tolerate further ischemia. This may support the potential for an individual and extended time window for vascular rescue therapies in acute ischemic stroke [8].

(cont'd) (NIHSS score 26). Intravenous TPA was started at 120 min from symptom onset using a standard dose of 0.9 mg/kg. At 10 min after TPA bolus, TCD showed terminal ICA recanalization with resumption of end-diastolic flow in the A1 ACA followed shortly by improvement in her level of consciousness. At 15 min of infusion, microembolic signals were heard in the M1 MCA accompanied with proximal M1 segment recanalization and resumption of low resistance end-diastolic flow towards the lenticulostriate perforating arteries. Clinically, her right leg began to move followed by antigravity strength in the distal arm and improved facial weakness (NIHSS score 18). TCD showed a continuing recanalization of the A1 ACA at 20 min, followed by resolution of her gaze preference and continued improvement in her right-sided weakness by 30 min (NIHSS score 15). At 35 min, she had complete M1 MCA recanalization with multiple microembolic signals suggesting continuing proximal clot dissolution. By 37 min, the patient could lift her arm with a mild drift, verbalize simple words and follow axial and extra-axial commands (NIHSS score 8). At 42 min of infusion, TCD showed developing reocclusion of the M1 MCA and dampening of the terminal ICA flow. At 44 min, the patient rapidly became drowsy and resumed her eye deviation, global aphasia and right hemiplegia (NIHSS score 24). Urgent DSA showed complete terminal ICA 'T'-type occlusion and an 80% ulcerated proximal ICA stenosis (DSA images inserted in the bottom right corner of Panel A).

Panel B. A 26-year-old Mexican man was seen in the Emergency Department at 2 h after symptom onset. He had fluctuating left-sided weakness and episodes of neglect. Intravenous TPA was initiated at 2.5 h after symptom onset. His NIHSS scores were changing between 1 to 11 points during one hour after TPA infusion. PMD-TCD images show continuing thrombus dissolution and reocclusion. DSA image insert shows two parts of a thrombus in the right MCA. Continuing reocclusion process was also seen during angiography at 4.5 h after symptom onset. Foreign body retrieval device was used to remove red thrombus from the MCA.

Panel C. Upper image (left to right) represent sequential TCD monitoring spectra of the distal right M1 MCA. At the time of TPA bolus, patient had NIHSS score of 15 points and a blunted (TIBI grade 2) residual flow signal suggesting MCA near-occlusion (cartoon). At 9 min after TPA bolus, TCD showed a stenotic (TIBI grade 4) flow signal with clusters of microemboli suggesting MCA clot dissolution (NIHSS score 13). At 14–21 min, TCD showed further MCA flow improvement to normal TIBI 5 flow grade indicating complete M1 MCA recanalization. At this time his NIHSS score decreased to 3 points. At 22 min, a sudden drop in MCA flow was detected (white arrow) suggesting reocclusion since the heart rate and blood pressure remained stable. This sudden M1 MCA obstruction was likely caused by a thrombus that lodged in the proximal MCA and then propagated to the site of insonation (next frame, NIHSS score 11). TCD shows a blunted (TIBI grade 2) flow signal with clusters of emboli and bruits. At 38 min after bolus, TCD shows a minimal (TIBI grade I) flow signal that suggests a complete M1 MCA reocclusion due to the absence of diastolic flow. Note continuing appearance of emboli during the last cardiac cycle. DSA image insert shows isolated MCA occlusion without evidence of ICA obstruction.

Case presentation

A 70-year-old man with past history of hypertension and paroxysmal atrial fibrillation had a sudden onset of left-sided weakness. Upon arrival, he had partial gaze deviation, hemianopsia, left-sided hemiparesis and neglect. His pretreatment NIHSS score was 15. Initial non-contrast head CT scan showed no hemorrhage and an ASPECTS score was 9 with an insular ribbon sign. The decision to give standard TPA therapy was made according to the NINDS rt-PA Stroke Study criteria. TPA bolus was given at 1 h and 30 min after stroke onset (Figure 1, panel C). Diagnostic TCD was completed before bolus, the worst residual flow signal was identified in the distal right M1 MCA, and continuous monitoring was performed for the duration of TPA infusion.

Diagnostic considerations

Clinical examination and head CT are consistent with an acute ischemia in the right MCA. This patient is an appropriate candidate for a standard intravenous TPA therapy within the first 3 h after stroke according to the NINDS rt-PA Stroke Study. Gaze preference, neglect, hemianopsia and right-sided hemiparesis indicate cortical involvement of most of the right MCA distribution and raise clinical suspicion of a proximal MCA occlusion. Bedside ultrasound was ordered to rapidly document proximal MCA occlusion and to start monitoring TPA infusion.

Ultrasound findings

At the time of bolus, TCD showed a blunted right M1 MCA flow signal (Figure 1, panel C, upper left Doppler spectra). Recanalization started within the next 9 min and a stenotic (TIBI flow grade 4) was detected. Complete right M1 MCA recanalization was diagnosed at 21 min. Note that although the right MCA has a mean flow velocity of 65 cm/s, the waveform still shows a delay in systolic flow acceleration that may indicate persistence of a more proximal hemodynamically significant obstruction in the ICA. At 22 min, TCD showed a sudden drop in the MCA flow most likely due to a new thrombus that lodged in the proximal MCA and then propagated to the distal portion of the M1 segment. This thrombus was most likely located in the ICA (a delayed systolic flow acceleration of the MCA waveform at 14 and 21 min. TCD then showed disappearance of the end-diastolic flow, indicating complete M1 MCA reocclusion.

Interpretation

TCD showed:

1 right M1 MCA near-occlusion;

2 stepwise and complete MCA recanalization during TPA infusion; and

3 early M1 MCA reocclusion during TPA infusion due to another thrombus that likely lodged from the ICA.

Correlative imaging

A non-contrast CT scan was repeated after deterioration to rule out intracerebral hemorrhage. CT scan showed no hemorrhage and no significant cerebral edema. Digital subtraction angiography (DSA) was performed 38 min after completion of TPA infusion and it showed a complete (TIMI grade I) right M1 MCA occlusion approximately 1 cm after its origin. No significant carotid stenosis or distal ICA thrombosis was found (Figure 1).

Differential diagnosis

TCD flow velocity may decrease due to a sudden drop in blood pressure. However, the vital signs were stable and our patient was not agitated or complaining of chest pain. Although TCD showed recanalization of this thrombus, the systolic flow acceleration was still somewhat delayed and continuing microembolic signals were heard (frames not shown in Figure 1). We initially thought that our patient had a proximal ICA stenosis or occlusion; however, DSA showed no ICA stenosis or thrombus. Therefore, it is likely that our patient had initially experienced embolization from the heart by a large thrombus. A part of it occluded the MCA, and a more proximal part was in the terminal ICA. As recanalization of the MCA thrombus occurred, the blood pressure moved a more proximal part of the thrombus from the ICA to MCA (note an abrupt disappearance of blood flow signals since flow obstruction occurred proximal to the site of insonation). In an experimental study, emboli introduced via a catheter into the proximal ICA favored lodging into the proximal MCA and its

branches, with the anterior cerebral artery (ACA) being affected in only 7% [9]. After re-embolization of the proximal MCA occurred, the thrombus propagated to the distal M1 MCA under pulsations of blood pressure and the patient redeveloped his neurologic deficit. This reocclusion occurred halfway into TPA infusion.

Management

Despite treatment with standard TPA therapy within the first 3 h after stroke onset, early reocclusion has occurred with re-establishment of the neurologic deficit (NIHSS 15–3–15 points). Although this patient had DFI, there was no sign of hypoattenuation of brain tissues or progression of cerebral edema on repeat CT. Therefore, this patient is a candidate for diagnostic invasive angiography that will help to decide whether an experimental intra-arterial clot-disrupting intervention is suitable. A prospective trial evaluating combined intravenous–intra-arterial thrombolysis is currently underway [10].

We explained to the patient the mechanism of redevelopment of his symptoms, and obtained an informed consent for intra-arterial thrombolysis. The disclosed risk of hemorrhage was estimated at 10%. Intra-arterial TPA was given according to the institutional review board (IRB)-approved protocol in 2-mg injections up to 22 mg total dose. After all 22 mg were infused, a TIMI grade III recanalization of the right MCA was achieved with a residual distal M1 MCA stenosis of approximately 50% possibly representing residual thrombosis.

Follow-up

Repeat neurologic examinations after intra-arterial thrombolysis showed significant neurologic improvement by 8 and 10 NIHSS points to a total score of 5 points at 24 h. The patient was discharged home on warfarin (target international normalized ratio 2–3) [11–13]. At 3 months follow-up, he had a modified Rankin score of 1. Repeat TCD showed normal velocity range in the right MCA without evidence of any significant residual stenosis. The patient continues to take warfarin due to paroxysmal atrial fibrillation detected with Holter monitoring.

References

1 Grotta JC, Welch KM, Fagan SC, Lu M, Frankel MR, Brott T, Levine SR, Lyden PD. Clinical deterioration following improvement in the NINDS rt-PA Stroke Trial. *Stroke* 2001; **32**: 661–8.

2 Davalos A, Toni D, Iweins F, Lesaffre E, Bastianello S, Castillo J. Neurological deterioration in acute ischemic stroke: potential predictors and associated factors in the European cooperative acute stroke study (ECASS) I. *Stroke* 1999; **30**: 2631–6.

3 Toni D, Fiorelli M, Zanette EM, Sacchetti ML, Salerno A, Argentino C, Solaro M, Fieschi C. Early spontaneous improvement and deterioration of ischemic stroke patients. A serial study with transcranial Doppler ultrasonography. *Stroke* 1998; **29**: 1144–8.

4 Toni D, Fiorelli M, Gentile M, Bastianello S, Sacchetti ML, Argentino C, Pozzilli C, Fieschi C. Progressing neurological deficit secondary to acute ischemic stroke. A study on predictability, pathogenesis, and prognosis. *Arch Neurol* 1995; **52**: 670–5.

5 Burgin WS, Alexandrov AV. Carotid thrombosis and re-occlusion. *Neurology* 2001; **56**: 568–70.

6 The NINDS rt-PA Stroke Study Group. Tissue plasminogen activator for acute ischemic stroke. *N Engl J Med* 1995; **333**: 1581–7.

7 Alexandrov AV, Grotta JC. Arterial re-occlusion in stroke patients treated with intravenous tissue plasminogen activator. *Neurology* 2002; **59**: 862–67.

8 Baron JC, von Kummer R, del Zoppo GJ. Treatment of acute ischemic stroke. Challenging the concept of rigid and universal time window. *Stroke* 1995; **26**: 2219–21.

9 Gacs G, Medrei FT, Bodosi M. Balloon catheter as a model of cerebral emboli in humans. *Stroke* 1982; **13**: 39–44.

10 Lewandowski CA, Frankel M, Tomsick TA, Broderick J, Frey J, Clark W, Starkman S, Grotta J, Spilker J, Khoury J, Brott T. Combined intravenous and intra-arterial r-TPA versus intra-arterial therapy of acute ischemic stroke. Emergency Management of Stroke (EMS) Bridging Trial. *Stroke* 1999; **30**: 2598–605.

11 Stroke Prevention in Atrial Fibrillation Investigators. Adjusted-dose warfarin versus low-intensity, fixed-dose warfarin plus aspirin for high-risk patients with atrial fibrillation: Stroke Prevention in Atrial Fibrillation III randomized clinical trial. *Lancet* 1996; **348**: 633–7.

12 Barnett HJM, Eliasziw M, Meldrum HE. Drug therapy: drugs and surgery in the prevention of ischemic stroke. *N Engl J Med* 1995; **332**: 238–2.

13 Hart RG, Benavente O, McBride R, Pearce LA. Antithrombotic therapy to prevent stroke in patients with atrial fibrillation: a meta-analysis. *Ann Intern Med* 2001; **12**: 613–24.

Extended window for thrombolysis

With the Stroke Treatment Team

Introduction

The current window for thrombolysis is determined by the time elapsed from symptom onset. The NINDS rt-PA Stroke Study established a 3-h window to effectively deliver intravenous tissue plasminogen activator (TPA) for stroke patients [1]. Overall, the European Cooperative Stroke Studies (ECASS) and the ATLANTIS trial were negative when intravenous TPA was given between 0 and 6 and 3–5 h after symptom onset [2–4]. However, a pooled analysis of the NINDS rt-PA Stroke Study, ECASS and ATLANTIS trials showed that select patients may benefit from intravenous TPA given up to 270 min after symptom onset [5], suggesting that beneficial arterial recanalization can be achieved within the first 5 h of stroke. The PROACT trial has shown that intra-arterial thrombolysis with prourokinase may be successfully performed up to 6 h after stroke onset [6]. These data suggest that the window for thrombolytic therapy may be longer than currently approved.

Although the shorter time to therapy from symptom onset is a strong predictor of TPA effectiveness during the first 3 h of ischemia [7], other markers of reversibility of ischemic damage are needed to identify patients who may benefit from thrombolysis given beyond the conventional time window. Data from experimental models of cerebral ischemia and anecdotal observations in human patients treated outside the conventional window for thrombolysis encourage an assessment of each subject's potential to respond to the intended therapeutic intervention [8]. This can be accomplished using simple and rapidly available tests that evaluate:

1 clinical stroke severity, i.e. NIHSS scores;

2 the site of arterial occlusion, residual flow and flow diversion with transcranial Doppler (TCD); and

3 the brain tissue condition, i.e. determined from a non-contrast computed tomography (CT) scan [9].

The value of magnetic resonance imaging (MRI)/MR angiography (MRA)/diffusion weighted imaging (DWI) and perfusion–diffusion mismatch measurements to discriminate reversible and irreversible tissue damage is also being tested in a prospective trial [10]. Generally, a lower intensity of DWI abnormality and perfusion greater than dif-fusion deficits (i.e. mismatch) indicate potentially salvageable tissue [10–13].

At the University of Texas, we have implemented an Institutional Review Board (IRB)-approved experimental protocol for compassionate use of thrombolysis and mechanical thrombus manipulation. This protocol was designed for patients who present outside the conventional window but after rapid clinical, CT, ultrasound or MRI assessments were considered to have a potential to respond to reperfusion therapies.

Eligibility criteria for this compassionate treatment protocol include:

1 time from symptom onset beyond 3 h or undetermined;

2 NIHSS score ≥ 4 points;

3 normal non-contrast CT scan or minimal signs of early ischemic changes such as loss of gray–white matter differentiation and/or sulcal effacement; and

4 the presence of persisting arterial occlusion on transcranial Doppler or angiography.

Contraindications include:

1 hypoattenuation of ischemic brain tissue on CT or early mass effect;

2 standard contraindications for intravenous TPA therapy; and

3 refusal or inability to give informed consent.

This experimental protocol for compassionate treatment allows various thrombolytic regimens including a low-dose intravenous TPA, primary intra-arterial thrombolysis with TPA or retavase, and a combination of intravenous and intra-arterial thrombolysis with or without additional mechanical clot disruption

and stenting of the residual stenosis. The choice of an experimental strategy is individualized dependent on the location and extent of arterial occlusion, clinical responses to initial flow improvement under ultrasound monitoring, and the presence of residual stenoses after thrombolysis.

The following case illustrates the clinical and instrumental evaluation of a patient presenting outside the conventional window for thrombolysis and the decision-making process associated with the choice of experimental therapies.

Case presentation

An 80-year-old African American man with no previous strokes and past history of hypertension and non-insulin-dependent diabetes had a sudden onset of right-sided weakness 6.5 h ago. Upon arrival, he has a gaze preference, neglect and right-sided hemiplegia with a total NIHSS score of 12 points. A non-contrast CT scan showed no hemorrhage and the ASPECTS score was 10.

Diagnostic considerations

Clinical examination and head CT are consistent with an acute ischemia in the left MCA. Intact speech and comprehension suggest MCA branch occlusion or good leptomeningeal collaterals. This patient is a candidate for our compassionate thrombolysis protocol since he has a significant neurologic deficit in the absence of early ischemic changes on CT despite the duration of ischemic symptoms longer than 6 h. Alternatively, since he is being evaluated at 6.5 h after stroke onset there is a chance that spontaneous recanalization of the proximal MCA may have occurred without signs of clinical improvement. In this situation, intravenous or local thrombolysis may carry a higher risk-to-benefit ratio since persisting neurologic deficits may be attributable to ischemic core rather than possibly large penumbra. The ASPECTS score of 10 points suggests an existing window for tissue rescue [9], and matching the deficit distribution with occlusion location may suggest the presence of flow collateralization and the possibility of an early clinical response to reperfusion. To determine whether a proximal arterial occlusion was still present, an urgent bedside ultrasound was performed.

Ultrasound findings

TCD showed a dampened TIBI grade 3 flow in the proximal left M1 MCA flow signal (Figure 1, left frame) and the absence of the distal left M1/M2 MCA flow signals.

Interpretation

TCD showed persisting occlusion of the left distal M1 MCA, and continuous TCD monitoring of the worst residual flow signals in the left MCA was initiated.

Differential diagnosis

This patient has a partial left MCA syndrome despite persisting arterial occlusion proximal to M2 subdivision. A disabling neurologic deficit and a normal CT scan make the compassionate use of thrombolysis under our experimental protocol justifiable and feasible. The following were the choices of further actions:
1 perform MRI, MRA, DWI and perfusion sequences to confirm M1 MCA occlusion, and if any perfusion–diffusion mismatch exists at this point, proceed with intra-arterial thrombolysis; or
2 give this patient a low-dose intravenous TPA (0.6 mg/kg, 15% accelerated bolus over 1 min, 85% infusion over 30 min) as soon as possible, continuously monitor TPA infusion by TCD and if the MCA occlusion persists, perform intra-arterial thrombolysis; or
3 urgently perform invasive angiography and administer intra-arterial thrombolysis if occlusion persists at this point.
As the Stroke Treatment Team members were debating pros and cons and available data to support each of these approaches, a spontaneous partial recanalization was detected by TCD. Flow velocity has increased in the proximal left MCA with signs of turbulence (Figure 2, left image), and a minimal flow signal (TIBI grade 1) has appeared at the depths corresponding to the M2 subdivision (Figure 2, right frame). The patient regained strength in the distal right leg and proximal arm, lowering the total NIHSS score to 6 points at 7.5 h after stroke onset. This early clinical recovery occurred in response to a minimal residual flow improvement with persisting distal M1 MCA occlusion demonstrating early recoverability of this patient and confirming the presence of salvageable brain tissue. It is speculated that continuous

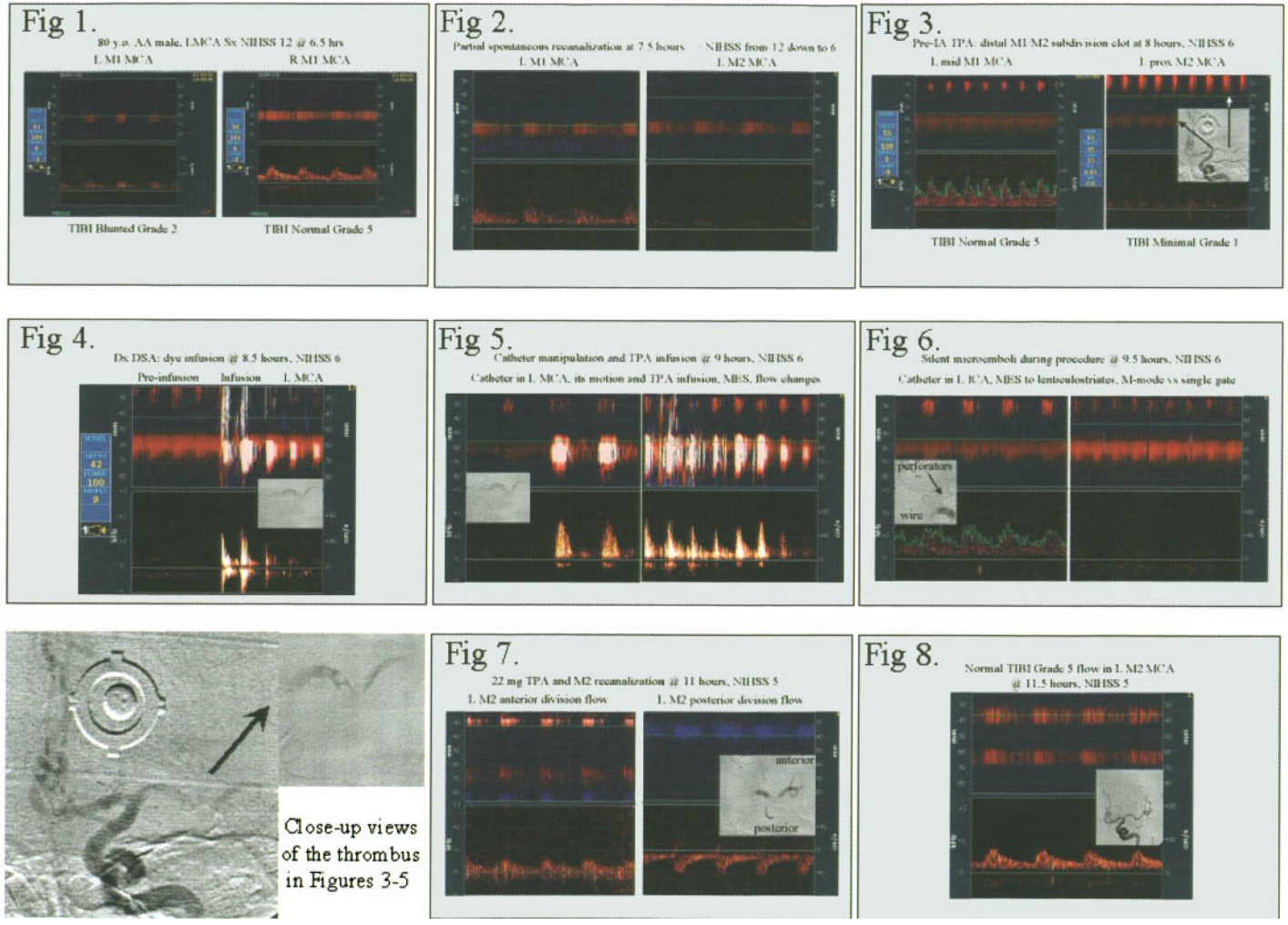

Figures 1–8 Sequential spectral transcranial Doppler and M-mode findings in an 80-year-old stroke patient presenting at 6.5 h after stroke onset.

exposure to ultrasound itself may induce some recanalization in stroke patients [14]. These clinical and ultrasound observations also suggest that if an MRI had been performed prior to partial recanalization, a perfusion–diffusion mismatch would likely have been present. At this point, an additional time delay to obtain MRI was felt to be unnecessary due to early clinical recovery. The decision was made to proceed directly with urgent angiography (option **3** above).

Correlative imaging

Urgent DSA showed a thrombus at the distal M1/M2 subdivision with TIMI grade I–II residual flow at the bifurcation (Figure 3). This thrombus had an irregular 'sausage-like' shape, completely obstructing one of the M2 branches (Figure 4). Continuous TCD monitoring was performed during angiography and Figures 4 and 5 illustrate TCD findings of multiple embolic signals in the M1 and M2 MCA segments as well as perforating arteries during contrast infusions and catheter manipulations.

Management

This patient received local intra-arterial thrombolysis with a total dose of 22 mg of TPA given with repeated 2 mL infusions delivered after mechanical clot manipulation with the catheter.

Follow-up

Repeat neurologic examinations during intra-arterial thrombolysis showed a stable neurologic deficit with a total NIHSS score of 6 points despite the length of intra-arterial thrombolysis (8.5–11.5 h). Intra-arterial TPA infusion began at 9 h and Figure 6 demonstrates residual flow signals around thrombus with catheter manipulation and drug infusion. TCD monitoring of intra-arterial drug infusion helped to determine a catheter position that allowed more residual flow into the thrombus between contrast injections. A partial TIMI grade II recanalization at the M2 MCA subdivision was achieved at 11 h (Figure 7), and a complete recanalization was seen at 11.5 h (Figure 8; an NIHSS score of 5 points at this time).

At 24 h, our patient had a total NIHSS score of 2 points, and no hemorrhagic transformation was found at 48 h after stroke onset. His modified Rankin score was 1 at 4 months after treatment. He receives aspirin with slow-release dipyridamole [15].

Conclusion

Skeptics may say that the observed early clinical response and outcome may have occurred naturally and it is impossible to determine the impact of intervention in case-by-case observations. This is true, indeed, and unlike randomized clinical trials, a case report bears little evidence, if any, but perhaps more than opinion. Clinical trials cannot be performed to test everything we do at the bedside. These trials are designed to test a hypothesis often developed through experimental treatment given to a few patients under informed consent.

The facts we disclose to those making the decision are the following:

1 The prognosis of a patient with an ischemic stroke and persisting proximal arterial occlusion if left untreated is grim (10% chance of complete recovery and up to 30–80% mortality rates dependent on the NIHSS scores and occlusion location).

2 At the same time, a treatment aimed at opening of an occluded vessel beyond the first 3 h may bear a risk of symptomatic or fatal hemorrhage of 10%.

3 The earlier the treatment is initiated and the earlier the vessel opens, the greater the chance of reversing the damage from cerebral ischemia.

References

1 The NINDS rt-PA Stroke Study Group. Tissue plasminogen activator for acute ischemic stroke. *N Engl J Med* 1995; **333**: 1581–7.

2 Hacke W, Kaste M, Fieschi C *et al.* Intravenous thrombolysis with recombinant tissue plasminogen activator for acute ischemic stroke: the European Cooperative Acute Stroke Study. *JAMA* 1995; **274**: 1017–25.

3 Hacke W, Kaste M, Fieschi C *et al.* Randomised double-blind placebo-controlled trial of thrombolytic therapy with intravenous alteplase in acute ischemic stroke (ECASS II): Second European–Australasian Acute Stroke Study Investigators. *Lancet* 1998; **352**: 1245–51.

4 Clarke WM, Wissman S, Albers GW, Jhamandas JH, Madden KP, Hamilton S. Recombinant tissue-type plasminogen activator (Alteplase) for ischemic stroke 3–5 hours after symptom onset. The ATLANTIS Study: a randomized controlled trial. Alteplase Thrombolysis for

Acute Noninterventional Therapy in Ischemic Stroke. *JAMA* 1999; **282**: 2019–26.

5 Brott TG, Kaste M, Albers GW. Analysis of the NINDS, ECASS I, ECASS II and ATLANTIS datasets. *Stroke* 2002; **33**: 340.

6 Furlan A, Higashida R, Wechsler L, Gent M, Rowley H, Kase C, Pessin M, Ahuja A, Callahan F, Clark WM, Silver F, Rivera F. Intra-arterial prourokinase for acute ischemic stroke. The PROACT II study: a randomized controlled trial. Prolyse in Acute Cerebral Thromboembolism. *JAMA* 1999; **282** (21): 2003–11.

7 Marler JR, Tilley BC, Lu M, Brott TG, Lyden PC, Grotta JC, Broderick JP, Levine SR, Frankel MP, Horowitz SH, Haley EC Jr, Lewandowski CA, Kwiatkowski TP. Early stroke treatment associated with better outcome: the NINDS rt-PA stroke study. *Neurology* 2000; **55**: 1649–55.

8 Baron JC, von Kummer R, del Zoppo GJ. Treatment of acute ischemic stroke. Challenging the concept of rigid and universal time window. *Stroke* 1995; **26**: 2219–21.

9 Barber PA, Demchuk AM, Zhang J, Buchan AM. Validity and reliability of a quantitative computed tomography score in predicting outcome of hyperacute stroke before thrombolytic therapy. *Lancet* 2000; **355**: 1670–4.

10 Albers GW. Advances in intravenous thrombolytic therapy for treatment of acute stroke. *Neurology* 2001; **57** (5 Suppl. 2): S77–81.

11 Moseley ME, Wendland MF, Kucharczyk. J. Magnetic resonance imaging of diffusion and perfusion. *Top Magn Reson Imaging* 1991; **3**: 50–67.

12 Warach SE. Tissue viability thresholds in acute stroke: the 4-factor model. *Stroke* 2001; **32**: 2640.

13 Kidwell CS, Saver JL, Mattiello J, Starkman S, Vinuela F, Duckwiler G, Gobin YP, Jahan R, Vespa P, Kalafut M, Alger JR. Thrombolytic reversal of acute human cerebral hemispheric injury shown by diffusion/perfusion magnetic resonance imaging. *Ann Neurol* 2000; **47**: 462–9.

14 Cintas P, Le Traon AP, Larrue V. High rate of recanalization of middle cerebral artery occlusion during 2-MHz transcranial color-coded Doppler continuous monitoring without thrombolytic drug. *Stroke* 2002; **33**: 626–8.

15 Diener HC, Cunha L, Forbes S, Silvenius J, Smets P, Lowenthal A. European Stroke Prevention Study 2. Dipyridamole and acetylsalicylic acid in secondary prevention of stroke. *J Neurol Sci* 1996; **143**: 1–10.

Index

Note: Page numbers in *italics* and bold represent figures/boxed material and tables respectively.